Mechanistic and inhibition studies on γ-butyrobetaine hydroxylase

A thesis submitted to the Board of the Faculty of Physical Sciences of the University of Oxford in partial fulfilment of the requirements for the degree of Doctor of Philosophy

Anna M. Rydzik

Merton College, University of Oxford

Hilary Term 2014

Abstract

Carnitine is an essential metabolite in the human body. It carries out several roles in human metabolism, including that in fatty acid metabolism. γ-Butyrobetaine hydroxylase (BBOX) is an Fe(II) and 2-oxoglutarate dependent oxygenase, which catalyses the final step of carnitine biosynthesis, i.e. hydroxylation of γ-butyrobetaine (GBB) to carnitine. Inhibition of BBOX has potential in the treatment for cardiovascular diseases.

The work described in this thesis focussed on mechanistic and inhibition aspects of BBOX catalysis. Firstly, a set of analytical tools for BBOX activity measurements was developed. The synthesis of fluorinated substrate analogues provided the basis for development of two assays for use *in vitro* with the isolated protein and in lysates, with detection by fluorescence or ^{19}F NMR, respectively. Furthermore, the use of ^{19}F NMR to monitor protein-ligand interactions was exemplified with the work on metallo-β-lactamases.

The developed fluoride-release assay was then used to screen a library of small molecules and led to recognition of scaffolds with potential applications as inhibitors. Further structure-activity relationship studies led to the identification of potent BBOX inhibitors, which were then evaluated for their activity in cells. The crystal structure of human BBOX with one of the lead inhibitors revealed that BBOX can undergo significant conformational changes, involving a movement of an active site loop. BBOX conformational flexibility may have a role in the GBB mediated substrate inhibition observed both with isolated protein and in cells.

In addition to the mechanistic and functional studies, the potential of BBOX as a biocatalytic tool was examined. BBOX has been shown to catalyse a hydroxylation of the symmetrical dialkyl piperidine carboxylic acids, leading to formation of up to three stereocentres in one reaction.

In the last part of this work properties of human BBOX were compared to BBOX from *Pseudomonas* sp. AK1, revealing differences in kinetic behaviour and substrate specificity. Novel substrates for bacterial BBOX were identified. *Pseudomonas sp AK1* BBOX was shown to hydroxylate amino acid analogues leading to formation of 1,2-amino alcohols.

Acknowledgements

I would like to thank my supervisor, Prof. Christopher J. Schofield, for inviting me to his lab. He has not only provided me with his guidance, 'crazy' ideas and interesting discussions, but has also given me the freedom to choose and pursue my own research directions (which he was still funding!).

My graduate studies in Oxford would not be possible without generous financial support from Dulverton Trust. In addition, the last months of my studies have been facilitated by a scholarship from the Vice Chancellors' Fund at the University of Oxford. I am indebted to the Trustees of both bodies for providing me with a great opportunity of becoming a member of the Oxford University.

I owe my gratitude to people with whom I have collaborated on various projects. The work on the γ-butyrobetaine hydroxylase would not be possible without Dr. Grazyna Kochan, who not only generously supplied me with a human enzyme, but also supported me with her advice throughout my D.Phil. Dr. Ivanhoe Leung has been of invaluable help with NMR experiments and discussions regarding the BBOX project. Dr. Armin Thalhammer has always been a source of great ideas and discussions. I also want to thank Dr. Jurgen Brem and Dr. Sander van Berkel for being one of the most enthusiastic people I have had the pleasure of working with. I owe my gratitude to all the people I have worked with and who are not mentioned by name above. I am also indebted to all who served me with their advice and critical discussions, even though not directly involved in my projects.

I am indebted to those who have given up their time to teach me new techniques. In particular, I would like to thank Dr. Luc Henry, Dr. Adam Hardy and Dr. Ruben Gomez-Castellanos for teaching me molecular biology; Dr. Michael McDonough and Dr. Rasheduzzaman Chowdhury for introducing me to the crystallisation procedures and solving BBOX structures; Dr. Ivanhoe Leung and Dr. Timothy Claridge for their help with the NMR spectroscopy; Dr. Nikita Loik for his patience with MS setup; Dr. Armin Thalhammer and Dr. Jurgen Brem for their assistance with fluorescence based techniques; WeiShen Aik and Dr. Akane Kawamaura for showing me how to work with tissue cultures; Dr. Steven Inglis for introducing me to the synthesis lab. Special thanks go to Dr. Radoslaw Lipinski, Dr. Adam Hardy, Dr. Sander van Berkel, Dr. Luc Henry and Dr. Carmen Domene for proof-reading this thesis. I would also like to thank other CJS group members who assisted me in any way during my studies.

I would like to thank my family and friends for their continuous support during past few years - especially my parents and sister, who constantly encouraged me in my efforts. I want to express my special thanks to Radek for his care and support during past years and for his patience with me during writing up. Despite the struggle we have had along the way and regardless of what awaits us in the future, I will always be grateful to him, because without him, I would not be where I am now.

Declaration

The work described in this thesis is entirely my own, except where I have either acknowledged help from a named person or given reference to a published source. Parts of this thesis have been published, as indicated in the end of the chapters. Written permission has been obtained from the publishers of any copyright figures for use in this thesis.

Contents

Abbreviations

2HG	2-hydroxyglutarate
2OG	2-oxoglutarate
2TY	2-tryptone/yeast extract
3-keto-GBB	3-carboxy-*N*,*N*,*N*-trimethyl-2-oxopropan-1-aminium
ACV	*N*-[(5*S*)-5-amino-5-carboxypentanoyl]-L-cysteinyl-D-valine
ALDH9	aldehyde dehydrogenase E3
ATP	adenosine triphosphate
BBOX	γ-butyrobetaine hydroxylase
BFA	3-bromo-1,1,1-trifluoroacetone
BIQ	bicyclic isoquinolinyl inhibitor
BlaB	metallo-β-lacatamase from *Chryseobacterium meningosepticum*
BLAST	basic local alignment search tool
Bn	benzyl
Boc	*tert*-butoxycarbonyl
CACT	carnitine-acylcarnitine translocase
CAR	L-carnitine
CARNF	(*R*)-3-carboxy-*N*-(fluoromethyl)-2-hydroxy-*N*,*N*-dimethylpropan-1-aminium
CAT	carnitine O-acetyltransferase
Cbz	carboxybenzyl
CDI	carbonyldiimidazole
CoA/ CoASH	coenzyme A
CODD	*C*-terminal oxygen dependent degradation domain
COSY	correlation spectroscopy
CPT I	carnitine palmitoyltransferase I
CPT II	carnitine palmitoyltransferase II
DAST	diethylaminosulfur trifluoride
DCM	dichloromethane
Deoxo-Fluor	bis(2-methoxyethyl)aminosulphur trifluoride
DMAP	4-dimethylamino pyridine
DMF	dimethylformamide
DM-NOFD	dimethyl-*N*-oxalyl-D-phenylalanine
DMOG	dimethyl-*N*-oxalyl-glycine
DMSO	dimethylsulphoxide
DSBH	double-stranded β-helix
E. coli	*Escherichia coli*
EDTA	ethylenediaminetetraacetic acid
ELSD	evaporative light scattering detection
ESI-MS	electrospray ionisation mass spectrometry
FIH	factor inhibiting hypoxia inducible factor
FBXL11	F-box and leucine-rich repeat protein 11
FBS	fetal bovine serum
GBB	γ-butyrobetaine
GBB-2	glycine betaine

GBB-3	2-carboxy-*N*,*N*,*N*-trimethylethan-1-aminium
GBB-5	4-carboxy-*N*,*N*,*N*-trimethylbutan-1-aminium
GBB-6	5-carboxy-*N*,*N*,*N*-trimethylpentan-1-aminium
GBB-CH3	*N*,*N*,*N*-trimethyl-4-oxopentan-1-aminium
GBB-NH(R)	(2*R*)-amino-γ-butyrobetaine
GBB-NH(S)	(*2S*)-amino-γ-butyrobetaine
GBB-OH	(2*S*)-hydroxy-γ-butyrobetaine
GBB-OMe	γ-butyrobetaine methyl ester
GBBF	(*3S*)-fluoro- γ-butyrobetaine
GBBNF	3-carboxy-*N*-(fluoromethyl)-*N*,*N*-dimethylpropan-1-aminium
hBBOX	human γ-butyrobetaine hydroxylase
HEPES	4-(2-hydroxyethyl)-1-piperazineethanesulfonic acid
HIF	hypoxia inducible factor
HMPA	hexamethylphosphoramide
HPLC	high-performance liquid chromatography
HSQC	heteronuclear single quantum coherence spectroscopy
HTMLA	hydroxytrimethyllysine aldolase
IPNS	isopenicillin N synthase
i-Pr	isopropyl
IPTG	isopropyl β-D-1-thiogalactopyranoside
JMJD	Jumonji domain containing protein
K_D	dissociation constant
KDM	Histone lysine demethylase
K_I	inhibition constant
K_M	Michaelis-Menten constant
LB	Luria-Bertani media
LC-MS	Liquid Chromatography Coupled Mass Spectroscopy
LHDMS	lithium bis(trimethylsilyl)amide
MBL	metallo-β-lactamase
MBP	maltose binding protein
MS	mass spectrometry
NADH	Nicotinamide Adenine Dinucleotide
NDM-1	New Delhi Metallo-β-lactamase 1
NMR	nuclear magnetic resonance
NOE	nuclear Overhauser effect
NOFD	*N*-oxalyl-D-phenylalanine
NOG	*N*-oxalylglycine
OD	optical density
ORF	open reading frame
P4H	prolyl 4-hydroxylase
PBP	Penicillin Binding Protein
PBS	phosphate buffered saline
PCA	pyridine carboxylic acid
PDB	protein data bank
PDCA	pyridinedicarboxylate
PHD	prolyl hydroxylase domain containing enzyme
PHF8	PHD finger protein 8
PLP	pyridoxal phosphate

psBBOX	γ-butyrobetaine hydroxylase from *Pseudomonas sp. AK1*
PyBOP	(Benzotriazol-1-yloxy)tripyrrolidinophosphonium hexafluorophosphate
SAM	*S*-adenosyl methionine
SAR	structure-activity relationships
SBL	serine-β-lactamase
SDS-PAGE	sodium dodecylsulphate polyacrylamide gel electrophoresis
SHMT	serine hydroxymethyltransferase
SPM-1	Sao Paulo Metallo-β-lactamase 1
TBS	*tert*-butyldimethylsilyl
TCA	tricarboxylic acid
TCEP	tris(2-carboxyethyl)phosphine
TEMED	tetramethylethylenediamine
TFA	trifluoroacetic acid
THF	tetrahydrofurane
THP	3-(2,2,2-trimethylhydraziniumyl)propionate
TMABA	4-*N*-trimethylaminobutyraldehyde
TMABA-DH	4-*N*-trimethylaminobutyraldehyde dehydrogenase
TMAO	trimethylamine-*N*-oxide
TML	N^{ϵ}, N^{ϵ}, N^{ϵ}-trimethyllysine
TML-OH	3-hydroxy-N^{ϵ}-trimethyllysine
TMLH	trimethyllysine hydroxylase
TMLNF	(*S*)-5-amino-5-carboxy-*N*-(fluoromethyl)-*N*,*N*-dimethylpentan-1-aminium
TMO-(R)	(*R*)-4-amino-4-carboxy-*N*,*N*,*N*-trimethylbutan-1-aminium
TMO-(S)	(*S*)-4-amino-4-carboxy-*N*,*N*,*N*-trimethylbutan-1-aminium
TOCSY	total correlation spectroscopy
TRIS	tris(hydroxymethyl)aminomethane
UPLC	ultra performance liquid chromatography
UTR	untranslated region
VHL	Von Hippel–Lindau tumour suppressor
wt	wild type

Standard abbreviations for nucleotides, amino acids and SI-units are used throughout.

Chapter 1

Introduction

Abstract

Chapter 1 provides an overview of the literature describing the physiological roles and metabolism of carnitine in animals, including humans. The current knowledge about enzymes involved in carnitine biosynthesis in animals is described, with a particular focus on trimethyllysine hydroxylase (TMLH) and γ-butyrobetaine hydroxylase (BBOX), which are 2-oxoglutarate dependent oxygenases that catalyse the first and the last step in carnitine biosynthesis. The role of carnitine in human metabolism is also discussed.

Contents

1 Carnitine – general information

1.1 Carnitine structure

L-Carnitine ((*3R*)-hydroxy-4-*N*,*N*,*N*-trimethylamino butyrate) is a low molecular weight molecule with high polarity and water-solubility. Carnitine was first characterised from muscle extracts in 1905 and is named after the Latin *carnis* (flesh). In 1962, the stereochemistry of the physiologically active form of carnitine was assigned as the L-(-) stereoisomer[1] (Fig. 1). Since then carnitine has been found to occur in most animals, some plants, yeast and microorganisms. The hydroxyl group of carnitine is of a great physiological relevance. The hydroxyl group can be *O*-acylated with acyl-coenzyme A activated derivatives in a carnitine acyltransferase catalysed process. In animals this process is essential as it facilitates fatty acid transport and the maintenance of acetyl group homeostasis. In healthy human, around 80% of carnitine is present in a free form in plasma.[1]

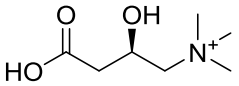

Figure 1 Structure of L-carnitine

1.2 Source of carnitine

Carnitine is considered to be a non-essential nutrient because it can be synthesised *in vivo* through a biosynthetic pathway, which is highly conserved across animals. However, in humans around 75% of the total carnitine is estimated to come from the diet and around 25% from endogenous biosynthesis.[2,3] The main food sources of carnitine include meat and dairy products.[4] In the case of those on a vegetarian diet, the blood serum concentrations of carnitine are lower than in the meat eating reference population.[5,6] Collectively, carnitine homeostasis is maintained through biosynthesis, dietary intake and reabsorption in the kidney.[4] Carnitine absorption is processed through active transport and diffusion.[7]

1.3 Tissue distribution and concentration

Carnitine is mainly found in heart and muscle tissue in animals including rats and pigs. Lower levels of carnitine are found in kidney, brain and testis.[8,9] The carnitine plasma concentrations in animals have been found to be sex and age dependent. In humans, carnitine plasma levels increase through the first year of life and stabilise until puberty at the level of 40 µM.[10-13] Subsequently, carnitine plasma levels increase in males, but not females, to reach adulthood levels of around 50 µM in males, which may suggest a role of sex hormones in the regulation of carnitine plasma levels.[11,14,15] In rats there are even more pronounced differences, with carnitine concentrations in males being almost twice as high as in females.[16]

2 Carnitine biosynthesis

A fully functional carnitine biosynthesis pathway has been identified in mammals, i.e. humans, mice and rats.[3,16] Sequence analyses indicate that *Drosophila melanogaster* and *Caenorhabditis elegans* have orthologs of the carnitine biosynthesis genes.[3] In some yeasts, i.e. *Nerosporra crassa*[17] and *Candida albicans*[18], a fully functional carnitine biosynthesis pathway has been characterised, while baker's yeast *Saccharomyces cerevisiae* is unable to biosynthesise carnitine endogenously, but can metabolise carnitine in growth media. Recently, evidence for carnitine biosynthesis in plants, i.e. *Arabidopsis thaliana* has been demonstrated.[19,20] To date there is no report of a full carnitine biosynthesis pathway in bacteria, however some species including certain *Pseudomonas* strains have been shown to contain the final enzyme of carnitine biosynthesis pathway – γ-butyrobetaine hydroxylase.[21-24]

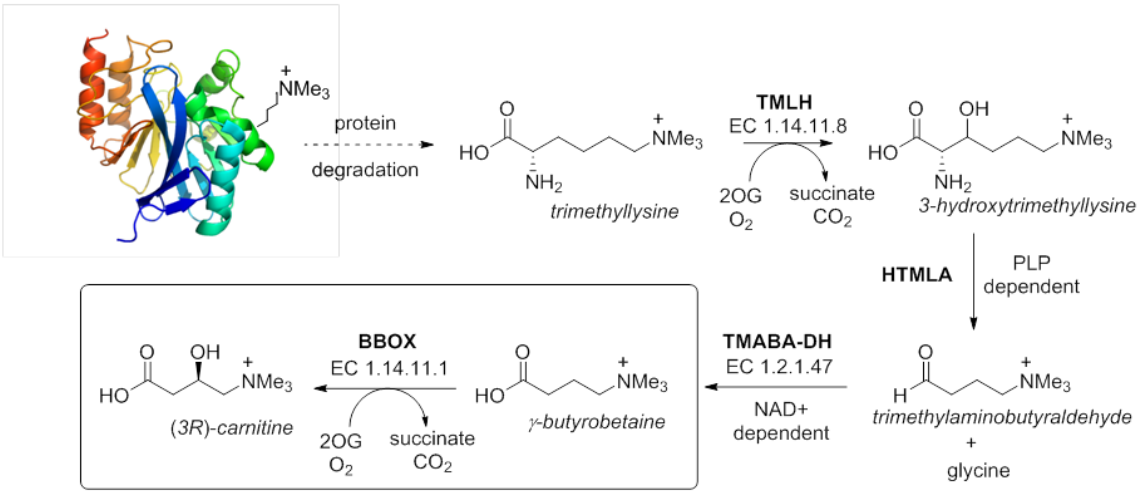

Figure 2 Enzymology of carnitine biosynthesis pathway.

Carnitine biosynthesis proceeds in four enzymatic steps, starting from N^{ϵ},N^{ϵ},N^{ϵ}-trimethyllysine (TML) (Fig. 2). The first step is catalysed by trimethyllysine hydroxylase (TMLH) and involves 2-oxoglutarate (2OG) and Fe(II) dependent hydroxylation of TML to 3-hydroxytrimethyllysine (TML-OH). TML-OH then undergoes aldolytic cleavage catalysed by pyridoxal-5'-phosphate (PLP) dependent hydroxytrimethyllysine aldolase. The resulting 4-trimethylaminobutyraldehyde (TMABA) is then oxidised to give γ-butyrobetaine (GBB) by NAD^+ dependent 4-trimethylaminobytyraldehyde dehydrogenase (TMABA-DH). The final step of carnitine biosynthesis involves hydroxylation of GBB to carnitine catalysed by the 2OG and Fe(II) dependent γ-butyrobetaine hydroxylase (BBOX).

2.1 Precursors

Carnitine biosynthesis originates from the essential amino acids lysine and methionine. It was shown that the *N*-methyl groups of carnitine originate from methionine,[25] which is used as a methyl donor in S-adenosylmethionine (SAM) dependent lysine methyltransferase.[26] The carbon backbone of carnitine was shown to originate from lysine.[27,28] In mammals, the main precursor of carnitine biosynthesis is N^{ϵ},N^{ϵ},N^{ϵ}-trimethyllysine (TML),[29,30] which is believed to originate from protein degradation. The availability of TML has been identified as the rate limiting step in carnitine biosynthesis.[1] Recently, it was reported that plant derived food contains substantial quantities of TML, and thus the dietary intake is likely the main source of TML in mammals.[31] However, previous observations suggested that endogenous TML is mainly excreted in the urine (>75%) and exogenous TML was not considered an efficient precursor of carnitine biosynthesis.[32-34] In line with those observations it is believed that TML is synthesised intercelluraly and converted into carnitine in the tissue of origin.[16] An interesting hypothesis arises from the identification of free lysine methyltransferase in *Neurospora crassa*,[35] although not yet identified the presence of a homologue of this enzyme in animals would enable conversion of free lysine to TML.

2.2 Tissue distribution of carnitine biosynthesis enzymes

The first three enzymatic steps of carnitine biosynthesis have been shown to occur in all studied human tissues, e.g. liver, brain, kidney, heart and skeletal muscle. However, the activity for γ-butyrobetaine hydroxylase has only been reported in the liver, kidney and to lesser extent in the brain.[36] The activity of γ-butyrobetaine hydroxylase in the liver was found to be age-dependent, with lower levels being observed in infants rising to maximal quantities in adult men. In contrast, activity of γ-butyrobetaine hydroxylase in the kidney did not depend on the age of subject as infants displayed adult levels of activity.[37] The other enzymes studied did not display age-dependency.

2.3 Trimethyllysine hydroxylase (TMLH)

Trimethyllysine hydroxylase (TMLH, E.C. 1.14.11.8) is the first enzyme of the carnitine biosynthesis pathway and is responsible for hydroxylation of N^{ϵ},N^{ϵ},N^{ϵ}-trimethyllysine (TML) to give 3-hydroxy-N^{ϵ},N^{ϵ},N^{ϵ}-trimethyllysine (TML-OH) (Scheme 1). TMLH belongs to the superfamily of 2-oxoglutarate (2OG) dependent oxygenases[38-40] and requires 2OG, Fe(II) and oxygen for catalytic activity.[41-43]

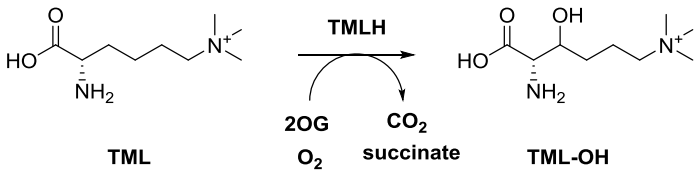

Scheme 1 TMLH catalysed hydroxylation of TML.

2.3.1 Discovery

TML was shown to be metabolised to give carnitine biosynthesis intermediates, i.e. γ-butyrobetaine aldehyde (TMABA) and γ-butyrobetaine (GBB) in whole rats[44] and in the isolated liver slices[30,45] in the early 1970s. The first observation of activity of semi-purified TMLH was described by Hulse and co-workers[46] who demonstrated that rat liver mitochondria were able to efficiently convert TML to 3-hydroxy-TML (TML-OH) in the presence of 2OG, Fe(II) and ascorbate. No enzymatic activity of this kind was found in the soluble fractions of the liver isolate.

2.3.2 Product identification

The identity of the product of TMLH catalysis was confirmed by periodate mediated oxidation of the hydroxylated compound, which yielded TMABA. Furthermore, a reaction of TML-OH with serine transhydroxymethylase (E.C. 2.1.2.1) also yielded TMABA and glycine as a second product.[46] The stereochemistry on the C-3 of TML-OH was not then directly assigned. However NMR work on 3-hydroxylysine diastereomers,[47] suggests the formation of the *erythro* isomer – (*2S, 3S*)-3-hydroxy-trimethyllysine.

2.3.3 Tissue distribution and localisation

TMLH activity has been found in human and rat liver, skeletal muscle, heart and brain tissues, with the highest activity being measured in kidney.[36,43] TMLH has been reported to be localised in the mitochondria as shown by differential centrifugation experiments[42,46] and subcellular fractionation using density gradient analyses.[48] Analysis of TMLH sequence has revealed the presence of *N*-terminal mitochondrial targeting sequence (MWYHKLLHQQSRLQNLMKRGDIAHGLRLSG).[49] The mitochondrial localisation of TMLH makes it unique among other carnitine biosynthesis enzymes, which otherwise are all localised in

the cytosol. Follow-up work has shown TMLH to be localised in the mitochondrial matrix.[49] TML-OH formation was shown to be limited by TML transport across the mitochondrial inner membrane and the existence of putative mitochondrial TML/ TML-OH transport system has been proposed.[49] Flux through carnitine biosynthesis pathway must be regulated, because the capacity of the carnitine biosynthesis exceeds a need for daily carnitine production.[50,51] The availability of TML is rate limiting for carnitine biosynthesis.[52,53] The presence of proposed TML/ TML-OH transport system could serve as an additional way of regulating carnitine biosynthesis.

2.3.4 Gene analysis

In humans the TMLH gene is located on the chromosome X (Xq28 region, between nucleotide positions 154495791 and 154372967) and is split into 8 exons.[54] Two alternatively spliced variants of TMLH, which are apparently ubiquitously expressed in humans have been cloned and expressed, to give proteins of 421 and 399 amino acids, respectively. Interestingly, in one of the splicing variants, one of the active site Fe(II) binding site residues appears to be mutated (H389R), which leads to loss of the hydroxylase activity.[55] Co-expression studies in HEK 293T kidney embryonic cells suggest that the non-active TMLH variant may act as a negative regulator of TMLH activity.[55]

2.3.5 Biochemical characterization of TMLH

TMLH initially was purified from rat kidney; subsequently cDNA encoding for rat TMLH was identified.[48] Based on this human and mouse cDNA TMLH homologues were identified. Human and rat TMLH have been produced in COS cells. Expression trials in yeast and *E. coli* were unsuccessful.

The gene encodes for a 405 amino acid protein with mass of 47.5 kDa, however the protein obtained from COS cell purification was found to have an apparent mass of 43 kDa. Inactive TMLH protein obtained from *S. cerevisiae* was found to have a mass of 47.5 kDa. It was therefore suggested that TMLH is expressed as a 47.5 kDa precursor, which is then processed to give a shorter product of 43 kDa upon transport to the mitochondria. Gel filtration and native gel electrophoresis analyses demonstrated protein with mass of 87 kDa, indicating that TMLH, similarly to BBOX, exists in a solution as a homodimer.[48] TMLH was found to have a broad pH optimum (6.5-7.5). The cofactor (i.e. TML, 2OG, Fe(II) dependencies of TMLH have been investigated by different groups. The results are summarised in Table 1.

Table 1 K_M values for TML, 2OG and Fe(II) as measured with TMLH from rat, mouse and *N. Crassa*.

TMLH source	Km values (mM)		
	TML	2OG	Fe(II)
Recombinant[a] rat TMLH[48]	1.1	0.109	0.054
Mouse liver homogenate[56]	0.164	0.605	0.004
Partially purified[b] TMLH from rat kidney[43]	0.10[c]	0.48	0.021
Partially purified[b] TMLH from rat liver[43]	0.10 [c]	0.48	0.020
Partially purified[b] TMLH from rat heart[43]	0.13 [c]	0.46	0.022
Partially purified[b] TMLH from rat skeletal muscle[43]	0.12 [c]	0.53	0.024
Rat kidney homogenate[42]	1.6	-	-
Recombinant[d] *Neurospora Crassa* TMLH[57]	0.33	0.133	0.46

[a] Recombinant rat TMLH expressed in COS-1 cells, [b] ammonium sulphate fractions were used, [c] The assay uses D,L-TML as a substrate [d] *Neurosporra crassa* TMLH expressed in *Saccharomyces cerevisiae.*

2.3.6 Inhibition of TMLH

Basic work on the influence of various substrate analogues and metals on BBOX was described by Stein *et al.*[43] The data for 2OG, TML and Fe(II) substitutes are summarized in Tables 2, 3 and 4, respectively. Measurements were performed with partially purified TMLH from rat kidney homogenates.

Table 2 Inhibition of TMLH from rat kidney by 2OG analogues.

Inhibitor	K_i
Succinate	3.0 mM
Citrate	3.9 mM
Oxalacetate	5.04 mM

Table 3 Inhibition of TMLH from rat kidney by TML analogues.

Inhibitor	K_i
2-*N*-Acetyl-6-*N*-trimethyl-L-lysine	0.2 mM
6-*N*-dimethyl-L-lysine	0.3 mM
6-*N*-monomethyl-L-lysine	0.45 mM
6-*N*-trimethyl-D-lysine	2.0 mM
L-Carnitine	3.5 mM
4-*N*-Trimethylaminobutyric acid	3.75 mM
3-Hydroxy-6-*N*-trimethyl-D,L-lysine	4.23 mM
L-Lysine	5.43 mM
Acetyl- L-Carnitine	No effect

Table 4 Inhibition of TMLH from rat kidney by Fe(II) analogues.

Inhibitor	K_i
$ZnCl_2$	2.86 µM
$CoCl_2$	5.8 µM
$CdCl_2$	15.63 µM
$NiCl_2$	18.57 µM
$MgCl_2$	No effect
$CaCl_2$	No effect

2.3.7 TMLH in disease

Meta-data analyses have shown that mutations in the TMLH gene are linked to autism.[58,59] As mentioned previously, TMLH is localized on the X chromosome in a highly unstable region.[54,55] Therefore, mutations in the TMLH gene have been found to affect male population to a higher extent.[60] Several defects in the TMLH encoding gene region have been identified[61,62] and linked with autistic phenotype of male subjects.[60] Some of those mutations were shown to lead to loss of TMLH function and impaired carnitine biosynthesis, with higher levels of TML detected in patients.[60]

2.4 Hydroxytrimethyllysine aldolase (HTMLA)

Hydroxytrimethyllysine aldolase (HTMLA) catalyses the aldolytic cleavage of TML-OH to yield γ-trimethylaminobytyraldehyde (TMABA) (Scheme 2). The process, like in the case of many other aldolases, appears to be dependent on pyridoxal 5'-phosphate (PLP), a derivative of pyridoxine (vitamin B_6).[16] The involvement of the PLP dependent enzyme in carnitine biosynthesis is supported by the observation that carnitine biosynthesis is inhibited by 1-amino-D-proline,[63] antagonist of vitamin B_6.[64] It was also shown that a diet low in vitamin B_6 leads to lowered carnitine levels in rat.[65,66]

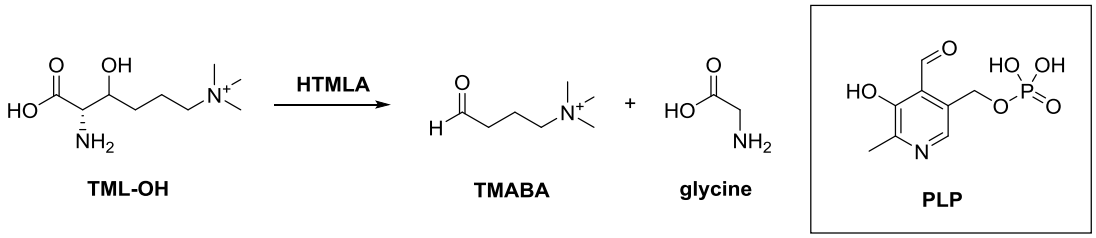

Scheme 2 HTMLA catalysed aldolytic cleavage of TML-OH. HTML is a PLP dependent enzyme.

2.4.1 Localization and tissue distribution

HTMLA is most likely a cytosolic enzyme, as its activity has been found almost exclusively in soluble fractions of cellular extracts. HTMLA activity can be detected in several human tissues, including liver, brain, kidney, heart and skeletal muscle homogenates.[36]

2.4.2 Identification

The gene encoding for HTMLA has not been yet identified in mammals, including humans. Serine methyltransferases are PLP-dependent enzymes, which catalyse conversion between serine and glycine. It was previously speculated that HTMLA might be similar to serine hydroxylmethyltransferase (SHMT), as an isolated SHMT was shown to convert TML-OH to TMABA.[67] Threonine aldolases, a PLP-dependent class of enzymes catalysing interconversion of threonine to glycine and acetaldehyde have been proposed as likely candidates for HTMLA homologues.[3]

2.4.2.1 *C. albicans* HTMLA

The complete carnitine biosynthesis pathway was assigned in yeast *Candida albicans*.[18] The studies have shown that one of two genes encoding threonine aldolase orthologs was encoding protein with HTMLA activity. However, even though disruption of any other gene from the carnitine biosynthesis pathway led to a block of carnitine biosynthesis, in the strains with the HTMLA gene disrupted some aldolytic cleavage of TML-OH could still be detected. Therefore, it was proposed that the conversion of TML-OH to TMABA might be promiscuous and can likely be catalysed by more than one enzyme.

2.5 Trimethylaminobutyraldehyde dehydrogenase (TMABA-DH)

Trimethylaminobutyraldehyde dehydrogenase (TMABA-DH, E.C. 1.2.1.47) is a NADH dependent enzyme, which catalyses the oxidation of TMABA to γ-butyrobetaine (GBB) (Scheme 3).

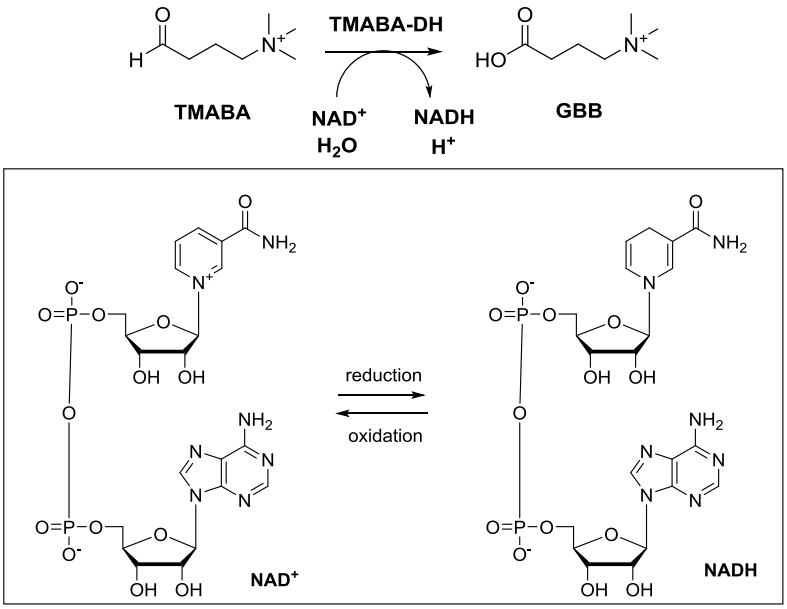

Scheme 3 TMABA-DH catalysed oxidation of TMABA to GBB. TMABA-DH is a NAD^+ dependent enzyme – structure of cofactor given below.

2.5.1 Tissue distribution and localization

In human tissues, the rate of TMABA dehydrogenation is highest in the liver, substantial in kidney, but lower in the brain, heart and in muscles.[36] TMABA-DH is localised in the cytosol. It has been first isolated from bovine liver.[68] Subsequently, TMABA-DH was purified from the rat liver, and after identification of the gene encoding for TMABA-DH, it was produced in *E. coli* as a MBP (maltose binding protein) fusion construct.[69] Recently, also TMABA-DH homologues from *Pseudomonas sp. 13CM* have been purified and characterised.[70,71]

2.5.2 Gene identification

The isolation and purification of rat liver TMABA-DH led to identification of the gene encoding for TMABA-DH in rats. The rat cDNA encodes a polypeptide of 494 amino acid residues, with calculated mass of 55 kDa.[69] BLAST analyses identified human aldehyde dehydrogenase 9 (ALDH9, E.C. 1.2.1.19) as a close homologue to rat TMABA-DH, with 92% sequence identity.[69] Subsequently, ALDH9 was reported to convert TMABA to GBB. Further kinetic analyses revealed similar parameters for rat TMABA-DH and human ALDH9, with high substrate specificity towards TMABA. Therefore, ADLH9[72-74] is the most likely candidate for TMABA-DH in humans.

2.6 γ-Butyrobetaine hydroxylase (BBOX)

γ-Butyrobetaine hydroxylase (BBOX, E.C. 1.14.11.1) catalyses the final step of carnitine biosynthesis, i.e. stereoselective[75] conversion of γ-butyrobetaine (GBB) to carnitine (Scheme 4).

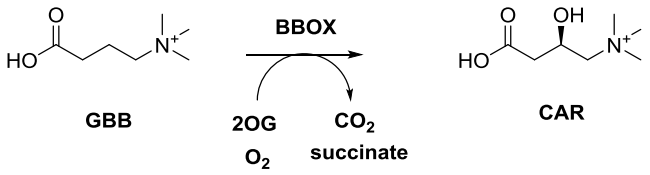

Scheme 4 BBOX catalysed hydroxylation of GBB to CAR.

2.6.1 Identification

In pioneering work, BBOX was partially purified from *Pseudomonas sp. AK1*,[22-24] which is a bacterial strain capable of growing on GBB as a sole source of carbon and nitrogen. Subsequently, BBOX was purified from rat[76] and calf liver[77], human kidney[78] and *Pseudomonas* cells. Recombinant human BBOX has been produced in *E. coli*[79] and baculovirus infected insect cells.[80]

2.6.2 Tissue distribution and localisation

BBOX is localised in the cytosol as suggested by various reports.[76,81,82] Paul *et al.*[83,84] have reported BBOX activity to be present in peroxisomes, however those results could not be reproduced and require further validation.[16] In mammals, expression of the gene encoding for BBOX is tissue specific. BBOX has been found in kidney, liver, brain and possibly in testis.[16] Significant levels of BBOX activity can be found in kidney or liver, depending on species studied; BBOX activity in humans is found mainly in the kidney, while in rat and mouse kidney activity has not been detected, with the liver being the main site of carnitine production.[85,86] It also appears that BBOX expression is developmentally regulated. Liver BBOX activity increases until reaching adulthood in rat liver.[87,88] In humans, BBOX liver activity is lower at early stage of development, however BBOX activity in the kidney is already present at birth.[89]

2.6.3 Gene identification

cDNA encoding for human BBOX comprises of an open reading frame (orf) of 1161 bp,[90] which encodes for a polypeptide of 387 amino acids and mass 44.7 kDa. The BBOX1 gene is localised on chromosome 11q14-15. Furthermore, a cDNA encoding for rat liver and mouse small intestinal enterocytes[91] BBOX was identified and characterised.[87] The transcription of the BBOX1 gene has been studied in the main sites of carnitine production in humans, i.e. the kidney, liver and brain. It has been shown that BBOX1 gene expression undergoes tissue specific regulation and that this regulation can occur during transcription initiation and mRNA maturation. Transcription initiation of the BBOX gene is regulated by 3 different promoters and

results in mRNAs, which differ in their 5' UTR, while mRNA maturation can be regulated by different polyadenylation mechanism, resulting in mRNAs with variations in their 3' UTR structure.[92] Recently, it has also been shown that maturation of BBOX1 mRNAs in rat liver is diet-dependent and affects carnitine levels in cells, i.e. high fat diet leads to different polyadenylation patterns and increased carnitine levels in liver.[93]

2.6.4 BBOX biochemical and structural characterisation

2.6.4.1 2-Oxoglutarate dependent oxygenases family introduction

Non-haem/ Fe(II) 2-oxoglutarate (2OG) dependent oxygenases form a large superfamily of enzymes, which in animals catalyse hydroxylations and *N*-demethylations (*via* *N*-CH_3 hydroxylation)[94,95] and are involved in a wide variety of biologically important processes,[39] including posttranslational chromatin modifications (histone demethylases), oxygen sensing (HIF hydroxylases), nucleic acid modifications or fatty acid metabolism. In plants and micro-organisms the range of 2OG oxygenase catalysed reactions is even broader and includes ring expansions and closures or desaturations.[94] 2OG oxygenases use 2OG as a co-substrate and couple its oxidative decarboxylation to two-electron oxidation of a substrate to give hydroxylated product, succinate and carbon dioxide. Fe(II) is an essential cofactor, which facilitates catalysis via formation of Fe(IV)-oxo species (Fig. 3). Structurally 2OG oxygenases contain a double-stranded β-helix (DSBH, jelly roll) fold that supports highly conserved Fe(II)-binding motif (HxD/E. . .H)[40,96,97] (Fig. 4). The carboxylate and oxo group of 2OG chelates metal in a bidentate manner and 2OG C-5 carboxylate is bound inside the active site pocket, including by electrostatic interactions.

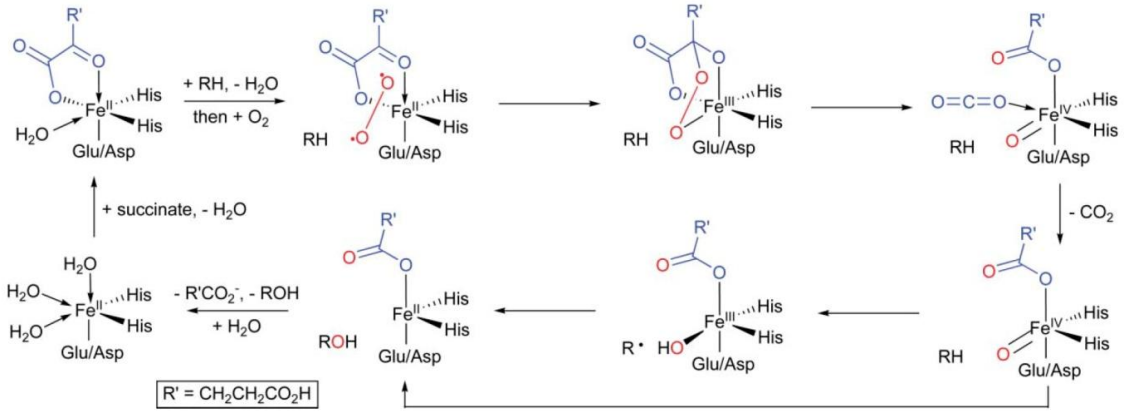

Figure 3 Proposed mechanism for hydroxylation, as catalysed by 2OG oxygenases. Picture from Kershaw *et al.*[98]

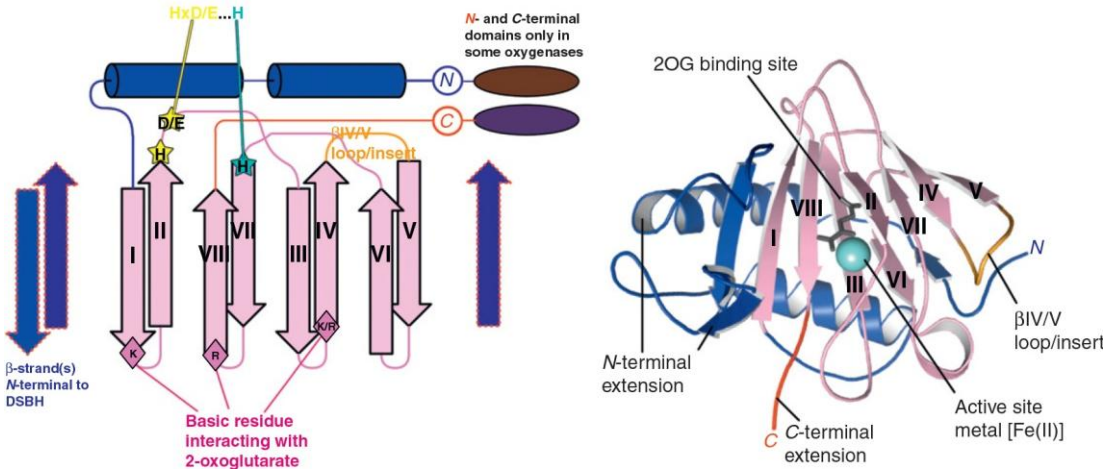

Figure 4 General structural architecture of 2OG oxygenases, as presented by two-dimensional topology of 2OG oxygenases and on three dimensional structure of AlkB (PDB id: 3BIE). Figure from Aik *et al.*[96]

2.6.4.2 Homology

There is a high sequence similarity (26%)[80] between BBOX and TMLH[80] (Fig. 5). BBOX, like TMLH belongs to the superfamily of 2OG dependent oxygenases and requires 2OG, Fe(II) and oxygen for catalysis.

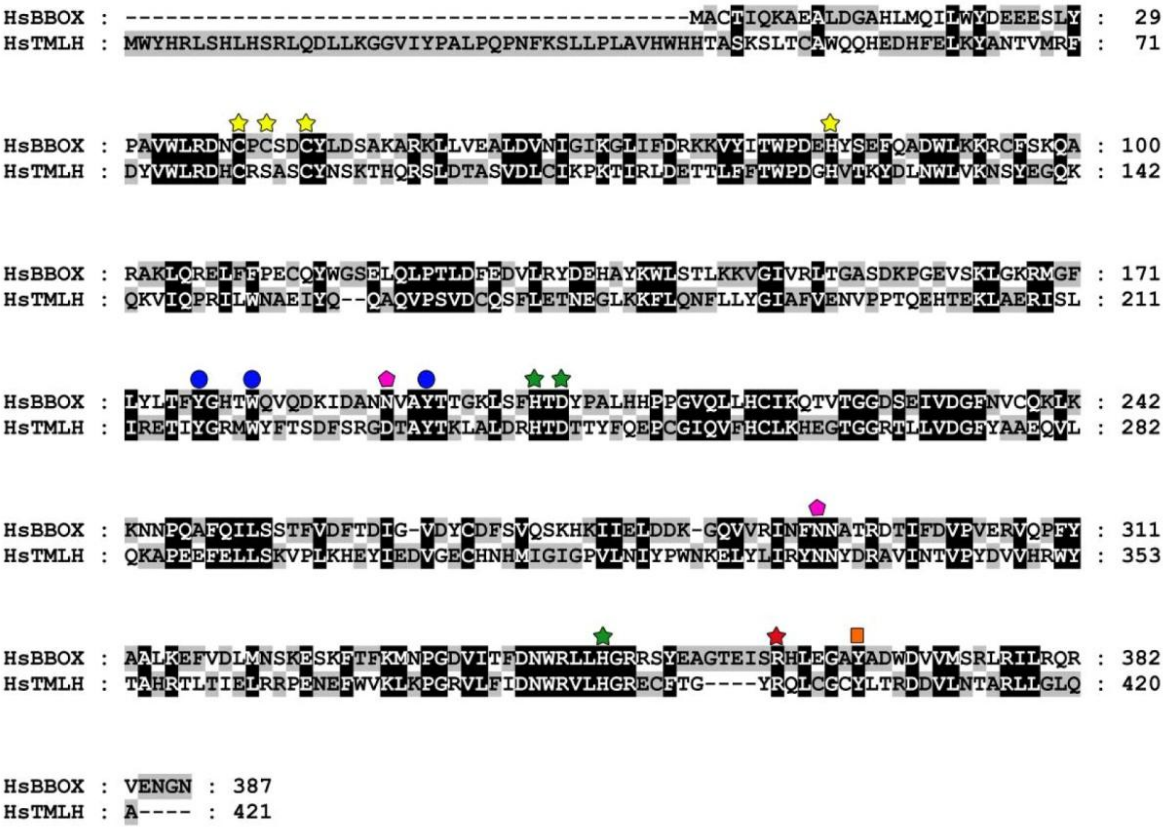

Figure 5 Sequence alignment of human BBOX (hBBOX gi|4502369) and human TMLH (hTMLH gi|8922625). Fe(II) ligating residues are indicated by green stars, Zn(II) ligating residues are indicated by yellow stars; the 2OG C5 interacting arginine is indicated by a red star, 'aromatic cage' residues involved in binding the Me_3N+- group of GBB are indicated by blue circles; GBB carboxylate interacting residues are indicated by magenta pentagons. The figure is adapted from Leung *et al.*[80]

2.6.5 Biochemical characterisation

BBOX isolated from rat liver, bovine liver and *Pseudomonas sp AK1* as well as recombinant human BBOX (purified from either Baculovirus infected insect cells or *E. coli*) was found to exist in a solution as a homodimer,[23,79,80] similarly to TMLH. Some early reports suggest that human BBOX purified from kidney can exist as 3 isoforms.[99] BBOX catalysis depends on 2-oxoglutarate (2OG), Fe(II) and oxygen – which is characteristic for enzyme belonging to the 2OG dependent oxygenase superfamily. The oxygen dependence of BBOX was reported by Lindstedt *et al.* for human kidney BBOX (K_M for O_2 was 5.5% vol). The reported K_M values for GBB and 2OG from different sources are summarised in Table 5.

Table 5 Kinetic parameters of BBOX from *Pseudomonas sp AK1*, rat liver and human.

BBOX source	K_M [mM]		remarks
	2OG	GBB	
Pseudomonas sp AK1	0.018	-	Ng *et al.*[100]
Pseudomonas sp AK1	0.5	2.4	Lindstedt *et al.*[24]
Rat liver	0.05	0.029	Wehbie *et al.*[101]; GBB substrate inhibition observed over 0.2 mM
Rat liver	0.5	-	Lindstedt *et al.*[102]
Rat liver	0.125	0.08	Galland *et al.*[76]; substrate inhibition was observed above 0.2 mM concentration of GBB and 1 mM 2OG
Human kidney	0.10, 0.13, 0.11	0.13, 0.11, 0.13	Lindstedt *et al.*[99]; K_M values are given for 3 different BBOX isoforms idetified
Human kidney	0.3	0.2	Lindstedt *et al.*[78]; GBB substrate inhibition observed after 0.5 mM
Recombinant human BBOX	-	0.0275	Tars *et al.*[79]; BBOX expressed in *E. coli*; no GBB substrate inhibition observed (concentrations measured were up to 0.3 mM)

BBOX activity was found to be stimulated by ascorbate and to a lesser extent by other reducing agents.[76,80,81,103] This is in agreement with the previously observed ascorbate-dependent activation reported for many other 2OG dependent oxygenases. Moreover, the carnitine biosynthesis has been shown to be dependent on ascorbate,[104] which is likely due to stimulation of activity of 2OG dependent oxygenases involved in carnitine biosynthesis, i.e. BBOX and TMLH. BBOX catalysis has been also reported to be stimulated by the presence of catalase.[105,106] Catalase catalyses decomposition of hydrogen peroxide to give water and oxygen. Stimulation of 2OG dependent oxygenases by catalase has been known and is attributed to its protective properties against reactive oxygen species, which might be generated either enzymatically or non-enzymatically in the enzyme active site. A similar effect on BBOX activity was observed with glutathione peroxidase.[107]

The inhibition of BBOX and its role in disease is further discussed in the introduction to Chapter 5 – Inhibition of BBOX.

2.6.6 Structural characterisation

Recently, crystal structures of human BBOX in the absence (PDB id: 3N6W)[79] and the presence of metal and substrate analogues (PDB id: 3O2G, 3MS5)[80] have been solved. The BBOX substrate structure was obtained as complex with Zn(II) (an Fe(II) surrogate), NOG (*N*-oxalylglycine, a close structural mimic of 2OG, which does not undergo decarboxylation) and GBB at a resolution of 1.82 Å (PDB id: 3O2G).[80] The structure revealed a homodimer, which is in agreement with previous in solution analyses. Each of the monomers comprised of *N*- and *C*-terminal domains linked by α-helix. The dimerisation occurred via *N*-terminal domain, which is unprecedented for 2OG dependent oxygenases. The *C*-terminal domain has a DSBH fold, which is characteristic for 2OG dependent oxygenases. The *N*-terminal domain contains contained unexpected zinc binding site, where Zn(II) was chelated by 3Cys-1His binding motif (Cys38, Cys40, Cys 43 and His 82). The active site metal is coordinated by three ligands: His202, Asp204 and His347 – a motif characteristic to most 2OG dependent oxygenases.[108] NOG is binding active site metal in a bidentate manner by one on the oxygens from C-1 carboxylate and the carbonyl oxygen. The C-5 carboxylate of NOG interacts with Arg360 as observed for other 2OG oxygenases. GBB is binding next to the metal, such that pro-*R* C-H bond at C-3 projects towards metal (in agreement with the *R*-stereochemistry of hydroxylation product – carnitine).

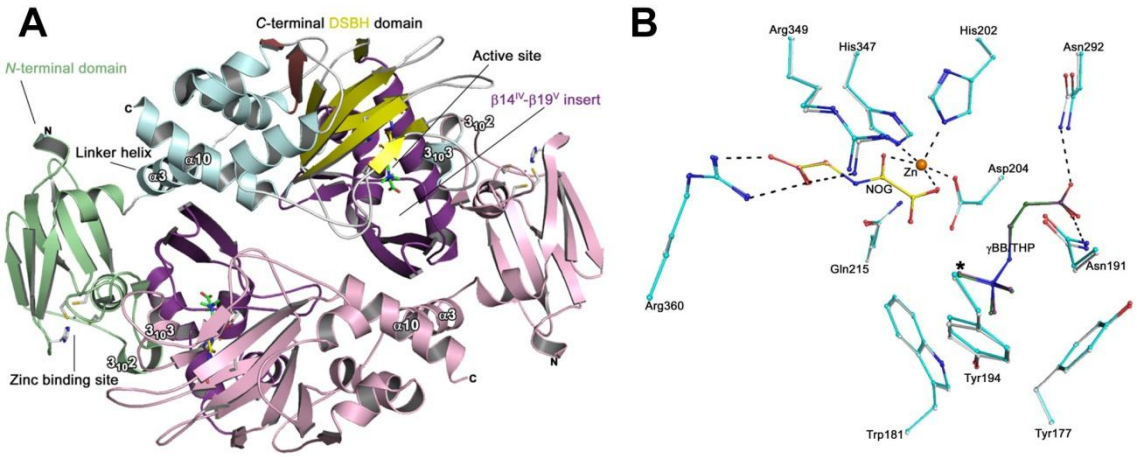

Figure 6 Views from a crystal structure of human BBOX in complex with Zn(II), GBB and NOG. A – The general fold of BBOX reveals a homodimer. Each of the monomers contains C-terminal domain with DSBH fold, containing active site and N-terminal zinc binding domain. B – View from active site of hBBOX with key residues responsible for metal and substrate binding. Figure adapted from Leung *et al*.[80]

3 Physiological role of carnitine

3.1 Role of carnitine in fatty acid metabolism

In animals fatty acids play an essential role as a primary energy source in many tissues, including in heart and skeletal muscles. Fat obtained from the diet is stored in the form of triglycerides, which can be hydrolysed to free fatty acids when needed to use as an energy source. Fatty acids are metabolized by the β-oxidation process in mitochondria. Carnitine is responsible for the transport of fatty acids through mitochondrial membrane.[7,109,110] The fatty acids, activated as acyl-CoA esters, undergo trans-esterification catalysed by carnitine palmitoyl transferase I (CPT I) to form *O*-acylated carnitine derivative.[111,112] The *O*-acylated carnitine is further transported through inner mitochondrial membrane by carnitine-acylcarnitine translocase (CACT).[113,114] Inside the mitochondrial matrix acyl-carinitine is a substrate for carnitine palmitoyl transferase II (CPT II), which catalyses hydrolysis of the acyl-carnitine esters with subsequent release of fatty acids and free carnitine.[113] The free carnitine can then be transported into the cytosol by the action of CACT and acyl-CoA enters β-oxidation.[115] Carnitine present in mitochondria can be also converted to short and medium chain length (C1-4) acyl-carnitines, through the action of carnitine acetyltransferase (CAT).[116-118] Products of CAT can then be transported into mitochondrial intermembrane space and cytosol via CACT.

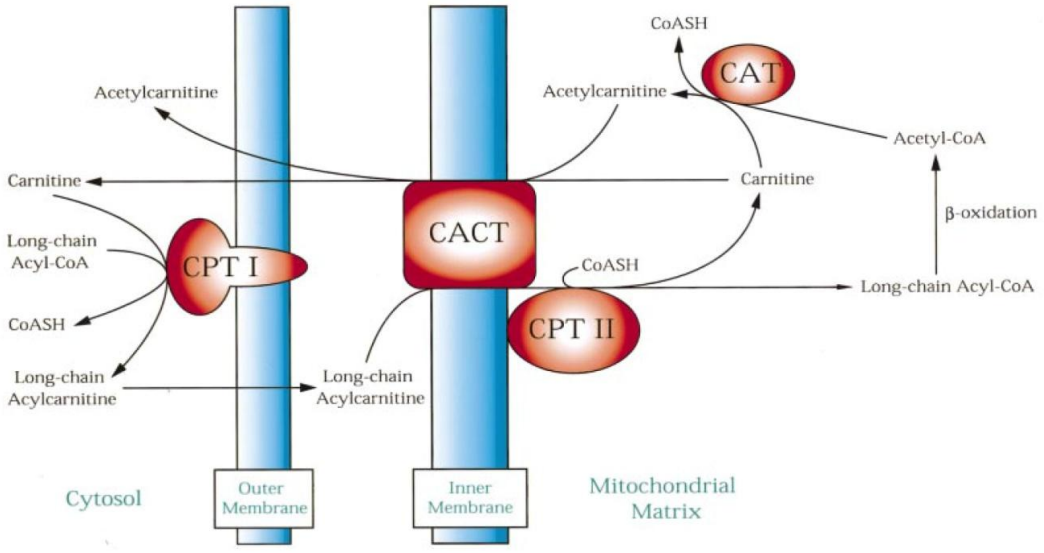

Figure 7 Enzymology of the carnitine-mediated transport of long-chain fatty acids into mitochondria. CPT I – carnitine palmitoyl transferase I – an enzyme located on the outer mitochondrial membrane, which catalyses the trans-esterification of acyl-CoA to give *O*-acyl carnitine esters. CACT – carnitine-acylcarnitine translocase is localized on the inner mitochondrial membrane and acts as a shuttle between mitochondrial matrix and intermambrane mitochondrial space for acyl-carnitine, carnitine and acetyl-carnitine. CPT II – carnitine palmitoyl transferase II is present in the mitochondrial matrix and is responsible for trans-esterification of acyl-carnitine to give acyl-CoA, which can enter the β-oxidation pathway. CAT – carnitine acetyl transferase is an mitochondrial enzyme with the ability to convert intramitochondrial carnitine to short and medium chain length (1-4 carbons) acyl-carnitines. Picture from Vaz *et al.*[115]

3.2 Modulating of acyl CoA-CoA ratio

Carnitine can be reversibly acylated with acyl groups derived from acyl-CoA pool. It has been shown that carnitine can act as a 'reservoir' of activated acyl units and modulate the ration of acetyl-CoA/ CoA.[119-121] In mitochondria free CoA plays various functions, including participation in the TCA cycle and in fatty acid β-oxidation, therefore decrease in free CoA levels can limit mitochondrial capacity for energy production (in particular, a high acyl-CoA/CoA ratio leads to inhibition of pyruvate dehydrogenase).[122,123] Carnitine induced decrease in acyl-CoA/ CoA ratio has been shown to activate pyruvate dehydrogenase and subsequently improve glucose metabolism in patients with diabetes.[124]

3.3 Metabolism of acyl groups

The *O*-acylation of carnitine is not limited to the acetyl group metabolism modulation.[121,125] The presence of the certain carnitine esters in blood of patients with metabolic disorders can be indicative of the disease and serve as a diagnostic tool.[126-130] In addition to inborn metabolic defects, carnitine homeostasis can be perturbed by several xenobiotics, e.g. drugs.[131] As an example can serve pivalic acid which is often used to modify drugs to improve their absorption. However, metabolism of pivalic acid leads to formation of stable pivalic acid – CoA ester, which cannot be further oxidised. Formation of a non-metabolizable acyl-CoA adduct is a typical step in the biotransformation of pivaloyl antibiotics.[132-135] The non-metabolizable pivaloyl esters can be transferred into carnitine and then transported out of the tissue and excreted with urine. It is proposed that analogous mechanism leads to a decrease in carnitine levels in the long term therapy with the anti-convulsant drug sodium valproate.[136-138]

3.4 Role of carnitine in peroxisomal fatty acid oxidation

Peroxisomal fatty acid oxidation is responsible for interconversion of long-chain and branched chain fatty acids into their chain-shortened forms with incomplete β-oxidation. Peroxisomes have been shown to oxidise long-chain fatty acids in a carnitine – dependent mechanism.[139,140] The medium-chain acyl-CoA products of peroxisomal oxidation have to be transported into mitochondria, where they can undergo complete oxidation. It has been demonstrated that carnitine (in the form of acyl-carnitine esters) plays a role in the transport of fatty acids between mitochondria and peroxisomes.[141-143]

4 Research outline

The research presented in this thesis focuses broadly on the last enzyme of the carnitine biosynthesis pathway – γ-butyrobetaine hydroxylase (BBOX). Work described in this thesis was aimed at:

- **Developing analytical tools to enable measurements of BBOX activity *in vitro*.** Chapter 2 describes development of two new assays employing fluorinated GBB analogues, which allow observation of BBOX activity both with isolated protein and in cell lysates.
- **Broadening the scope of ^{19}F NMR based methodologies in protein-ligand interaction studies.** Chapter 3 presents how fluorinated proteins (as opposed to fluorinated ligands) can be used for monitoring protein ligand – interactions on the example of New Delhi Metallo-β-lactamase I and the series of identified inhibitors.
- **Investigating the potential of BBOX as a tool for biocatalysis.** Chapter 4 describes identification of novel cyclic substrate for BBOX, which upon hydroxylation undergoes dessymetrisation with subsequent formation of up to three new stereocentres.
- **Identification of small molecule scaffolds for use as BBOX inhibitors.** Chapter 5 focuses on medium throughput screening of small molecules libraries and identification of lead inhibitor compounds and their evaluation for activity in cells.
- **Comparison of properties of BBOX from human and bacteria.** Chapter 6 presents a work on BBOX from *Pseudomonas sp. AK1*. The kinetic properties and substrate specificity of both human and bacterial BBOX are compared.

References

1. Hoppel, C. The role of carnitine in normal and altered fatty acid metabolism. *American Journal of Kidney Disease* **41**, S4-12 (2003).
2. Rebouche, C.J. Carnitine function and requirements during the life cycle. *The FASEB Journal* **6**, 3379-86 (1992).
3. Strijbis, K., Vaz, F.M. & Distel, B. Enzymology of the carnitine biosynthesis pathway. *IUBMB Life* **62**, 357-62 (2010).
4. Rebouche, C.J. Kinetics, pharmacokinetics, and regulation of L-carnitine and acetyl-L-carnitine metabolism. in *Carnitine: The Science Behind a Conditionally Essential Nutrient*, Vol. 1033 (eds. Alesci, S. et al.) 30-41 (New York Acad Sciences, New York, 2004).
5. Etzioni, A., Levy, J., Nitzan, M., Erde, P. & Benderly, A. Systemic carnitine deficiency exacerbated by a strict vegetarian diet. *Archives of Disease in Childhood* **59**, 177-179 (1984).
6. Lombard, K.A., Olson, A.L., Nelson, S.E. & Rebouche, C.J. Carnitine status of lactoovovegetarians and strict vegetarian adults and children. *The American Journal of Clinical Nutrition* **50**, 301-6 (1989).
7. Ramsay, R.R., Gandour, R.D. & van der Leij, F.R. Molecular enzymology of carnitine transfer and transport. *Biochimica et Biophysica Acta (BBA) - Protein Structure and Molecular Enzymology* **1546**, 21-43 (2001).
8. Fischer, M., Keller, J., Hirche, F., Kluge, H., Ringseis, R. & Eder, K. Activities of γ-butyrobetaine dioxygenase and concentrations of carnitine in tissues of pigs. *Comparative Biochemistry and Physiology Part A: Molecular & Integrative Physiology* **153**, 324-331 (2009).
9. Marquis, N.R. & Fritz, I.B. The Distribution of Carnitine, Acetylcarnitine, and Carnitine Acetyltransferase in Rat Tissues. *Journal of Biological Chemistry* **240**, 2193-2196 (1965).
10. Borum, P.R. Variation in tissue carnitine concentrations with age and sex in the rat. *Biochemical Journal* **176**, 677-681 (1978).
11. Schmidt-Sommerfeld, E., Werner, D. & Penn, D. Carnitine plasma concentrations in 353 metabolically healthy children. *European Journal of Pediatrics* **147**, 356-360 (1988).
12. Buchta, R., Nyhan, W.L., Broock, R. & Schragg, P. Carnitine in adolescents. *Journal of Adolescent Health* **14**, 440-441 (1993).
13. Güneral, F. Serum and urine total, free and acylcarnitine levels related to age: assessment of renal handling of carnitine. *The Turkish journal of pediatrics* **37**, 217-222 (1995).
14. Cederblad, G. Plasma carnitine and body composition. *Clinica Chimica Acta* **67**, 207-212 (1976).
15. Takiyama, N. & Matsumoto, K. Age- and Sex-Related Differences of Serum Carnitine in a Japanese Population. *Journal of the American College of Nutrition* **17**, 71-74 (1998).
16. Vaz, F.M. & Wanders, R.J. Carnitine biosynthesis in mammals. *Biochemical Journal* **361**, 417-29 (2002).
17. Kaufman, R.A. & Broquist, H.P. Biosynthesis of carnitine in Neurospora crassa. *Journal of Biological Chemistry* **252**, 7437-9 (1977).
18. Strijbis, K., van Roermund, C.W., Hardy, G.P., van den Burg, J., Bloem, K., de Haan, J., van Vlies, N., Wanders, R.J., Vaz, F.M. & Distel, B. Identification and characterization of a complete carnitine biosynthesis pathway in Candida albicans. *The FASEB Journal* **23**, 2349-59 (2009).
19. Rippa, S., Zhao, Y., Merlier, F., Charrier, A. & Perrin, Y. The carnitine biosynthetic pathway in Arabidopsis thaliana shares similar features with the pathway of mammals and fungi. *Plant Physiology and Biochemistry* **60**, 109-114 (2012).
20. Bourdin, B., Adenier, H. & Perrin, Y. Carnitine is associated with fatty acid metabolism in plants. *Plant Physiology and Biochemistry* **45**, 926-931 (2007).
21. Kleber, H.P. Bacterial carnitine metabolism. *FEMS Microbiol Lett* **147**, 1-9 (1997).

22. Lindstedt, G., Lindstedt, S., Midtvedt, T. & Tofft, M. The Formation and Degradation of Carnitine in Pseudomonas*. *Biochemistry* **6**, 1262-1270 (1967).
23. Lindstedt, G., Lindstedt, S. & Nordin, I. Purification and properties of gamma-butyrobetaine hydroxylase from Pseudomonas sp AK 1. *Biochemistry* **16**, 2181-8 (1977).
24. Lindstedt, G., Lindstedt, S. & Tofft, M. Gamma-butyrobetaine hydroxylase from Pseudomonas sp AK 1. *Biochemistry* **9**, 4336-42 (1970).
25. Tanphaichitr, V., Horne, D.W. & Broquist, H.P. Lysine, a Precursor of Carnitine in the Rat. *Journal of Biological Chemistry* **246**, 6364-6366 (1971).
26. Paik, W.K. & Kim, S. Protein methylation. *Science* **174**, 114-9 (1971).
27. Tanphaichitr, V. & Broquist, H.P. Role of Lysine and ε-N-Trimethyllysine in Carnitine Biosynthesis : II. STUDIES IN THE RAT. *Journal of Biological Chemistry* **248**, 2176-2181 (1973).
28. Horne, D.W., Tanphaichitr, V. & Broquist, H.P. Role of Lysine in Carnitine Biosynthesis in Neurospora crassa. *Journal of Biological Chemistry* **246**, 4373-4375 (1971).
29. LaBadie, J., Dunn, W.A. & Aronson, N.N. Hepatic synthesis of carnitine from protein-bound trimethyl-lysine. Lysosomal digestion of methyl-lysine-labelled asialo-fetuin. *Biochemical Journal* **160**, 85-95 (1976).
30. Dunn, W.A., Rettura, G., Seifter, E. & Englard, S. Carnitine biosynthesis from gamma-butyrobetaine and from exogenous protein-bound 6-N-trimethyl-L-lysine by the perfused guinea pig liver. Effect of ascorbate deficiency on the in situ activity of gamma-butyrobetaine hydroxylase. *Journal of Biological Chemistry* **259**, 10764-10770 (1984).
31. Servillo, L., Giovane, A., Cautela, D., Castaldo, D. & Balestrieri, M.L. Where Does Nε-Trimethyllysine for the Carnitine Biosynthesis in Mammals Come from? *PLoS ONE* **9**, e84589 (2014).
32. Rebouche, C.J. & Engel, A.G. Significance of renal gamma-butyrobetaine hydroxylase for carnitine biosynthesis in man. *Journal of Biological Chemistry* **255**, 8700-5 (1980).
33. Melegh, B., Hermann, R. & Bock, I. Generation of hydroxytrimethyllysine from trimethyllysine limits the carnitine biosynthesis in premature infants. *Acta Pædiatrica* **85**, 345-350 (1996).
34. Melegh, B., Toth, G., Adamovich, K., Szekely, G., Gage, D.A. & Bieber, L.L. Labeled trimethyllysine load depletes unlabeled carnitine in premature infants without evidence of incorporation. *Biology of the Neonate* **76**, 19-25 (1999).
35. Borum, P.R. & Broquist, H.P. Purification of S-adenosylmethionine: epsilon-N-L-lysine methyltransferase. The first enzyme in carnitine biosynthesis. *Journal of Biological Chemistry* **252**, 5651-5 (1977).
36. Rebouche, C.J. & Engel, A.G. Tissue distribution of carnitine biosynthetic enzymes in man. *Biochimica et Biophysica Acta* **630**, 22-9 (1980).
37. Olson, A.L. & Rebouche, C.J. gamma-Butyrobetaine hydroxylase activity is not rate limiting for carnitine biosynthesis in the human infant. *Journal of Nutrition* **117**, 1024-31 (1987).
38. Prescott, A.G. & Lloyd, M.D. The iron(II) and 2-oxoacid-dependent dioxygenases and their role in metabolism. *Natural Product Reports* **17**, 367-383 (2000).
39. Loenarz, C. & Schofield, C.J. Expanding chemical biology of 2-oxoglutarate oxygenases. *Nature Chemical Biology* **4**, 152-6 (2008).
40. McDonough, M.A., Loenarz, C., Chowdhury, R., Clifton, I.J. & Schofield, C.J. Structural studies on human 2-oxoglutarate dependent oxygenases. *Current Opinion in Structural Biology* **20**, 659-672 (2010).
41. Sachan, D.S. & Broquist, H.P. Synthesis of carnitine from ε-N-trimethyllysine in post mitochondrial fractions of Neurospora crassa. *Biochemical and Biophysical Research Communications* **96**, 870-875 (1980).
42. Sachan, D.S. & Hoppel, C.L. Carnitine biosynthesis. Hydroxylation of N6-trimethyl-lysine to 3-hydroxy-N6-trimethyl-lysine. *Biochemical Journal* **188**, 529-534 (1980).

43. Stein, R. & Englard, S. Properties of rat 6-N-trimethyl-l-lysine hydroxylases: Similarities among the kidney, liver, heart, and skeletal muscle activities. *Archives of Biochemistry and Biophysics* **217**, 324-331 (1982).
44. Cox, R.A. & Hoppel, C.L. Biosynthesis of carnitine and 4-N-trimethylaminobutyrate from 6-N-trimethyl-lysine. *Biochemical Journal* **136**, 1083-1090 (1973).
45. Cox, R.A. & Hoppel, C.L. Carnitine biosynthesis in rat liver slices. *Biochimica et Biophysica Acta (BBA) - General Subjects* **362**, 403-413 (1974).
46. Hulse, J.D., Ellis, S.R. & Henderson, L.M. Carnitine biosynthesis. beta-Hydroxylation of trimethyllysine by an alpha-ketoglutarate-dependent mitochondrial dioxygenase. *Journal of Biological Chemistry* **253**, 1654-1659 (1978).
47. Novak, R.F., Swift, T.J. & Hoppel, C.L. N6-Trimethyl-lysine metabolism. Structural identification of the metabolite 3-hydroxy-N6-trimethyl-lysine. *Biochemical Journal* **188**, 521-527 (1980).
48. Vaz, F.M., Ofman, R., Westinga, K., Back, J.W. & Wanders, R.J.A. Molecular and Biochemical Characterization of Rat ε-N-Trimethyllysine Hydroxylase, the First Enzyme of Carnitine Biosynthesis. *Journal of Biological Chemistry* **276**, 33512-33517 (2001).
49. van Vlies, N., Ofman, R., Wanders, R.J.A. & Vaz, F.M. Submitochondrial localization of 6-N-trimethyllysine dioxygenase − implications for carnitine biosynthesis. *FEBS Journal* **274**, 5845-5851 (2007).
50. Davis, A.T. & Hoppel, C.L. Effect of starvation on the disposition of free and peptide-linked trimethyllysine in the rat. *The Journal of nutrition* **116**, 760-767 (1986).
51. Rebouche, C.J., Lehman, L.J. & Olson, L. epsilon-N-trimethyllysine availability regulates the rate of carnitine biosynthesis in the growing rat. *The Journal of nutrition* **116**, 751-759 (1986).
52. Carter, A.L. & Frenkel, R. The role of the kidney in the biosynthesis of carnitine in the rat. *Journal of Biological Chemistry* **254**, 10670-10674 (1979).
53. Bøhmer, T. Conversion of butyrobetaine to carnitine in the rat in vivo. *Biochimica et Biophysica Acta (BBA) - General Subjects* **343**, 551-557 (1974).
54. Monfregola, J., Napolitano, G., Conte, I., Cevenini, A., Migliaccio, C., D'Urso, M. & Ursini, M.V. Functional characterization of the TMLH gene: promoter analysis, in situ hybridization, identification and mapping of alternative splicing variants. *Gene* **395**, 86-97 (2007).
55. Monfregola, J., Cevenini, A., Terracciano, A., Vlies, N.v., Arbucci, S., Wanders, R.J.A., D'Urso, M., Vaz, F.M. & Ursini, M.V. Functional analysis of TMLH variants and definition of domains required for catalytic activity and mitochondrial targeting. *Journal of Cellular Physiology* **204**, 839-847 (2005).
56. van Vlies, N., Wanders, R.J.A. & Vaz, F.M. Measurement of carnitine biosynthesis enzyme activities by tandem mass spectrometry: Differences between the mouse and the rat. *Analytical Biochemistry* **354**, 132-139 (2006).
57. Swiegers, J.H., Vaz, F.M., Pretorius, I.S., Wanders, R.J. & Bauer, F.F. Carnitine biosynthesis in Neurospora crassa: identification of a cDNA coding for epsilon-N-trimethyllysine hydroxylase and its functional expression in Saccharomyces cerevisiae. *FEMS Microbiology Letters* **210**, 19-23 (2002).
58. Lim, Elaine T., Raychaudhuri, S., Sanders, Stephan J., Stevens, C., Sabo, A., MacArthur, Daniel G., Neale, Benjamin M., Kirby, A., Ruderfer, Douglas M., Fromer, M. *et al.* Rare Complete Knockouts in Humans: Population Distribution and Significant Role in Autism Spectrum Disorders. *Neuron* **77**, 235-242 (2013).
59. Rosti, R.O., Sadek, A.A., Vaux, K.K. & Gleeson, J.G. The genetic landscape of autism spectrum disorders. *Developmental Medicine & Child Neurology* **56**, 12-18 (2014).
60. Nava, C., Lamari, F., Heron, D., Mignot, C., Rastetter, A., Keren, B., Cohen, D., Faudet, A., Bouteiller, D., Gilleron, M. *et al.* Analysis of the chromosome X exome in patients with autism spectrum disorders identified novel candidate genes, including TMLHE. *Transl Psychiatry* **2**, e179 (2012).

61. Celestino-Soper, P.B.S., Shaw, C.A., Sanders, S.J., Li, J., Murtha, M.T., Ercan-Sencicek, A.G., Davis, L., Thomson, S., Gambin, T., Chinault, A.C. *et al.* Use of array CGH to detect exonic copy number variants throughout the genome in autism families detects a novel deletion in TMLHE. *Human Molecular Genetics* **20**, 4360-4370 (2011).
62. Celestino-Soper, P.B., Violante, S., Crawford, E.L., Luo, R., Lionel, A.C., Delaby, E., Cai, G., Sadikovic, B., Lee, K., Lo, C. *et al.* A common X-linked inborn error of carnitine biosynthesis may be a risk factor for nondysmorphic autism. *Proceedings of the National Academy of Sciences U S A* **109**, 7974-81 (2012).
63. Dunn, W.A., Aronson, N.N. & Englard, S. The effects of 1-amino-D-proline on the production of carnitine from exogenous protein-bound trimethyllysine by the perfused rat liver. *Journal of Biological Chemistry* **257**, 7948-7951 (1982).
64. Sasaoka, K., Ogawa, T., Moritoki, K. & Kimoto, M. Antivitamin B-6 effect of 1-aminoproline on rats. *Biochimica et Biophysica Acta (BBA) - General Subjects* **428**, 396-402 (1976).
65. Khan-Siddiqui, L. & Bamji, M.S. Effect of riboflavin or pyridoxine deficiency on tissue carnitine levels in rats. *Nutrition Research* **7**, 445-448 (1987).
66. Cho, Y.O. & Leklem, J.E. In vivo evidence for a vitamin B-6 requirement in carnitine synthesis. *The Journal of nutrition* **120**, 258-265 (1990).
67. Henderson, L.M., Nelson, P.J. & Henderson, L. Mammalian enzymes of trimethyllysine conversion to trimethylaminobutyrate. *Federation proceedings* **41**, 2843-2847 (1982).
68. Hulse, J.D. & Henderson, L.M. Carnitine biosynthesis. Purification of 4-N'-trimethylaminobutyraldehyde dehydrogenase from beef liver. *Journal of Biological Chemistry* **255**, 1146-1151 (1980).
69. Vaz, F.M., Fouchier, S.W., Ofman, R., Sommer, M. & Wanders, R.J.A. Molecular and Biochemical Characterization of Rat γ-Trimethylaminobutyraldehyde Dehydrogenase and Evidence for the Involvement of Human Aldehyde Dehydrogenase 9 in Carnitine Biosynthesis. *Journal of Biological Chemistry* **275**, 7390-7394 (2000).
70. Hassan, M., Okada, M., Ichiyanagi, T. & Mori, N. 4-N-trimethylaminobutyraldehyde dehydrogenase: purification and characterization of an enzyme from Pseudomonas sp. 13CM. *Bioscience Biotechnology and Biochemistry* **72**, 155-62 (2008).
71. Bari, M.R., Hassan, M., Akai, N., Arima, J. & Mori, N. Gene cloning and biochemical characterization of 4-N-trimethylaminobutyraldehyde dehydrogenase II from Pseudomonas sp. 13CM. *World Journal of Microbiology and Biotechnology* **29**, 683-692 (2013).
72. Abe, T., Takada, K., Ohkawa, K. & Matsuda, M. Purification and characterization of a rat brain aldehyde dehydrogenase able to metabolize gamma-aminobutyraldehyde to gamma-aminobutyric acid. *Biochemical Journal* **269**, 25-29 (1990).
73. Lin, S.W., Chen, J.C., Hsu, L.C., Hsieh, C.-L. & Yoshida, A. Human γ-Aminobutyraldehyde Dehydrogenase (ALDH9): cDNA Sequence, Genomic Organization, Polymorphism, Chromosomal Localization, and Tissue Expression. *Genomics* **34**, 376-380 (1996).
74. Kikonyogo, A. & Pietruszko, R. Aldehyde dehydrogenase from adult human brain that dehydrogenates gamma-aminobutyraldehyde: purification, characterization, cloning and distribution. *Biochemical Journal* **316**, 317-324 (1996).
75. Englard, S., Blanchard, J.S. & Midelfort, C.F. Gamma-butyrobetaine hydroxylase - stereochemical course of the hydroxylation. *Biochemistry* **24**, 1110-1116 (1985).
76. Galland, S., Le Borgne, F., Guyonnet, D., Clouet, P. & Demarquoy, J. Purification and characterization of the rat liver gamma-butyrobetaine hydroxylase. *Molecular and Cellular Biochemistry* **178**, 163-168 (1998).
77. Kondo, A., Blanchard, J.S. & Englard, S. Purification and properties of calf liver γ-butyrobetaine hydroxylase. *Archives of Biochemistry and Biophysics* **212**, 338-346 (1981).

78. Lindstedt, G., Lindstedt, S. & Nordin, I. gamma - Butyrobetaine hydroxylase in human kidney. *Scandinavian Journal of Clinical & Laboratory Investigation* **42**, 477-485 (1982).
79. Tars, K., Rumnieks, J., Zeltins, A., Kazaks, A., Kotelovica, S., Leonciks, A., Sharipo, J., Viksna, A., Kuka, J., Liepinsh, E. *et al.* Crystal structure of human gamma-butyrobetaine hydroxylase. *Biochemical and Biophysical Research Communications* **398**, 634-639 (2010).
80. Leung, I.K.H., Krojer, T.J., Kochan, G.T., Henry, L., von Delft, F., Claridge, T.D.W., Oppermann, U., McDonough, M.A. & Schofield, C.J. Structural and Mechanistic Studies on gamma-Butyrobetaine Hydroxylase. *Chemistry & Biology* **17**, 1316-1324 (2010).
81. Lindsted.G & Lindsted.S. Cofactor requirements of gamma-butyrobetaine hydroxylase from rat liver. *Journal of Biological Chemistry* **245**, 4178-& (1970).
82. Erfle, J.D. Hydroxylation of γ-butyrobetaine by rat and ovine tissues. *Biochemical and Biophysical Research Communications* **64**, 553-557 (1975).
83. Paul, H.S., Sekas, G. & Adibi, S.A. Carnitine biosynthesis in hepatic peroxisomes - demonstration of gamma-butyrobetaine hydroxylase activity. *European Journal of Biochemistry* **203**, 599-605 (1992).
84. Paul, H.S., Sekas, G. & Adibi, S.A. A new metabolic role for hepatic peroxisomes - biosynthesis of carnitine. *Clinical Research* **38**, A354-A354 (1990).
85. Englard, S. & Carnicero, H.H. γ-Butyrobetaine hydroxylation to carnitine in mammalian kidney. *Archives of Biochemistry and Biophysics* **190**, 361-364 (1978).
86. Englard, S. Hydroxylation of γ-butyrobetaine to carnitine in human and monkey tissues. *FEBS Letters* **102**, 297-300 (1979).
87. Galland, S., Le Borgne, F., Bouchard, F., Georges, B., Clouet, P., Grand-Jean, F. & Demarquoy, J. Molecular cloning and characterization of the cDNA encoding the rat liver gamma-butyrobetaine hydroxylase. *Biochimica et Biophysica Acta (BBA) - Molecular and Cell Biology of Lipids* **1441**, 85-92 (1999).
88. Hahn, P. The development of carnitine synthesis from γ-butyrobetaine in the rat. *Life Sciences* **28**, 1057-1060 (1981).
89. Olson, A.L. & Rebouche, C.J. gamma-Butyrobetaine hydroxylase activity is not rate limiting for carnitine biosynthesis in the human infant. *The Journal of nutrition* **117**, 1024-1031 (1987).
90. Vaz, F.M., van Gool, S., Ofman, R., Ijlst, L. & Wanders, R.J.A. Carnitine Biosynthesis: Identification of the cDNA Encoding Human γ-Butyrobetaine Hydroxylase. *Biochemical and Biophysical Research Communications* **250**, 506-510 (1998).
91. Shekhawat, P.S., Sonne, S., Carter, A.L., Matern, D. & Ganapathy, V. Enzymes involved in l-carnitine biosynthesis are expressed by small intestinal enterocytes in mice: Implications for gut health. *Journal of Crohn's and Colitis* **7**, e197-e205 (2013).
92. Rigault, C., Le Borgne, F. & Demarquoy, J. Genomic structure, alternative maturation and tissue expression of the human BBOX1 gene. *Biochimica et Biophysica Acta (BBA) - Molecular and Cell Biology of Lipids* **1761**, 1469-1481 (2006).
93. Rigault, C., Le Borgne, F., Tazir, B., Benani, A. & Demarquoy, J. A high-fat diet increases l-carnitine synthesis through a differential maturation of the Bbox1 mRNAs. *Biochimica et Biophysica Acta (BBA) - Molecular and Cell Biology of Lipids* **1831**, 370-377 (2013).
94. Hausinger, R.P. Fe(II)/α-ketoglutarate-dependent hydroxylases and related enzymes. *Critical Reviews in Biochemistry and Molecular Biology* **39**, 21-68 (2004).
95. Walport, L.J., Hopkinson, R.J. & Schofield, C.J. Mechanisms of human histone and nucleic acid demethylases. *Current Opinion in Chemical Biology* **16**, 525-34 (2012).
96. Aik, W., McDonough, M.A., Thalhammer, A., Chowdhury, R. & Schofield, C.J. Role of the jelly-roll fold in substrate binding by 2-oxoglutarate oxygenases. *Current Opinion in Structural Biology* **22**, 691-700 (2012).

97. Chowdhury, R., McDonough, M.A., Mecinovic, J., Loenarz, C., Flashman, E., Hewitson, K.S., Domene, C. & Schofield, C.J. Structural basis for binding of hypoxia-inducible factor to the oxygen-sensing prolyl hydroxylases. *Structure* **17**, 981-9 (2009).
98. Kershaw, N.J., Caines, M.E.C., Sleeman, M.C. & Schofield, C.J. The enzymology of clavam and carbapenem biosynthesis. *Chemical Communications*, 4251-4263 (2005).
99. Lindstedt, S. & Nordin, I. Multiple forms of gamma-butyrobetaine hydroxylase (EC 1.14.11.1). *Biochemical Journal* **223**, 119-127 (1984).
100. Ng, S.F., Hanauske-Abel, H.M. & Englard, S. Cosubstrate binding site of Pseudomonas sp. AK1 gamma-butyrobetaine hydroxylase. Interactions with structural analogs of alpha-ketoglutarate. *Journal of Biological Chemistry* **266**, 1526-1533 (1991).
101. Wehbie, R.S., Punekar, N.S. & Lardy, H.A. Rat liver .gamma.-butyrobetaine hydroxylase catalyzed reaction: influence of potassium, substrates, and substrate analogs on hydroxylation and decarboxylation. *Biochemistry* **27**, 2222-2228 (1988).
102. Lindstedt, G. & Lindstedt, S. Cofactor requirements of gamma-butyrobetaine hydroxylase from rat liver. *Journal of Biological Chemistry* **245**, 4178-86 (1970).
103. Lindsted.G, Lindsted.S & Tofft, M. Gamma-butyrobetaine hydroxylase from Pseudomonas-sp-AK-1. *Biochemistry* **9**, 4336-& (1970).
104. Rebouche, C.J. Ascorbic acid and carnitine biosynthesis. *The American Journal of Clinical Nutrition* **54**, 1147S-1152S (1991).
105. Blanchard, J.S. & Englard, S. Studies on the irreversible inactivation of gamma-butyrobetaine hydroxylase - the effect of catalase. *Federation Proceedings* **40**, 1670-1670 (1981).
106. Blanchard, J.S., Englard, S. & Kondo, A. Gamma-butyrobetaine hydroxylase - a unique protective effect of catalase. *Archives of Biochemistry and Biophysics* **219**, 327-334 (1982).
107. Punekar, N.S., Wehbie, R.S. & Lardy, H.A. gamma-Butyrobetaine hydroxylase and the protective role of glutathione peroxidase. *Journal of Biological Chemistry* **262**, 6720-6724 (1987).
108. Clifton, I.J., McDonough, M.A., Ehrismann, D., Kershaw, N.J., Granatino, N. & Schofield, C.J. Structural studies on 2-oxoglutarate oxygenases and related double-stranded beta-helix fold proteins. *Journal of Inorganic Biochemistry* **100**, 644-69 (2006).
109. McGarry, J.D. & Brown, N.F. The Mitochondrial Carnitine Palmitoyltransferase System — From Concept to Molecular Analysis. *European Journal of Biochemistry* **244**, 1-14 (1997).
110. McGarry, J.D. The mitochondrial carnitine palmitoyltransferase system: its broadening role in fuel homoeostasis and new insights into its molecular features. *Biochemical Society transactions* **23**, 321-324 (1995).
111. Norum, K.R. & Bremer, J. The Localization of Acyl Coenzyme A-Carnitine Acyltransferases in Rat Liver Cells. *Journal of Biological Chemistry* **242**, 407-411 (1967).
112. Norum, K.R., Farstad, M. & Bremer, J. The submitochondrial distribution of acid: CoA ligase (AMP) and palmityl-CoA: Carnitine palmityltransferase in rat liver mitochondria. *Biochemical and Biophysical Research Communications* **24**, 797-804 (1966).
113. Violante, S., IJlst, L., te Brinke, H., Tavares de Almeida, I., Wanders, R.J.A., Ventura, F.V. & Houten, S.M. Carnitine palmitoyltransferase 2 and carnitine/acylcarnitine translocase are involved in the mitochondrial synthesis and export of acylcarnitines. *The FASEB Journal* **27**, 2039-2044 (2013).
114. Indiveri, C., Iacobazzi, V., Tonazzi, A., Giangregorio, N., Infantino, V., Convertini, P., Console, L. & Palmieri, F. The mitochondrial carnitine/acylcarnitine carrier: Function, structure and physiopathology. *Molecular Aspects of Medicine* **32**, 223-233 (2011).
115. Vaz, F.M. & Wanders, R.J.A. Carnitine biosynthesis in mammals. *Biochemical Journal* **361**, 417-429 (2002).
116. Violante, S., Ijlst, L., Ruiter, J., Koster, J., van Lenthe, H., Duran, M., de Almeida, I.T., Wanders, R.J., Houten, S.M. & Ventura, F.V. Substrate specificity of human carnitine

acetyltransferase: Implications for fatty acid and branched-chain amino acid metabolism. *Biochimica et Biophysica Acta* **1832**, 773-9 (2013).
117. Bremer, J. Carnitine--metabolism and functions. *Physiological Reviews* **63**, 1420-1480 (1983).
118. Jogl, G. & Tong, L. Crystal Structure of Carnitine Acetyltransferase and Implications for the Catalytic Mechanism and Fatty Acid Transport. *Cell* **112**, 113-122 (2003).
119. Rebouche, C.J. & Seim, H. Carnitine metabolism and its regulation in microorganisms and mammals. Vol. 18 39-61 (1998).
120. Ramsay, R.R. & Arduini, A. The Carnitine Acyltransferases and Their Role in Modulating Acyl-CoA Pools. *Archives of Biochemistry and Biophysics* **302**, 307-314 (1993).
121. Ramsay, R.R. & Zammit, V.A. Carnitine acyltransferases and their influence on CoA pools in health and disease. *Molecular Aspects of Medicine* **25**, 475-493 (2004).
122. Hansford, R.G. Studies on inactivation of pyruvate dehydrogenase by palmitoylcarnitine oxidation in isolated rat heart mitochondria. *Journal of Biological Chemistry* **252**, 1552-60 (1977).
123. Brass, E.P. Interaction of carnitine and propionate with pyruvate oxidation by hepatocytes from clofibrate-treated rats: importance of coenzyme A availability. *Journal of Nutrition* **122**, 234-40 (1992).
124. Capaldo, B., Napoli, R., Di Bonito, P., Albano, G. & Sacca, L. Carnitine improves peripheral glucose disposal in non-insulin-dependent diabetic patients. *Diabetes Research Clinical and Practice* **14**, 191-5 (1991).
125. Steiber, A., Kerner, J. & Hoppel, C.L. Carnitine: a nutritional, biosynthetic, and functional perspective. *Molecular Aspects of Medicine* **25**, 455-473 (2004).
126. Minkler, P.E., Kerner, J., North, K.N. & Hoppel, C.L. Quantitation of long-chain acylcarnitines by HPLC/fluorescence detection: application to plasma and tissue specimens from patients with carnitine palmitoyltransferase-II deficiency. *Clinica Chimica Acta* **352**, 81-92 (2005).
127. Roe, C.R., Hoppel, C.L., Stacey, T.E., Chalmers, R.A., Tracey, B.M. & Millington, D.S. Metabolic response to carnitine in methylmalonic aciduria. An effective strategy for elimination of propionyl groups. *Arch Dis Child* **58**, 916-20 (1983).
128. Ogier de Baulny, H. & Saudubray, J.M. Branched-chain organic acidurias. *Semin Neonatol* **7**, 65-74 (2002).
129. Roe, C.R., Millington, D.S., Maltby, D.A., Kahler, S.G. & Bohan, T.P. L-carnitine therapy in isovaleric acidemia. *Jornal of Clinical Investigation* **74**, 2290-5 (1984).
130. Chalmers, R.A., Roe, C.R., Stacey, T.E. & Hoppel, C.L. Urinary excretion of l-carnitine and acylcarnitines by patients with disorders of organic acid metabolism: evidence for secondary insufficiency of l-carnitine. *Pediatr Res* **18**, 1325-8 (1984).
131. Arrigoni-Martelli, E. & Caso, V. Carnitine protects mitochondria and removes toxic acyls from xenobiotics. *Drugs Exp Clin Res* **27**, 27-49 (2001).
132. Holme, E., Greter, J., Jacobson, C.E., Lindstedt, S., Nordin, I., Kristiansson, B. & Jodal, U. Carnitine deficiency induced by pivampicillin and pivmecillinam therapy. *Lancet* **2**, 469-73 (1989).
133. Holme, E., Jodal, U., Linstedt, S. & Nordin, I. Effects of pivalic acid-containing prodrugs on carnitine homeostasis and on response to fasting in children. *Scand J Clin Lab Invest* **52**, 361-72 (1992).
134. Brass, E.P., Mayer, M.D., Mulford, D.J., Stickler, T.K. & Hoppel, C.L. Impact on carnitine homeostasis of short-term treatment with the pivalate prodrug cefditoren pivoxil. *Clin Pharmacol Ther* **73**, 338-47 (2003).
135. Brass, E.P. Pivalate-generating prodrugs and carnitine homeostasis in man. *Pharmacol Rev* **54**, 589-98 (2002).
136. Rozas, I., Camina, M.F., Paz, J.M., Alonso, C., Castro-Gago, M. & Rodriguez-Segade, S. Effects of acute valproate administration on carnitine metabolism in mouse serum and tissues. *Biochemical Pharmacology* **39**, 181-5 (1990).

137. Perrott, J., Murphy, N.G. & Zed, P.J. L-carnitine for acute valproic acid overdose: a systematic review of published cases. *Ann Pharmacother* **44**, 1287-93 (2010).
138. Farkas, V., Bock, I., Cseko, J. & Sandor, A. Inhibition of carnitine biosynthesis by valproic acid in rats--the biochemical mechanism of inhibition. *Biochemical Pharmacology* **52**, 1429-33 (1996).
139. Ferdinandusse, S., Mulders, J., L, I.J., Denis, S., Dacremont, G., Waterham, H.R. & Wanders, R.J. Molecular cloning and expression of human carnitine octanoyltransferase: evidence for its role in the peroxisomal beta-oxidation of branched-chain fatty acids. *Biochemical and Biophysical Research Communications* **263**, 213-8 (1999).
140. Buechler, K.F. & Lowenstein, J.M. The involvement of carnitine intermediates in peroxisomal fatty acid oxidation: a study with 2-bromofatty acids. *Arch Biochem Biophys* **281**, 233-8 (1990).
141. Bieber, L.L., Emaus, R., Valkner, K. & Farrell, S. Possible functions of short-chain and medium-chain carnitine acyltransferases. *Federation Proceedings* **41**, 2858-62 (1982).
142. Jakobs, B.S. & Wanders, R.J. Fatty acid beta-oxidation in peroxisomes and mitochondria: the first, unequivocal evidence for the involvement of carnitine in shuttling propionyl-CoA from peroxisomes to mitochondria. *Biochemical and Biophysical Research Communications* **213**, 1035-41 (1995).
143. Verhoeven, N.M., Roe, D.S., Kok, R.M., Wanders, R.J., Jakobs, C. & Roe, C.R. Phytanic acid and pristanic acid are oxidized by sequential peroxisomal and mitochondrial reactions in cultured fibroblasts. *Journal of Lipid Research* **39**, 66-74 (1998).

Chapter 2

Development of assays for BBOX activity *in vitro*

Abstract

Chapter 2 describes the development of assays to measure BBOX activity *in vitro* and in crude cell lysates. An analogue of GBB fluorinated at C-3 (GBBF) was synthesised and determined to be a good substrate for BBOX. GBBF was found to be oxidised by BBOX with subsequent release of fluoride ions, which could then be quantified using a fluorescein based probe. The assay was optimised to high throughput format for use in inhibitor discovery (as described in Chapter 5). The second part of Chapter 2 describes the synthesis of fluoromethylated intermediates of carnitine biosynthesis – fluoromethyl GBB (GBBNF) and fluoromethyl TML (TMLNF). GBBNF was evaluated as a substrate for BBOX and its utility was exemplified by BBOX activity assays with purified enzyme and in crude bacterial cell lysates as followed by ^{19}F NMR.

Contents

1 Introduction

1.1 Assays for 2OG dependent oxygenases

2OG dependent oxygenases catalyse a wide range of reactions, some of high biological significance[1] (as discussed in Chapter 1). Therefore a range of assays to measure 2OG dependent oxygenases activity have been developed.[2] These assays can be broadly divided into those measuring co-substrate (2OG, oxygen)/co-product (succinate, CO_2) consumption/production and those where measurement of oxidised product formation or substrate consumption is measured. The first approach is general for all 2OG dependent oxygenases as it relies on the conserved role of 2OG and oxygen as substrates and succinate and CO_2 as co-products of 2OG dependent oxygenase catalysis.[3] The most common assays are based on detection of [^{14}C]-labelled CO_2 or succinate[4-7]; however other detection techniques have also been employed, including LC-MS,[6] spectroscopic[8-11] or electrochemical assays.[12,13] In most cases, direct product detection is used, but indirect methods, such as succinate detection by enzyme-coupled assays were also developed.[14,15] The main drawback of 2OG decarboxylation assays is in the assumption of a direct correlation between 2OG decarboxylation and substrate oxidation. This can be a major problem, as it has been shown that 2OG dependent oxygenases can catalyse 2OG decarboxylation independent of substrate hydroxylation (uncoupled turnover).[16-19] In some cases, this reaches significantly high values, e.g. when poor substrate is used.[1,20] Assays specific for particular 2OG dependent oxygenases detect substrate hydroxylation or other type of oxidation. In the case of histone demethylases, formaldehyde, which is a product formed after *N*-CH_3 hydroxylation followed by elimination, can be detected using a formaldehyde dehydrogenase coupled assay.[21-23] Other assays for oxidised product detection employ MS,[24,25] NMR[11] or antibody based methods which rely on fluorescence[26]/luminescence[27] detection.

1.2 Assays for γ-butyrobataine hydroxylase activity

As discussed in section 1.1, BBOX activity can be assayed using methods that are generic for 2OG dependent oxygenases, e.g. employing [^{14}C]-labeled 2OG.[28,29] Since carnitine is a widely studied metabolite, several methods for determination of its concentration in body fluids/tissue preparation exist.[30] Apart from detection of radiolabelled carnitine, methods using carnitine acetyl transferase coupled with [^{14}C]-acetyl-CoA are used.[31] One of the most convenient methods employs tandem mass spectrometry, which has been extensively used to determine carnitine concentrations in biological fluids.[32-35] Activity of BBOX is usually measured using labelled GBB.[36] As an alternative, the activity of BBOX can be determined using a two-step procedure, where carnitine from non-labelled GBB is measured employing a radioisotopic assay.[37,38] Recently, NMR has also been used

to determine BBOX activity.[39] However, these techniques are often not high throughput (and therefore not suitable for setting up a large inhibitor screening platform), require difficult to access or expensive reagents (e.g. radiolabelled substrates), can suffer from background interference (e.g. ^{1}H NMR assays are usually difficult to use in cell lysates) or have to account for the possible interference of the tested inhibitor with other assay components (this is especially important in the case of coupled enzymatic assays). Therefore, the development of a BBOX assay that overcomes these issues was undertaken.

1.3 Literature precedents on fluorinated substrates of 2OG dependent oxygenases

Fluorinated substrate analogues have previously been used as probes to determine enzymatic activity,[40] and as mechanistic probes.[41] There are a few examples of the use fluorinated substrate analogues to study 2OG dependent oxygenases. Isopenicillin N synthase is a 2OG dependent oxygenase which catalyses the formation of bicyclic isopenicillin N from *δ*-(L-*α*-aminoadipoyl)-L-cysteinyl-D-valine (ACV), and is reported to eliminate hydrogen fluoride from a fluorinated ACV analogue (Scheme 1). The reaction is proposed to occur through a novel catalytic mechanism, where the enzyme acts as a Lewis acid (though a radical mechanism is also possible).[42]

Previous studies on the hypoxia-inducible factor prolyl hydroxylase domain containing enzyme 2 (PHD2)[43] and a collagen prolyl 4-hydroxylase (P4H)[44] have reported that these oxygenases can accept substrate analogues that are fluorinated on the same carbon as that undergoing hydroxylation. For both P4H and PHD2, it was shown that peptides containing (*4S*)-4-fluoroproline are hydroxylated to yield peptidyl-4-oxoproline concomitant with the release of a fluoride ion (Scheme 2).

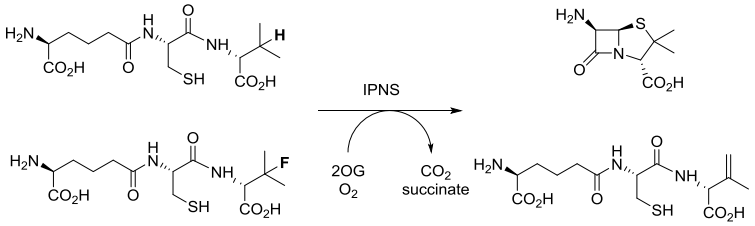

Scheme 1 IPNS catalyse elimination of hydrogen fluoride from a fluorinated analogue of natural substrate ACV.

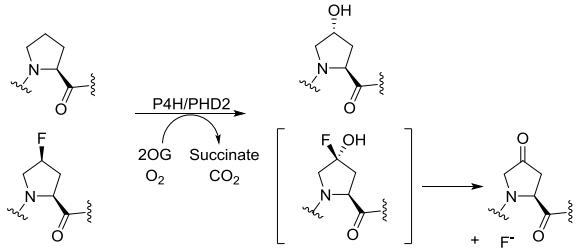

Scheme 2 P4H and PHD2 catalyse the hydroxylation of peptidyl-(*4S*)-4-fluoroproline to give peptidyl-4-ketoproline with the concomitant release of a fluoride ion.

2 Development of a fluoride release assay for BBOX

2.1 Fluoride detection

2.1.1 The choice of the probe

As described before, similarly to other 2OG dependent oxygenases like PHD2 or P4H, BBOX can catalyse turnover of a fluorinated substrate analogue (GBBF) with subsequent fluoride ion release. To establish a functional assay an appropriate detection method for fluoride ions has to be chosen. Detection of fluoride has, to date, attracted considerable attention, as fluoride is a common additive in toothpaste and drinking water. There are several detection methods described in the literature, including potentiometry, ^{19}F NMR and the use of chromogenic probes. Use of chromogenic or fluorogenic probes presents easy to use and low cost methods of analysis.[45] Therefore, for these studies fluorescein based probe (**1**) was chosen (Fig. 1). The TBS-protected spirolactone form of the probe is non-fluorescent, however fluoride mediated desilylation yields an open-ring native fluorescein and the rise of the fluorescence signal can be easily followed. The probe was previously used to assign fluoride concentrations in toothpaste samples and was shown to have high sensitivity, satisfactory tolerance to water content (up to 30%) and works well at pH 7.0, which would be convenient for enzymatic assays. Initial tests of probe (**1**) on aqueous fluoride ion solutions demonstrated that the fluorescence signal is proportional to the fluoride ion content in the solution (Fig. 1).

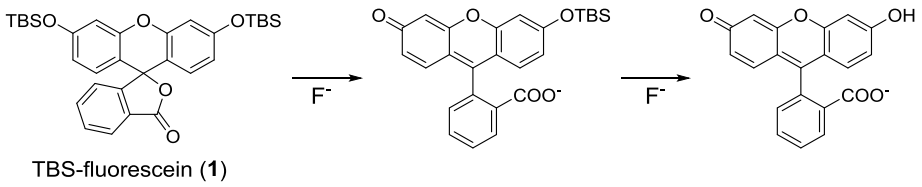

Scheme 3 Cleavage of TBS-fluorescein probe (**1**) by fluoride ions.

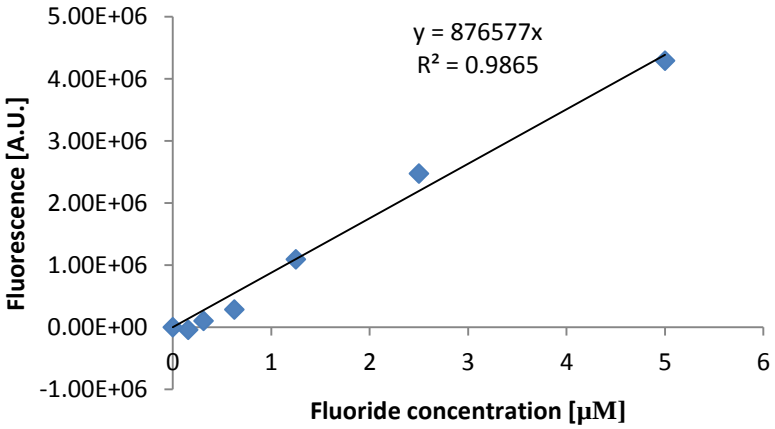

Figure 1 Fluorescence signal is directly proportional to the fluoride concentration in the solution.

2.1.2 Optimisation of fluoride detection

Conditions of fluoride detection by the TBS-fluorescein probe (**1**) were optimised for best performance in the assay. The standard assay consisted of an aqueous solution containing fluoride ions, which was incubated with a constant amount of probe in an organic solvent. After a fixed incubation time, a reaction was quenched by addition of HEPES buffer pH 7.0 (reading buffer), prior to fluorescence readout. Normalized fluorescence signal was calculated by subtracting the fluorescence signal for a control solution (which did not contain fluoride ions) from produced fluorescence signal.

Firstly, the type of aqueous solution containing fluoride ions was investigated. Detection of fluoride ions in water or Tris-HCl buffer (50 mM, pH 7.0) was performed. Tris-HCl buffer was chosen as this buffer was suitable for BBOX assays. The fluorescence background levels (solution with no fluoride ion added) were found to be similar in water or Tris, suggesting that the buffer has little influence on fluoride detection. In the buffered solution, the curve is steeper than in water alone and saturates at lower fluoride concentrations; increased sensitivity of the probe with 0-20 µM of fluoride is observed in Tris buffer (Fig. 2). Reaction of fluoride with the probe is carried out in an organic solvent-water mixture.

Several organic solvents were tested as a media to initially dissolve the probe (Fig. 3). The best results were obtained with DMSO, which gave highest fluorescence signal and less non-specific probe decomposition (measured in a sample which did not contain fluoride ions and denoted as a background signal). The ratio of aqueous solution containing fluoride ions to DMSO solution of a probe was next determined. Generally, higher amounts of DMSO gave better results, however 70% of DMSO still gave satisfactory results and mixtures containing >70% can be used in assays (Fig. 4).

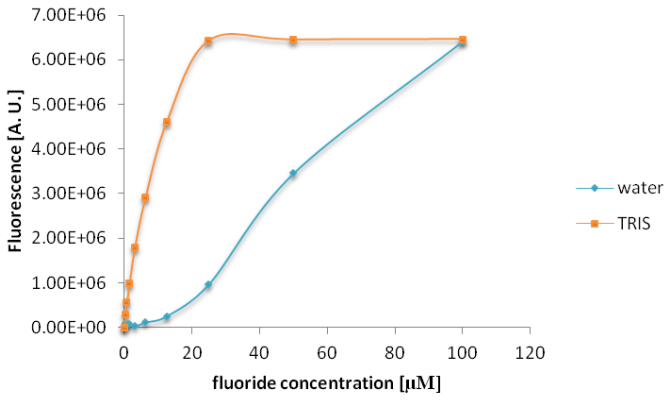

Figure 2 Dependence of the fluorescence signal on fluoride concentration, when fluoride ions were in water or 50 mM Tris buffer.

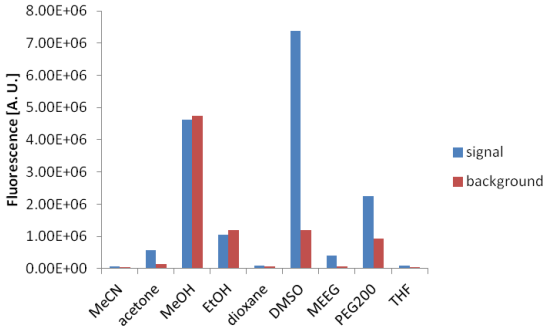

Figure 3 Dependence of fluorescence signal on the type of organic solvent used for incubations with TBS-fluorescein probe (blue). Red bars represent non specific TBS-fluorescein probe deprotection, when no fluoride ions are present in the solution.

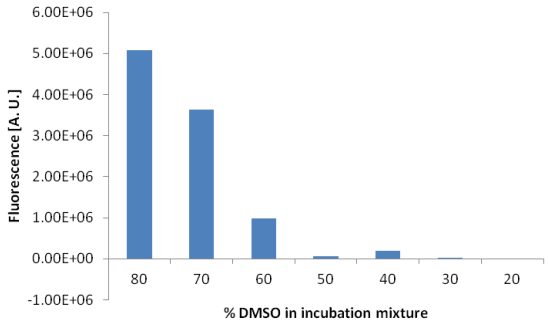

Figure 4 Dependence of the fluorescence signal on the amount of DMSO in the incubation mixture.

The incubation time of fluoride ions with the probe was investigated: longer incubation times gave better results. However, incubation for too long led to an increase in the background signal, originating from unspecific decomposition of the probe (Fig. 5). 50 mM HEPES pH 7.0 was chosen as the reading buffer because of the low background signal obtained and a good signal/noise ratio (Fig. 6). The amount of reading buffer does not seem to affect fluorescence signal (Fig. 7). Also, increasing the temperature of the incubation from room temperature (25°C) to 37°C did not significantly affect the efficiency of the deprotection reaction (Fig. 8).

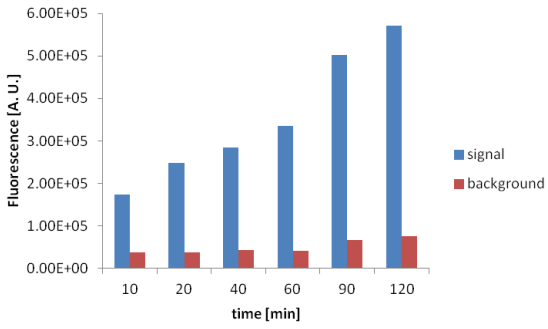

Figure 5 Dependence of fluorescence signal on incubation time.

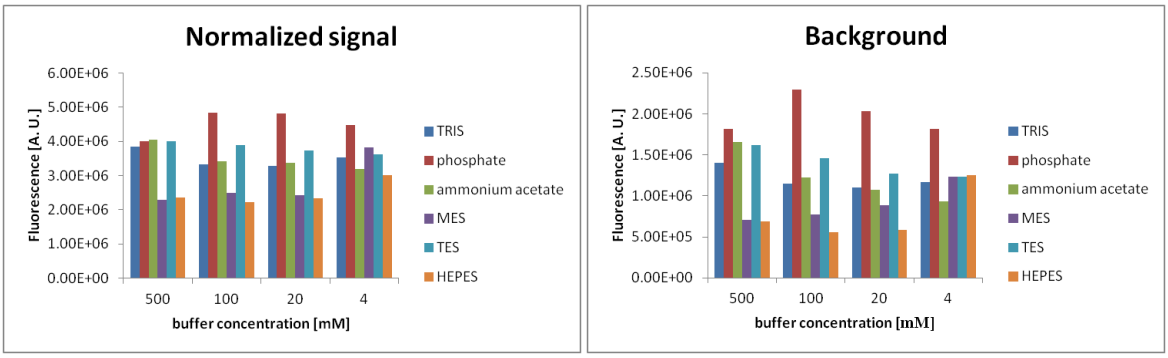

Figure 6 Dependence of fluorescence signal of fluoride containing sample (left) and sample without fluoride (right) on the type and concentration of reading buffer used.

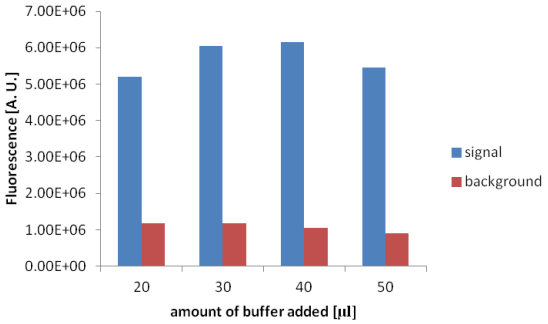

Figure 7 Dependence of fluorescence signal on the amount of reading buffer (HEPES 50 mM pH 7.0) added.

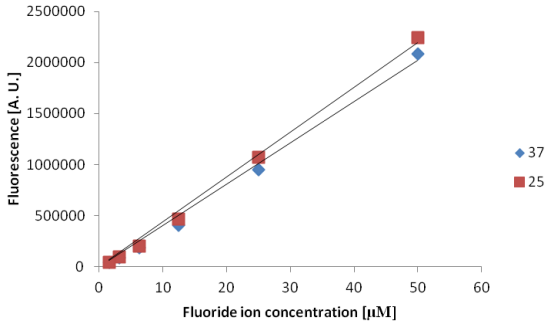

Figure 8 Dependence of fluorescence signal on fluoride ion concentrations for 25°C and 37°C incubations.

2.2 Synthesis of fluorinated BBOX substrates

2.2.1 Substrate design

Based on previous work on PHD2 and P4H, fluorinated BBOX substrate which might undergo BBOX catalysed fluoride release was determined to be (*3S*)-fluoro-GBB (GBBF, (**2**)) (Scheme 4). During the BBOX catalytic cycle, the pro-(*R*) hydrogen is abstracted therefore the (*3S*)-fluoro-GBB should be a preferential substrate over the (*3R*)-fluoro-GBB (R-GBBF, (**3**)).

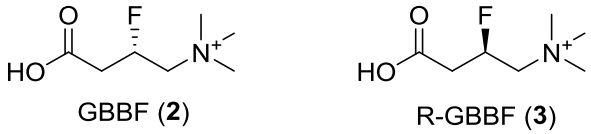

Scheme 4 Structure of fluorinated GBB analogues.

2.2.2 Synthetic approaches towards 3-fluoro carboxylic acid synthesis

The synthesis of β-fluorinated acid derivatives by direct fluorodehydroxylation can be challenging because fluoride is a relatively strong base that induces elimination to give α,β-unsaturated compounds. Several routes based on 3-hydroxy-4-aminobutyric acid derivatives were investigated. Direct fluorodehydroxylation of suitably protected precursors resulted in either no fluorination product being formed or loss of fluoride during deprotection. These attempts are summarised in Scheme 5. Fluorination of carnitine ester (**5**) with diethylaminosulphur trifluoride (DAST) led to the formation of the elimination product only (Scheme 5A). When the *N*-Cbz protected ester of 4-aminobutyric acid (**9**) was used the desired fluorinated product (**10**) was obtained; however only a small amount of the desired product could be detected (Scheme 5B). Treatment of the doubly *N*-Cbz protected 4-aminobutyric acid derivative (**12**) with DAST gave the cyclised oxazolidinone product (**13**) (Scheme 5C). Reaction of *N*-phthaloyl derivative (**15**) gave the desired fluorinated product (**16a**) in a satisfactory yield, however the product of elimination (**16b**) could also be observed (Scheme 5D). However, attempted deprotection of (**16a**) resulted in the loss of the fluoride. The results for the attempted fluorination reactions of various derivatives are summarised in Table 1.

Table 1 Fluorodehydroxylation of 3-hydroxy-γ-aminobutyric acid derivatives.

subst.	DAST (eq.)	HF/pyr. (eq.)	Isolated yield %		
			fluorination	elimination	starting material
(**15**)	2	8	50	10 (E only)	22
(**15**)	0	8	0	0	quant.
(**15**)	2	0	46	36 (E:Z=1:1)	0
(**9**)	2	8	2	-	-
(**12**)	2	8	0	0	0
(**5**)	2	8	0	quant. (E only)	0

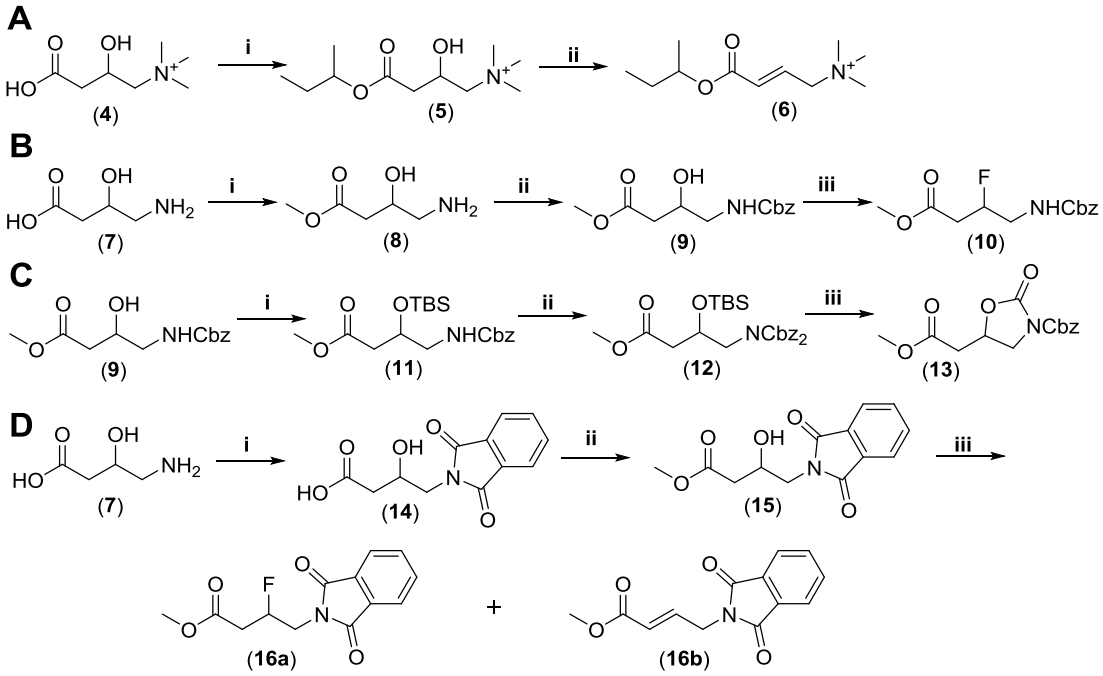

Scheme 5 Conditions: (A) i. 2-butanol, HCl, reflux; ii. (Diethylamino)sulphur trifluoride (DAST), HF/pyridine; (B) i. MeOH, reflux, HCl; ii. Benzyl chloroformate (CbzCl), $NaHCO_3$, H_2O, EtOAc; iii. DAST, HF/pyridine; (C) i. *tert*-Butyldimethylsilyl trifluoromethanesulphonate, pyridine; ii. CbzCl, LHDMS, THF, HMPA. iii. DAST, HF/pyridine; (D) i Phthalic anhydride, toluene, Dean-Stark conditions; ii. MeOH, HCl, iii. DAST, HF/pyridine.

In addition to the persisting problem of HF elimination to the corresponding α,β-unsaturated carboxylic acid derivative, the approaches described above would not allow for stereoselective introduction of fluoride. A single enantiomer of GBBF is required for enzymatic assays, as the potential inhibitory properties of R-GBBF could complicate data analysis. Therefore a route where fluoride is introduced prior to the carboxylic acid was investigated (Scheme 6). Starting from (*R*) and (*S*)-phenylalanine, (*3S*)-fluoro-GBB (**2**) and (*3R*)-fluoro-GBB (**3**) were prepared. In this synthetic route, ring opening of an aziridinium ion intermediate by a fluoride ion to give regioisomers (**20**) and (**20'**) was utilised.[46] A carboxylic acid functionality was introduced at a late stage of the synthetic route by ruthenium mediated oxidative degradation of the phenyl ring. The final products GBBF and R-GBBF were obtained by exhaustive *N*-methylation of amino acids (**24a**) and (**24b**) respectively. Final transformation quantitatively yielded the desired products, as judged by ^{1}H NMR spectroscopy, which were desalted by HPLC.

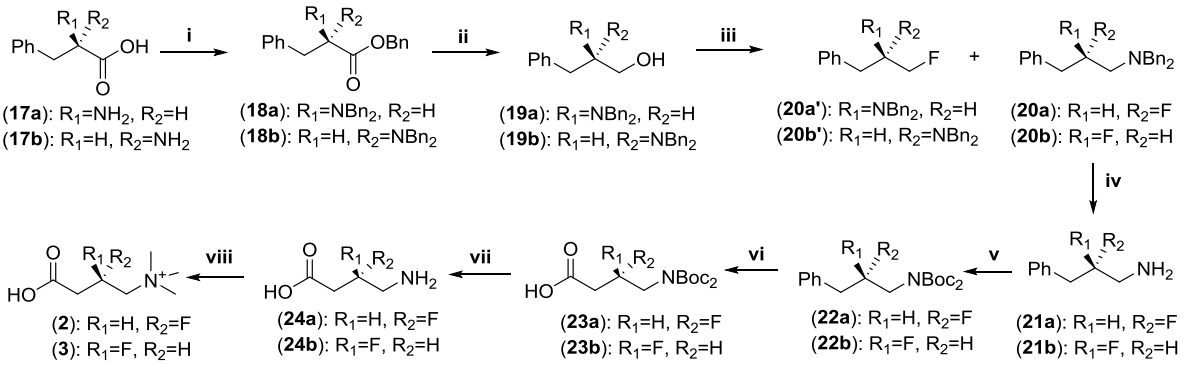

Scheme 6 Synthesis of (*3S*)-3-fluoro-GBB (GBBF, (**2**)) and (*3R*)-3-fluoro-GBB (R-GBBF, (**3**)). Reagents and conditions: i. BnBr, K_2CO_3, EtOH, H_2O, 62%; ii. $LiAlH_4$, THF, 76%; iii. Deoxo-Fluor™, CH_2Cl_2, 46%; iv. H_2, Pd(C), MeOH, 84%; v. Boc_2O, DMAP, MeCN, 88%; vi. $RuCl_3$, $NaIO_4$, CCl_4/MeCN/H_2O, 52%; vii. CH_2Cl_2, HCl, 54%; viii. CH_3I, K_2CO_3, MeOH, 11%.

2.3 Evaluation of GBBF as a BBOX substrate

GBBF was evaluated by ^{1}H NMR for BBOX catalysed oxidation and was found to be a substrate (Fig. 9). ^{1}H NMR studies revealed the formation of 3-keto-4-(trimethylammonio)butanoate (**25**) with subsequent decarboxylation leading to *N*,*N*,*N*-trimethylamino acetone (**26**) (Fig. 9). ^{19}F-NMR analyses revealed that the only detectable fluorine containing species formed in reaction of (*S*)-GBBF with BBOX are fluoride ions (Fig. 9B). This observation is consistent with previous studies in which BBOX was shown to catalyse the hydroxylation of (*S*)-carnitine, an analogue of (*S*)-GBBF, to give 3-keto-4-(trimethylammonio)butanoate (**25**) and water.[39]

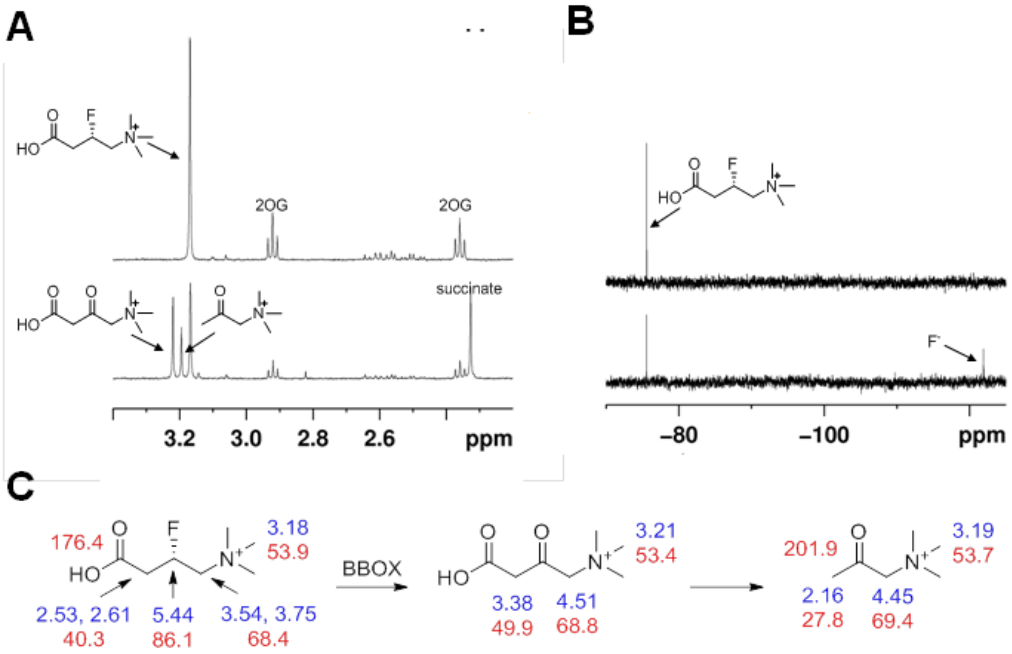

Figure 9 BBOX catalysed oxidation of GBBF as observed by ^{1}H (A) and ^{19}F (B) NMR. ^{1}H (blue) and ^{13}C (red) assignments of GBBF oxidation products (C).

In contrast, (*R*)-GBBF was found to be a poor BBOX substrate (<5% conversion after 3 hours under standard assay conditions, as monitored by ^{1}H and ^{19}F NMR). Products of the reaction of (*R*)-GBBF were observed to be the same as for the reaction of its enantiomer, as judged by ^{1}H and ^{19}F NMR analyses. The observation that GBBF (**2**) is a BBOX substrate is consistent with crystallographic studies revealing that the pro-(*R*) C-H bond of GBB is directed towards the iron centre which is responsible for hydroxylation to give (*R*)-carnitine.[39] Assuming this reaction proceeds via C-H bond oxidation, the observation that R-GBBF (**3**) is a substrate (albeit a poor one) implies that R-GBBF (**3**) can adopt catalytically productive arrangements other than those observed in the reported BBOX–GBB complex crystal structure.[39]

2.4 Use of fluoride release assay

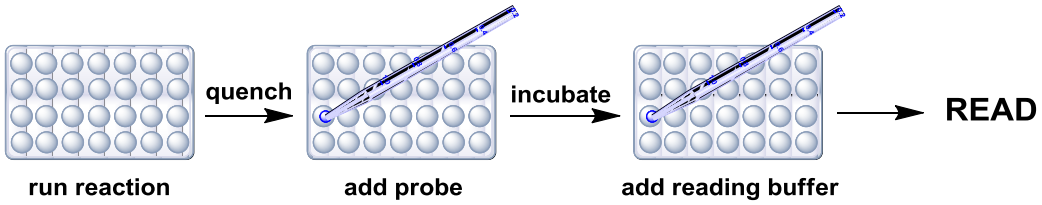

Scheme 7 Flow chart of fluoride release assay.

As discussed before, the fluoride release assay (Scheme 7) can be used to follow BBOX catalysed GBBF oxidation and to obtain kinetic parameters. The K_M values obtained for 2OG and GBBF (**2**) were 0.3 mM and 28 µM respectively (Table 2), which are comparable to the values obtained by NMR using GBB under similar conditions (Fig. 10).[47]

Table 2 Kinetic parameters of BBOX catalysed GBBF oxidation and 2OG turnover as observed by fluoride release assay and ^{1}H NMR.

	Fluoride release assay			NMR assay		
	K_M [µM]	V_{max} [µM/s]	K_{cat} [1/s]	K_M [µM]	V_{max} [µM/s]	K_{cat} [1/s]
2OG	470	0.055	0.55	150	0.039	0.39
GBBF (**2**)	83	0.062	0.62	12	0.010	0.10

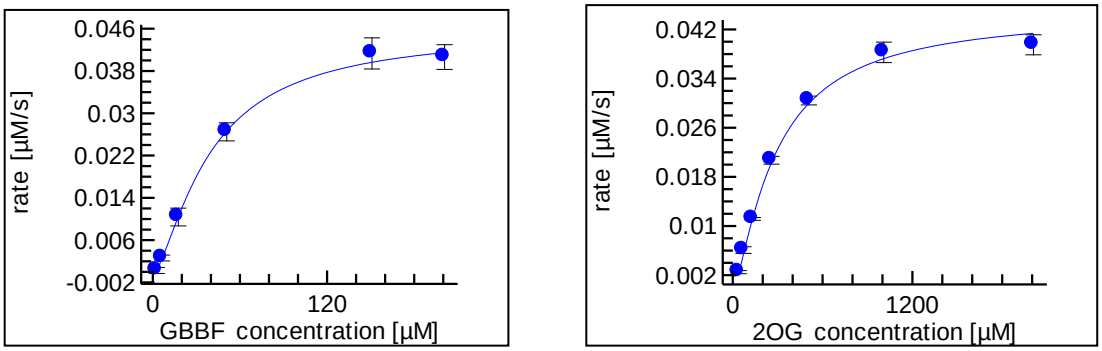

Figure 10 Curve fit for kinetic parameters of BBOX catalysed GBBF oxidation measured with fluoride release assay. Data fitted with Michaelis-Menten model.

Previous kinetic studies have shown that the activity of human BBOX is stimulated by potassium ions and reducing agents.[48] The results obtained with the fluoride release assay reveal that human BBOX has the same requirements when GBBF is used; potassium ions and reducing agents such as ascorbate increase activity (Fig. 11). Thus, high-throughput and quantitative determination of enzyme kinetics for BBOX appear feasible with the fluorinated substrate analogues.

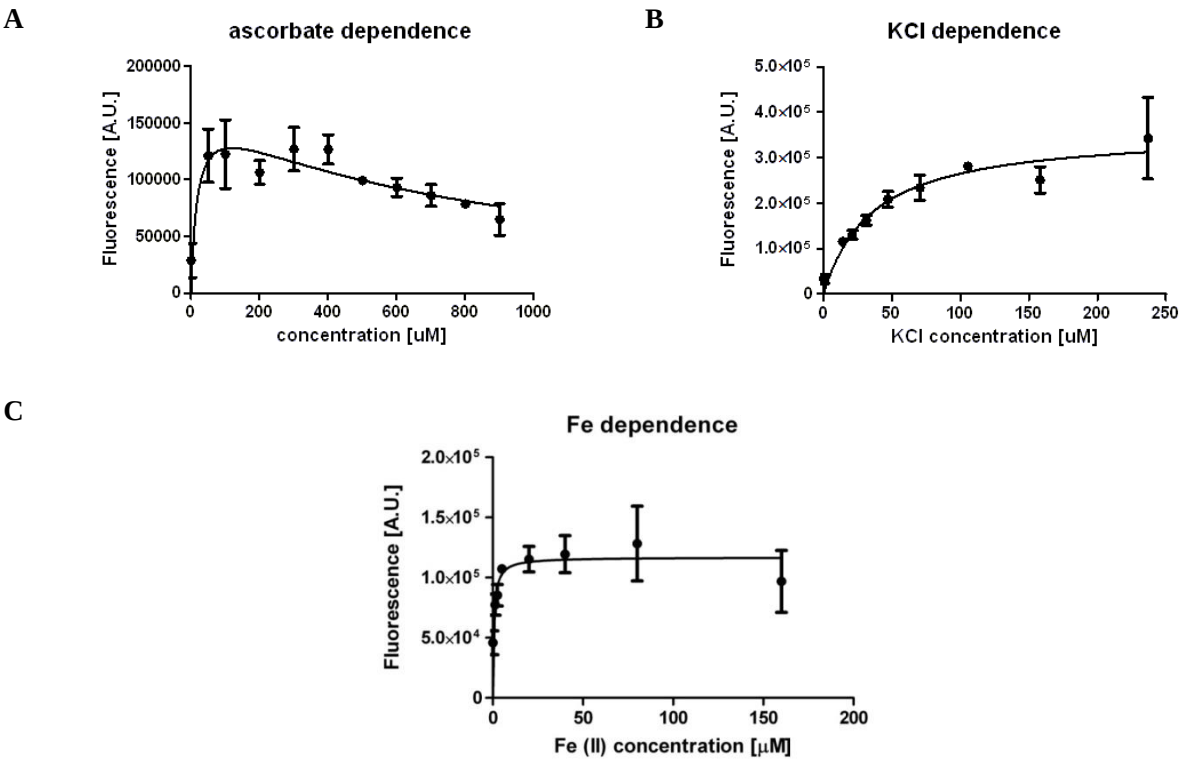

Figure 11 Effects of ascorbate, KCl and Fe(II) on BBOX activity as measured by fluoride release assay. (A) Ascorbate stimulates (*S*)-GBBF turnover (K_M = 18.5 μM); (B) KCl stimulates BBOX activity (K_M = 35.5 μM); (C) Fe(II) dependence (K_M = 0.68 μM).

The next step was to investigate the applicability of the assay to inhibitor screening. Therefore, IC_{50} values for potential inhibitors of BBOX were determined. By monitoring the change in fluorescence intensity at different inhibitor concentrations, sigmoidal curves for inhibition were observed. Initially, BBOX inhibition by 3-(2,2,2-trimethylhydrazine)propionate ((THP)[49], which is marketed as cardioprotective drug targeted at BBOX) and *N*-oxalylglycine (NOG, which is a generic 2OG oxygenase inhibitor) was evaluated. IC_{50} values of 30 μM and 315 μM for THP and NOG respectively were obtained using the fluoride release assay and were consistent with the values obtained previously by NMR using recombinant human BBOX.[39] Aromatic inhibitors such as pyridine 2,4-dicarboxylate (2,4-PDCA) and a bicyclic isoquinolinyl inhibitor (BIQ)[2,50], which is being investigated as an inhibitor of human prolyl-4-hydroxylases, were then tested. Using the fluoride release assay, it was found that they are also inhibitors for BBOX, with IC_{50} values of 100 μM and 14 μM, respectively (Fig. 12).

Table 3 Inhibition of BBOX as measured by fluoride release and ^{1}H NMR assays

Name	Structure	IC_{50} fluoride assay [µM]	IC_{50} NMR assay [µM]
BIQ	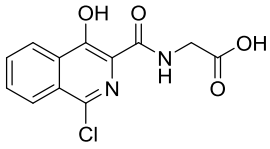	18	22
NOG	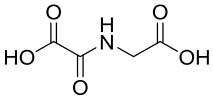	390	124
2,4-PDCA	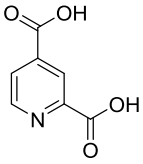	82	-
THP	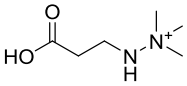	65	34

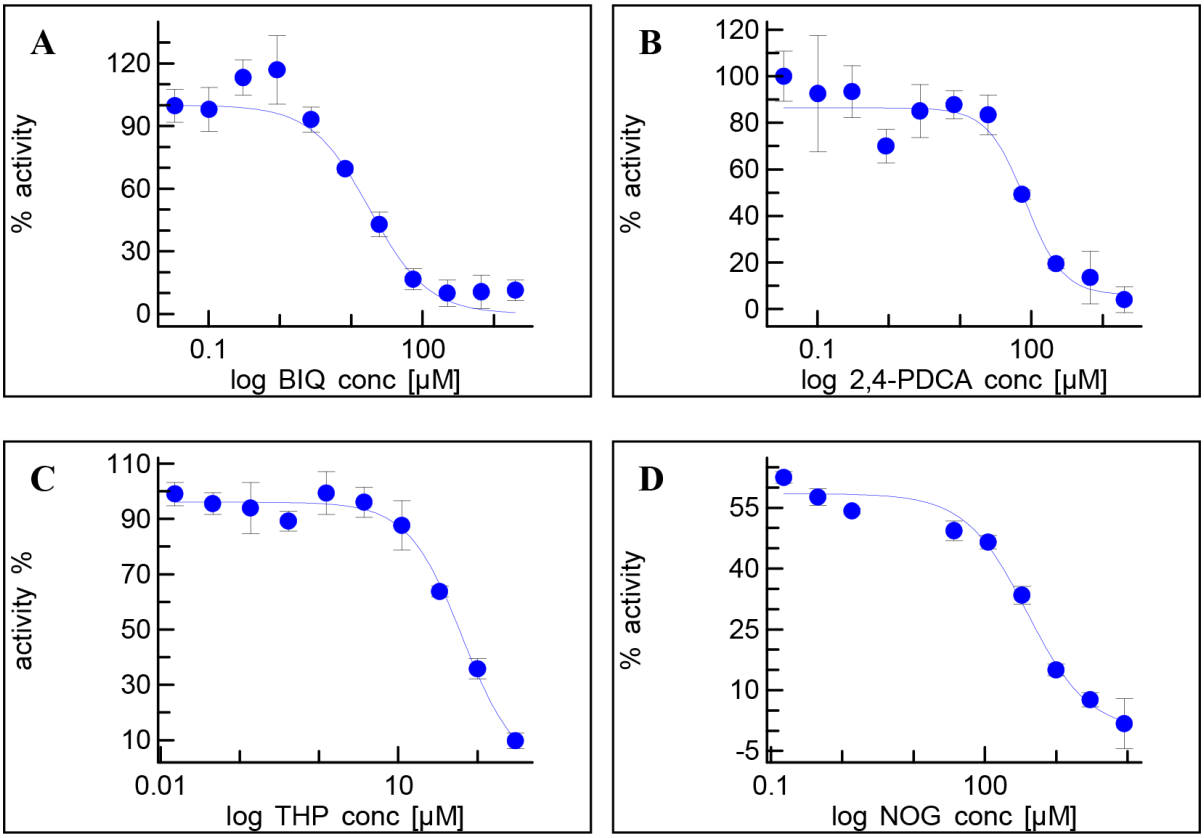

Figure 12 BBOX inhibition by BIQ, 2,4-PDCA, THP and NOG. Data fitted with 4-parameter logistic model (dose-response).

2.5 Application of the fluoride release assay for other enzymes

Use of the fluoride release assay was investigated for PHD2, which, as mentioned previously, was reported to accept a fluorinated peptide analogue as a substrate to yield the 4-oxoprolyl product (Scheme 2)[44]. The reaction of PHD2 with an appropriate peptide substrate bearing a cis-4-fluoroprolyl residue at the canonical hydroxylation site was carried out. The amount of fluoride released could be quantified by using the chemical probe (Fig. 13). Therefore, the utility of the fluorescence-based fluoride detection assay was demonstrated for 2OG-dependent oxygenases other than BBOX, accepting oligomeric substrates, and presents an alternative for available PHD2 screening platforms.

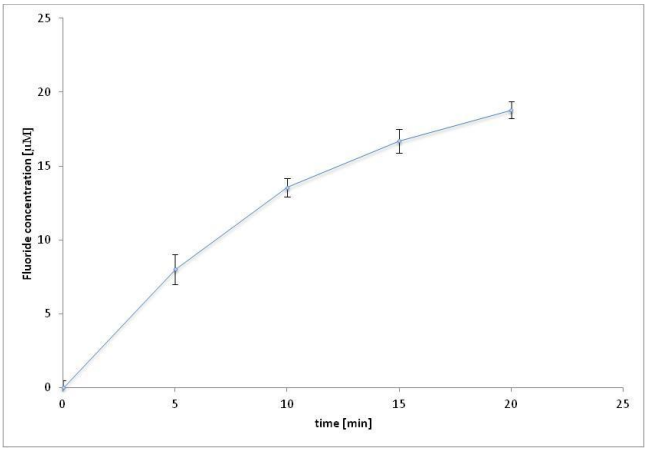

Figure 13 Fluoride is released when 4-fluoro Pro CODD peptide (F-CODD) is reacted with human PHD2[51]. The reaction mixture contained: 4 µM PHD2, 50 µM Fe (II), 200 µM F-CODD, 300 µM 2OG, 500 µM ascorbate, 50 mM Tris pH=7.5. The sequence of F-CODD is DLDLEMLAXYIPMDDDFQL where X is a 4-fluorinated prolyl residue.

3 Fluoromethylated intermediates of carnitine biosynthesis

Organofluorine compounds are widely used in chemistry and chemical biology. Their applications include the modification of physicochemical and conformational properties of small molecules, and uses in radiomedicine[52] as tracers or labels for NMR studies.[40,53] ^{19}F NMR is emerging as a valuable tool for studying biochemical processes *in vitro* and *in vivo.*[54] The principle advantage of ^{19}F NMR is the absence of endogenous fluorinated species in most living organisms eliminates the problem of background interference and signal overlap. However, the use of ^{19}F NMR is often limited by the availability of appropriately labelled fluorinated compounds. In this section, synthesis and evaluation of fluorinated intermediates of carnitine biosynthesis, in particular GBB, are discussed.

3.1 Synthesis of monofluoromethylated GBB and TML

Various approaches to the incorporation of fluorine into small molecules are available, however reagents for electrophilic monofluoromethylation are limited.[55] Prakash *et al.* reported an air and moisture stable electrophilic fluoromethylation reagent (**27**) (Fig. 14) that reacts under mild conditions[56] with various nucleophiles, including amines.[56,57]

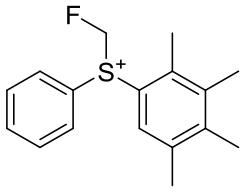

Figure 14 Structure of fluoromethylating reagent (**27**).

Reagent (**27**) was used in the preparation of fluoromethylated GBB (GBBNF, (**29**)) and trimethyllysine (TMLNF, (**31**)), starting from appropriately protected *N*,*N*-dimethylated precursors, as shown in Scheme 8.

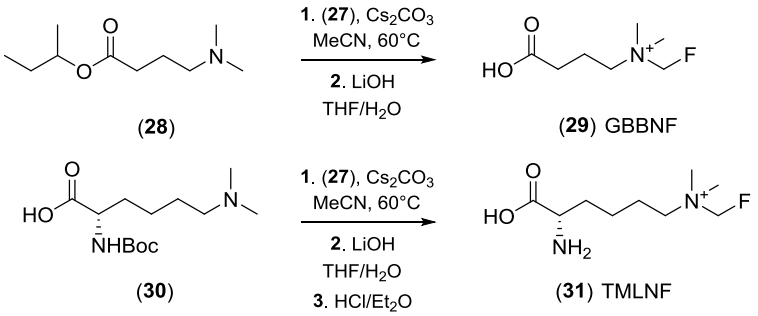

Scheme 8 Preparation of *N*-CH_2F derivatives of GBB and TML.

3.2 Evaluation of GBBNF as a BBOX substrate

The fluoromethylated GBB analogue (GBBNF, (**29**)) was evaluated using NMR in reaction with purified recombinant human BBOX (hBBOX) *in vitro*. GBBNF (**29**) was found to be an hBBOX substrate, as demonstrated by ^{1}H NMR analyses (Fig. 15), undergoing hydroxylation at the C3 position to give a fluoromethylated carnitine analogue (**32**).

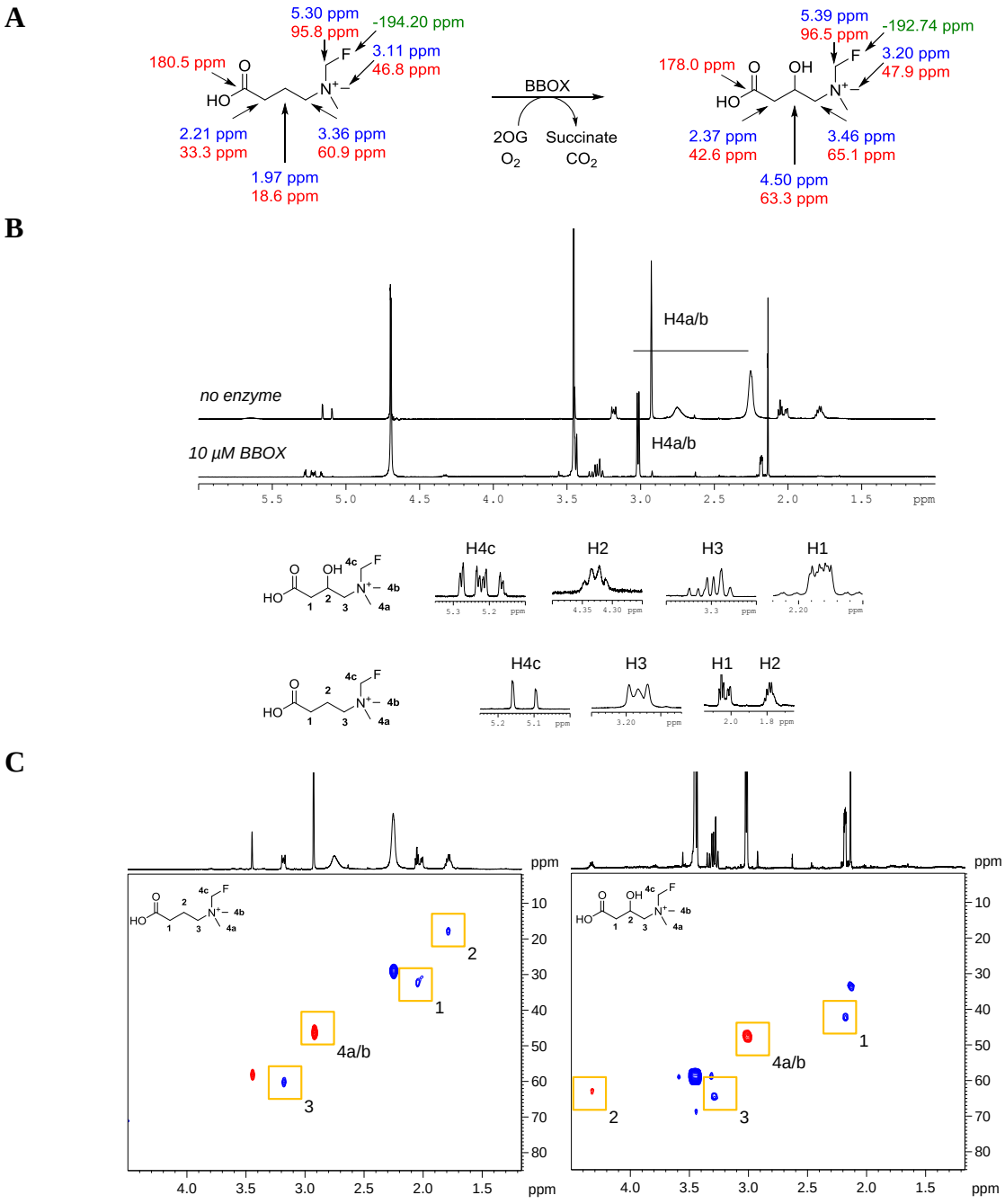

Figure 15 Assignments of BBOX catalysed GBBNF (**27**) hydroxylation. A – ^{1}H (blue), ^{19}F (green) and ^{13}C (red). B – ^{1}H NMR spectra of GBBNF (**27**) and enzymatic reaction mixture. C – ^{1}H-^{13}C HSQC spectra of GBBNF (**27**) and enzymatic reaction mixture.

The kinetic parameters reported in this section were obtained using ^{1}H NMR. Comparison of the initial rates of hydroxylation of GBB, GBBNF (**29**) and GBBF (**2**) by BBOX revealed that GBBNF (**29**) is a better substrate than GBBF (**2**) (Table 4, Fig. 16). The initial hydroxylation rate of GBBNF (**29**) is ~65% of the initial hydroxylation rate of GBB, while GBBF (**2**) is hydroxylated at ~20% of the initial rate of GBB. The K_M and k_{cat} values also reveal that the properties of GBBNF (**29**) as a substrate are closer to those of GBB than GBBF (**2**) (Table 4).

Levels of 'uncoupled' 2OG turnover for GBB and its fluorinated analogues were examined by comparing the rates of succinate formation with the rate of hydroxylation. The results showed GBBNF (**29**) to be similar to GBB (ratio of succinate formation to hydroxylation 1.1 for GBB vs 1.3 for GBBNF), whereas with GBBF (**2**), the ratio of uncoupled/coupled turnover was around two (Table 4). As for GBB, GBBF (**2**) displays substantial substrate inhibition (apparent K_i values in the micromolar range – see Table 4). Interestingly, the extent of substrate inhibition by GBBNF (**29**) was much less than for GBB or GBBF (**2**) (Fig. 17). The mechanism of substrate inhibition of hBBOX is unknown, but is of interest as it may be involved in regulating carnitine biosynthesis in cells, which is further discussed in Chapters 5 and 6.

Table 4 Kinetic parameters of fluorinated GBB analogues.

		GBB	GBBF (**2**)	GBBNF (**27**)
rate [µM/s]	Hydroxylation	0.123	0.027	0.083
	Succinate formation	0.162	0.063	0.097
Ratio of succinate formation to hydroxylation		1.1	2	1.3
Kinetic parameters	K_M [µM]	4.2	19.8	16.6
	k_{cat} [1/s]	0.83	0.14	0.30
	K_i [µM]	24.5	135	-

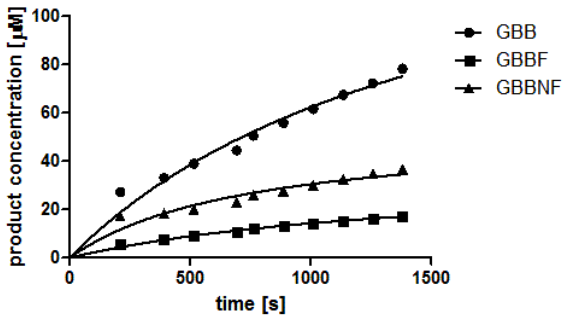

Figure 16 Time courses of BBOX catalysed oxidation of GBB, GBBNF (**27**) and GBBF (**2**) obtained by NMR.

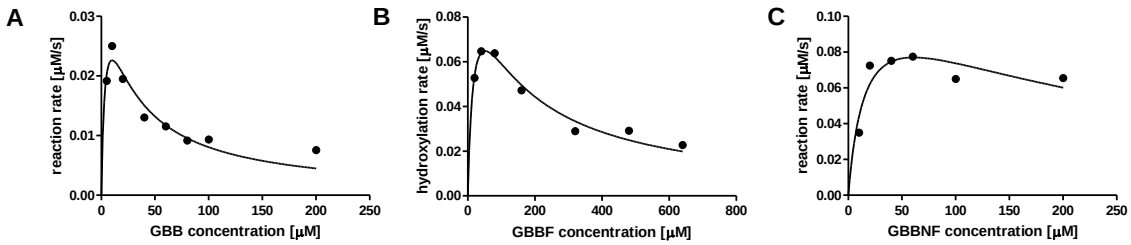

Figure 17 Dependence of the initial rate of hydroxylation on GBB analogue concentration.

3.3 Application of GBBNF for ^{19}F NMR assays *in vitro*

BBOX catalysed GBBNF (**29**) hydroxylation can be followed by ^{19}F NMR. The fluorine chemical shift of the product is distinctively different from the observed shift of the substrate. In these compounds, the ^{19}F resonance appears with a 1:1:1 triplet fine structure, not as a singlet. This structure arises from coupling of the fluorine to the adjacent quadrupolar ^{14}N nucleus (I = 1, 99.6% abundance) and is apparent because the highly symmetrical tetrahedral environment of the ^{14}N centre suppresses rapid quadrupolar relaxation that, in less symmetrical environments, leads to loss of coupling fine structure. ^{19}F NMR was also employed for IC_{50} measurements. BBOX inhibition by THP[58], which is an inhibitor and competitive substrate for BBOX[39] was again investigated. The obtained IC_{50} value (82 µM) is similar to that obtained by ^{1}H NMR (34 µM) and fluoride release (65 µM) assays.

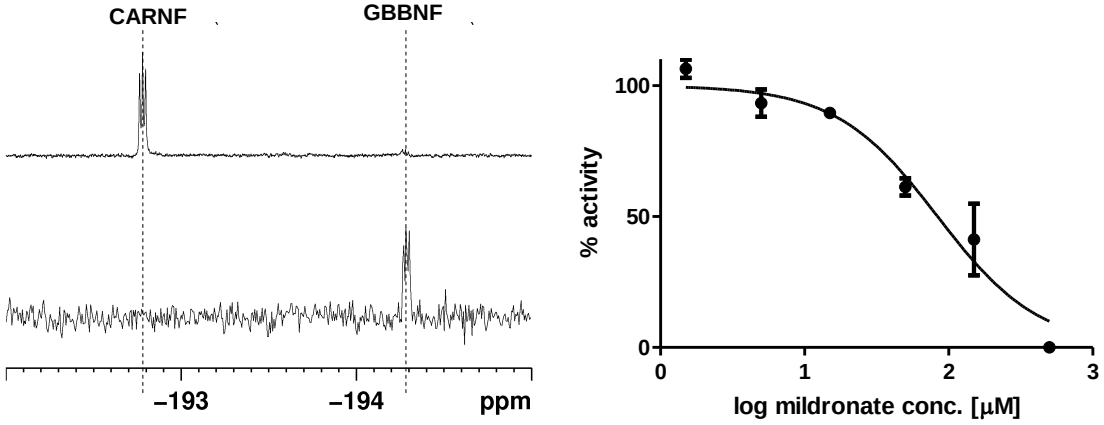

Figure 18 BBOX catalysed reaction of GBBNF can be followed by ^{19}F NMR (left). IC_{50} curve of BBOX inhibition by THP obtained by ^{19}F NMR with GBBNF (right).

3.4 Following BBOX activity in cell lysates

In the previous section, ^{19}F NMR *in vitro* assays with GBBNF were shown to be useful for BBOX activity studies. However, an advantage of ^{19}F NMR is its ability to monitor specific BBOX reaction without the interference of any other non-fluorinated assay components. This makes it suitable for more biologically relevant assay conditions. *E. coli* BL21 (DE3) cells producing a prokaryotic BBOX homologue from *Pseudomonas* sp. AK1 (psBBOX) were used to test turnover of GBBNF in

cell lysates. In crude cell lysate GBBNF was observed to be converted to fluorinated carnitine analogue (CARNF) and the conversion was 2OG dependent (Fig. 19).

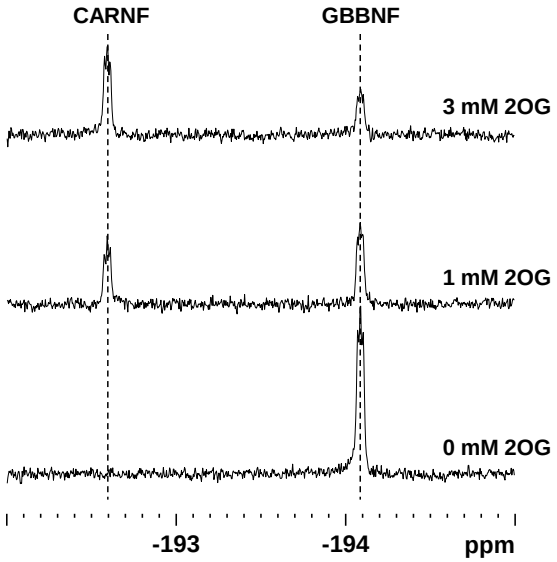

Figure 19 Turnover of GBBNF in cell lysates is dependent on the amount of 2OG added.

E. coli BL21 (DE3) cells were transformed with the pCOLD I plasmid bearing the psBBOX gene (further discussed in Chapter 6). 100 mL cultures were incubated for 4 h at 37 °C and were then induced with 0.2 mM IPTG (isopropyl β-D-1-thiogalactopyranoside) and incubated for a fixed amount of time at 15°C, harvested, treated with GBBNF and 2OG and analysed by ^{19}F NMR. The extent of GBBNF conversion was found to be also dependent on the amount of psBBOX present in the extracts (Fig. 20).

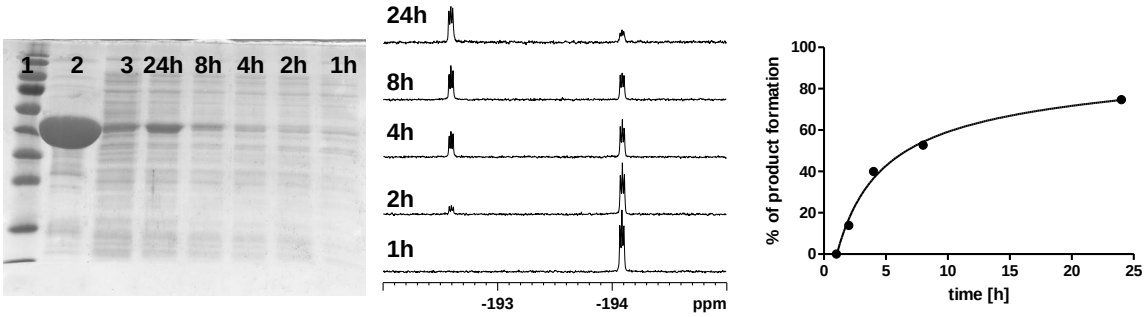

Figure 20 SDS-PAGE gel shows lysate samples from cells harvested at various times after IPTG induction (lanes 4-8). Molecular weight marker (lane 1), BBOX sample (lane 2) and uninduced cells harvested after 24 h (lane 3) are shown. BBOX activity in cell lysates were quantified by ^{19}F NMR. GBBNF conversion in cell lysate plotted against time elapsed from induction by IPTG was fitted with equation: y=a-bln(x+c), where a=7.8, b=-21.6, c=-0.34 and R^2=0.97 (OriginPro 8.5.1 software).

4 Summary and perspective

Synthetic routes towards GBB analogues fluorinated in position 3 of the main carbon chain and the *N*-methyl group were developed. The fluorinated GBB analogues were evaluated as BBOX substrates. (*3S*)-fluoro-GBB was oxidised by BBOX, with subsequent fluoride release. This was used for the development of a fluorescence based assay for BBOX activity measurements. It was shown that the method can be applied to other 2OG dependent oxygenases, i.e. PHD2, which catalysed turnover of a peptidyl substrate containing fluoro proline. These results open up the possibility of examining fluorinated substrate analogues for other 2OG dependent oxygenases and further assay development. The *N*-methyl fluorinated analogue GBBNF was shown to undergo hydroxylation analogously to GBB itself. Its use was exemplified by following BBOX catalysed turnover *in vitro* and in cell lysates by means of ^{19}F NMR. Overall, two efficient assays for assessing the extent of BBOX activity were developed, the assays can be used for high throughput *in vitro* inhibition studies on BBOX, as well as in cellular studies on carnitine biosynthesis.

5 Acknowledgements

Human BBOX used in these studies was supplied by Dr. Grażyna T. Kochan (Structural Genomics Consortium, Oxford). Entire NMR work for the fluoride release assay section and part of the NMR work on GBBNF section (NMR involving bacterial cell lysates and IC_{50} for THP) was done by Dr. Ivanhoe K.H. Leung (Department of Chemistry, University of Oxford). Fluoromethylating agent (26) was synthesised by Dr. Armin Thalhammer (Department of Chemistry, University of Oxford). The fluorinated CODD derivative was synthesised by Naomi Rippengale (Department of Chemistry, University of Oxford).

Work included in this chapter was published in an altered form:

- A. M. Rydzik, I. K. H. Leung, G. T. Kochan, A. Thalhammer, U. Oppermann, T. D. W. Claridge, C. J. Schofield, *ChemBioChem* **2012**, *13*, 1559-1563.
- A. M. Rydzik, I. K. H. Leung, A. Thalhammer, G. T. Kochan, T. D. W. Claridge, C. J. Schofield, *ChemComm* **2014**, *50*, 1175-1177.

6 Experimental section

6.1 NMR

^{1}H NMR assays were performed on a Bruker AVIII 700 with inverse TCI cryoprobe using 3 mm MATCH tubes. Pulses were calibrated for ^{1}H spectra using single-pulse nutation method (Bruker pulsecal routine). Water suppression was achieved using the excitation sculpting method. ^{19}F NMR assays were performed on a Bruker AVII 500.

6.2 Optimisation of fluoride ion detection

Unless otherwise stated, default conditions are 40 µl probe (5 µM stock, final concentration 2 µM), 10 µl of fluoride ion solution (20 µM stock, final concentration 2 µM) in Tris-HCl (50 mM, pH=7.0) was quenched with 50 µl of HEPES buffer (50 mM, pH=7.0) after 1 hour the incubation. Fluorescence was measured immediately after addition of buffer to samples. Normalized signals were calculated as the fluorescence signal (average of triplicate) minus the fluorescence signal for a control with no fluoride ion added (average of triplicate).

6.3 Enzymatic assays

6.3.1 Reagents

Reagents were purchsed from Sigma-Aldrich unless otherwise stated. Tris-d_{11} was from Cambridge Isotopes. Standard solution of Tris d_{11} buffer was 50 mM in H_2O pH 7.5 and contained 0.1% NaN_3 to prevent microbial growth. 2OG was used as a sodium salt, ascorbate as potassium salt, and GBB as hydrochloride salt. Fe(II) stock solution was prepared by dissolving $Fe(NH_4)_2(SO_4)_2$ in 20 mM HCl solution to final concentration of 100 mM.

6.3.2 Fluoride-release assays

Enzymatic reactions were performed with the following final concentrations: 40 µM (*S*)-GBBF (**2**), 40 µM ammonium iron(II) sulphate hexahydrate, 250 µM ascorbate, 160 µM potassium chloride, 500 µM 2-oxoglutarate disodium salt, 100 nM BBOX and 50 mM Tris·HCl buffer (pH 7.5). Reagents and BBOX were mixed at room temperature in a 96-well plate, and the reaction was initiated by the addition of 2OG. The reaction was quenched by addition of 20% acetonitrile. The quenched reaction mixture (20 µL) was then transferred to a separate solid black 96-well round-bottom plate, and was incubated with bis(tert-butyldimethylsilyloxy) fluorescein (**1**) (80 µL, 5 µM) for 1 h at room temperature. HEPES buffer (50 µL, 50 mM, pH 7.0) was then added, and the mixture was incubated for a further 2 min prior to fluorescence being measured by using an EnVision Multilabel plate reader (PerkinElmer) fitted with FITC FP 480/30 (480 nm, bandwidth 30 nm) and FITC FP 535/40 emission (535 nm, bandwidth 40 nm) filters. For each enzymatic reaction, a

corresponding control containing all reagents but no enzyme was also recorded. The normalised fluorescence signal was defined as the observed fluorescence signal minus the control signal.

6.3.3 Kinetic assays for GBBF by fluoride release

Standard kinetic assays were conducted at 298 K in solutions containing (*S*)-GBBF (**2**) (40 µM), ammonium iron(II) sulphate hexahydrate (40 µM), ascorbic acid disodium salt (250 µM), potassium chloride (160 µM), 2-oxoglutarate disodium salt (500 µM), BBOX (100 nM) and Tris·HCl buffer (50 mM, pH 7.5). Reactions were initiated by the addition of 2OG. All measurements were repeated four times.

6.3.4 Inhibition assays by fluoride release

Inhibition assays were conducted at 298 K in solutions containing (*S*)-GBBF (40 µM), ammonium iron(II) sulphate hexahydrate (40 µM), ascorbic acid disodium salt (250 µM), potassium chloride (160 µM), 2-oxoglutarate disodium salt (500 µM), BBOX (100 nM) and Tris·HCl buffer (50 mM, pH 7.5) and varying concentrations of inhibitor. Reactions were initiated by 2OG addition, and quenched by the addition of 20% acetonitrile after 10 min.

6.3.5 Kinetic assays for GBBNF by ^{1}H NMR

^{1}H NMR hydroxylation/succinate formation assays contained: GBB analogue 100 µM, 2OG 500 µM, ascorbate 500 µM, KCl 200 mM, Fe(II) 50 µM, enzyme 400 nM, buffer: Tris-d_{11} 50mM pH 7.5 in H_2O, 10% D_2O. Reactions were performed in a final volume of 160 µL, initiated by addition of enzyme, and then followed by ^{1}H NMR in real time. ^{1}H NMR K_M measurements were made using analogous conditions but with a saturating concentration of 2OG (1 mM).

6.3.6 Kinetic assays for GBBNF by ^{19}F NMR

^{19}F NMR inhibition assays used the following conditions: GBBNF 150 µM, 2OG 100 µM, ascorbate 500 µM, KCl 80 mM, Fe(II) 40 µM, enzyme 25 nM, buffer: Tris-d_{11} 50 mM pH 7.5 in H_2O. Samples were prepared in final volume of 0.4 mL. Reaction was initiated by addition of hBBOX and quenched after 10 min by addition of 0.1 mL of CD_3CN.

6.3.7 GBBNF cell lysate assays

E. coli BL21 (DE3) cells were transformed with a pCOLD I plasmid bearing the psBBOX gene. 100 mL cultures were grown in 2TY media containing ampicillin as a selection marker for 4 h at 37°C with shaking until the OD_{600} reached 0.5 and then induced with 0.2 mM IPTG (isopropyl β-D-1-thiogalactopyranoside) and incubated overnight (15°C). Cells were pelleted by centrifuging 7000 rpm for 10 min at 4°C. The cell pellet was then re-suspended in 5 times weight of binding buffer (50 mM HEPES pH 7.6, 0.5 M NaCl, 5 mM imidazole) and lysed by sonication. The lysate was centrifuged and the supernatant used in further experiments. SDS-PAGE molecular weight marker was from Thermo Scientific (PageRuler Prestained Protein Ladder 10-170 kDa). NMR samples were

prepared by addition of 10% 50 mM Tris-d_{11} D_2O pH 7.5, 10% 50 mM Tris-d_{11} H_2O pH 7.5, 0.5 mM trifluoroacetic acid as a chemical shift reference, 1 mM fluoromethyl GBB and 3 mM 2OG.

6.4 Data processing

NMR data were processed using TopSpin 3.1 software (Bruker). Kinetic analyses were done using GraphPad Prism software and XLFit software. Standard Michaelis-Menten model was used for the fits of kinetic data and 4-Parameter Logistic Model (XLfit) for dose-response inhibition curve fitting.

6.5 Synthesis

6.5.1 Reagents

General synthetic considerations are according to Synthesis section in Appendix 1. Reagents were from Acros, Aldrich, Fluka, Lancaster, TCI, Fluorochem and used as supplied. Solvents for chemical transformation, work-up and chromatography were from Rathburn (HPLC grade) and used without further purification. Dry solvents were from Aldrich or prepared by filtration through columns containing activated aluminium oxide under argon.

6.5.2 Synthesis of TBS-fluorescein probe (1)

6.5.2.1 3',6'-Bis((tert-butyldimethylsilyl)oxy)-4a',9a'-dihydro-3H-spiro[isobenzofuran-1,9'-xanthen]-3-one

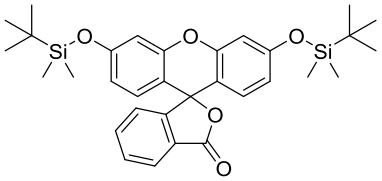

To a solution of fluorescein (1.0 g, 3.01 mmol) in dichloromethane (20 ml) was added 2,6-lutidine (870 µl, 7.52 mmol, 2.5 eq) followed by the dropwise addition of *tert*-butyldimethylsilyl triflate (1.52 ml, 6.62 mmol, 2.2 eq). The resulting suspension was stirred for 3 h at room temperature, then was diluted with dichloromethane, washed 3 times with water, dried over Na_2SO_4 and concentrated *in vacuo*. The crude residue was purified by flash column chromatography on silica to give **2** as a white solid (520 mg, 0.93 mmol, 31%).

mp 76-79°C (lit. 154-155°C[59]); TLC 8:2 hexane/EtOAc R_f= 0.55, ^{1}H NMR (500 MHz, *CDCl*$_3$) δ ppm 8.02 (1 H, d, *J*=7.5 Hz, ArH), 7.67 (1 H, td, *J*=7.5, 1.0 Hz, ArH), 7.62 (1 H, td, *J*=7.5, 1.0 Hz, ArH), 7.19 (1 H, d, *J*=7.5, Hz, ArH), 6.74 (2 H, d, *J*=2.5 Hz, ArH), 6.64 (2 H, d, *J*=8.5 Hz, ArH), 6.53 (2 H, dd, *J*=8.5, 2.5 Hz, ArH), 0.99 (18 H, s, C(C*H*$_3$)$_3$), 0.24 (6 H, s, Si-C*H*$_3$), 0.23 (6 H, s, Si-C*H*$_3$); ^{13}C NMR (125 MHz, *CDCl*$_3$) δ ppm 169.5, 157.6, 153.1, 152.3, 134.9, 129.6, 129.0, 126.8, 124.9, 124.0, 116.6, 112.0, 107.6, 83.3, 25.6, 18.2, -4.4; IR ν_{max} (neat)/cm^{-1} 2955, 2930, 1768, 1629, 1560, 1179, 839; LRMS (ESI$^-$, *m/z*) 262.08 [M-H].

6.5.3 Intermediates for fluorodehydroxylation

6.5.3.1 4-Sec-butoxy-2-hydroxy-*N*,*N*,*N*-trimethyl-4-oxobutan-1-aminium (5)

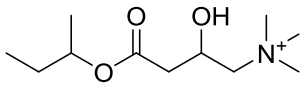

A solution of DL-carnitine chloride (4 g, 20.0 mmol) in 2-butanol (20 ml) was treated with 10 ml of a 2 M solution of HCl in Et_2O. The resultant mixture was stirred at reflux overnight. Then the mixture was cooled and evaporated several times with acetone to afford **5** as clear oil (4.82 g, 19.0 mmol, 95%).

^{1}H NMR (400 MHz, *$CDCl_3$*) δ ppm 4.90 (1 H, br. s., OH), 4.73 - 4.83 (1 H, m), 4.58 - 4.70 (1 H, m), 3.79 - 3.56 (2 H, m), 3.46 (9 H, s, 3×CH_3), 2.55 - 2.79 (2 H, m), 1.37 - 1.67 (2 H, m), 1.13 - 1.22 (3 H, m), 0.81 - 0.94 (3 H, m); ^{13}C NMR (101 MHz, *$CDCl_3$*) δ ppm 170.7, 73.1, 62.7, 54.9, 40.2, 28.7, 19.4, 9.7; IR ν_{max} (film)/cm^{-1} 3385, 2975, 1720, 1643, 1479, 1293, 1179, 1094; LRMS (ESI$^+$, *m/z*) 218.19 [M$^+$]; HRMS (ESI$^+$) $C_{11}H_{24}NO_3^+$ requires 218.1751, found [M+Na$^+$] 218.1751.

6.5.3.2 (*E*)-4-*sec*-butoxy-*N*,*N*,*N*-trimethyl-4-oxobut-2-en-1-aminium (6)

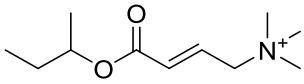

5 (200 mg, 0.92 mmol) was mixed in anhydrous dichloromethane at -10°C and HF-pyridine (134 µl, 7.36 mmol, 8 eq) was added, followed by dropwise addition of DAST (243 µl, 1.84 mmol, 2eq). The mixture was stirred overnight and then nitrogen was bubbled through solution to remove HF. A 10% aqueous solution of K_2CO_3 was added until the pH 7. The resultant mixture was concentrated *in vacuo*. The crude product was analysed by ^{1}H NMR and used without further purification. The analysis has shown the presence of the elimination product as its *E*-isomer.

^{1}H NMR (200 MHz, *$(CD_3)_2CO$*) δ ppm 7.09 (1 H, dt, *J*=15.5, 7.5 Hz), 6.61 (1 H, dt, *J*=15.5, 1.0 Hz), 4.86 - 4.99 (1 H, m), 4.81 (2 H, dd, *J*=7.5, 1.0 Hz), 3.51 (9 H, s, *N*-CH_3), 2.04 - 2.14 (2 H, m), 1.26 (3 H, d, *J*=6.5 Hz), 0.87 - 0.98 (3 H, m).

6.5.3.3 Methyl 4-(benzyloxycarbonylamino)-3-hydroxybutanoate (9)

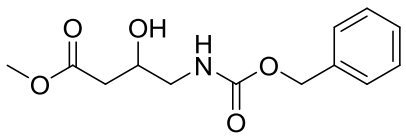

4-aminobutyric acid (500 mg, 4.20 mmol) was dissolved in MeOH (10 ml), and 3 ml of 2 M solution of HCl in Et_2O were added and the resulting mixture was stirred at reflux overnight. The reaction mixture was concentrated *in vacuo* and the residue was dissolved in a solution of $NaHCO_3$ (1.4 g, 16.8 mmol, 4 eq) in water (10 ml). Ethyl acetate was added (10 ml), followed by dropwise addition of benzyl chloroformate at 0°C. The resulting mixture was stirred overnight at room temperature.

The aqueous phase was separated, washed with ethyl acetate, and the combined organics were dried over $MgSO_4$, concentrated *in vacuo* and subjected to column chromatography on silica to afford **9** as a colourless oil (897 mg, 3.36 mmol, 80%).

TLC 7:3 hexane/EtOAc R_f= 0.10; ^{1}H NMR (400 MHz, *CDCl$_3$*) δ ppm 7.16 - 7.43 (5 H, m, ArH), 5.31 - 5.48 (1 H, m, NH), 5.10 (2 H, s), 4.05 - 4.21 (1 H, m), 3.70 (3 H, s), 3.55 (1 H, br. s., OH), 3.39 (1 H, ddd, *J*=14.0, 6.5, 3.5 Hz), 3.18 (1 H, ddd, *J*=13.0, 6.0, 1.0 Hz), 2.49 (2 H, d, *J*=8.0 Hz); ^{13}C NMR (101 MHz, *CDCl$_3$*) δ ppm 172.8, 157.0, 136.4, 128.5, 128.2, 128.1, 67.4, 66.9, 51.9, 45.9, 38.4; IR ν_{max} (film)/cm^{-1} 3357, 2953, 1719, 1533, 1439, 1258, 1171, 1003; LRMS (ESI$^+$, *m/z*) 290.11 [M+Na$^+$]; HRMS (ESI$^+$) $C_{13}H_{17}NNaO_5$ requires 290.0999, found [M+Na$^+$] 290.1003.

6.5.3.4 Methyl 4-(benzyloxycarbonylamino)-3-fluorobutanoate (10)

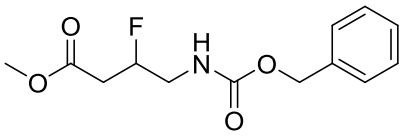

10 was synthesised following the procedure used for the synthesis of fluorinated derivative **16a**. Starting from alcohol **9** (100 mg, 0.37 mmol) a small amount of yellow oil was isolated (~2 mg, 0.0074 mmol, <2%) which was characterized only by ^{1}H NMR due to small amount of material and some remaining impurities.

^{1}H NMR (400 MHz, *CDCl$_3$*) δ ppm 7.34 - 7.40 (5 H, m, ArH), 5.12 (2 H, s), 4.52 (1 H, m, $J_{H\text{-}F}$=48.0), 3.90 (1 H, br. s, NH), 3.70 (3 H, s, CH_3), 3.71-3.78 (2 H, m), 2.68 (2 H, m).

6.5.3.5 Methyl 4-(benzyloxycarbonylamino)-3-(tert-butyldimethylsilyloxy)butanoate (11)

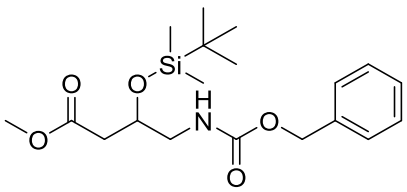

To a stirred solution of **9** (300 mg, 1.12 mmol, 1 eq) in anhydrous CH_2Cl_2 at 0°C was added pyridine (271 µl, 3.38 mmol, 3 eq), followed by the addition of *tert*-butyldimethylsilyl trifluoromethanesulphonate (283 µl, 1.23 mmol, 1.1 eq). The resultant mixture was stirred at room temperature for 3 h before being quenched with a saturated aqueous solution of ammonium chloride. The phases were separated and the aqueous phase extracted with CH_2Cl_2. The combined organic phases were washed with brine, dried over $MgSO_4$, concentrated and purified by flash column chromatography on silica to afford **11** as a colourless oil (195 mg, 0.51 mmol, 46%).

TLC 7:3 hexane/EtOAc R_f= 0.55; ^{1}H NMR (500 MHz, *CDCl$_3$*) δ ppm 7.30 - 7.41 (5 H, m, ArH), 5.06 - 5.19 (2 H, m), 5.00 (1 H, br. s., NH), 4.18 - 4.32 (1 H, m), 3.67 (3 H, s, OCH_3), 3.23 - 3.38 (2 H, m), 2.49 (2 H, d, *J*=6.0 Hz), 0.87 (9 H, s, *t*BuSi), 0.05 (3 H, s, CH_3-Si), 0.08 (3 H, s, CH_3-Si); ^{13}C NMR (125 MHz, *CDCl$_3$*) δ ppm 171.5, 156.5, 136.4, 128.5, 128.1, 68.2, 66.8, 51.6, 46.5, 40.0, 25.7,

17.9, -4.8, -5.0; IR ν_{max} (film)/cm^{-1} 2953, 2931, 1732, 1522, 1255, 115; LRMS (ESI$^+$, *m/z*) 404.18 [M+Na$^+$]; HRMS (ESI$^+$) $C_{19}H_{31}NNaO_5Si$ requires 404.1864, found [M+Na$^+$] 404.1864.

6.5.3.6 1,1-Dibenzyl 4-methyl 3-(*tert*-butyldimethylsilyloxy)butane-1,1,4-tricarboxylate (12)

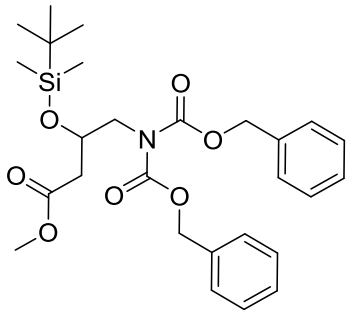

To a stirred solution of **11** (185 mg, 0.49 mmol) in a mixture of anhydrous THF (8 ml) and hexamethylphosphoramide (1.5 ml) at -78°C was added lithium bis(trimethylsilyl)amide (640 µl, 0.64 mmol, 1.3 eq, 1 M solution in tetrahydrofuran) dropwise and the resultant mixture was stirred for 15 min. Benzyl chloroformate (100 µl, 0.69 mmol, 1.4 eq) was added dropwise and the mixture was stirred for a further 30 min at -78°C. The reaction was quenched with a saturated aqueous solution of ammonium chloride. The phases were separated and the aqueous layer washed with ethyl acetate. The combined organic extracts were dried over $MgSO_4$, filtered and concentrated *in vacuo*. Purification by flash column chromatography on silica afforded **12** as a colourless oil (65mg, 0.13 mmol, 27%).

TLC 7:3 hexane/EtOAc R_f= 0.60;^{1}H NMR (500 MHz, *CDCl$_3$*) δ ppm 7.29 - 7.43 (10 H, m, ArH), 5.24 (4 H, s), 4.37 (1 H, tt, *J*=6.5 Hz), 3.89 (1 H, dd, *J*=14.0, 7.0 Hz), 3.76 (1 H, dd, *J*=14.0, 6.5 Hz), 3.62 (3 H, s, OMe), 2.45 (2 H, d, *J*=6.5 Hz), 0.82 (9 H, s, *t*BuSi), -0.03 (3 H, s, Si-CH$_3$), -0.06 (3 H, s, Si-CH$_3$); ^{13}C NMR (125 MHz, *CDCl$_3$*) δ ppm 171.4, 153.5, 135.1, 128.6, 128.4, 128.4, 68.9, 67.3, 51.6, 51.3, 40.8, 25.6, 17.8, -5.0, -5.3; IR ν_{max} (film)/cm^{-1} 2954, 2856, 2360, 1741, 1701, 1437, 1386, 1215, 1167; LRMS (ESI$^+$, *m/z*) 538.24 [M+Na$^+$]; HRMS (ESI$^+$) $C_{27}H_{37}NNaO_7Si$ requires 538.2232, found [M+Na$^+$] 538.2233.

6.5.3.7 Benzyl 5-(2-methoxy-2-oxoethyl)-2-oxooxazolidine-3-carboxylate (13)

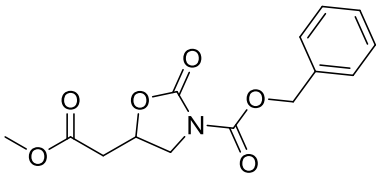

13 was synthesised following the procedure used for the synthesis of **16a**. Starting from **12** (58 mg, 0.11 mmol) a pale yellow oil was isolated (23 mg, 0.078 mmol, 71%).

TLC 6:4 hexane/EtOAc Rf= 0.25; ^{1}H NMR (400 MHz, *CDCl$_3$*) δ ppm 7.32 - 7.46 (5 H, m, ArH), 5.30 (2 H, s), 4.84 - 4.98 (1 H, m), 4.21 (1 H, dd, *J*=10.5, 8.5 Hz), 3.74 - 3.78 (1 H, m), 3.73 (3 H, s, OCH_3), 2.92 (1 H, dd, *J*=17.0, 5.5 Hz), 2.73 (1 H, dd, *J*=17.0, 7.5 Hz); ^{13}C NMR (101MHz, *CDCl$_3$*) δ ppm 169.2, 151.0, 150.7, 134.8, 128.7, 128.4, 69.3, 68.8, 52.3, 48.4, 38.7; IR ν_{max} (film)/cm^{-1} 1819, 1732, 1439, 1297, 1213, 1067; LRMS (ESI$^+$, *m/z*) 316.11 [M+Na$^+$].

6.5.3.8 Methyl 4-(1,3-dioxoisoindolin-2-yl)-3-hydroxybutanoate (15)

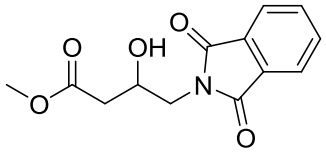

4-Aminobutyric acid (2.0 g, 16.8 mmol) and phthalic anhydride (3.0 g, 20.30 mmol, 1.2 eq) were suspended in toluene (20 ml). The mixture was refluxed in a Dean-Stark apparatus. The resultant red residue was filtered and the toluene was removed *in vacuo*. The mixture was co-evaporated several times with hexane and left overnight in dichloromethane. The solid which precipitated was filtered off and the filtrate was concentrated and redissolved in anhydrous methanol (30 ml). Then 4 ml of a 2 M solution of HCl in Et_2O were added and the resulting solution was stirred for 24 h. The solvent was removed *in vacuo* and the residue dissolved in ethyl acetate. Undissolved material was removed by filtration and the filtrate concentrated *in vacuo*. Purification by flash column chromatography on silica afforded **15** as a white solid (850 mg, 3.23 mmol, 19% over 2 steps).

mp 123-125°C (lit. 124-126°C[60]); TLC 8:2 hexane/EtOAc R_f= 0.35, ^{1}H NMR (400 MHz, *CDCl$_3$*) δ ppm 7.86 (2 H, dd, *J*=5.5, 3.0 Hz, ArH), 7.74 (2 H, dd, *J*=5.5, 3.0 Hz, ArH), 4.30 - 4.44 (1 H, m), 3.89 (1 H, dd, *J*=14.0, 7.0 Hz), 3.79 (1 H, dd, *J*=14.0, 4.5 Hz), 3.72 (3 H, s), 3.25 (1 H, br. s., OH), 2.61 (1 H, dd, *J*=16.5, 4.0 Hz), 2.53 (1 H, dd, *J*=16.5, 8.5 Hz); ^{13}C NMR (101 MHz, *CDCl$_3$*) δ ppm 172.2, 168.6, 134.2, 131.9, 123.5, 66.6, 51.9, 42.9, 38.8; IR ν_{max} (KBr disc)/cm^{-1} 3481, 2952, 1770, 1467, 1396, 1192, 1058; LRMS (ESI$^-$, *m/z*) 262.08 [M-H].

6.5.3.9 Methyl 4-(1,3-dioxoisoindolin-2-yl)-3-fluorobutanoate (16a)

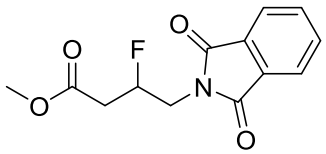

To a stirred solution of **15** (200 mg, 0.76 mmol) in anhydrous CH_2Cl_2 was added HF-pyridine (111 µl, 6.08 mmol, 8 eq) at 0°C, followed by DAST (201 µl, 1.52 mmol, 2 eq). The reaction was stirred for 2 days at room temperature. Water was added and the aqueous phase was extracted with CH_2Cl_2. The combined organic phases were washed with brine, dried and purified by flash column chromatography on silica to afford **16a** as a white solid (100 mg, 0.38 mmol, 50%). Byproduct **20'**

(white solid, 18 mg, 0.075 mmol, 10%, *E* isomer only) and starting material (43 mg, 0.16 mmol, 22%) were also isolated.

mp 73-75°C; TLC 6:4 hexane/EtOAc R_f= 0.50, ^{1}H NMR (500 MHz, *CDCl$_3$*) δ ppm 7.89 (2 H, dd, *J*=5.5, 3.0 Hz, ArH), 7.75 (2 H, dd, *J*=5.5, 3.0 Hz, ArH), 5.33 – 5.14 (1 H, m, J_{H-F}=47.5 Hz), 4.07 (1 H, ddd, *J*=17.0, 14.5, 7.0 Hz), 3.92 (1 H, ddd, *J*=23.0, 14.0, 4.0 Hz), 3.73 (3 H, s), 2.65 - 2.86 (2 H, m); ^{13}C NMR (125 MHz, *CDCl$_3$*) δ ppm 169.60 (1 C, d, *J*=6.7 Hz), 167.95, 134.22, 131.83, 123.53, 87.13 (1 C, d, *J*=175.5 Hz), 52.11, 40.88 (1 C, d, *J*=24.0 Hz), 37.88 (1 C, d, *J*=24.0 Hz); ^{19}F NMR (377 MHz, *CDCl$_3$*) δ ppm -185.57 (1 F, m); IR ν_{max} (KBr disc)/cm^{-1} 1776, 1716, 1425, 1284, 1089; LRMS (ESI$^+$, *m/z*) 288.07 [M+Na$^+$]; HRMS (ESI$^+$) $C_{13}H_{12}FNaNO_4$ requires 288.0643, found [M+Na$^+$] 288.0644.

6.5.3.10 (*E*)-methyl 4-(1,3-dioxoisoindolin-2-yl)but-2-enoate (16b)

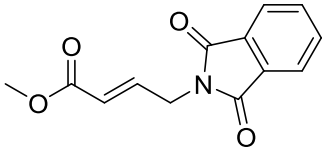

mp 100-102°C (lit. 104-105°C[61]); TLC 6:4 hexane/EtOAc R_f= 0.50; ^{1}H NMR (400 MHz, *CDCl$_3$*) δ ppm 7.88 (2 H, dd, *J*=5.5, 3.0 Hz, ArH), 7.76 (2 H, dd, *J*=5.5, 3.0 Hz, ArH), 6.94 (1 H, dt, *J*=16.0, 5.0 Hz), 5.92 (1 H, dt, *J*=15.5, 1.5 Hz), 4.45 (2 H, dd, *J*=5.5, 1.5 Hz), 3.72 (3 H, s); ^{13}C NMR (101 MHz, *CDCl$_3$*) δ ppm 167.9, 166.0, 141.0, 134.3, 131.9, 123.5, 122.8, 51.7, 38.2; IR ν_{max} (KBr disc)/cm^{-1} 1774, 1715, 1422, 1278, 1197, 1178, 986; LRMS (ESI$^-$, *m/z*) 244.06 [M-H].

6.5.4 Synthesis of GBBF (2) and R-GBBF (3)

6.5.4.1 (*R*)-benzyl 2-(dibenzylamino)-3-phenylpropanoate[62] (18a)

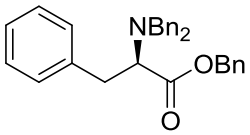

18a was synthesised following the literature procedure[62]. To a solution of D-phenylalanine (2.0 g, 12.12 mmol) in EtOH (80 ml) and H_2O (20 ml) was added Na_2CO_3 (3.85 g, 36.36 mmol, 3 eq), followed by a solution of benzyl bromide (5.04 ml, 42.42 mmol, 3.5 eq) in EtOH (20 ml) over 30 min. The mixture was stirred overnight at reflux, before being cooled to room temperature. Ethanol was removed *in vacuo* and the remaining mixture was diluted with water (80 ml) and diethyl ether (50 ml). The aqueous layer was washed twice with ether. The combined organic extracts were dried over $MgSO_4$ and concentrated *in vacuo*. Purification by flash column chromatography on silica afforded **18a** (3.25 g, 7.48 mmol, 62%) as a colourless oil.

TLC 8:2 hexane/EtOAc; R_f= 0.55, ^{1}H NMR (400 MHz, *CDCl*$_3$) δ ppm 7.37 - 7.47 (4 H, m, ArH), 7.15 - 7.32 (14 H, m, ArH), 7.03 - 7.11 (2 H, m, ArH), 5.30 (1 H, d, *J*=12.0 Hz, C*H*'H"-O), 5.18 (1 H, d, *J*=12.0 Hz, CH'*H*"-O), 3.99 (2 H, d, *J*=14.0 Hz, CH_2-N), 3.79 (1 H, t, *J*=7.5 Hz), 3.61 (2 H, d, *J*=14.0 Hz, CH_2-N), 3.21 (1 H, dd, *J*=14.0, 7.5 Hz), 3.07 (1 H, dd, *J*=14.0, 8.0 Hz); ^{13}C NMR (101 MHz, *CDCl*$_3$) δ ppm 172.2, 139.3, 138.1, 136.0, 129.5, 128.7, 128.6, 128.5, 128.3, 128.2, 128.2, 127.0, 126.3, 66.1, 62.4, 54.5, 35.7; IR ν_{max} (film)/cm^{-1} 3063, 3029, 3005, 2845, 2808, 1730, 1495, 1454, 1160, 1029; LRMS (ESI$^+$, *m/z*) 436.26 [M+H]; $[\alpha]^{20}_D$=+131.3 (c=1 in $CHCl_3$).

6.5.4.2 (*S*)-benzyl 2-(dibenzylamino)-3-phenylpropanoate[62] (18b)

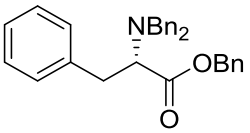

18b was synthesised following the procedure used for **18a**. Starting from L-phenylalanine (4.0 g, 24.24 mmol) **18b** was obtained as a colourless oil (9.36 g, 22.14 mmol, 91%).

TLC 8:2 hexane/EtOAc R_f= 0.55, ^{1}H NMR (400 MHz, *CDCl*$_3$) δ ppm 7.37 - 7.47 (4 H, m, ArH), 7.15 - 7.32 (14 H, m, ArH), 7.03 - 7.11 (2 H, m, ArH), 5.30 (1 H, d, *J*=12.1 Hz, C*H*'H"-O), 5.18 (1 H, d, *J*=12.0 Hz, CH'*H*"-O), 3.99 (2 H, d, *J*=14.0 Hz, CH_2-N), 3.79 (1 H, t, *J*=7.5 Hz), 3.61 (2 H, d, *J*=14.0 Hz, CH_2-N), 3.21 (1 H, dd, *J*=14.0, 7.3 Hz), 3.07 (1 H, dd, *J*=14.0, 8.0 Hz); ^{13}C NMR (101 MHz, *CDCl*$_3$) δ ppm 172.2, 139.3, 138.1, 136.0, 129.5, 128.7, 128.6, 128.5, 128.3, 128.2, 128.2, 127.0, 126.3, 66.1, 62.4, 54.5, 35.7; IR ν_{max} (film)/cm^{-1} 3063, 3029, 3005, 2845, 2808, 1730, 1495, 1454, 1160, 1029; LRMS (ESI$^+$, *m/z*) 436.26 [M+H]; $[\alpha]^{20}_D$=-131.5 (c=1 in $CHCl_3$).

6.5.4.3 (*R*)-2-(dibenzylamino)-3-phenylpropan-1-ol[62] (19a)

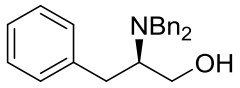

To a stirred suspension of $LiAlH_4$ (524 mg, 13.8 mmol, 2eq) in THF (50 ml) at 0°C under an atmosphere of nitrogen was added a solution of **18a** (3.0 g, 6.90 mmol) in THF (10 ml) and the resulting mixture was stirred for 1 hour at 0°C. Then water was added until gas effervescence had stopped. THF was removed *in vacuo* and the resultant mixture was extracted with Et_2O (3×50 ml). The combined organic extracts were dried over Na_2SO_4 and concentrated *in vacuo*. Purification by flash column chromatography on silica gave **19a** (1.80 g, 5.22 mmol, 76%) as a white solid.

mp 67-70°C (lit. 69-71°C[62]); TLC 8:2 hexane/EtOAc; R_f= 0.45, ^{1}H NMR (400 MHz, *CDCl*$_3$) δ ppm 7.08 - 7.42 (15 H, m, ArH), 3.96 (2 H, d, *J*=13.0 Hz, CH_2-N), 3.47 - 3.61 (3 H, m, CH_2-N, C*H*'H"-OH), 3.32 - 3.43 (1 H, m), 3.07 - 3.20 (2 H, m, Ph-C*H*'H", CH'*H*"-OH), 3.04 (1 H, br. s., OH), 2.39 - 2.55 (1 H, m, Ph-CH'*H*"); ^{13}C NMR (101 MHz, *CDCl*$_3$) δ ppm 139.2, 139.1, 129.0, 129.0, 128.6, 127.3, 126.3, 60.9, 60.4, 53.3, 31.8; IR ν_{max} (KBr disc)/cm^{-1} 3460, 1601, 1582, 1494, 1029; LRMS (ESI$^+$, *m/z*) 354.21 [M+Na$^+$]; $[\alpha]^{20}_D$=-57.4 (c=1 in $CHCl_3$).

6.5.4.4 (*S*)-2-(dibenzylamino)-3-phenylpropan-1-ol[62] (19b)

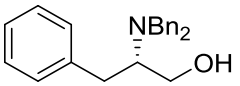

19b was synthesised following the procedure used for **19a**. Starting from **18b** (9.0 g, 20.7 mmol) **19b** was obtained as a white solid (4.70 g, 13.63 mmol, 66%).

mp 67-70°C (lit. 69-71°C[62]); TLC 8:2 hexane/EtOAc R_f= 0.45, ^{1}H NMR (400 MHz, *CDCl*$_3$) δ ppm 7.08 - 7.42 (15 H, m, ArH), 3.96 (2 H, d, *J*=13.0 Hz, CH_2-N), 3.47 - 3.61 (3 H, m, CH_2-N, C*H*'H"-OH), 3.32 - 3.43 (1 H, m), 3.07 - 3.20 (2 H, m, Ph-C*H*'H", CH'*H*"-OH), 3.04 (1 H, br. s., OH), 2.39 - 2.55 (1 H, m, Ph-CH'*H*"); ^{13}C NMR (101 MHz, *CDCl*$_3$) δ ppm 139.2, 139.1, 129.0, 129.0, 128.6, 127.3, 126.3, 60.9, 60.4, 53.3, 31.8; IR ν_{max} (KBr disc)/cm^{-1} 3460, 1601, 1582, 1494, 1029; LRMS (ESI$^+$, *m/z*) 354.21 [M+Na$^+$]; $[\alpha]^{20}_D$=+56.0 (c=1 in $CHCl_3$).

6.5.4.5 (*S*)-*N*,*N*-dibenzyl-2-fluoro-3-phenylpropan-1-amine[46] (20a)

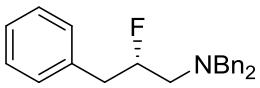

To a solution of **19a** (1.5 g, 4.35 mmol) in anhydrous CH_2Cl_2 (40 ml) at -10°C under an atmosphere of nitrogen was added a solution of Deoxo-Fluor (802 µl, 4.35 mmol, 1eq) in anhydrous CH_2Cl_2 (5 ml) dropwise over 15 min. The resulting mixture was allowed to warm to room temperature and stirred for 24 h. The reaction was quenched with 10% aqueous K_2CO_3 solution and the organic phase was separated, dried over Na_2SO_4 and concentrated *in vacuo*. Purification by flash column

chromatography on silica afforded **20a** (700 mg, 2.02 mmol, 46%) as a colourless oil. As a by-product compound **20a'** was isolated as a colourless oil (145 mg, 0.42 mmol, 10%) and starting material was also recovered (450 mg, 1.31 mmol, 30%).

TLC 2:1 hexane/CH_2Cl_2; R_f= 0.50, ^{1}H NMR (400 MHz, *CDCl$_3$*) δ ppm 7.32 - 7.43 (8 H, m, ArH), 7.22 - 7.32 (5 H, m, ArH), 7.15 (2 H, d, *J*=7.0 Hz, ArH), 4.87 (2 H, dquin, *J*=5.5, *J*=48.5 Hz), 3.72 (4 H, s, NCH_2Ph), 2.92 (1 H, d, *J*=6.0 Hz), 2.84 - 2.88 (1 H, m), 2.78 - 2.83 (1 H, m), 2.71 - 2.78 (1 H, m); ^{13}C NMR (101 MHz, *CDCl$_3$*) δ ppm 139.3, 137.4, 137.4, 129.3, 129.0, 128.4, 128.3, 127.0, 126.5, 94.4, 92.7, 59.1, 56.5, 39.9, 39.7; ^{19}F NMR (377 MHz, *CDCl$_3$*) δ ppm -179.91 (1 F, m); IR ν_{max} (film)/cm^{-1} 3062, 3028, 2949, 2802, 2719, 1644, 1605, 1495, 1454, 1028; LRMS (ESI$^+$, *m/z*) 334.20 [M+H]; $[\alpha]^{20}_D$=-6.3 (c=1 in $CHCl_3$).

6.5.4.6 (*R*)-*N*,*N*-dibenzyl-1-fluoro-3-phenylpropan-2-amine 20a'

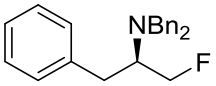

TLC 2:1 hexane/ CH_2Cl_2; R_f= 0.50, ^{1}H NMR (400 MHz, *CDCl$_3$*) δ ppm 7.21 - 7.38 (13 H, m, ArH), 7.12 (2 H, d, *J*=7.0 Hz, ArH), 4.58 (2 H, m, *J*=47.0Hz), 3.77 - 3.91 (4 H, m, CH_2N), 3.10 - 3.25 (1 H, m), 3.03 (1 H, dd, *J*=13.5, 6.0 Hz, Ph-C*H*'H"), 2.86 (1 H, dd, *J*=13.5, 8.5 Hz, Ph-CH'*H*"); ^{13}C NMR (101 MHz, *CDCl$_3$*) δ ppm 140.0, 139.4, 129.4, 128.6, 128.4, 128.3, 126.9, 126.2, 84.4, 82.7, 59.4, 59.2, 54.5, 33.1, 33.1; ^{19}F NMR (377 MHz, *CDCl$_3$*) δ ppm -226.16 (1 F, m);

IR ν_{max} (film)/cm^{-1} 3062, 3027, 2954, 2803, 1494, 1454, 1029; LRMS (ESI$^+$, *m/z*) 334.20 [M+H].

6.5.4.7 (*R*)-*N*,*N*-dibenzyl-2-fluoro-3-phenylpropan-1-amine[46] (20b)

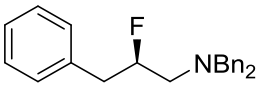

20b was synthesised following the procedure used for **20a**. Starting from **19b** (4.6 g, 13.34 mmol) **20b** was obtained as a colourless oil (3.42 g, 9.86 mmol, 74%). Along with major product by-product **20b'** was also isolated (727 mg, 2.10 mmol, 16%).

TLC 2:1 hexane/CH_2Cl_2 R_f= 0.45 ^{1}H NMR (400 MHz, *CDCl$_3$*) δ ppm 7.32 - 7.43 (8 H, m, ArH), 7.22 - 7.32 (5 H, m, ArH), 7.15 (2 H, d, *J*=7.0 Hz, ArH), 4.87 (2 H, dquin, *J*=5.5, *J*=48.5 Hz), 3.72 (4 H, s, NCH_2), 2.92 (1 H, d, *J*=6.0 Hz), 2.84 - 2.88 (1 H, m), 2.78 - 2.83 (1 H, m), 2.71 - 2.78 (1 H, m); ^{13}C NMR (101 MHz, *CDCl$_3$*) δ ppm 139.3, 137.4, 137.4, 129.3, 129.0, 128.4, 128.3, 127.0, 126.5, 94.4, 92.7, 59.1, 56.5, 39.9, 39.7; ^{19}F NMR (377 MHz, *CDCl$_3$*) δ ppm -179.91 (1 F, m); IR ν_{max} (film)/cm^{-1} 3062, 3028, 2949, 2802, 2719, 1644, 1605, 1495, 1454, 1028; LRMS (ESI$^+$, *m/z*) 334.20 [M+H]; $[\alpha]^{20}_D$=+6.5 (c=1 in $CHCl_3$).

6.5.4.8 (*S*)-N,N-dibenzyl-1-fluoro-3-phenylpropan-2-amine 20b'

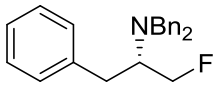

TLC 2:1 hexane/CH_2Cl_2 R_f= 0.45, ^{1}H NMR (400 MHz, *CDCl*$_3$) δ ppm 7.21 - 7.38 (13 H, m, ArH), 7.12 (2 H, d, *J*=7.0 Hz, ArH), 4.58 (2 H, m, *J*=47.0Hz), 3.77 - 3.91 (4 H, m, CH_2N), 3.10 - 3.25 (1 H, m, H8), 3.03 (1 H, dd, *J*=13.5, 6.0 Hz, Ph-C*H*'H"), 2.86 (1 H, dd, *J*=13.5, 8.5 Hz, Ph-CH'*H*"); ^{13}C NMR (101 MHz, *CDCl*$_3$) δ ppm 140.0, 139.4, 129.4, 128.6, 128.4, 128.3, 126.9, 126.2, 84.4, 82.7, 59.4, 59.2, 54.5, 33.1, 33.1; ^{19}F NMR (377 MHz, *CDCl*$_3$) δ ppm -226.16 (1 F, m); IR ν_{max} (film)/cm^{-1} 3062, 3027, 2954, 2803, 1494, 1454, 1029; LRMS (ESI$^+$, *m/z*) 334.20 [M+H].

6.5.4.9 (S)-2-fluoro-3-phenylpropan-1-amine[46] (21a)

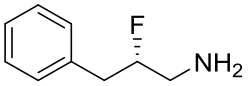

To a solution of **20a** (1.04 g, 3.12 mmol) in methanol (20 ml) under an atmosphere of nitrogen was added palladium (10% on carbon, 104 mg). The resulting mixture was stirred under positive pressure of hydrogen for 12 h and then was filtered through a pad of celite. The filtrate was concentrated *in vacuo* to afford **21a** (400 mg, 2.61 mmol, 84%) as a colourless oil. Compound was used without further purification.

^{1}H NMR (400 MHz, *CDCl*$_3$) δ ppm 7.19 - 7.37 (5 H, m, ArH), 4.55 - 4.78 (1 H, m), 2.81 - 3.08 (4 H, m), 1.47 (2 H, s, NH_2); ^{13}C NMR (101 MHz, *CDCl*$_3$) δ ppm 129.3, 128.5, 128.5, 128.1, 127.1, 126.7, 45.8, 45.6, 39.1, 38.9; ^{19}F NMR (377 MHz, *CDCl*$_3$) δ ppm -186.01 (1 F, m); IR ν_{max} (film)/cm^{-1} 2993, 1589, 1482, 1456, 1150, 1034; LRMS (ESI$^+$, *m/z*) 154.11 [M+H].

6.5.4.10 (*R*)-2-fluoro-3-phenylpropan-1-amine[46] (21b)

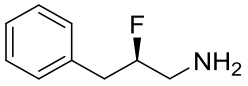

21b was synthesised following the procedure used for **21a**. Starting from **20b** (3.35 g, 9.64 mmol) **21b** was obtained as a colourless oil (1.24 g, 8.10 mmol, 84%). Compound was used without further purification.

^{1}H NMR (400 MHz, *CDCl*$_3$) δ ppm 7.19 - 7.37 (5 H, m, ArH), 4.55 - 4.78 (1 H, m), 2.81 - 3.08 (4 H, m), 1.47 (2 H, s, NH_2); ^{13}C NMR (101 MHz , *CDCl*$_3$) δ ppm 129.3, 128.5, 128.5, 128.1, 127.1, 126.7, 45.8, 45.6, 39.1, 38.9; ^{19}F NMR (377 MHz, *CDCl*$_3$) δ ppm -186.01 (1 F, m); IR ν_{max} (film)/cm^{-1} 2993, 1589, 1482, 1456, 1150, 1034; LRMS (ESI$^+$, *m/z*) 154.11 [M+H].

6.5.4.11 (*S*)-di-tert-butyl 2-fluoro-3-phenylpropyliminodicarbonate[46] (22a)

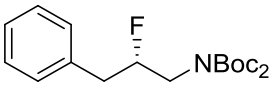

Boc_2O (1.0 g, 4.56 mmol, 4 eq) and DMAP (21 mg, 0.17 mmol, 0.15 eq) were added to a solution of **21a** (190 mg, 1.14 mmol) in acetonitrile (5 ml). The resulting mixture was stirred overnight at reflux, before being cooled to room temperature. Acetonitrile was removed *in vacuo* and crude mixture was dissolved in diethyl ether, washed with water, dried over $MgSO_4$ and concentrated *in vacuo*. Purification by flash column chromatography on silica afforded **22a** (367 mg, 1.00 mmol, 88%) as a colourless oil.

TLC 96:4 hexane/EtOAc R_f= 0.25, ^{1}H NMR (400 MHz, *CDCl$_3$*) δ ppm 7.18 - 7.36 (5 H, m, ArH), 4.90 (1 H, m, $J_{H\text{-}F}$ = 50.0 Hz), 4.00 (1 H, ddd, *J*=14.5, 13.0, 8.5 Hz), 3.59 - 3.77 (1 H, m), 2.82 - 3.05 (2 H, m), 1.48 (18 H, s, $C(CH_3)_3$); ^{13}C NMR (101 MHz, *CDCl$_3$*) δ ppm 152.5, 136.4, 129.3, 128.5, 126.7, 92.5 (d, *J*=176.0), 82.6, 49.5 (d, *J*=22.5), 39.4, 39.2, 28.0; ^{19}F NMR (377 MHz, *CDCl$_3$*) δ ppm -186.42 (1 F, m); IR ν_{max} (film)/cm^{-1} 2980, 2935, 1749, 1699, 1643, 1429, 1365, 1145; LRMS (ESI$^+$, *m/z*) 354.25 [M+H]; $[\alpha]^{20}_D$=+32.2 (c=1 in $CHCl_3$).

6.5.4.12 (R)-di-tert-butyl 2-fluoro-3-phenylpropyliminodicarbonate[46] (22b)

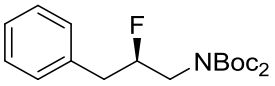

22b was synthesised following the procedure used for **22a**. Starting from **21b** (1.2 g, 7.84 mmol) **22b** was obtained as a colourless oil (2.51 g, 7.11 mmol, 91%).

TLC 96:4 hexane/EtOAc R_f= 0.25, ^{1}H NMR (400 MHz, *CDCl$_3$*) δ ppm 7.18 - 7.36 (5 H, m, ArH), 4.90 (1 H, m, $J_{H\text{-}F}$ = 50.0 Hz), 4.00 (1 H, ddd, *J*=14.5, 13.0, 8.5 Hz), 3.59 - 3.77 (1 H, m), 2.82 - 3.05 (2 H, m), 1.48 (18 H, s, $C(CH_3)_3$); ^{13}C NMR (101 MHz, *CDCl$_3$*) δ ppm 152.5, 136.4, 129.3, 128.5, 126.7, 92.5 (d, *J*=176.0), 82.6, 49.5 (d, *J*=22.5), 39.4, 39.2, 28.0; ^{19}F NMR (377 MHz, *CDCl$_3$*) δ ppm -186.42 (1 F, m); IR ν_{max} (film)/cm^{-1} 2980, 2935, 1749, 1699, 1643, 1429, 1365, 1145; LRMS (ESI$^+$, *m/z*) 354.25 [M+H]; $[\alpha]^{20}_D$=-32.8 (c=1 in $CHCl_3$).

6.5.4.13 (*S*)-4-(bis(tert-butoxycarbonyl)amino)-3-fluorobutanoic acid[46] (23a)

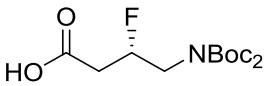

$NaIO_4$ was added (3.66 g, 17.1 mmol, 18eq) to a solution of **22a** (350 mg, 0.95 mmol) in a mixture of CCl_4 (8 ml), acetonitrile (8 ml) and H_2O (10 ml). The resulting mixture was treated with $RuCl_3 \cdot H_2O$ (13 mg, 0.057 mmol, 0.06eq) and stirred vigorously for 3 days. The reaction mixture was then filtered through celite, solids were washed with EtOAc and the filtrate was concentrated *in vacuo*. Purification by flash column chromatography on silica gave **23a** (175 mg, 0.49 mmol, 52%) as a colourless oil.

TLC 7:3 hexane/EtOAc R_f= 0.10, ^{1}H NMR (400 MHz, *CDCl$_3$*) δ ppm 5.12 (1 H, ddt, *J*=48.0, 7.5, 3.5 Hz), 4.03 (1 H, td, *J*=15.0, 7.5 Hz), 3.73 - 3.87 (1 H, m), 2.61 - 2.81 (2 H, m), 1.51 (18 H, s, C(CH$_3$)$_3$); ^{13}C NMR (101 MHz, *CDCl$_3$*) δ ppm 174.5, 152.5, 88.2 (d, *J*=174.0 Hz), 83.1, 48.7 (d, *J*=24.0 Hz), 37.8, 28.0; ^{19}F NMR (377 MHz, *CDCl$_3$*) δ ppm -186.30 (1 F, m); IR ν_{max} (film)/cm^{-1} 2985, 2934, 1785, 1429, 1370, 1237, 1121; LRMS (ESI$^-$, *m/z*) 320.10 [M-H]; $[\alpha]^{20}_D$=+37.6 (c=1 in $CHCl_3$).

6.5.4.14 (*R*)-4-(bis(tert-butoxycarbonyl)amino)-3-fluorobutanoic acid[46] (23b)

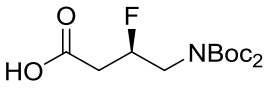

23b was synthesised following the procedure used for **23a**. Starting from **22b** (200 mg, 0.54 mmol) **23b** was obtained as a colourless oil (79 mg, 0.22 mmol, 40%).

TLC 7:3 hexane/EtOAc R_f= 0.10, ^{1}H NMR (400 MHz, *CDCl$_3$*) δ ppm 5.12 (1 H, ddt, *J*=48.0, 7.5, 3.5 Hz), 4.03 (1 H, td, *J*=15.0, 7.5 Hz), 3.73 - 3.87 (1 H, m), 2.61 - 2.81 (2 H, m), 1.51 (18 H, s, C(CH$_3$)$_3$); ^{13}C NMR (101 MHz, *CDCl$_3$*) δ ppm 174.5, 152.5, 88.2 (d, *J*=174.0 Hz), 83.1, 48.7 (d, *J*=24.0 Hz), 37.8, 28.0; ^{19}F NMR (377 MHz, *CDCl$_3$*) δ ppm -186.30 (1 F, m); IR ν_{max} (film)/cm^{-1} 2985, 2934, 1785, 1429, 1370, 1237, 1121; LRMS (ESI$^-$, *m/z*) 320.10 [M-H]; $[\alpha]^{20}_D$=-38.2 (c=1 in $CHCl_3$).

6.5.4.15 (*S*)-4-amino-3-fluorobutanoic acid[46] (24a)

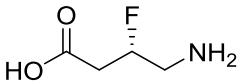

To a solution of **23a** (215 mg, 0.67 mmol) in CH_2Cl_2 (3 ml) were added 3ml of 1 M solution of HCl in Et_2O and the resultant mixture was stirred overnight. Then nitrogen was bubbled through the reaction mixture until complete removal of volatiles. The resulting white solid residue was dissolved in a small amount of EtOH and crystallized from EtOH/Et_2O to afford **24a** (57 mg, 0.36 mmol, 54%) as white crystals.

mp 114-116°C (lit. 116-118°C[46]); ^{1}H NMR (400 MHz, *D$_2$O*) δ ppm 5.13 (1 H, m, J_{H-F}=49.0 Hz), 3.14 - 3.34 (2 H, m), 2.67 - 2.82 (2 H, m); ^{13}C NMR (101 MHz, *D$_2$O*) δ ppm 172.4, 87.5 (d, *J*=171.0 Hz), 42.7 (d, *J*=21.0 Hz), 37.0 (d, *J*=22.5 Hz); IR ν_{max} (KBr disc)/cm^{-1} 3028, 1701, 1611, 1508, 1448, 1306, 1036; ^{19}F NMR (377 MHz, *D$_2$O*) δ ppm -189.55 (1 F, m); LRMS (ESI$^+$, *m/z*) 122.10 [M+H]; $[\alpha]^{20}_D$=34.6 (c=1 in MeOH).

6.5.4.16 Synthesis of (*R*)-4-amino-3-fluorobutanoic acid[46] (24b)

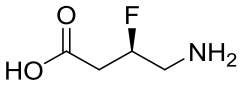

24b was synthesised following the procedure used for **24a**. Starting from **23b** (50 mg, 0.16 mmol) **24b** was obtained as a colourless oil (16 mg, 0.10 mmol, 66%).

mp 114-116°C (lit. 116-118°C[46]); ^{1}H NMR (400 MHz, D_2O) δ ppm 5.13 (1 H, m, $J_{H\text{-}F}$=49.0 Hz), 3.14 - 3.34 (2 H, m), 2.67 - 2.82 (2 H, m); ^{13}C NMR (101 MHz, D_2O) δ ppm 172.4, 87.5 (d, *J*=171.0 Hz), 42.7 (d, *J*=21.0 Hz), 37.0 (d, *J*=22.5 Hz); IR ν_{max} (KBr disc)/cm^{-1} 3028, 1701, 1611, 1508, 1448, 1306, 1036; ^{19}F NMR (377 MHz, D_2O) δ ppm -189.55 (1 F, m); LRMS (ESI$^+$, *m/z*) 122.10 [M+H]; $[\alpha]^{20}_{D}$=-34.1 (c=1 in MeOH).

6.5.4.17 (*S*)-3-carboxy-2-fluoro-*N,N,N*-trimethylpropan-1-aminium (GBBF, 2)

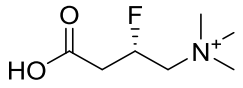

Methyl iodide (48 µl, 0.77 mmol, 4eq) was added to a stirred solution of **24a** (30 mg, 0.19 mmol) and K_2CO_3 (54 mg, 0.38 mmol, 2eq) in MeOH (3 ml). The mixture was stirred for 24 h before pH was brought to 7 with 1M HCl. The resulting mixture was concentrated *in vacuo* and half of it was purified by HPLC (reverse phase column, gradient 50% of B in 15 min, retention time 10.8 min). Fractions containing the product were concentrated *in vacuo* to give **2** as an off-white oil (~2 mg, 0.01 mmol, 11%), which was then redissolved in water and freeze-dried.

^{1}H NMR (700 MHz, D_2O) δ ppm 5.44 (1 H, m, $J_{H\text{-}F}$=50.5 Hz), 3.75-3.54 (2 H, m), 3.18 (9 H, s, NCH_3); 2.61 - 2.53 (2 H, m); ^{13}C NMR (176 MHz, D_2O) δ ppm 176.5 (C=O), 86.1 (C-F), 68.4 (CH_2-N), 53.9 (3×CH_3), 40.3 (C-COOH); ^{19}F NMR (377 MHz, D_2O) δ ppm -75.57 (1 F, m); LRMS (ESI$^+$, *m/z*) 164.12 [M]; HRMS (ESI$^+$) $C_7H_{15}FNO_2^+$ requires 164.1081, found [M] 164.1082.

6.5.4.18 (*R*)-3-carboxy-2-fluoro-*N,N,N*-trimethylpropan-1-aminium (3)

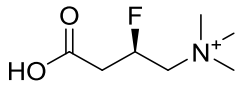

3 was synthesised following the procedure used for **2** starting from **24b** (10 mg, 0.06 mmol). **3** was obtained as an off-white oil (~1.5 mg, 0.008 mmol, 12%).

^{1}H NMR (700 MHz, D_2O) δ ppm 5.44 (1 H, m, $J_{H\text{-}F}$=50.5 Hz), 3.75-3.54 (2 H, m), 3.18 (9 H, s, NCH_3); 2.61 - 2.53 (2 H, m); ^{13}C NMR (176 MHz, D_2O) δ ppm 176.5 (C=O), 86.1 (C-F), 68.4 (CH_2-N), 53.9 (3×CH_3), 40.3 (C-COOH); ^{19}F NMR (377 MHz, D_2O) δ ppm -75.57 (1 F, m); LRMS (ESI$^+$, *m/z*) 164.12 [M]; HRMS (ESI$^+$) $C_7H_{15}FNO_2^+$ requires 164.1081, found [M] 164.1082.

6.5.5 Synthesis of fluoromethylated analogues of GBB and TML

6.5.5.1 Sec-butyl 4-(dimethylamino)butanoate hydrochloride (28)

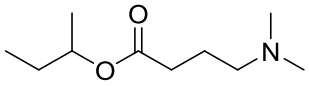

4-(Dimethylamino)butanoic acid (1 g, 5.97 mmol) was dissolved in 2-butanol (7 mL) and treated with 3.25 mL of 2 M solution of HCl in Et_2O. The mixture was refluxed overnight. The resultant solution was then cooled, concentrated *in vacuo* and then coevaporated several times with acetone to afford (**28**) (1.24 g, 5.55 mmol, 93%) as a colourless oil.

^{1}H NMR (400 MHz; $CDCl_3$) δ =4.71 - 4.88 (1 H, m), 3.00 - 3.14 (2 H, m), 2.82 (3 H, s, CH_3), 2.81 (3 H, s, CH_3), 2.43 (2 H, t, *J*=7.0 Hz), 2.04 - 2.22 (2 H, m), 1.40 - 1.66 (2 H, m), 1.17 (3 H, d, *J*=6.5 Hz), 0.85 (3 H, t, *J*=7.5 Hz) ppm. ^{13}C NMR (101 MHz; $CDCl_3$) δ = 171.6, 73.1, 69.5, 56.9, 42.8, 31.9, 30.9, 28.7, 19.4, 9.7 ppm. FT-IR ν_{max} (film) 3407, 2974, 2698, 1724, 1469, 1380, 1204 cm^{-1}. HRMS (ESI-TOF) calcd for $C_{10}H_{22}NO_2$ [M+H$^+$]: 188.1645, found: 188.1645.

6.5.5.2 3-Carboxy-*N*-(fluoromethyl)-*N*, *N*-dimethylpropan-1-aminium) chloride (29)

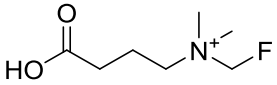

Cs_2CO_3 (655 mg, 2.01 mmol, 1.5 eq) was added to a solution of (**28**) (300 mg, 1.34 mmol) in dry MeCN (20 mL) and the resulting mixture was stirred vigorously. (**26**) (970 mg, 2.68 mmol, 2 eq) was added and the mixture was stirred overnight at 50°C. The reaction mixture was then filtered and the filtrate was extracted with cyclohexane and coevaporated several times with methanol and CH_2Cl_2 to afford 4-sec-butoxy-*N*-(fluoromethyl)-*N*,*N*-dimethyl-4-oxobutan-1-aminium) tetrafluoroborate (**28a**) (320 mg, 1.04 mmol, 78%) as a yellow oil.

^{1}H NMR (500 MHz; $CDCl_3$) δ = 5.38 (2 H, d, *J*=45.0 Hz, C*H*$_2$F), 4.82 (1 H, m), 3.40 - 3.55 (2 H, m), 3.21 (6 H, s, 2×CH_3), 2.45 (2 H, t, *J*=6.5 Hz), 2.02 - 2.11 (2 H, m), 1.44 - 1.68 (2 H, m), 1.20 (3 H, d, *J*=6.5 Hz), 0.88 (3 H, t, *J*=7.5 Hz) ppm. ^{13}C NMR (126 MHz; $CDCl_3$) δ = 171.7, 97.0, 95.2, 73.2, 60.8, 47.1, 30.1, 28.7, 19.3, 17.5, 9.7 ppm. FT-IR ν_{max} (film) 2976, 2360, 2341, 1724, 1382, 1056 cm^{-1}. HRMS (ESI-TOF) calcd for $C_{11}H_{23}FNO_2^+$ [M$^+$]: 220.1707, found: 220.1708.

To a solution of (**28a**) (320 mg, 1.04 mmol) in H_2O (5 mL) $LiOH{\cdot}H_2O$ (218 mg, 5.20 mmol, 5 eq) was added and the mixture was stirred overnight at room temperature. The solvent was co-evaporated several times with methanol and CH_2Cl_2, the residue was suspended in MeOH and filtered. The filtrate was concentrated *in vacuo*, redissolved in water and brought to pH 7 by 1M aqueous solution of HCl. The aqueous solution was subjected to purification by HPLC (C18 column, solvent system: A – H_2O, 0.05% CF_3COOH, B – MeCN, 0.1% CF_3COOH; gradient 50% of B in 15 min, retention time 10.5 min, ELSD detection). Fractions containing the product were concentrated *in vacuo* to give (**29**) (50 mg, 24%) as a white hygroscopic solid.

^{1}H NMR (250 MHz; MeOH) δ = 8.39 (1H, s, OH), 5.44 (2H, d, *J* = 45.0 Hz, C*H*$_2$F), 3.43 - 3.54 (2H, m), 3.21 (3H, s, CH_3), 3.20 (3H, s, CH_3), 2.40 (2H, t, *J* = 7.0 Hz), 1.99 - 2.16 (2H, m) ppm. ^{13}C NMR (126 MHz; D_2O) δ = 180.5, 95.8, 60.9, 46.8, 33.3, 18.6. ^{19}F NMR (377 MHz; $CDCl_3$) δ = -193.7 ppm. HRMS (ESI-TOF) calcd for $C_7H_{15}FNO_2^+$ [M^+]: 164.1081, found: 164.1081.

6.5.5.3 *N*$^{\varepsilon}$,*N*$^{\varepsilon}$-Dimethyl-*N*$^{\varepsilon}$-fluoromethyl-L-lysine (31)

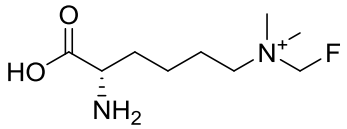

A 50-mL round-bottom flask was charged with *N*-Boc dimethyllysine (Bachem, Weil am Rhein, Germany; 100 mg, 0.36 mmol, 1 equiv.) and Cs_2CO_3 (180 mg, 0.55 mmol, 1.5 equiv.) in CH_3CN (10 mL). The reaction mixture was stirred vigorously at room temperature, then monofluoromethyl sulphonium salt (**26**) (400 mg, 1.09 mmol, 3 equiv.) was added in one portion. The resultant suspension was stirred at 60°C overnight and filtered. The filtrate was extracted with cyclohexane (3 × 10 mL) and co-evaporated with MeOH and CH_2Cl_2. The residue was dissolved in CF_3COOH /MeOH (1:1 v/v, 10 mL) and a solution of LiOH (50 mg) in water (10 mL) was added. The reaction mixture was stirred at room temperature (4 h), then co-evaporated with MeOH and CH_2Cl_2. The residue was suspended in MeOH, filtered and the filtrate was concentrated *in vacuo*. The resultant residue was purified by reverse phase HPLC (C18 column, solvent system: A – H_2O, 0.05% CF_3COOH, B – MeCN, 0.1% CF_3COOH; gradient 50% of B in 15 min, retention time 14 min, ELSD detection). Fractions containing product were freeze-dried to yield *N*-Boc-*N*$^{\varepsilon}$,*N*$^{\varepsilon}$-dimethyl-*N*$^{\varepsilon}$-fluoromethyl-L-lysine (**31a**) (36 mg, 0.09 mmol, 24%) as a yellow hygroscopic solid. ^{1}H NMR (700 MHz; D_2O) δ = 5.27 (2H, d, *J*=45.0 Hz, C*H*$_2$F), 4.04 (1H, m, C*H*NH), 3.36 (2H, t, *J*=10.0 Hz, C*H*$_2$N$^+$), 3.08 (3H, s, CH_3), 3.08 (3H, s, CH_3), 1.75 (4H, m), 1.40 (2H, m), 1.36 (9H, s, $C(CH_3)_3$) ppm. The obtained solid (**31a**) was treated with 5 mL of 2M solution of HCl in Et_2O and stirred at room temperature (2 h). Solvent were evaporated to give (**31**) as white hygroscopic solid (HCl salt, 22 mg, 0.08 mmol, 90%).

^{1}H NMR (700 MHz; D_2O) δ = 5.26 (2H, d, *J*=45.0 Hz, C*H*$_2$F), 3.87 (1H, t, *J*=6.5, C*H*NH), 3.36 (2H, m, C*H*$_2$N$^+$), 3.07 (6H, s, 2×CH_3), 1.90 (2H, m), 1.79 (2H, m), 1.42 (2H, m) ppm. ^{13}C NMR (136 MHz; D_2O) δ = 172.4, 96.0 (d, *J*=45.0 Hz), 61.0, 53.0, 47.1, 29.2, 21.2, 21.1 ppm. ^{19}F NMR (377 MHz; $CDCl_3$) δ = -193.7 ppm. $[\alpha]_D^{20} =$ +5.1 (c = 0.5 in MeOH). HRMS (ESI-TOF) calcd for $C_9H_{20}FN_2O_2^+$ [M^+]: 207.1503, found: 207.1504.

References

1. Hausinger, R.P. Fe(II)/α-ketoglutarate-dependent hydroxylases and related enzymes. *Critical Reviews in Biochemistry and Molecular Biology* **39**, 21-68 (2004).
2. Rose, N.R., McDonough, M.A., King, O.N.F., Kawamura, A. & Schofield, C.J. Inhibition of 2-oxoglutarate dependent oxygenases. *Chemical Society Reviews* **40**, 4364-4397 (2011).
3. McDonough, M.A., Loenarz, C., Chowdhury, R., Clifton, I.J. & Schofield, C.J. Structural studies on human 2-oxoglutarate dependent oxygenases. *Current Opinion in Structural Biology* **20**, 659-672 (2010).
4. Hewitson, K.S., McNeill, L.A., Riordan, M.V., Tian, Y.-M., Bullock, A.N., Welford, R.W., Elkins, J.M., Oldham, N.J., Bhattacharya, S., Gleadle, J.M. *et al.* Hypoxia-inducible Factor (HIF) Asparagine Hydroxylase Is Identical to Factor Inhibiting HIF (FIH) and Is Related to the Cupin Structural Family. *Journal of Biological Chemistry* **277**, 26351-26355 (2002).
5. Zhang, J.-H., Qi, R.C.C., Chen, T., Chung, T.D.Y., Stern, A.M., Hollis, G.F., Copeland, R.A. & Oldenburg, K.R. Development of a Carbon Dioxide-Capture Assay in Microtiter Plate for Aspartyl-β-hydroxylase. *Analytical Biochemistry* **271**, 137-142 (1999).
6. Kaule, G. & Günzler, V. Assay for 2-oxoglutarate decarboxylating enzymes based on the determination of [1-14C]succinate: Application to prolyl 4-hydroxylase. *Analytical Biochemistry* **184**, 291-297 (1990).
7. Wirthner, R., Balamurugan, K., Stiehl, D.P., Barth, S., Spielmann, P., Oehme, F., Flamme, I., Katschinski, D.M., Wenger, R.H. & Camenisch, G. Determination and modulation of prolyl-4-hydroxylase domain oxygen sensor activity. *Methods in Enzymology* **435**, 43-60 (2007).
8. Price, J.C., Barr, E.W., Glass, T.E., Krebs, C. & Bollinger, J.M. Evidence for Hydrogen Abstraction from C1 of Taurine by the High-Spin Fe(IV) Intermediate Detected during Oxygen Activation by Taurine:α-Ketoglutarate Dioxygenase (TauD). *Journal of the American Chemical Society* **125**, 13008-13009 (2003).
9. Price, J.C., Barr, E.W., Tirupati, B., Bollinger, J.M. & Krebs, C. The First Direct Characterization of a High-Valent Iron Intermediate in the Reaction of an α-Ketoglutarate-Dependent Dioxygenase: A High-Spin Fe(IV) Complex in Taurine/α-Ketoglutarate Dioxygenase (TauD) from Escherichia coli†. *Biochemistry* **42**, 7497-7508 (2003).
10. Price, J.C., Barr, E.W., Hoffart, L.M., Krebs, C. & Bollinger, J.M. Kinetic Dissection of the Catalytic Mechanism of Taurine:α-Ketoglutarate Dioxygenase (TauD) from Escherichia coli†. *Biochemistry* **44**, 8138-8147 (2005).
11. Flashman, E., Hoffart, L.M., Hamed, R.B., Bollinger, J.M., Jr., Krebs, C. & Schofield, C.J. Evidence for the slow reaction of hypoxia-inducible factor prolyl hydroxylase 2 with oxygen. *FEBS Journal* **277**, 4089-99 (2010).
12. Ehrismann, D., Flashman, E., Genn, D.N., Mathioudakis, N., Hewitson, K.S., Ratcliffe, P.J. & Schofield, C.J. Studies on the activity of the hypoxia-inducible-factor hydroxylases using an oxygen consumption assay. *Biochemical Journal* **401**, 227-234 (2007).
13. Mirica, L.M., McCusker, K.P., Munos, J.W., Liu, H.-w. & Klinman, J.P. 18O Kinetic Isotope Effects in Non-Heme Iron Enzymes: Probing the Nature of Fe/O2 Intermediates. *Journal of the American Chemical Society* **130**, 8122-8123 (2008).
14. Valle, A.B.F., Panek, A.D. & Mattoon, J.R. Colorimetric determination of succinic acid using yeast succinate dehydrogenase. *Analytical Biochemistry* **91**, 583-599 (1978).
15. Luo, L., Pappalardi, M.B., Tummino, P.J., Copeland, R.A., Fraser, M.E., Grzyska, P.K. & Hausinger, R.P. An assay for Fe(II)/2-oxoglutarate-dependent dioxygenases by enzyme-coupled detection of succinate formation. *Analytical Biochemistry* **353**, 69-74 (2006).
16. Hewitson, K.S., Granatino, N., Welford, R.W., McDonough, M.A. & Schofield, C.J. Oxidation by 2-oxoglutarate oxygenases: non-haem iron systems in catalysis and signalling. *Philos Trans A Math Phys Eng Sci* **363**, 807-28; discussion 1035-40 (2005).
17. Schofield, C.J. & Zhang, Z. Structural and mechanistic studies on 2-oxoglutarate-dependent oxygenases and related enzymes. *Current Opinion in Structural Biology* **9**, 722-731 (1999).

18. Prescott, A.G. & Lloyd, M.D. The iron(II) and 2-oxoacid-dependent dioxygenases and their role in metabolism. *Natural Product Reports* **17**, 367-383 (2000).
19. Costas, M., Mehn, M.P., Jensen, M.P. & Que, L. Dioxygen Activation at Mononuclear Nonheme Iron Active Sites: Enzymes, Models, and Intermediates. *Chemical Reviews* **104**, 939-986 (2004).
20. Flashman, E., Davies, S.L., Yeoh, K.K. & Schofield, C.J. Investigating the dependence of the hypoxia-inducible factor hydroxylases (factor inhibiting HIF and prolyl hydroxylase domain 2) on ascorbate and other reducing agents. *Biochemical Journal* **427**, 135-142 (2010).
21. Tsukada, Y.-i., Fang, J., Erdjument-Bromage, H., Warren, M.E., Borchers, C.H., Tempst, P. & Zhang, Y. Histone demethylation by a family of JmjC domain-containing proteins. *Nature* **439**, 811-816 (2006).
22. Couture, J.-F., Collazo, E., Ortiz-Tello, P.A., Brunzelle, J.S. & Trievel, R.C. Specificity and mechanism of JMJD2A, a trimethyllysine-specific histone demethylase. *Nature Structural Biology* **14**, 689-695 (2007).
23. Roy, T.W. & Bhagwat, A.S. Kinetic studies of Escherichia coli AlkB using a new fluorescence-based assay for DNA demethylation. *Nucleic Acids Research* **35**, e147 (2007).
24. Rose, N.R., Ng, S.S., Mecinović, J., Liénard, B.t.M.R., Bello, S.H., Sun, Z., McDonough, M.A., Oppermann, U. & Schofield, C.J. Inhibitor Scaffolds for 2-Oxoglutarate-Dependent Histone Lysine Demethylases⊥. *Journal of Medicinal Chemistry* **51**, 7053-7056 (2008).
25. Flashman, E., Davies, S.L., Yeoh, K.K. & Schofield, C.J. Investigating the dependence of the hypoxia-inducible factor hydroxylases (factor inhibiting HIF and prolyl hydroxylase domain 2) on ascorbate and other reducing agents. *Biochemical Journal* **427**, 135-42 (2010).
26. Dao, J.H., Kurzeja, R.J.M., Morachis, J.M., Veith, H., Lewis, J., Yu, V., Tegley, C.M. & Tagari, P. Kinetic characterization and identification of a novel inhibitor of hypoxia-inducible factor prolyl hydroxylase 2 using a time-resolved fluorescence resonance energy transfer-based assay technology. *Analytical Biochemistry* **384**, 213-223 (2009).
27. Kawamura, A., Tumber, A., Rose, N.R., King, O.N., Daniel, M., Oppermann, U., Heightman, T.D. & Schofield, C. Development of homogeneous luminescence assays for histone demethylase catalysis and binding. *Analytical Biochemistry* **404**, 86-93 (2010).
28. Lindstedt, G. & Lindstedt, S. Cofactor requirements of gamma-butyrobetaine hydroxylase from rat liver. *Journal of Biological Chemistry* **245**, 4178-86 (1970).
29. Lindstedt, G., Lindstedt, S. & Tofft, M. Gamma-butyrobetaine hydroxylase from Pseudomonas sp AK 1. *Biochemistry* **9**, 4336-42 (1970).
30. Marzo, A. & Curti, S. l-Carnitine moiety assay: an up-to-date reappraisal covering the commonest methods for various applications. *Journal of Chromatography B: Biomedical Sciences and Applications* **702**, 1-20 (1997).
31. Cederblad, G., Holm, J., Lindstedt, G., Lindstedt, S., Nordin, I. & Schersten, T. gamma-Butyrobetaine hydroxylase activity in human and ovine liver and skeletal muscle tissue. *FEBS Letters* **98**, 57-60 (1979).
32. Millington, D.S., Kodo, N., Norwood, D.L. & Roe, C.R. Tandem mass spectrometry: a new method for acylcarnitine profiling with potential for neonatal screening for inborn errors of metabolism. *Journal of Inherited Metabolic Disease* **13**, 321-4 (1990).
33. Vreken, P., van Lint, A.E., Bootsma, A.H., Overmars, H., Wanders, R.J. & van Gennip, A.H. Rapid diagnosis of organic acidemias and fatty-acid oxidation defects by quantitative electrospray tandem-MS acyl-carnitine analysis in plasma. *Advances in Experimental Medicine and Biology* **466**, 327-37 (1999).
34. Kodo, N., Millington, D.S., Norwood, D.L. & Roe, C.R. Quantitative assay of free and total carnitine using tandem mass spectrometry. *Clinica Chimica Acta* **186**, 383-390 (1990).
35. Stevens, R.D., Hillman, S.L., Worthy, S., Sanders, D. & Millington, D.S. Assay for Free and Total Carnitine in Human Plasma Using Tandem Mass Spectrometry. *Clinical Chemistry* **46**, 727-729 (2000).
36. Englard, S., Horwitz, L.J. & Mills, J.T. A simplified method for the measurement of gamma-butyrobetaine hydroxylase activity. *Journal of Lipid Research* **19**, 1057-63 (1978).

37. Vaz, F.M., van Gool, S., Ofman, R., Ijlst, L. & Wanders, R.J. Carnitine biosynthesis: identification of the cDNA encoding human gamma-butyrobetaine hydroxylase. *Biochemical and Biophysical Research Communication* **250**, 506-10 (1998).
38. Barth, P.G., Scholte, H.R., Berden, J.A., Van der Klei-Van Moorsel, J.M., Luyt-Houwen, I.E., Van 't Veer-Korthof, E.T., Van der Harten, J.J. & Sobotka-Plojhar, M.A. An X-linked mitochondrial disease affecting cardiac muscle, skeletal muscle and neutrophil leucocytes. *Journal of Neurological Science* **62**, 327-55 (1983).
39. Leung, I.K.H., Krojer, T.J., Kochan, G.T., Henry, L., von Delft, F., Claridge, T.D.W., Oppermann, U., McDonough, M.A. & Schofield, C.J. Structural and Mechanistic Studies on gamma-Butyrobetaine Hydroxylase. *Chemistry & Biology* **17**, 1316-1324 (2010).
40. Dalvit, C. Ligand- and substrate-based 19F NMR screening: Principles and applications to drug discovery. *Progress in Nuclear Magnetic Resonance Spectroscopy* **51**, 243-271 (2007).
41. Goldstein, J.A., Cheung, Y.-F., Marletta, M.A. & Walsh, C. Fluorinated substrate analogs as stereochemical probes of enzymic reaction mechanisms. *Biochemistry* **17**, 5567-5575 (1978).
42. Grummitt, A.R., Rutledge, P.J., Clifton, I.J. & Baldwin, J.E. Active-site-mediated elimination of hydrogen fluoride from a fluorinated substrate analogue by isopenicillin N synthase. *Biochemical Journal* **382**, 659-666 (2004).
43. Loenarz, C., Mecinovic, J., Chowdhury, R., McNeill, L.A., Flashman, E. & Schofield, C.J. Evidence for a Stereoelectronic Effect in Human Oxygen Sensing. *Angewandte Chemie-International Edition* **48**, 1784-1787 (2009).
44. Gorres, K.L. & Raines, R.T. Direct and continuous assay for prolyl 4-hydroxylase. *Analytical Biochemistry* **386**, 181-185 (2009).
45. Cametti, M. & Rissanen, K. Recognition and sensing of fluoride anion. *Chemical Communications*, 2809-2829 (2009).
46. Deniau, G., Slawin, A.M.Z., Lebl, T., Chorki, F., Issberner, J.P., van Mourik, T., Heygate, J.M., Lambert, J.J., Etherington, L.A., Sillar, K.T. *et al.* Synthesis, conformation and biological evaluation of the enantiomers of 3-fluoro-gamma-aminobutyric acid ((R)- and (S)-3F-GABA): An analogue of the neurotransmitter GABA. *ChemBioChem* **8**, 2265-2274 (2007).
47. Rydzik, A.M., Leung, I.K.H., Kochan, G.T., Thalhammer, A., Oppermann, U., Claridge, T.D.W. & Schofield, C.J. Development and Application of a Fluoride-Detection-Based Fluorescence Assay for γ-Butyrobetaine Hydroxylase. *ChemBioChem* **13**, 1559-1563 (2012).
48. Wehbie, R.S., Punekar, N.S. & Lardy, H.A. Rat-Liver Gamma-Butyrobetaine Hydroxylase Catalyzed Reaction - Influence of Potassium, Substrates, and Substrate-Analogs on Hydroxylation and Decarboxylation. *Biochemistry* **27**, 2222-2228 (1988).
49. Simkhovich, B.Z., Shutenko, Z.V., Meirena, D.V., Khagi, K.B., Mezapuke, R.J., Molodchina, T.N., Kalvins, I.J. & Lukevics, E. 3-(2,2,2-Trimethylhydrazinium)Propionate (Thp) - a Novel Gamma-Butyrobetaine Hydroxylase Inhibitor with Cardioprotective Properties. *Biochemical Pharmacology* **37**, 195-202 (1988).
50. Warshakoon, N.C., Wu, S.D., Boyer, A., Kawamoto, R., Sheville, J., Renock, S., Xu, K., Pokross, M., Zhou, S., Winter, C. *et al.* Structure-based design, synthesis, and SAR evaluation of a new series of 8-hydroxyquinolines as HIF-1 alpha prolyl hydroxylase inhibitors. *Bioorganic & Medicinal Chemistry Letters* **16**, 5517-5522 (2006).
51. McNeill, L.A., Flashman, E., Buck, M.R.G., Hewitson, K.S., Clifton, I.J., Jeschke, G., Claridge, T.D.W., Ehrismann, D., Oldham, N.J. & Schofield, C.J. Hypoxia-inducible factor prolyl hydroxylase 2 has a high affinity for ferrous iron and 2-oxoglutarate. *Molecular Biosystems* **1**, 321-324 (2005).
52. Purser, S., Moore, P.R., Swallow, S. & Gouverneur, V. Fluorine in medicinal chemistry. *Chemical Society Reviews* **37**, 320-330 (2008).
53. Vulpetti, A. & Dalvit, C. Fluorine local environment: from screening to drug design. *Drug Discovery Today* **17**, 890-7 (2012).

54. Chen, H., Viel, S., Ziarelli, F. & Peng, L. 19F NMR: a valuable tool for studying biological events. *Chemical Society Reviews* (2013).
55. Hu, J., Zhang, W. & Wang, F. Selective difluoromethylation and monofluoromethylation reactions. *Chemical Communications*, 7465-7478 (2009).
56. Prakash, G.K.S., Ledneczki, I., Chacko, S. & Olah, G.A. Direct electrophilic monofluoromethylation. *Organic Letters* **10**, 557-560 (2008).
57. Prakash, G.K.S. & Chacko, S. Novel nucleophilic and electrophilic fluoroalkylation methods. *Current Opinion in Drug Discovery and Development* **11**, 793-802 (2008).
58. Dambrova, M., Liepinsh, E. & Kalvinsh, I. Mildronate: Cardioprotective action through carnitine-lowering effect. *Trends in Cardiovascular Medicine* **12**, 275-279 (2002).
59. Yang, X.F., Ye, S.J., Bai, Q. & Wang, X.Q. A fluorescein-based fluorogenic probe for fluoride ion based on the fluoride-induced cleavage of tert-butyldimethylsilyl ether. *Journal of Fluorescence* **17**, 81-87 (2007).
60. Denmark, S.E. & Ahmad, M. Carbonylative ring opening of terminal epoxides at atmospheric pressure. *Journal of Organic Chemistry* **72**, 9630-9634 (2007).
61. Baker, J.T. & Sifniades, S. Synthesis and Properties of Pyrrolin-2-Ones. *Journal of Organic Chemistry* **44**, 2798-2800 (1979).
62. Obrien, P., Powell, H.R., Raithby, P.R. & Warren, S. Investigation of the configurational stability of lithiated phosphine oxides using the Hoffmann test: X-ray structures of (2S(*),3S(*),4R(*))2-(N,N-dibenzylamino)-4-diphenylphosphinoyl-1-phenylp entan-3-ol and (2S(*),4S(*))-2-(N,N-dibenzylamino)-4-diphenylphinoyl-1-phenylpentan-3-o ne. *Journal of the Chemical Society-Perkin Transactions 1*, 1031-1039 (1997).

Chapter 3

^{19}F NMR studies on fluorinated proteins

Abstract

Chapter 3 describes the development of a method for the selective fluorination of proteins involved in the inactivation of antibiotics and its application to studying conformational changes. The NDM-1 and SPM-1 – metallo-β-lactamases involved in bacteria antibiotic resistance were labelled with a single fluorinated tag close to the active site. ^{19}F NMR studies on those model systems indicate how metal and ligand binding can affect a local conformation of a protein. The method was used to determine binding constants and investigate the binding mode for several ligands, as well as allowed tracking mobile loop movements and differentiate between different metal bound species.

Contents

1 Introduction

1.1 Use of ^{19}F NMR to study biological systems

Organofluorine compounds have substantial applications in chemistry and chemical biology; their applications include the modification of physicochemical and conformational properties of small molecules, and uses in radiomedicine as tracers[1] or labels for NMR studies.[2,3] Whereas the size of the fluorine atom is close to hydrogen (van der Waals' radius 1.47 Å for fluorine versus 1.20 Å for hydrogen), its electronic properties are similar to those of the hydroxyl group and therefore fluorine substitutions in organic molecules are often used as hydroxyl group mimics. Fluorine containing derivatives are widely used in medicine and agriculture,[4] with 20-25% of drugs produced containing at least one fluorine atom.[1] Equally, increased interest in fluorine containing organic compounds was followed by development of synthetic strategies to achieve selective fluorinations.[5] These advances in fluorine chemistry enabled the construction of fluorinated probes for enzymatic reactions, metabolic processes and biotransformations.

^{1}H, ^{13}C and ^{15}N solution state NMR experiments are widely used to provide data on protein structure and dynamics. However, ^{19}F NMR was recognized as an invaluable tool to study protein systems and metabolic processes under biological conditions,[6-9] where traditional NMR techniques would suffer from signal overlap. Fluorinated organic compounds are almost absent in the nature (from *de novo* biosynthesis), therefore even in complex biological mixtures intrinsic fluorine signals are not present. ^{19}F has a 100% natural abundance, spin ½ and magnetogyric ratio at a level of 83% of proton, which translates into reasonably high sensitivity of NMR detection. Compared to ^{1}H, ^{19}F has a much broader chemical shift range and its sensitivity to local environment is much higher (fluorine nucleus is surrounded by 9 electrons rather than single electron in the case of hydrogen). Therefore monitoring subtle changes in an examined system, e.g. weak binding events, enzyme folding and conformational exchange is usually possible to a much greater extent.

1.2 Protein modifications

Proteins are targets of most existing pharmaceuticals and are likely to remain so in the foreseeable future. High resolution methods for assessing protein 3D structure, i.e. protein crystallography and NMR are mainly used for determining ligand binding modes; however, these are time-consuming and in the case of X-ray crystallography provide only static datasets. There is an urgent need for protein-observed methods allowing determination of not only ligand affinities, but also binding modes in solution. An attractive approach to study protein structure and dynamics is represented by ^{19}F-NMR.[7-9] Several synthetic strategies to fluorinated amino acid analogues are available.[10] Incorporation of fluorinated amino acid derivatives into biopolymers can be achieved through a variety of different methods, including chemical modifications, preparation of fusion proteins by

native ligation and biosynthetic incorporation by microorganisms.[6,9,11] Biosynthetic methods typically rely on the use of auxotrophic bacterial strains (e.g. tryptophan) and supplementing its fluorinated version into media. However, this method labels proteins uniformly in multiple positions. In certain cases site-specific labelling is preferred in studying particular protein systems (e.g. for large protein systems, where uniform labelling leads to complicated spectra). Multiple modifications can also perturb protein folding/stability, leading to systems with distinctively different properties than the native ones. Site-directed biosynthetic labelling methods include *in vitro* incorporation of unnatural amino acids employing modified aminoacyl-tRNA synthases,[12,13] and chemical posttranslational modification of nucleophilic amino acid side chains, e.g. cysteine[14] or lysine[15] and to lesser extent serine and threonine.[9] Chemical tagging avoids problems associated with biosynthetic incorporation, such as low expression yields linked to toxicity of fluorinated precursors and insufficient uptake by aminoacyl-tRNA synthases. The most common targets of chemical tagging are cysteine residues due to their high nucleophilicity. Modification strategies include alkylations, disulphide bond formation or amide/thioester exchange.[6] One of those strategies is represented by alkylation of cysteine residues employing 3-bromo-1,1,1-trifluoroacetone (BFA), which was successfully used in studies of both soluble[16-18] and membrane proteins.[14,19,20]

1.3 Metallo-β-lactamases and antibiotic resistance

The increasing problem of antibiotic resistance is a major public health concern,[21] rendering the development of new antimicrobials an re-emerging area.[22,23] To date a majority of clinically used antibiotics contain the β-lactam motif and target cell-wall biosynthesis. The mode of action of β-lactams is based on irreversible binding to a nucleophilic serine residue in the active site of PBPs (Penicillin Binding Proteins), which catalyse a transpeptidation reaction in the cell wall biosynthesis. However, bacteria have evolved mechanisms of resistance towards β-lactams, with β-lactamase mediated hydrolysis being a major issue.[24-26] β-Lactamase enzymes are divided into four classes (A-D) based on DNA sequence similarity.[26,27] Long-considered as being of little clinical relevance, metallo-β-lactamases (MBLs[26], class B enzymes) are now presenting a serious global threat to almost all β-lactam antibiotics. Unlike the serine β-lactamases (SBLs), the MBLs are structurally and mechanistically unrelated to PBPs, and are unlikely to be inhibited by current mechanism-based SBL inhibitors (e.g. clavulanic acid).

MBLs are further divided into three different subclasses (B1, B2 and B3), in part reflecting their number of Zn(II) ions and sequence and/or structural similarities.[27] All MBLs present a characteristic αβ/βα sandwich fold and in addition, B1 and B2 subclasses present considerable sequence similarity to each other and rather low sequence similarity to subclass B3 enzymes. Enzymes belonging to B1 subclass are considered the most clinically relevant enzymes because of their broad range substrate recognitions.[24] B1 enzymes bind two Zn(II) ions and are located both on chromosomally and mobile genetic elements (plasmids, transposons). The B2 subclass contains only

chromosomally encoded MBLs with environmental maritime origin. These enzymes are activated only in the presence of β-lactams. B2 enzymes share on average 11% similarity to B1 enzymes. Enzymes belonging to the B2 subclass are all mono-Zn enzymes. The second metal binding site is altered because of the mutation. These B2 enzymes are also known as "true carbapenemases" because they present a specific substrate hydrolysing profile. They have low activity against penicillins and cephalosporins and sometimes they can even be inhibited by these substrates.[28] The B3 enzymes are also di-Zn containing enzymes, not presenting any substrate specificity and are mostly chromosomally located. However, in the last two years new plasmid mediated B3 MBLs were reported.[29]

Due to variations in MBL structures, including conformational changes involving active site loop movements,[30] the identification of broad spectrum MBL inhibitors is very challenging. Moreover, inhibitor discovery is hampered by lack of appropriate assays for MBLs and related proteins, especially those accounting for conformational changes upon inhibitor binding.

1.4 New Delhi Metallo-β-Lactamase (NDM-1)

NDM-1 (New Delhi Metallo-β-lactamase-1) was originally found in 2008 in New Delhi in a *Klebsiella pneumoniae* isolate. Later it spread across the word, including India, Pakistan and the United Kingdom.[31] NDM-1 is a flagship example of clinically relevant MBL,[31] with pathogens carrying the NDM-1 gene, often referred to as a 'super bug'. It is able to inactivate almost all clinically used β-lactam based antibiotics (except monobactams, e.g. aztreonam), including carbapenems, utilizing different metal cofactors and possibly differential mechanisms based on reaction conditions.[32]

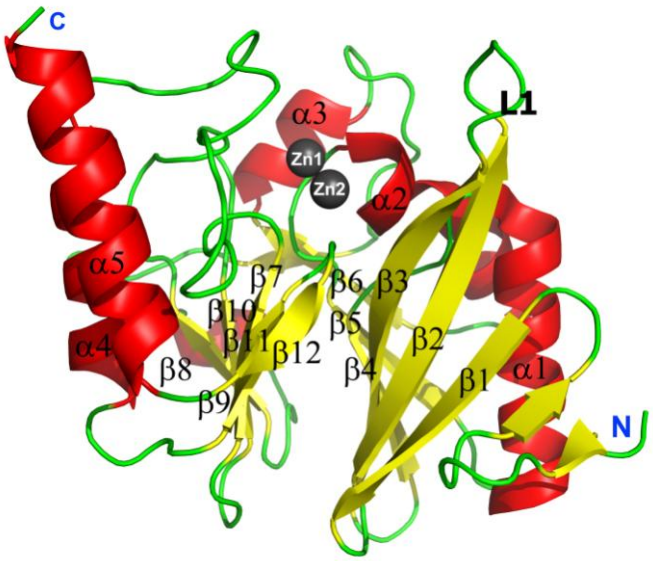

Figure 1 Overall fold of NDM-1-di-Zn(II) complex. L1 loop flanks NDM-1 active site. The figure was generated using di-Zn(II)-NDM-1 crystal structure (PDB id: 3SPU[33]).

1.5 São Paulo metallo-β-lactamase (SPM-1)

SPM-1 was originally found in São Paulo, Brasil on a chromosome of a *Pseudomonas aeruginosa* isolate.[34] Currently, SPM-1 represents a major clinical and public health problem in South America.[35,36] In Brasil, SPM-1 is the main MBL and its 35% presence in *P. aeruginosa* clinical isolates caused several outbreaks to date. The high mortality rate associated with bacteria carrying the SPM-1 gene (bla_{SPM-1}) is based mainly on the resistance of *P. aeruginosa* containing bla_{SPM-1} (60%) to all clinically used antibiotics.[37] Moreover, SPM-1 is interesting from the perspective that it presents similarities to both B1 and B2 subclasses of MBLs – it binds 2 zinc ions (characteristic for B1 class enzymes) and possesses α3 loop insert characteristic for B2 class enzymes.

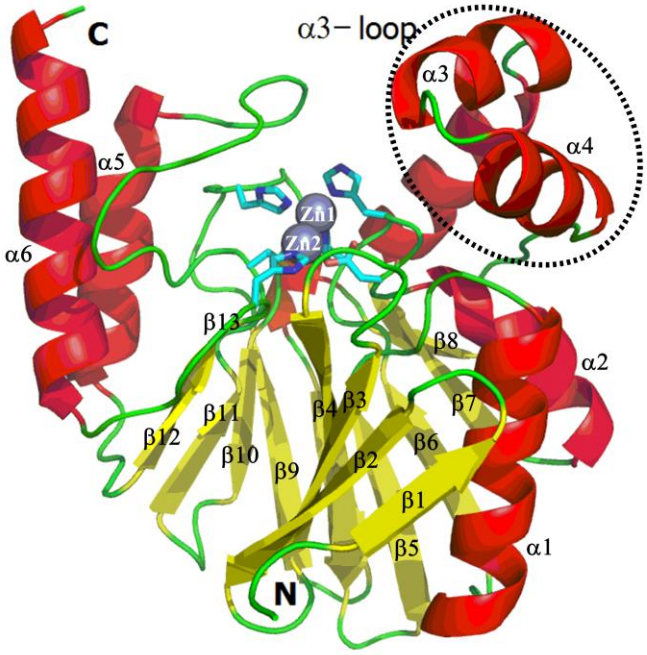

Figure 2 Overall fold of SPM-1-di-Zn(II) complex. The figure was generated using di-Zn(II)-SPM-1 crystal structure (PDB id: 2FHX[38]).

2 Studies on NDM-1

2.1 Conformation of the loop

Movements in loops that flank the MBL active site are proposed to be important in substrate/inhibitor binding.[32,39,40] In order to introduce a ^{19}F label into NDM-1, the L1 loop (residues 65-73 between strands β2 and β3, Fig. 3) was chosen, because differences in crystal structures imply that it is conformationally mobile. The apparent absence of exposed cysteine side chain in the NDM-1 (which contains only one cysteine at its active site), suggested that cysteine thiol modification may be suitable for ^{19}F label incorporation. NDM-1 cysteine variant, modified in the L1 loop (M67C) was produced. Pleasingly, cysteine 67 of the NDM-1 M67C variant was site selectively modified by treatment with 3-bromo-1,1,1-trifluoroacetone (BFA) (Fig. 4) to give the $–S-CH_2(CO)CF_3$ adduct (denoted as NDM-1*) as confirmed by LC-MS analyses (Fig. 5).

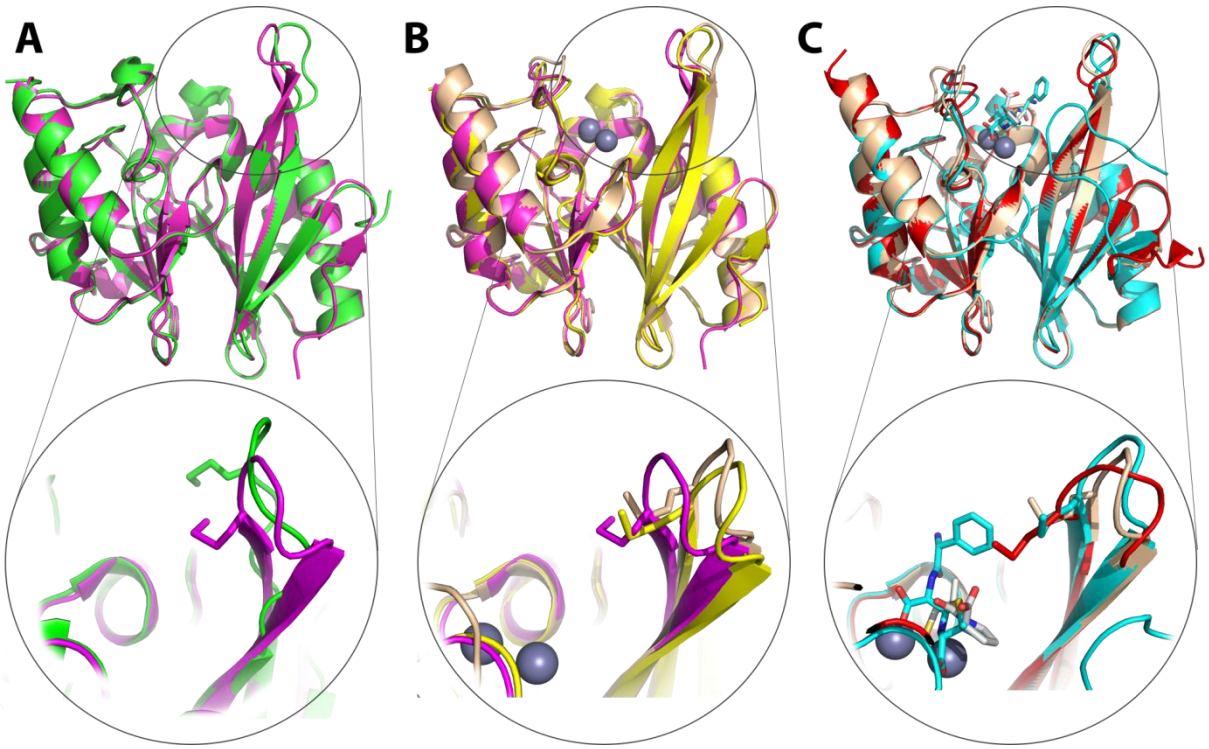

Figure 3 Overlay of views derived from different NDM-1 crystal structures. The L1 loop (circled) can adopt different conformations dependent on metallation state or ligands bound. A – Comparison of two different apo NDM-1 structures 3RKK[39] (green) and 3SBL[39] (magenta) reveals conformational flexibility of the loop in the apo protein. B – Comparison of apo NDM-1 (3SBL, magenta), mono-Zn(II) NDM-1 complex (3SFP[39], yellow) and di-Zn(II) NDM-1 complex (3SPU[33], wheat) demonstrates that loops can adopt different conformations in different protein metallation states. C – Comparison of NDM-1-di-Zn(II) complex (3SPU, wheat), NDM-1-di-Zn(II) in complex with hydrolysed ampicillin (3Q6X[40], blue) and NDM-1-di-Zn(II) in complex with L-captopril (4EXS[41], red) shows the L1 loop can adopt different conformation depending on the ligand bound. Close-up shots show the position of Met67 on the L1 loop.

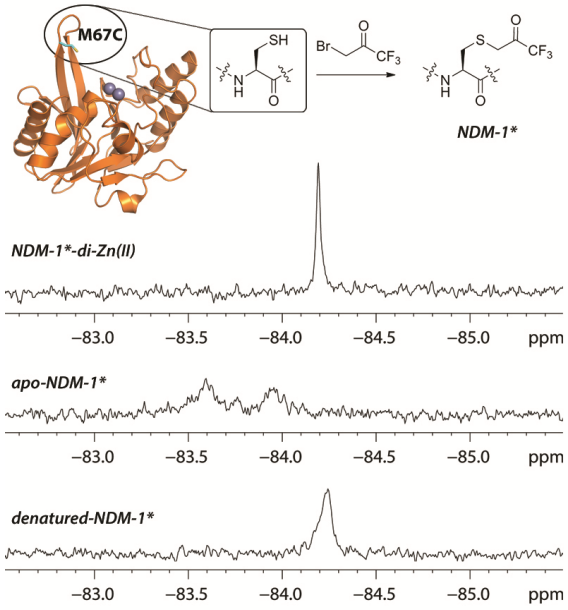

Figure 4 Unique signal patterns depending on the conformational and metallation state of NDM-1*. Site-specific labelling of M67C NDM-1 with 3-bromo-1,1,1-trifluoroacetone (BFA). ^{19}F-NMR spectra of NDM-1*-di-Zn(II) complex, apo-NDM-1* and denatured NDM-1* (obtained by incubation with 2M guanidinium chloride).

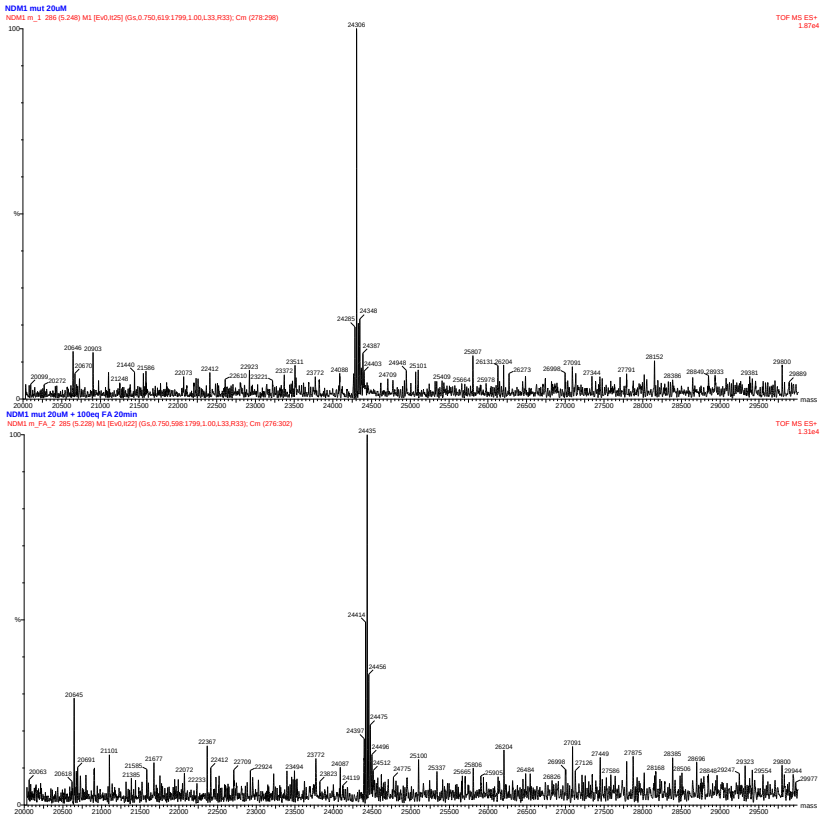

Figure 5 MS spectra of NDM-1 M67C (top) and NDM-1 M67C labelled with BFA (3-bromo-1,1,1-trifluoro acetone) (bottom). The observed mass difference (+129) corresponds to attachment of a single BFA label per molecule of NDM-1 M67C. Spectra were acquired using a Waters LCT Premier instrument fitted with TOF analyser. The electrospray ionisation mode was used.

Several crystallographically assessed conformations of the L1 loop in the apo, metal- and/or ligand bound states of MBLs have been reported, and are proposed to participate in the positioning of ligands at the active site (Fig. 3). The ^{19}F-NMR spectrum of di-Zn(II) bound NDM-1* displays a single peak belonging to the protein, suggesting that di-Zn(II) NDM-1* exists at least predominantly in a single distinct conformation, or the loop movement is very fast on the NMR timescale yielding signal with averaged shift (Fig. 4).[42] To further characterise the label's position within the protein's 3D structure, its solvent accessibility was tested. ^{19}F-NMR chemical shifts are highly sensitive to local chemical environment and even small differences in dielectric properties of a solvent, i.e. change of H_2O to D_2O, can result in change of chemical shift.[6,43] The change in ^{19}F chemical shift is proportional to the molar fraction of D_2O in H_2O and the extent of that phenomenon is dependent on accessibility of the fluorine containing moiety to solvent molecules. Measurements of chemical shift change of NDM-1* label and TFA (internal standard) as a function of D_2O content revealed that the label was sensitive to solvent interactions in 85% compared to TFA (Fig. 6); consistent with the largely solvent exposed Met67 residue in the NDM-1 active site.

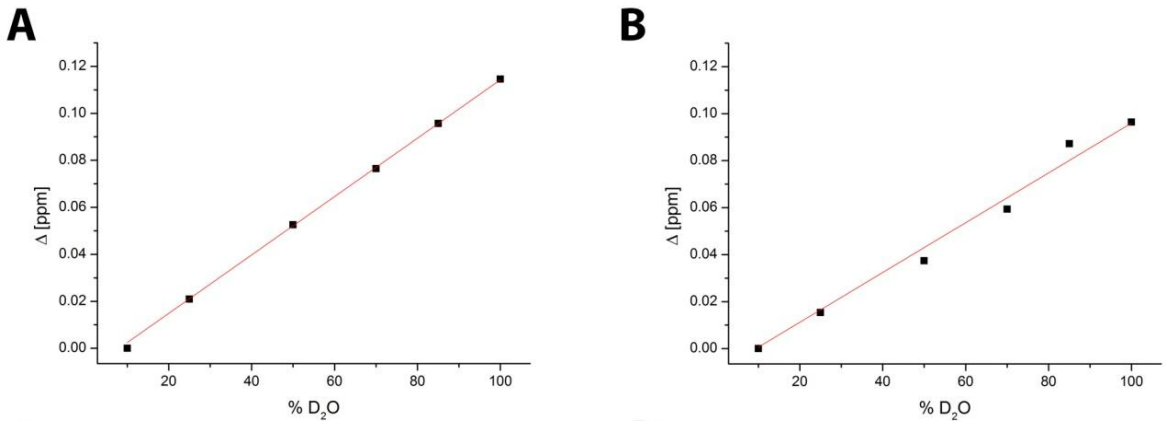

Figure 6 Solvent exposure experiments. Dependence of change in signal chemical shift for (A) CF_3COOH (TFA) internal standard present in the solution of di-Zn(II)-NDM-1* and (B) di-Zn(II)-NDM-1* label. TFA sample describes fully exposed CF_3 signal. Data were fitted with linear function using OriginPro 8.5.1. Obtained fits are as follows: A – y=0.00124x-0.01, R2>0.99; B – y=0.00106x-0.01, R2>0.98; Percentage solvent exposure of the NDM-1* label was calculated as a ratio of linear fit slope obtained for NDM-1* to analogous slope for TFA present in a sample (which was set to 100% as a fully exposed small molecule signal).

Removal of the Zn(II) ions from the NDM-1* active site, using 10 mM EDTA, led to the observation of broader signals, reflecting at least two conformers, in an intermediate exchange system (exchange rates are referred to NMR time scales throughout text), indicated by significant line broadening (Fig. 4). Metal sequestering from the active site was noticeably slower in the presence of inhibitor D-captopril, which ligates via its thiol group to both active site zinc ions (Fig. 7).

Upon denaturation, using 2M guanidinium chloride, a broadened signal was obtained (Fig. 7). The change in signal shape likely reflects the average chemical environment of the label in an unfolded NDM-1*. These initial studies show application of ^{19}F NMR for the time-resolved monitoring of ligand induced changes at the NDM-1 active site.

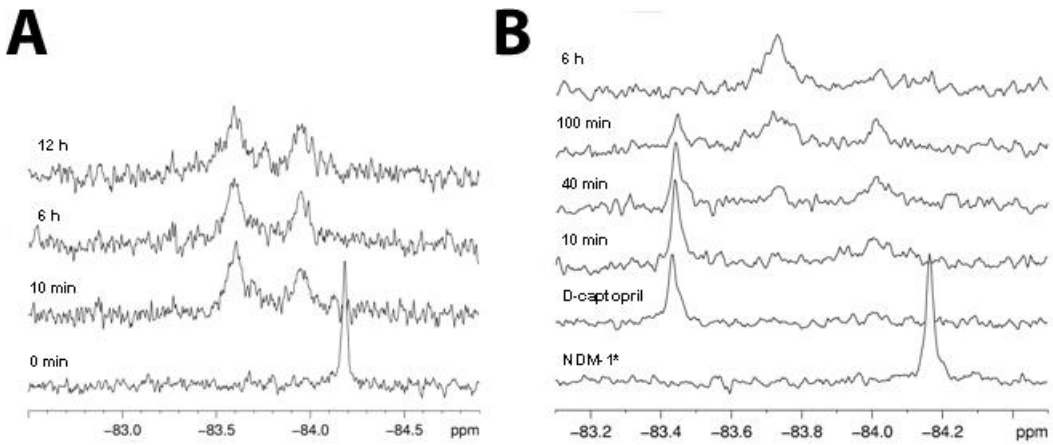

Figure 7 Time course analyses of NDM-1* treatment with EDTA. A – Sequestering metal from the NDM-1*-di-Zn(II) complex by 10 mM EDTA is rapid. B – Treatment of the NDM-1*-di-Zn(II)-D-captopril complex with 10 mM EDTA leads to slow deterioration of the initial complex and appearance of peaks characteristic to apo protein.

2.2 Ligand binding

In order to investigate whether conformational changes upon ligand binding could be monitored by ^{19}F NMR, we carried out assays with di-Zn(II)-NDM-1* and different ligands.

2.2.1 Slow exchange system

Both L- and D-captopril (Fig. 8) have been reported as potent NDM-1 inhibitors with the IC_{50} values of 202 µM and 7.9 µM, respectively.[44] Titration of NDM-1* with both isomers, followed by ^{19}F-NMR measurements, provided a direct read-out of ligand-enzyme complex formation (Fig. 9). For both L- and D-captopril the appearance of a distinctive peak of di-Zn(II)-NDM-1* complex with the inhibitor could be observed, with increasing peak areas upon titration with ligand. This scenario is characteristic for slow exchange system, signifying both captopril isomers as strong binders.[42]

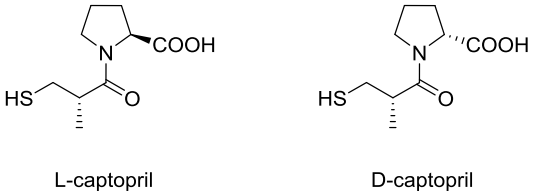

Figure 8 Structure of L- and D-captopril.

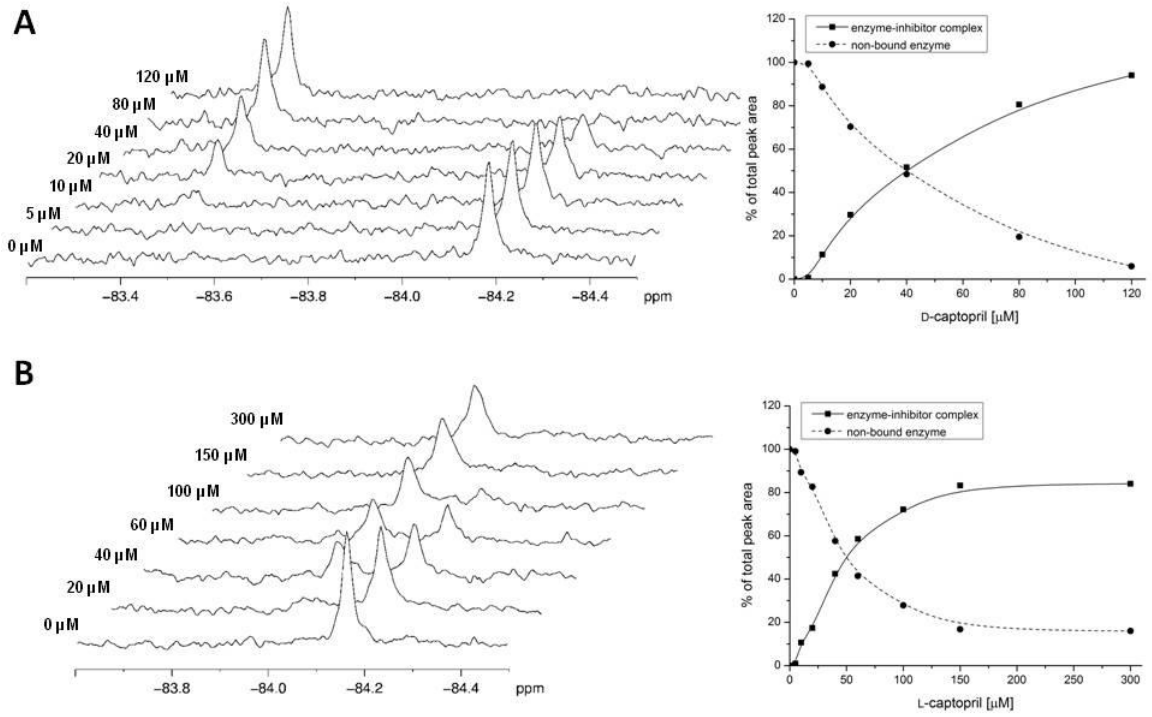

Figure 9 Binding of D- and L-captopril to NDM-1* (A and B, respectively) followed by ^{19}F NMR.

2.2.2 K_D fitting

^{19}F-NMR titration data were used to calculated K_D values for binding of both captopril isomers. Values were calculated following the changes in the peak area, using a modified version of the function for specific binding.[45,46] K_D is ligand-enzyme dissociation constant described by equation:

$$\text{(Equation 1)}\ K_D = \frac{[L][P]}{[LP]},$$

where [L], [P], [LP] are equilibrium concentrations of the free ligand, free protein and ligand-protein complex, respectively. Non-bound ligand [L] and protein [P] concentration are equal to total ligand [L_0] and protein [P_0] concentrations minus the ligand-protein complex:

$$\text{(Equation 2)}\ [L] = [L_0] - [LP],\ \text{(Equation 3)}\ [P] = [P_0] - [LP]$$

Therefore equation (1) can be written as:

$$\text{(Equation 4)}\ K_D = \frac{([L_0]-[LP])([P_0]-[LP])}{[LP]},$$

which after rearrangement gives:

$$\text{(Equation 5)}\ [LP]^2 - [LP]([L_0] + [P_0] + K_D) + [L_0][P_0] = 0$$

and can be solved as a quadratic equation to give:

$$\text{(Equation 6)}\ [LP] = \frac{([L_0]+[P_0]+K_D)-\sqrt{([L_0]+[P_0]+K_D)^2-4[L_0][P_0]}}{2}$$

Variable is defined as ratio of ligand-protein complex to sum of ligand-protein complex and free protein:

$$\text{(Equation 7)}\ y = \frac{[LP]}{[LP]+[P]}$$

Which using equation 3 can be written as:

$$\text{(Equation } \mathbf{8}\text{)}\ y = \frac{[LP]}{[P_0]}$$

Substituting [LP] with equation **6** we obtain K_D fitting function:

$$\text{(Equation } \mathbf{9}\text{)}\ y = \frac{([L_0]+[P_0]+K_D)-\sqrt{([L_0]+[P_0]+K_D)^2-4[L_0][P_0]}}{2[P_0]}$$

where $[P_0]$ is fixed concentration of protein solution used in the experiment and $[L_0]$ is ligand concentration titrated into solution.

Equation **9** was used to fit binding curves for L- and D-captopril (OriginPro 8.5.1). Molar fraction of protein-ligand complex ($X_{complex}$) was used as the dependent variable. Here, X was calculated as ratio of integrals corresponding to protein-ligand complex and sum of integrals corresponding to non-bound protein and protein-ligand complex. K_D values of 34.1±5.6 μM and 57.3±3.4 μM were obtained for D- and L-captopril, respectively (Fig. 10).

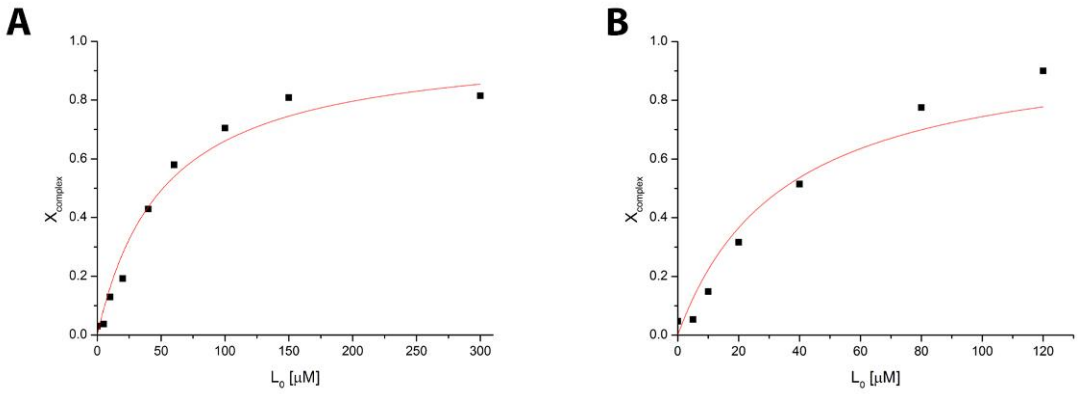

Figure 10 K_D measurements using ^{19}F NDM-1*. Molar fraction of protein-ligand complex (L-captopril (A) and D-captopril (B)) as a function of free ligand concentration. Data were fitted using equation **9**.

The crystal structure of NDM-1 in complex with L-captopril also revealed that its thiol is positioned to chelate both active site Zn(II) ions and that its side chain carboxylate interacts with Asn220 of NDM-1 (Fig. 11).[41] The precise binding mode of D-captopril to NDM-1 is unknown; however, it is likely that its thiol group interacts with two Zn(II) ions in the active site analogously to L-captopril.[47] D-Captopril can likely interact with other conserved residues, i.e. Glu123 and/or Gln152 (Fig. 11), similar to captopril binding to another metallo-β-lactamase BlaB.[48]

The observed change in the ^{19}F chemical shift upon titration of di-Zn(II)-NDM-1* is much larger for D-captopril than for L-captopril indicating a more significant change of the environment upon binding of D-captopril. Analysis of available structures together with the predicted D-captopril binding mode (Fig. 11), suggests that this difference may reflect more substantial ligand-binding induced movement of the L1 loop in the case of D-captopril. In support of this hypothesis, solvent exposure experiments with D-captopril showed that the di-Zn(II)-NDM1*-D-captopril complex has a decreased exposure of 73% relative to the TFA response, as compared to 85% for the di-Zn(II)-

NDM1* (Fig. 12B), consistent with an induced loop closure upon D-captopril binding. In contrast, no change in solvent exposure for di-Zn(II)-NDM-1*-L-captopril complex compared to di-Zn(II)-NDM-1* was observed (Fig. 12C).

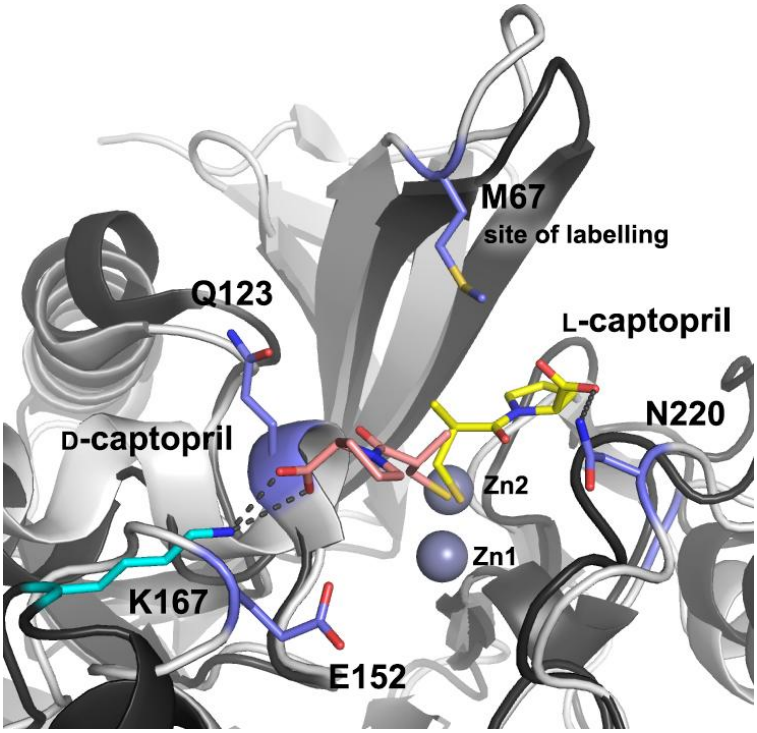

Figure 11 The different chemical shifts for L- and D- captopril likely reflect different binding modes. View from crystallographic analyses of NDM-1 complexed with di-Zn(II) and L-captopril (PDB id: 4EXS). The L-captopril (yellow) interacts with Asn220. Binding of D-captopril (pink) is modeled based on a structure of D-captopril complexed with the BlaB MBL (PDB id: 1M2X).

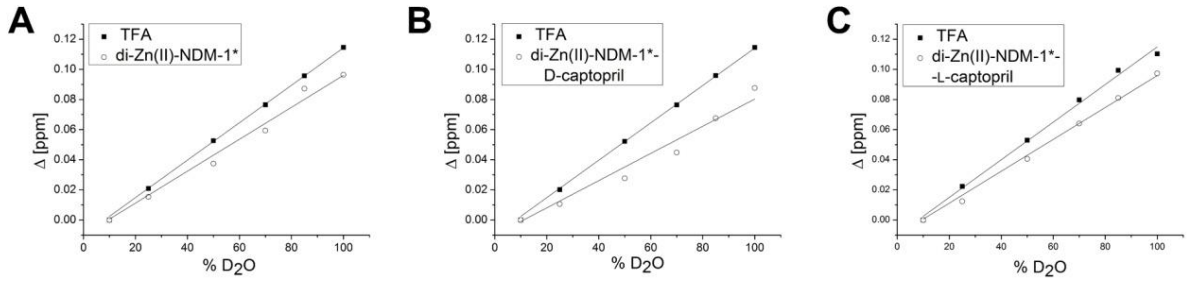

Figure 12 Monitoring the change in ^{19}F chemical shift as a function of D_2O content. A – Change in chemical shift for CF_3COOH (TFA) (■) and di-Zn(II)-NDM-1* (○), fitted with linear functions giving (■) y=0.00124x-0.01, R^2>0.99 and (○) y=0.00106x-0.01, R^2>0.98. B – Change in chemical shift for TFA (■) and the di-Zn(II)-NDM-1*-D-captopril complex (○), fitted with linear functions giving (■) y=0.00124x-0.01, R^2>0.99 and (○) y=0.00090x-0.01, R^2>0.98. C – Change in chemical shift for TFA (■) and the di-Zn(II)-NDM-1*-L-captopril complex (○), fitted with linear functions giving (■) y=0.00125x-0.01, R^2>0.99 and (○) y=0.00106x-0.01, R^2>0.99. The percentage solvent exposure of the NDM-1* label was calculated as a ratio of the slope obtained for the NDM-1* complex relative to the analogous slope for TFA in the sample (set to 100% as a fully exposed small molecule signal).

2.2.3 Competition studies

^{19}F-NMR measurements were applied to study the competition between the binding of L- and D-captopril. A rise in peak intensity of the signal assigned to the D-captopril-NDM-1* complex was observed when L-captopril-NDM-1* complex was titrated with D-captopril (Fig. 13), consistent with a lower IC_{50} for D- as compared to L-captopril,[44] indicating the ^{19}F-NMR can discriminate between different binding modes.

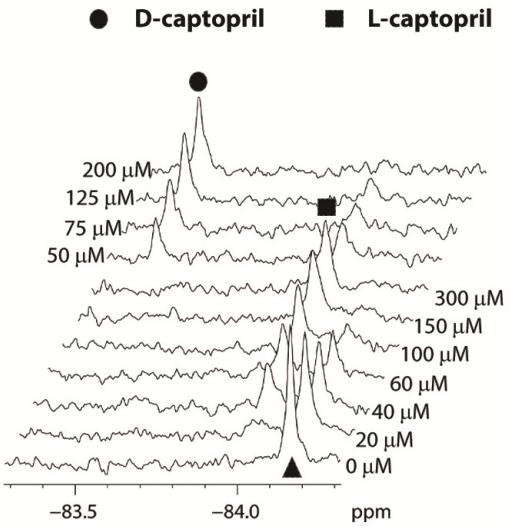

Figure 13 Titration of NDM-1*-di-Zn(II) (▲) with L-captopril leads to appearance of a distinctive peak (■) corresponding to a NDM-1*-di-Zn(II)-L-captopril complex. L-Captopril can be displaced from a NDM-1* by D-captopril as indicated by the appearance of a peak characteristic for the NDM-1*-di-Zn(II)-D-captopril complex (●).

2.2.4 Weak binding ligands

Applicability of ^{19}F NMR method to monitor binding of weak inhibitors was tested, i.e. enantiomeric isoquinolines (**1**) and (**2**), which were shown to inhibit NDM-1.[49] Upon titration of NDM-1* with isoquinoline (**1**) a change in chemical shift and slight line broadening was observed, corresponding to an average of both free NDM-1* and NDM-1*-(**1**) complex peaks (Fig. 14). This phenomenon, in contrast to slow exchange systems as was shown for both captoprils, is characteristic for a fast exchange system.[42] Titration of (**2**) resulted in significant line broadening upon complex formation (Fig. 14) typical for an intermediate exchange system. These results are in good agreement with IC_{50} data; i.e. (**2**) is a better inhibitor than (**1**) (IC_{50} 61 μM for (**1**) and 47 μM for (**2**)[49]). Displacement of the weaker binding ligand (**2**) by a stronger binder (i.e. D-captopril) led to the formation of NDM-1*-D-captopril complex (Fig. 15).

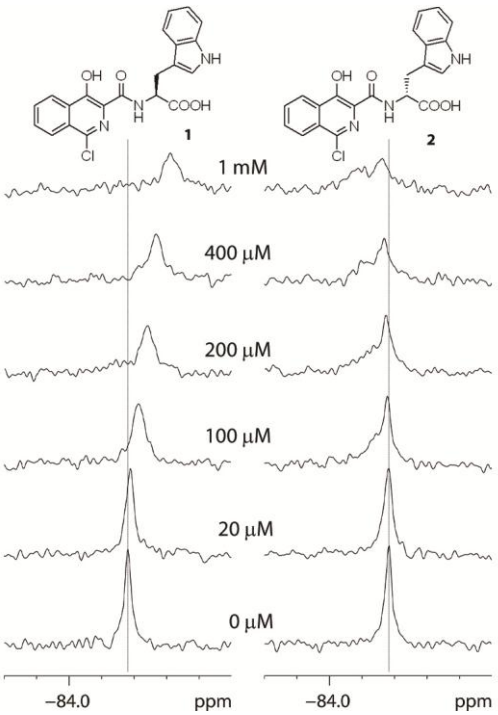

Figure 14 ^{19}F NMR identification of different modes of ligand binding. Titration of di-Zn(II)-NDM-1* (70 µM) with isoquinoline (**1**) and (**2**).

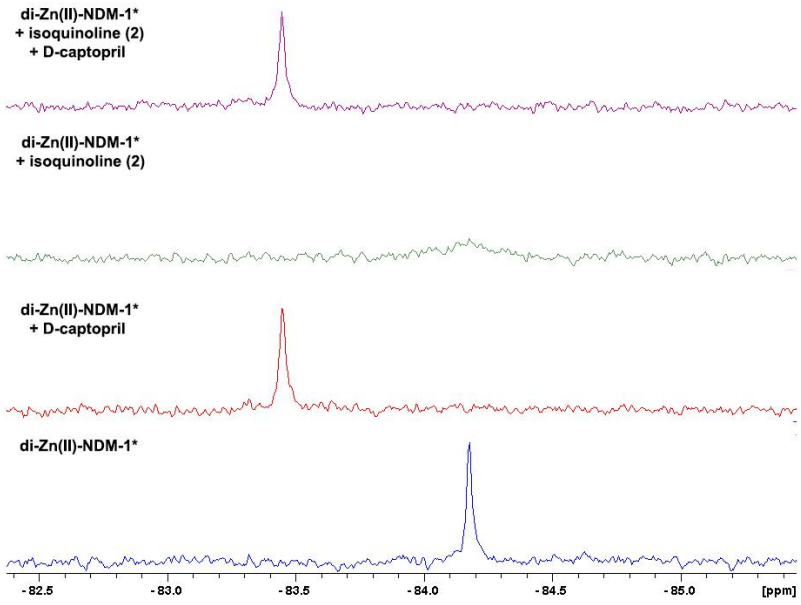

Figure 15 ^{19}F NMR spectra of di-Zn(II)-NDM-1* treated with isoquinoline (**2**). The fluorine signal recovers after addition of D-captopril.

Data obtained for isoquinoline (**1**) allowed for binding isotherm fitting using the equation **9** defining the dependent variable as $\Delta_{obs}/\Delta_{max}$ (where $\Delta_{obs} = \delta_0 - \delta_{obs}$ and $\Delta_{max} = \delta_0 - \delta_{max}$ and δ_0, δ_{obs}, δ_{max} are chemical shifts of the initial protein peak, observed peak and peak with maximal shift corresponding to saturated protein-ligand complex, respectively), resulting in a K_D of 170 µM (Fig. 16).

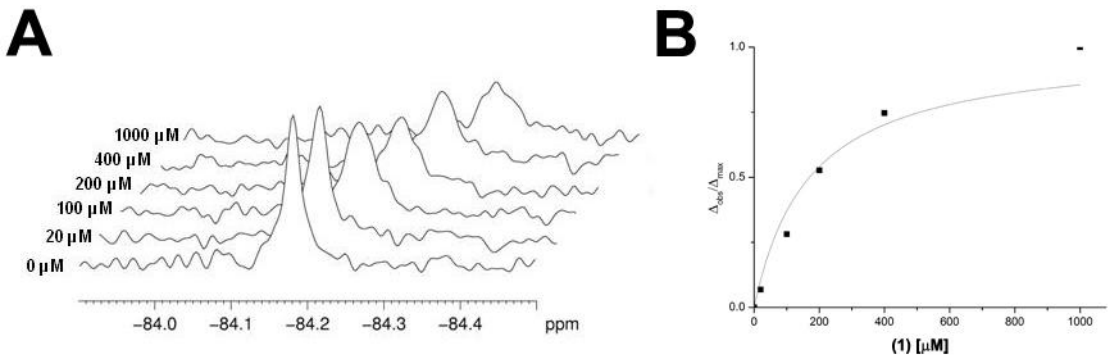

Figure 16 Formation of the NDM-1*-isoquinoline (**1**) complex as followed by ^{19}F NMR. K_D curve fit for isoquinoline (**1**) binding to NDM-1*.

2.2.5 Ligands with multiple binding modes

Other thiol-containing benzoic acids, i.e. thiosalicylic acid (**3**) and 3,5-bis(mercaptomethyl)benzoic acid (**4**) which have been reported to be broad spectrum MBL inhibitors,[50] were tested for binding to NDM-1* using the ^{19}F detection method. Unlike captoprils, upon binding of both compound (**3**) and (**4**) two peaks were observed in their respective ^{19}F-NMR spectra (Fig. 17).

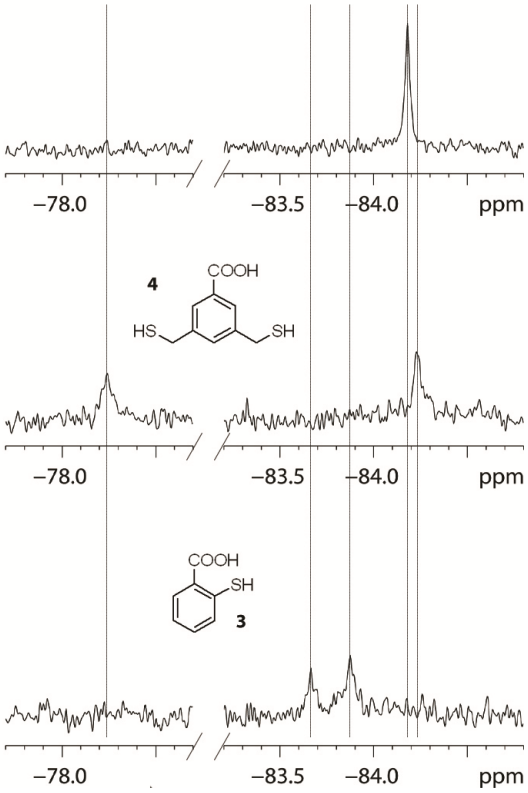

Figure 17 ^{19}F NMR aids identification of different modes of ligand binding. Titration of di-Zn(II)-NDM-1* (70 µM) with thiols (**3**) and (**4**) (160 µM for both (**3**) and (**4**)) – multiple modes of binding were observed for both thiol-based inhibitors.

The observed signal for thiol (**3**) was found close to the original NDM-1* signal and presumably represents a fast exchange system complex. The second signal observed at higher frequency also represents a fast exchange system, however, the larger change in chemical shift suggests that the phenyl ring interacts with the flexible L1 loop containing the label (similar to L-captopril). In the case of thiol (**4**) two binding modes were observed, one of which represents a similar fast exchange system as for thiol (**3**), and another signal significantly deshielded (Fig. 17). Presumably, this species corresponds to a significant conformational change of the flexible L1 loop.

2.2.6 Ligands which does not bind

In an era of emerging antibiotic resistance, including the evolution of MBLs, significant efforts are directed to the development of novel antibiotics, including β-lactams, which are not substrates for MBLs. Monobactams, e.g. aztreonam (Fig. 18), are a class of β-lactams that are not hydrolysed by MBLs[51] and have been reported not to inhibit NDM-1.[39] It was, however, shown that ^{15}N-labelled Bc-II binds aztreonam in a non-productive manner.[51] To reveal potential active site binding of aztreonam to NDM-1* a titration experiment using up to 2.5 mM aztreonam was performed. No chemical shift was observed upon the presence of aztreonam which suggests that aztreonam has no active site interaction.

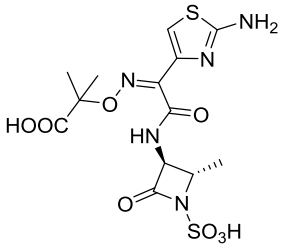

Figure 18 Structure of aztreonam.

2.3 Metal binding

MBLs contain either one, or more commonly, two catalytically productive active site metal ions[40]. However, there is uncertainty about the order of binding, and in some cases, the exact metal content.[52-54]

Metal binding to NDM-1 was investigated by titrating apo-NDM-1* with Zn(II). Upon Zn(II) addition, the broad peaks of the apo form disappeared and a rise of signals corresponding to species assigned as mono- or di-Zn(II) bound NDM-1* complexes was observed (Fig. 19). Mono and di-Zn(II) bound species were observed even at low zinc concentrations, suggesting rapid sequential metal binding. The ratio between mono and di-Zn(II) complexes was similar up to one equivalent of metal added, likely reflecting the difference between affinities of two metal binding sites.[40]

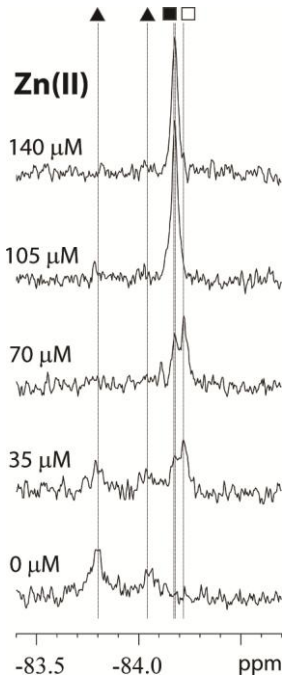

Figure 19 Titration of apo-NDM-1* with Zn(II). ▲ = apo-NDM-1* signals; apparent metal bound species: ■ = NDM-1*-di-Zn(II); □ = NDM-1*-mono-Zn(II).

2.4 DMSO titration defines active site

It has been shown that organic solvents can bind in empty cavities of enzymes and can be used as detection probes to identify the possible binding sites.[55,56] To demonstrate the effect of DMSO on the NDM-1 active site the change in chemical shift of the label and TFA as a function of increasing DMSO concentration was measured. The shift of the label was found to be much more sensitive to increasing DMSO content than the shift of the TFA signal, indicating that DMSO binds weakly in the active site (Fig. 20).

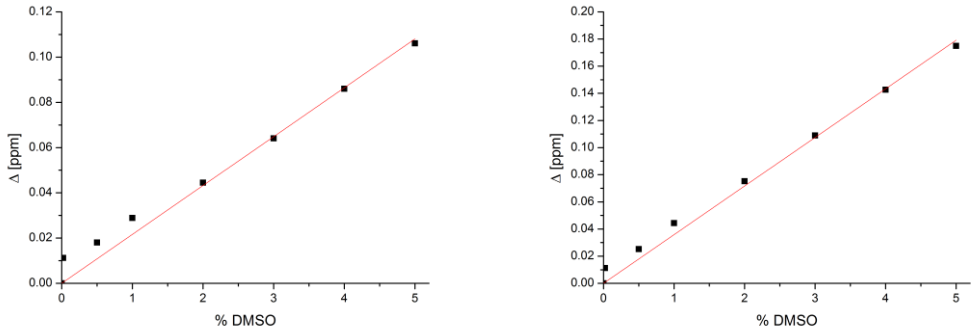

Figure 20 Left – change in chemical shift of TFA signal induced by increasing concentration of DMSO (y=0.02161x, R^2>0.99). Right – change in chemical shift of NDM-1* signal induced by increasing concentration of DMSO (y=0.03582x, R^2>0.99).

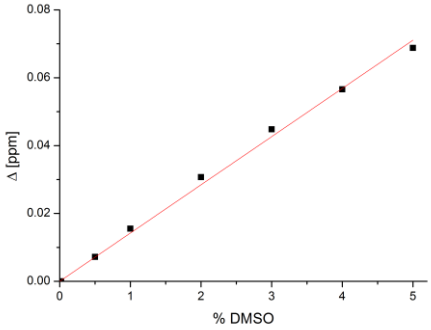

Figure 21 Change in chemical shift of NDM-1* signal induced by increasing concentration of DMSO, normalized to TFA chemical shift change (y=0.01421x, R^2>0.99).

The DMSO binding curve was used to evaluate whether the change of chemical shift upon binding of inhibitors described in this chapter is not only attributed to the effect of an increasing concentration of DMSO. Moreover, binding of DMSO demonstrates that a sulphoxide moiety can be a good starting point for further design of inhibitors of NDM-1 and related MBLs. The sensitivity of this ^{19}F NMR based method will allow screening of other fragments with different functional groups to identify novel scaffolds for inhibitor discovery.

3 Studies on SPM-1

3.1 Mobile loop

São Paolo Metallo-β-lactamase -1 (SPM-1) was proposed to be a structural hybrid between B1 and B2 MBL classes. Characteristic to the B1 subclass it binds two metal ions, while in the sequence of SPM-1 a central insertion (α3 and α4 region, 24 AA) was found which is defined as a conserved α-helix characteristic for B2 MBLs (Fig. 22). Deletion of the central insertion reduces activity of the enzyme (from 2.5 to 370 fold), implying an important role of this loop in the catalytic activity of SPM-1.[38] This central insertion is also held responsible for the 'open' conformation for SPM-1 as compared to the generally 'closed' conformations of all B2 enzymes (Fig. 22), however, recently it was shown by X-ray crystallography that α3 loop region of SPM-1 can adopt either an open[38] or closed conformation.

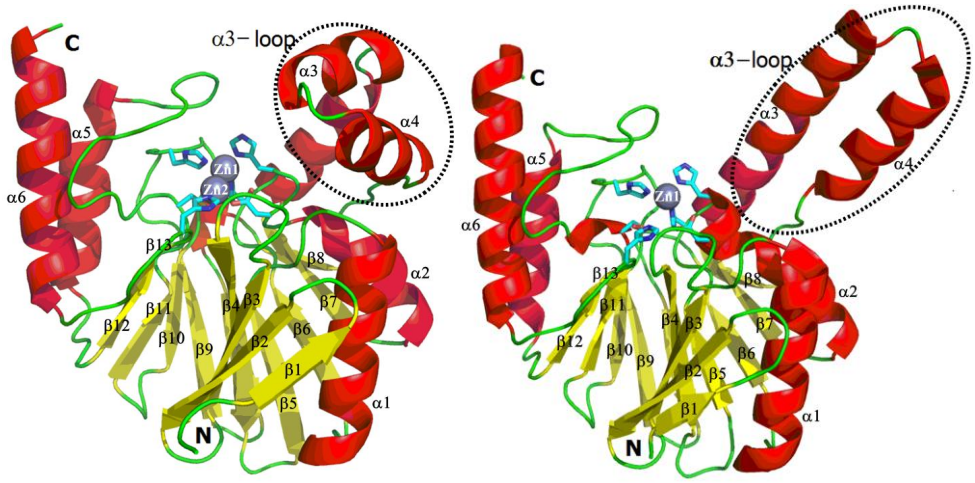

Figure 22 View from crystal structures of SPM-1 in "closed" (unpublished data from Dr. Jürgen Brem) "open" (PDB id: 2FHX) conformations.

3.2 SPM-1 labelling

Studying the dynamics of protein structures in solution by means of ^{19}F NMR gives the unique opportunity to observe conformational equilibriums of the proteins. To study the observed α3 loop movement of SPM-1 in solution, ^{19}F NMR experiments on a strategically labelled SPM-1 variant were performed. A Y152C mutant was designed, introducing an exposed cysteine residue on the edge of the α3 loop (Fig. 23), which was envisaged to provide detailed information about the α3 loop behaviour in solution. Production of the Y152C mutant followed by chemical modification using 3-bromo-1,1,1-trifluoroacetone yielded the fluorine-labelled SPM-1 mutant (SPM-1*), as was confirmed by MS analysis (Fig. 24).

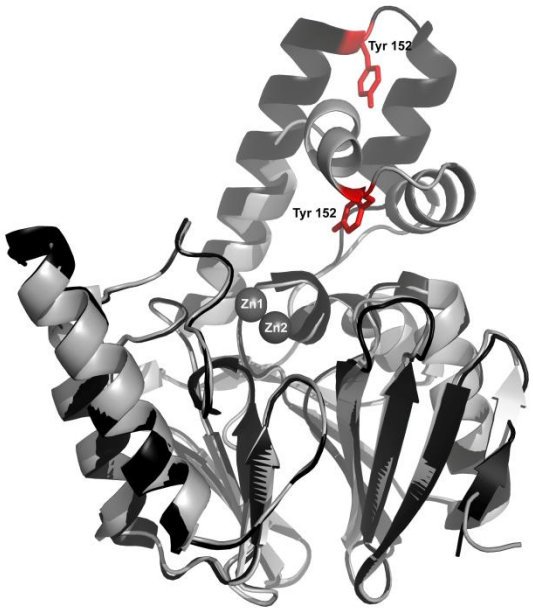

Figure 23 View from SPM-1 'closed' and 'open' form with the labelling site marked in red.

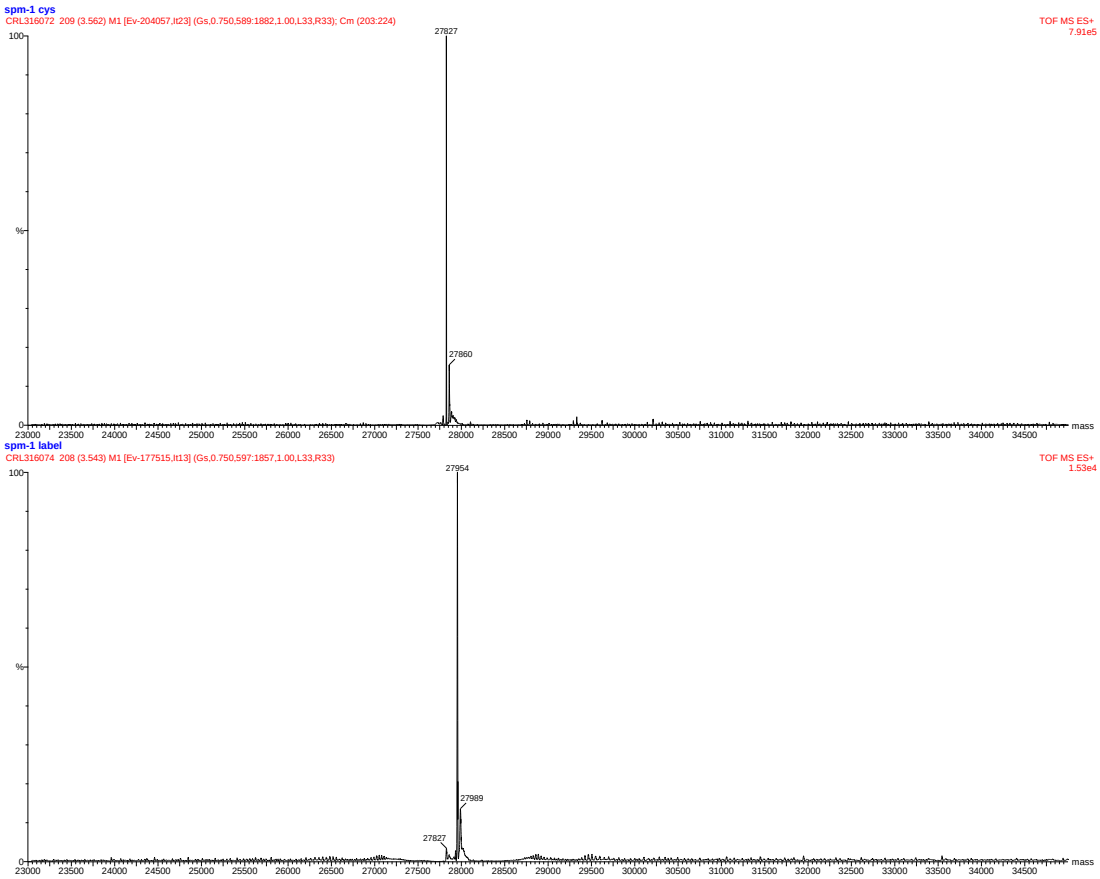

Figure 24 MS spectra of SPM-1 Y152C (top) and SPM-1 Y152C labelled with BFA (3-bromo-1,1,1-trifluoro acetone) (bottom). The observed mass difference (+127) corresponds to attachment of a single BFA label per a molecule of SPM-1 Y152C. Spectra were acquired using a Waters LCT Premier instrument fitted with TOF analyser. The electrospray ionisation mode was used.

3.3 ^{19}F NMR studies on SPM-1*

^{19}F NMR analysis on di-Zn(II)-SPM-1* gave two distinct fluorine signals (-72 ppm and -83 ppm) (Fig. 25). MS analysis demonstrated that only one site was labelled, therefore the label exists in two distinctive conformations, which are in a slow exchange system. Upon denaturation with 2M guanidinium chloride only one, broadened signal was observed, with a similar chemical shift compared to that obtained by denaturation of NDM-1* (Fig. 26).

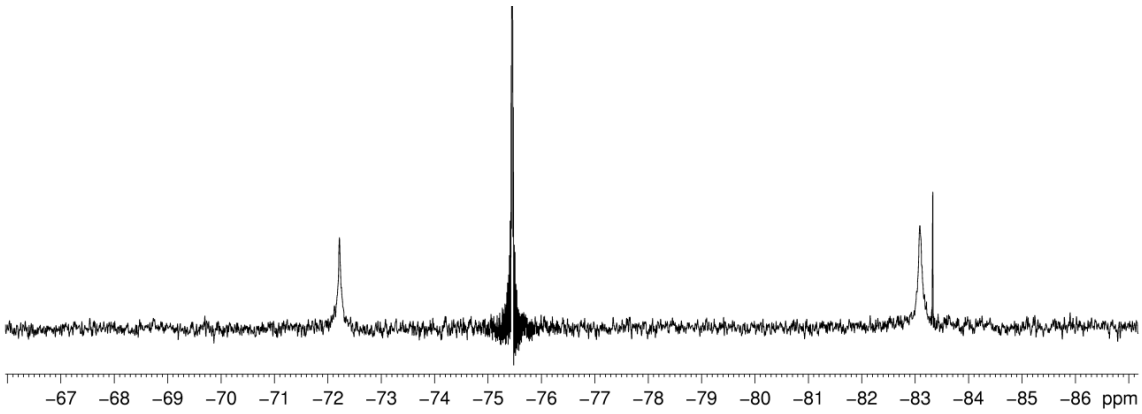

Figure 25 ^{19}F NMR spectra of SPM-1* (80 µM protein, 50 µM TFA standard, Tris 50 mM pH 7.5, 200 mM NaCl, 10% D_2O). Signals (from left to right) correspond to SPM-1*, TFA, SPM-1* and excess of labelling agent.

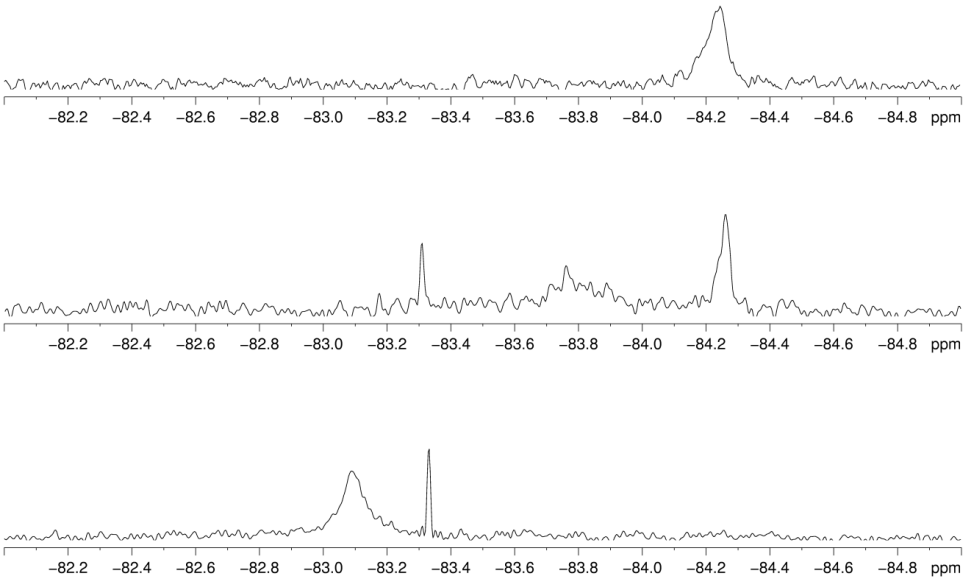

Figure 26 Comparison of ^{19}F NMR spectra of denatured NDM-1*, denatured SPM-1*, native SPM-1* (from top to bottom).

3.4 Solvent exposure experiments

Determination of the solvent accessibility for each signal of SPM-1* revealed that the signal at -72 ppm is as sensitive to the isotope content of the solvent system as TFA, corresponding to a 99% exposure of the ^{19}F label. The signal at -83 ppm presented significantly lower sensitivity (58% exposure of the ^{19}F label), suggesting this label is more concealed in the SPM-1* active site (Fig. 27).

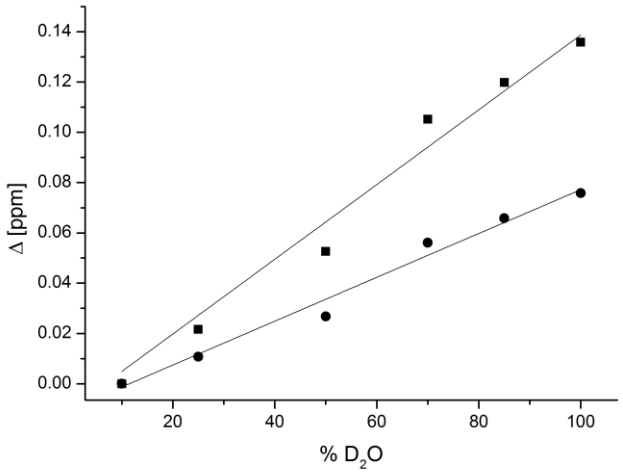

Figure 27 Change of ^{19}F chemical shift dependent on D_2O content in H_2O reveals different sensitivities for the -83 ppm and -72 ppm signals to solvent isotopic composition. Measured shifts were referenced to TFA shift under same conditions.

3.5 Saturation transfer experiments

In order to further elucidate which signal corresponds to the 'open' or 'closed' conformation of the enzyme, the saturation transfer experiments were performed (Fig. 27, Table 1). The basis of this experiment is irradiation of one signal with a low power pulse, which leads to a decrease of its intensity. However, if the irradiated signal is connected to another signal by chemical exchange (e.g. in case of two conformers), then the intensity of second signal should also decrease.

At 298K only a minimal decrease in the intensity of both ^{19}F signals of SPM-1* was observed (28% and 5% for signals at -72 and -83 ppm, respectively, when opposite signals irradiated) (Table 1). When the temperature was increased to 320K a higher percentage of response was detected (70% and 25% for signals at -72 and -83 ppm, respectively, when opposite signals irradiated) (Table 1). This is consistent with a higher mobility of the flexible loop at increased temperatures. The overall exchange between the two loop states is slow with a frequency $< 5 \cdot 10^3$ s^{-1} judging from the differences in frequency between the two interchangeable signals.

Table 1 Summary of saturation transfer experiment data.

Temp. [K]	decrease in -72 ppm peak intensity when -83 ppm peak saturated	decrease in -83 ppm peak intensity when -72 ppm peak saturated	ratio of peak intensities (-72/-83 ppm)
298	28%	5%	1:2
320	70%	25%	1:4

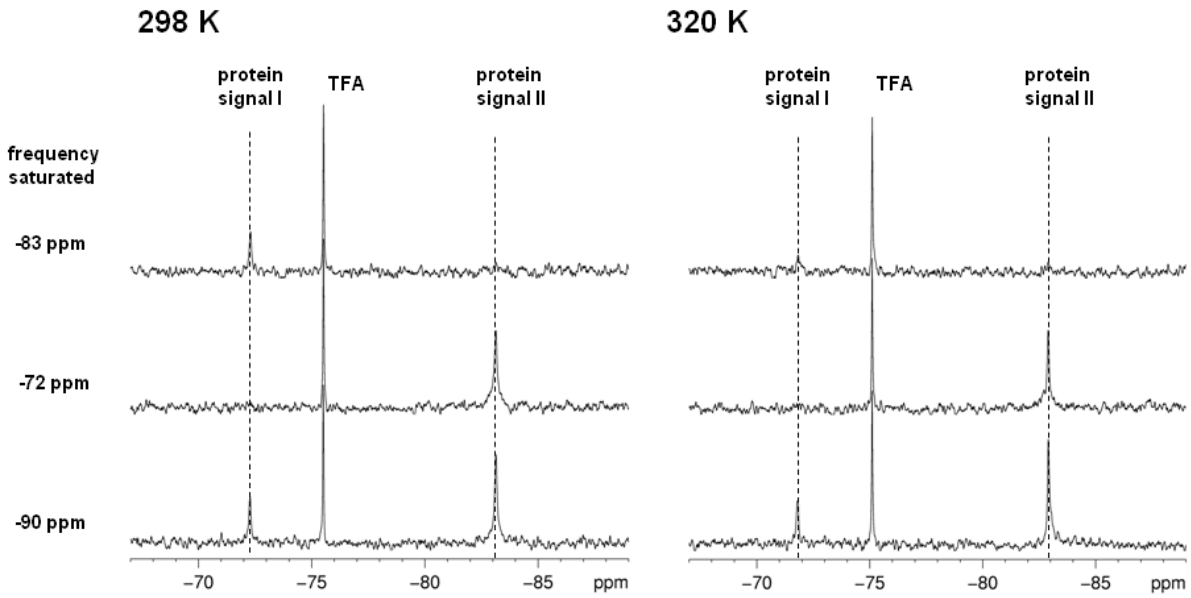

Figure 28 Saturation transfer experiments on di-Zn(II)-SPM-1*.

4 Summary and perspective

A robust ^{19}F-NMR method for the determination of specific ligand-metal binding to the NDM-1 active site was developed. This technique enables determination of binding constants, assessing type and number of ligand binding modes and tracking ligand-induced loop movements. In combination with conventional screening methods, this technique paves the way for the rapid identification of a clinically relevant MBL inhibitor. The same method was applied to elucidate a predicted loop movement in the SPM-1. The described method should also be readily applicable to study many other proteins.

5 Acknowledgements

NDM-1 and SPM-1 protein variants used in these studies were produced by Dr Jürgen Brem (Department of Chemistry, University of Oxford). IC_{50} measurements for isoquinoline derivatives (**1**) and (**2**) were measured by Dr Jürgen Brem. I would like to thank Dr Jürgen Brem and Dr Sander van Berkel (Department of Chemistry, University of Oxford) for their guidance and discussion regarding MBLs biochemistry and Dr Timothy Claridge (Department of Chemistry, University of Oxford) for his help with NMR experiments and data interpretation.

Part of the work described in this chapter has been published in:

- A. M. Rydzik, J. Brem, S. S. van Berkel, I. Pfeffer, A. Makena, T. D. W. Claridge, C. J. Schofield, *Angewandte Chemie International Edition* **2014**, 53, 3129–3133.
- S. S. van Berkel, J. Brem, A. M. Rydzik, R. Salimraj, R. Cain, A. Verma, R. J. Owens, C. W. Fishwick, J. Spencer, C. J. Schofield, *Journal of Medicinal Chemistry* **2013**, 56, 6945-6953.

6 Experimental section

6.1 Protein labelling

An appropriate cysteine-containing protein was treated with tris-(2-carboxyethyl)phosphine **(**TCEP, final concentration 2 mM), then incubated on ice (5 min) and buffered exchanged into phosphate buffer (50 mM, pH 7.0, 200 mM NaCl). A concentrated stock of 100 mM 3-bromo-1,1,1-trifluoroacetone (Sigma-Aldrich) reagent in phosphate buffer was prepared freshly prior to the reaction. Protein sample (0.15 mM) was treated with 3-bromo-1,1,1-trifluoroacetone (final concentration 2 mM) and incubated for 10 min at room temperature, prior to buffer exchange into Tris buffer (50 mM, pH 7.5, 200 mM NaCl). Buffer exchanges were performed using a PD-10 desalting column (GE Healthcare).

6.2 MS analyses

Protein MS spectra were acquired using following parameters:

System: Waters LCT instrument fitted with TOF analyser, ESI mode and HP1100 chromatography system (Agilent).

Column: ProSwift RP-4H analytical column (1×50 mm, Thermo Scientific).

Solvents system: solvent A – water 0.1% formic acid, solvent B – acetonitrile 0.1% formic acid.

Gradient:

time	% A	Flow rate [ml/min]
0.00	95	0.4
0.50	95	0.4
4.50	5	0.4
6.50	5	0.4
7.50	95	0.4
10.00	95	0.4

Calibration: Protein spectra were calibrated against myoglobin standard. Mass accuracy <5ppm with internal calibration. Resolution: 5000 Da.

Blank wash sample: *i*-PrOH

Tuning file parameters: sample cone 25V, extraction cone 5V, RF lens 255, desolvatation temperature: 300°C, source temperature: 100°C

MS method: 0-10 min, mass range 300-1800 Da, ESI+, Tof MS, MS scan mode

Pressure limit: 2500 psi

6.3 NMR

6.3.1 Instrumentation

NMR measurements were conducted using a Bruker AVII 500 spectrometer equipped with a 5mm z-gradient triple resonance inverse $^{1}H/^{19}F(^{13}C)$ TXI probe operating at 298K using 5 mm diameter NMR tubes (Norell). $^{19}F\{^{1}H\}$ decoupled spectra were recorded using inverse-gated Waltz-16 ^{1}H decoupling with rf field of 3.125 kHz. ^{19}F 90^{o} pulse lengths were 11 μs and spectra were typically obtained using 768 scans and a recovery delay of 1s. Data were processed with 3 Hz Lorentzian line broadening using TopSpin 3.1 software (Bruker) and were referenced to the internal trifluoroacetic acid (TFA) standard (-75.45 ppm).

6.3.2 Sample preparation

Samples contained NDM-1*-di-Zn(II) complex (80 μM, unless otherwise stated) in Tris buffer (50 mM, pH 7.5) supplemented with 200 mM NaCl and 10% D_2O. TFA (50 μM) was used as an internal standard. All inhibitor incubations were compared to appropriate NDM-1* samples containing same amount of DMSO, but no inhibitor, to ensure change of chemical shift was not the sole effect of increasing DMSO concentration. The DMSO titration curve was prepared for reference (see main text). Samples for SPM-1* experiments were prepared in an analogous way.

6.3.3 Metal binding experiments

Apo NDM-1* was obtained by incubation of NDM-1*-di-Zn(II) complex with 10 mM EDTA in Tris buffer (50 mM pH 7.5) supplemented with 200 mM NaCl (12 h, 4°C). The solution was then buffer exchanged into fresh Tris buffer (50 mM pH 7.5) supplemented with 200 mM NaCl to remove excess EDTA. Samples for metal titrations were containing 70 μM NDM-1* and 50 μM TFA as an internal standard.

References

1. Purser, S., Moore, P.R., Swallow, S. & Gouverneur, V. Fluorine in medicinal chemistry. *Chemical Society Reviews* **37**, 320-330 (2008).
2. Vulpetti, A. & Dalvit, C. Fluorine local environment: from screening to drug design. *Drug Discov Today* **17**, 890-7 (2012).
3. Dalvit, C. Ligand- and substrate-based 19F NMR screening: Principles and applications to drug discovery. *Progress in Nuclear Magnetic Resonance Spectroscopy* **51**, 243-271 (2007).
4. Müller, K., Faeh, C. & Diederich, F. Fluorine in pharmaceuticals: Looking beyond intuition. *Science* **317**, 1881-1886 (2007).
5. Ojima, I. Exploration of fluorine chemistry at the multidisciplinary interface of chemistry and biology. *Journal of Organic Chemistry* **78**, 6358-6383 (2013).
6. Kitevski-LeBlanc, J.L. & Prosser, R.S. Current applications of 19F NMR to studies of protein structure and dynamics. *Prog Nucl Magn Reson Spectrosc* **62**, 1-33 (2012).
7. Cobb, S.L. & Murphy, C.D. 19F NMR applications in chemical biology. *Journal of Fluorine Chemistry* **130**, 132-143 (2009).
8. Chen, H., Viel, S., Ziarelli, F. & Peng, L. (19)F NMR: a valuable tool for studying biological events. *Chemical Society Reviews* **42**, 7971-82 (2013).
9. Gerig, J.T. Fluorine NMR of proteins. *Progress in Nuclear Magnetic Resonance Spectroscopy* **26, Part 4**, 293-370 (1994).
10. Qiu, X.-L. & Qing, F.-L. Recent Advances in the Synthesis of Fluorinated Amino Acids. *European Journal of Organic Chemistry* **2011**, 3261-3278 (2011).
11. Frieden, C., Hoeltzli, S.D. & Bann, J.G. The preparation of 19F-labeled proteins for NMR studies. *Methods in Enzymology* **380**, 400-15 (2004).
12. Jackson, J.C., Hammill, J.T. & Mehl, R.A. Site-specific incorporation of a (19)F-amino acid into proteins as an NMR probe for characterizing protein structure and reactivity. *Journal of the American Chemical Society* **129**, 1160-6 (2007).
13. Jones, D.H., Cellitti, S.E., Hao, X., Zhang, Q., Jahnz, M., Summerer, D., Schultz, P.G., Uno, T. & Geierstanger, B.H. Site-specific labeling of proteins with NMR-active unnatural amino acids. *Journal of Biomolecular NMR* **46**, 89-100 (2010).
14. Luchette, P.A., Prosser, R.S. & Sanders, C.R. Oxygen as a paramagnetic probe of membrane protein structure by cysteine mutagenesis and 19F NMR spectroscopy. *Journal of the American Chemical Society* **124**, 1778-1781 (2002).
15. Adriaensens, P., Box, M.E., Martens, H.J., Onkelinx, E., Put, J. & Gelan, J. Investigation of protein structure by means of 19F-NMR. A study of hen egg-white lysozyme. *European Journal of Biochemistry* **177**, 383-394 (1988).
16. Huestis, W.H. & Raftery, M.A. Bromotrifluoroacetone alkylates hemoglobin at cysteine β93. *Biochemical and Biophysical Research Communications* **81**, 892-899 (1978).
17. Thomas, M.R. & Boxer, S.G. 19F NMR of trifluoroacetyl-labeled cysteine mutants of myoglobin: Structural probes of nitric oxide bound to the H93G cavity mutant. *Biochemistry* **40**, 8588-8596 (2001).
18. Critz, W.J. & Martinez-Carrion, M. Sulphydryl group modification of aspartate aminotransferase with 3-bromo-1,1,1-trifluoropropanone during catalysis. *Biochemistry* **16**, 1554-1558 (1977).
19. Oxenoid, K., Sönnichsen, F.D. & Sanders, C.R. Topology and secondary structure of the N-terminal domain of diacylglycerol kinase. *Biochemistry* **41**, 12876-12882 (2002).
20. Hellmich, U.A., Pfleger, N. & Glaubitz, C. 19F-MAS NMR on proteorhodopsin: Enhanced protocol for site-specific labeling for general application to membrane proteins. *Photochemistry and Photobiology* **85**, 535-539 (2009).
21. Fisher, J.F., Meroueh, S.O. & Mobashery, S. Bacterial resistance to beta-lactam antibiotics: compelling opportunism, compelling opportunity. *Chemical Reviews* **105**, 395-424 (2005).
22. O'Connell, K.M.G., Hodgkinson, J.T., Sore, H.F., Welch, M., Salmond, G.P.C. & Spring, D.R. Combating Multidrug-Resistant Bacteria: Current Strategies for the Discovery of Novel Antibacterials. *Angewandte Chemie International Edition* **52**, 10706-10733 (2013).

23. McKenna, M. Antibiotic resistance: the last resort. *Nature* **499**, 394-6 (2013).
24. Cornaglia, G., Giamarellou, H. & Rossolini, G.M. Metallo-beta-lactamases: a last frontier for beta-lactams? *Lancet Infectious Diseases* **11**, 381-93 (2011).
25. Walsh, T.R., Toleman, M.A., Poirel, L. & Nordmann, P. Metallo-beta-lactamases: the quiet before the storm? *Clinical Microbioly Reviews* **18**, 306-25 (2005).
26. Bebrone, C. Metallo-beta-lactamases (classification, activity, genetic organization, structure, zinc coordination) and their superfamily. *Biochemical Pharmacology* **74**, 1686-701 (2007).
27. Bush, K. & Jacoby, G.A. Updated functional classification of beta-lactamases. *Antimicrobial Agents and Chemotherapy* **54**, 969-76 (2010).
28. Zervosen, A., Valladares, M.H., Devreese, B., Prosperi-Meys, C., Adolph, H.-W., Mercuri, P.S., Vanhove, M., Amicosante, G., van Beeumen, J., Frère, J.-M. *et al.* Inactivation of Aeromonas hydrophila metallo-β-lactamase by cephamycins and moxalactam. *European Journal of Biochemistry* **268**, 3840-3850 (2001).
29. Yong, D., Toleman, M.A., Giske, C.G., Cho, H.S., Sundman, K., Lee, K. & Walsh, T.R. Characterization of a new metallo-beta-lactamase gene, bla(NDM-1), and a novel erythromycin esterase gene carried on a unique genetic structure in Klebsiella pneumoniae sequence type 14 from India. *Antimicrobial Agents and Chemotherapy* **53**, 5046-54 (2009).
30. Moali, C., Anne, C., Lamotte-Brasseur, J., Groslambert, S., Devreese, B., Van Beeumen, J., Galleni, M. & Frere, J.M. Analysis of the importance of the metallo-beta-lactamase active site loop in substrate binding and catalysis. *Chemistry & Biology* **10**, 319-29 (2003).
31. Kumarasamy, K.K., Toleman, M.A., Walsh, T.R., Bagaria, J., Butt, F., Balakrishnan, R., Chaudhary, U., Doumith, M., Giske, C.G., Irfan, S. *et al.* Emergence of a new antibiotic resistance mechanism in India, Pakistan, and the UK: a molecular, biological, and epidemiological study. *Lancet Infectious Diseases* **10**, 597-602 (2010).
32. Kim, Y., Cunningham, M.A., Mire, J., Tesar, C., Sacchettini, J. & Joachimiak, A. NDM-1, the ultimate promiscuous enzyme: substrate recognition and catalytic mechanism. *FASEB Journal* **27**, 1917-27 (2013).
33. King, D. & Strynadka, N. Crystal structure of New Delhi metallo-beta-lactamase reveals molecular basis for antibiotic resistance. *Protein Science* **20**, 1484-91 (2011).
34. Toleman, M.A., Simm, A.M., Murphy, T.A., Gales, A.C., Biedenbach, D.J., Jones, R.N. & Walsh, T.R. Molecular characterization of SPM-1, a novel metallo-beta-lactamase isolated in Latin America: report from the SENTRY antimicrobial surveillance programme. *Journal of Antimicrobial Chemotherapy* **50**, 673-9 (2002).
35. Polotto, M., Casella, T., de Lucca Oliveira, M.G., Rubio, F.G., Nogueira, M.L., de Almeida, M.T. & Nogueira, M.C. Detection of P. aeruginosa harboring bla CTX-M-2, bla GES-1 and bla GES-5, bla IMP-1 and bla SPM-1 causing infections in Brazilian tertiary-care hospital. *BMC Infectious Diseases* **12**, 176 (2012).
36. Zavascki, A.P., Gaspareto, P.B., Martins, A.F., Goncalves, A.L. & Barth, A.L. Outbreak of carbapenem-resistant Pseudomonas aeruginosa producing SPM-1 metallo-{beta}-lactamase in a teaching hospital in southern Brazil. *Journal of Antimicrobial Chemotherapy* **56**, 1148-1151 (2005).
37. Fonseca, E.L., Freitas Fdos, S. & Vicente, A.C. The colistin-only-sensitive Brazilian Pseudomonas aeruginosa clone SP (sequence type 277) is spread worldwide. *Antimicrobial Agents and Chemotherapy* **54**, 2743 (2010).
38. Murphy, T.A., Catto, L.E., Halford, S.E., Hadfield, A.T., Minor, W., Walsh, T.R. & Spencer, J. Crystal structure of Pseudomonas aeruginosa SPM-1 provides insights into variable zinc affinity of metallo-beta-lactamases. *Journal of Molecular Biology* **357**, 890-903 (2006).
39. Kim, Y., Tesar, C., Mire, J., Jedrzejczak, R., Binkowski, A., Babnigg, G., Sacchettini, J. & Joachimiak, A. Structure of apo- and monometalated forms of NDM-1--a highly potent carbapenem-hydrolyzing metallo-beta-lactamase. *PLoS One* **6**, e24621 (2011).
40. Zhang, H. & Hao, Q. Crystal structure of NDM-1 reveals a common beta-lactam hydrolysis mechanism. *FASEB Journal* **25**, 2574-82 (2011).

41. King, D.T., Worrall, L.J., Gruninger, R. & Strynadka, N.C.J. New Delhi Metallo-β-Lactamase: Structural Insights into β-Lactam Recognition and Inhibition. *Journal of the American Chemical Society* **134**, 11362-11365 (2012).
42. Bain, A.D. Chemical exchange in NMR. *Progress in Nuclear Magnetic Resonance Spectroscopy* **43**, 63-103 (2003).
43. Kitevski-LeBlanc, J.L., Evanics, F. & Prosser, R.S. Approaches for the measurement of solvent exposure in proteins by 19F NMR. *Journal of Biomolecular NMR* **45**, 255-264 (2009).
44. Guo, Y., Wang, J., Niu, G., Shui, W., Sun, Y., Zhou, H., Zhang, Y., Yang, C., Lou, Z. & Rao, Z. A structural view of the antibiotic degradation enzyme NDM-1 from a superbug. *Protein Cell* **2**, 384-94 (2011).
45. Fielding, L. NMR methods for the determination of protein–ligand dissociation constants. *Progress in Nuclear Magnetic Resonance Spectroscopy* **51**, 219-242 (2007).
46. Morton, C.J., Pugh, D.J.R., Brown, E.L.J., Kahmann, J.D., Renzoni, D.A.C. & Campbell, I.D. Solution structure and peptide binding of the SH3 domain from human Fyn. *Structure* **4**, 705-714 (1996).
47. Antony, J., Gresh, N., Olsen, L., Hemmingsen, L., Schofield, C.J. & Bauer, R. Binding of D- and L-captopril inhibitors to metallo-β-lactamase studied by polarizable molecular mechanics and quantum mechanics. *Journal of Computational Chemistry* **23**, 1281-1296 (2002).
48. García-Sáez, I., Hopkins, J., Papamicael, C., Franceschini, N., Amicosante, G., Rossolini, G.M., Galleni, M., Frère, J.-M. & Dideberg, O. The 1.5-Å Structure of Chryseobacterium meningosepticum Zinc β-Lactamase in Complex with the Inhibitor, D-Captopril. *Journal of Biological Chemistry* **278**, 23868-23873 (2003).
49. van Berkel, S.S., Brem, J., Rydzik, A.M., Salimraj, R., Cain, R., Verma, A., Owens, R.J., Fishwick, C.W., Spencer, J. & Schofield, C.J. Assay Platform for Clinically Relevant Metallo-beta-lactamases. *Journal of Medicinal Chemistry* **56**, 6945-53 (2013).
50. Liénard, B.M.R., Garau, G., Horsfall, L., Karsisiotis, A.I., Damblon, C., Lassaux, P., Papamicael, C., Roberts, G.C.K., Galleni, M., Dideberg, O. *et al.* Structural basis for the broad-spectrum inhibition of metallo-β- lactamases by thiols. *Organic and Biomolecular Chemistry* **6**, 2282-2294 (2008).
51. Poeylaut-Palena, A.A., Tomatis, P.E., Karsisiotis, A.I., Damblon, C., Mata, E.G. & Vila, A.J. A minimalistic approach to identify substrate binding features in B1 Metallo-β-lactamases. *Bioorganic & Medicinal Chemistry Letters* **17**, 5171-5174 (2007).
52. de Seny, D., Heinz, U., Wommer, S., Kiefer, M., Meyer-Klaucke, W., Galleni, M., Frere, J.M., Bauer, R. & Adolph, H.W. Metal ion binding and coordination geometry for wild type and mutants of metallo-beta -lactamase from Bacillus cereus 569/H/9 (BcII): a combined thermodynamic, kinetic, and spectroscopic approach. *Journal of Biological Chemistry* **276**, 45065-45078 (2001).
53. Siemann, S., Badiei, H.R., Karanassios, V., Viswanatha, T. & Dmitrienko, G.I. 68Zn isotope exchange experiments reveal an unusual kinetic lability of the metal ions in the di-zinc form of IMP-1 metallo-beta-lactamase. *Chemical Commununications*, 532-5344 (2006).
54. Periyannan, G.R., Costello, A.L., Tierney, D.L., Yang, K.-W., Bennett, B. & Crowder, M.W. Sequential Binding of Cobalt(II) to Metallo-β-lactamase CcrA†. *Biochemistry* **45**, 1313-1320 (2005).
55. Liepinsh, E. & Otting, G. Organic solvents identify specific ligand binding sites on protein surfaces. *Nature Biotechnology* **15**, 264-268 (1997).
56. Dalvit, C., Floersheim, P., Zurini, M. & Widmer, A. Use of organic solvents and small molecules for locating binding sites on proteins in solution. *Journal of Biomolecular NMR* **14**, 23-32 (1999).

Chapter 4

BBOX catalysed oxidative desymmetrisation

Abstract

Chapter 4 describes the studies on the BBOX catalysed oxidation of cyclic GBB analogues. Cyclic GBB analogues, i.e. *N*,*N*-dialkyl isonipecotic acid derivatives, were shown to be hydroxylated by human BBOX to give a single diastereomer. BBOX catalysed hydroxylation led to the desymmetrisation of the starting materials and consequent formation of up to three new stereocentres in one step. The conformations of starting materials and oxidation products in water were assigned by 1D and 2D NMR techniques. A crystal structure of *N*,*N*-dimethyl isonipecotic acid in complex with human BBOX was obtained, which allowed further rationalization of the stereochemistry assigned by the in-solution techniques.

Contents

1 Introduction

1.1 Enzyme catalysed desymmetrisations

Enzymes are among the most selective catalysts known for chemical transformations, including the preparation of optically active compounds.[1,2] Desymmetrisation is defined as a modification which eliminates one or more of the substrate's elements of symmetry.[3] Amongst various synthetic efforts towards enantioselective desymmetrisation,[4] enzyme-mediated catalysis presents an attractive option. The mild reaction conditions, under which most enzymes operate, means that their reactions are less affected by unwanted side reactions including epimerisation, isomerisation, and racemisation. Moreover, enzymes can provide a highly asymmetric host environment, which can enable high stereoselectivity of catalysed transformations.

Enzymes catalysing redox reactions have been used for *meso*-desymmetrisation.[1] However, there are few examples of the use of isolated enzymes involving the oxidation of unactivated C-H bonds[5] for desymmetrisation, with most of such transformations being catalysed by cytochrome P450-dependent monooxygenases.[6]

1.2 2OG dependent oxygenases and biocatalytic transformations

2-Oxoglutarate and Fe(II) dependent dioxygenases[7] are a diverse superfamily of enzymes, which perform various oxidative transformations, including stereospecific hydroxylations. Even though various highly enantio- and stereoselective processes are within the range of 2OG oxygenases reactivity, their biocatalytic potential has not been widely exploited, especially on an industrial scale. Most of the biocatalytically used 2OG dependent oxygenases are employed in biosynthesis of their prime substrates, e.g. synthesis of scopolamine through hydroxylation of hyoscyamine by hyoscyamine 6-β hydroxylase.[8] An interest in 2OG oxygenase catalysed processes is nourished by the possibility of the synthesis of new unnatural amino acids, e.g. hydroxylated derivatives of arginine,[9] tryptophan,[10] phenylalanine,[11] leucine,[12-14] proline[15] and many others. Proline hydroxylases are a subfamily of 2OG oxygenases, which are reported to catalyse hydroxylation of probably the most diverse range of substrates to date[16-18] and which have been used for the commercial production of hydroxyprolines.

2 BBOX catalysed hydroxylation of cyclic GBB analogues

2.1 Substrate screening

To explore the biocatalytic potential of BBOX, a set of cyclic GBB analogues has been screened as potential BBOX substrates using an MS-based assay. Subsequently *N*,*N*-dimethylisonipecotic acid (**1**) has been identified as a human BBOX substrate. Screening of other related heterocyclic motifs revealed substrate preferences for BBOX. The enzyme requires a quaternary ammonium centre for reactivity – neither isonipecotic acid (**2**) nor *N*-methyl isonipecotic acid (**3**) were substrates for BBOX. Analogues with additional modifications in the piperidine ring (e.g. unsaturated analogue (**4**), or methylated analogue (**5**)) were not substrates for BBOX. The carboxylate has to be positioned at C4 of piperidine ring – analogue (**10**) with the carboxylate at C3 was not hydroxylated by BBOX. In addition, 5-membered ring analogues did not support hydroxylation. The analogues screened as BBOX substrates are summarised in Fig. 1.

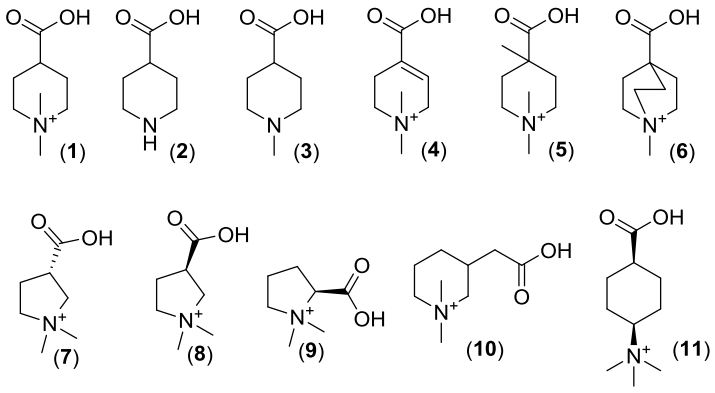

Figure 1 Cyclic GBB analogues screened as BBOX substrates.

2.2 *N*,*N*-Dimethylisonipecotic acid is a BBOX substrate

In the sample of (**1**) treated with BBOX, MS analyses have shown the presence of a +16 peak (compared to the initial mass of the substrate), most likely corresponding to the hydroxylation product (Fig. 2). To date, a few GBB analogues have been reported as BBOX substrates, i.e. 3-fluoro GBB and *N*-fluoromethyl GBB (Chapter 2), δ-valerobetaine and β-propionobetaine (Chapter 6). However, they are all linear compounds. The reaction of BBOX with cyclic GBB analogues is unprecedented, and therefore further studies on BBOX catalysed hydroxylation of analogue (**1**) are of great interest. In particular, the conformation of the substrate required for efficient binding in a BBOX active site and the stereochemical structure of the obtained product have to be investigated.

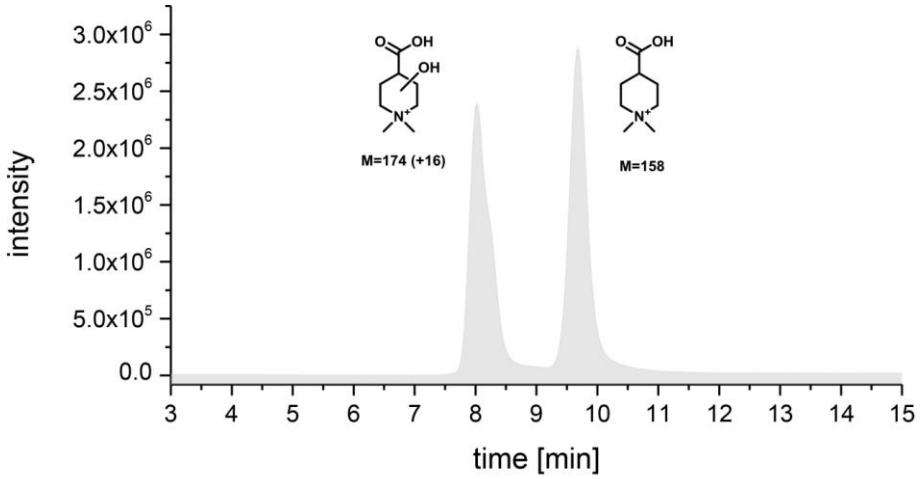

Figure 2 LC-MS chromatogram of the reaction of BBOX with *N*,*N*-dimethylisonipecotic acid (**1**). Spectra were recorded in mass range 120-300 Da (scan mode), single ion mode used in parallel to monitor masses: 158 (substrate, rt = 9.68 min) and 174 (product, rt = 8.02 min).

2.3 Conformational analysis of *N*,*N*–dimethylnipecotic acid

Firstly, the in-solution conformation of the substrate – *N*,*N*-dimethyl isonipecotic acid (**1**) was investigated by NMR methods. The ^{1}H NMR spectrum of (**1**) in D_2O at room temperature displayed only one distinctive set of peaks, likely corresponding to one conformer (Fig. 3). The position of the H4, adjacent to the carboxylic group, was assigned as axial, based on the coupling constant pattern (J_{aa} = 11.2 Hz, J_{ae} = 4.6 Hz). The overall signal pattern was characteristic for a chair conformation (Fig. 3). The identity of signals was further confirmed by assignment of ^{13}C NMR shifts for (**1**) using ^{1}H-^{13}C HSQC spectra (Fig. 4).

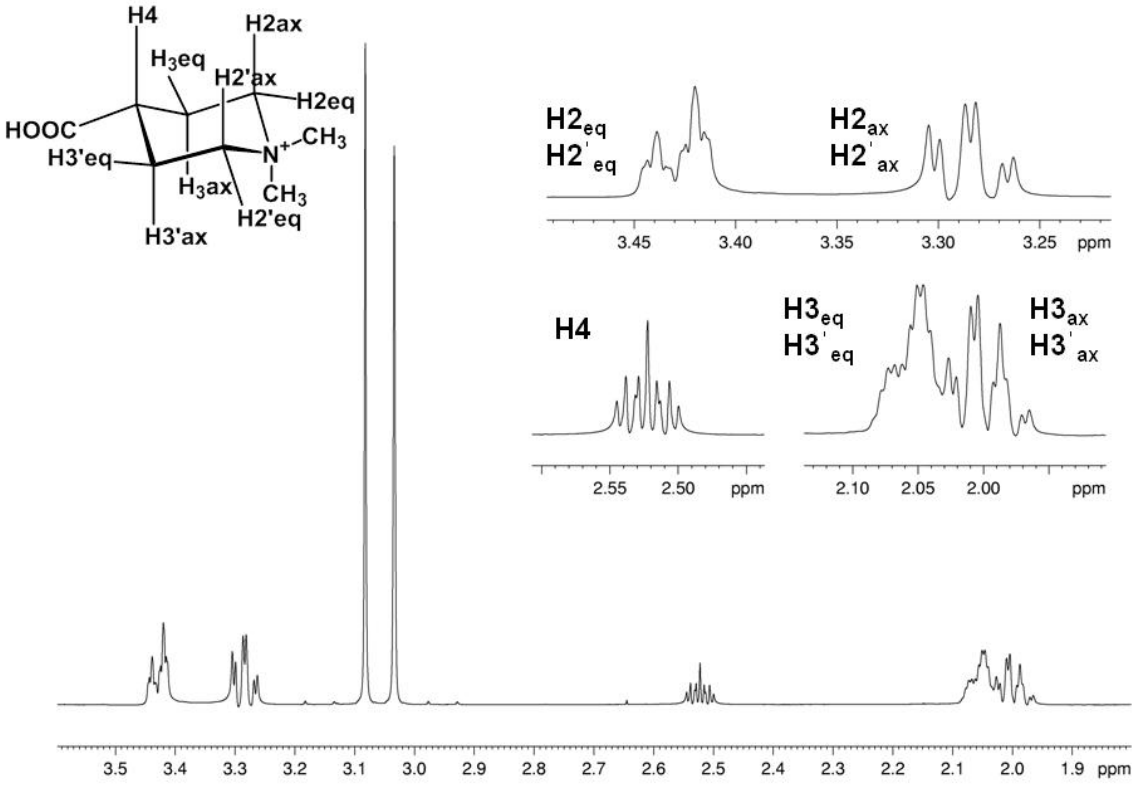

Figure 3 Conformation of *N*,*N*-dimethyl isonipecotic acid (**1**) as assigned by ^{1}H NMR. ^{1}H NMR (700 MHz, D_2O) δ ppm 3.43 (2H, dt, *J* = 13.1, 3.7 Hz, H_{2eq}, $H_{2'eq}$), 3.28 (2H, td, *J* = 12.7, 3.6 Hz, H_{2ax}, $H_{2'ax}$), 3.08 (3H, s, CH_3), 3.03 (3H, s, CH_3), 2.64 (1H, tt, *J* = 11.2, 4.6 Hz, H_4), 2.09-2.02 (2H, m, H_{3eq}, $H_{3'eq}$), 2.02-1.96 (2H, m, H_{3ax}, $H_{3'ax}$).

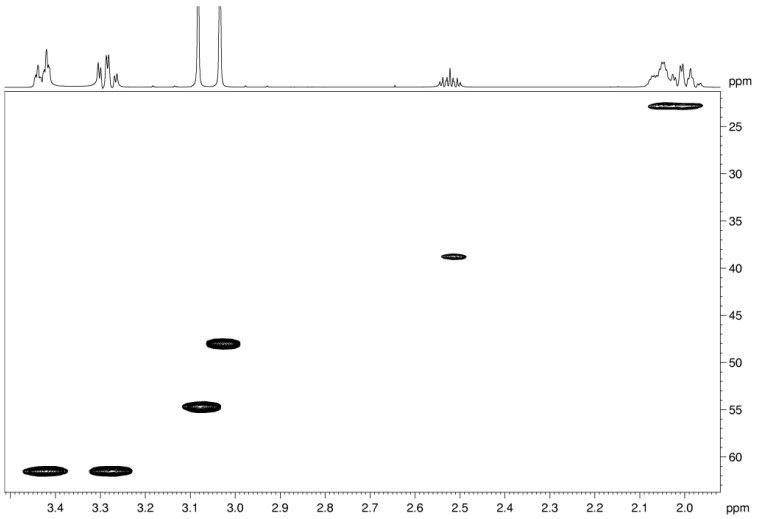

Figure 4 Conformation of *N*,*N*-dimethyl isonipecotic acid (**1**) as assigned by ^{1}H-^{13}C HSQC. ^{13}C NMR (from HSQC signals) (176 MHz, D_2O) δ ppm 61.5 (C_2, $C_{2'}$), 54.7 (CH_3), 47.9 (CH_3), 38.7 (C_4), 22.7 (C_3, $C_{3'}$).

2.4 Crystal structure of BBOX in complex with *N*,*N*-dimethyl isonipecotic acid

Having established what conformation (**1**) adopts in an aqueous solution, the actual mode of binding of (**1**) to BBOX was investigated. Human BBOX was crystallised with *N*,*N*-dimethylisonipecotic acid (**1**) and NOG (*N*-oxalyl glycine – a non reactive structural mimic of 2OG) in the presence of Ni(II) (a Fe(II) surrogate). A crystal structure obtained at 1.9 Å resolution (H32 space group, PDB id: 4CWD) reveals a homodimer, as observed in the case of the crystal structure of BBOX in complex with GBB and NOG (PDB id: 3O2G)[19] and solution analyses.[20]

The overall fold of the enzyme is very similar to that obtained for the human BBOX structure in complex with GBB, NOG and Zn(II) (PDB id: 3O2G)[19] (Fig. 5A). The active site loop, which was proposed to move upon substrate binding,[21] is in the closed position as in the GBB complexed structure. The positioning of an active site residues in the BBOX.(**1**).NOG.Ni(II) complex structure is very similar to those in a BBOX.GBB.NOG.Zn(II) structure (PDB id: 3O2G). The position of the metal, 2OG and substrate binding residues is well conserved, demonstrating that (**1**) does not perturb significantly interactions within the active site and the overall BBOX folding. A view from the active site of BBOX.(**1**).NOG.Ni(II) complex has also shown that (**1**) is bound in the chair conformation, with the carboxylate in the equatorial position (pro-*S*) (Fig. 5C), as suggested by in-solution NMR analyses. The conformational arrangement of the hydroxylated site of (**1**) is essentially identical with the position of the hydroxylation site of GBB (Fig. 5B). Part of the typical catalytic cycle of 2OG dependent oxygenases involves a step in which hydrogen is abstracted from the substrate and the corresponding radical is formed. The abstracted hydrogen is usually pointing towards the active site iron. In the BBOX.(**1**).NOG.Ni(II) complex, the equatorial H3 (pro-*R*) of analogue (**1**) is pointing towards the metal in the active site and therefore it is likely to be abstracted in the catalytic cycle. Thus, (*3R*)-hydroxy-(*4S*)-isonipecotic acid is likely a candidate for the hydroxylation product of BBOX catalysed turnover of (**1**).

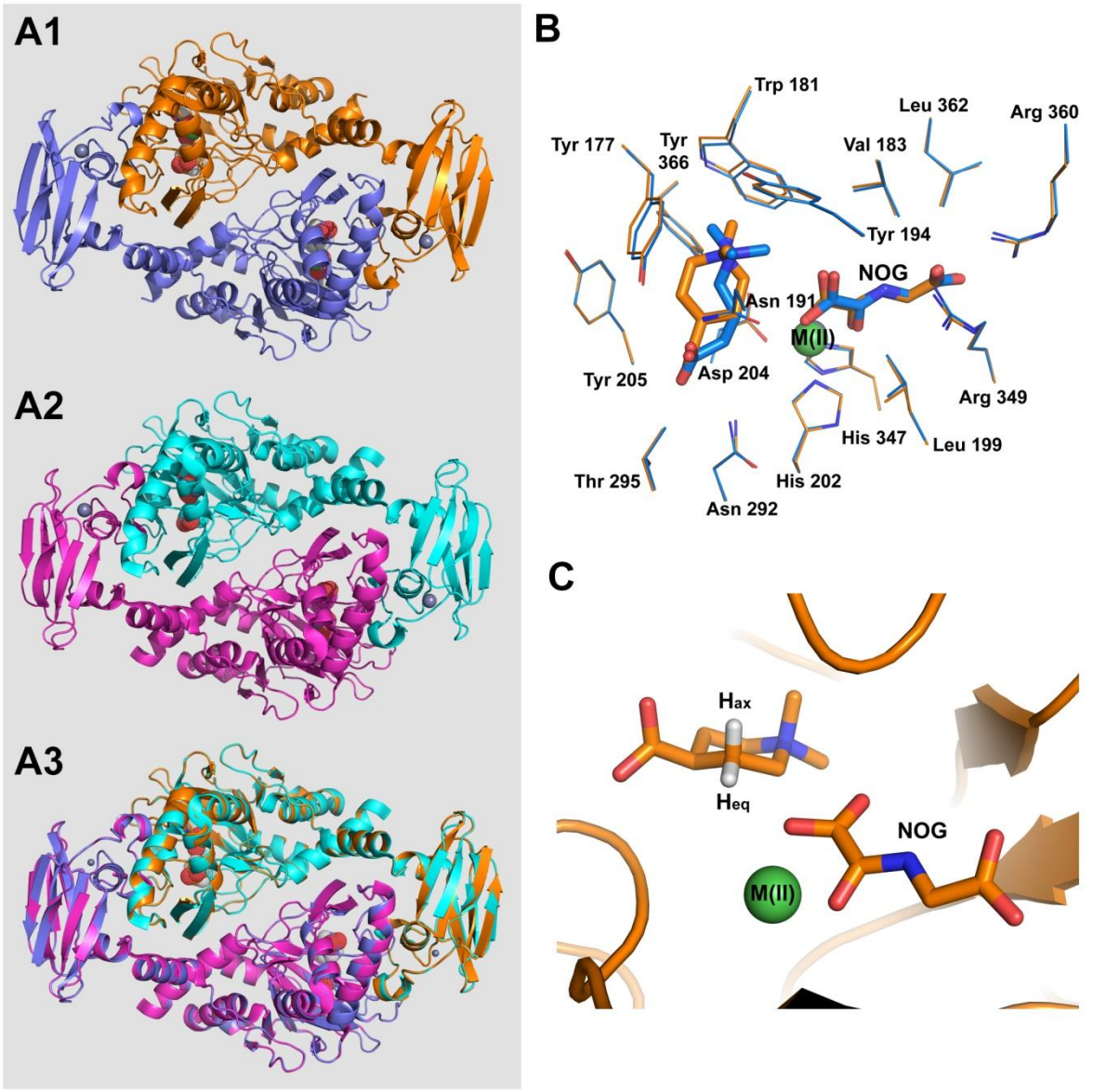

Figure 5 Views from the crystal structure of human BBOX in complex with *N*,*N*-dimethylisonipecotic acid (**1**), NOG and Ni(II). A – The overall structure of the BBOX.(**1**).NOG.Ni(II) complex dimer (PDB id: 4CWD) (A1), BBOX.GBB.NOG.Zn(II) complex dimer (PDB id: 3O2G) (A2) and the overlay of both dimers reveal high structural similarity of both complexes. B – Overlay of the active sites of BBOX.(**1**).NOG.Ni(II) complex (orange) and BBOX.GBB.NOG.Zn(II) complex (blue) demonstrates similar positioning of substrates and metal binding amino acids. C – View from the active site of BBOX.(**1**).NOG.Ni(II) complex demonstrates equatorial H3 is position towards metal, and thus this position is likely prone to hydroxylation during catalytic cycle.

2.5 Reaction of BBOX with *N*,*N*–dimethyl isonipecotic acid

The assignment of BBOX catalysed hydroxylation of (**1**) was analysed by NMR. Upon treatment of (**1**) with BBOX in the mixture containing 2OG, Fe(II) and KCl, a second set of peaks characteristic for cyclic GBB analogue was observed. Furthermore, 2OG was decarboxylated to succinate, in agreement with the 2OG dependent oxygenases mechanism. *N*,*N*–Dimethyl isonipecotic acid (**1**) gave only one product upon reaction with BBOX, which was assigned as 3-hydroxy-*N*,*N*-dimethylisonipecotic acid (Scheme 1) with the aid of ^{1}H NMR (Fig. 6) and ^{1}H-^{13}C HSQC spectra of reaction mixture (Fig. 7). The analysis of the coupling constants revealed that both hydrogens linked to the same carbons as the carboxylate and hydroxyl groups were in the axial positions (C_4-H: J_{aa} = 12.4 Hz, J_{aa} = 10.5 Hz, J_{ae} = 4.7 Hz; C_3-H: J_{aa} = 10.8 Hz × 2, J_{ae} = 4.7 Hz). This is in agreement with crystallographic analyses, suggesting formation of (*3R*)-hydroxy-(*4S*)-isonipecotic acid. Because no double hydroxylation was observed in the *in vitro* assays, it is proposed that the crystal structure likely reflects the only productive positioning of the substrate (**1**) in the BBOX active site, and so enables proposed assignment of the absolute stereochemistry of the obtained product.

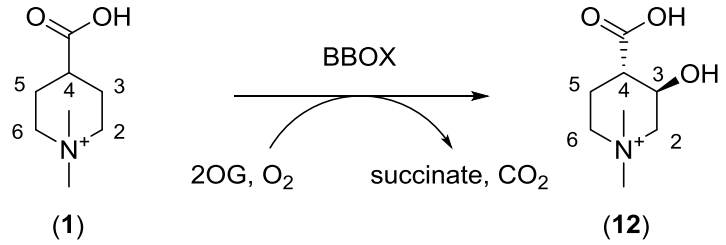

Scheme 1 BBOX catalysed hydroxylation of *N*,*N*- dimethyl isonipecotic acid. Reaction conditions: 0.5 mM *N*,*N*-dimethyl isonipecotic acid (**1**), 0.8 mM 2OG, 80 mM KCl, 50 μM Fe(II), 8 μM hBBOX, Tris-d_{11} 50 mM pH 7.5 D_2O.

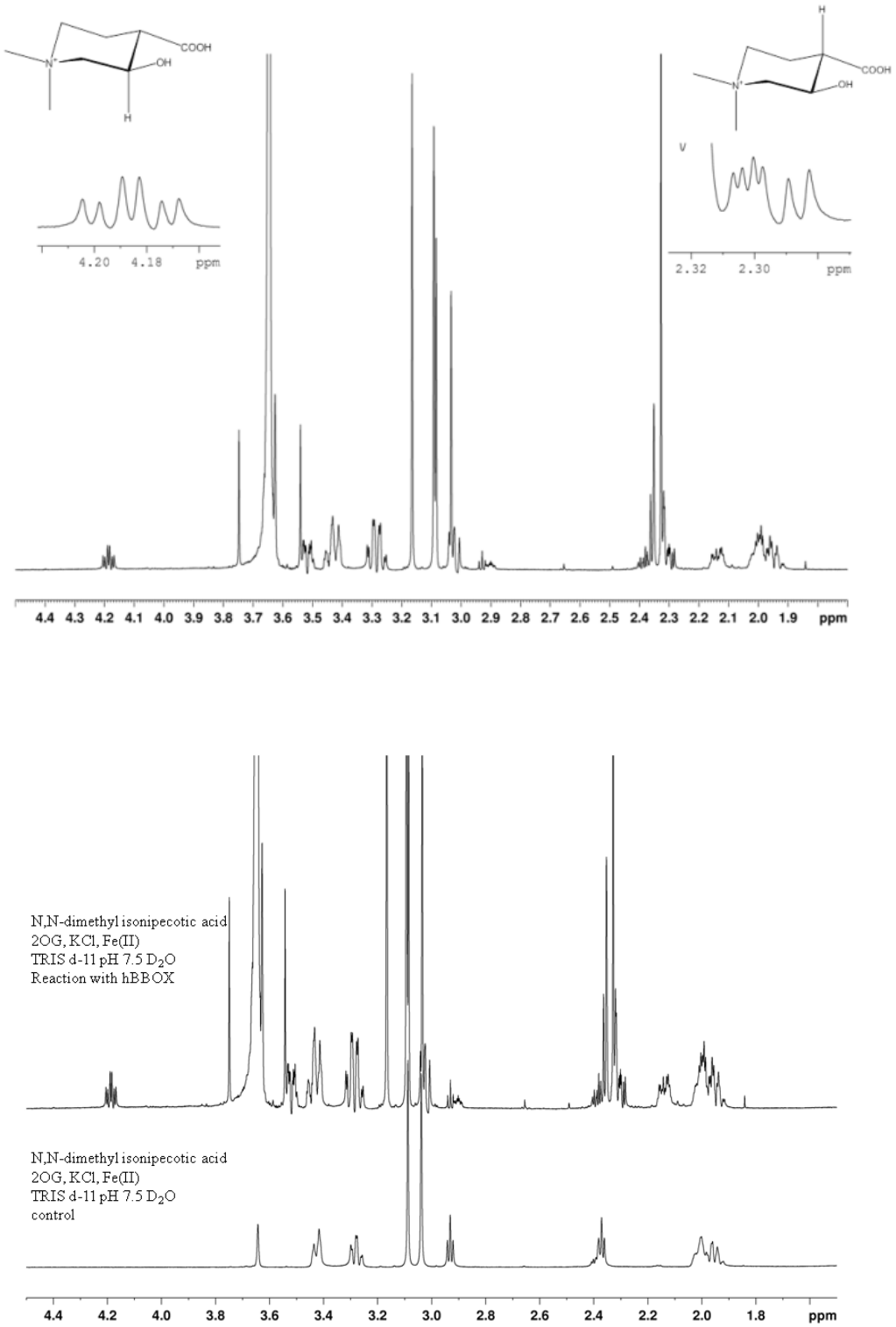

Figure 6 ^{1}H NMR assignments of the BBOX catalysed hydroxylation of *N*,*N*-dimethyl isonipecotic acid (**1**) (top). Overlay of reaction and mixture before enzyme added (bottom). ^{1}H NMR (700 MHz, D_2O) δ ppm 4.18 (1H, td, *J* = 10.8, 4.7 Hz, H_3), 3.54-3.49 (1H, m, H_2), 3.47-3.42 (1H, m, H_{6eq}), 3.33-3.28 (1H, m, H_{6ax}), 3.16 (3H, s, CH_3), 3.09 (3H, s, CH_3), 3.04-3.00 (1H, m, $H_{2'}$), 2.30 (1H, ddd, *J* = 12.4, 10.5, 4.7 Hz, H_4), 2.17-2.11 (1H, m, H_5), 1.97 (1H, m, $H_{5'}$).

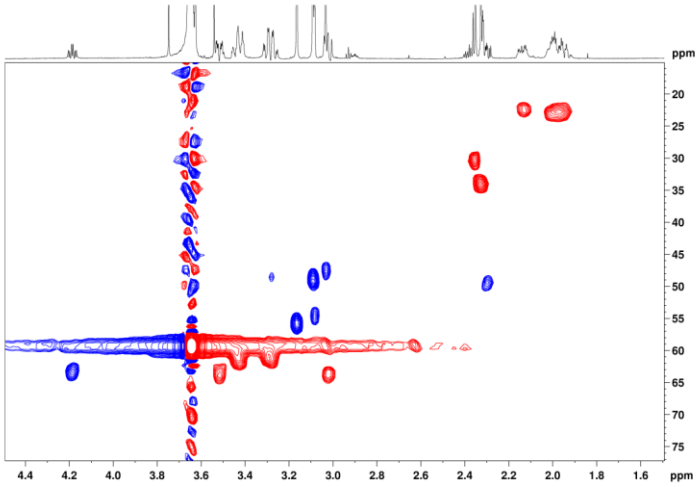

Figure 7 ^{1}H-^{13}C HSQC spectra of *N*,*N* – dimethyl isonipecotic acid (**1**) reaction with BBOX. ^{13}C NMR (from HSQC signals) (176 MHz, D_2O) δ ppm 63.7 (C_2), 63.4 (C_3), 61.8 (C_6), 54.7 (CH_3), 49.5 (C_4), 47.5 (CH_3), 22.52 (C_5).

2.6 *N*-Methyl-*N*-ethyl isonipecotic acid is a BBOX substrate

Following the example of *N*,*N*-dimethyl isonipecotic acid (**1**), it was investigated if any other alkylated isonipecotic acid derivative could serve as a BBOX substrate. The precedent of *N*-fluoromethyl GBB (described in Chapter 2) demonstrated that analogues with larger *N*-substituents than methyl group can also be accepted as BBOX substrates. Therefore, the *N*-methyl-*N*-ethylisonipecotic acid (**13**) was of interest, in particular because its hydroxylation could lead to simultaneous formation of three stereocentres. The MS analyses have shown the appearance of a +16 peak in the BBOX treated sample of *N*-ethyl-*N*-methyl isonipecotic acid (**13**) (Fig. 8).

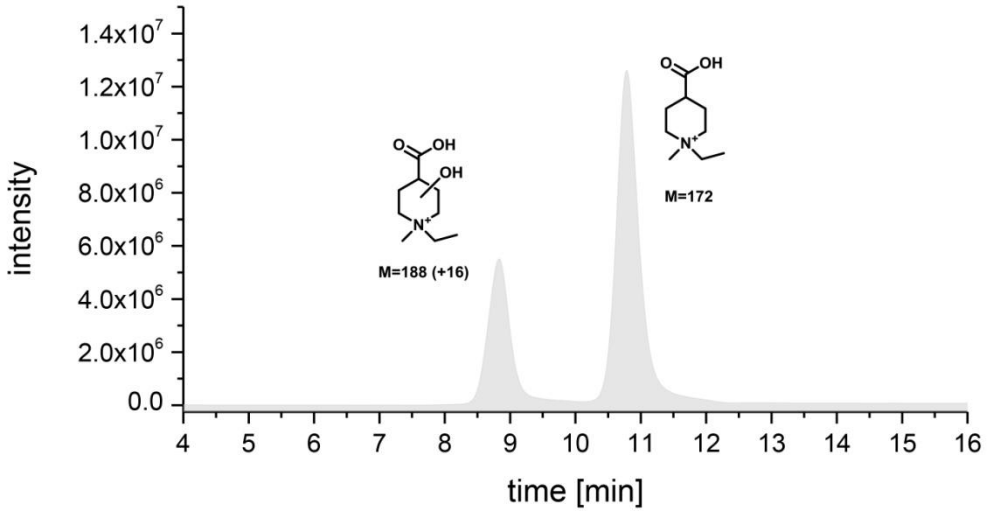

Figure 8 LC-MS chromatogram of the reaction of BBOX with *N*-methyl-*N*-ethylisonipecotic acid (**13**). Spectra were recorded in mass range 120-300 Da (scan mode), single ion mode used in parallel to monitor masses: 172 (substrate, rt = 10.79 min) and 188 (product, rt = 8.86 min).

2.6.1 Conformational assignments of *N*-methyl-*N*-ethylisonipecotic acid (13)

N-Methyl-*N*-ethylisonipecotic acid (**13**) was prepared from commercially available *N*-methyl isonipecotic acid (**3**) and *N*-ethyl isonipecotic acid (**14**). In both cases, the resulting product was a mixture of two isomers (Scheme 2).

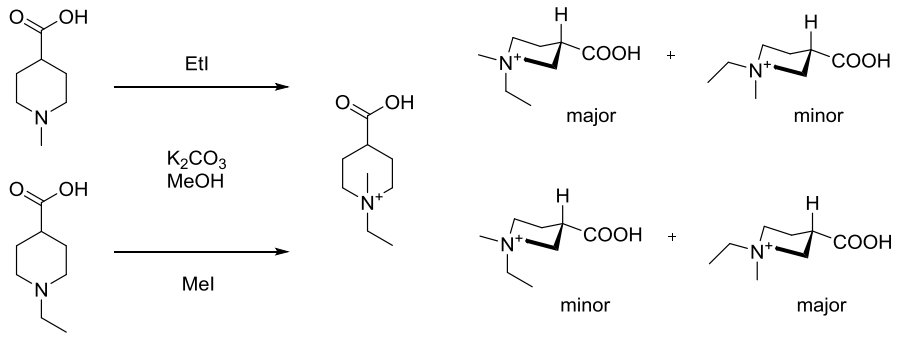

Scheme 2 Synthesis of *N*-ethyl-*N*-methyl isonipecotic acid (**5**).

The identity of the isomers was assigned using NMR spectroscopy. The methyl group position was confirmed by an nOe signal pattern (Fig. 9). A proton attached to C4, adjacent to the carboxylate was assigned to be axial in both isomers of (**13**) by the coupling constants pattern (isomer A: J_{aa} = 10.2 Hz, J_{ae} = 5.1 Hz; isomer B: J_{aa} = 11.5 Hz, J_{ae} = 4.8 Hz) (Fig. 10 and 11).

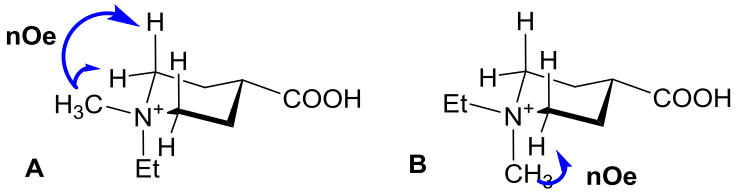

Figure 9 nOe correlations for isomers of *N*-ethyl-*N*-methyl isonipecotic acid.

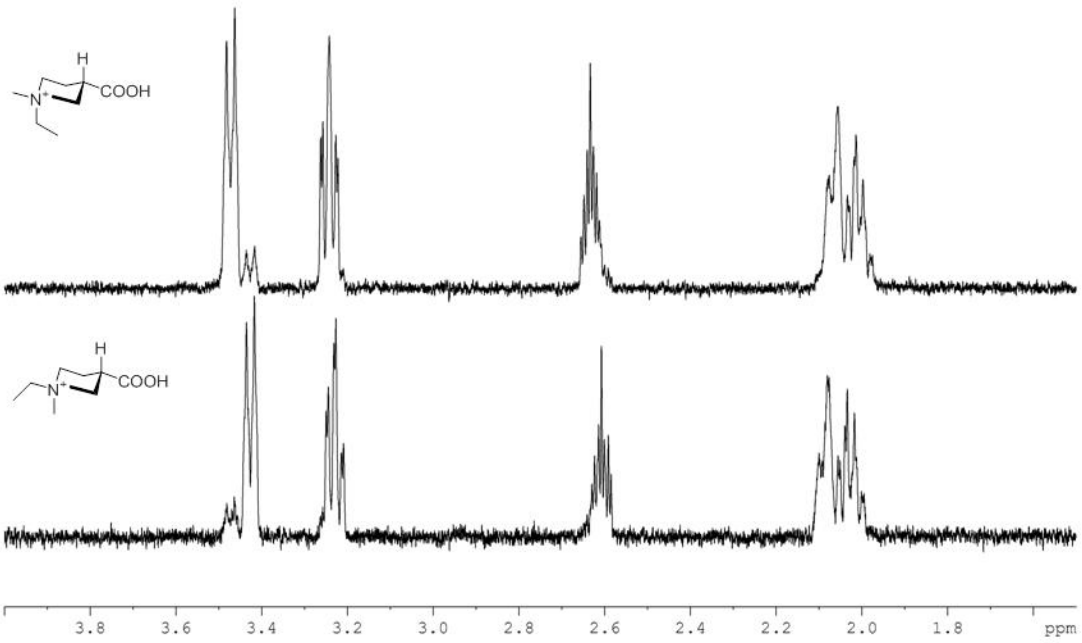

Figure 10 1D TOCSY spectra for *N*-ethyl-*N*-methylisonipecotic acid (**13**) isomers.

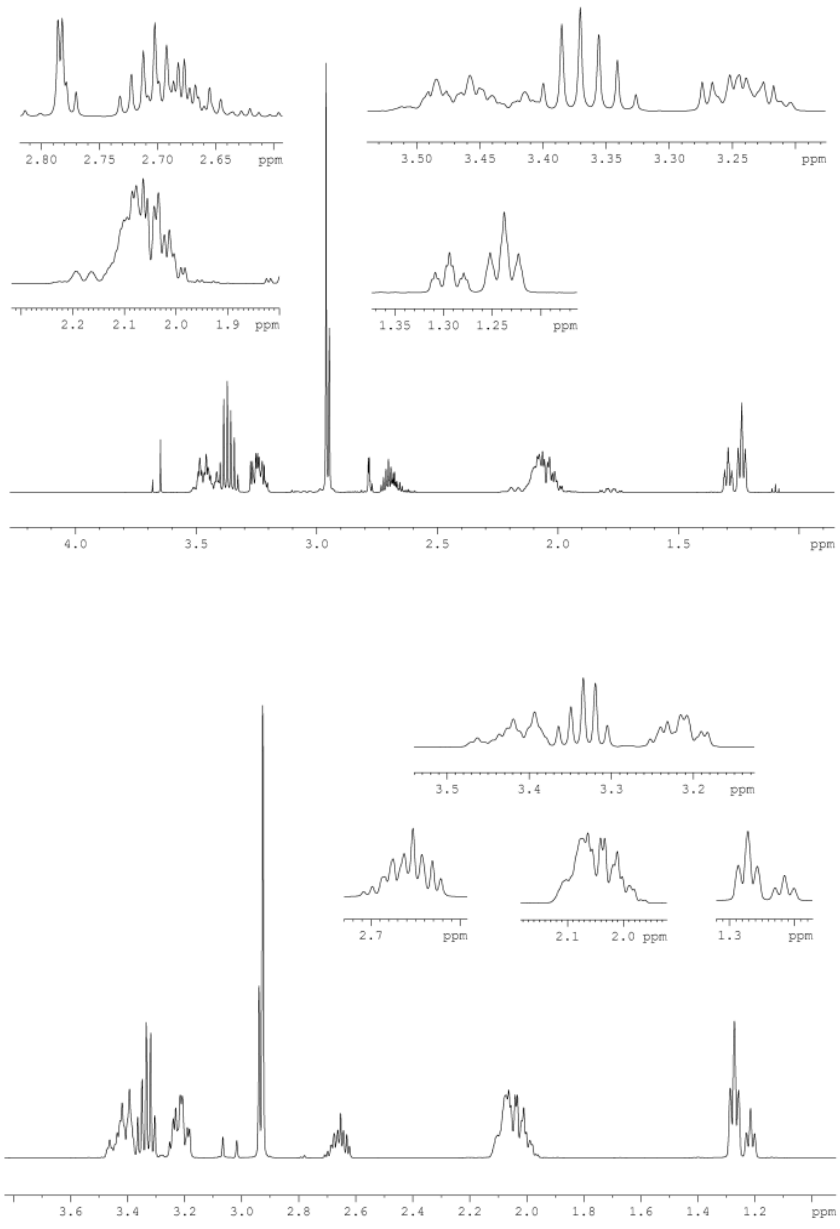

Figure 11 ^{1}H NMR spectra of *N*,*N*-methyl ethyl isonipecotic acid (**13**) obtained by alkylation of *N*-methyl isonipecotic acid (top) or *N*-ethyl isonipecotic acid (bottom). Isomer A: ^{1}H NMR (700 Hz, D_2O) δ ppm 3.47 (2H, dt, *J* = 13.3, 4.4 Hz, H_{2eq}, $H_{2'eq}$), 3.38 (2H, q, *J* = 7.5 Hz, CH_2CH_3), 3.24 (2H, td, *J* = 11.5, 3.8 Hz, H_{2ax}, $H_{2'ax}$), 2.96 (3H, s, CH_3), 2.63 (1H, tt, *J* = 10.2, 5.1 Hz, H_4), 2.12-1.99 (4H, m, H_{3eq}, $H_{3'eq}$, H_{3ax}, $H_{3'ax}$), 1.25 (3H, t, J = 7.8, CH_2CH_3). ^{13}C NMR (from HSQC signals) (176 MHz, D_2O) δ ppm 59.3 (C_2, $C_{2'}$), 53.7 (CH_2CH_3), 50.8 (CH_3), 37.8 (C_4), 22.2 (C_3, $C_{3'}$), 6.44 (CH_2CH_3). Isomer B: ^{1}H NMR (700 Hz, D_2O) δ ppm 3.43 (2H, dt, *J* = 13.5, 3.8 Hz, H_{2eq}, $H_{2'eq}$), 3.35 (2H, q, *J* = 7.5 Hz, CH_2CH_3), 3.22 (2H, td, *J* = 13.1, 3.6 Hz, H_{2ax}, $H_{2'ax}$), 2.95 (3H, s, CH_3), 3.03 (3H, s, CH_3), 2.61 (1H, tt, *J* = 11.5, 4.8 Hz, H_4), 2.12-1.99 (4H, m, H_{3eq}, $H_{3'eq}$, H_{3ax}, $H_{3'ax}$), 1.30 (3H, t, J = 7.8, CH_2CH_3).

2.6.2 Product assignment

The structure of the product of BBOX catalysed hydroxylation of (**13**) was assigned with the aid of NMR spectroscopy. It appears that isomers A and B of (**13**) act differently in the BBOX catalysed hydroxylation. Analogue (**13a**) is a preferred substrate for BBOX, while (**13b**) is almost non-reactive. The small amount of hydroxylation product for (**13b**) was obtained at high concentrations of BBOX (>40 µM). The reaction of (**13a**) with BBOX yielded a single diastereomer: (*1R,3R,4S*)-4-carboxy-1-ethyl-3-hydroxy-1-methylpiperidin-1-ium (**15a**) (Fig. 12). The conformation of (**15a**) was assigned from coupling constants pattern in ^{1}H NMR (Fig. 13). The reaction gave a product with equatorial carboxylate (H4 axial; J_{aa} = 12.2 Hz, J_{aa} = 10.4 Hz, J_{ae} = 4.8 Hz) and equatorial hydroxyl group (H3 axial; J_{aa} = 10.4 Hz × 2, J_{ae} = 4.4 Hz) (Fig. 13), similarly to the reaction of *N,N*-dimethyl isonipecotic acid (**1**) with BBOX.

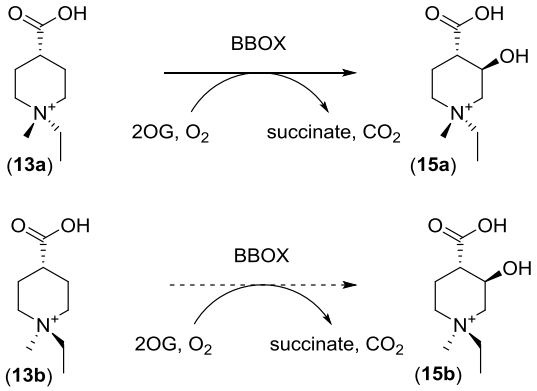

Figure 12 BBOX catalysed hydroxylation of *N*-methyl, *N*-ethyl isonipecotic acid (**13**) conformers.

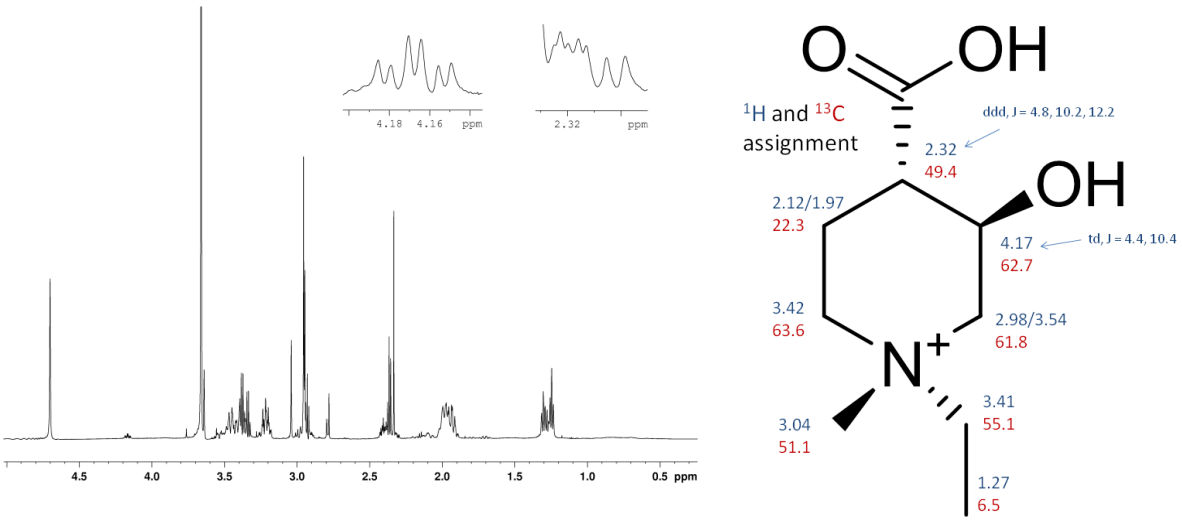

Figure 13 ^{1}H and ^{13}C NMR assignments of product of BBOX catalysed hydroxylation of *N*-methyl-*N*-ethyl isonipecotic acid (**13**).

3 BBOX catalysed oxidations of cyclic GBB analogues

3.1 Kinetic analyses of cyclic BBOX substrates

Analogues (**1**) and (**13a**) were evaluated as BBOX substrates in comparison to GBB (Table 1). In the case of both cyclic analogues the initial rate was around two times slower than the one measured for GBB. The amount of uncoupled 2OG turnover was similar to the amount recorded for GBB catalysed hydroxylation (Table 1). For the *N*,*N*-dimethyl isonipecotic acid (**1**) further kinetic measurements were done. K_M value of 25 µM was obtained, which is slightly higher than the K_M for GBB (4 µM). The V_{max} was 0.040 µM/s and k_{cat} 0.15 1/s, which is lower than the value obtained for a GBB (k_{cat} 0.83 1/s). Interestingly, the substrate inhibition was observed only above 0.2 mM of (**1**), while for GBB substrate inhibition occurs over 20 µM of GBB concentration.

Table 1 Initial rates of product formation in reaction of BBOX with GBB and cyclic analogues (**4**) and (**5a**)

substrate	Initial rate of hydroxylation [µM/s]	Initial rate of succinate formation [µM/s]
GBB	0.130	0.162
(**1**)	0.059	0.078
(**13a**)	0.041	0.077

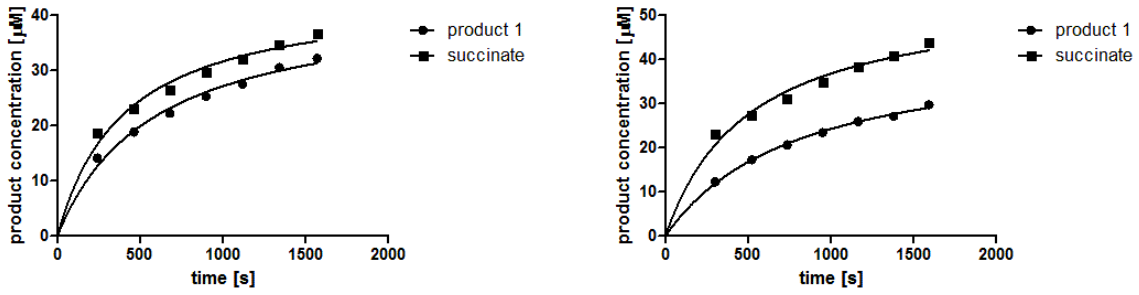

Figure 14 Time course of BBOX catalysed oxidation of (**1**) (left) and (**13a**) (right).

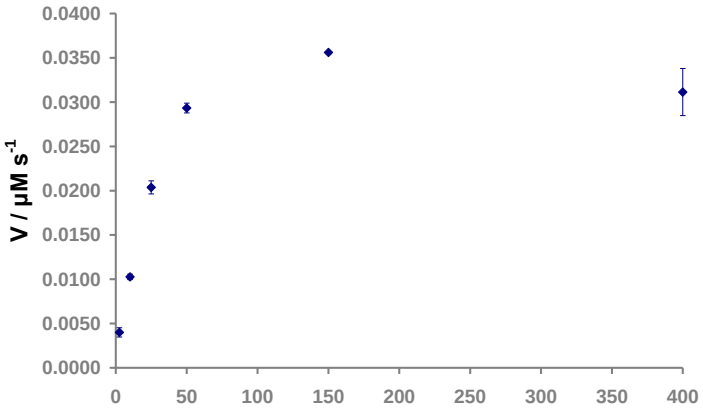

Figure 15 Dependence of the initial reaction rate on the concentration of cyclic GBB analogue (**1**).

4 Conformational assignments of other isonipecotic acid derivatives

When *N*-methyl isonipecotic (**3**) was ethylated the mixture of product isomers was A:B=2:1. The methylation of *N*-ethyl isonipecotic acid (**14**) led to mixture of isomers: A and B, with the ratio of 1:3. The difference in the product distribution might be caused by the different conformations of the substrates (**3**) and (**14**). Therefore the conformations of isonipecotic acid (**2**), *N*-methyl isonipecotic acid (**3**) and *N*-ethylisonipecotic acid (**14**) were examined. The conformational equilibria in the isonipecotic acid derivatives were not previously studied in detail. The conformation of such systems in physiological conditions is of interest, as they were shown to be GABA receptor agonists/antagonists[22-25].

4.1 Conformation of piperidine

The conformation of piperidine in a solution has been studied since 1960[26]. The preference for the chair conformation was quite clear; however the relative position of the hydrogen and lone pair on the nitrogen was questionable. Most of the studies supported equatorial position of N-H group[27], however that effect may be solvent dependent[26]. Piperidine was shown to undergo conformational exchange through ring inversion and nitrogen inversion (Fig. 16).

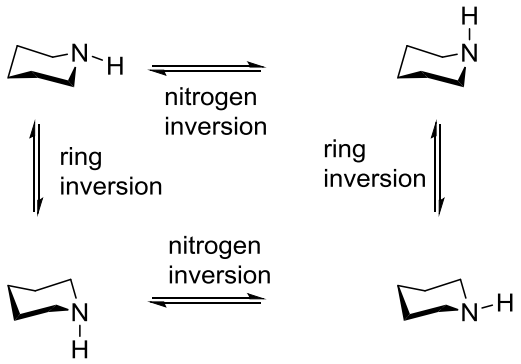

Figure 16 Conformations of piperidine.

4.2 Conformation of isonipecotic acid

The conformational equilibria of piperidine analogue – isonipecotic acid, were studied. A similar equilibrium can exist for isonipecotic acid (**2**), however the main form present in an aqueous solution was determined to be a chair conformation with the equatorial carboxylate. The carboxylate position was assigned from the coupling constants pattern in the ^{1}H NMR (Fig. 17). The proton at C4 was determined to be axial (H4: J_{aa} = 11.3 Hz, J_{ae} = 3.8 Hz).

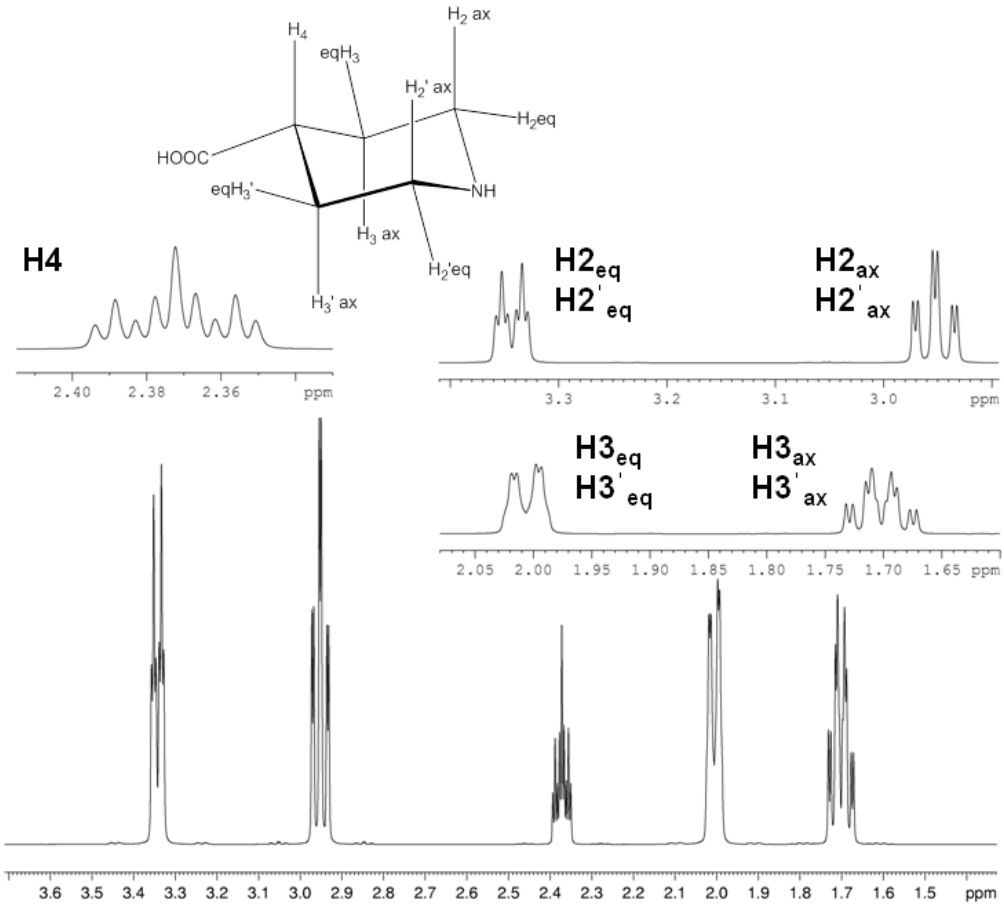

Figure 17 Conformation of isonipecotic acid (**1**) as assigned by ^{1}H NMR. ^{1}H NMR (700 MHz, D_2O) δ ppm 3.34 (2H, dt, *J* = 3.7, 13.0 Hz, H_{2eq}, $H_{2'eq}$), 2.95 (2H, td, *J* = 3.2, 12.6 Hz, H_{2ax}, $H_{2'ax}$), 2.37 (1H, tt, *J* = 3.8, 11.3 Hz, H_{4ax}), 2.03-1.98 (2H, m, H_{3eq}, $H_{3'eq}$), 1.74-1.67 (2H, m, H_{3ax}, $H_{3'ax}$).

4.3 Conformation of *N*-methyl isonipecotic acid

In general, there are four possible chair conformations of *N*-methyl isonipecotic acid (**3**), all interconvertible through ring inversion or nitrogen inversion (Fig. 18).

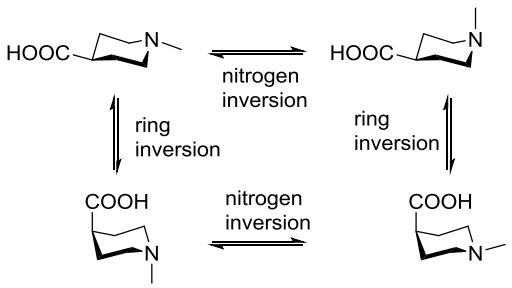

Figure 18 Possible conformations of *N*-methyl isonipecotic acid (**3**).

^{1}H NMR spectroscopy allows observation of two distinguishable conformations present at room temperature, one being predominant with a ratio of 3.5:1 of the major to the minor form of the compound (Fig. 19-22).

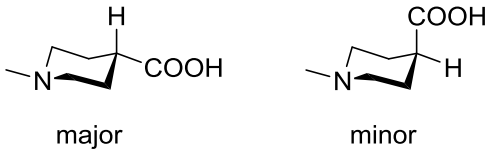

Figure 19 Structure of *N*-methyl isonipecotic acid (**3**) and its two chair conformations existing at room temperature.

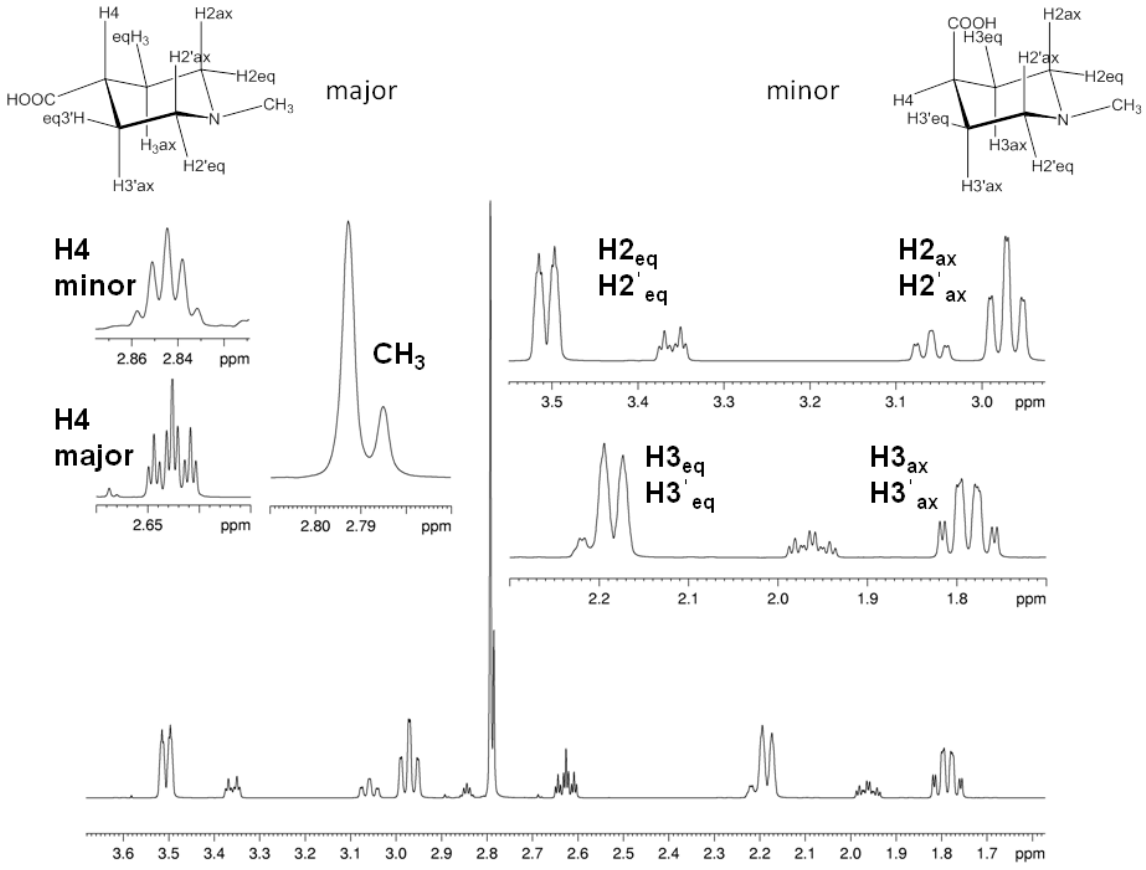

Figure 20 Conformations of *N*-methyl isonipecotic acid (**3**) as assigned by ^{1}H NMR. Major: ^{1}H NMR (700 MHz, D_2O) δ ppm 3.51 (2H, dt, *J* = 12.8, 1.9 Hz, H_{2eq}, $H_{2'eq}$), 2.97 (2H, td, *J* = 13.1, 2.2 Hz, H_{2ax}, $H_{2'ax}$), 2.79 (3H, s, CH_3), 2.63 (1H, tt, *J* = 12.4, 3.7 Hz, H_4), 2.18 (2H, dt, *J* = 14.8, 1.9 Hz, H_{3eq}, $H_{3'eq}$), 1.83-1.75 (2H, m, H_{3ax}, $H_{3'ax}$). Minor: ^{1}H NMR (700 MHz, D_2O) δ ppm 3.36 (2H, dt, *J* = 13.1, 4.1 Hz, H_{2eq}, $H_{2'eq}$), 3.06 (2H, td, *J* = 12.5, 2.5 Hz, H_{2ax}, $H_{2'ax}$), 2.84 (1H, q, *J* = 4.6 Hz, H_4), 2.78 (3H, s, CH_3), 2.20 (2H, m, H_{3eq}, $H_{3'eq}$), 1.96 (2H, ddt, *J* = 15.7, 11.4, 4.5 Hz, H_{3ax}, $H_{3'ax}$).

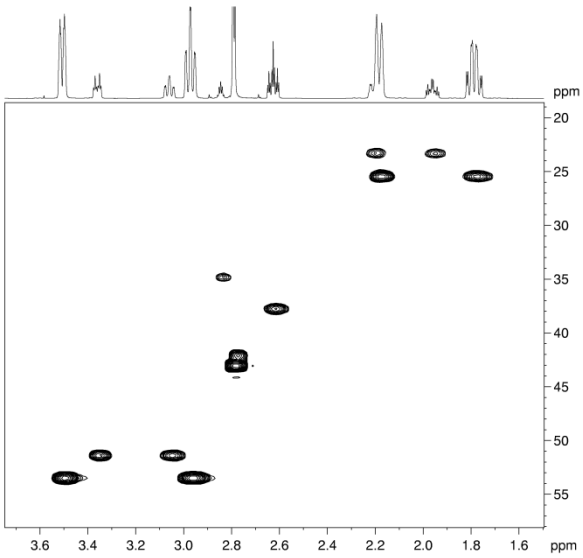

Figure 21 ^{1}H-^{13}C HSQC spectrum of *N*-methyl isonipecotic acid (**3**). Major: ^{13}C NMR (from HSQC signals) (176 MHz, D_2O) δ ppm 53.44 (C_2, $C_{2'}$), 43.06 (CH_3), 37.75 (C_4), 25.38 (C_3, $C_{3'}$). Minor: ^{13}C NMR (from HSQC signals) (176 MHz, D_2O) δ ppm 51.36 (C_2, $C_{2'}$), 42.09 (CH_3), 34.79 (C_4), 23.20 (C_3, $C_{3'}$).

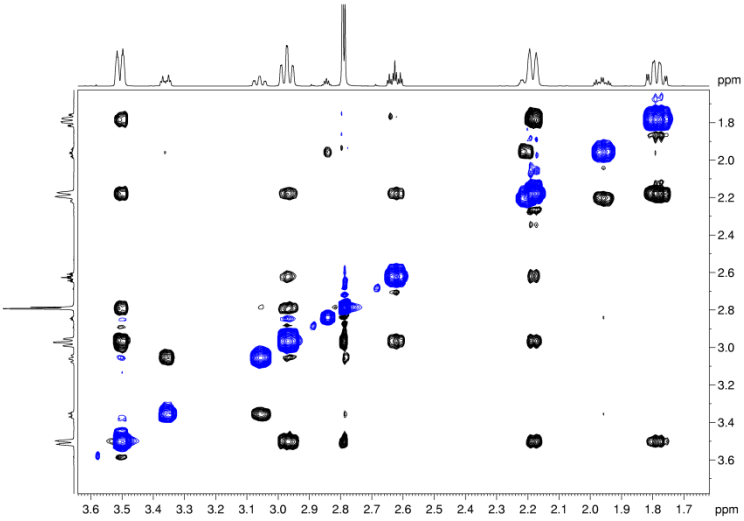

Figure 22 ^{1}H-^{1}H nOe spectrum of *N*-methyl isonipecotic acid (**3**).

4.3.1 Carboxylate position

The conformational position of the carboxylate was assigned from coupling constants of H4. The major form shows a typical pattern for an axial proton with signal at 2.63 ppm, being observed as a triplet of triplets with coupling constants of J_{aa}=12.4 and J_{ae}=3.7 Hz. In the minor isomer the H4 signal is shifted downfield to 2.84 ppm, which is characteristic for equatorial substituents. The signal also becomes broader with J_{ee} and J_{ea} coupling constants of equal value of 4.6 Hz. Thus, the carboxylate described as being in the axial position for the minor isomer (Fig. 20).

4.3.2 Methyl group position

The methyl group position was assigned from nOe spectra. nOe signals were observed between the *N*-methyl group and both axial and equatorial protons H2 and H2'. However, no nOe was observed between the methyl group and H3 nor the H3' protons, suggesting an absence of 1,3-diaxial interactions, which would be observed if the methyl group was in the axial position. Therefore the major conformational position of the methyl group was assigned as being equatorial for both conformers. For the major conformer one set of nOe experiments with variable mixing time was recorded. Plotting the relative peak intensity of the nOe between methyl group and $H3_{eq}$ or $H3_{ax}$ versus mixing time (referred to as a PANIC approach[28,29]) enables identification of direct and indirect nOe signals. The indirect nOe signal can be identified by the presence of a lag phase for short mixing times (when the nOe is not allowed to develop properly). The resultant plot suggest direct nOe between the methyl group and neighbouring axial protons and indirect correlations to the axial protons, which further confirms the equatorial position of the methyl group.

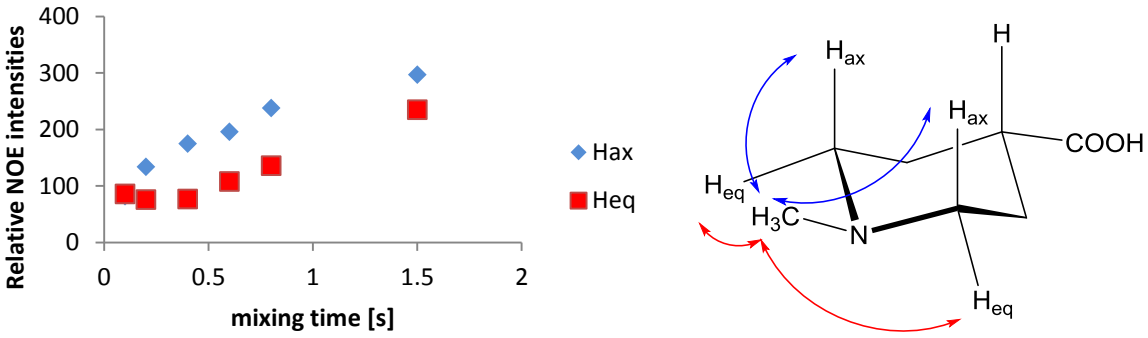

Figure 23 nOe assignments of the methyl group position in the *N*-methyl isonipecotic acid (**2**).

4.3.3 *p*K_a measurments

pK_a measurements were conducted for the major and minor form by monitoring chemical shift change of H4 signal under different pH range. Both forms were assigned *p*K_a = 4.0 (Fig. 24).

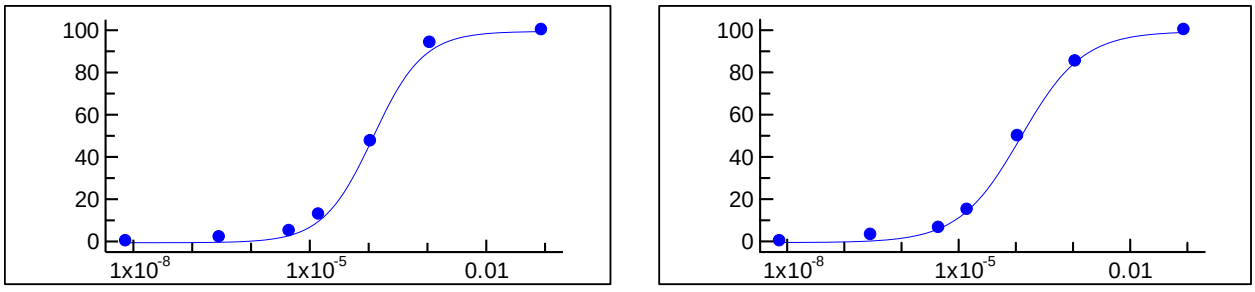

Figure 1 *p*K_a measurements – concentration of [H^+] as a function of % of chemical shift of H4 signal for major (left) and minor (right) isomer.

4.4 *N*-Ethylisonipecotic acid

N-Ethylisonipecotic acid (**14**) is, similarly to the *N*-methyl derivative, existing as two distinguishable conformers (Fig. **25**). Coupling constants patterns in the ^{1}H NMR (Fig. 26) similar to those obtained for *N*-methyl isonipecotic acid (**3**) suggest analogue (**14**) adopts similar conformation to (**3**). The ratio of major to minor conformer was like in case of (**3**) 3.5:1.

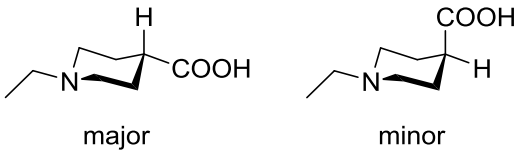

Figure 25 Structure of *N*-ethyl isonipecotic acid (**3**) and its two chair conformations existing at room temperature.

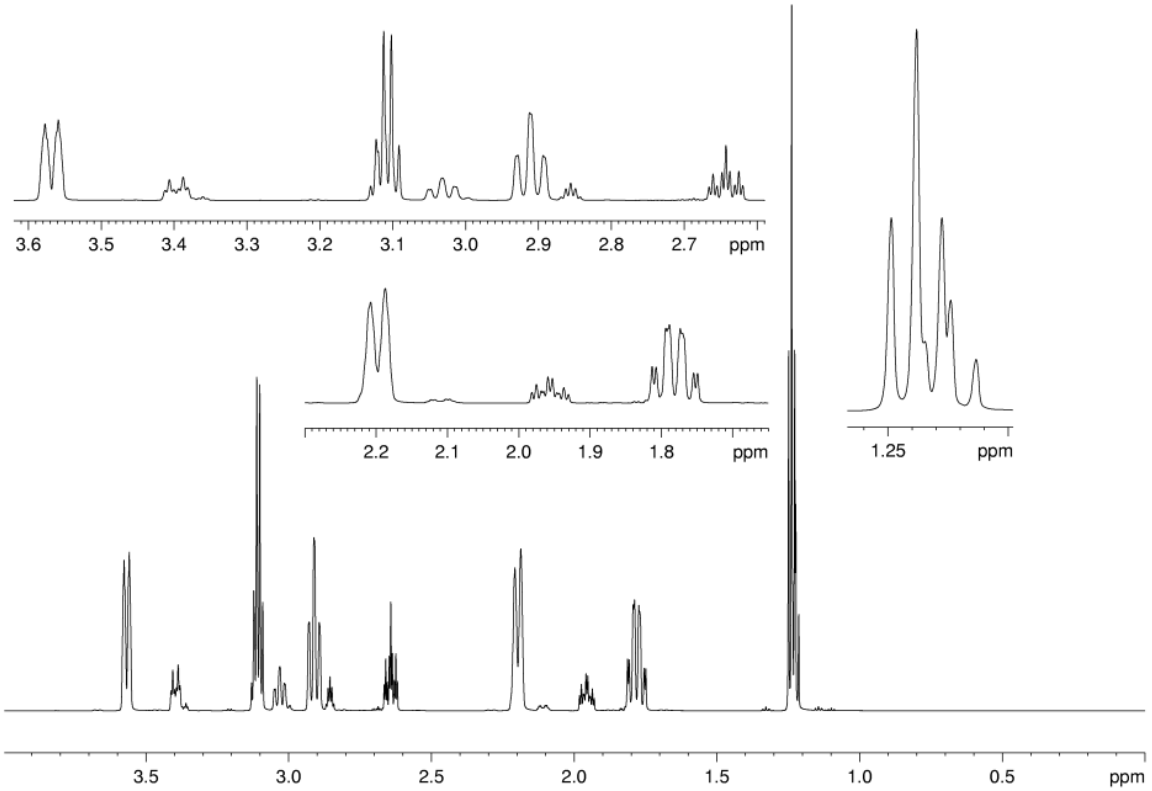

Figure 26 Conformations of *N*-ethyl isonipecotic acid (**3**) as assigned by ^{1}H NMR. Major: ^{1}H NMR (700 MHz, D_2O) δ ppm 3.57 (2H, dt, *J* = 12.8, 1.9 Hz, H_{2eq}, $H_{2'eq}$), 3.11 (2H, q, *J* = 7.3 Hz, C*H*$_2$CH$_3$), 2.91 (2H, td, *J* = 13.1, 1.9 Hz, H_{2ax}, $H_{2'ax}$), 2.64 (1H, tt, *J* = 12.3, 3.8 Hz, H_4), 2.24-2.16 (2H, m, H_{3eq}, $H_{3'eq}$), 1.83-1.74 (2H, m, H_{3ax}, $H_{3'ax}$), 1.24 (2H, q, *J* = 7.3 Hz, CH$_2$C*H*$_3$). Minor: ^{1}H NMR (700 MHz, D_2O) δ ppm 3.40 (2H, dt, *J* = 13.2, 4.0 Hz, H_{2eq}, $H_{2'eq}$), 3.12 (2H, q, *J* = 7.3 Hz, C*H*$_2$CH$_3$ overlapped with the corresponding signal of major isomer), 3.03 (2H, td, *J* = 12.7, 2.8 Hz, H_{2ax}, $H_{2'ax}$), 2.86 (1H, q, *J* = 4.7 Hz, H_4), 2.24-2.16 (2H, m, overlapped with signal for major isomer, H_{3eq}, $H_{3'eq}$), 1.96 (2H, ddt, *J* = 4.5, 11.6, 15.7 H_{3ax}, $H_{3'ax}$), 1.22 (3H, t, *J* = 7.3, CH$_2$C*H*$_3$).

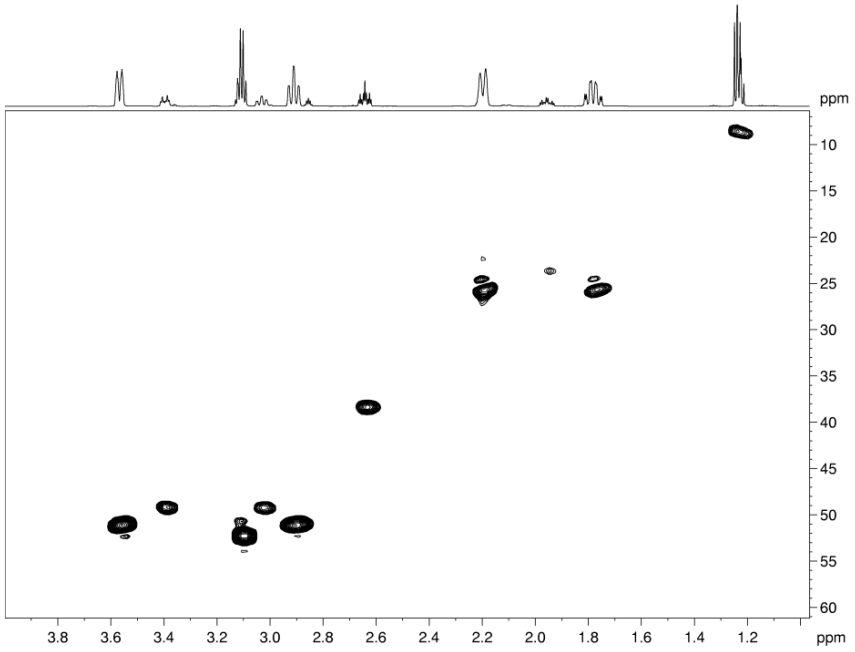

Figure 27 ^{1}H-^{13}C HSQC spectrum of *N*-ethyl isonipecotic acid (**14**). Major: ^{13}C NMR (from HSQC signals) (176 MHz, D_2O) δ ppm 52.21 (CH_2CH_3), 51.09 (C_2, $C_{2'}$), 38.28 (C_4), 25.64 (C_3, $C_{3'}$), 8.48 (CH_2CH_3). Minor: ^{13}C NMR (from HSQC signals) (176 MHz, D_2O) δ ppm 50.67 (CH_2CH_3), 49.17 (C_2, $C_{2'}$), 35.76 (C_4), 23.61 (C_3, $C_{3'}$), 8.81 (CH_2CH_3).

4.5 Influence of *N*-methylation on isonipecotic acid derivatives conformations

The analysis of coupling constants of H4 in the isonipecotic acid (**2**), *N*-methyl isonipecotic acid (**3**), and dialkylated isonipecotic acids (**1**) and (**13**) reveals that with the increasing *N*-methylation status J_{aa} are becoming smaller and J_{ae} larger (Fig. 28). The observed change in coupling constant values is usually connected to 6-membered ring flattening resulting in change of angles between neighbouring protons. The tendency to change coupling constant values can be observed upon methylation of nitrogen, i.e. isonipecotic acid (**2**) and its monomethylated form (**3**) display clear splitting pattern characteristic for axial protons, while for *N*,*N*-dimethyl isonipecotic acid (**1**) and *N*,*N*-ethylmethyl isonipecotic acid (**13**) as the coupling constant values become closer to each other, the pattern starts to resemble a septet (Fig. 28).

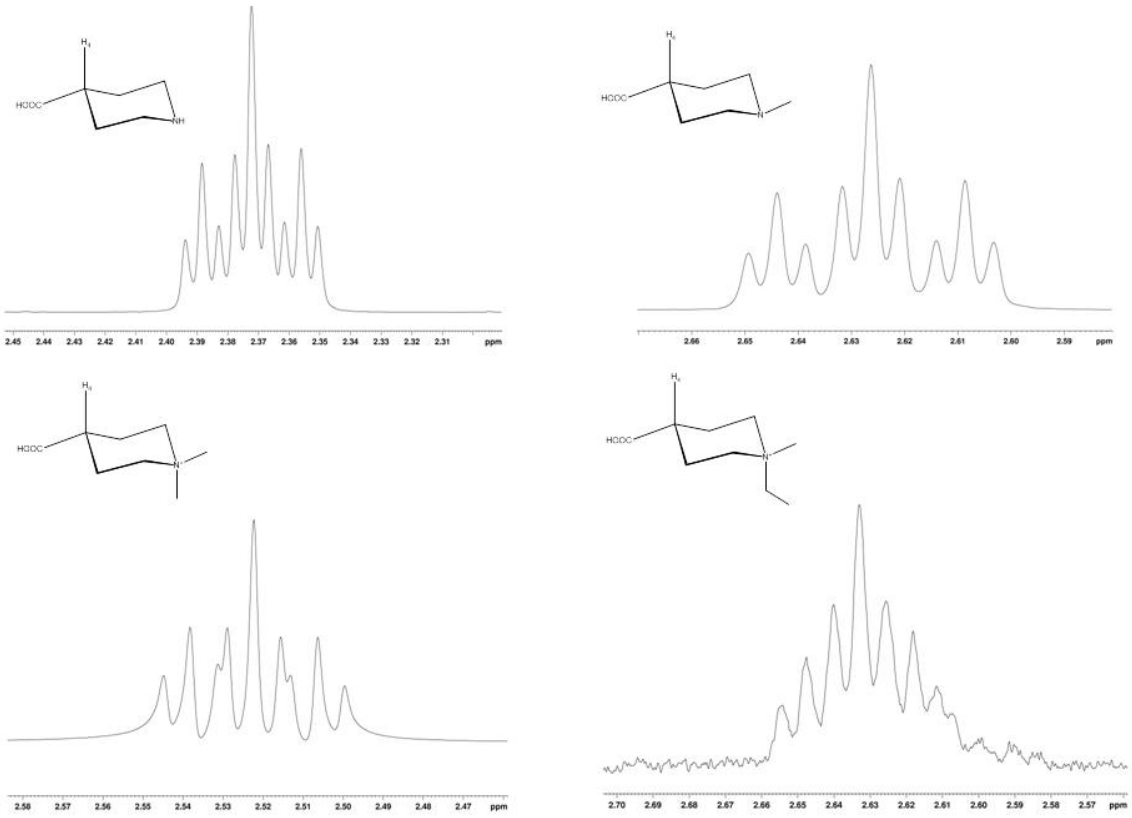

Figure 28 ^{1}H NMR signal of H4 in isonipecotic acid (**1**), *N*-methyl isonipecotic acid (**2**), *N*, *N* – dimethyl isonipecotic acid (**4**) and *N*-ethyl, *N*-methyl isonipecotic acid (**5**).

5 Summary and perspective

BBOX was shown to catalyse a desymmetrisation of *N*,*N*-dialkyl isonipecotic acids, with the simultaneous production of up to three chiral centres in one reaction. The conformation of the piperidine-based starting materials and the corresponding oxidation products in solution was studied by means of 1D and 2D NMR techniques. BBOX can be used as a valuable catalyst for the synthesis of chiral quaternary ammonium salts, for use as chiral phase-transfer catalysts or chiral auxiliaries. The results highlight the potential of 2OG dependent oxygenases for desymmetrisation of achiral compounds with concomitant introduction of multiple chiral centres. The limitations in the range of accepted substrates can be further addressed by the modifications of naturally occurring enzymes, especially with the constantly growing amount of structural information available on 2OG dependent oxygenases. Thus, 2OG dependent oxygenases have considerable potential both for the production of chiral starting materials for high-value chemical production, and for the late stage oxidations of bioactive compounds.

6 Acknowledgements

Human BBOX used in these studies was supplied by Dr. Grazyna T. Kochan (Structural Genomics Consortium, Oxford). K_M measurement for analogue (**1**) was done by Dr. Ivanhoe K.H. Leung (Department of Chemistry, University of Oxford). Dr Ivanhoe Leung is acknowledged for useful discussions on NMR assignments of GBB analogues hydroxylation products and Dr. Nikita Loik (Department of Chemistry, University of Oxford) for his assistance and advice on initial MS screen in search for BBOX substrates. Crystal structure of BBOX in complex with N,N-dimethyl isonipecotic acid was solved by Dr. Michael McDonough (Department of Chemistry, University of Oxford).

7 Experimental section

7.1 NMR

NMR assays were performed on Bruker AVIII 700 with inverse TCI cryoprobe using 3 mm MATCH tubes. Pulses were calibrated using single-pulse nutation method (Bruker pulsecal routine). Water suppression was achieved using the excitation sculpting method.

7.1.1 Hydroxylation product assignment

Hydroxylation reactions were performed using the following conditions: 0.8 mM 2OG (disodium salt), 80 mM KCl, 50 µM Fe(II) (used as an $(NH_4)_2Fe(SO_4)_2$ salt and prepared freshly before reaction start), 0.2 mM GBB analogue in 50 mM TRIS-d11 pH 7.5 in D_2O. Reaction was started by addition of human BBOX to the final concentration of 8 µM. Mixture was incubated overnight and then products were assigned using ^{1}H and ^{1}H-^{13}C HSQC NMR.

7.1.2 Time course assays

Time course assays were run using the following conditions: GBB/GBB analogue 100 µM, 2OG 0.5 mM (disodium salt), ascorbate 0.5 mM (mono potassium salt), KCl 200 mM, Fe(II) 50 µM (used as an $(NH_4)_2Fe(SO_4)_2$ salt and prepared freshly before reaction start) in 50 mM TRIS d-11 pH 7.5, 10% D_2O. Reaction was initiated by the addition of human BBOX to the final concentration of 400 nM. First spectrum was measured after 210 sec from the reaction start. Each spectrum was measured with 16 transients.

7.2 MS

7.2.1 Initial screen

Initial screens for BBOX substrates were performed on Waters LCT Premier Instrument, employing Electron impact Chemical Ionisation, fitted with time of flight (ToF) analyser. Samples were measured using direct injection (no column attached) and analysed for the presence of a +16 peak.

Enzymatic assays were run in the following conditions: 100 µM substrate, 1 mM 2-oxoglutarate disodium salt, 100 µM Fe(II) ($Fe(NH_4)_2(SO_4)_2$ salt, solution prepared fresh before experiment from concentrated stock in 20 mM HCl), 200 mM KCl, 500 µM ascorbic acid sodium salt, 1 µM enzyme, buffer: 50 mM phosphate pH 7.0, final volume 200 µL. Each assay contained samples run with BBOX and control with no enzyme added.

7.2.2 LC-MS method

Chromatographic separation of the GBB analogues was performed using mixed mode chromatography. Chromatographic separation was performed using an Aquity UPLC system (Waters). Column: PrimeSep 200 mixed mode, 2.1×250mm, particles 5µm (SIELC, Prospect Heights, US). Mobile phase: Solvent A – 9:1 H_2O-acetonitrile mixture, 0.05% formic acid, solvent B

– 8:2 H_2O-acetonitrile mixture, 0.2% formic acid. Gradient: Linear gradient from 0% to 100% B in 25 min, column reconditioning: 25-26 min from 0% to 100% A, 26-30 min 100% A. Flow rate: 0.3 mL/min. Injection volume 10 µL. Detection was performed using a Waters Quattro Micro instrument (triple quadrupole MS, electrospray ionisation, positive ion mode). The single ion mode was used and scan mode was running in parallel as a control. The reaction samples were prepared as described in the method for initial MS screening.

7.3 Crystallography

Crystallization was performed in 24-well plates; hanging drops were equilibrated against 400 µl of reservoir solution. Drops consisted of 1 µl reservoir solution and 1 µl protein solution. The reservoir solution contained: 0.2 M ammonium citrate, 1 mM $NiSO_4$, 4% 1, 6-diaminohexane, 19% PEG 3350. Protein (20 mg/ml) was in TRIS buffer (50 mM pH 7.5) containing 200 mM NaCl and was supplemented with 5 mM N, N- dimethylisonipecotic acid (**4**) and 10 mM NOG (100 mM stock solutions in TRIS 50 mM, pH adjusted to 7.0) prior to crystallization. Crystals formed after a week were used for micro seeding to yield bigger crystals which formed overnight. No crystals were observed in the presence of GBB. Crystals were flash cooled in liquid nitrogen using 25% glycerol in mother liquor as a cryoprotectant.

7.4 Synthesis

7.4.1 General information

Non-methylated precursors and *N*-methyl isonipecotic acid and *N*-ethyl isonipecotic acid were from Sigma-Aldrich.

7.4.2 General procedure for synthesis cyclic GBB analogues

The appropriate amino acid (1 equiv.) was dissolved in methanol (5 mL) along with K_2CO_3 (4 equiv.), treated with an excess of iodomethane (5 equiv.) and stirred at room temperature for 24 h. The methanol was evaporated, and the resultant residue dissolved in water (1 mL) and acidified with concentrated HCl. The mixture was stirred for 1 h and then washed with diethyl ether. Water was then evaporated *in vacuo* and the resultant residue was purified by HPLC (preparative C-18 reverse phase column; gradient: 50% B in 15 min, where A – water, 0.05% formic acid, B – acetonitrile, 0.1% formic acid; fractions containing product identified using Evaporative Light Scattering Detection (ELSD). The desired fractions were combined and freeze-dried to yield the product as a highly hygroscopic solid. Due to low level of compound recovery after HPLC purification, some of the assays used crude products if pure by ^{1}H NMR (which contained compound and KCl mixture, concentration of organic sample was determined by ^{1}H NMR). Due to small amount of purified product IR spectra and optical rotation values are not reported. Melting points are not given due to highly hygroscopic nature of the obtained material.

7.4.3 4-carboxy-1,1-dimethylpiperidin-1-ium (1)

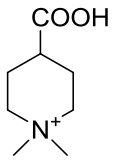

The trifluoroacetic acid (TFA) salt of desired product (11 mg, 0.04 mmol, 10%) was obtained starting from isonipecotic acid (50 mg, 0.39 mmol) and following the general procedure.

^{1}H NMR (700 MHz, D_2O) δ = 3.47 (dt, *J*=13.0, 3.0 Hz, 2 H), 3.33 (td, *J*=12.5, 3.5 Hz, 2 H), 3.12 (s, 3 H), 3.07 (s, 3 H), 2.67 (tt, *J*=10.5, 5.0 Hz, 1 H), 2.10 - 2.17 (m, 2 H), 2.01 - 2.10 (m, 2 H) ppm, ^{13}C NMR (126 MHz, D_2O) δ = 177.8, 61.4, 54.1, 48.1, 37.3, 22.3 ppm. HRMS (ESI-TOF) calcd for $C_8H_{16}NO_2^+$ [M^+]: 158.1176, found: 158.1168.

7.4.4 4-carboxy-1-ethyl-1-methylpiperidin-1-ium (14)

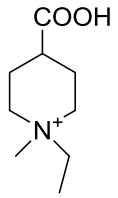

The trifluoroacetic acid (TFA) salt of desired product (9 mg, 0.03 mmol, 8%) was obtained starting from isonipecotic acid (50 mg, 0.39 mmol) and following the general procedure. The compound was obtained as a mixture of isomers.

Major conformer was assigned by NMR: ^{1}H NMR (700 MHz, D_2O) δ ppm 3.47 (2H, dt, *J* = 13.3, 4.4 Hz, H_{2eq}, $H_{2'eq}$), 3.38 (2H, q, *J* = 7.5 Hz, C*H*$_2$CH$_3$), 3.24 (2H, td, *J* = 11.5, 3.8 Hz, H_{2ax}, $H_{2'ax}$), 2.96 (3H, s, CH_3), 3.03 (3H, s, CH_3), 2.63 (1H, tt, *J* = 10.2, 5.1 Hz, H_4), 2.12-1.99 (4H, m, H_{3eq}, $H_{3'eq}$, H_{3ax}, $H_{3'ax}$), 1.25 (3H, t, J = 7.8, CH$_2$C*H*$_3$).

^{13}C NMR (from HSQC signals) (176 MHz, D_2O) δ ppm 59.3 (C_2, $C_{2'}$), 53.7 (*C*H$_2$CH$_3$), 50.8 (CH_3), 37.8 (C_4), 22.2 (C_3, $C_{3'}$), 6.44 (CH$_2$*C*H$_3$). HRMS (ESI-TOF) calcd for $C_9H_{18}NO_2^+$ [M^+]: 172.1332, found: 172.1338.

7.4.5 4-carboxy-1,1-dimethyl-1,2,3,6-tetrahydropyridin-1-ium (4)

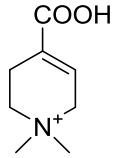

The trifluoroacetic acid (TFA) salt of desired product (14 mg, 0.05 mmol, 12%) was obtained starting from isonipecotic acid (50 mg, 0.39 mmol) and following the general procedure.

^{1}H NMR (700 MHz, D_2O) δ = 6.77 - 6.83 (m, 1 H), 4.07 (q, *J*=2.5 Hz, 2 H), 3.50 (t, *J*=6.5 Hz, 2 H), 3.10 (s, 6 H), 2.65 - 2.72 (m, 2 H) ppm, ^{13}C NMR (126 MHz, D_2O) δ = 168.4, 129.1, 127.6, 60.7, 58.2, 51.7, 19.5 ppm. HRMS (ESI-TOF) calcd for $C_8H_{14}NO_2^+$ [M^+]: 156.1019, found: 156.1013.

7.4.6 4-carboxy-1,1,4-trimethylpiperidin-1-ium (5)

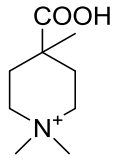

The trifluoroacetic acid (TFA) salt of desired product (10 mg, 0.03 mmol, 8%) was obtained starting from 4-methylisonipecotic acid (50 mg, 0.39 mmol) and following the general procedure.

^{1}H NMR (700 MHz, D_2O) δ = 3.47 (dt, *J*=13.5, 4.0 Hz, 2 H), 3.35 (td, *J*=3.0, 12.5 Hz, 2 H), 3.16 (s, 6 H), 2.32 (d, J=15.5, 2 H), 1.95 (ddt, J=3.5, 11.0, 15.5, 2 H), 1.35 (s, 3 H) ppm, ^{13}C NMR (126 MHz, D_2O, from HSQC signals) δ = 59.8, 54.3, 49.2, 28.2, 24.2 ppm. HRMS (ESI-TOF) calcd for $C_9H_{18}NO_2^+$ [M^+]: 172.1332, found: 172.1325.

7.4.7 4-carboxy-1-methylquinuclidin-1-ium (6)

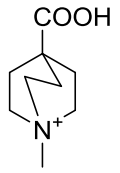

The trifluoroacetic acid (TFA) salt of desired product (16 mg, 0.05 mmol, 13%) was obtained starting from 1-aza-bicyclo[2.2.2]octane-4-carboxylic acid (50 mg, 0.39 mmol) and following the general procedure.

^{1}H NMR (700 MHz, D_2O) δ = 3.47 (t, *J*=7.5 Hz, 6 H), 2.96 (s, 3 H), 2.17 (t, *J*=7.5 Hz, 6 H) ppm, ^{13}C NMR (126 MHz, D_2O, from HSQC signals) δ = 56.3, 51.6, 25.8 ppm. HRMS (ESI-TOF) calcd for $C_9H_{18}NO_2^+$ [M^+]: 170.1176, found: 170.1179.

7.4.8 (*S*)-3-carboxy-1,1-dimethylpyrrolidin-1-ium (7)

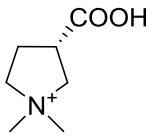

The trifluoroacetic acid (TFA) salt of desired product (10 mg, 0.04 mmol, 9%) was obtained starting from (*S*)-pyrrolidine-3-carboxylic acid (50 mg, 0.43 mmol) and following the general procedure.

^{1}H NMR (700 MHz, D_2O) δ = 3.72 - 3.82 (m, 2 H), 3.52 - 3.62 (m, 3 H), 3.15 (s, 3 H), 3.12 (s, 3 H), 2.53 - 2.62 (m, 1 H), 2.39 - 2.47 (m, 1 H) ppm, ^{13}C NMR (126 MHz, D_2O) δ = 175.5, 66.4, 65.3, 40.5, 52.2, 26.5 ppm. HRMS (ESI-TOF) calcd for $C_7H_{14}NO_2^+$ [M^+]: 144.1019, found: 144.1013.

7.4.9 (*R*)-3-carboxy-1,1-dimethylpyrrolidin-1-ium (8)

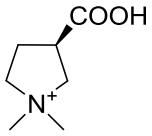

The trifluoroacetic acid (TFA) salt of desired product (13 mg, 0.05 mmol, 12%) was obtained starting from (*R*)-pyrrolidine-3-carboxylic acid (50 mg, 0.43 mmol) and following the general procedure.

^{1}H NMR (700 MHz, D_2O) δ = 3.72 - 3.82 (m, 2 H), 3.52 - 3.62 (m, 3 H), 3.15 (s, 3 H), 3.12 (s, 3 H), 2.53 - 2.62 (m, 1 H), 2.39 - 2.47 (m, 1 H) ppm, ^{13}C NMR (126 MHz, D_2O) δ = 175.5, 66.4, 65.3, 40.5, 52.2, 26.5 ppm. HRMS (ESI-TOF) calcd for $C_7H_{14}NO_2^+$ [M^+]: 144.1019, found: 144.1019.

7.4.10 (*R*)-2-carboxy-1,1-dimethylpyrrolidin-1-ium (9)

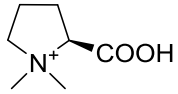

The trifluoroacetic acid (TFA) salt of desired product (10 mg, 0.04 mmol, 9%) was obtained starting from (*R*)-proline (50 mg, 0.43 mmol) and following the general procedure.

^{1}H NMR (700 MHz, D_2O) δ = 4.27 (t, *J*=9.5 Hz, 1 H), 3.68 (ddd, *J*=11.5, 8.5, 3.5 Hz, 1 H), 3.53 (q, *J*=9.5 Hz, 1 H), 3.27 (s, 3 H), 3.07 (s, 3 H), 2.46 - 2.54 (m, 1 H), 2.28 - 2.36 (m, 1 H), 2.07 - 2.20 (m, 2 H) ppm, ^{13}C NMR (126 MHz, D_2O) δ = 169.0, 74.2, 67.8, 52.2, 46.2, 24.6, 18.5 ppm. HRMS (ESI-TOF) calcd for $C_7H_{14}NO_2^+$ [M^+]: 144.1019, found: 144.1015.

7.4.11 3-(carboxymethyl)-1,1-dimethylpiperidin-1-ium (10)

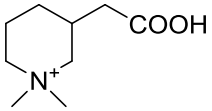

The trifluoroacetic acid (TFA) salt of desired product (10 mg, 0.03 mmol, 9%) was obtained starting from (*S*)- 3-piperidinecarboxylic acid (50 mg, 0.35 mmol) and following the general procedure.

^{1}H NMR (700 MHz, D_2O) δ = 3.41 (t, *J*=15.5 Hz, 2 H), 3.15 (t, *J*=13.0 Hz, 1 H), 3.08 (s, 3 H), 3.05 (s, 3 H), 2.94 (t, *J*=12.5 Hz, 1 H), 2.36 - 2.44 (m, 1 H), 2.31 (qd, *J*=16.5, 6.5 Hz, 2 H), 1.87 - 1.98 (m, 2 H), 1.79 - 1.87 (m, 1 H), 1.16 (qd, *J*=13.0, 4.0 Hz, 1 H) ppm, ^{13}C NMR (126 MHz, D_2O) δ = 175.6, 65.8, 62.4, 56.7, 47.4, 37.2, 27.9, 26.8, 19.7 ppm. HRMS (ESI-TOF) calcd for $C_9H_{18}NO_2^+$ [M^+]: 172.1332, found: 172.1332.

7.4.12 4-carboxy-N,N,N-trimethylcyclohexan-1-aminium (11)

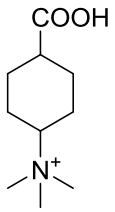

The trifluoroacetic acid (TFA) salt of desired product (11 mg, 0.04 mmol, 11%) was obtained starting from 4-aminocyclohexane-1-carboxylic acid (50 mg, 0.35 mmol) and following the general procedure.

^{1}H NMR (700 MHz, D_2O) δ = 3.28 (tt, *J*=11.5, 3.5 Hz, 1 H), 2.97 (s, 9 H), 2.71 (td, *J*=4.5, 2.5 Hz, 1 H), 2.25 (d, *J*=14.0 Hz, 2 H), 2.06 - 2.12 (m, 2 H), 1.52 - 1.64 (m, 4 H) ppm, ^{13}C NMR (126 MHz, D_2O) δ = 178.8, 73.7, 50.5, 36.8, 25.4, 22.3 ppm. HRMS (ESI-TOF) calcd for $C_{10}H_{20}NO_2^+$ [M^+]: 186.1489, found: 186.1482.

References

1. Garcia-Urdiales, E., Alfonso, I. & Gotor, V. Update 1 of: Enantioselective enzymatic desymmetrizations in organic synthesis. *Chemical Reviews* **111**, PR110-80 (2011).
2. Garcia-Urdiales, E., Alfonso, I. & Gotor, V. Enantioselective enzymatic desymmetrizations in organic synthesis. *Chemical Reviews* **105**, 313-54 (2005).
3. Schoffers, E., Golebiowski, A. & Johnson, C.R. Enantioselective synthesis through enzymatic asymmetrization. *Tetrahedron* **52**, 3769-3826 (1996).
4. C. Willis, M. Enantioselective desymmetrisation. *Journal of the Chemical Society, Perkin Transactions 1*, 1765-1784 (1999).
5. Hollmann, F., Arends, I.W.C.E., Buehler, K., Schallmey, A. & Buhler, B. Enzyme-mediated oxidations for the chemist. *Green Chemistry* **13**, 226-265 (2011).
6. Munzer, D.F., Meinhold, P., Peters, M.W., Feichtenhofer, S., Griengl, H., Arnold, F.H., Glieder, A. & de Raadt, A. Stereoselective hydroxylation of an achiral cyclopentanecarboxylic acid derivative using engineered P450s BM-3. *Chemical Communications*, 2597-2599 (2005).
7. Hausinger, R.P. Fe(II)/α-ketoglutarate-dependent hydroxylases and related enzymes. *Critical Reviews in Biochemistry and Molecular Biology* **39**, 21-68 (2004).
8. Cardillo, A.B., Talou, J.R. & Giulietti, A.M. Expression of Brugmansia candida Hyoscyamine 6beta-Hydroxylase gene in Saccharomyces cerevisiae and its potential use as biocatalyst. *Microbial Cell Factories* **7**, 17 (2008).
9. Yin, X. & Zabriskie, T.M. VioC is a non-heme iron, α-ketoglutarate-dependent oxygenase that catalyzes the formation of 3S-hydroxy-L-arginine during viomycin biosynthesis. *ChemBioChem* **5**, 1274-1277 (2004).
10. Windahl, M.S., Petersen, C.R., Christensen, H.E.M. & Harris, P. Crystal structure of tryptophan hydroxylase with bound amino acid substrate. *Biochemistry* **47**, 12087-12094 (2008).
11. Nakata, H., Yamauchi, T. & Fujisawa, H. Phenylalanine hydroxylase from Chromobacterium violaceum. Purification and characterization. *Journal of Biological Chemistry* **254**, 1829-1833 (1979).
12. Hibi, M., Kawashima, T., Sokolov, P.M., Smirnov, S.V., Kodera, T., Sugiyama, M., Shimizu, S., Yokozeki, K. & Ogawa, J. L-Leucine 5-hydroxylase of Nostoc punctiforme is a novel type of Fe(II)/α-ketoglutarate-dependent dioxygenase that is useful as a biocatalyst. *Applied Microbiology and Biotechnology* **97**, 2467-2472 (2013).
13. Hibi, M., Kawashima, T., Kasahara, T., Sokolov, P.M., Smirnov, S.V., Kodera, T., Sugiyama, M., Shimizu, S., Yokozeki, K. & Ogawa, J. A novel Fe(II)/α-ketoglutarate-dependent dioxygenase from Burkholderia ambifaria has β-hydroxylating activity of N-succinyl L-leucine. *Letters in Applied Microbiology* **55**, 414-419 (2012).
14. Kodera, T., Smirnov, S.V., Samsonova, N.N., Kozlov, Y.I., Koyama, R., Hibi, M., Ogawa, J., Yokozeki, K. & Shimizu, S. A novel l-isoleucine hydroxylating enzyme, l-isoleucine dioxygenase from Bacillus thuringiensis, produces (2S,3R,4S)-4-hydroxyisoleucine. *Biochemical and Biophysical Research Communications* **390**, 506-510 (2009).
15. Baldwin, J.E., Field, R.A., Lawrence, C.C., Merritt, K.D. & Schofield, C.J. Proline-4-hydroxylase: Stereochemical course of the reaction. *Tetrahedron Letters* **34**, 7489-7492 (1993).
16. Shibasaki, T., Sakurai, W., Hasegawa, A., Uosaki, Y., Mori, H., Yoshida, M. & Ozaki, A. Substrate selectivities of proline hydroxylases. *Tetrahedron Letters* **40**, 5227-5230 (1999).
17. Klein, C. & Hüttel, W. A Simple Procedure for Selective Hydroxylation of L-Proline and L-Pipecolic Acid with Recombinantly Expressed Proline Hydroxylases. *Advanced Synthesis & Catalysis* **353**, 1375-1383 (2011).
18. Hara, R. & Kino, K. Characterization of novel 2-oxoglutarate dependent dioxygenases converting l-proline to cis-4-hydroxy-l-proline. *Biochemical and Biophysical Research Communications* **379**, 882-886 (2009).

19. Leung, I.K.H., Krojer, T.J., Kochan, G.T., Henry, L., von Delft, F., Claridge, T.D.W., Oppermann, U., McDonough, M.A. & Schofield, C.J. Structural and Mechanistic Studies on gamma-Butyrobetaine Hydroxylase. *Chemistry & Biology* **17**, 1316-1324 (2010).
20. Galland, S., Le Borgne, F., Guyonnet, D., Clouet, P. & Demarquoy, J. Purification and characterization of the rat liver gamma-butyrobetaine hydroxylase. *Molecular and Cellular Biochemistry* **178**, 163-168 (1998).
21. Rydzik, A.M., Chowdhury, R., Kochan, G.T., Williams, S.T., McDonough, M.A., Kawamura, A. & Schofield, C.J. Modulating carnitine levels by targeting its biosynthesis - selective inhibition of [gamma]-butyrobetaine hydroxylase. *Chemical Science* (2014).
22. Krogsgaard-Larsen, P., Falch, E., Schousboe, A., Curtist, D.R. & †, D.L. Piperidine-4-sulphonic Acid, a New Specific GAB A Agonist. *Journal of Neurochemistry* **34**, 756-759 (1980).
23. Krogsgaard-Larsen, P. Inhibitors of the GABA uptake systems. *Molecular and Cellular Biochemistry* **31**, 105-121 (1980).
24. Krehan, D., Frølund, B., Krogsgaard-Larsen, P., Kehler, J., Johnston, G.A.R. & Chebib, M. Phosphinic, phosphonic and seleninic acid bioisosteres of isonipecotic acid as novel and selective GABAC receptor antagonists. *Neurochemistry International* **42**, 561-565 (2003).
25. Croucher, M.J., Meldrum, B.S. & Krogsgaard-Larsen, P. Anticonvulsant activity of GABA uptake inhibitors and their prodrugs following central or systemic administration. *European Journal of Pharmacology* **89**, 217-228 (1983).
26. Blackburne, I.D., Katritzky, A.R. & Takeuchi, Y. Conformation of piperidine and of derivatives with additional ring hetero atoms. *Accounts of Chemical Research* **8**, 300-306 (1975).
27. Anet, F.A.L. & Yavari, I. Nitrogen inversion in piperidine. *Journal of the American Chemical Society* **99**, 2794-2796 (1977).
28. Hu, H. & Krishnamurthy, K. Revisiting the initial rate approximation in kinetic NOE measurements. *Journal of Magnetic Resonance* **182**, 173-177 (2006).
29. Macur, S., Farmer Ii, B.T. & Brown, L.R. An improved method for the determination of cross-relaxation rates from NOE data. *Journal of Magnetic Resonance (1969)* **70**, 493-499 (1986).

Chapter 5

Inhibition of human BBOX

Abstract

Chapter 5 describes studies aimed at finding inhibitors of BBOX and their validation for use in cellular studies. BBOX is a therapeutic target in cardiovascular medicine. However, to date no highly potent and selective human BBOX inhibitor has been identified. A set of over 600 potential inhibitors of 2OG dependent oxygenases were screened against BBOX using the fluoride release assay. This work led to the identification of lead scaffolds, including 3-hydroxy-2-picolinic acid and isoquinoline derivatives. Further optimisation led to the identification of a potent inhibitor of BBOX, which was shown to lower carnitine levels in a cellular assay. A crystal structure of the inhibitor with BBOX revealed an active site loop movement, which may be relevant in the BBOX catalytic mechanism and helps to rationalize GBB substrate inhibition observed both with isolated BBOX and in cells. Other scaffolds, including hydroxythiazole based compounds were also evaluated as BBOX inhibitors leading to the identification of highly potent inhibitors. Moreover, a set of GBB analogues was screened against BBOX *in vitro* and in cells, which led to identification of novel agents that reduce carnitine levels in cells. Finally, the inhibition of BBOX by targeting its zinc binding domain was examined. The results indicate that *N*-terminal zinc binding domain is indispensible for BBOX folding and activity.

Contents

1 Introduction

1.1 Role of carnitine in cardiac metabolism

Cardiac ischemia and related conditions are major causes of mortality in many countries.[1] In the normal heart, glucose and fatty acid metabolisms are tightly regulated, with fatty acids acting as a main source of energy; however, in the failing heart this homeostasis is perturbed.[2] A shift towards glucose oxidation under ischemic conditions was shown to aid cardiac efficiency and improve heart function in both the long and short term[3] (glucose metabolism is linked with less oxygen consumption per molecule of ATP produced[2]). The manipulation of the preferred cellular energy source is therefore of interest with respect to pharmacological intervention in cardiovascular disease. Several approaches for inhibiting fatty acid metabolism have been employed, including targeting pools of free fatty acid by acting on their transport into mitochondria or β-oxidation.[2]

In the human body carnitine is mainly obtained from the diet, with its endogenous biosynthesis being listed as a secondary source. Despite this, the carnitine biosynthesis pathway is a highly conserved enzymatic path across all animals (including carnivores, which are ensured constant carnitine uptake from consumed meat). Recently, carnitine biosynthesis has been shown to be induced by fat-rich diet[4] and regulated by thyroid hormones, which altered BBOX activity in liver.[5] Therefore it can be proposed that the endogenous carnitine biosynthesis provides fine regulation of carnitine levels, with effects on preferred energy source utilisation. Consequently, manipulation of the ratio between glucose and the fatty acid metabolism could potentially be achieved by modulating carnitine biosynthesis. It has also been proposed that high levels of carnitine in red meat can cause heart disease via metabolism of carnitine leading to production of trimethylamine *N*-oxide (TMAO), which promotes arteriosclerosis.[6] Therefore inhibition of carnitine biosynthesis is of interest in the treatment and prevention of cardiovascular disease.

1.2 Previous work on BBOX inhibitors

To date, there is little precedent for the inhibition of human BBOX. The existing reports focus on GBB analogues,[7,8] which are all relatively weak inhibitors and attracted more attention as probes for enzyme mechanistic studies[9] rather than possible cell based tools or drug candidates. The existing data on BBOX inhibition are summarized below.

1.2.1 Inhibitors of human BBOX

To date, there is one clinically used agent, which is targeted specifically at human carnitine system. It is marketed by a Latvian company Grindeks under the name Mildronate (THP, MET-88).[10,11] Mildronate is sold as a cardioprotective drug in Russia and some of the Eastern European countries. Even though it was initially targeted at BBOX, it has been shown to be a rather weak inhibitor of BBOX *in vitro* (IC_{50} value of 60 μM[12]/ 12 μM[13]) and also a competitive substrate.[14,15] 3-

Hydroxypropionic acid, glucose and succinic acid were major metabolites identified in plasma after oral treatment with Mildronate.[16] Other reports suggested that Mildronate acts as an inhibitor of carnitine acetyltransferase[17] and can influence the neural system.[18] Mildronate is a close structural mimic of both GBB and carnitine (Scheme 1), which may explain non-specificity of its mode of action, as it can probably interact with more than one GBB/carnitine binding proteins or transporters.

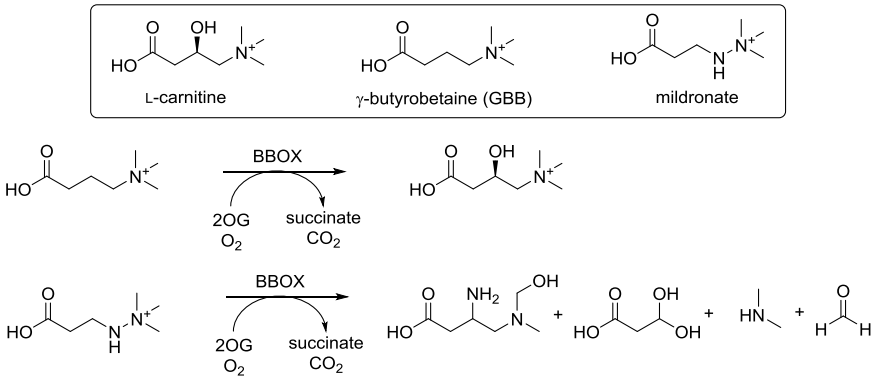

Scheme 1 Structures of carnitine, γ-butyrobetaine and Mildronate. Mildronate is a close structural mimic of γ-butyrobetaine (GBB) and carnitine. Both GBB and Mildronate are BBOX substrates. In the case of Mildronate multiple products of BBOX catalysis are observed.[14]

1.2.2 Inhibitors of BBOX from *Pseudomonas sp. AK1*

Most of the inhibition studies on BBOX have been done on the *Pseudomonas sp. AK1* enzyme, presumably because of its availability compared to human or animal BBOX (an expression system for human BBOX was established only recently[14] and prior to that, animal BBOX was obtained by isolation from the appropriate organs,[19] while bacterial homologue was isolated from Pseudomonas cultures[20]). However, the results may not be directly translatable into the human BBOX system as there are differences between kinetic properties and substrate selectivity of *Pseudomonas sp. AK1* and human BBOX (see Chapter 6). The main classes of inhibitors investigated were derived from BBOX susbtrate structures.

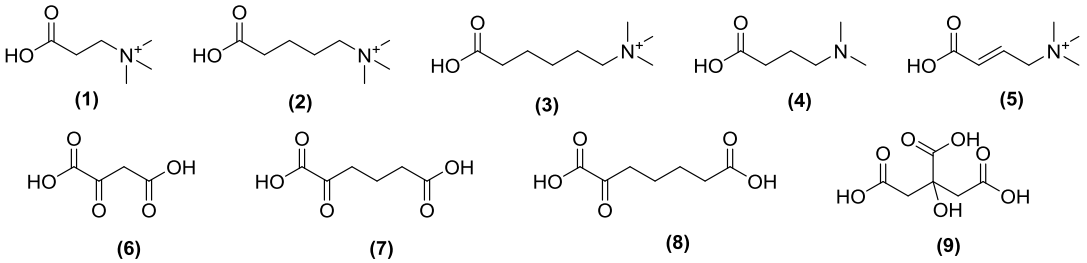

Figure 1 Structure of inhibitors of BBOX from *Pseudomonas sp. AK1* as decribed by Lindsted *et al.*[20]

Lindsted *et al.*[20] identified several GBB analogues as inhibitors of *Pseudomonas sp. AK1* BBOX (percentege inhibition at 11.4 mM inhibitor concentration is given in parentheses): 3-trimetylamino propionate ((**1**), 18%), 5-trimethylaminovalerate ((**2**), 30%), 6-trimethylaminocaproate ((**3**), 23%), 4-dimethylaminobutyrate ((**4**), 41%), 4-trimethylaminocrotonate ((**5**), 50%) (analogues (**1**)-(**5**), Fig. 1).

In the same work 2OG analogues were shown to inhibit BBOX (percentage inhibition at 11.4 mM inhibitor concentration is given in parentheses): oxaloacetate ((**6**), 40%), 2-ketoadipate ((**7**), 20%), 2-ketopimelate ((**8**), 80%), citrate ((**9**), 50%) (analogues (**6**)-(**9**), Fig. 1). An excess of the following metal ions were also shown to be inhibitory (percentage inhibition at 0.57 mM metal concentration is given in parentheses): Mg^{2+} (5%), Ca^{2+} (12%), Cr^{3+} (18%), Mn^{2+} (35%), Co^{2+} (93%), Ni^{2+} (92%), Cu^{2+} (80%), Zn^{2+} (93%), Cd^{2+} (86%), Hg^{2+} (80%).

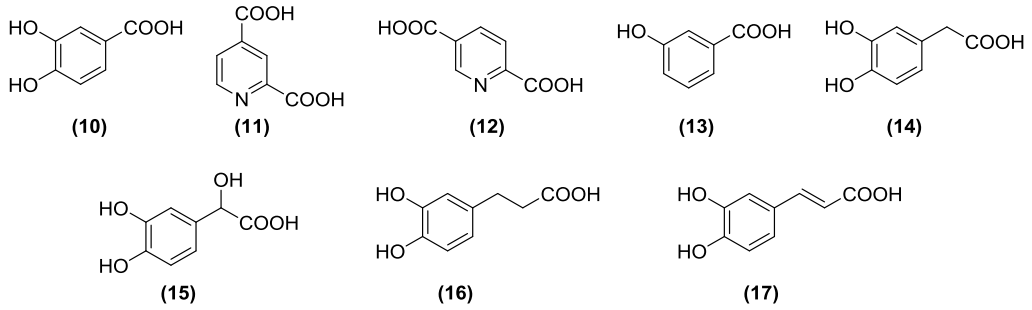

Figure 2 Inhibitors of BBOX from *Pseudomonas sp. AK1* as identified by Ng *et al.*[21]

In addition, several analogues of 2OG, i.e. pyridinecarboxylic acids and benzoic acids were used to map the 2OG binding site of *Pseudomonas sp. AK1* BBOX.[21] These studies identified 3,4-dihydroxybenzoate ((**10**), K_i=0.6 μM) and pyridine 2,4-dicarboxylate ((**11**), K_i=0.2 μM) as the most potent inhibitors. Pyridine 2,5-dicarboxylate ((**12**), K_i=0.014 mM), 3-hydroxybenzoate ((**13**), K_i=0.02 mM), 3,4-dihydroxyphenylacetate ((**14**), K_i=0.013 mM), 3,4-dihydroxymandelate ((**15**), K_i=0.028 mM), 3,4-dihydroxypropionate ((**16**), K_i=0.020 mM) and 3,4-dihydroxycinnamate ((**17**), K_i=0.006 mM) were also identified as good inhibitors (Figure 2).

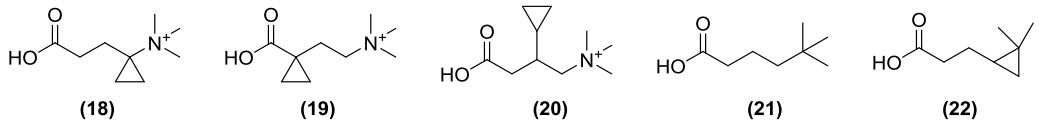

Figure 3 Structures of *Pseudomonas sp. AK1* BBOX inhibitors described by Ng *et al.*[21] and Ziering *et al*[8].

GBB analogues were also used as mechanistic probes to investigate BBOX-catalysed reaction. A series of cyclopropyl substituted GBB analogues (compounds (**18**)-(**20**), Fig. 3) were synthesised with a view to use them as 'free radical clock' probes for radical transition states.[7] Analogues (**18**) and (**20**) were identified as competitive inhibitors, with K_i values of 12.9 mM and 7.9 mM, respectively. Analogue (**19**) was found to be a noncompetitive inhibitor. Ziering *et al*. identified 5,5-dimethylhexanoic acid (**21**) and 3-(2,2-dimethylcyclopropyl)propanoic acid (**22**) (Fig. 3) as inhibitors of *Pseudomonas sp. AK1* BBOX.[8] Analogue (**21**) was a competitive inhibitor with K_i=0.16 mM and also a poor substrate for BBOX. Analogue (**22**) was a competitive inhibitor (K_i=0.22 mM) and was shown to inactivate BBOX (the inactivation was oxygen and 2OG dependent).

1.2.3 Inhibitors of BBOX from rat liver

Rat liver BBOX was studied for cofactor requirements and inhibition. Whebie *et al.*[22] identified 3-bromo-2-oxoglutarate (**23**) as a BBOX substrate which was a non-competitive inhibitor in respect of 2OG and irreversibly inactivated enzyme at high concentrations (1 mM). Work by Lindsted[23] identified several metal chelators as inhibitors of BBOX (percentage inhibition at 0.05 mM concentration of compound is given in parentheses): 1,10-phenanthroline ((**24**), 80%), 2,2'-dipirydine ((**25**), 70%), EDTA ((**26**), 70%) dithiazone ((**27**), 35%) and catechol-3,5-sulfonate ((**28**), 95%) (Fig. 4). Rutin (**29**) and Quercetin (**30**) inhibited rat liver BBOX by 70% and 60%, respectively at 0.125 mM inhibitor concentration. The following metal chelators were identified as inhibitors at higher concentrations (percentage inhibition at 0.5 mM concentration of compound is given in parentheses): 8-hydroxyquinoline (**31**, 99%), dihydroxyethylaminoacetic acid (**32**, 60%) and sodium diethyldithiocarbamate (**33**, 25%). The structures of rat liver BBOX inhibitors are shown in Fig. 4. Similarly to *Pseudomonas sp. AK1* BBOX studies, the influence of metal ions on the activity of rat liver BBOX was investigated.[23] The following metal ions were found to inhibit rat liver BBOX at 0.14 mM concentration (percentage inhibition given in parentheses): V^{3+} (70%), Co^{2+} (90%), Cu^{2+} (50%), Zn^{2+} (70%). The best inhibitor was Ni^{2+} which inhibited BBOX by 40% when used at 0.014 mM.

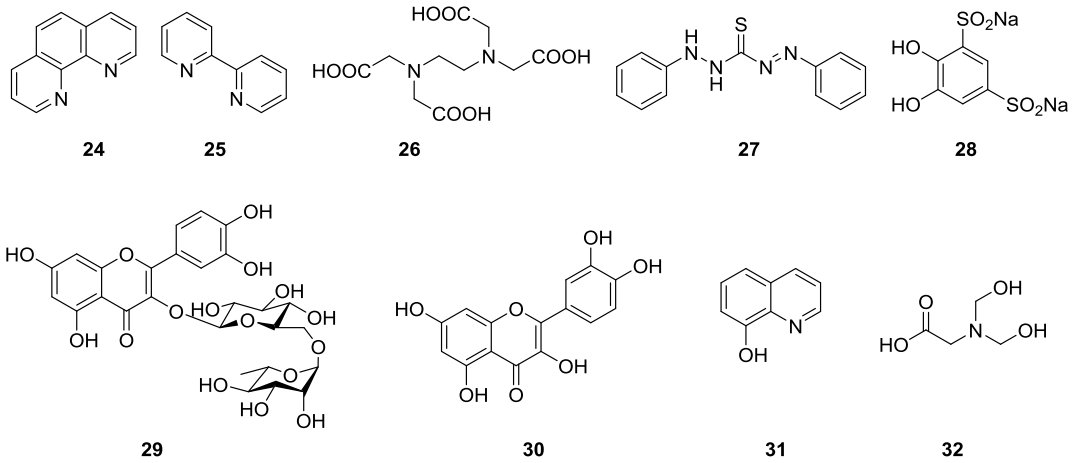

Figure 4 Structures of the rat liver BBOX inhibitors as described by Lindsted.[23]

2 Assays for BBOX inhibition

2.1 *In vitro* assays

In this work, inhibition of human BBOX was measured by the fluoride release assay, as discussed in Chapter 2. Additional measurements were performed using a ^{1}H NMR based method as discussed in Chapter 6. A fluoride release assay allows for fast screening in the 384-well plate format and therefore was used for assessment of potency of large panel of potential inhibitors, as well as IC_{50} values determination. The most promising inhibitors were then also assessed using the ^{1}H NMR assay, which enables the use of GBB, instead of GBBF and therefore assessment of inhibitor behaviour in conditions closer to the physiological ones.

2.2 Cell-based assays

Measurements of the levels of carnitine and associated metabolites were done using an LC-MS based assay. The separation method for the carnitine biosynthesis intermediates was developed using chromatography on a mixed-mode resin (reverse phase and ion exchange, Primesep column), followed by the detection by mass spectrometry (Fig. 5). Several human cell lines were screened for the presence of carnitine and associated metabolites. Carnitine was detected in the following cell lines: HEK 293T kidney embryonic cells, MCF7 breast cancer cells, RCC4 renal carcinoma cells (both VHL deficient and expressing VHL), 786-0 renal carcinoma cells (both VHL deficient and expressing VHL). In contrast, no carnitine could be detected in HeLa cervical carcinoma cell and U2OS osteosarcoma cell samples. Further study was done on HEK 293T cells due to high levels of carnitine present and cell line robustness.

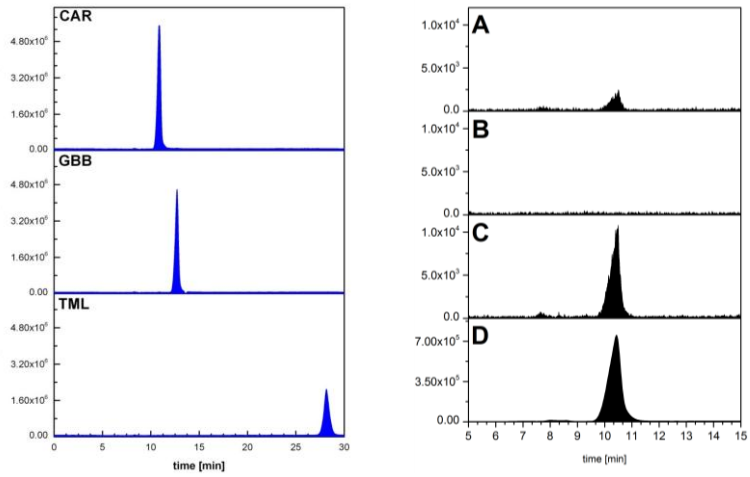

Figure 5 Left: Carnitine biosynthesis pathway standards were analysed using the developed cell-assay conditions. The assay enables good separation of trimethyllysine, γ-butyrobetaine and carnitine. 100 µM standards: CAR – carnitine, GBB – γ-butyrobetaine, TML – trimethyllysine. Spectra were recorded in mass range 120-300 Da (scan mode), single ion mode used in parallel to monitor masses: 189.2 (TML), 162.2 (CAR), 146.2 (GBB). Right: Analysis of the carnitine content in HEK 293T cell lysates. A – cells incubated with 125 µM of Mildronate B – cells incubated with 500 µM Mildronate, C – control cell sample with no additives, D – carnitine standard.

2.3 Binding assay

A binding assay was developed based on BBOX intrinsic fluorescence quenching, as observed upon titration with 3-hydroxypyridine based inhibitors (Fig. 6). The method was optimised for use in a 96-well plate format. Fluorescence was measured on a Pherastar FS plate reader (BMG Labtech) using the following parameters: excitation 280 nm, emission 350 nm, 5 µM BBOX, 20 µM Fe(II) and variable concentration of the compounds. Assays were performed in 50 mM Tris buffer pH 7.5 containing 200 mM NaCl in total volume of 50 µL per well. The fluorescence signal was defined as the measured fluorescence of the protein-ligand complex minus the signal of the compound in the absence of BBOX.

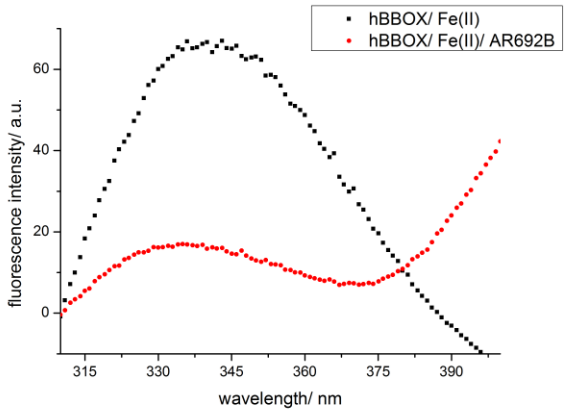

Figure 6 Fluorescence measurements. Fluorescence emission spectra of the BBOX/Fe(II) complex compared to BBOX/Fe(II)/AR692B complex. Excitation 270 nm, emission 310-400 nm. Spectra were measured using 10 µM BBOX, 20 µM Fe(II) and 20 µM AR692B.

3 Broad screen in search of BBOX inhibitors

A broad screen of different classes of potential human BBOX inhibitors was performed employing the fluoride release assay. In total, over 600 small molecules were screened, providing comprehensive information on useful scaffolds for further development (Fig. 7). Each class is further discussed in this chapter.

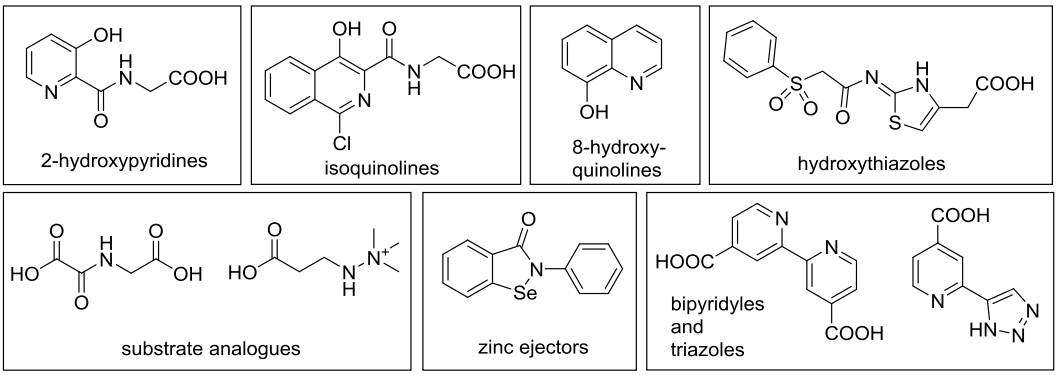

Figure 7 Structural classes of inhibitors screened against human BBOX.

4 Inhibition of BBOX by 2-hydroxypyridine analogues

4.1 2-Hydroxypyridines as inhibitors of BBOX

A broad screen identified 3-hydroxypicolinic acid (PCA) derivative (**33**) as a good inhibitor of BBOX (IC_{50} 6.2 μM) and a promising lead inhibitor molecule (Fig. 8A). The glycine moiety (CH_2COOH) of (**33**) was assumed to bind analogously to the $(CH_2)_2COOH$ group of 2OG. Analyses of an existing crystal structure of BBOX[14] revealed the presence of an unoccupied hydrophobic pocket directly adjacent to the 2OG methylene binding region and located on the interior of the active site (Fig. 8B).

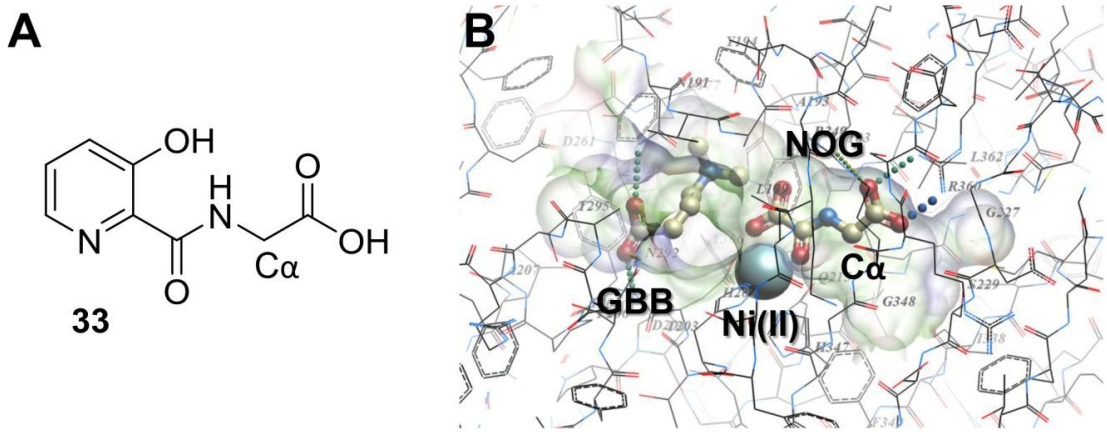

Figure 8 A – Structure of a lead compound (**33**) with 3-hydroxypyridine scaffold. B – Active site of human BBOX with GBB, NOG (N-oxalyl glycine – a close structural mimetic of 2OG) and Ni(II) bound (PDB id: 3O2G).

Therefore analogues of (**1**) derivatised at the Cα position of the modified amino acid were prepared. Analogues were synthesised by amide coupling of 3-hydroxy-2-picolininc acid and a desired amino acid methyl ester, using 1,1ˈ-carbonyldiimidazole (CDI) as a coupling agent (Scheme 2).

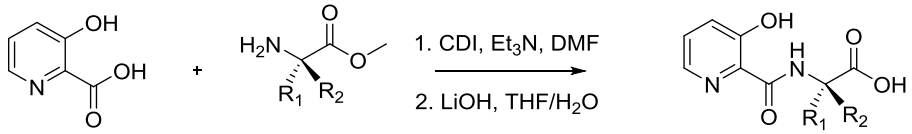

Scheme 2 Synthesis of 3-hydroxy-2-picolinic acid derivatives.

It was found that derivatisation of glycine at its *pro*-(*S*), but not *pro*-(*R*), position led to increased potency (Fig. 9). Amongst the Cα side chains tested, in general the bulky, aromatic ones, such as phenyl (**34a**) or 3-indole (**35a**) were preferred. With alkyl moieties, such as methyl (**37a**) or isopropyl (**38a**), no significant improvement in potency was observed compared to unsubstituted analogue (**33**). An improvement in potency was also observed with glutamic acid derivative (**40a**). In contrast, all analogues with (*R*)-stereochemistry side chain were much weaker inhibitors than their

(*S*)-substituted counterparts. The alanine (**37b**) and glutamic acid (**40b**) derivatives still retained some of their inhibitory properties, presumably because of small size and relative flexibility of side chain. Interestingly, for the aspartic acid derivatives, the (*R*)-substituted analogue (**41b**) was more potent than the (*S*) one (**41a**), which could possibly be attributed to the specific interactions of carboxylate of (**41b**) within the BBOX active site. The IC_{50} data are summarized in Table 1.

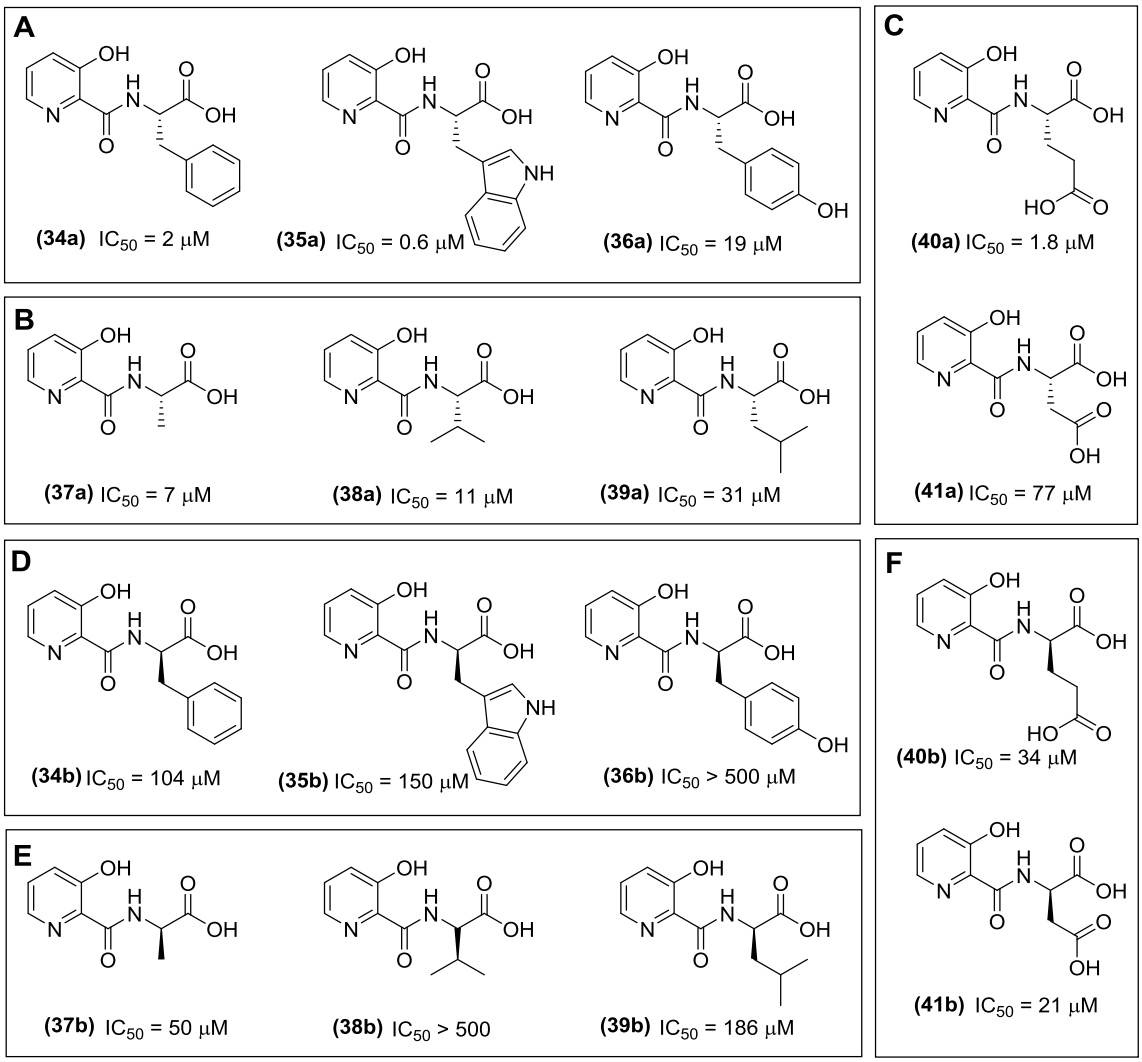

Figure 9 Effects of structural variations on inhibitor activity. The A – Aromatic side chains can improve potency ((**34a**) and (**35a**)) or lead to decrease in activity (**36a**). B – The tested alkyl side chains do not improve potency ((**37a**) and (**38a**)) and in case of the isobutyl side chain (**39a**) potency is lower than the template compound. C – The presence of a carboxylate side chain can improve potency, depending on the chain length. D –E – The activity of analogues with the (*R*)-stereocentre at Cα is lower than the (*S*) side chain enantiomers.

Table 1 Inhibitory properties of 3-hydroxy-2-picolinic acid conjugates with amino acids.

code	R_1	R_2	IC_{50} [µM]
33	H	H	6.2±2.7
34a	CH_2Ph	H	2.0±0.2
34b	H	CH_2Ph	104±21
35a	CH_2-(3-indole)	H	0.52±0.09
35b	H	CH_2-(3-indole)	150±16
36a	CH_2Ph(4-OH)	H	19.2±4.4
36b	H	CH_2Ph(4-OH)	>1000
37a	CH_3	H	7.4±1.4
37b	H	CH_3	49.5±9.7
38a	$CH(CH_3)_2$	H	10.7±1.5
38b	H	$CH(CH_3)_2$	754±63
39a	$CH_2CH(CH_3)_2$	H	31.0±9.3
39b	H	$CH_2CH(CH_3)_2$	186±20
40a	$(CH_2)_2COOH$	H	1.8±0.26
40b	H	$(CH_2)_2COOH$	34.0±2.9
41a	CH_2COOH	H	76.6±10.3
41b	H	CH_2COOH	21.2±8.9
42	CH_2-(4-imidazole)	H	126±10

4.2 Further SAR investigation of 3-hydroxypyridine based analogues

On the basis of structural work on 2OG oxygenase-inhibitor complexes,[24,25] it was predicted that analogue (**33**) would bind to the BBOX active site iron atom via its carbonyl group and either its pyridine-nitrogen or C-3 hydroxyl group (Fig. 10).

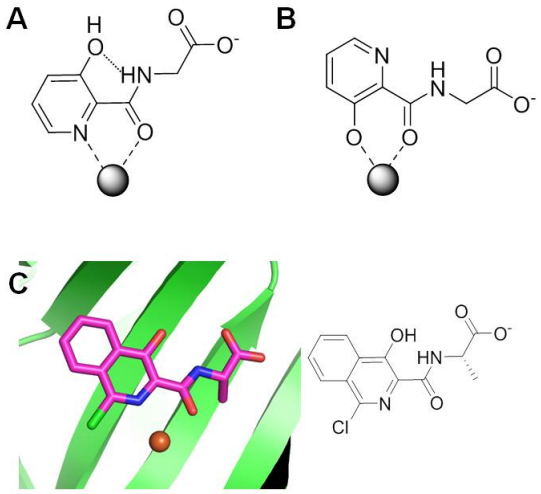

Figure 10 A, B – Possible binding modes of the 3-hydroxypyridine scaffold. C – Binding mode A was modelled based on a crystal structure of a related 2OG dependent Hypoxia-Inducible Factor Prolyl Hydroxylase 2 (PHD2/ EGLN1) in a complex with *N*-[(1-chloro-4-hydroxyisoquinolin-3-yl)carbonyl]alanine (PDB code: 4BQY).[26]

Further structure-activity relationship studies revealed that, both the pyridine-nitrogen and the C-3 hydroxyl group are essential for binding. Analogues lacking either hydroxyl (**45**) or pyridine nitrogen (**44**) did not retain their inhibitory properties (Fig. 11A). The structure lacking a carboxylate was not active either (Fig. 11B). When the bulky side chain was present, analogues lacking either the pyridine-nitrogen or C-3 hydroxyl group retained some of the activity, whilst analogues lacking a side chain carboxylate were inactive (Fig. 11B). Note, that analogue (**47**) lacking hydroxyl group was more potent than analogue (**48**), which does not possess pyridine nitrogen. Therefore the predominant mode of binding probably involves carbonyl and pyridine nitrogen (Fig. 11B).

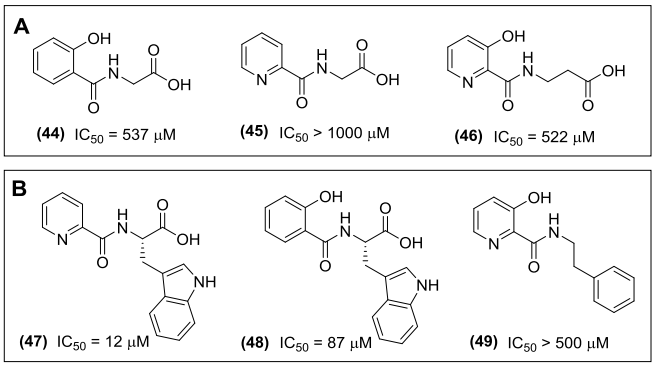

Figure 11 A – Effects of pyridine nitrogen, phenolic hydroxyl and carboxylate on activity of the template compound. B – Effects of the pyridine nitrogen, phenolic hydroxyl, and carboxylate on activity of compounds with aromatic side chain.

Table 2 Inhibitory properties of 2-carboxypyridine (PCA) derivatives.

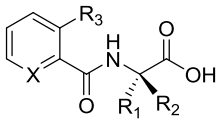

code	X	R_1	R_2	R_3	IC_{50} [μM]
44	H	COOH	H	OH	536.8±110.2
45	N	COOH	H	H	>1000
46	N	CH_2COOH	H	OH	522±61
47	N	COOH	CH_2-(3-indole)	H	12.5±3.1
48	H	COOH	CH_2-(3-indole)	OH	87.6±27.3
49	N	H	CH_2Ph	OH	>1000

4.3 Development of AR692B

Having established that aromatic Cα side chains promote good inhibitory properties of PCA derivatives, a methodology for further introduction of various side chains was developed. This was achieved via coupling to *S*-alkylated cysteines, which allows synthesis of a broad range of derivatives with defined stereochemistry at Cα position. Following this route, a set of analogues with varying pyridine side chains was synthesised (Scheme 3).

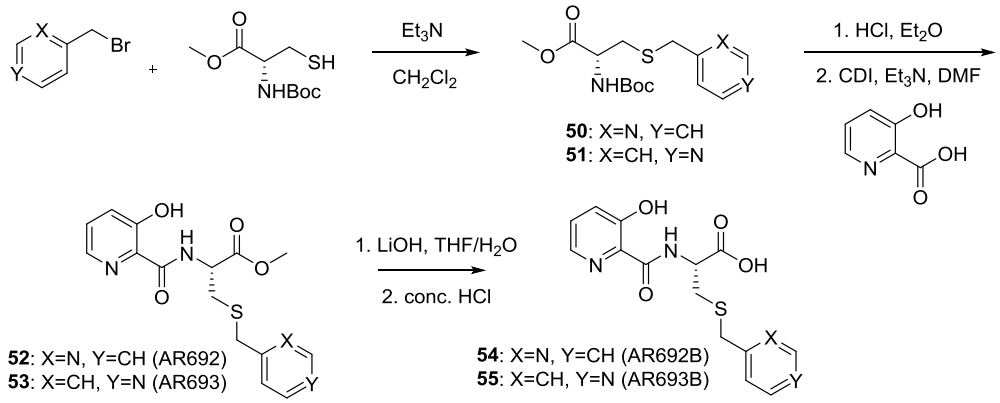

Scheme 3 Synthesis of AR692B and AR693B.

Both AR692B and AR693B were potent BBOX inhibitors, with IC_{50} values of 0.47±0.06 µM and 0.72±0.19 µM. AR692B was chosen for further studies.

4.4 Evaluation of AR692B

4.4.1 Inhibition

The fluoride release assay uses a fluorinated BBOX substrate analogue which has a slightly higher K_M value than GBB (20 µM vs. 4 µM) and also leads to a certain level of uncoupling between 2OG decarboxylation and substrate hydroxylation,[12] so that higher quantities of 2OG are used (assays were performed at 500 µM 2OG concentration). Therefore, the kinetic properties of AR692B were also examined using an ^{1}H NMR assay, in which the native substrate (GBB) and 2OG at its K_M value[12] (150 µM) were used (as described in Section 2.1). With this assay the IC_{50} value was 153 nM.

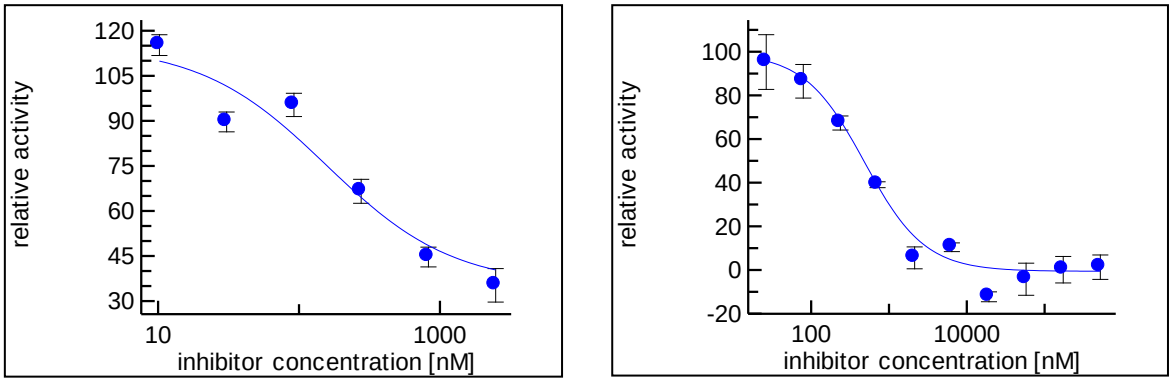

Figure 12 Dose – response curve for inhibition of BBOX by AR692B as measured by the ^{1}H NMR assay (left panel) and the fluoride release assay (right panel).

4.4.2 Competition experiments

AR692B was found to be a competitive inhibitor of BBOX with respect to both 2OG and GBB as established by employing the ^{1}H NMR assay (Fig. 13).

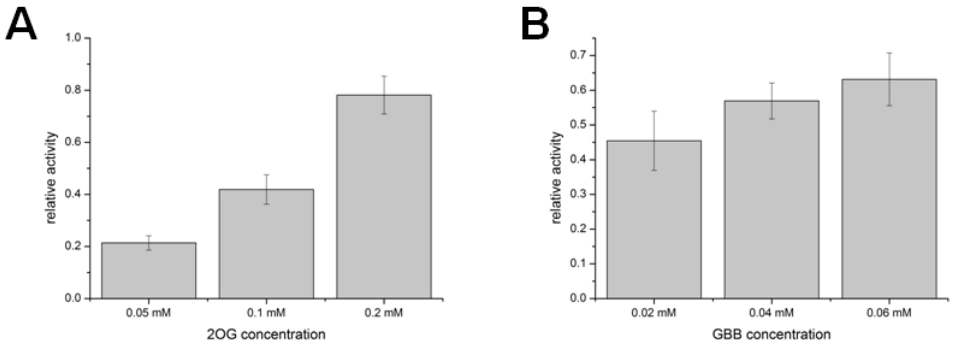

Figure 13 BBOX inhibition by AR692B is dependent on both 2OG and GBB concentrations. A – Increasing the 2OG concentration leads to an increase in BBOX activity (at constant inhibitor concentration). B – Increasing the GBB concentration leads to an increase in BBOX activity (at constant inhibitor concentration) Experiments were performed employing the NMR assay as described for IC_{50} measurements. Values are given as the ratio of carnitine formation in the reaction containing inhibitor to control reaction with no inhibitor added.

4.4.3 Binding experiments

The binding of AR692B and related compounds to BBOX was measured using the fluorescence quenching assay as described in Section 2.3 of this chapter. The obtained K_D value for AR692B binding to BBOX was 0.50±0.07 μM (Fig. 14), signifying AR692B as a relatively strong BBOX binder. Following the same methodology binding constants of (**33**) and (**34a**) to BBOX were also measured, giving K_D values of 10.8±0.8 μM and 1.3±0.3 μM, respectively (Fig. 14).

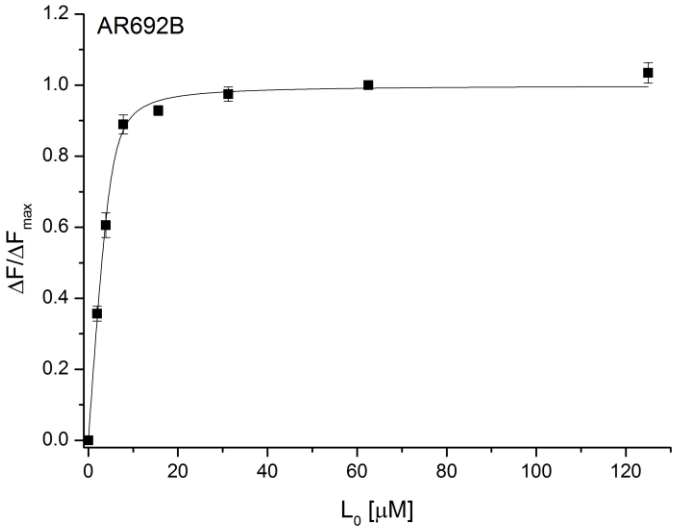

Figure 14 Binding curve of AR692B to BBOX.

4.4.4 Selectivity screen

AR692B was tested against a panel of seven other human 2OG oxygenases including lysine-specific histone demethylases (KDMs) and the hypoxia inducible factor (HIF) hydroxylases. Inhibitors used as positive controls were as follow: IOX1 (5-carboxy-8-hydroxyquinoline), IC_{50} 1.7 μM (JMJD2A),[27] 12.6 μM (PHF8),[28] 14.3 μM (PHD2),[27] 20.5 μM (FIH);[27] 2,4-PDCA (2,4-pyridine dicarboxylic acid) IC_{50} 4.1 μM (FBXL11),[28] 8 μM (JMJD1A),[28] 33 μM (JMJD3).[28] The screening method and conditions were as reported.[27-29] AR692B was inactive against the tested KDMs at 100 μM, and had only weak affinity towards the catalytic domain of the HIF prolyl hydroxylase 2 isoform (PHD2) (Table 3), with an IC_{50} of 28 μM (Fig. 15). The reduced effect on PHD2 activity when compared to BBOX activity likely reflects the relatively tight 2OG binding pocket of PHD2[30] compared to that of BBOX, which hinders binding of the bulky side chain of AR692B.

Table 3 Inhibition of human 2OG dependent oxygenases by AR692B.

Enzyme	Other nomenclature	Function	substrate	% inhibition at 100uM	±STDEV
JMJD2A	KDM4A	H3K9/36 demethylase	H3K9me3 a.a.7-14	9.4	7.0
PHF8	KDM7B	H3K9/27me2/1 demethylase	H3K9me2 a.a.1-28	13.9	1.7
FBXL11	KDM2A	H3K36me2/1 demethylase	H3K36me2 a.a. 31-43	0.00	0.01
JMJD1A	KDM3A	H3K9me2/1 demethylase	H3K9me2 a.a 1-28	-0.02	0.01
JMJD3	KDM6B	H3K27 demethylase	H3K27me3 a.a. 14-35	26.3	3.0
PHD2	EGLN1	HIF hydroxylase	CODD HIF1a 19-mer	72.5	5.0
FIH	HIF1AN	HIF hydroxylase	CADD HIF2a 36-mer	5.0	1.6

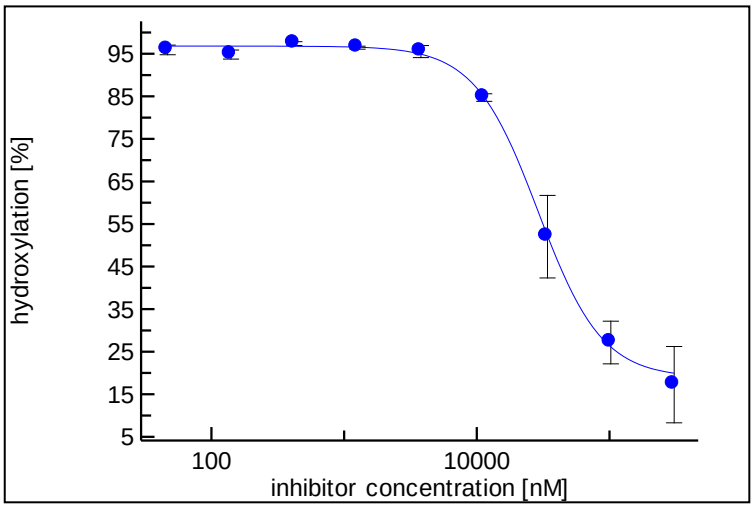

Figure 15 Dose – response curve for inhibition of PHD2 by AR692B as measured by the MALDI based assay.

4.4.5 Cell based studies

The activity of AR692B in cell culture was evaluated using the assay as described in Section 2.2 of this chapter. Because AR692B displayed lower activity in cells compared to the *in vitro* assays with isolated protein, prodrug forms of AR692B with increased lipophilicity were investigated, i.e. methyl (AR692, (**52**)) and octyl ester (AR780, (**5**)) derivatives. Octyl ester was synthesised as shown in Scheme 4.

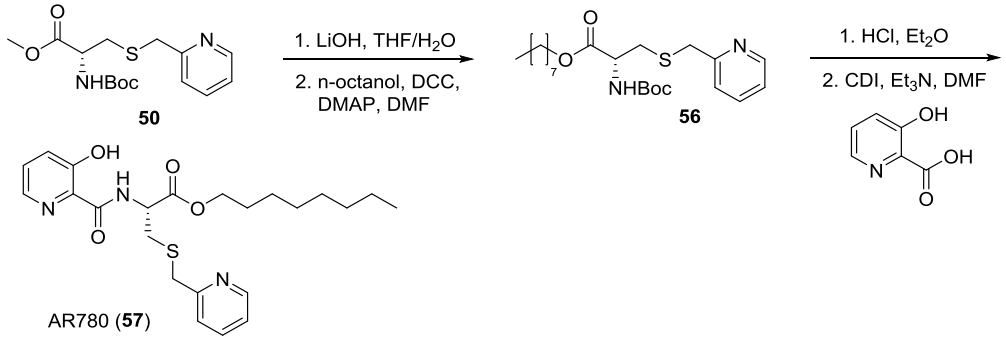

Scheme 4 Synthesis of AR780.

Studies on HEK 293T cells demonstrated that both AR692B and AR692 were not cytotoxic up to concentrations of 0.5 mM; whereas AR780 induced reduction in cell growth and survival at concentrations > 0.06 mM. Both AR692B and AR692 induced > 40% reduction in carnitine levels at 100 μM. The octyl ester AR780 was more potent with ~ 60% reduction of free carnitine levels when used at 10 μM and > 75% reduction at 50 μM (Fig. 16). The improved cellular potency of the octyl ester (AR780) is likely due to its increased cell permeability. Mildronate was less active than AR780 giving 63% reduction of carnitine levels at 50 μM and 30% reduction at 20 μM (Table 4). Mildronate was not active below 5 μM. Both methyl and octyl ester derivatives were inactive against BBOX in an *in vitro* assay, suggesting that they are hydrolysed to AR692B in cells.

Table 4 Inhibition of carnitine biosynthesis in HEK 293T cells.

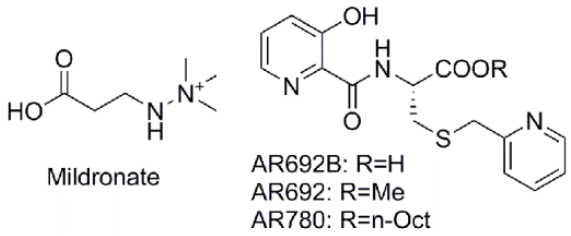

Compound	Concentration of compound [μM]	Carnitine levels*
AR692	100	52 ± 4
AR692	300	33 ± 3
AR692B	100	57 ± 9
AR780	50	21 ± 7
AR780	10	40 ± 4
Mildronate	50	37 ±10
Mildronate	20	70 ± 6

*Measured carnitine levels are given as percentage of free carnitine levels obtained for cells dosed with DMSO (control). Control was set to 100% (SEM ± 13%).

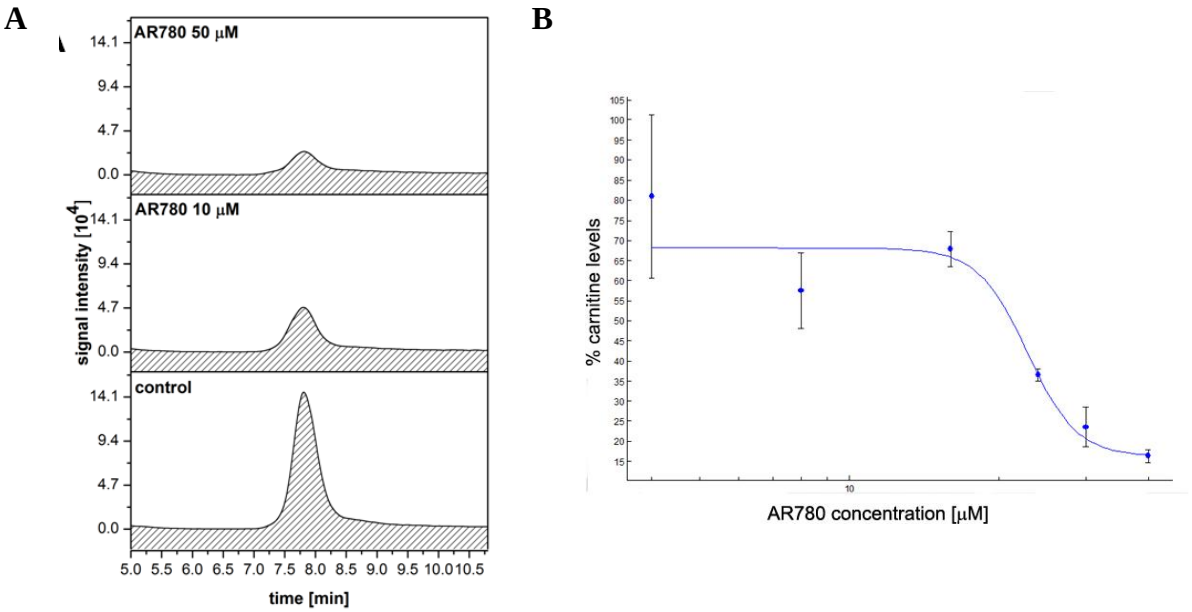

Figure 16 Inhibition of carnitine biosynthesis in HEK 293T cells. A – LC-MS chromatogram of carnitine peak in cells incubated with AR780 and control cells with no compound added. B – The dependency of carnitine levels on AR780 doses in cells (IC_{50} value of 22 μM). Spectra were recorded in the mass range 120-300 Da (scan mode), single ion mode was used in parallel to monitor the following m/z values: 189.2 (TML), 162.2 (CAR), 146.2 (GBB). Mildronate run as a control, displayed 39±3% carnitine levels, when used at 50 μM. Each point represents the mean of three independent cell samples, error bars represent standard deviation from the mean.

4.5 Crystal structure of BBOX in complex with AR692B

To get more insight into the mechanism of BBOX inhibition by AR692B, a crystal structure of human BBOX in complex with Ni(II) (an Fe(II) surrogate) and AR692B was obtained ($P2_12_12_1$ space group, 2.8 Å resolution, PDB code: 4C8R). The overall fold of BBOX in complex with AR692B is similar to the fold of the previously reported BBOX structures (PDB id: 3O2G, 3N6W), i.e. is comprised of eight β-strands (βI-VIII), surrounded by structural elements common to other 2OG-dependent oxygenases and some specific to the BBOX subfamily (DSBH: the core double stranded β-helix of the 2OG oxygenases, which has eight β-strands, I→VIII[31,32]). BBOX did not crystallise in the presence of GBB and AR692B, likely reflecting a competitive mode of AR692B inhibition relative to GBB as well as 2OG. The structure consists of three homodimers (six BBOX molecules per asymmetric unit). In all of the six chains, additional difference density (F_o-F_c), assigned as AR692B, was observed at the active site (Fig. 17). In all six monomers the active site metal is chelated in a bidentate fashion by the AR692B pyridine nitrogen (*trans* to His347) and the side chain carbonyl oxygen (*trans* to Asp204) of AR692B, in addition to the conserved HXD ..H motif and a water molecule. The AR692B carboxylate side chain is positioned to form electrostatic interactions with the guanidinium group of Arg360, similarly to the C-5 carboxylate of 2OG.[14] The pyridine ring of the C-4 side chain appears to have two different binding modes (binding mode I and II, Fig. 18) (from the thioether bond) – the binding mode with >70% occupancy was modelled based on the OMIT F_o-F_c electron density maps (Fig. 18).

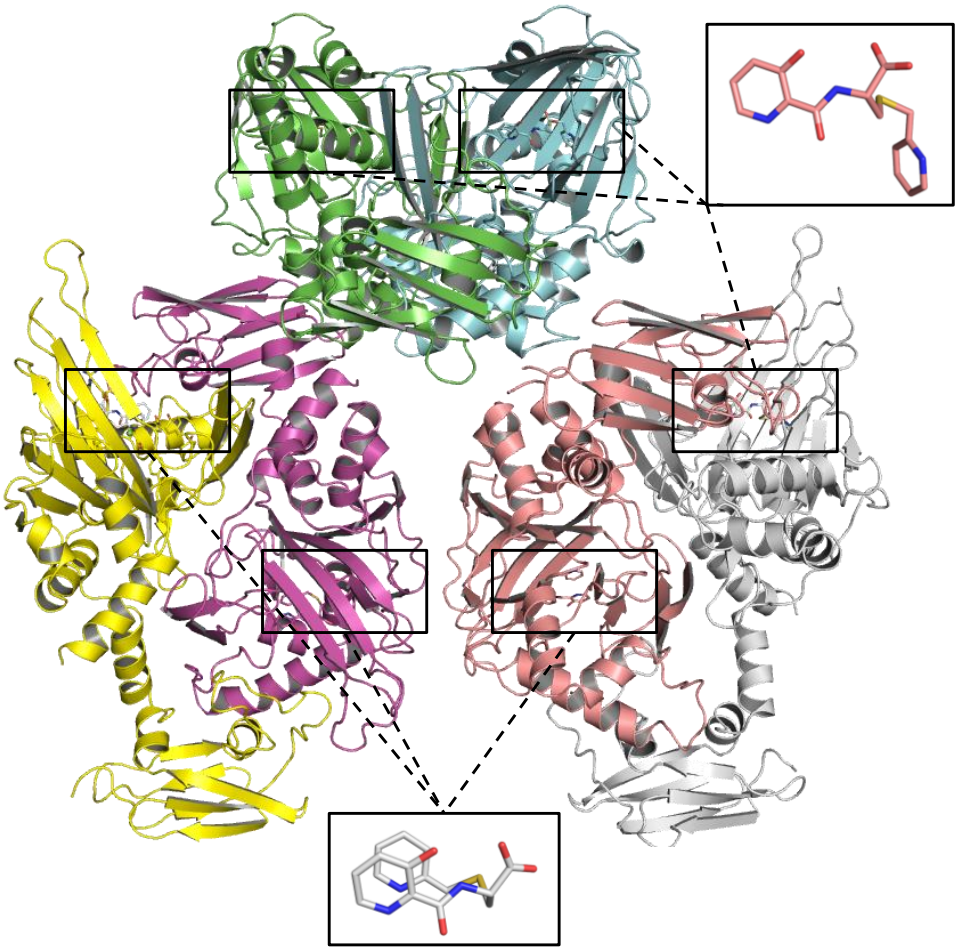

Figure 17 View from a crystal structure of the BBOX.Ni(II).AR692B complex (PDB code: 4C8R) showing the molecules in each asymmetric unit (six molecules per asymmetric unit, organised as three dimers). The inhibitor in grey sticks corresponds to binding mode I and that in pink sticks corresponds to binding mode II.

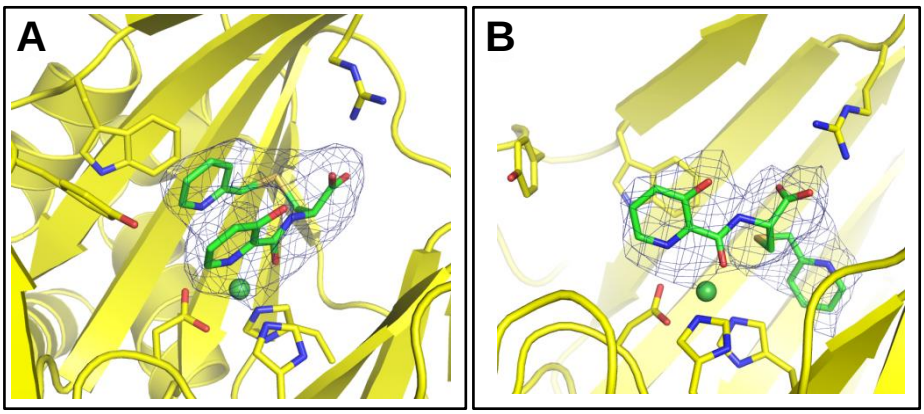

Figure 18 Electron density maps (OMIT F_o-F_c map contoured to 3σ) for ligand binding modes I and II.

In conformer I (modelled in three monomers), the AR692B aromatic side chain is positioned between the metal-coordinating pyridine ring of AR692B and a hydrophobic region of BBOX formed by the side chains of Tyr177, Trp181 and Val183 (Fig. 18A). Such a 'U-shaped' inhibitor binding mode is unprecedented in available 2OG oxygenases inhibitor complexes. In conformer II, the aromatic side chain is positioned to interact in the hydrophobic cleft (adjacent to the 2OG methylene group binding site) formed by the hydrophobic side chains of Leu217 (DSBH β-III), Ile338 and Phe340 (DSBH β-III) (Fig. 18B).

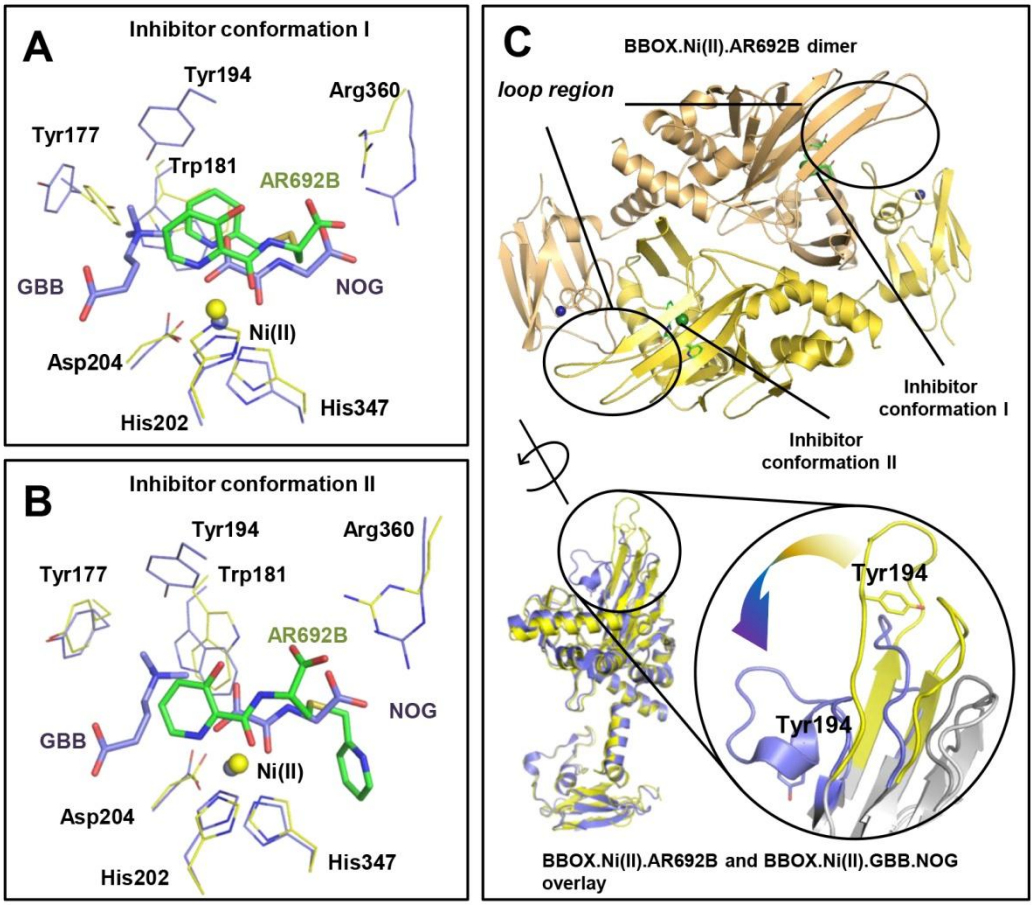

Figure 1 AR692B inhibits BBOX via a structurally unusual mechanism. The inhibitor adopts two different conformations (shown in panels A and B) when complexed with BBOX. In three of the monomers in the asymmetric unit, the inhibitor 'folds back' on itself to form a sandwich-type structure stabilised by inter- and intra-molecular π-stacking interactions involving both of its pyridine rings and Trp181, Tyr 177 protein residues. In the alternative binding mode observed in the three other monomers of the asymmetric unit, the thioether linked pyridine side chain occupies a hydrophobic pocket adjacent to the 2OG binding site. Overlays of BBOX.AR692B complex (yellow) and BBOX.GBB.NOG complex (blue) reveals a steric clash of inhibitor with GBB. NOG (*N*-oxalylglycine) is a close structural mimic of 2OG. C – BBOX functions as a dimer. Overlay of BBOX.Ni(II).NOG.GBB (blue, PDB: 3O2G) and BBOX.Ni(II).AR692B (yellow, PDB: 4C8R) complexes reveals substantial movement of the 'βI/βII loop' (observed in both conformers). Note, the position of Tyr194 changes from an 'open' (yellow) to a 'closed' (blue) conformation upon binding of GBB, leading to the formation of the trimethyl ammonium binding pocket.

4.5.1 Flexible active site loop

Substantial conformational differences can be observed between structures with and without substrate/inhibitor bound (PDB ID: 3O2G/3N6W) (Fig. 20). The metal-coordinating pyridine of AR692B causes a steric clash with a loop (residues 183-199, 'βI/βII loop') involved in GBB binding (in the case of both binding modes of AR692B). In the BBOX.GBB.NOG complex structure this loop contains a short 3_{10} helix linking DSBH strands βI and βII (residues 183-199, 'βI/βII loop'). The Tyr194 residue found in the 'βI/βII loop' is part of an aromatic cage that interacts with the GBB trimethyl ammonium group via hydrophobic and π-cation interactions[33-35] and acts as a 'lid' that encloses the GBB binding site (Fig. 19C). The clash between AR692B and the 'βI/βII loop' causes this part of the structure to unfold and form extended βI and βII strands (Fig. 19C, 20).

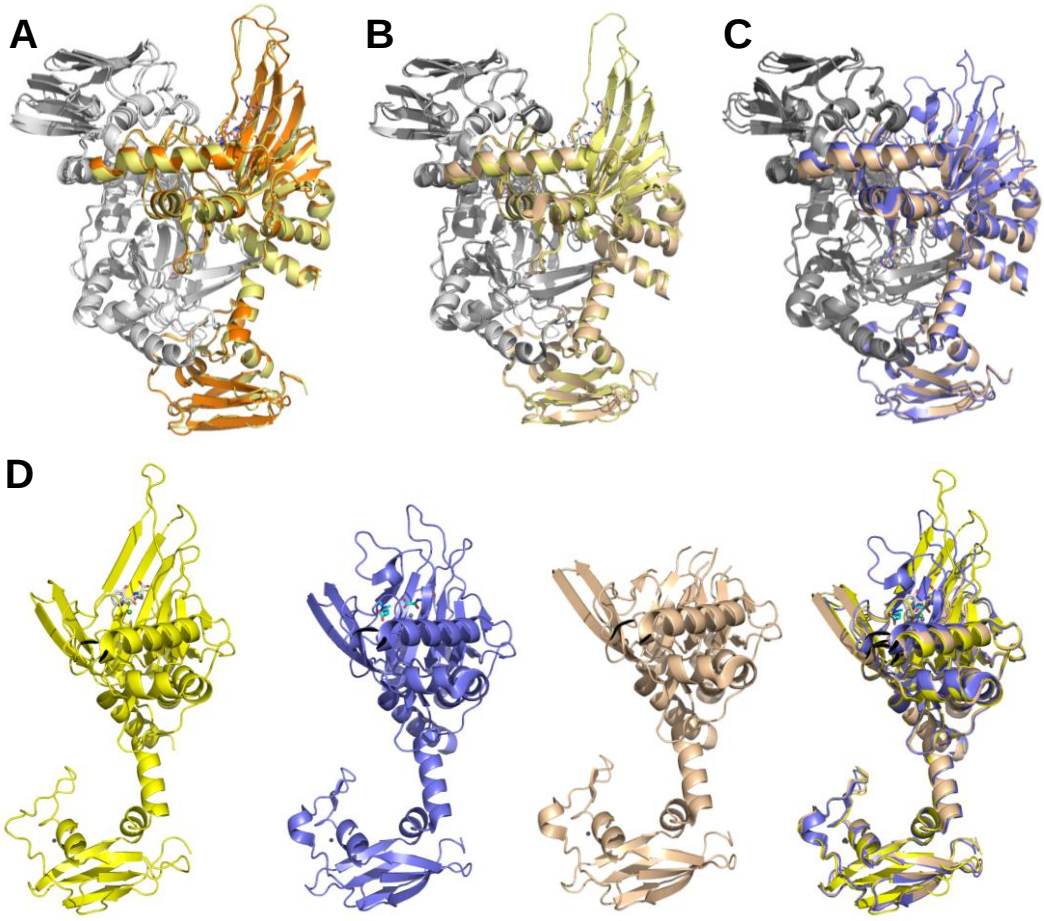

Figure 20 Structural differences in BBOX monomers observed on ligand binding. BBOX.Ni(II).AR692B – binding mode 1 (yellow, PDB code: 4C8R), BBOX.Ni(II).AR692B – binding mode 2 (orange, PDB code: 4C8R), BBOX apo structure (pink, PDB code: 3N6W), BBOX.Ni(II).NOG.GBB (blue, PDB code: 3O2G). A-C: Overlay of BBOX crystal structures D – comparison of corresponding monomers.

4.5.2 Active site loop and mechanism of catalysis

The 'βI/βII loop' can adopt various conformations – an 'open' form with AR692B, loop is apparently unstructured in the BBOX apo form[13] (PDB ID: 3N6W) – and folds to isolate the active site once GBB is bound[14] (PDB ID: 3O2G). These observations suggest that conformational flexibility is an important feature of BBOX catalysis. The 'closed' conformation is likely stabilised by π-cation interactions of the trimethyl ammonium group of GBB with the side chains of the aromatic cage amino acids. As judged from the structure of BBOX in complex with AR692B (which is a 2OG mimetic), 2OG likely does not stabilise the βI/βII loop in a 'closed' conformation, and thus enables binding of GBB substrate after that of 2OG. It was reported that BBOX is inhibited by high concentrations of its substrate GBB *in vitro.*[14,36] Analysis of the available crystal structures reveals that neither GBB nor 2OG appear to (at least efficiently) bind to BBOX once the 'βI/βII loop' is in the closed conformation, because the active site is inaccessible. The observed substrate inhibition may be due to GBB binding prior to 2OG (Fig. 21) and disrupting the ordered sequential mechanism of the 2OG oxygenases,[37] i.e. initial GBB binding prevents that of 2OG, by supporting a 'closed' loop conformation.

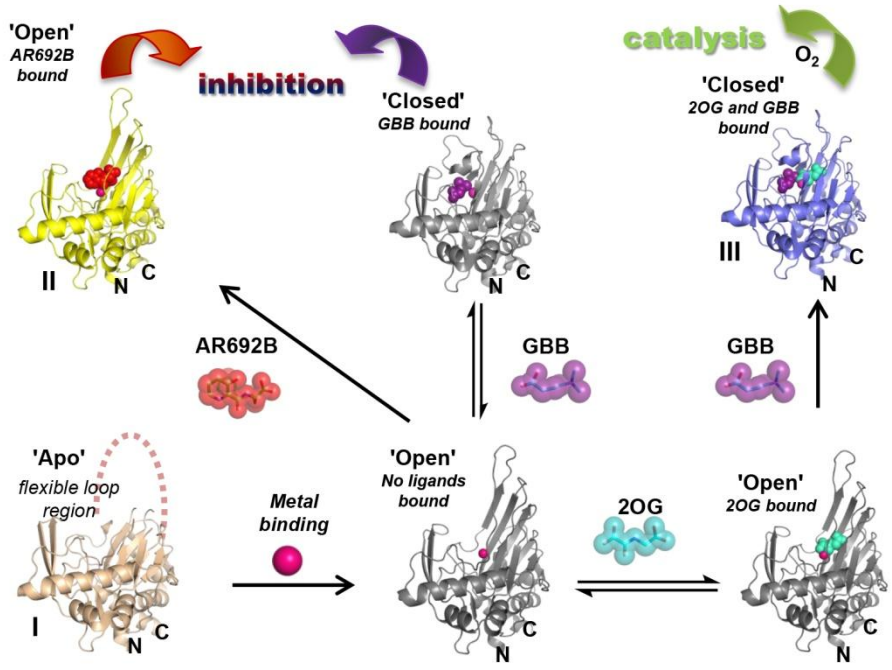

Figure 21 Conformational changes during BBOX inhibition/catalysis. The combined BBOX structures imply a flexible loop (residues 183-199, 'βI/βII loop') can fold to enclose the active site. During catalysis 2OG binding is followed by GBB, then binding of O_2. Binding of GBB stabilizes the 'closed' conformation by π-cation interactions in an aromatic cage (Figure 2C). BBOX substrate inhibition may occur when GBB binds prior to 2OG and 'closed' loop conformation is stabilized hindering 2OG binding. Binding of AR692 competes with both 2OG and GBB and induces the open loop conformation. Only the catalytic domain is shown (residues 106 – 384); grey structures represent predicted conformations with modelled ligands. The catalytic domains in structures II and III have an active site metal bound (Ni(II)), while the structure of the apo-catalytic domain (I) does not have active site metal bound. Metals are shown as pink spheres. PDB codes of BBOX complexes: I –3N6W (in this structure the loop was unresolved), II – 4C8R, III – 3O2G.

In order to investigate the biological significance of GBB-mediated BBOX inhibition, cell-based experiments were conducted. GBB was shown to reduce carnitine levels by ~50% when used at 20 µM (Fig. 22), supporting the proposal that GBB-mediated substrate inhibition of BBOX may be involved in a negative feedback mechanism.

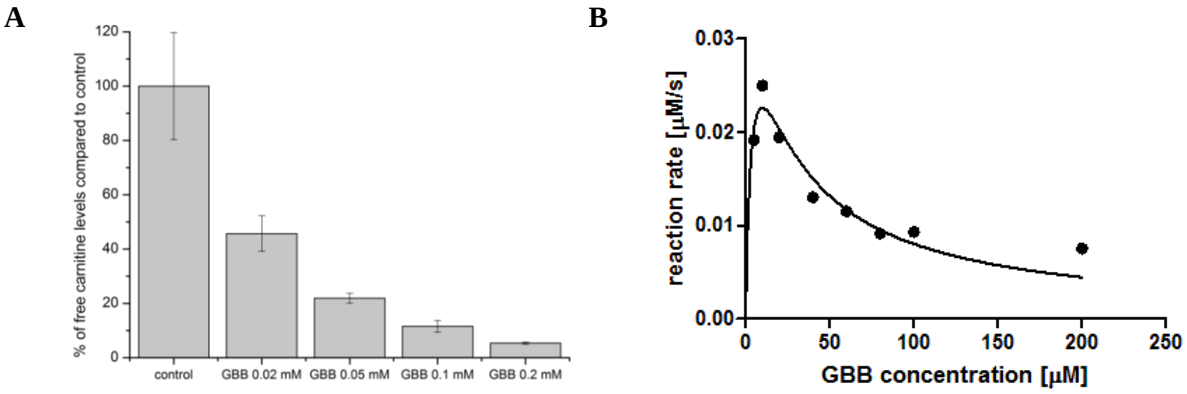

Figure 22 Inhibition of carnitine biosynthesis by GBB. Cells were cultured with additional GBB added to the media. Cells incubated with GBB have shown decrease in levels of free carnitine compared to control free carnitine levels (panel A). These observations are consistent with *in vitro* data showing an inhibitory effect of GBB on BBOX activity at concentrations above 20 µM (panel B).

4.6 Inhibition by other pyridine based compounds

In addition to 3-hydroxy picolinic acid-containing analogues, other pyridine-based scaffolds were tested for BBOX inhibition, e.g. pyridine dicarboxylates (PDCA analogues (**58**)-(**62**), Table 5). These were previously shown to inhibit 2OG-dependent oxygenases, including histone demethylases. However, none of these scaffolds were potent inhibitors of human BBOX. This observation is interesting as 2,4-PDCA (**59**) and 2,5-PDCA (**60**) were demonstrated to inhibit BBOX from *Pseudomonas sp. AK1*. In contrast, 3,4-dihydroxybenzoic acid derivatives, which were one of the most potent inhibitors of BBOX from *Pseudomonas sp. AK1* are also relatively good inhibitors of human BBOX (analogues (**63**)-(**65**), Table 5).

The derivatives of 2-picolinic acid substituted at position 5 or 6 of the pyridine ring were also tested. In general, the analogues that carry a hydroxyl group at position 3 tolerated bulky substituents at position 5 (analogues (**66**)-(**68**)). The analogues substituted in position 5 or 6 but without the 3-hydroxyl were not active (analogues (**70**)-(**74**)).

Table 5 Inhibition of human BBOX by pyridine dicarboxylates and related compounds.

no	name	structure	IC_{50} [µM]
58	2,3-PDCA	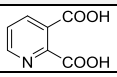	>500
59	2,4-PDCA	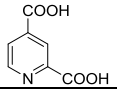	>200
60	2,5-PDCA	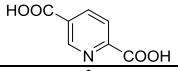	>200
61	2,6-PDCA	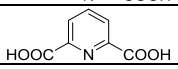	>200
62	3,4-PDCA	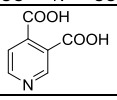	>500
63	3,4-dihydroxybenzoic acid	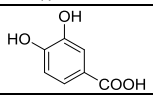	12.7±2.6
64	3,4-dihydroxyphenylacetic acid	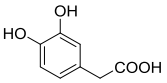	28.5±8.2
65	3,4-dihydroxycinnamic acid	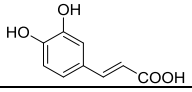	26.2±8.9

Table 6 Inhibition of human BBOX by analogues of 2-picolinic acids derivatised on the pyridine ring.

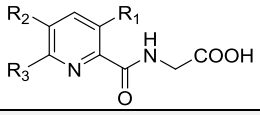

no	R1	R2	R3	RA%*
66	OH	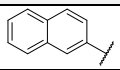	H	48
67	OH	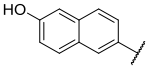	H	48
68	OH	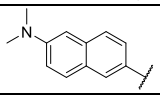	H	51
69	OH	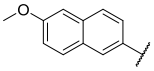	H	90
70	H	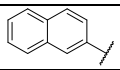	H	92
71	H	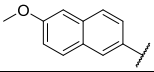	H	91
72	H	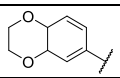	H	77
73	H	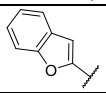	H	93
74	H	H		96

RA = % residual activity corresponds to the activity of BBOX when inhibitor was present at 50 µM compared to the activity of BBOX without inhibitor.

5 Inhibition of BBOX by isoquinolines and quinolines

5.1 Isoquinoline analogues

The broad screen identified isoquinoline analogue (**75**) as a inhibitor of BBOX (IC_{50} 30 μM). In order to explore this lead further, a series of isoquinoline analogues was synthesised (Scheme 5). Similar to the pyridine derivatives, removal of the nitrogen or hydroxyl group from the *N*-acyl aromatic ring led to loss of potency (Fig. 23). In the isoquinoline series, C-α side chains with the (*S*)-stereochemistry were also preferred over those with the (*R*)-stereochemistry. However, in contrast to the pyridine series, small side chains were preferred in the case of the hydroxy-isoquinolines, with the methyl-substituted compound having the best inhibitory properties (Table 7, analogue (**77a**)). Isoquinolines retained their inhibitory properties, providing they were functionalised with a hydroxyl group in the meta- position to the isoquinoline nitrogen (Fig. 23). As opposed to the 3-hydroxy-2-picolinic acid series, removal of the pyridine nitrogen seemed to have less impact and did not lead to complete loss of potency (Fig. 23). Collectively, these results imply that isoquinolines may bind to BBOX in a different mode than the hydroxypyridine series.

Table 7 Inhibition of BBOX by isoquinoline analogues derivatised at Cα.

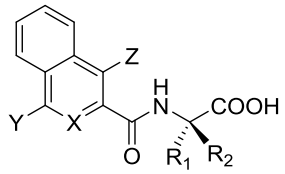

no	X	Y	Z	R_1	R_2	IC_{50} [μM]
75	N	Cl	OH	H	H	30.2±6.4
76a	N	Cl	OH	CH_2-3-indole	H	11.4±0.84
76b	N	Cl	OH	H	CH_2-3-indole	33.4±4.5
77a	N	Cl	OH	CH_3	H	5.8±0.77
77b	N	Cl	OH	H	CH_3	72.6±11.6
78a	N	Cl	OH	$CH(CH_3)_2$	H	99.6±22.0
78b	N	Cl	OH	H	$CH(CH_3)_2$	115±39
79a	N	Cl	OH	$CH_2CH(CH_3)_2$	H	89.2±14.5
79b	N	Cl	OH	H	$CH_2CH(CH_3)_2$	49.1±7.9
80a	N	Cl	OH	CH_2Ph	H	13.6±0.77
80b	N	Cl	OH	H	CH_2Ph	62.6±11.6
81a	N	Cl	OH	$(CH_2)_2COOH$	H	418±96
81b	N	Cl	OH	H	$(CH_2)_2COOH$	380±35
82a	N	Cl	OH	CH_2COOH	H	459±82
82b	N	Cl	OH	H	CH_2COOH	628±102
83	N	H	H	H	H	>1000
84	H	H	OH	H	H	207±12
85	H	H	OH	CH_2-3-indole	H	83±24

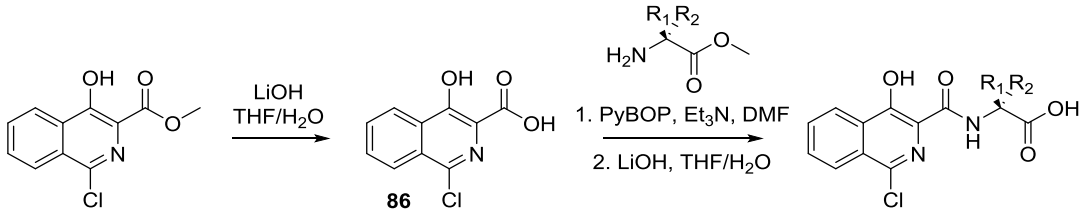

Scheme 5 Synthesis of isoquinoline analogues.

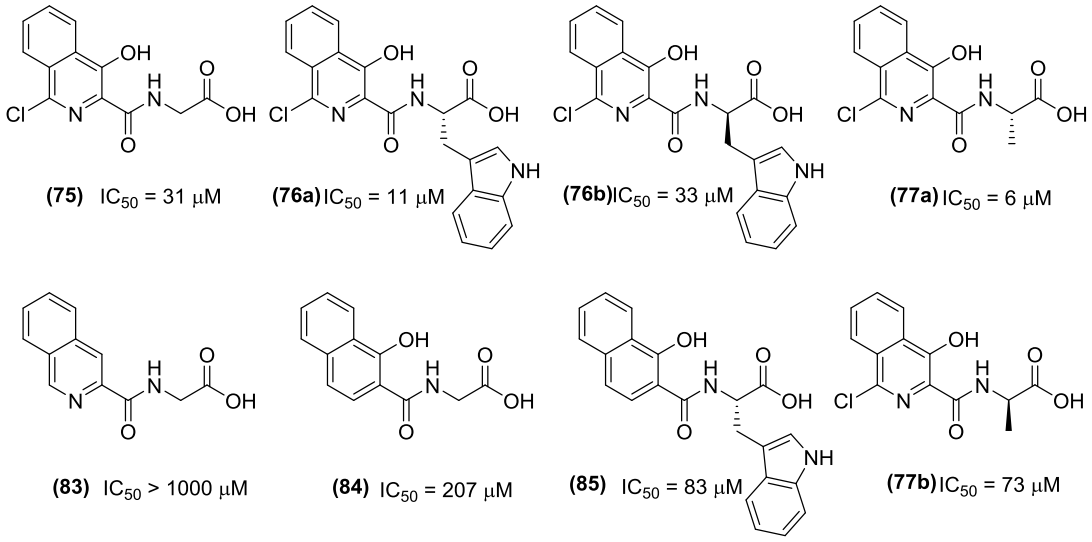

Figure 23 Isoquinoline series analogues display relatively good BBOX inhibitory properties, with IC_{50} values in the low micromolar region. For isoquinolines, as for the pyridines, removal of the pyridine-nitrogen (**84**) or hydroxyl (**83**) group leads to loss of potency. Unlike the pyridinyl-series, small side chains (**77a**) are preferred; however the (*S*)-stereochemistry was still favoured (**76a**, **77a**). Analogues with bulky aromatic side chains attached were less potent inhibitors and the difference between potency of (*S*)-analogue (**77a**) and (*R*)-analogue (**77b**) was less profound than in the case of methyl substituent.

5.2 Quinoline analogues

Quinoline analogues, as opposed to isoquinoline containing scaffolds, were relatively poor BBOX inhibitors, with the exception of 2-carboxy-8-hydroxyquinoline (**86**), which had IC_{50} value of 15.8 μM. Interestingly, 5-carboxy-8-hydroxyquinoline (**88**) and 4-carboxy-8-hydroxyquinoline (**89**), which were shown to be broad spectrum histone demethylase inhibitors and to some extent inhibit other 2OG dependent oxygenases (prolyl hydroxylases and DNA modification enzymes),[28] inhibited BBOX only in the high micromolar range, with IC_{50} values of 196 and 111 μM, respectively (Table 8). 2-Carboxy-3-hydroxyquinoline derivative (**96**) is a ring-expanded analogue of 3-hydroxy-2-picolinic acid based scaffold (**33**). (**33**) was a potent inhibitor of BBOX with IC_{50} value of 6.2 μM. Surprisingly, analogue (**96**) did not inhibit BBOX even at high micromolar concentrations.

Table 8 Inhibition of BBOX by quinoline containing analogues.

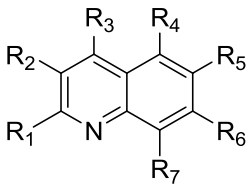

no	R_1	R_2	R_3	R_4	R_5	R_6	R_7	% RA	IC_{50} [µM]
86	COOH	H	H	H	H	H	OH	-	15.8±1.4
87	H	H	H	H	H	COOH	OH	-	149±12
88	H	H	H	COOH	H	H	OH	-	196
89	H	H	COOH	H	H	H	OH	-	111
90	H	H	H	SO_3H	H	H	OH	95±9	-
91	H	H	H		H	H	OH	50±8	-
92	H	H	H	Cl	H	H	OH	83±22	-
93	COOH	OH	H	H	H	H	H	-	152±40
94	COOH	H	OH	H	H	H	H	-	>1000
95	COOH	OH	OH	H	H	H	H	-	179.2±18
96	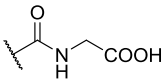	OH	H	H	H	H	H	-	>1000
97	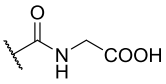	H	H	H	H	H	OH	-	190±15
98	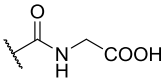	H	H	H	H	H	H	97±7	-
99	H	H	H	H	H	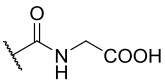	OH	-	338±42

RA = % residual activity corresponds to the activity of BBOX when inhibitor was present at 50 µM compared to the activity of BBOX without inhibitor.

6 Inhibition of BBOX by hydroxythiazoles

6.1 Initial screen hit

The initial broad screen identified a known PHD2 (prolyl hydroxylase domain protein 2) inhibitor[38] with the hydroxythiazole scaffold (**100**) as inhibitor of BBOX with IC_{50} in low micromolar range (IC_{50} 12.5 µM). Therefore this scaffold was further investigated.

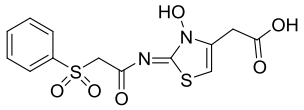

(**100**)

Figure 24 Structure of hydroxythiazole (**100**).

6.2 Structure – activity relationship studies with hydroxythiazoles

6.2.1 Variations in linker

Structure-activity relationship studies as a set of hydroxythiazoles identified several features, including linker properties, as important for potency. The most potent analogues had thioether or sulphonyl linkage (analogues (**100**) and (**101**), respectively), while analogues with amine or carbon linkage were not active (analogues (**102**) and (**103**)) (Table 9). The analogues with extended linker were examined, revealing longer linkages could be also accommodated, provided they contain a sulphonyl or thioether moiety (Table 10).

Table 9 Effects of the linker atom on the potency of hydroxythiazole based inhibitors.

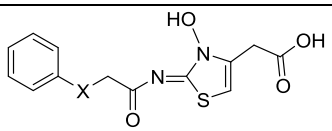

no	X	IC_{50} [µM]
100	SO_2	12±5
101	S	4.7±0.2
102	NH	>50
103	CH_2	>50

Table 10 Effects of the linker on the potency of hydroxythiazole based inhibitors.

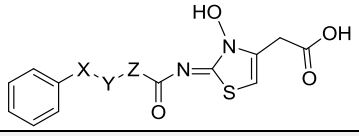

no	X	Y	Z	IC_{50} [µM]
104	SO_2	CH_2	CH_2	7.5±1.0
105	CH_2	SO_2	CH_2	5.9±5.9
106	CH_2	CH_2	SO_2	3.7±0.8
107	CH_2	CH_2	CH_2	>50
108	CH_2	S	CH_2	3.1±0.8

6.2.2 Variations in thiazole ring

N-Hydroxylation was found to be vital for the hydroxythiazole inhibitory properties – analogue (**109**), where thiazole core was not hydroxylated, did not inhibit BBOX at 50 μM concentration (Table 11). Substitutions at the carbon adjacent to the sulphur atom of thiazole ring were not tolerated, as shown with the examples of analogues (**110**) and (**111**) (Table 11).

Table 11 Effects of the substitutions in the thiazole ring on the potency of inhibitors.

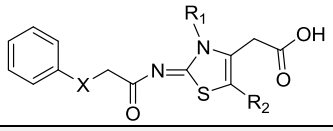

no	X	R_1	R_2	IC_{50} [μM]
100	SO_2	OH	H	12±5
109	SO_2	H	H	>50
110	SO_2	OH	CH_3	>50
101	S	OH	H	4.7±0.2
111	S	OH	CH_3	>50

6.2.3 Modifications on CH_2 adjacent to carboxylate

The analogues mono-substituted at CH_2 adjacent to carboxylate remained potent inhibitors, even with a bulky substituents, such as benzyl group (analogues (**114**) and (**118**)). Di-substitutions were not tolerated, as shown on the example of dimethyl substituted analogues (**115**) and (**119**) (Table 12).

Table 12 Effects of the substituents on the carbon adjacent to the carboxylate on the inhibitory properties of hydroxythiazoles.

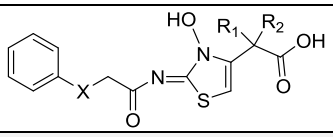

no	X	R_1	R_2	IC_{50} [μM]
100	SO_2	H	H	12±5
112	SO_2	CH_3	H	6.0±0.8
113	SO_2	iPr	H	13±2
114	SO_2	CH_2Ph	H	15±1
115	SO_2	CH_3	CH_3	>50
101	S	H	H	4.7±0.2
116	S	CH_3	H	3.3±2.2
117	S	iPr	H	13±2
118	S	CH_2Ph	H	>50
119	S	CH_3	CH_3	>50

6.2.4 Variations in the aromatic side chain

Several hydroxythiazole analogues with various aromatic side chains were examined. Substitution of the aromatic side chain with a methyl group (**136**) or a cyclohexyl group (**155**) resulted in a loss of activity. In general, analogues with phenyl ring (substituted or unsubstituted) or a naphthyl ring were potent inhibitors. Bulky substitutions within the phenyl ring (e.g. biphenyl analogues) were still active in the series with short linkage (e.g. analogues (**130)**, (**171**) – Table 13 and 15); in a series with CH_2 extended linker these substitutions resulted in loss of the activity (e.g. analogues (**150**), (**192**) – Table 14 and 16).

The most potent analogue (IC_{50} 0.63 µM) contained a phenyl ring substituted in position 4 with the CN group (**146**). The CN group is quite small and has been demonstrated to make polar interactions with proteins within narrow pockets,[39] so may be well accomodated into the BBOX active site.

Table 13 Effects of different side chains on the activity of hydroxythiazole inhibitors with a sulphonyl linkage.

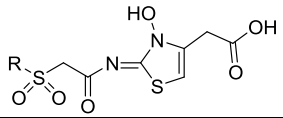

no	R	IC_{50} [µM]	no	R	IC_{50} [µM]
120		11±1	**129**	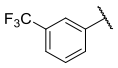	1.6±0.3
121	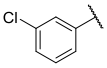	2.6±0.4	**130**	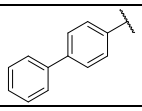	12±28
122	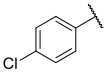	1.6±0.3	**131**	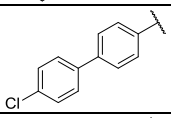	>50
123	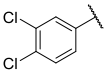	1.8±0.6	**132**	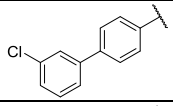	>50
124	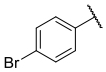	1.0±0.3	**133**	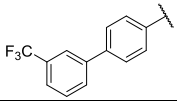	>50
125	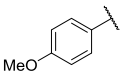	9.9±3.6	**134**	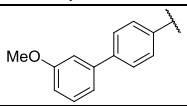	>50
126	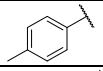	16±3	**135**	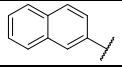	2.7±0.8
127	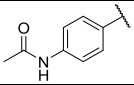	14±4	**136**	CH_3	>50
128	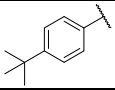	>50	**137**		3.2±0.9

Table 14 Effects of different side chains on the activity of hydroxythiazole inhibitors with a methylene extended sulphonyl linkage.

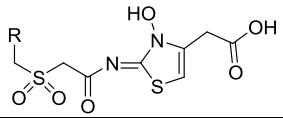

no	R	IC_{50} [µM]	no	R	IC_{50} [µM]
138		5.9±5.9	**147**	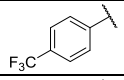	1.3±0.2
139		4.2±0.8	**148**	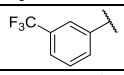	3.9±0.4
140		7.1±0.9	**149**	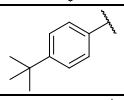	>50
141		6.6±1.5	**150**	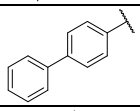	>50
142		2.7±1.3	**151**	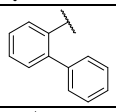	>50
143		3.3±0.5	**152**		12±3
144	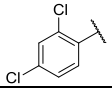	8.4±1.6	**153**	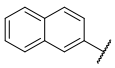	9.2±1.5
145		1.2±0.2	**154**	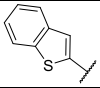	4.7±1.8
146	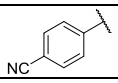	0.63±0.10	**155**		>50

Table 15 Effects of different side chains on the activity of hydroxythiazole inhibitors with thioether linkage.

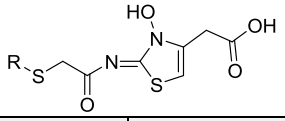

no	R	IC_{50} [µM]	no	R	IC_{50} [µM]
156		12±2	**165**	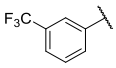	16±4
157	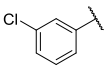	35±2	**166**	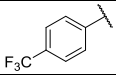	88±7
158	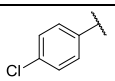	2.6±0.8	**167**		4±1
159	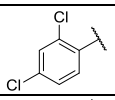	8.3±1.1	**168**	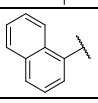	5.3±3.7
160	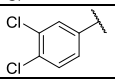	5.5±1.1	**169**	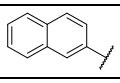	4.8±2.9

161	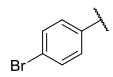	5.1±4.2	**170**	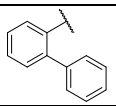	7.7±1.1
162	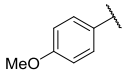	>50	**171**	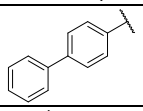	8.1±1.9
163		5.1±2.1	**172**	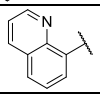	>50
164	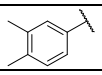	>50			

Table 16 Effects of different side chains on the activity of hydroxythiazole inhibitors with methylene extended thioether linkage.

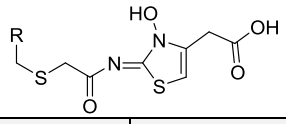

no	R	IC_{50} [µM]	no	R	IC_{50} [µM]
173		>50	**184**		>50
174		32±6	**185**	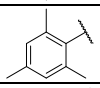	9.1±0.9
175		14±2	**186**	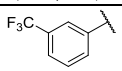	>50
176		>50	**187**	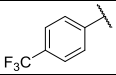	38±9
177	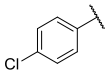	>50	**188**	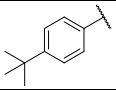	>50
178	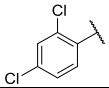	>50	**189**		>50
179	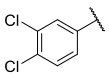	15±4	**190**	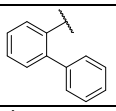	>50
180	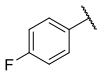	27±8	**191**	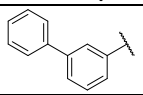	>50
181		50±1	**192**	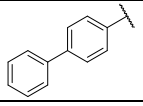	>50
182	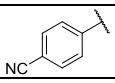	4.1±0.9	**193**	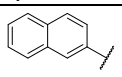	>50
183		>50	**194**	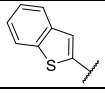	>50

6.2.5 Therapeutic perspectives

In conclusion, hydroxythiazole based analogues present a good scaffold for BBOX inhibition. However, these analogues were shown to inhibit also other 2OG dependent oxygenases,[38] which may raise a problem of selectivity. In particular, hydroxythiazoles are potent inhibitors of PHD2. PHD2 is a cellular oxygen sensor[40,41] and participates in the differentiation of metabolism under normoxic/hypoxic conditions. PHD2 catalyses the hydroxylation of HIF-1α (Hypoxia inducible factor subunit 1α) proline residue, supporting degradation of this transcription factor.[42,43] It was shown that stabilisation of HIF family members provides protection against ischemia-induced protein damage.[44] Therefore, the dual action of hydroxythiazole based inhibitors on BBOX and PHD2 may be of interest in the treatment of ischemia related heart conditions.

7 Inhibition of BBOX by substrate analogues

7.1 Screening of GBB analogues

Following the success of Mildronate as a clinically used BBOX inhibitor, other GBB-like compounds were assayed for the inhibition of BBOX. Analogues were screened using the fluoride release assay as described (Section 2.1 and 12.2.1) % RA values used in this section correspond to the residual activity of BBOX when inhibitor was present at 50 µM compared to the activity of BBOX without inhibitor. Substrate inhibition of BBOX by GBB was at a level of 45±6 % RA (when GBB was used at 50 µM).

7.1.1 GBB analogues with variable chain length

The GBB analogues where the chain length is shorter or longer that GBB (i.e. (**195**), (**1**), (**2**), (**3**)), did not inhibit BBOX when used at 50 µM concentration (Table 17). It was found that unsaturated GBB analogue (**5**), previously identified as an inhibitor of BBOX from *Pseudomonas sp AK1* also inhibited human BBOX. The unsaturated methyl ester (**196**) was a BBOX inhibitor, however less potent than its free carboxylate form (Table 18).

Table 17 Inhibition of BBOX by GBB analogues with different chain lenghts.

no	Structure	% RA
195	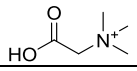	94±10
1	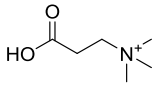	89±10
2	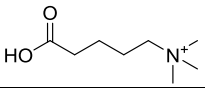	98±8
3	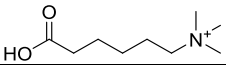	105±8

Table 18 Inhibition of BBOX by unsaturated GBB analogues.

no	Structure	% RA
5	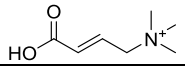	11±4
196	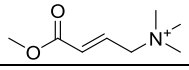	53±6
197	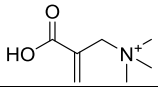	110±5

7.1.2 Chain substituted GBB analogues

Substitutions in the aliphatic chain of GBB did not lead to potent inhibitors of BBOX (analogues (**198**)-(**206**)); however some inhibition was observed both in case of 2- and 3-substituted derivatives (Table 19). L-Carnitine (**199**) was shown to weakly inhibit BBOX, while almost no inhibition could be observed in case of D-carnitine (**198**). In general, (*3R*)-substitutions lead to more potent inhibitors than (*3S*) analogues (Table 19). In the case of 2-substituted analogues, both (*2S*) and (*2R*) derivatives were moderately good inhibitors (analogues (**203**)-(**205**)). N^{ε}-trimethyllysine (**206**), a precursor of carnitine biosynthesis did not inhibit BBOX (Table 19).

Table 19 Inhibition of BBOX by chain-substituted GBB analogues.

no	Structure	% RA
198	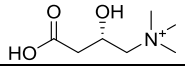	90±7
199	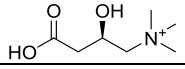	71±4
200	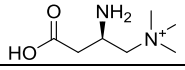	81±5
201	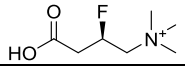	70±12
202	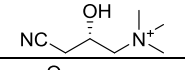	106±7
203	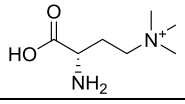	66±10
204	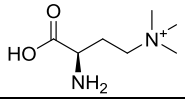	72±3
205	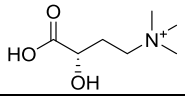	73±6
206	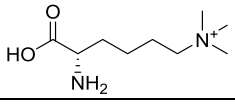	103±11

7.1.3 GBB analogues with modified carboxylate moiety

Replacement of the carboxylate with a keto moiety (**207**) led to loss of activity. The methyl ester (**208**) was also a less potent inhibitor than GBB itself (Table 20). Only the hydroxamic acid derivative (**209**) was quite good inhibitor, compared to the other tested GBB analogues.

Table 20 Inhibition of BBOX by carboxylate modified GBB analogues.

no	Structure	% RA
207	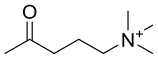	98±2
208	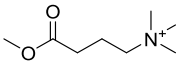	65±5
209	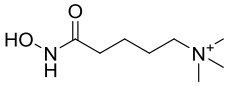	37±4

7.1.4 GBB analogues with modifications in trimethyl ammonium moiety

In general, replacement of the trimethyl ammonium group of GBB was not well tolerated and led to loss of inhibitory properties. Analogues with aromatic rings were tested in the hope that they could form interactions within the BBOX hydrophobic pocket constituted of several aromatic side chains, responsible for binding of trimethyl ammonium group of GBB. However, those did not display any inhibitory properties (i.e. analogues **214-216**, Table 21). Only dimethyl GBB (**4**) displayed some weak inhibition, probably due to possible protonation of the nitrogen atom, resulting in positively charged group, capable of forming π-cation interactions within the BBOX hydrophobic pocket.[14]

Table 21 Inhibition of BBOX by trimethyl ammonium modified GBB analogues.

no	Structure	% RA
4	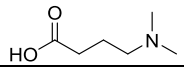	86±4
210	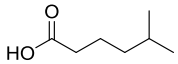	96±7
211	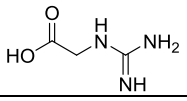	106±5
212	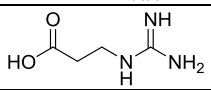	104±6
213	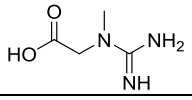	100±7
214	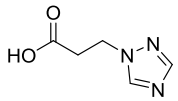	116±11
215	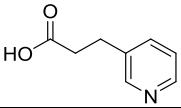	95±8
216	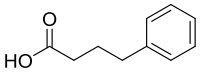	103±11
217	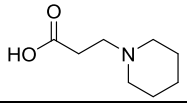	71±6
218	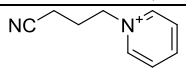	92±3

7.1.5 Mildronate analogues

Structural variations of Mildronate were also examined as an attempt to improve BBOX inhibition properties. It was revealed that the analogue where trimethylammonium was replaced by *tert*-butyl group (**220**) was still a good BBOX inhibitor, while dimethyl Mildronate analogue (**222**) was not active under the assay conditions (Table 22). This might indicate that steric requirements (presence of 3 methyl groups) are as important as charge requirements (presence of trimethylammonium group) for analogue binding to BBOX. Analogue where nitrogen was replaced with oxygen (**221**) was not active.

Table 22 Inhibition of BBOX by Mildronate analogues.

no	Structure	% RA
219	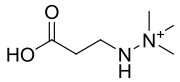	48±1
220	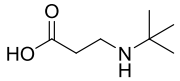	50±6
221	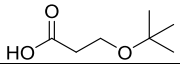	90±6
222	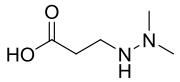	105±2

7.1.6 Acetylcholine analogue

Acetylcholine analogues were examined as BBOX inhibitors, due to their close structural resemblance to GBB, however none of them was found to inhibit BBOX under the assay conditions (Table 23).

Table 23 Inhibition of BBOX by acetylcholine analogues.

no	Structure	% RA
223	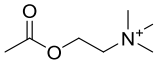	113±5
224	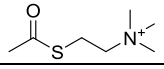	92±2
225	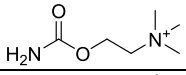	104±16
226	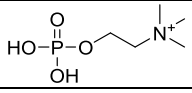	98±6

7.1.7 Cyclic GBB analogues

5-Membered and 6-membered cyclic GBB analogues were examined as BBOX inhibitors (Table 24 and 25). Analogues (**228**), (**231**) and (**234**) were identified as potential inhibitors of BBOX.

Table 24 Inhibition of BBOX by cyclic GBB analogues with a 5-membered ring.

no	Structure	% RA
227	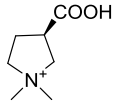	97±8
228	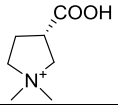	64±6
229	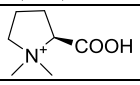	95±2
230	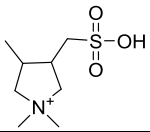	88±7

Table 25 Inhibition of BBOX by cyclic GBB analogues with a 6-membered ring.

no	Structure	% RA	no	Structure	% RA
231	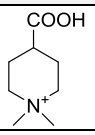	50±12	**237**	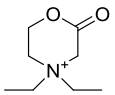	93±13
232	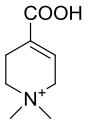	99±2	**238**	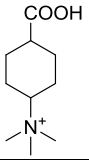	99±6
233	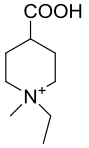	90±3	**239**	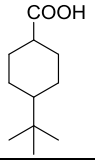	94±20
234	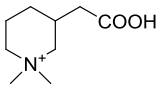	42±9	**240**	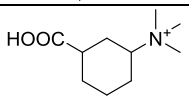	105±6
235	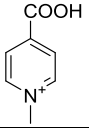	88±11	**241**	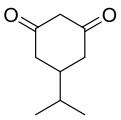	74±8
236	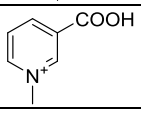	82±10			

7.1.8 Daminozide analogues

A plant growth regulator, daminozide (**242**) was demonstrated to be an inhibitor of KDM2/7 family of human JmjC histone demethylases.[29] Analogues of daminozide were examined as BBOX inhibitors because of their close resemblance to GBB/Mildronate structure. None of the tested analogues demonstrated any BBOX inhibitory activity (Table 26).

Table 26 Inhibition of BBOX by daminozide analogues.

no	Structure	% RA*	IC_{50} [µM]
242	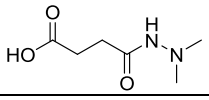	83±7	-
243	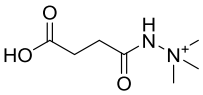	85±5	-
244	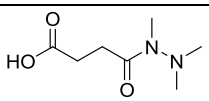	71±7	-
245	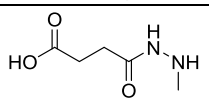	6±5	120
246	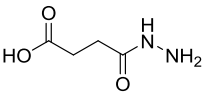	14±10	290
247	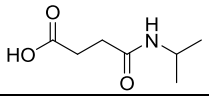	107±5	-
248	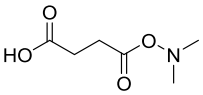	14±6	-
249	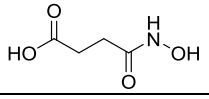	24±5	-
250	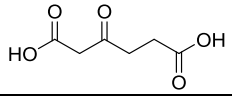	19±3	-
251	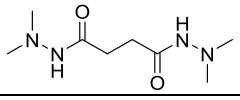	99±9	-

* %RA when 0.5 mM of inhibitor was used.

8 Modulating of carnitine levels in cell

8.1 Regulation of carnitine levels by Mildronate

8.1.1 Influence of Mildronate on different cell lines

Mildronate is a clinically used agent with carnitine lowering properties. The influence of Mildronate on carnitine levels in different cell types was examined. HEK 293T kidney embryonic cells, MCF7 breast cancer cells, RCC4 renal carcinoma cells (both VHL deficient and expressing VHL), 786-0 renal carcinoma cells (both VHL deficient and expressing VHL) were tested. The results revealed that Mildronate decreases carnitine levels across a range of different cell lines to a similar extent (Fig. 25).

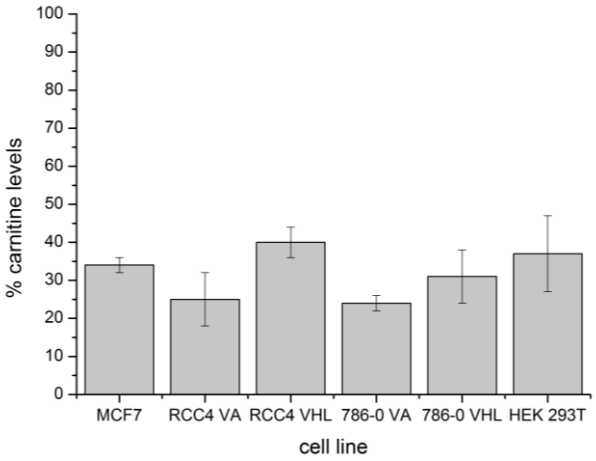

Figure 25 Decrease of carnitine levels in different cell lines by 50 μM Mildronate. % Carnitine levels are defined as percentage of carnitine in the Mildronate treated cells compared to carnitine levels in non-treated cells. Carnitine levels were as follows: MCF7 - 34±2%, RCC4 VA - 25±7%, RCC4 VHL - 40±4%, 786-0 VA - 24±2%, 786-0 VHL - 31±7%, HEK 293T - 37±10%.

8.2 GBB analogues can decrease carnitine levels in cell

GBB analogues that were good inhibitors of BBOX *in vitro* were tested for their influence on carnitine levels in cells. Surprisingly, hydroxamic acid (**209**) did not lower cell carnitine content as it may have been expected from one of the best *in vitro* inhibitors in the GBB analogue set. Moreover, the Mildronate analogue (**253**) did not show any effect on carnitine levels, consistent with its *in vitro* activity (Table 27). Unsaturated analogue (**5**) had a carnitine lowering effect similar to that of Mildronate. Analogues (**252**), (**254**) and (**234**) were the best carnitine lowering agents. However, in this set, only analogue (**254**) was a potent BBOX inhibitor *in vitro*, which suggest analogues (**252**) and (**234**) likely decrease carnitine levels through a mechanism different from BBOX inhibition.

Table 27 Inhibition of BBOX by selected GBB analogues *in vitro* and their effect on the carnitine levels in cell.

no	Structure	IC_{50} [μM]*	% carnitine levels**	
			50 μM	10 μM
219	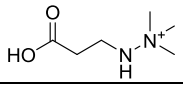	62±10	48±3	-
4	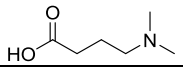	>150	-	-
5	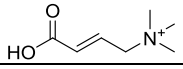	8.7±1.1	42±2	-
196	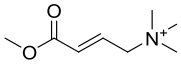	122±24	-	-
252	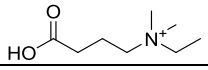	42±15	6.4±0.3	13±1
220	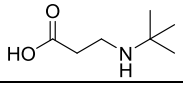	63±14	-	-
253	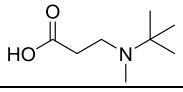	46±14	91±6	104±2
254	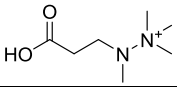	2.3±0.6	15±0.3	34±4
209	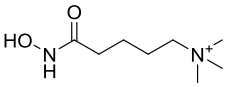	26±8	80±3	73±3
228	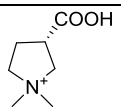	97±20	-	-
231	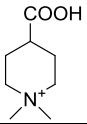	>150	-	-
234	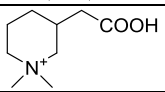	67±7	3.4±0.2	8.8±0.6

*IC_{50} as measured with recombinant human BBOX by fluoride release assay; **carnitine levels in HEK293T cells treated with 50 μM or 10 μM compound, relative to carnitine levels in control cells with no inhibitor added.

8.3 Influence of 2OG dependent oxygenase inhibitors on carnitine levels in cell

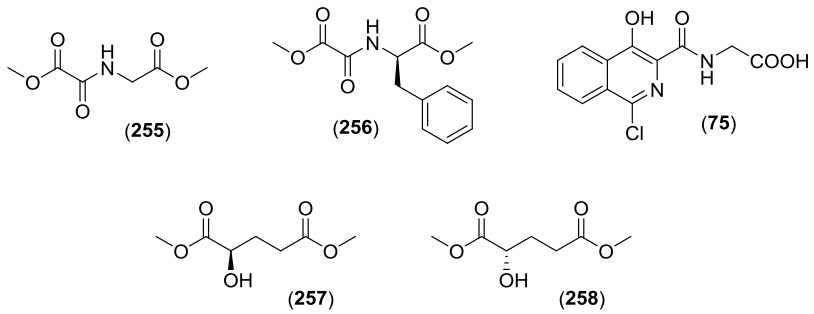

Figure 26 Structures of cell permeable derivatives of 2OG dependent oxygenases inhibitors.

8.3.1 DMOG and analogues

2OG analogues, including *N*-oxalylglycine (NOG), are known 2OG dependent oxygenases inhibitors. The influence of NOG on carnitine levels in cells was tested employing a cell permeable derivative dimethyl-NOG (DMOG, **255**). The results revealed that DMOG had only small influence on the carnitine levels in cells, even at high concentrations of the inhibitor (up to 1 mM), which is consistent with high IC_{50} value obtained for DMOG in assay with isolated BBOX (IC_{50} > 200 μM) (Fig. 27).

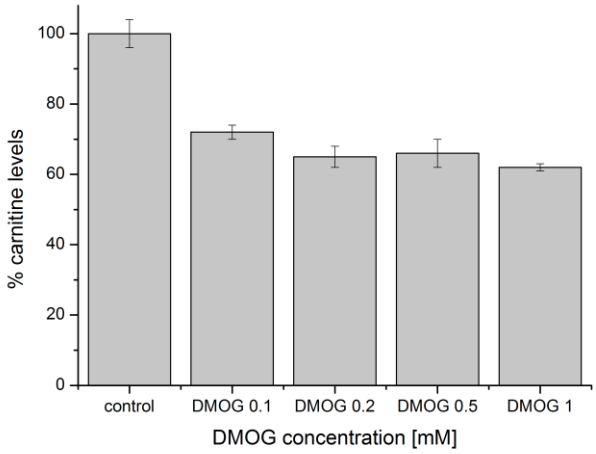

Figure 27 Influence of DMOG on the carnitine levels in cell. Carnitine levels were as follows: control - 100±4%, DMOG 0.1 mM - 72±2%, DMOG 0.2 mM - 65±3%, DMOG 0.5 mM - 66±4%, DMOG 1mM - 62±1%.

The NOG derivative, D-phenyl-*N*-oxalylglycine (NOFD) – an inhibitor of 2OG dependent asparaginyl hydroxylase FIH[45,46] – was also tested in the cell based assay. To improve cell uptake, the dimethyl derivative DM-NOFD (**256**) was used; however, no reduction in carnitine levels was observed at 0.2 mM of DM-NOFD. Similarly, the isoquinoline analogue (**75**), which was found to be an inhibitor of 2OG dependent prolyl hydroxylase PHD2[24,47-49] as well as inhibitor of BBOX with moderate potency (IC_{50} 30 μM), did not affect carnitine levels in cells when used at 0.2 mM concentration.

8.3.2 2HG

2-Hydroxyglutarate (2HG) is a 2OG analogue associated with certain cancer types and often referred to as an oncometabolite[50,51]. It was suggested 2HG may act as a competitive inhibitor of 2OG dependent oxygenases. Both its enantiomers are weak BBOX inhibitors (IC_{50} of 97 µM and 11 mM for (*S*) and (*R*)-2HG, respectively)[52]. Therefore the effect of high concentrations (1 mM) of (*R*)-2HG (**257**) and (*S*)-2HG (**258**) on the carnitine levels in cell was examined, however no significant change in carnitine levels was observed (Fig. 28).

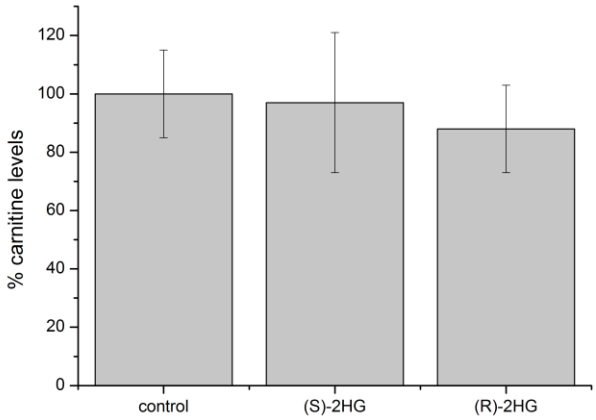

Figure 28 Influence of (*R*)- and (*S*)-2HG on the carnitine levels in cell. Carnitine levels were as follows: control - 100±15%, (*S*)-2HG - 97±24%, (*R*)-2HG - 88±15%.

9 Inhibition through ejection of structural zinc

9.1 Zinc binding domains in 2OG dependent oxygenases

Structural studies have revealed that 2OG oxygenases contain a conserved double stranded β-helix (DSBH) core which supports the residues responsible for Fe(II) and 2OG binding[31,32,53]. However many 2OG oxygenases contain additional domains which also have the ability to bind metals, in particular zinc finger type domains. The functions of zinc binding domains are diverse and in some cases they have been shown to be required for folding and catalytic activity, e.g. in histone demethylase KDM4A the C-terminal zinc finger is required for activity and conformational stability and is likely involved in substrate binding[54,55]. There are also examples of 2OG dependent oxygenases where zinc finger type domains are not required for catalysis; some of these are responsible for mediating protein-protein interactions, e.g. the *N*-terminal zinc finger of prolyl hydroxylase protein domain 2 (PHD2)[56] and the zinc binding domain(s) of the TET family DNA hydroxylases[57].

9.2 BBOX zinc binding domain

As observed both in solution and by crystallographic analyses[14], BBOX is mainly present as a homodimer, with each monomer containing *N*- and *C*- terminal domains (Fig. 29). The *C*-terminal BBOX domain has a DSBH core fold and contains the active site, with the Fe(II), 2OG and GBB binding residues. The *N*-terminal domain contains the Zn(II) binding site, where the Zn(II) is chelated by a Cys_3-His motif (Cys38, Cys 40, Cys43 and His 82). The zinc binding residues are highly conserved in BBOX from different species (Fig. 30) and have been shown to be responsible for BBOX dimerization[14]; however, the influence of the presence of Zn(II) on BBOX catalytic activity has not been previously investigated.

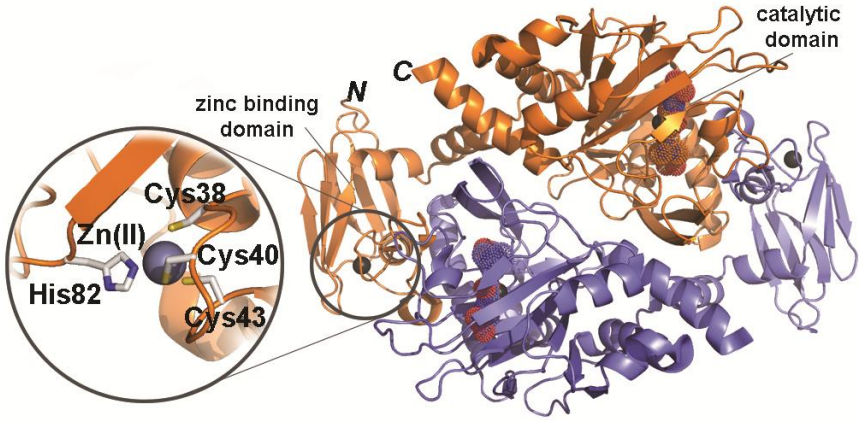

Figure 29 View from a crystal structure of BBOX in complex with GBB, NOG (*N*-oxalylglycine – a mimic of 2OG) and Zn(II) (PDB id: 3O2G). BBOX is a homodimer comprising of catalytic domain where Fe(II) and substrates bind and zinc binding domain. The close up shows the Zn(II) binding site of one monomer.

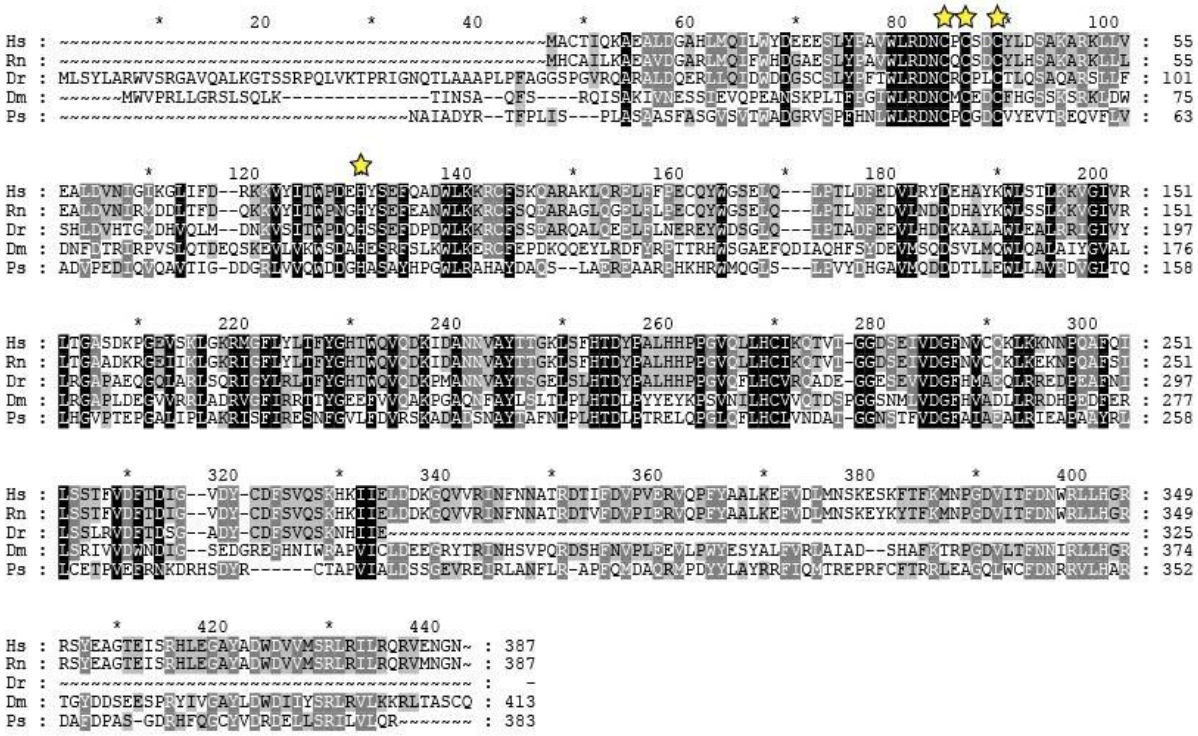

Figure 30 Alignment of BBOX sequences from *Homo sapiens* (Hs, gi 4502369), *Rattus norvegicus* (Rn, gi 12018320), *Danio rerio* (Dr, gi 62955403), *Drosophila melanogaster* (Dm, gi 221329931), *Pseudomonas sp. AK1* (Ps, gi 231642) reveals conserved cysteine and histidine residues forming the zinc binding domain.

9.3 Inhibition of BBOX by selenium and sulphur-containing zinc ejectors

Selenium and sulphur based compounds are reported to be effective zinc ejectors, due to their demonstrated ability to interact with cysteine-residues involved in Zn(II) binding in many proteins. A set of potential zinc ejectors was examined for their ability to inhibit BBOX (Table 28). As a positive control, an isoquinoline derivative BIQ (**75**) was used. BIQ has been previously reported to inhibit BBOX[12] and other 2OG dependent oxygenases[58] through chelating active site Fe(II) ion and interacting with specific active site residues.[24,59-61] Compounds (**259**)-(**265**) were inhibitors of BBOX; the IC_{50} values were found to be dependent on the time of preincubation prior to reaction (Table 28, Fig. 31), i.e. consistent with mechanism involving irreversible ejection of structural zinc. Interestingly, ebselen (**259**) was the most potent inhibitor with IC_{50} value of 0.5 μM. Ebselen is known to be an effective zinc ejector, as shown on the example of metallothionein[62] and human histone demethylase KDM4A.[55] Ebselen is currently in late stage clinical development for stroke treatment.[63-65] The observation that ebselen inhibits BBOX is interesting from a therapeutic perspective, because inhibition of BBOX has been shown to aid in recovery after acute stroke.

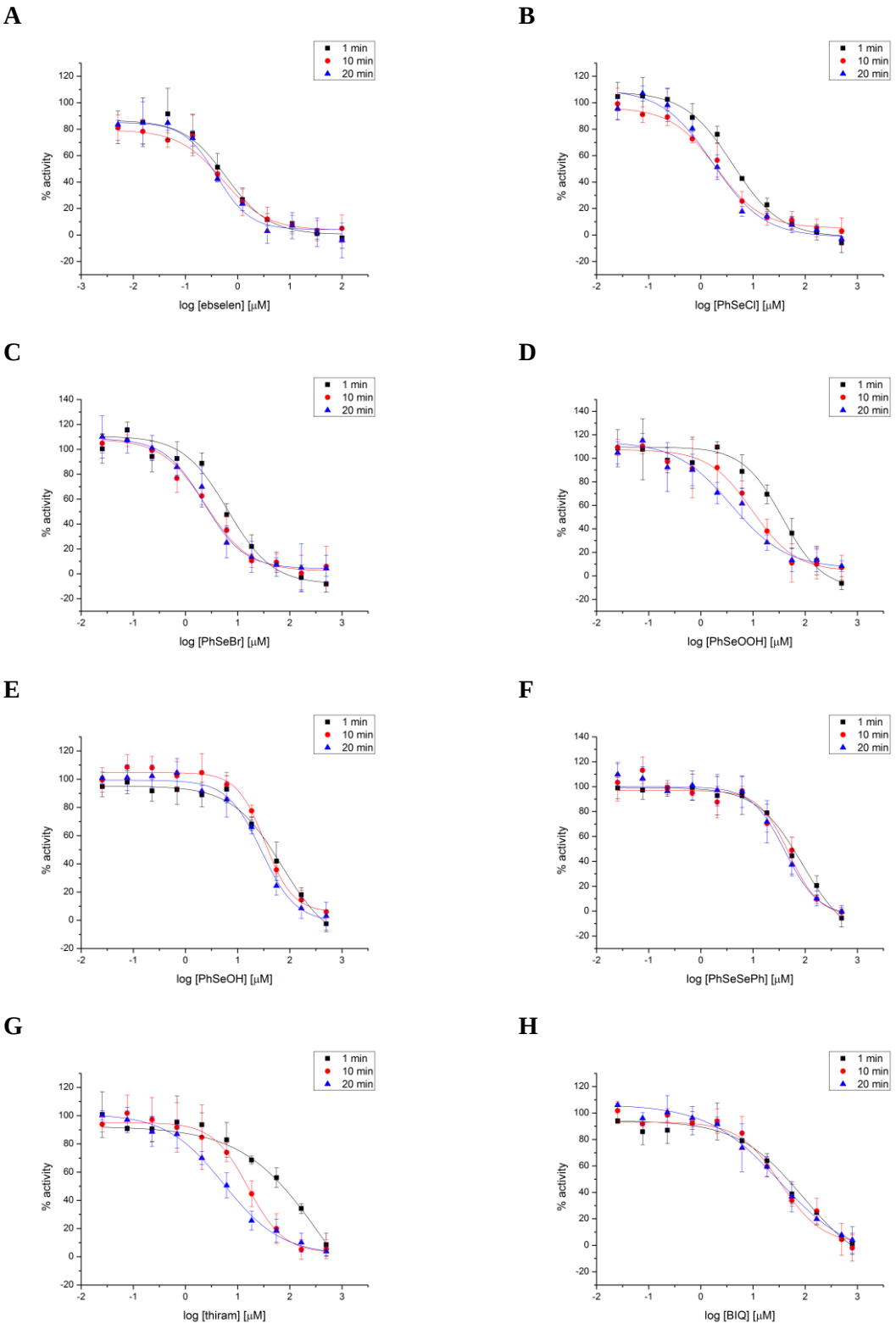

Figure 31IC_{50} curves for inhibition of BBOX by A – ebselen, B – PhSeCl, C – PhSeBr, D – PhSeOOH, E – PhSeOH, F – PhSeSePh, G – thiram, H – BIQ. Curves obtained after 1, 10 and 20 min of inhibitor preincubation with BBOX

Table 28 Inhibition of BBOX by zinc ejectors. IC_{50} values are given for the 1, 10 and 20 min preincubation of the compound with BBOX.

compound	structure	IC_{50} BBOX [µM]		
		1 min	10 min	20 min
Ebselen (**259**)	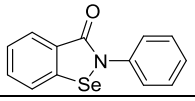	0.59±0.11	0.55±0.08	0.46±0.07
PhSeCl (**260**)	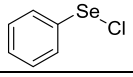	5.1±0.6	2.2±0.3	1.9±0.3
PhSeBr (**261**)	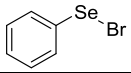	7.0±1.7	2.4±0.4	2.6±0.3
PhSeOOH (**262**)	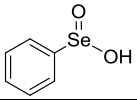	35±7	10±2	5.0±1.8
PhSeOH (**263**)	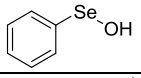	54±11	34±3	26±3
PhSeSePh (**264**)	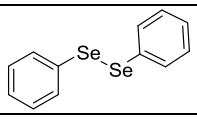	55±5	33±9	39±6
Thiram (**265**)	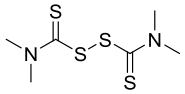	160±67	16±2	5.5±8
BIQ (**75**)	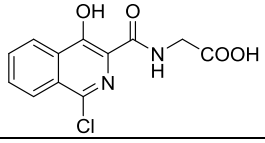	36±4	33±9	32±13
Na_2SeO_4 (**266**)	-	>500	-	-
Na_2SeO_3 (**267**)	-	>500	-	-
Saccharin (**268**)	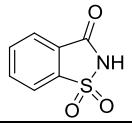	>500	-	-

9.4 Zinc ejection by analogues (259)-(265)

Having shown that selenium and sulphur containing compounds were BBOX inhibitors, the Zn(II) ejection from BBOX induced by analogues (**259**)-(**265**) was examined (Fig. 32-34). The work employed a fluorescence based assay, wherein the amount of Zn(II) was quantified by measuring the increase in fluorescence upon binding of Zn(II) to a Zn(II) specific probe. As expected compounds (**259**)-(**265**) ejected Zn(II) in a time and dose-dependent manner (Fig. 32-34). PhSeCl (**260**), PhSeBr (**261**) and PhSeOOH (**262**) were the most effective zinc ejectors, consistent with their good inhibitory properties and increased potency with increasing pre-incubation times (Table 28). PhSeOH (**263**) and PhSeSePh (**264**) were apparently poor zinc ejectors, consistent with their relatively high IC_{50} values. A control experiment demonstrated that no Zn(II) ejection was triggered by BIQ (**75**), in good agreement with a mechanism involving binding to the active site iron of 2OG oxygenases. Interestingly, thiram (**265**) displayed sigmoidal dependence of free Zn(II) on time,

which suggests a cooperative mechanism of zinc-released form BBOX. Surprisingly, ebselen (**259**) displayed only moderate ability to eject zinc under the standard assay conditions. This observation suggests the mode of BBOX inhibition by ebselen (**259**) may be more complex than simply Zn(II) ejection.

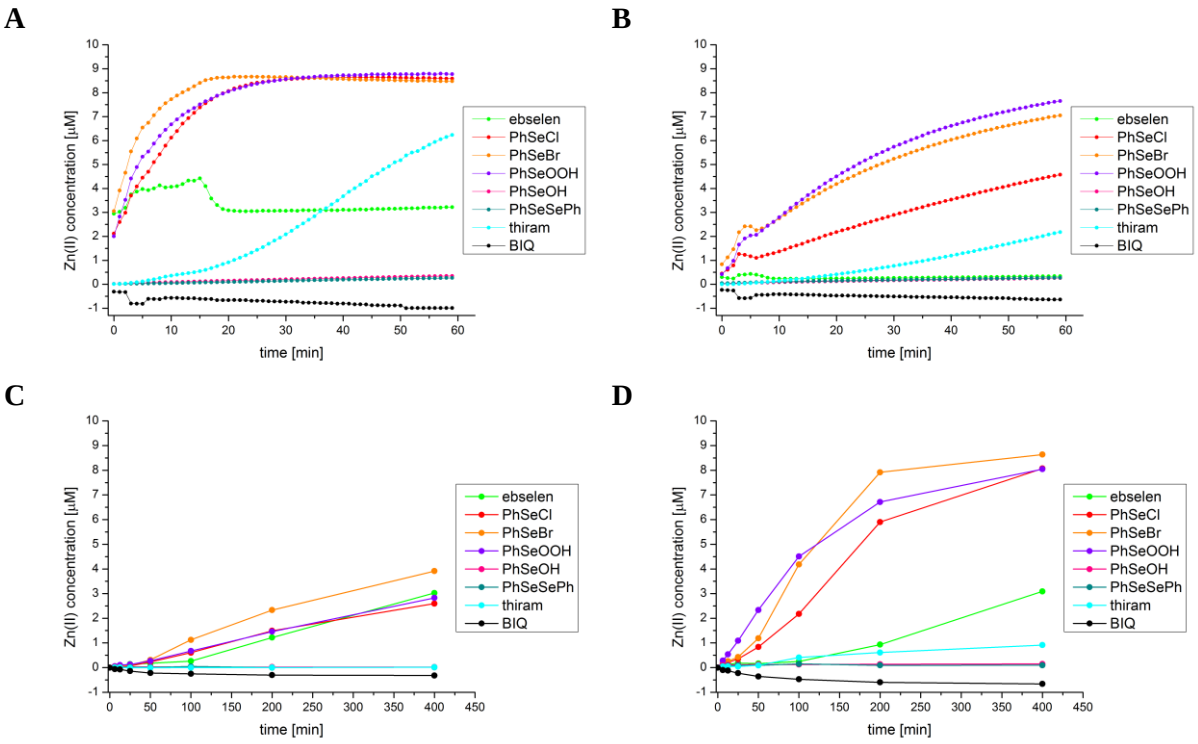

Figure 32 Ejection of zinc from BBOX by analogues (**259**)-(**265**) and (**75**). Time course of Zn(II) ejection from BBOX by 0.4 mM (A) and 0.1 mM (B) of inhibitor (**259**)-(**265**) and (**75**). Dose-response curves for zinc ejection from BBOX by (**259**)-(**265**) and (**75**) as measured after 1 min (C) and 20 min (D) of incubation of BBOX with an inhibitor.

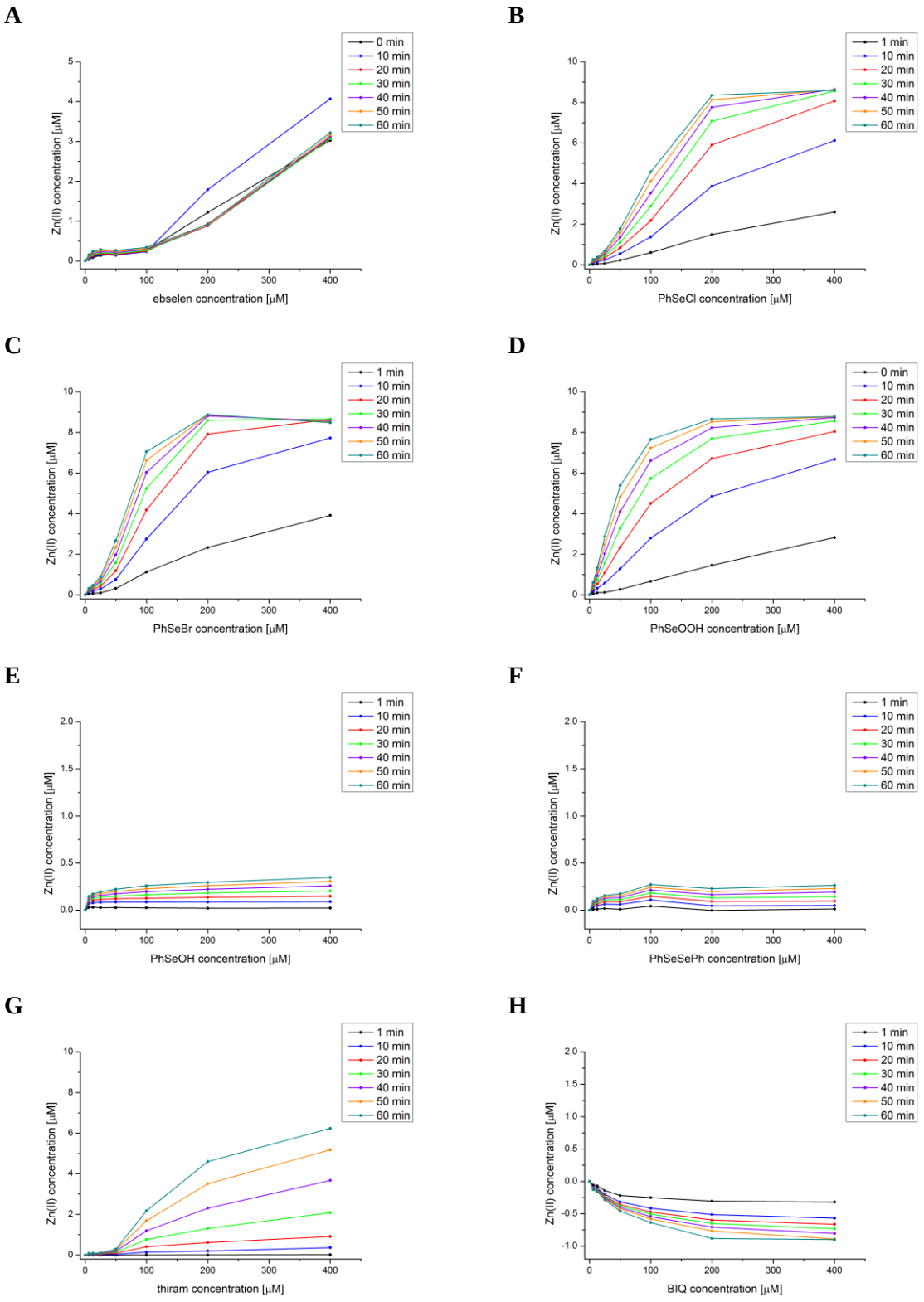

Figure 33 Dependency of the amount of Zn(II) release on the concentration of an inhibitor. A – ebselen, B – PhSeCl, C – PhSeBr, D – PhSeOOH, E – PhSeOH, F – PhSeSePh, G – thiram, H – BIQ. The curves are derived from signal obtained after 1, 10, 20, 30, 40, 50 and 60 min incubation of BBOX (10 μM) with inhibitor.

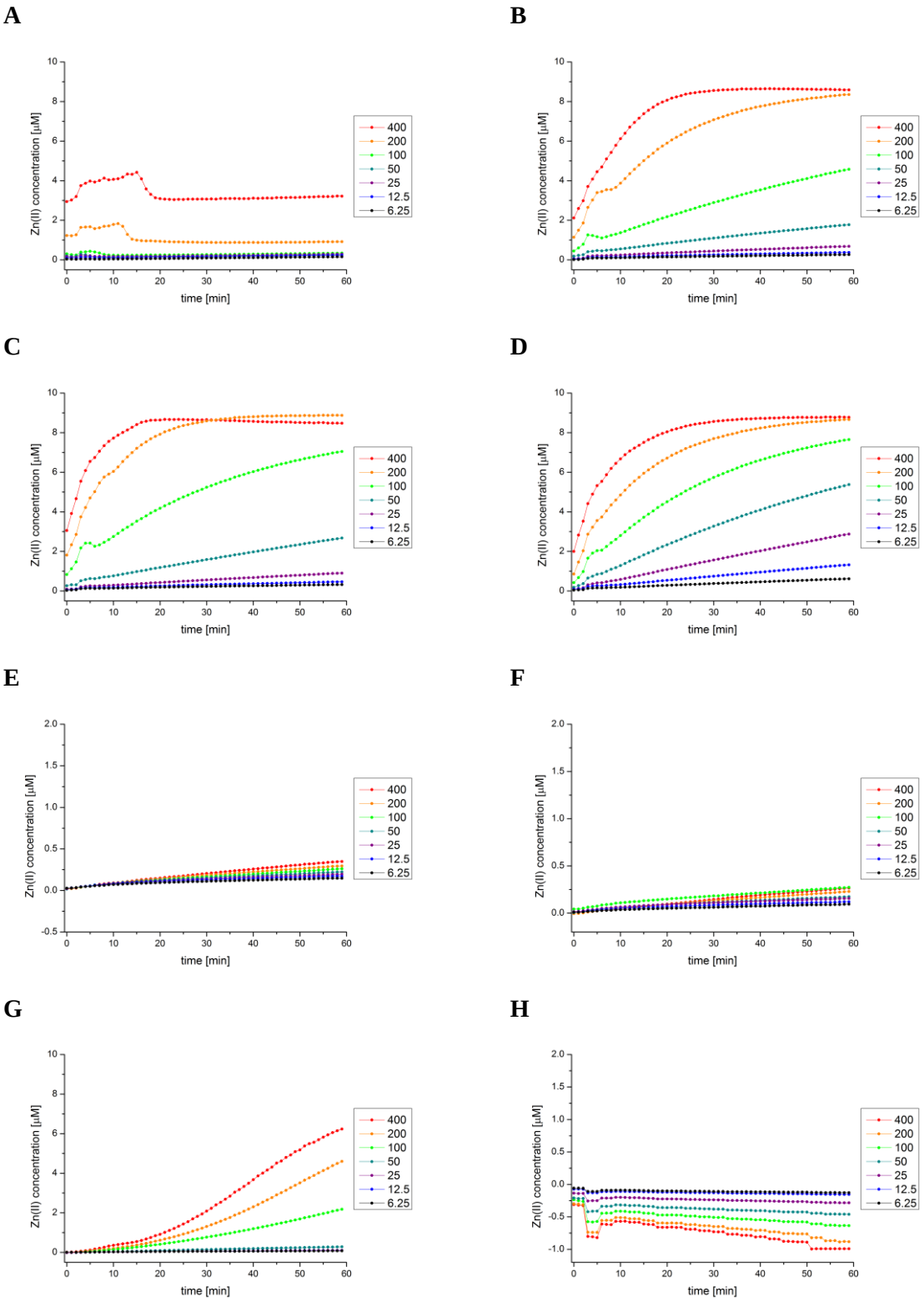

Figure 34 Time course of Zn(II) release with time, using increasing concentrations of inhibitors. A – ebselen, B – PhSeCl, C – PhSeBr, D – PhSeOOH, E – PhSeOH, F – PhSeSePh, G – thiram, H – BIQ. The inhibitor concentrations used were 6.25, 12.5, 25, 50, 100, 200 and 400 µM.

9.5 Binding studies

To further investigate the interactions of compounds **259**-**265** with BBOX, we carried out binding assays. The binding was determined by quenching of intrinsic tryptophan fluorescence of BBOX upon binding of an inhibitor (Section 2.3). The binding of the compounds correlated with their inhibitory potencies, with ebselen (**259**), followed by PhSeCl (**260**), PhSeBr (**261**) and PhSeOOH (**262**) being the best binders (Fig. 35). Binding studies were also conducted on BBOX which did not contain Fe(II) in the active site; as anticipate in this case binding of the control inhibitor BIQ (**75**) was very weak. Binding of BIQ (**75**) was greatly improved after addition of an Fe(II) to the measured solution, consistent with the proposed mechanism of inhibition of BBOX by BIQ (**75**), involving coordination of the active site Fe(II). Binding of the sulphur/selenium containing compounds (**259**-**265**), including ebselen (**259**) (Fig. 36), was not significantly changed by the presence of an added Fe(II), suggesting they probably do not interact within the active site of BBOX, but rather with the Zn chelating cysteine residues following their previously proposed mechanism of action.

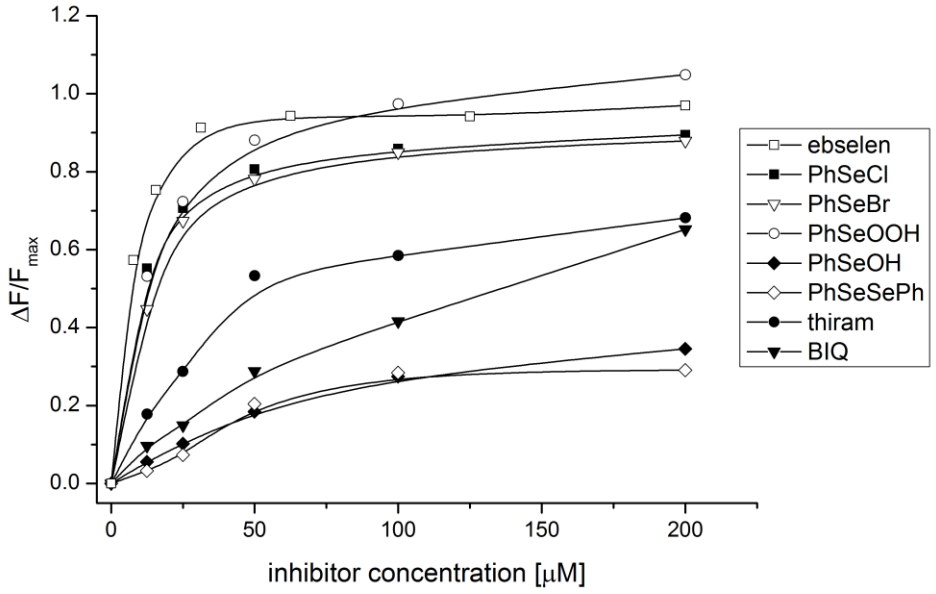

Figure 35 Binding of compounds **259**-**265** to BBOX (in the absence of Fe(II) in the active site) as determined by intrinsic fluorescence quenching of BBOX – comparison of binding of analogues **259**-**265**.

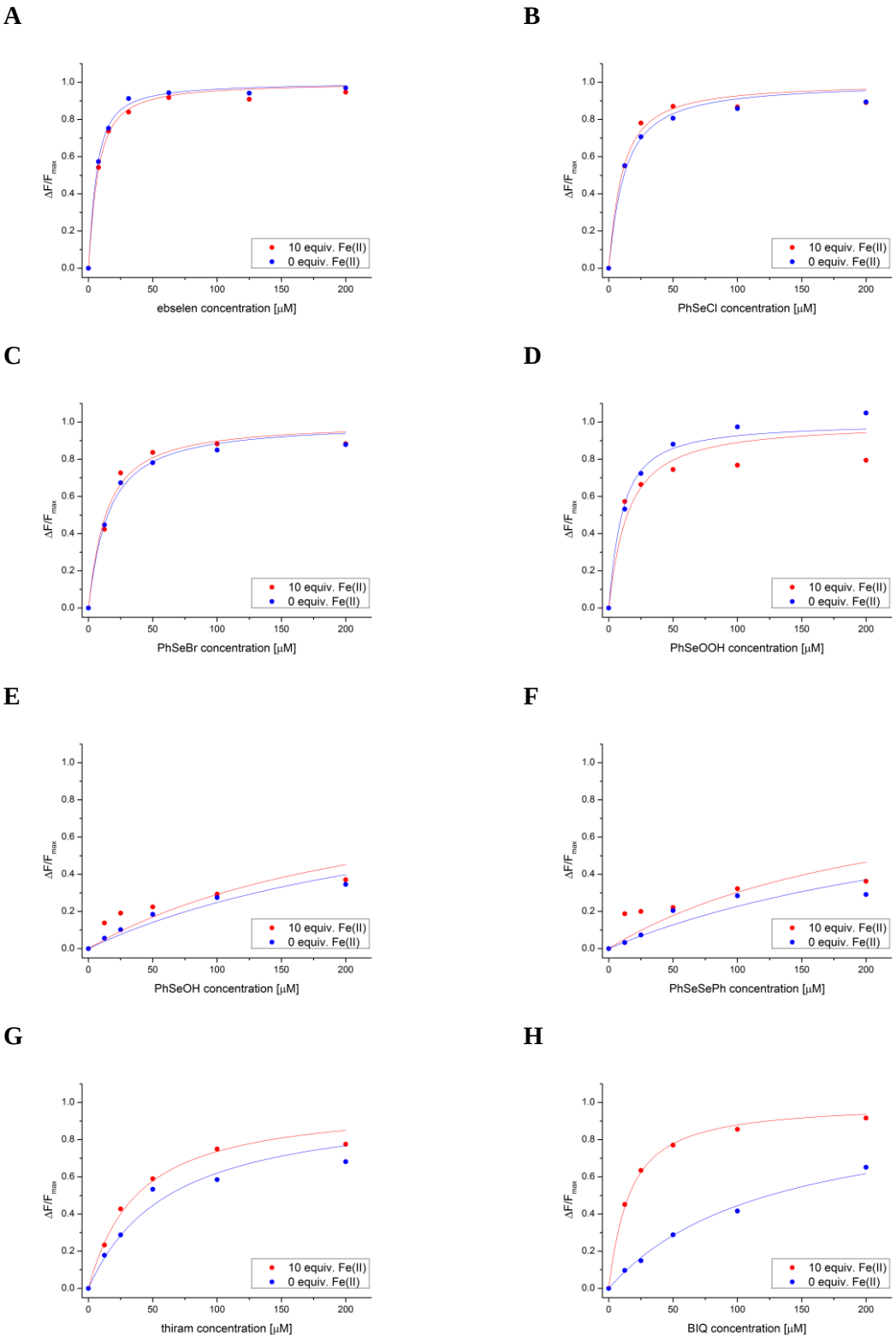

Figure 36 Changes in BBOX fluorescence upon titration with inhibitors. A – ebselen, B – PhSeCl, C – PhSeBr, D – PhSeOOH, E – PhSeOH, F – PhSeSePh, G – thiram, H – BIQ. BBOX concentration was 5 μM. Blue curves represent binding to apo BBOX (no Fe(II)) and the red curves represent binding to BBOX (5 μM) incubated with Fe(II) (50 μM).

Table 29 K_D values for binding of inhibitors to apo BBOX and BBOX/Fe(II) complex, as determined by fluorescence quenching binding assays.

compound	$K_{D\ BBOX}$ [μM]	$K_{D\ BBOX/Fe(II)}$ [μM]
Ebselen (**259**)	3.6±0.2	4.6±0.4
PhSeCl (**260**)	9.4±1.1	7.5±1.1
PhSeBr (**261**)	13±1	11±2
PhSeOOH (**262**)	7.6±1.1	12±3
PhSeOH (**263**)	>200	>200
PhSeSePh (**264**)	>200	>200
Thiram (**265**)	59±8	35±3
BIQ (**75**)	122±63	13±1

* Data were fitted with equation: $y=(([L_0]+[P_0]+K_D)-(([L_0]+[P_0]+K_D)^2-4[L_0][P_0])^{0.5})/(2[P_0])$, where $[L_0]$ is total concentration of ligand and $[P_0]$ is total concentration of the protein (OriginPro 8.5.1).

9.6 Mass spectrometry analyses

Mass spectrometry (MS) analyses were carried out to investigate potential covalent modifications of BBOX by the most potent inhibitors ((**259**)-(**262**)). It was envisaged that BBOX-SSeR' bonds may survive under LC-MS chromatography and ionisation conditions. Indeed in MS spectra of BBOX treated with one equivalent of PhSeCl (**263**), PhSeBr (**261**) and PhSeOOH (**262**) a single covalent modification was observed, corresponding to a PhSe- group mass shift (+156) (Fig. 37), i.e. reaction with a cysteinyl thiol. In the case of ebselen (**259**), even after prolonged (24 h) incubation, only small amounts of covalent modification were detected (+274 peak, Fig. 37); however at high concentrations of ebselen (10 equiv.), BBOX underwent multiple apparent covalent modifications corresponding to nine ebselen molecules bound per BBOX molecule (Fig. 38). Non-denaturing MS analyses (Fig. 39) suggested that ebselen can bind at low concentrations forming adducts stable under MS conditions (80 V cone voltage). Thus, ebselen may inhibit both by covalent and non-covalent mechanism.

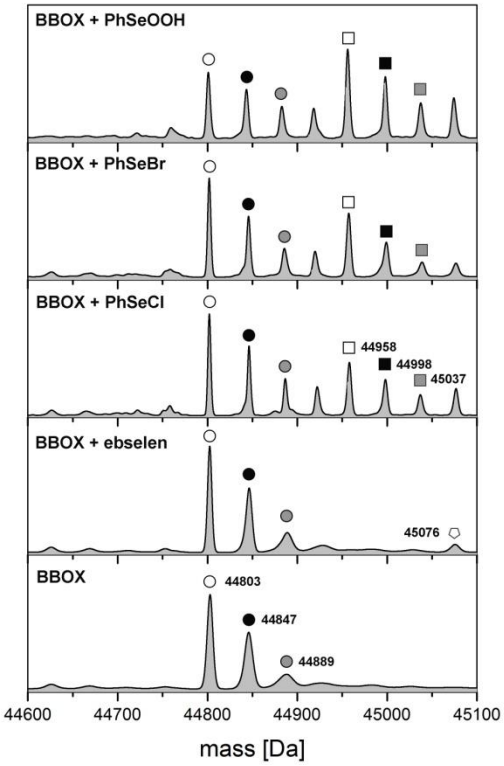

Figure 37 MS analyses for binding of inhibitors **259**-**262** to BBOX. Denaturing MS reveals analogues **260**-**262** likely covalentely modify BBOX when used in a 1:1 enzyme : inhibitor ratio. Note relatively little binding was observed for ebselen (**259**).

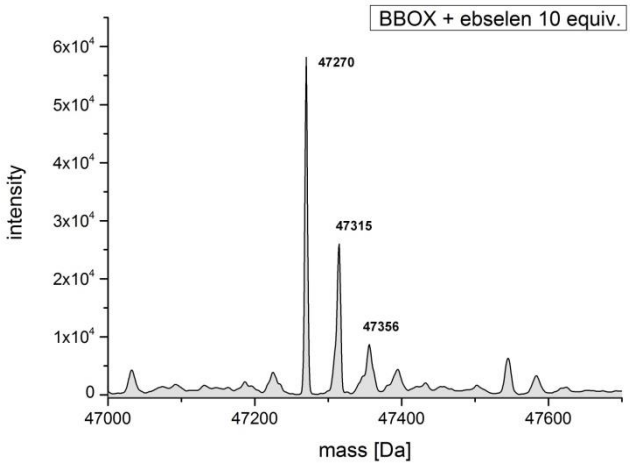

Figure 38 Denaturing MS analyses of BBOX treated with an excess of ebselen. BBOX incubated with 10 equiv. of ebselen displays a mass shift (+2467) corresponding to addition of 9 molecules of ebselen. This observation is consistent with the number of cysteine residues present in the BBOX construct used.

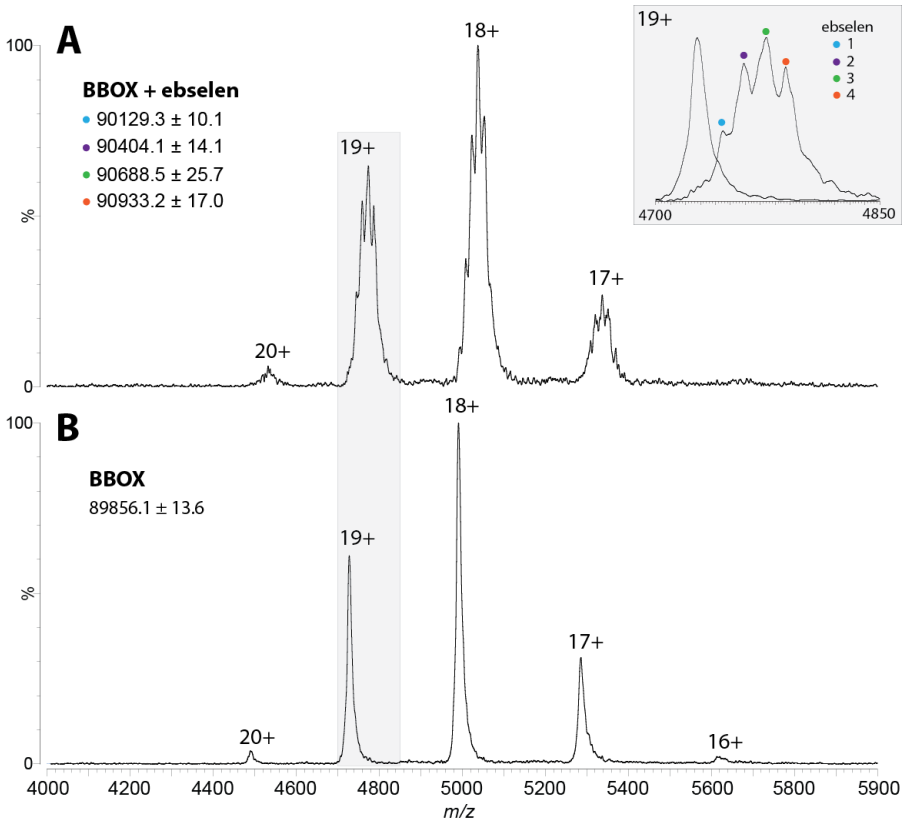

Figure 39 Non-denaturing MS analyses of BBOX treated with 2 equiv. of ebselen. In the absence of ebselen a single peak is detected for each charge state and corresponds to the apo-form (B). BBOX incubated with ebselen at low concentrations was found to non-covalently bind up to four ebselen molecules (A). The deconvoluted masses of the bound form are shown and are in agreement with these stochiometries (inset; overlay of 19+ charge state).

9.7 Summary of zinc ejection studies

In summary, it was demonstrated that selenium and sulphur containing compounds can inhibit BBOX catalysis. The mechanism likely involve covalent modification of one or more cysteine residues following removal of the structural Zn(II). The results imply that a functional zinc binding domain is indispensible for BBOX catalysis, as for some 2OG dependent histone demethylases, e.g. KDM4A.[55] New inhibitors of BBOX were identified, with ebselen – a clinical trial candidate for the treatment of acute stroke – being particularly potent. Because BBOX inhibition is reported to aid recovery after cardiac dysfunctions, the therapeutic effect of ebselen could thus, at least in part, be due to BBOX inhibition.

10 Summary and perspectives

A set of new assays for assessing inhibitor binding, zinc ejection from BBOX and determination of cellular carnitine contents was developed. The assays will aid further studies on BBOX and related proteins. The new set of assay tools enabled identification of scaffolds for potential BBOX inhibitors. Further synthetic development gave the first potent BBOX inhibitor (AR692B), whose prodrug form was demonstrated to lower carnitine levels in cultured cells. A crystal structure of human BBOX in complex with AR692B revealed interesting features – the compound displayed two binding modes, one of which featured an intermolecular π-stacked conformation, unprecedented in 2OG dependent oxygenases. Moreover, the overall fold of BBOX changed upon inhibitor binding, raising questions about the role of active site loop movement in the catalytic cycle. The investigation of other scaffolds like quinolines, isoquinolines or hydroxythiazoles led to the identification of other potent inhibitors, most likely exhibiting different binding modes to BBOX. Screening of a library of GBB analogues led to the identification of structural motifs important for GBB binding. These results may aid the development of GBB-based BBOX inhibitors and/or alternative substrates for biosynthetic purposes. Among GBB analogues, the most effective cell carnitine lowering agents were discovered – which is of interest from a therapeutic perspective. Finally, inhibition studies using zinc ejectors revealed that N-terminal zinc binding domain of BBOX is indispensible for BBOX conformational stability and activity. Ebselen – a drug candidate for treatment of stroke, was identified as a potent BBOX inhibitor with an unusual mode of inhibition. Interestingly, cardioprotective properties of ebselen may be, at least in part, due to the inhibition of BBOX activity.

11 Acknowledgements

Purified human BBOX stocks used in these studies was supplied by Dr. Grażyna T. Kochan (Structural Genomics Consortium, Oxford).

2PCA, quinoline and isoquinoline series

X-ray crystallography data on BBOX-AR692B complex were collected and solved by Dr. Rasheduzzaman Chowdhury (Department of Chemistry, University of Oxford). Selectivity screen of AR692B on the panel of other 2OG oxygenases was performed by Sophie Williams (Department of Chemistry, University of Oxford). Compounds (**66**)-(**74**) and (**98**) were synthesised by Marina Demetriades (Department of Chemistry, University of Oxford). Compounds (**90**) and (**91**) were synthesised by Dr. Clarisse Lejeune (Department of Chemistry, University of Oxford).

Hydroxythiazole series

Hydroxythiazoles used in the BBOX inhibition studies were supplied by Dr. Philip Tagari (Amgen) and Dr. Clarisse Lejeune (analogues (**109**), (**113**), (**114**), (**117**), (**118**)).

GBB analogues series

Analogues (**222**) and (**240**) were synthesised by Luc Henry (Department of Chemistry, University of Oxford). Analogues (**248**) and (**251**) were synthesised by Dr. Clarisse Lejeune. Analogues (**243**)-(**247**), (**249**) and (**250**) were synthesised by Dr. Ester Woon (Department of Chemistry, University of Oxford).

Zinc ejection

Non-denaturing MS analyses were carried out by Dr. Weston Struwe (Department of chemistry, University of Oxford). Dr Jürgen Brem Department of Chemistry, University of Oxford) assisted in the development of the BBOX binding assay.

The work included in this chapter has been published in an altered form:

- A. M. Rydzik, R. Chowdhury, G. T. Kochan, S. T. Williams, M. A. McDonough, A. Kawamura, C. J. Schofield, *Chemical Science* **2014**, 5, 1765-1771.
- R. J. Hopkinson, A. Tumber, C. Yapp, R. Chowdhury, W. Aik, K. H. Che, X. S. Li, J. B. L. Kristensen, O. N. F. King, M. C. Chan, K. K. Yeoh, H. Choi, L. J. Walport, C. C. Thinnes, J. T. Bush, C. Lejeune, A. M. Rydzik, *et al.*, *Chemical Science* **2013**, *4*, 3110-3117.
- N. R. Rose, E. C. Y. Woon, A. Tumber, L. J. Walport, R. Chowdhury, X. S. Li, O. N. F. King, C. Lejeune, S. S. Ng, T. Krojer, M. C. Chan, A. M. Rydzik, R. J. Hopkinson, K. H. Che, M. Daniel, C. Strain-Damerell, C. Gileadi, G. Kochan, I. K. H. Leung, J. Dunford, K. K. Yeoh, P. J. Ratcliffe, N. Burgess-Brown, F. von Delft, S. Muller, B. Marsden, P. E. Brennan, M. A. McDonough, U. Oppermann, R. J. Klose, C. J. Schofield, A. Kawamura, *Journal of Medicinal Chemistry* **2012**, *55*, 6639-6643.

12 Experimental section

12.1 NMR

NMR assays were performed on Bruker AVIII 700 with inverse TCI cryoprobe using 3 mm MATCH tubes. Pulses were calibrated using single-pulse nutation method (Bruker pulsecal routine). Water suppression was achieved using the excitation sculpting method.

12.1.1 General conditions for NMR assays

40 µM GBB, 150 µM 2OG, 500 µM ascorbate, 200 mM KCl, 50 µM Fe(II), BBOX 50 nM, TRIS d-11 50 mM pH 7.5, 10% D_2O, 0.01% NaN_3, final volume 160 µl. Error calculated as standard deviation from data derived from eight different time points per reaction.

12.1.1.1 Conditions for substrate competition experiments

The following conditions were used: 50 µM GBB (for 2OG competition experiment), 150 µM 2OG (for GBB competition experiment), 500 µM ascorbate, 200 mM KCl, 50 µM Fe(II), 400 nM AR692B, 50 nM BBOX, 50 mM TRIS d_{11} pH 7.5, 10% D_2O, 0.01% NaN_3.

12.2 Fluoride release assays

The fluorinated GBB analogue (GBBF) and TBS-protected fluorescein probe were synthesised as described in Chapter 2. Other reagents were from Sigma-Aldrich. Reactions were performed in a final volume of 10 µl (black 384-well plates, clear, flat bottom, Grenier BioOne). The following final concentrations of reagents were used: 40 µM GBBF (fluorinated analogue of GBB), 500 µM 2OG (disodium salt, Sigma-Aldrich), 250 µM ascorbate (potassium salt, Sigma-Aldrich), 160 mM KCl, 40 µM Fe(II) ($Fe(NH_4)_2(SO_4)_2$ salt, prepared fresh as a 100 mM solution in 20 mM HCl and added to the reaction mixture just prior to the initiation of the assay), BBOX 200 nM. Reactions were performed in 50 mM TRIS buffer pH 7.0, initiated by addition of BBOX to the mixture containing all cofactors and inhibitor and quenched after 10 min by addition of TBS-fluorescein probe in DMSO (40 µl, to a final concentration of 5 µM). The plate was then sealed and incubated for 60 min at room temperature prior to addition of 10 µl of 50 mM HEPES buffer pH 7.0. The resultant signal was read up to 5 min after addition of HEPES buffer using an EnVision Multilabel plate reader (Perkin Elmer) fitted with FITC FP 480/30 (480 nm, bandwidth 30 nm) and FITC FP 535/40 emission (535 nm, bandwidth 40 nm) filters. For each reaction, controls containing all reagents except BBOX (negative control) or inhibitor (positive control) were recorded. The normalised fluorescence signal was defined as the observed fluorescence signal minus the negative control signal. Percentage activity was calculated as a ratio of normalised signal for reaction containing inhibitor to positive control signal. Errors were calculated as standard deviations from four separate measurements. IC_{50} data were fitted using XLfit software (IDBS Solutions) using 4-parameter logistic model (sigmoidal dose-response with variable slope).

12.2.1 Fluoride release assay protocol for inhibition with preincubation

Procedure was as for the standard fluoride release assay, with the exception that reactions were initiated by addition of a mixture containing all cofactors to a solution of BBOX and the inhibitor (preincubated for 0, 10 or 20 min prior to the start of the reaction).

12.3 Cell based assays

12.3.1 Cell culture

HEK 293T cells were cultured in Dulbecco's modified Eagle medium (DMEM) (Lonza/ BioWhittaker, supplemented with 4.5 g/L glucose) with a Penicillin/ Streptomycin antibiotic mixture (Sigma, 0.1 mg/mL Streptomycin and 100 units/mL Penicillin), 2 mM GlutaMAX (Gibco) and 10% FBS (PAA) in 10 cm sterile Petri dishes. When cells reached confluence, the media was removed and cells washed twice with PBS (Lonza). The pellet was re-suspended in 6 mL of PBS and split into 6 new Petri dishes (1 mL of cell suspension each (~3×10^6)) with 10 mL of media containing desired additives. Cells were grown for 48 h (37°C, 5% CO_2). Media was discarded and cells washed 3 times with 5 mL of PBS, cells were scraped and centrifuged for 5 min at 1000 rpm. The supernatant was removed and the pellet was frozen at -80°C. Before measurement the pellet was incubated on ice with 100 mL of PBS for 20 min. Cells were re-suspended in PBS by vortexing and lysed in sonication water bath (5 cycles of 1sec sonication-1 sec break) and spun down at 14800 rpm for 10 min. Supernatants were collected and transferred to MS vials for measurement.

12.3.2 MS method for cell analyses

Chromatographic separation of the carnitine biosynthesis metabolites was performed using mixed mode chromatography. Chromatographic separation was performed using an Aquity UPLC system (Waters). Column: PrimeSep 200 mixed mode, 2.1×250 mm, particles 5 μm (SIELC, Prospect Heights, US). Mobile phase: Solvent A – 9:1 H_2O-acetonitrile mixture, 0.05% formic acid, solvent B – 8:2 H_2O-acetonitrile mixture, 0.2% formic acid. Gradient: Linear gradient from 0% to 100% B in 25 min, column reconditioning: 25-26 min from 0% to 100% A, 26-30 min 100% A. Flow rate: 0.3 mL/min. Injection volume 10 μL. Detection was performed using a Waters Quattro Micro instrument (triple quadrupole MS, electrospray ionisation, positive ion mode). The single ion mode was used and scan mode was running in parallel as a control.

12.4 Fluorescence binding assays

Fluorescence was measured using a Pherastar FS plate reader (BMG Labtech) using following parameters: excitation 280 nm, emission 350 nm, 5 μM BBOX, 20 μM Fe(II) and variable concentration of tested compound. Assays were performed in 50 mM Tris buffer pH 7.5 containing 200 mM NaCl in total volume of 50 μL per well in 96-well plates (Greiner, black, bottom: flat, clear). Measurements were done in triplicates, error bars represent standard deviation from mean.

The concentration of inhibitor was plotted against $\Delta F_{obs}/\Delta F_{max}$, where ΔF_{obs} is the observed decrease in fluorescence signal and ΔF_{max} is maximum measured decrease in fluorescence signal (decrease in fluorescence signal when the saturation was reached compared to initial fluorescence measurement for BBOX alone). Data were fitted with equation: $y = (([L_0]+[P_0]+K_D)-(([L_0]+[P_0]+K_D)^2-4[L_0][P_0])^{0.5})/(2[P_0])$, where $[L_0]$ is total concentration of ligand and $[P_0]$ is total concentration of the protein (OriginPro 8.5.1).

12.5 Zinc ejection assays

Zinc(II) concentrations were determined by measuring the increase in fluorescence upon binding of Zn(II) to the Zn(II)-specific fluorophore FluoZin™-3 (Invitrogen). Fluorescence was measured using a Pherastar FS plate reader (BMG Labtech) using the following parameters: excitation 485 nm, emission 520 nm. Assays generally contained 10 µM BBOX, 10 µM FluoZin-3 probe and variable concentration of the tested compound in 50 mM Tris-HCl buffer pH 7.5 with a final volume of 50 µL in 96-well plates (Greiner, black, bottom: flat, clear). A calibration curve was obtained between 0-10 µM Zn(II) in the presence of 10 µM BBOX (the shape of the curve was shown to be affected by the presence of BBOX). Readings were performed in 60 cycles at rate of 1 min per cycle.

12.6 Denaturing mass spectrometry

Samples were prepared by treatment of BBOX (10 µM) in 50 mM Tris-HCl buffer pH 7.5, containing 200 mM NaCl, with inhibitor to final concentration of 10 µM (total vol. 50 µL). Samples were run on Waters LCT Premier XE Spectrometer equiped with electrospray interface coupled to an Agilent 1100 Series HPLC with a CTC-autosampler inlet system. The column used was Merck Chromolith® C-18 2 x 5 mm column (Merck). Samples were kept at 4°C before injection and run with a gradient from 5% B to 100% B in A over 5 min (solvent A – water, 0.1% formic acid; B – acetonitrile).

12.7 Non-denaturing mass spectrometry

Native mass spectrometry measurements of BBOX were performed on a modified Synapt G1 HDMS ion mobility instrument (Waters Co., Manchester UK) as previously described[66]. The MS instrument parameters were as follows: capillary voltage 1.3 kV, cone voltage 80 V, extraction cone 1.0 V, trap collision voltage 5.0 V, trap DC bias voltage 15 V, trap gas flow 3.0 mL/min, IMS gas flow 40mL/min. 5µM BBOX was buffer-exchanged into 200mM ammonium acetate pH 7.4 using Micro BioSpin 6 columns (BioRad, UK). Ebselen (diluted in 200mM ammonium acetate with 0.05% DMSO) was added immediately prior to MS. Data analysis was performed using MassLynx v4.1 software.

12.8 Selectivity screen conditions

The enzyme activities of JMJD2A, JMJD1A, PHF8, FBXL11, JMJD3, FIH and PHD2 were measured by relative demethylation/hydroxylation of known substrate peptides using Matrix-assisted laser-desorption/ionization (MALDI) time-of-flight (TOF) mass spectrometry (MS), Waters. The reaction mixture composition varied as optimised for each reaction (JMJD2A, FBXL11 – 1 µM enzyme, 10 µM peptide, 50 mM HEPES pH 7.5, 200 µM 2-oxyglutarate (disodium salt, Sigma), 10 µM $FeSO_4 \times 7\ H_2O$, 100 µM sodium ascorbate (Sigma); JMJD1A, PHF8, JMJD3 with additional 150 mM NaCl; FIH and PHD2, in TRIS pH 7.5, 100 mM NaCl). Enzyme, sodium ascorbate and Fe(II) were incubated with 100 µM AR692B for 15 min before adding peptide and 2-oxoglutarate mix. Reaction was incubated for 20 min at 25°C, quenched with MeOH and spotted using α-Cyano-4-hydroxycinnamic acid (CHCA) matrix. Inhibition was calculated relative to the activity of a null-inhibitor control.

12.9 Crystallography

Crystallisation was performed in 24-well plates; hanging drops were equilibrated against 400 µl of reservoir solution. Drops consisted of 1 µl reservoir solution and 1 µl protein solution. The reservoir solution contained: 0.2 M ammonium citrate, 1 mM $NiSO_4$, 2% 1,6-diaminohexane, 19% PEG 3350. Protein (20 mg/ml) was in TRIS buffer (50 mM pH 7.5) containing 200 mM NaCl and was supplemented with 5 mM AR692B (100 mM solution in TRIS 50 mM, pH adjusted to 7.0) prior to crystallisation. Crystals formed after a week were used for micro seeding to yield bigger crystals which formed overnight. No crystals were observed in the presence of GBB. Crystals were flash cooled in liquid nitrogen using 25% glycerol in the mother liquor as a cryoprotectant. A dataset for BBOX.Ni.AR692B complex was collected at the Diamond beamline I02 with a Pilatus 6M detector. Difficulties in data processing arose, as there was a crack/warping in the crystal. Therefore, data were integrated and scaled using only the most intense spots setting a $I/\sigma I$ cut-off of 3.0 and using HKL2000.[67] The structure was solved by molecular replacement using PHASER [68] (search model PDB ID: 3O2G). Parameter and topology files for AR692B were generated using PRODRG [69] for refinement in CNS.[70] Iterative cycles of model building in COOT [71] and slowcool-simulated annealing refinement using the maximum-likelihood function and bulk-solvent modeling in CNS proceeded until the R_{cryst}/R_{free} no longer decreased. PROCHECK [72] was used to monitor the geometric quality of the model between refinement cycles.

Table 30 Crystallographic data processing, refinement statistics of the BBOX.Ni(II).AR692B complex.

Measurement	**BBOX.Ni(II).AR692B**
PDB acquisition code	4C8R
Data collection	
Space Group	$P2_12_12_1$
Cell dimensions a,b,c (Å)	195.744
	91.659
	167.132
Resolution (Å)	48.42 – 2.82 (2.90 – 2.82)*
No. of unique reflections	71043 (7115)*
Completeness (%)	97.8 (99.3)*
Redundancy	3.7 (3.5)*
R_{sym}**	0.203 (0.801)*
Mean I/σ(I)	4.0 (1.9)*
Wilson B value ($Å^2$)	58.9
Refinement	
R_{factor}	0.215
R_{free}	0.244
R.m.s. deviation	
Bond length, Å	0.009
Bond angle, °	1.3

*Highest resolution shell shown in parenthesis.

**$R_{sym} = \sum|I-\langle I\rangle|/\sum I$, where I is the intensity of an individual measurement and $\langle I\rangle$ is the average intensity from multiple observations.

12.10 Synthesis

12.10.1 Reagents

General synthetic considerations are according to Synthesis section in the Appendix 1. Reagents were from Acros, Aldrich, Fluka, Lancaster, TCI, Fluorochem and used as supplied. Solvents for chemical transformation, work-up and chromatography were from Rathburn at HPLC grade and used without further purification. Anhydrous solvents were from Aldrich or prepared by filtration through columns containing activated aluminium oxide under argon.

12.10.2 General procedure for preparation of amino acids conjugates of 3-hydroxypicolinic acid

3-Hydroxypicolinic acid (300 mg, 2.16 mmol) and CDI (420 mg, 2.59 mmol, 1.2 eq) were stirred in anhydrous DMF (3 mL) for 10 min, prior to the addition of solution of amino acid methyl ester (2.59 mmol, 1.2 eq) and Et_3N (320 µL, 2.27 mmol, 1.05 eq) in DMF (3 mL). The resultant mixture was stirred overnight at room temperature. Upon reaction completion, most of the DMF was evaporated *in vacuo* and the resultant residue was suspended in CH_2Cl_2 (10 mL) and washed with H_2O (3 x 5 mL). The organic phase was dried over $MgSO_4$, filtered and subjected to the column chromatography (Biotage SNAP KP-SIL™ 25 g cartridge, eluent system: cHex/EtOAc). The obtained product was dissolved in a mixture of THF/H_2O (1:1, 6 mL) and subsequently treated with $LiOH \cdot H_2O$ (450 mg, 10.8 mmol, 5 eq). The reaction was stirred at room temperature for 12 h. THF was evaporated *in vacuo* and the remaining aqueous solution was neutralized with conc. HCl. If precipitate was formed it was filtered-off and dried *in vacuo* to yield the desired product. In case no precipitate was formed, the aqueous solution was extracted with EtOAc (3 x 10 mL). The combined organic layers were dried over $MgSO_4$, filtered and evaporated *in vacuo* to yield the desired product.

12.10.2.1 (3-Hydroxypicolinoyl)glycine (33)[73]

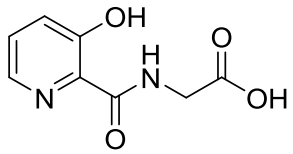

The desired compound (33) was obtained as a white solid (178 mg, 0.91 mmol, 42%) from 3-hydroxypicolinic acid (300 mg, 2.16 mmol).

^{1}H NMR (400 MHz, DMSO-d_6) δ = 12.28 (br. s., 1 H, OH), 9.33 (t, *J*=6.0 Hz, 1 H, NH), 8.18 (dd, *J*=4.5, 1.5 Hz, 1 H), 7.55 (dd, *J*=8.5, 4.5 Hz, 1 H), 7.43 (dd, *J*=8.5, 1.5 Hz, 1 H), 3.99 (d, *J*=6.0 Hz, 2 H, CH_2) ppm. ^{13}C NMR (101 MHz, DMSO-d_6) δ = 171.4, 169.8, 158.0, 140.9, 131.8, 130.2, 126.9, 41.5 ppm. Mp = 136-139 °C (lit. 169-170°C) [73]. HRMS (ESI-TOF) calcd for $C_8H_8N_2NaO_4$ [M+Na$^+$]: 219.0376, found: 219.0366. FT-IR ν_{max} (neat): 3234, 3017, 1608, 1519, 1404, 1344, 816, 662 cm^{-1}.

12.10.2.2 (3-Hydroxypicolinoyl)-L-phenylalanine (34a)

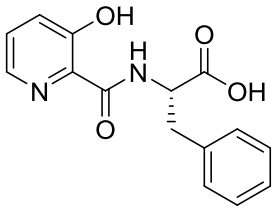

The desired compound (34a) was obtained as a white solid (277 mg, 0.97 mmol, 45%) from 3-hydroxypicolinic acid (300 mg, 2.16 mmol).

^{1}H NMR (400 MHz, $CDCl_3$) δ = 8.48 (br. s., 1 H, NH), 8.05 (br. s., 1 H), 7.10 - 7.40 (m, 8 H), 5.06 (q, *J*=7.0 Hz, 1 H, CH), 3.35 (dd, *J*=14.0, 5.5 Hz, 1 H, CHC*H*'H''), 3.24 (dd, *J*=14.0, 7.0 Hz, 1 H, CHCH'*H*'') ppm. ^{13}C NMR (101 MHz, $CDCl_3$) δ = 175.9, 168.5, 157.9, 139.8, 135.5, 130.7, 129.3, 129.0, 128.7, 127.3, 126.5, 53.0, 37.7 ppm. Mp = 116-118 °C. $[\alpha]^{20}_{D}$ = +25.6 (c = 0.1 in MeOH). HRMS (ESI-TOF) calcd for $C_{15}H_{14}N_2NaO_4$ [M+Na^+]: 309.0846, found: 309.0834. FT-IR ν_{max} (neat): 3344, 3027, 1727, 1635, 1272, 637 cm^{-1}.

12.10.2.3 (3-Hydroxypicolinoyl)-D-phenylalanine (34b)

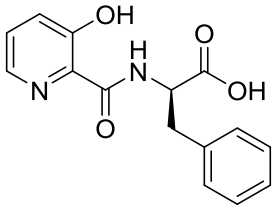

The desired compound (34b) was obtained as a white solid (246 mg, 0.86 mmol, 40%) from 3-hydroxypicolinic acid (300 mg, 2.16 mmol).

^{1}H NMR (400 MHz, $CDCl_3$) δ = 8.48 (br. s., 1 H, NH), 8.05 (br. s., 1 H), 7.10 - 7.40 (m, 8 H), 5.06 (q, *J*=7.0 Hz, 1 H, CH), 3.35 (dd, *J*=14.0, 5.5 Hz, 1 H, CHC*H*'H''), 3.24 (dd, *J*=14.0, 7.0 Hz, 1 H, CHCH'*H*'') ppm. ^{13}C NMR (101 MHz, $CDCl_3$) δ = 175.9, 168.5, 157.9, 139.8, 135.5, 130.7, 129.3, 129.0, 128.7, 127.3, 126.5, 53.0, 37.7 ppm. Mp = 123-126 °C. $[\alpha]^{20}_{D}$ = -23.2 (c = 0.1 in MeOH). HRMS (ESI-TOF) calcd for $C_{15}H_{14}N_2NaO_4$ [M+Na^+]: 309.0846, found: 309.0835. FT-IR ν_{max} (neat): 3345, 3032, 1727, 1635, 1265, 639 cm^{-1}.

12.10.2.4 (3-Hydroxypicolinoyl)-L-tryptophan (35a)[73]

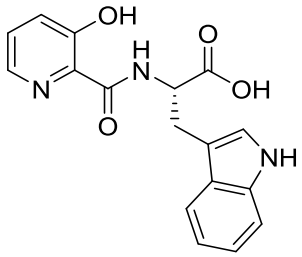

The desired compound (35a) was obtained as a yellow solid (295 mg, 0.91 mmol, 35%) from 3-hydroxypicolinic acid (300 mg, 2.16 mmol).

^{1}H NMR (400 MHz, CD_3OD) δ = 8.28 (br. s., 1 H), 7.77 - 7.93 (m, 2 H), 7.53 (dd, *J*=7.5, 3.5 Hz, 1 H), 7.28 - 7.39 (m, 1 H), 7.11 - 7.18 (m, 1 H), 7.03 - 7.11 (m, 1 H), 6.88 - 7.00 (m, 1 H), 4.99 - 5.06 (m, 1 H, CH), 3.41 - 3.58 (m, 2 H, CH_2) ppm. ^{13}C NMR (101 MHz, CD_3OD) δ = 172.1, 156.9, 137.0, 136.4, 132.5, 130.2, 127.6, 123.8, 121.6, 118.9, 118.1, 111.5, 108.7, 54.1, 27.3 ppm. Mp = 170-174 °C (lit. 109-111 °C)[73]. $[\alpha]^{20}_{D}$ = +7.6 (c = 0.2 in MeOH). HRMS (ESI-TOF) calcd for $C_{17}H_{15}N_3NaO_4$ [M+Na^+]: 348.0955, found: 348.0947. FT-IR ν_{max} (neat): 3328, 1715, 1522, 1324, 1198, 779cm^{-1}.

12.10.2.5 (3-Hydroxypicolinoyl)-D-tryptophan (35b)

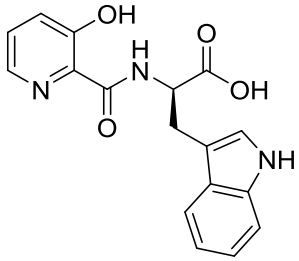

The desired compound (35b) was obtained as a yellow solid (287 mg, 0.89 mmol, 34%) from 3-hydroxypicolinic acid (300 mg, 2.16 mmol).

^{1}H NMR (400 MHz, CD_3OD) δ = 8.28 (br. s., 1 H), 7.77 - 7.93 (m, 2 H), 7.53 (dd, *J*=7.5, 3.5 Hz, 1 H), 7.28 - 7.39 (m, 1 H), 7.11 - 7.18 (m, 1 H), 7.03 - 7.11 (m, 1 H), 6.88 - 7.00 (m, 1 H), 4.99 - 5.06 (m, 1 H, CH), 3.41 - 3.58 (m, 2 H, CH_2) ppm. ^{13}C NMR (101 MHz, CD_3OD) δ = 172.1, 156.9, 137.0, 136.4, 132.5, 130.2, 127.6, 123.8, 121.6, 118.9, 118.1, 111.5, 108.7, 54.1, 27.3 ppm. Mp = 180-182 °C. $[\alpha]^{20}_{D}$ = -7.9 (c = 0.2 in MeOH). HRMS (ESI-TOF) calcd for $C_{17}H_{16}N_3O_4$ [M+H^+]: 326.1135, found: 326.1128. FT-IR ν_{max} (neat): 3329, 1715, 1618, 1518, 1324, 1198, 778 cm^{-1}.

12.10.2.6 (3-Hydroxypicolinoyl)-L-tyrosine (36a)

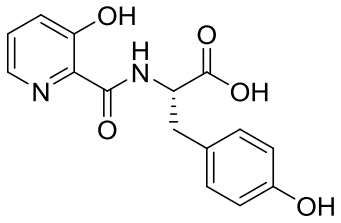

The desired compound (36a) was obtained as a white solid (294 mg, 0.97 mmol, 45%) from 3-hydroxypicolinic acid (300 mg, 2.16 mmol).

^{1}H NMR (400 MHz, CD_3OD) δ = 8.10 (dd, *J*=4.5, 1.0 Hz, 1 H), 7.44 (dd, *J*=8.5, 4.5 Hz, 1 H), 7.34 (dd, *J*=8.5, 1.0 Hz, 1 H), 7.05 (d, *J*=8.5 Hz, 2 H), 6.69 (d, *J*=8.5 Hz, 2 H), 4.84 (dd, *J*=7.0, 5.5 Hz, 1 H, CH), 3.23 (dd, *J*=14.0, 5.5 Hz, 1 H, C*H*'H''), 3.13 (dd, *J*=14.0, 7.0 Hz, 1 H, CH'*H*'') ppm. ^{13}C NMR (101 MHz, CD_3OD) δ = 173.1, 168.7, 158.0, 156.5, 140.0, 131.2, 130.4, 129.1, 127.4, 126.2, 115.3, 53.5, 36.6 ppm. Mp = 123-125 °C. $[\alpha]^{20}_D$ = +41.6 (c = 0.2 in MeOH). HRMS (ESI-TOF) calcd for $C_{15}H_{14}N_2NaO_5$ [M+Na^+]: 325.0795, found: 325.0782. FT-IR ν_{max} (neat): 3497, 2941, 1674, 1534, 1275, 1132, 836, 637 cm^{-1}.

12.10.2.7 (3-Hydroxypicolinoyl)-D-tyrosine (36b)

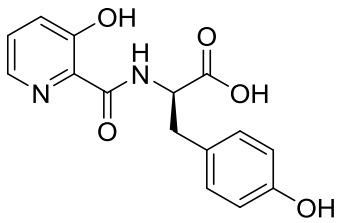

The desired compound (36b) was obtained as a white solid (294 mg, 0.97 mmol, 45%) from 3-hydroxypicolinic acid (300 mg, 2.16 mmol).

^{1}H NMR (400 MHz, DMSO-d_6) δ = 8.93 (d, *J*=8.5 Hz, 1 H, NH), 8.15 (dd, *J*=4.5, 1.5 Hz, 1 H), 7.52 (dd, *J*=8.5, 4.5 Hz, 1 H), 7.40 (dd, *J*=8.5, 1.0 Hz, 1 H), 7.01 (d, *J*=8.5 Hz, 2 H), 6.62 (d, *J*=8.5 Hz, 2 H), 4.57 - 4.72 (m, 1 H, CH), 3.04 - 3.15 (m, 2 H, CH_2) ppm. ^{13}C NMR (101 MHz, DMSO-d_6) δ = 172.6, 168.7, 157.6, 156.4, 140.5, 131.1, 130.5, 129.9, 127.6, 126.6, 115.6, 53.8, 35.7 ppm. Mp = 123-125 °C. $[\alpha]^{20}_D$ = -40.9 (c = 0.2 in MeOH). HRMS (ESI-TOF) calcd for $C_{15}H_{14}N_2NaO_5$ [M+Na^+]: 325.0795, found: 325.0783. FT-IR ν_{max} (neat): 3488, 2941, 1674, 1276, 1132, 636 cm^{-1}.

12.10.2.8 (3-Hydroxypicolinoyl)-L-alanine (37a)[73]

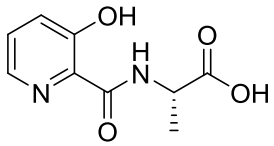

The desired compound (37a) was obtained as a white solid (190 mg, 0.91 mmol, 42%) from 3-hydroxypicolinic acid (300 mg, 2.16 mmol).

^{1}H NMR (400 MHz, DMSO-d_6) δ = 12.26 (s, 1 H, OH), 9.17 (d, *J*=7.5 Hz, 1 H, NH), 8.19 (dd, *J*=4.5, 1.0 Hz, 1 H), 7.55 (dd, *J*=8.5, 4.5 Hz, 1 H), 7.43 (dd, *J*=8.5, 1.0 Hz, 1 H), 4.49 (quin, *J*=7.5×4 Hz, 1 H, CH), 1.45 (d, *J*=7.5 Hz, 3 H, CH_3) ppm. ^{13}C NMR (101 MHz, DMSO-d_6) δ = 174.1, 169.1, 158.1, 140.9, 131.7, 130.2, 126.9, 48.4, 17.8 ppm. Mp = 188-190 °C (187-189 °C)[73]. $[\alpha]^{20}_D$ = +24.4 (c = 0.5 in MeOH). HRMS (ESI-TOF) calcd for $C_9H_{10}N_2NaO_4$ [M+Na$^+$]: 233.0533, found: 233.0524. FT-IR ν_{max} (neat): 3354, 2947, 1729, 1596, 1187, 698 cm^{-1}.

12.10.2.9 (3-Hydroxypicolinoyl)-D-alanine (37b)

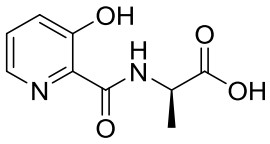

The desired compound (37b) was obtained as a white solid (170 mg, 0.81 mmol, 37%) from 3-hydroxypicolinic acid (300 mg, 2.16 mmol).

^{1}H NMR (400 MHz, DMSO-d_6) δ = 12.26 (s, 1 H, OH), 9.17 (d, *J*=7.5 Hz, 1 H, NH), 8.19 (dd, *J*=4.5, 1.0 Hz, 1 H), 7.55 (dd, *J*=8.5, 4.5 Hz, 1 H), 7.43 (dd, *J*=8.5, 1.0 Hz, 1 H), 4.49 (quin, *J*=7.5×4 Hz, 1 H, CH), 1.45 (d, *J*=7.5 Hz, 3 H, CH_3) ppm. ^{13}C NMR (101 MHz, DMSO-d_6) δ = 174.1, 169.1, 158.1, 140.9, 131.7, 130.2, 126.9, 48.4, 17.8 ppm. Mp = 195-196 °C. $[\alpha]^{20}_D$ = -24.7 (c = 0.5 in MeOH). HRMS (ESI-TOF) calcd for $C_9H_{10}N_2NaO_4$ [M+Na$^+$]: 233.0533, found: 233.0522. FT-IR ν_{max} (neat): 3354, 2947, 1730, 1627, 1596, 1187, 701 cm^{-1}.

12.10.2.10 (3-Hydroxypicolinoyl)-L-valine (38a)

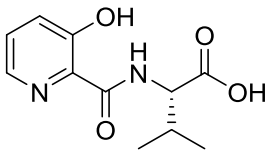

The desired compound (38a) was obtained as a white solid (180 mg, 0.76 mmol, 35%) from 3-hydroxypicolinic acid (300 mg, 2.16 mmol).

^{1}H NMR (400 MHz, $CDCl_3$) δ = 8.48 (br. s., 1 H, NH), 8.01 - 8.12 (m, 1 H), 7.23 - 7.41 (m, 2 H), 4.70 (dd, *J*=8.5, 4.5 Hz, 1 H, C*H*CO_2H), 2.32 - 2.49 (m, 1 H, C*H*$(CH_3)_2$), 1.05 (br. s., 3 H, CH_3), 1.03 (br. s., 3 H, CH_3) ppm. ^{13}C NMR (101 MHz, $CDCl_3$) δ = 176.2, 168.6, 157.9, 139.6, 130.8,

128.9, 126.5, 56.8, 31.1, 19.1, 17.7 ppm. Mp = 81-83 °C. $[\alpha]^{20}_{D}$ = +36.9 (c = 0.3 in MeOH). HRMS (ESI-TOF) calcd for $C_{11}H_{14}N_2NaO_4$ [M+Na^+]: 261.0846, found: 261.0844. FT-IR ν_{max} (neat): 3348, 2964, 1728, 1647, 1528, 1451, 805 cm^{-1}.

12.10.2.11 (3-Hydroxypicolinoyl)-D-valine (38b)

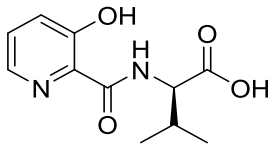

The desired compound (38b) was obtained as a white solid (196 mg, 0.83 mmol, 38%) from 3-hydroxypicolinic acid (300 mg, 2.16 mmol).

^{1}H NMR (400 MHz, $CDCl_3$) δ = 10.65 (br. s., 1 H, OH), 8.46 (d, *J*=8.0 Hz, 1 H, NH), 8.10 (dd, *J*=4.0, 1.0 Hz, 1 H), 7.37 (dd, *J*=8.5, 4.5 Hz, 1 H), 7.32 (d, *J*=8.0 Hz, 1 H), 4.72 (dd, *J*=9.0, 5.0 Hz, 1 H, C*H*CO_2H), 2.40 (sptd, *J*=6.8×6, 5.5 Hz, 1 H, C*H*$(CH_3)_2$), 1.07 (d, *J*=7.0 Hz, 3 H, CH_3), 1.06 (d, *J*=7.0 Hz, 3 H, CH_3) ppm. ^{13}C NMR (101 MHz, $CDCl_3$) δ = 176.2, 168.6, 157.9, 139.6, 130.8, 128.9, 126.5, 56.8, 31.1, 19.1, 17.7 ppm. Mp = 73-77 °C. $[\alpha]^{20}_{D}$ = -36.5 (c = 0.3 in MeOH). HRMS (ESI-TOF) calcd for $C_{11}H_{14}N_2NaO_4$ [M+Na^+]: 261.0846, found: 261.0846. FT-IR ν_{max} (neat): 3378, 3340, 2965, 2874, 1740, 1647, 1528, 1451, 1339, 806 cm^{-1}.

12.10.2.12 (3-Hydroxypicolinoyl)-L-leucine (39a)

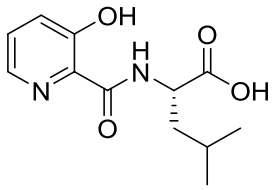

The desired compound (39a) was obtained as a white solid (230 mg, 0.91 mmol, 42%) from 3-hydroxypicolinic acid (300 mg, 2.16 mmol).

^{1}H NMR (400 MHz, DMSO-d_6) δ = 11.82 (br. s., 1 H, OH), 8.31 (d, *J*=8.5 Hz, 1 H, NH), 8.09 (d, *J*=4.5 Hz, 1 H), 7.35 - 7.40 (m, 1 H), 7.30 - 7.35 (m, 1 H), 4.70 - 4.89 (m, 1 H, C*H*COOH), 1.70 - 1.95 (m, 3 H, CH_2, C*H*$(CH_3)_2$), 1.01 (br. s, 3 H, CH_3), 0.99 (br. s, 3 H, CH_3) ppm. ^{13}C NMR (101 MHz, DMSO-d_6) δ = 177.4, 168.7, 157.9, 139.7, 130.9, 128.9, 126.3, 50.3, 41.0, 24.9, 22.8, 21.7 ppm. Mp = 93-95 °C. $[\alpha]^{20}_{D}$ = +7.4 (c = 0.1 in MeOH). HRMS (ESI-TOF) calcd for $C_{12}H_{16}N_2NaO_4$ [M+Na^+]: 275.1002, found: 275.1003. FT-IR ν_{max} (neat): 3372, 2961, 1724, 1654, 1445, 1295, 632 cm^{-1}.

12.10.2.13 (3-Hydroxypicolinoyl)-D-leucine (39b)

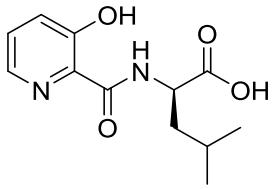

The desired compound (39b) was obtained as a white solid (200 mg, 0.79 mmol, 37%) from 3-hydroxypicolinic acid (300 mg, 2.16 mmol).

^{1}H NMR (400 MHz, DMSO-d_6) δ = 11.82 (br. s., 1 H, OH), 8.31 (d, *J*=8.5 Hz, 1 H, NH), 8.09 (d, *J*=4.5 Hz, 1 H), 7.35 - 7.40 (m, 1 H), 7.30 - 7.35 (m, 1 H), 4.70 - 4.89 (m, 1 H, C*H*COOH), 1.70 - 1.95 (m, 3 H, CH_2, CH(CH_3)$_2$), 1.01 (br. s, 3 H, CH_3), 0.99 (br. s, 3 H, CH_3) ppm. ^{13}C NMR (101 MHz, DMSO-d_6) δ = 177.4, 168.7, 157.9, 139.7, 130.9, 128.9, 126.3, 50.3, 41.0, 24.9, 22.8, 21.7 ppm. Mp = 90-92 °C. $[\alpha]^{20}_D$ = -7.8 (c = 0.1 in MeOH). HRMS (ESI-TOF) calcd for $C_{12}H_{16}N_2NaO_4$ [M+Na$^+$]: 275.1002, found: 275.0998. FT-IR ν_{max} (neat): 3372, 2961, 1724, 1654, 1445, 1295, 632 cm^{-1}.

12.10.2.14 (3-Hydroxypicolinoyl)-L-glutamic acid (40a)

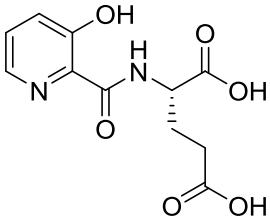

The desired compound (40a) was obtained as a pink solid (170 mg, 0.63 mmol, 24%) from 3-hydroxypicolinic acid (300 mg, 2.16 mmol).

^{1}H NMR (400 MHz, CD_3OD) δ = 8.15 (d, *J*=4.5 Hz, 1 H), 7.46 (dd, *J*=8.5, 4.5 Hz, 1 H), 7.36 (d, *J*=8.5 Hz, 1 H), 4.71 (dd, *J*=8.5, 4.5 Hz, 1 H, CH), 2.43 - 2.52 (m, 2 H, CH_2COOH), 2.31 - 2.43 (m, 1 H, CHCH'H''), 2.08 - 2.22 (m, 1 H, CHCH'H'') ppm. ^{13}C NMR (101 MHz, CD_3OD) δ = 175.3, 173.3, 169.3, 158.1, 140.0, 131.3, 129.2, 126.2, 51.6, 30.1, 27.1 ppm. Mp = 73-75 °C. $[\alpha]^{20}_D$ = +6.3 (c = 0.1 in MeOH). HRMS (ESI-TOF) calcd for $C_{11}H_{12}N_2NaO_6$ [M+Na$^+$]: 291.0588, found: 291.0576. FT-IR ν_{max} (neat): 3366, 2961, 2931, 1733, 1647, 1527, 1239, 1149, 806, 700 cm^{-1}.

12.10.2.15 (3-Hydroxypicolinoyl)-D-glutamic acid (40b)

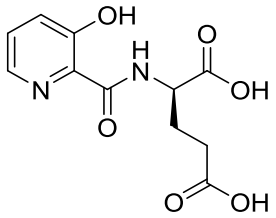

The desired compound (40b) was obtained as a pink solid (140 mg, 0.53 mmol, 20%) from 3-hydroxypicolinic acid (300 mg, 2.16 mmol).

^{1}H NMR (400 MHz, CD_3OD) δ = 8.15 (d, *J*=4.5 Hz, 1 H), 7.46 (dd, *J*=8.5, 4.5 Hz, 1 H), 7.36 (d, *J*=8.5 Hz, 1 H), 4.71 (dd, *J*=8.5, 4.5 Hz, 1 H, CH), 2.43 - 2.52 (m, 2 H, C*H*$_2$COOH), 2.31 - 2.43 (m, 1 H, CHC*H*'H''), 2.08 - 2.22 (m, 1 H, CHCH'*H*'') ppm. ^{13}C NMR (101 MHz, CD_3OD) δ = 175.3, 173.3, 169.3, 158.1, 140.0, 131.3, 129.2, 126.2, 51.6, 30.1, 27.1 ppm. Mp = 84-87 °C. $[\alpha]^{20}_{D}$ = -6.8 (c = 0.1 in MeOH). HRMS (ESI-TOF) calcd for $C_{11}H_{12}N_2NaO_6$ [M+Na$^+$]: 291.0588, found: 291.0585. FT-IR ν_{max} (neat): 3363, 2961, 1715, 1645, 1526, 1448, 1187, 1119, 801 cm^{-1}.

12.10.2.16 (3-Hydroxypicolinoyl)-L-aspartic acid (41a)

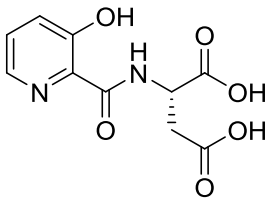

The desired compound (41a) was obtained as a pink solid (185 mg, 0.73 mmol, 28%) from 3-hydroxypicolinic acid (300 mg, 2.16 mmol).

^{1}H NMR (400 MHz, CD_3OD) δ = 8.13 (dd, *J*=4.5, 1.5 Hz, 1 H), 7.45 (dd, *J*=8.5, 4.5 Hz, 1 H), 7.35 (d, *J*=8.5 Hz, 1 H), 4.99 (m, 1H, CH overlapped with H_2O, assigned from ^{1}H-^{1}H COSY and ^{1}H-^{13}C HSQC spectra), 3.09 (dd, *J*=17.0, 5.5 Hz, 1 H, C*H*'H''), 2.98 (dd, *J*=17.0, 5.0 Hz, 1 H, CH'*H*'') ppm. ^{13}C NMR (101 MHz, CD_3OD) δ = 173.2, 172.6, 169.0, 158.0, 140.1, 131.3, 129.2, 126.1, 48.4, 35.8 ppm. Mp = 196-198 °C. $[\alpha]^{20}_{D}$ = +36.7 (c = 0.3 in MeOH). HRMS (ESI-TOF) calcd for $C_{10}H_{10}N_2NaO_6$ [M+Na$^+$]: 277.0431, found: 277.0426. FT-IR ν_{max} (neat): 3053, 1611, 1517, 1322, 1206, 802 cm^{-1}.

12.10.2.17 (3-Hydroxypicolinoyl)-D-aspartic acid (41b)

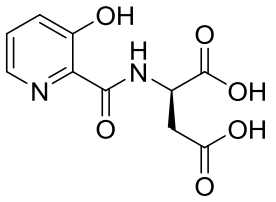

The desired compound (41b) was obtained as a pink solid (150 mg, 0.60 mmol, 23%) from 3-hydroxypicolinic acid (300 mg, 2.16 mmol).

^{1}H NMR (400 MHz, CD_3OD) δ = 8.13 (dd, *J*=4.5, 1.5 Hz, 1 H), 7.45 (dd, *J*=8.5, 4.5 Hz, 1 H), 7.35 (d, *J*=8.5 Hz, 1 H), 4.99 (m, 1H, CH overlapped with H_2O, assigned from ^{1}H-^{1}H COSY and ^{1}H-^{13}C HSQC spectra), 3.09 (dd, *J*=17.0, 5.5 Hz, 1 H, C*H*'H''), 2.98 (dd, *J*=17.0, 5.0 Hz, 1 H, CH'*H*'') ppm. ^{13}C NMR (101 MHz, CD_3OD) δ = 173.2, 172.6, 169.0, 158.0, 140.1, 131.3, 129.2, 126.1, 48.4, 35.8 ppm. Mp = 196-199 °C. $[\alpha]^{20}_{D}$ = -35.6 (c = 0.3 in MeOH). HRMS (ESI-TOF) calcd for $C_{10}H_{10}N_2NaO_6$ [M+Na$^+$]: 277.0431, found: 277.0424. FT-IR ν_{max} (neat): 3053, 1615, 1517, 1325, 1206, 803 cm^{-1}.

12.10.2.18 (3-Hydroxypicolinoyl)-L-histidine (43)

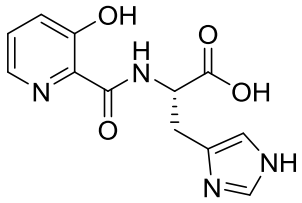

The desired compound (43) was obtained as a white solid (250 mg, 0.91 mmol, 35%) from 3-hydroxypicolinic acid (300 mg, 2.16 mmol).

^{1}H NMR (400 MHz, D_2O) δ = 8.49 (s, 1 H), 8.23 (d, *J*=5.0 Hz, 1 H), 7.99 (d, *J*=9.0 Hz, 1 H), 7.85 (dd, *J*=9.0, 5.5 Hz, 1 H), 7.22 (s, 1 H), 4.92 (dd, *J*=7.5, 5.0 Hz, 1 H, CH), 3.39 (dd, *J*=15.5, 5.0 Hz, 1 H, C*H*'H''), 3.29 (dd, *J*=15.5, 7.5 Hz, 1 H, CH'*H*'') ppm. ^{13}C NMR (101 MHz, D_2O) δ = 173.2, 160.7, 157.5, 135.8, 134.9, 133.9, 130.8, 128.7, 127.8, 117.7, 52.9, 26.6 ppm. Mp = 222-225 °C. $[\alpha]^{20}_{D}$ = -9.6 (c = 0.2 in MeOH). HRMS (ESI-TOF) calcd for $C_{12}H_{12}N_4O_4$ [M+H$^+$]: 277.0931, found: 277.0928. FT-IR ν_{max} (neat): 3217, 2460, 1720, 1658, 1523, 810, 621 cm^{-1}.

12.10.2.19 (2-Hydroxybenzoyl)glycine (44)[74]

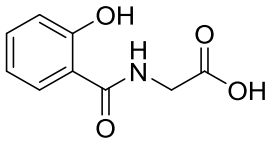

The desired compound (44) was obtained as a white solid (205 mg, 0.98 mmol, 45%) starting from salicylic acid (300 mg, 2.17 mmol) and following the general procedure.

^{1}H NMR (400 MHz, DMSO-d_6) δ = 12.24 (s, 1 H, OH), 9.15 (t, *J*=5.5 Hz, 1 H, NH), 7.89 (dd, *J*=8.0, 1.5 Hz, 1 H), 7.42 (ddd, *J*=8.5, 7.5, 1.5 Hz, 1 H), 6.82 - 7.01 (m, 2 H), 4.00 (d, *J*=6.0 Hz, 2 H, CH_2) ppm. ^{13}C NMR (101 MHz, DMSO-d_6) δ = 171.4, 169.2, 160.0, 134.3, 128.7, 119.3, 117.8, 115.8, 41.5 ppm. Mp = 165-167 °C (lit. 150-152 °C)[74]. HRMS (ESI-TOF) calcd for $C_9H_9NaNO_4$ [M+Na$^+$]: 218.0424, found: 218.0414. FT-IR ν_{max} (neat): 3389, 3345, 1705, 1607, 1546, 1234, 793 cm^{-1}.

12.10.2.20 Picolinoylglycine (45)[73]

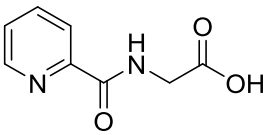

The desired compound (45) was obtained as a white solid (293 mg, 1.63 mmol, 40%) starting from picolinic acid (500 mg, 4.07 mmol) and following the general procedure.

^{1}H NMR (400 MHz, DMSO-d_6) δ = 9.01 (t, *J*=6.0 Hz, 1 H, NH), 8.65 (d, *J*=4.5 Hz, 1 H), 7.95 - 8.07 (m, 2 H), 7.61 (ddd, *J*=7.0, 5.0, 1.5 Hz, 1 H), 3.99 (d, *J*=6.0 Hz, 2 H, CH_2) ppm. ^{13}C NMR (101 MHz, DMSO-d_6) δ = 171.9, 165.0, 150.2, 149.4, 138.7, 127.6, 122.8, 41.8 ppm. Mp = 180-183 °C (lit. 119-121 °C)[73]. HRMS (ESI-TOF) calcd for $C_8H_8NaN_2O_3$ [M+Na$^+$]: 203.0427, found: 203.0427. FT-IR ν_{max} (neat): 3335, 2933, 2160, 1751, 1633, 1532, 1196, 671 cm^{-1}.

12.10.2.21 3-(3-Hydroxypicolinamido)propanoic acid (46)

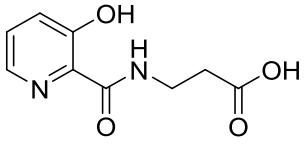

The desired compound (46) was obtained as a white solid (204 mg, 0.97 mmol, 45%) from 3-hydroxypicolinic acid (300 mg, 2.16 mmol).

^{1}H NMR (400 MHz, DMSO-d_6) δ = 9.12 (t, *J*=6.0 Hz, 1 H, NH), 8.16 (dd, *J*=4.5, 1.5 Hz, 1 H), 7.54 (dd, *J*=8.5, 4.5 Hz, 1 H), 7.44 (dd, *J*=8.5, 1.5 Hz, 1 H), 3.52 (td, *J*=7.0, 6.0 Hz, 2 H, NHC*H*$_2$), 2.56 (t, *J*=7.0 Hz, 2 H, CH_2CO_2H) ppm. ^{13}C NMR (101 MHz, DMSO-d_6) δ = 173.7, 168.9, 158.0, 140.4, 131.8, 130.1, 127.2, 35.5, 34.3 ppm. Mp = 175-177 °C. HRMS (ESI-TOF) calcd for $C_9H_{10}N_2NaO_4$

[M+Na$^+$]: 233.0533, found: 233.0523. FT-IR ν_{max} (neat): 3354, 3107, 2933, 2166, 1713, 1664, 1397, 672 cm^{-1}.

12.10.2.22 Picolinoyl-L-tryptophan (47)[75]

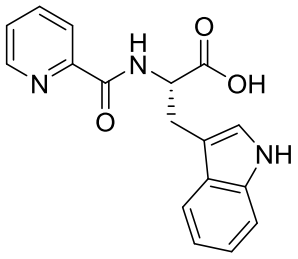

The desired compound (47)[75] was obtained as a white solid (478 mg, 1.55 mmol, 38%) starting from picolinic acid (500 mg, 4.07 mmol) and following the general procedure.

^{1}H NMR (400 MHz, DMSO-d_6) δ = 10.88 (br. s., 1 H), 8.67 (d, *J*=8.0 Hz, 1 H), 8.60 (d, *J*=4.5 Hz, 1 H), 7.93 - 8.09 (m, 2 H), 7.56 - 7.63 (m, 1 H), 7.52 (d, *J*=8.0 Hz, 1 H), 7.32 (d, *J*=8.1 Hz, 1 H), 7.14 (d, *J*=2.0 Hz, 1 H), 7.05 (t, *J*=7.5 Hz, 1 H), 6.92 (t, *J*=7.5 Hz, 1 H), 4.73 - 4.84 (m, 1 H), 3.36 (d, *J*=6.0 Hz, 2 H) ppm. ^{13}C NMR (101 MHz, DMSO-d_6) δ = 173.8, 164.2, 150.1, 149.4, 138.8, 137.0, 128.1, 127.7, 124.6, 122.7, 121.8, 119.2, 119.2, 112.3, 110.2, 53.7, 27.7 ppm. Mp = 144-146 °C. $[\alpha]^{20}_D$ = +10.2 (c = 0.2 in MeOH). HRMS (ESI-TOF) calcd for $C_{17}H_{15}NaN_3O_3$ [M+Na$^+$]: 332.1006, found: 332.0993. FT-IR ν_{max} (neat): 3353, 1724, 1657, 1521, 1211, 741 cm^{-1}.

12.10.2.23 (2-Hydroxybenzoyl)-L-tryptophan (48)

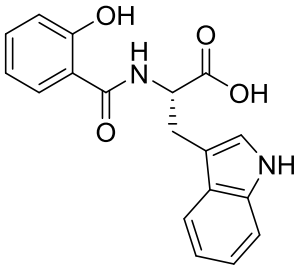

The desired compound (48)[75] was obtained as a white solid (339 mg, 1.05 mmol, 48%) starting from salicylic acid (300 mg, 2.17 mmol) and following the general procedure.

^{1}H NMR (400 MHz, DMSO-d_6) δ = 11.98 (br. s., 1 H, OH), 10.91 (d, *J*=1.5 Hz, 1 H, NH), 9.01 (d, *J*=7.5 Hz, 1 H, NH), 7.94 (dd, *J*=8.0, 1.5 Hz, 1 H), 7.57 (d, *J*=7.5 Hz, 1 H), 7.29 - 7.43 (m, 2 H), 7.18 (d, *J*=2.5 Hz, 1 H), 7.05 (td, *J*=7.5, 1.0 Hz, 1 H), 6.85 - 7.01 (m, 3 H), 4.63 - 4.84 (m, 1 H, CH), 3.31 (m, 2 H, CH_2) ppm. ^{13}C NMR (101 MHz, DMSO-d_6) δ = 174.0, 168.4, 159.7, 137.0, 134.5, 129.8, 128.0, 124.5, 121.8, 119.7, 119.3, 119.0, 118.0, 116.8, 112.3, 110.6, 54.2, 27.6 ppm. Mp = 130-133 °C. $[\alpha]^{20}_D$ = -11.9 (c = 0.2 in MeOH). HRMS (ESI-TOF) calcd for $C_{16}H_{18}NaN_2O_4$ [M+Na$^+$]: 347.1002, found: 347.0992. FT-IR ν_{max} (neat): 3395, 1718, 1597, 1490, 1215, 741 cm^{-1}.

12.10.2.24 3-Hydroxy-N-phenethylpicolinamide (49)

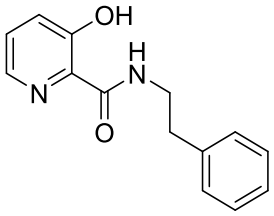

The desired compound (49) was obtained as yellow oil (290 mg, 1.19 mmol, 55%) by coupling 3-hydroxypicolinic acid (300 mg, 2.16 mmol) with 2-phenylethan-1-amine (300 µl, 2.38 mmol, 1.1eq) and following the general procedure.

^{1}H NMR (400 MHz, $CDCl_3$) δ = 12.24 (s, 1 H, OH), 8.15 (br. s., 1 H, NH), 8.02 (dd, *J*=4.0, 2.0 Hz, 1 H), 7.21 - 7.39 (m, 7 H), 3.60 - 3.83 (m, 2 H, CH_2), 2.96 (t, *J*=7.3 Hz, 2 H, CH_2) ppm. ^{13}C NMR (101 MHz, $CDCl_3$) δ = 168.8, 157.8, 139.5, 138.5, 131.5, 128.8, 128.7, 128.6, 126.6, 126.0, 40.3, 35.8 ppm. HRMS (ESI-TOF) calcd for $C_{14}H_{14}N_2NaO_2$ [M+Na^+]: 265.0947, found: 265.0949. FT-IR ν_{max} (neat): 3370, 3027, 1647, 1531, 1447, 1296, 808 cm^{-1}.

12.10.3 Synthesis of AR692B and derivatives

12.10.3.1 Methyl N-(tert-butoxycarbonyl)-S-(pyridin-2-ylmethyl)-L-cysteinate (50)[76]

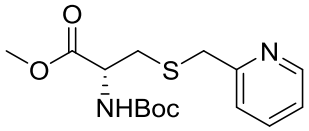

Et_3N (1.69 mL, 12.15 mmol, 2.5 eq) was added dropwise to a stirred solution of 2-(bromomethyl)pyridine hydrobromide (1.29 g, 5.10 mmol, 1.05 eq) in anhydrous DCM (10 mL). Methyl (tert-butoxycarbonyl)-L-cysteinate (1 mL, 4.86 mmol, 1 eq) was dissolved in 5 mL of DCM and added to 2-(bromomethyl)pyridine solution dropwise at 0 °C. The resultant mixture was stirred overnight at room temperature. The DCM was then evaporated *in vacuo* and remaining residue was subjected to column chromatography on silica (Biotage SNAP KP-SIL™ 50 g cartridge, cHex/EtOAc). Solvents were evaporated to yield the desired compound as a yellow oil (1.19 g, 3.65 mmol, 75%).

^{1}H NMR (400 MHz, $CDCl_3$) δ = 8.49 - 8.58 (m, 1 H, ArH), 7.65 (td, *J*=8.0, 2.0 Hz, 1 H, ArH), 7.30 (d, *J*=8.0 Hz, 1 H, ArH), 7.17 (ddd, *J*=7.5, 5.0, 1.0 Hz, 1 H, ArH), 5.92 (d, *J*=7.5 Hz, 1 H, NH), 4.42 - 4.61 (m, 1 H, CH), 3.85 (s, 2 H, SCH_2), 3.71 (s, 3 H, OCH_3), 2.94 (d, *J*=5.3 Hz, 2 H, CH*CH_2*), 1.43 (s, 9 H, $C(CH_3)_3$) ppm, ^{13}C NMR (101 MHz, $CDCl_3$) δ = 171.6, 158.0, 155.4, 149.2, 137.0, 123.2, 122.2, 79.9, 53.6, 52.5, 38.2, 33.9, 28.3 ppm. $[\alpha]^{20}_D$ = -27.2 (c = 0.5 in MeOH). HRMS (ESI-TOF) calcd for $C_{15}H_{22}N_2NaO_4S$ [M+Na^+]: 349.1192, found: 349.1199. FT-IR ν_{max} (neat): 2978, 1747, 1712, 1159, 730 cm^{-1}.

12.10.3.2 Methyl N-(tert-butoxycarbonyl)-S-(pyridin-4-ylmethyl)-L-cysteinate (51)[77]

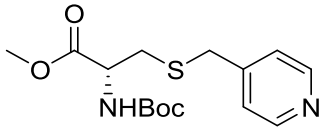

Et_3N (1.69 mL, 12.15 mmol, 2.5 eq) was added dropwise to a stirred solution of 2-(bromomethyl)pyridine hydrobromide (1.29 g, 5.10 mmol, 1.05 eq) in anhydrous DCM (10 mL). Methyl (tert-butoxycarbonyl)-L-cysteinate (1 mL, 4.86 mmol, 1 eq) was dissolved in 5 mL of DCM and added to 2-(bromomethyl)pyridine solution dropwise at 0 °C. The resultant mixture was stirred overnight at room temperature. DCM was evaporated *in vacuo* and remaining residue was subjected to column chromatography on silica (Biotage SNAP KP-SIL™ 50 g cartridge, cHex/EtOAc). The solvents were evaporated to yield the desired compound as a yellow oil (1.08 g, 3.32 mmol, 68%).

^{1}H NMR (400 MHz, $CDCl_3$) δ = 8.55 (d, *J*=5.5 Hz, 2 H), 7.25 (d, *J*=5.5 Hz, 2 H), 5.32 (d, *J*=7.0 Hz, 1 H, NH), 4.46 - 4.62 (m, 1 H, CH), 3.75 (s, 3 H, OCH_3), 3.69 (s, 2 H, SCH_2), 2.89 (dd, *J*=14.0, 4.5 Hz, 1 H, CHC*H*'H''), 2.78 (dd, *J*=14.0, 5.5 Hz, 1 H, CHCH'*H*''), 1.46 (s, 9 H, $C(CH_3)_3$) ppm, ^{13}C NMR (126 MHz, $CDCl_3$) δ = 171.3, 155.2, 149.4, 148.2, 124.6, 80.5, 53.1, 52.8, 35.5, 33.9, 28.3

ppm. $[\alpha]^{20}_D$ = -34.0 (c = 0.3 in MeOH). HRMS (ESI-TOF) calcd for $C_{15}H_{22}N_2NaO_4S$ $[M+Na^+]$: 349.1192, found: 349.1193. FT-IR ν_{max} (neat): 3191, 2982, 1743, 1708, 1604, 1163, 740 cm^{-1}.

12.10.3.3 Methyl N-(3-hydroxypicolinoyl)-S-(pyridin-2-ylmethyl)-L-cysteinate (AR692, 52)

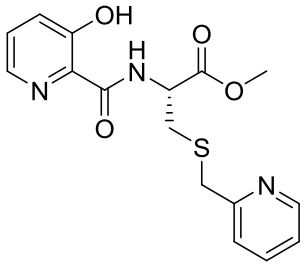

Methyl *N*-(tert-butoxycarbonyl)-*S*-(pyridin-2-ylmethyl)-L-cysteinate (2.35 g, 7.20 mmol, 1 eq) was treated with a 1M solution of HCl in Et_2O (20 mL) and stirred overnight at room temperature. The reaction mixture was evaporated *in vacuo* and dissolved in 5 mL of anhydrous DMF. Et_3N (1.5 mL, 10.8 mmol, 1.5 eq) was then added. The resultant solution was added to a mixture of commercially available 3-hydroxypicolinic acid (1.00 g, 7.20 mmol, 1 eq) stirred with CDI (1.40 g, 8.64 mmol, 1.2 eq) in anhydrous DMF (5 mL) for 15 min prior to addition of the amine solution in DMF. After stirring for 24 h at room temperature the DMF was evaporated *in vacuo* and the remaining residue was taken up in 20 mL DCM and washed 3 times with 10 mL of water. The organic layer was dried over $MgSO_4$, evaporated *in vacuo* and subjected to column chromatography on silica (Biotage SNAP KP-SIL™ 50 g cartridge, cHex/EtOAc). The solvent was evaporated to yield the desired compound as a yellow oil (1.12 g, 3.24 mmol, 45%).

^{1}H NMR (400 MHz, $CDCl_3$) δ = 11.76 (s, 1 H, OH), 8.81 (d, *J*=8.0 Hz, 1 H, NH), 8.47 - 8.59 (m, 1 H), 8.10 (dd, *J*=4.5, 1.5 Hz, 1 H), 7.61 (td, *J*=7.5, 2.0 Hz, 1 H), 7.25 - 7.43 (m, 3 H), 7.14 (m, 1 H), 4.88 - 5.04 (m, 1 H, CH), 3.89 (d, *J*=2.8 Hz, 2 H, SCH_2), 3.79 (s, 3 H, OCH_3), 3.09 (m, 2 H, $CHCH_2$) ppm, ^{13}C NMR (101 MHz, $CDCl_3$) δ = 170.6, 168.7, 157.9, 157.8, 149.4, 139.8, 136.8, 131.1, 128.9, 126.0, 123.1, 122.1, 52.8, 51.7, 38.2, 33.3 ppm. $[\alpha]^{20}_D$ = -37.2 (c = 0.1 in MeOH). HRMS (ESI-TOF) calcd for $C_{16}H_{17}N_3NaO_4S$ $[M+Na^+]$: 370.0832, found: 370.0836. FT-IR ν_{max} (neat): 3370, 2953, 1743, 1648, 1526, 1473, 701 cm^{-1}.

12.10.3.4 Methyl N-(3-hydroxypicolinoyl)-S-(pyridin-4-ylmethyl)-L-cysteinate (53)

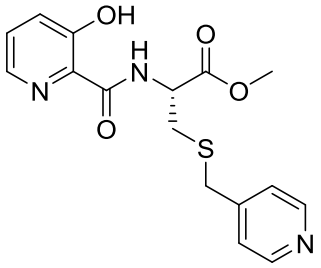

Methyl *N*-(tert-butoxycarbonyl)-*S*-(pyridin-4-ylmethyl)-L-cysteinate (430 mg, 1.32 mmol, 1 eq) was treated with a 1M solution of HCl in diethyl ether (5 mL) and stirred overnight at room temperature.

The reaction mixture was evaporated *in vacuo* and dissolved in 3 mL of the anhydrous DMF followed by the addition of Et_3N (275 µL, 1.98 mmol, 1.5 eq). The resultant solution was added to a mixture of commercially available 3-hydroxypicolinic acid (186 mg, 1.32 mmol, 1 eq) stirred with CDI (255 mg, 1.58 mmol, 1.2 eq) in anhydrous DMF (3 mL) for 15 min prior to addition of the amine solution in DMF. After stirring for 24h at room temperature DMF was evaporated *in vacuo* and remaining residue was taken up in 10 mL of DCM and washed 3 times with 5 mL of water. The organic layer was dried over $MgSO_4$, evaporated *in vacuo* and subjected to the column chromatography on silica (Biotage SNAP KP-SIL™ 25 g cartridge, eluent system cHex/EtOAc). Solvent was evaporated to yield the desired compound as a yellow oil (183 mg, 0.53 mmol, 40%).

^{1}H NMR (400 MHz, $CDCl_3$) δ = 11.66 (br. s., 1 H, OH), 8.66 (d, *J*=8.0 Hz, 1 H, NH), 8.53 - 8.59 (m, 2 H), 8.14 (dd, *J*=4.5, 1.5 Hz, 1 H), 7.30 - 7.44 (m, 4 H), 4.92 - 5.02 (m, 1 H, CH), 3.82 (s, 3 H, OCH_3), 3.77 (s, 2 H, SCH_2), 2.92 - 3.10 (m, 2 H, CHC*H*$_2$) ppm, ^{13}C NMR (101 MHz, $CDCl_3$) δ = 170.3, 168.7, 157.9, 149.1, 147.8, 140.0, 130.8, 129.1, 126.2, 124.3, 53.0, 51.4, 35.5, 33.5 ppm. $[\alpha]^{20}_D$ = -33.4 (c = 0.1 in MeOH). HRMS (ESI-TOF) calcd for $C_{16}H_{18}NO_4S$ [M+H$^+$]: 348.1013, found: 348.1005. FT-IR ν_{max} (neat): 3370, 3067, 2954, 1744, 1647, 1523, 701 cm^{-1}.

12.10.3.5 N-(3-hydroxypicolinoyl)-S-(pyridin-2-ylmethyl)-L-cysteine (AR692B, 54)

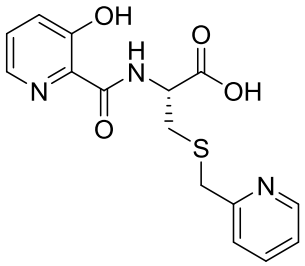

Methyl *N*-(3-hydroxypicolinoyl)-*S*-(pyridin-2-ylmethyl)-L-cysteinate (**53**) (200 mg, 0.58 mmol) was stirred overnight with $LiOH{\cdot}H_2O$ (120 mg, 2.90 mmol, 5eq) in a mixture of THF (2 mL) and water (2 mL). The THF was evaporated *in vacuo* and the resultant aqueous solution was acidified with concentrated HCl. Upon acidification product precipitated as a white solid, which was filtered off and dried under vacuum to yield the desired compound (153 mg, 0.46 mmol, 80%).

^{1}H NMR (400 MHz, DMSO-*d*$_6$) δ = 12.17 (br. s., 1 H, OH), 9.28 (d, *J*=8.0 Hz, 1 H, NH), 8.46 (dd, *J*=5.0, 1.0 Hz, 1 H), 8.21 (dd, *J*=4.5, 1.0 Hz, 1 H), 7.73 (td, *J*=7.5, 2.0 Hz, 1 H), 7.57 (dd, *J*=8.5, 4.5 Hz, 1 H), 7.46 (dd, *J*=8.5, 1.0 Hz, 1 H), 7.39 (d, *J*=8.0 Hz, 1 H), 7.18 - 7.28 (m, 1 H), 4.64 - 4.83 (m, 1 H, CH), 3.86 (d, *J*=4.5 Hz, 2 H, SCH_2), 3.06 - 3.13 (m, 2 H, CHC*H*$_2$) ppm, ^{13}C NMR (101 MHz, DMSO-*d*$_6$) δ = 171.8, 169.0, 158.7, 157.7, 149.4, 140.6, 137.4, 131.2, 130.0, 126.6, 123.5, 122.6, 51.7, 37.3, 32.4 ppm. Mp = 165-167 °C. $[\alpha]^{20}_D$ = -26.8 (c = 0.1 in MeOH). HRMS (ESI-TOF) calcd for $C_{15}H_{15}N_3NaO_4S$ [M+Na$^+$]: 356.0675, found: 356.0677. FT-IR νmax (neat): 3362, 1721, 1649, 1530, 1445, 702 cm^{-1}.

12.10.3.6 N-(3-hydroxypicolinoyl)-S-(pyridin-4-ylmethyl)-L-cysteine (AR693B, 55)

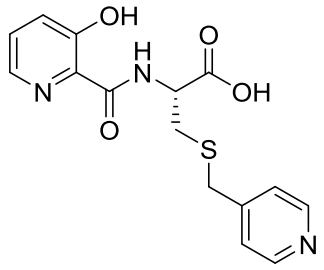

Methyl *N*-(3-hydroxypicolinoyl)-*S*-(pyridin-4-ylmethyl)-L-cysteinate (50 mg, 0.15 mmol) was stirred overnight with $LiOH \cdot H_2O$ (30 mg, 0.73 mmol, 5eq) in a mixture of THF (1 mL) and water (1 mL). The THF was evaporated *in vacuo* and the resultant aqueous solution was acidified with concentrated HCl. Upon acidification the product precipitated as a white solid, which was filtered off and dried under the vacuum to yield the desired compound (30 mg, 0.087 mmol, 58%).

^{1}H NMR (400 MHz, DMSO-d_6) δ = 12.12 (br. s., 1 H, OH), 9.24 (d, *J*=8.5 Hz, 1 H, NH), 8.47 - 8.57 (m, 2 H), 8.20 (dd, *J*=4.5, 1.5 Hz, 1 H), 7.57 (dd, *J*=8.5, 4.5 Hz, 1 H), 7.45 (dd, *J*=8.5, 1.5 Hz, 1 H), 7.38 - 7.41 (m, 2 H), 4.67 (td, *J*=8.5, 4.5 Hz, 1 H, CH), 3.81 (br. s, 2 H, SCH_2), 2.95 - 3.08 (m, 2 H, CHCH_2) ppm, ^{13}C NMR (101 MHz, DMSO-d_6) δ = 171.6, 169.0, 157.7, 149.5, 149.1, 140.6, 131.1, 130.0, 126.6, 124.8, 51.7, 34.4, 32.4 ppm. Mp = 190-192 °C. $[\alpha]^{20}_D$ = -23.4 (c = 0.1 in MeOH). HRMS (ESI-TOF) calcd for $C_{15}H_{15}N_3NaO_4S$ [M+Na^+]: 356.0675, found: 356.0678. FT-IR ν_{max} (neat): 3368, 1645, 1515, 1448, 1298, 701 cm^{-1}.

12.10.3.7 Octyl N-(tert-butoxycarbonyl)-S-(pyridin-2-ylmethyl)-L-cysteinate (56)

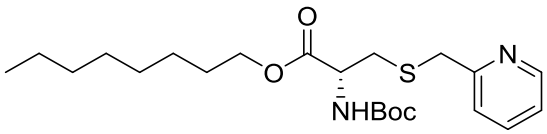

A solution of methyl *N*-(tert-butoxycarbonyl)-*S*-(pyridin-2-ylmethyl)-L-cysteinate (1.70 g, 5.45 mmol, 1 eq) in THF (10 mL) was treated with 20 mL of a 1M solution of LiOH in water and stirred overnight at room temperature. The THF was evaporated and resultant aqueous solution brought to pH 7.0 with concentrated HCl and extracted 3 times with 10 mL of DCM. The organic layer was dried over $MgSO_4$ and evaporated. Obtained residue was mixed with DCC (1.70 g, 8.17 mmol, 1.5 eq) and DMAP (200 mg, 1.64 mmol, 0.3 eq) in anhydrous DMF (15 mL) prior to the dropwise addition of n-octanol (4.3 mL, 27.3 mmol, 5eq). After 12 h the DMF was evaporated and remaining residue taken into DCM (20 mL) and washed with H_2O (3×10 mL). Organic layer was dried over $MgSO_4$, evaporated and subjected to column chromatography on silica (Biotage SNAP KP-SIL^{TM} 50 g cartridge, cHex/EtOAc). Solvents were evaporated to yield the desired compound as a yellow oil (1.30 g, 3.07 mmol, 56%).

^{1}H NMR (400 MHz, $CDCl_3$) δ = 8.54 - 8.66 (m, 1 H), 7.89 (t, *J*=7.0 Hz, 1 H), 7.54 (d, *J*=8.0 Hz, 1 H), 7.35 - 7.46 (m, 1 H), 5.80 (d, *J*=7.0 Hz, 1 H, NH), 4.53 (d, *J*=5.0 Hz, 1 H, CH), 4.15 (t, *J*=6.5

Hz, 2 H, OCH_2), 4.06 (d, *J*=3.5 Hz, 2 H, SCH_2), 2.94 - 3.09 (m, 2 H, CHC*H*$_2$), 1.61 - 1.68 (m, 2 H), 1.47 (s, 9 H, $C(CH_3)_3$), 1.26 - 1.36 (m, 10 H), 0.90 (t, *J*=6.1 Hz, 3 H, CH_2CH_3) ppm, ^{13}C NMR (126 MHz, $CDCl_3$) δ = 170.9, 156.8, 155.4, 145.7, 140.5, 125.0, 123.3, 80.1, 66.0, 53.7, 35.9, 34.4, 32.8, 31.8, 29.2, 28.5, 28.4, 25.8, 22.7, 14.1 ppm. $[\alpha]^{20}_D$ = -20.5 (c = 0.2 in MeOH). HRMS (ESI-TOF) calcd for $C_{22}H_{36}N_2NaO_4S$ [M+Na^+]: 447.2288, found: 447.2283. FT-IR ν_{max} (neat): 2926, 2856, 1714, 1435, 1165, 748 cm^{-1}.

12.10.3.8 Octyl N-(3-hydroxypicolinoyl)-S-(pyridin-2-ylmethyl)-L-cysteinate (AR780, 57)

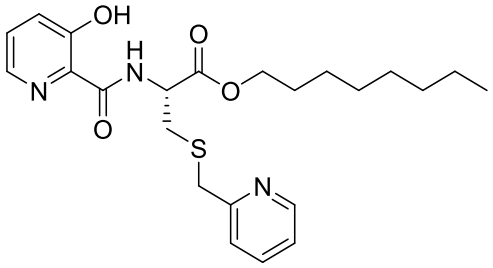

Octyl *N*-(tert-butoxycarbonyl)-*S*-(pyridin-2-ylmethyl)-L-cysteinate (0.93 g, 2.20 mmol, 1 eq) was treated with a 1M solution of HCl in Et_2O (10 mL) and stirred overnight at room temperature. The reaction mixture was evaporated *in vacuo* and dissolved in 7 mL of anhydrous DMF followed by addition of Et_3N (460 µL, 3.3 mmol, 1.5 eq). The resultant solution was added to the mixture of commercially available 3-hydroxypicolinic acid (370 mg, 2.64 mmol, 1.2 eq) stirred with CDI (430 mg, 2.64 mmol, 1.2 eq) in anhydrous DMF (7 mL) for 15 min prior to the addition of the amine solution in DMF. After stirring for 24h at room temperature DMF was evaporated *in vacuo* and remaining residue was taken up in DCM (20 mL) and washed with H_2O (3×10 mL). Organic layer was dried over $MgSO_4$, evaporated *in vacuo* and subjected to column chromatography on silica (Biotage SNAP KP-SIL^{TM} 25 g cartridge, eluent system cHex/EtOAc). The solvent was evaporated to yield the desired compound as a yellow oil (290 mg, 0.66 mmol, 30%). ^{1}H NMR (400 MHz, $CDCl_3$) δ = 11.70 (s, 1 H, OH), 8.71 (d, *J*=8.5 Hz, 1 H, NH), 8.43 - 8.49 (m, 1 H), 8.03 (dd, *J*=4.0, 1.5 Hz, 1 H), 7.60 (td, *J*=7.5, 2.0 Hz, 1 H), 7.27 - 7.33 (m, 2 H), 7.23 (dd, *J*=8.5, 1.5 Hz, 1 H), 7.12 (ddd, *J*=7.5, 5.0, 0.5 Hz, 1 H), 4.87 (ddd, *J*=8.5, 6.5, 5.0 Hz, 1 H, CH), 4.12 (td, *J*=7.0, 1.0 Hz, 3 H, OCH_2), 3.88 (br. s, 2 H, SCH_2), 3.07 (dd, *J*=14.0, 5.0 Hz, 1 H, CHC*H*'H''), 3.00 (dd, *J*=14.0, 6.5 Hz, 1 H, CHCH'*H*''), 1.58 (quin, *J*=7.0 Hz, 2 H), 1.17 - 1.26 (m, 10 H), 0.77 - 0.85 (m, 3 H, CH_2CH_3) ppm, ^{13}C NMR (101 MHz, $CDCl_3$) δ = 170.1, 168.7, 157.8, 157.6, 148.4, 139.9, 137.6, 131.1, 128.9, 126.0, 123.6, 122.3, 66.2, 51.8, 37.6, 33.5, 31.7, 29.1, 28.5, 25.8, 22.6, 14.1 ppm. $[\alpha]^{20}_D$ = -38.1 (c = 0.2 in MeOH). HRMS (ESI-TOF) calcd for $C_{23}H_{31}N_3NaO_4S$ [M+Na^+]: 468.1927, found: 468.1934. FT-IR ν_{max} (neat): 3372, 2957, 2926, 2854, 1739, 1649, 1570, 1470, 1179, 701 cm^{-1}.

12.10.4 General procedure for synthesis of amino acids conjugates of 1-chloro-4-hydroxyisoquinolines

1-Chloro-4-hydroxyisoquinoline-3-carboxylic acid (300 mg, 1.35 mmol), amino acid methyl ester (1.2 eq), PyBOP (1.2 eq) and Et_3N (1.5 mmol) were dissolved in the anhydrous DMF (5 mL) and subsequently stirred at room temperature for 24h. Upon completion of the reaction the DMF was evaporated *in vacuo* and the resultant residue was suspended in CH_2Cl_2 (20 mL) and washed with H_2O (2 x 10 mL). The organic phase was dried over $MgSO_4$, filtered and subjected to column chromatography (Biotage SNAP KP-SIL™ 25 g cartridge, eluent system: cHex/EtOAc, ratio for elution of each methyl ester is given along with characterization of final product). The obtained product was dissolved in a mixture of THF/H_2O (1:1, 10 mL) and subsequently treated with LiOH · H_2O (5 eq). The reaction was stirred at room temperature for 12 h. The THF was evaporated *in vacuo* and the remaining aqueous solution was neutralized with conc. HCl. If a precipitate was formed, it was filtered-off and dried *in vacuo* to yield the desired product. In case no precipitate was formed, the aqueous solution was extracted with EtOAc (3 x 10 mL). The combined organic layers were dried over $MgSO_4$, filtered and evaporated *in vacuo* to yield desired product.

12.10.4.1 1-Chloro-4-hydroxyisoquinoline-3-carboxylic acid (86)[78]

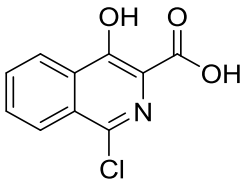

Commercially available methyl 1-chloro-4-hydroxyisoquinoline-3-carboxylate (5.0 g, 21.0 mmol) was dissolved in a mixture of H_2O and THF (1:1, 50 mL) and treated with lithium hydroxide (LiOH · H_2O, 4.42 g, 0.21 mol, 10 eq). The reaction was stirred at room temperature for 24h. The THF was evaporated and resulting water solution extracted with EtOAc (2 x 20 mL). The aqueous phase was acidified with conc. HCl (pH = 1) and subsequently extracted with EtOAc (3 x 20 mL). The combined organic extracts were dried over $MgSO_4$, filtered, and evaporated *in vacuo* to yield the desired compound as a white solid (4.47 g, 95%).

^{1}H NMR (400 MHz, DMSO-d_6): δ = 8.31-8.36 (m, 1H, ArH), 8.21-8.25 (m, 1H, ArH), 7.96-8.01 (m, 2H, ArH) ppm. ^{13}C NMR (101 MHz, DMSO-d_6) δ = 171.5, 156.0, 138.8, 132.1, 131.8, 129.1, 128.8, 125.9, 123.2, 119.5 ppm. Mp = 202-205°C (194-196 °C)[78]. HRMS (ESI-TOF) calcd. for $C_{10}H_6ClNO_3$ [M+H$^+$]: 221.9963, found: 221.9958. FT-IR ν_{max} (neat): 2966, 1656, 1312, 1233, 768 cm^{-1}.

12.10.4.2 2-(1-Chloro-4-hydroxyisoquinoline-3-carboxamido)acetic acid (75)[79]

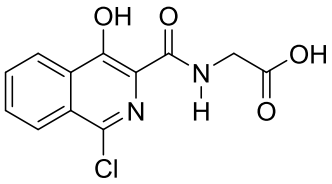

The desired compound (75)[79] was obtained as a white solid (175 mg, 46%) starting from 1-chloro-4-hydroxyisoquinoline-3-carboxylic acid (300 mg, 1.35 mmol).

^{1}H NMR (400 MHz, DMSO-d_6) δ = 9.16 (t, *J*=6.0 Hz, 1 H, NH), 8.30 (m, 1 H, ArH) 8.24 (m, 1 H, ArH), 7.84 - 8.09 (m, 2 H, ArH) 4.02 (d, *J*=6.0 Hz, 2 H, CH_2) ppm, ^{13}C NMR (101 MHz, DMSO-d_6) δ = 171.4, 169.6, 155.1, 139.4, 132.6, 132.5, 130.3, 129.3, 126.9, 123.8, 121.3, 41.7 ppm. Mp = 212-214 °C, HRMS (ESI-TOF) calcd for $C_{12}H_9ClN_2NaO_4$ [M+Na$^+$]: 303.0144, found: 303.0143, FT-IR ν_{max} (neat): 3402, 2915, 1712, 1641, 1354, 1255, 794 cm^{-1}.

12.10.4.3 (*S*)-2-(1-chloro-4-hydroxyisoquinoline-3-carboxamido)-3-(1H-indol-3-yl)propanoic acid (76a)[80]

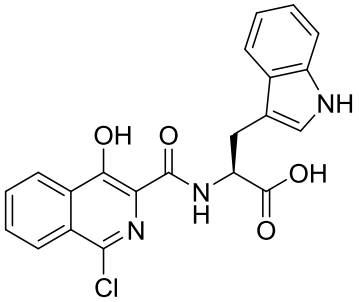

The desired compound (76a) was obtained as an off-white solid (232 mg, 42%) starting from 1-chloro-4-hydroxyisoquinoline-3-carboxylic acid (300 mg, 1.35 mmol).

^{1}H NMR (400 MHz, DMSO-d_6) δ = 13.50 (s, 1H, OH), 10.93 (s, 1H, NH indole), 8.80 (d, *J* = 8.1 Hz, 1H, NH), 8.30 - 8.38 (m, 1H, ArH), 8.24 - 8.30 (m, 1H, ArH), 7.93 - 8.08 (m, 2H, ArH), 7.58 (d, *J* = 8.0 Hz, 1H, ArH), 7.33 (d, *J* = 8.0 Hz, 1H, ArH), 7.19 (d, *J* = 2.0 Hz, 1H, H7), 7.05 (t, *J* = 7.0 Hz, 1H, ArH), 6.95 (t, *J* = 7.5 Hz, 1H, ArH), 4.83 (td, *J* = 7.5, 5.0 Hz, 1H, H5), 3.46 (overlapping with water signal, 2H, H6, determined by HSQC) ppm. ^{13}C NMR (176 MHz, DMSO-d_6) δ = 172.9, 168.7, 154.7, 139.0, 136.6, 132.3, 132.3, 129.9, 129.0, 127.7, 126.6, 124.2, 123.5, 121.5, 120.8, 119.0, 118.7, 111.9, 109.8, 53.3, 26.9 ppm. Mp = 205-208 °C (lit. 205-208 °C)[80], $[\alpha]^{20}_D$ = -21.7 (c = 0.133 in DMSO). HRMS (ESI-TOF) calcd for $C_{21}H_{16}ClN_3NaO_4$ [M+Na$^+$]: 432.0722, found: 432.0737. FT-IR ν_{max} (neat): 3365, 1718, 1633, 1529, 1320, 768 cm^{-1}.

12.10.4.4 (*R*)-2-(1-chloro-4-hydroxyisoquinoline-3-carboxamido)-3-(1H-indol-3-yl)propanoic acid (76b)[80]

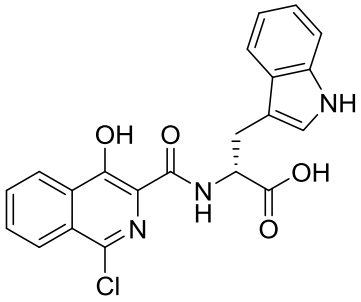

The desired compound (76b) was obtained as a white solid (249 mg, 45%) starting from 1-Chloro-4-hydroxyisoquinoline-3-carboxylic acid (300 mg, 1.35 mmol).

^{1}H NMR (400 MHz, DMSO-d_6) δ = 13.50 (s, 1H, OH), 10.93 (s, 1H, NH indole), 8.80 (d, *J* = 8.0 Hz, 1H, NH), 8.30 - 8.38 (m, 1H, ArH), 8.24 - 8.30 (m, 1H, ArH), 7.93 - 8.08 (m, 2H, ArH), 7.58 (d, *J* = 8.0 Hz, 1H, ArH), 7.33 (d, *J* = 8.0 Hz, 1H, ArH), 7.19 (d, *J* = 2.0 Hz, 1H, H7), 7.05 (t, *J* = 7.0 Hz, 1H, ArH), 6.95 (t, *J* = 7.5 Hz, 1H, ArH), 4.83 (td, *J* = 7.5, 5.0 Hz, 1H, H5), 3.46 (overlapped with water signal, 2H, H6, determined by HSQC) ppm. ^{13}C NMR (176 MHz, DMSO-d_6) δ = 172.9, 168.7, 154.7, 139.0, 136.6, 132.3, 132.3, 129.9, 129.0, 127.7, 126.6, 124.2, 123.5, 121.5, 120.8, 119.0, 118.7, 111.9, 109.8, 53.3, 26.9 ppm. Mp = 212-214 °C (lit. 212-214 °C)[80], $[\alpha]^{20}_D$ = 24.9 (c = 0.088 in DMSO). HRMS (ESI-TOF) calcd for $C_{21}H_{16}ClN_3NaO_4$ [M+Na$^+$]: 432.0722, found: 432.0729. FT-IR ν_{max} (neat): 3362, 1634, 1529, 1319, 770 cm^{-1}.

12.10.4.5 (*S*)-2(1-Chloro-4-hydroxyisoquinoline-3-carboxamido)propanoic acid (77a)[81]

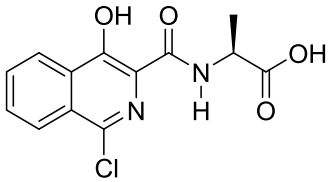

The desired compound (77a) was obtained as a white solid (145 mg, 38%) starting from 1-chloro-4-hydroxyisoquinoline-3-carboxylic acid (300 mg, 1.35 mmol).

^{1}H NMR (400 MHz, DMSO-d_6) δ = 9.15 (d, *J*=7.5 Hz, 1 H, NH), 8.39 - 8.45 (m, 1 H, ArH), 8.32 - 8.39 (m, 1 H, ArH), 8.02 - 8.10 (m, 2 H, ArH), 4.63 (quin, *J*=7.5 Hz, 1 H, CH), 1.55 (d, *J*=7.5 Hz, 3 H, CH_3) ppm, ^{13}C NMR (101 MHz, DMSO-d_6) δ = 173.7, 168.7, 154.9, 139.0, 132.3, 132.2, 130.0, 129.0, 126.6, 123.5, 120.9, 48.1, 17.4 ppm. Mp =195-198 °C (lit. 178-180 °C) [81], $[\alpha]^{20}_D$ = -11.7 (c = 0.100 in DMSO). HRMS (ESI-TOF) calcd for $C_{13}H_{10}ClN_2O_4$ [M-H$^+$]: 293.0335, found: 293.0327, FT-IR ν_{max} (neat): 3440, 3372, 1735, 1620, 1547, 1361, 1286, 770 cm^{-1}.

12.10.4.6 (*R*)-2(1-Chloro-4-hydroxyisoquinoline-3-carboxamido)propanoic acid (77b)[81]

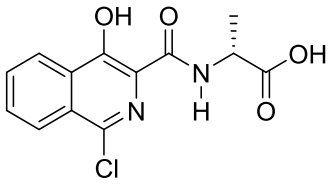

The desired compound (77b) was obtained as a white solid (148 mg, 40%) starting from 1-chloro-4-hydroxyisoquinoline-3-carboxylic acid (300 mg, 1.35 mmol).

^{1}H NMR (400 MHz, DMSO-d_6) δ = 9.15 (d, *J*=7.5 Hz, 1 H, NH), 8.39 - 8.45 (m, 1 H, ArH), 8.32 - 8.39 (m, 1 H, ArH), 8.02 - 8.10 (m, 2 H, ArH), 4.63 (quin, *J*=7.5 Hz, 1 H, CH), 1.55 (d, *J*=7.5 Hz, 3 H, CH_3) ppm, ^{13}C NMR (101 MHz, DMSO-d_6) δ = 173.7, 168.7, 154.9, 139.0, 132.3, 132.2, 130.0, 129.0, 126.6, 123.5, 120.9, 48.1, 17.4 ppm. Mp =191-193 °C (lit. 116-118 °C)[81], $[\alpha]^{20}_D$ = +10.5 (c = 0.100 in DMSO). HRMS (ESI-TOF) calcd for $C_{13}H_{10}ClN_2O_4$ [M-H$^+$]: 293.0335, found: 293.0329, FT-IR ν_{max} (neat): 3441, 3370, 1735, 1622, 1544, 1361, 1286, 772 cm^{-1}.

12.10.4.7 (*S*)-Methyl 2-(1-chloro-4-hydroxyisoquinoline-3-carboxamido)-3-methylbutanoic acid (78a)[82]

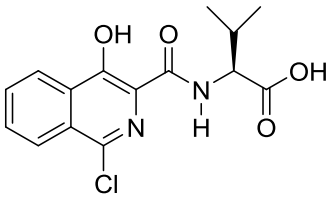

The desired compound (78a) was obtained as a white solid (148 mg, 34%) starting from 1-chloro-4-hydroxyisoquinoline-3-carboxylic acid (300 mg, 1.35 mmol).

^{1}H NMR (400 MHz, DMSO-d_6) δ = 8.55 (d, *J*=8.5 Hz, 1 H, NH), 8.40 (m, 1 H, ArH), 8.35 (m, 1 H, ArH), 8.06 (m, 2 H, ArH), 4.49 (dd, *J*=8.5, 5.5 Hz, 1 H, C*H*CO_2H), 2.38 (sptd, *J*=7.0×4, 5.5 Hz, 1 H, C*H*$(CH_3)_2$), 1.04 (d, *J*=7.0 Hz, 3 H, CH_3), 1.03 (d, *J*=7.0 Hz, 3 H, CH_3) ppm, ^{13}C NMR (101 MHz, DMSO-d_6) δ = 172.6, 168.7, 154.8, 139.2, 132.4, 132.3, 130.0, 129.1, 126.6, 123.5, 120.6, 57.6, 30.6, 19.5, 18.6 ppm. Mp =165-168°C (lit. 178-180 °C)[82], $[\alpha]^{20}_D$ = +16.7 (c = 0.100 in DMSO). HRMS (ESI-TOF) calcd for $C_{15}H_{15}ClNaN_2O_4$ [M+H$^+$]: 345.0613, found: 345.0611, FT-IR ν_{max} (neat): 3447, 3373, 2965, 1759, 1572, 1259, 776 cm^{-1}.

12.10.4.8 (*R*)-Methyl 2-(1-chloro-4-hydroxyisoquinoline-3-carboxamido)-3-methylbutanoic acid (78b)[82]

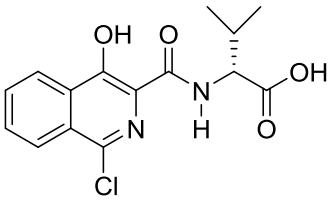

The desired compound (78b) was obtained as a white solid (165 mg, 38%) starting from 1-chloro-4-hydroxyisoquinoline-3-carboxylic acid (300 mg, 1.35 mmol).

^{1}H NMR (400 MHz, DMSO-d_6) δ = 8.55 (d, *J*=8.5 Hz, 1 H, NH), 8.40 (m, 1 H, ArH), 8.35 (m, 1 H, ArH), 8.06 (m, 2 H, ArH), 4.49 (dd, *J*=8.5, 5.5 Hz, 1 H, C*H*CO_2H), 2.38 (sptd, *J*=7.0×4, 5.5 Hz, 1 H, C*H*$(CH_3)_2$), 1.04 (d, *J*=7.0 Hz, 3 H, CH_3), 1.03 (d, *J*=7.0 Hz, 3 H, CH_3) ppm, ^{13}C NMR (101 MHz, DMSO-d_6) δ = 172.6, 168.7, 154.8, 139.2, 132.4, 132.3, 130.0, 129.1, 126.6, 123.5, 120.6, 57.6, 30.6, 19.5, 18.6 ppm. Mp =172-175°C (lit. 178-180 °C)[82], $[\alpha]^{20}_D$ = -18.1 (c = 0.100 in DMSO). HRMS (ESI-TOF) calcd for $C_{15}H_{15}ClNaN_2O_4$ [M+H$^+$]: 345.0613, found: 345.0614, FT-IR ν_{max} (neat): 3447, 3373, 2965, 1759, 1572, 1259, 776 cm^{-1}.

12.10.4.9 (*S*)-2-(1-chloro-4-hydroxyisoquinoline-3-carboxamido)-4-methylpentanoic acid (79a)[80]

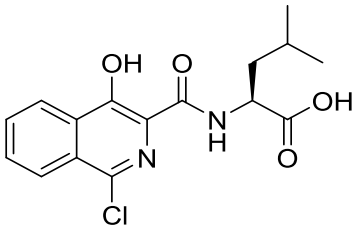

The desired compound (79a) was obtained as an off-white solid (160 mg, 35%) starting from 1-chloro-4-hydroxyisoquinoline-3-carboxylic acid (300 mg, 1.35 mmol).

^{1}H NMR (400 MHz, DMSO-d_6) δ = 13.67 (br. s., 1H, OH), 9.03 (d, *J* = 8.5 Hz, 1H, NH), 8.29 - 8.35 (m, 1H, ArH), 8.24 - 8.29 (m, 1H, ArH), 7.91 - 8.06 (m, 2H, ArH), 4.44 - 4.66 (m, 1H, H5), 1.96 (m, 1H, H6'), 1.54 - 1.77 (m, 2H, H6'', H7), 0.91 (d, *J* = 6.0 Hz, 3H, H8), 0.92 (d, *J* = 6.0 Hz, 3H, H9) ppm. ^{13}C NMR (101 MHz, DMSO-d_6) δ = 174.0, 169.7, 155.3, 139.4, 132.6, 132.6, 130.4, 129.4, 126.9, 123.8, 121.2, 51.1, 39.6 (overlapped with DMSO signal), 25.4, 23.8, 22.1 ppm. Mp = 158-160 °C (lit. 158-160 °C)[80], $[\alpha]^{20}_D$ = 13.4 (c = 0.104 in DMSO). HRMS (ESI-TOF) calcd for $C_{16}H_{17}ClN_2NaO_4$ [M+Na$^+$]: 359.0769, found: 359.0763. FT-IR ν_{max} (neat): 3380, 2966, 1656, 1312, 1233, 768 cm^{-1}.

12.10.4.10 (*R*)-2-(1-chloro-4-hydroxyisoquinoline-3-carboxamido)-4-methylpentanoic acid (79b)[80]

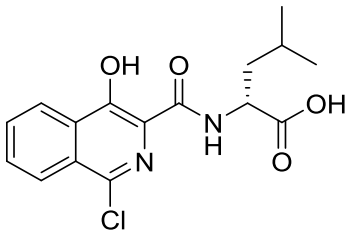

The desired compound (79b) was obtained as an off-white solid (146 mg, 32%) starting from 1-chloro-4-hydroxyisoquinoline-3-carboxylic acid (300 mg, 1.35 mmol).

^{1}H NMR (400 MHz, DMSO-d_6) δ = 13.67 (br. s., 1H, OH), 9.03 (d, *J* = 8.5 Hz, 1H, NH), 8.29 - 8.35 (m, 1H, ArH), 8.24 - 8.29 (m, 1H, ArH), 7.91 - 8.06 (m, 2H, ArH), 4.44 - 4.66 (m, 1H, H5), 1.96 (m, 1H, H6'), 1.54 - 1.77 (m, 2H, H6", H7), 0.91 (d, 3H, *J* = 6.0 Hz, H8), 0.92 (d, *J* = 6.0 Hz, 3H, H9) ppm. ^{13}C NMR (101 MHz, DMSO-d_6) δ = 174.0, 169.7, 155.3, 139.4, 132.6, 132.6, 130.4, 129.4, 126.9, 123.8, 121.2, 51.1, 39.6 (overlapped with DMSO signal), 25.4, 23.8, 22.1 ppm. Mp = 157-159 °C (lit. 157-159 °C)[80], $[\alpha]^{20}_D$ = -12.6 (c = 0.095 in DMSO). HRMS (ESI-TOF) calcd for $C_{16}H_{17}ClN_2NaO_4$ [M+Na$^+$]: 359.0769, found: 359.0765. FT-IR ν_{max} (neat): 3379, 2968, 1656, 1312, 1233, 768 cm^{-1}.

12.10.4.11 (*S*)-2-(1-Chloro-4-hydroxyisoquinoline-3-carboxamido)-3-phenylpropanoic acid (80a)[61]

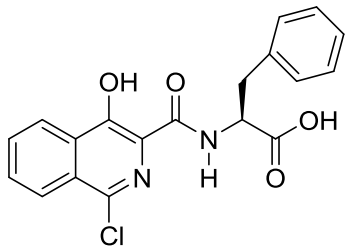

The desired compound (80a) was obtained as a white solid (219 mg, 44%) starting from 1-chloro-4-hydroxyisoquinoline-3-carboxylic acid (300 mg, 1.35 mmol).

^{1}H NMR (400 MHz, DMSO-d_6) δ = 8.99 (d, *J*=8.5 Hz, 1 H, NH), 8.37 (m, 1 H, ArH), 8.32 (m, 1 H, ArH), 8.03 (m, 2 H, ArH), 7.32 (m, 4 H, PhH), 7.25 (m, 1 H, PhH), 4.86 (dt, *J*=8.5, 7.0 Hz, 1 H, CH), 3.35 (d, *J*=7.0 Hz, 2 H, CH_2Ph) ppm, ^{13}C NMR (101 MHz, DMSO-d_6) δ = 172.5, 168.8, 154.8, 139.0, 137.8, 132.3, 132.3, 129.9, 129.6, 129.0, 128.8, 127.1, 126.6, 123.4, 120.7, 53.6, 36.4 ppm. Mp =180-183 °C (lit. 185-188 °C)[61], $[\alpha]^{20}_D$ = -31.1 (c = 0.100 in DMSO). HRMS (ESI-TOF) calcd for $C_{19}H_{15}ClNaN_2O_4$ [M+H$^+$]: 393.0613, found: 393.0610, FT-IR ν_{max} (neat): 3448, 3360, 2931, 1736, 1570, 1259, 773 cm^{-1}.

12.10.4.12 (*R*)-2-(1-Chloro-4-hydroxyisoquinoline-3-carboxamido)-3-phenylpropanoic acid (80b)[61]

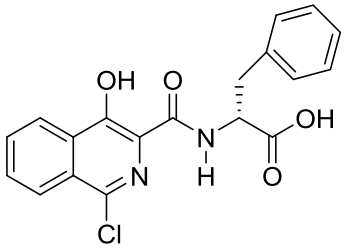

The desired compound (80b) was obtained as a white solid (205 mg, 41%) starting from 1-chloro-4-hydroxyisoquinoline-3-carboxylic acid (300 mg, 1.35 mmol).

^{1}H NMR (400 MHz, DMSO-d_6) δ = 8.99 (d, *J*=8.5 Hz, 1 H, NH), 8.37 (m, 1 H, ArH), 8.32 (m, 1 H, ArH), 8.03 (m, 2 H, ArH), 7.32 (m, 4 H, PhH), 7.25 (m, 1 H, PhH), 4.86 (dt, *J*=8.5, 7.0 Hz, 1 H, CH), 3.35 (d, *J*=7.0 Hz, 2 H, CH_2Ph) ppm, ^{13}C NMR (101 MHz, DMSO-d_6) δ = 172.5, 168.8, 154.8, 139.0, 137.8, 132.3, 132.3, 129.9, 129.6, 129.0, 128.8, 127.1, 126.6, 123.4, 120.7, 53.6, 36.4 ppm. Mp =168-171 °C (lit. 184-186 °C)[61], $[\alpha]^{20}_D$ = +29.7 (c = 0.100 in DMSO). HRMS (ESI-TOF) calcd for $C_{19}H_{15}ClNaN_2O_4$ [M+H$^+$]: 393.0613, found: 393.0612, FT-IR ν_{max} (neat): 3449, 3359, 2931, 1736, 1574, 1260, 770 cm^{-1}.

12.10.4.13 (*S*)-2-(1-chloro-4-hydroxyisoquinoline-3-carboxamido)pentanedioic acid (81a)[80]

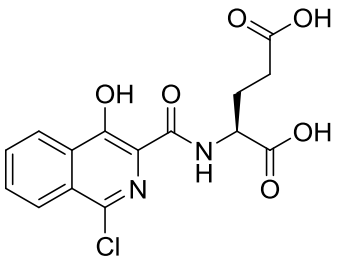

The desired compound (81a) was obtained as a cream white solid (133 mg, 28%) starting from 1-chloro-4-hydroxyisoquinoline-3-carboxylic acid (300 mg, 1.35 mmol).

^{1}H NMR (400 MHz, DMSO-d_6) δ = 13.63 (br. s., 1H, OH), 9.14 (d, *J* = 8.0 Hz, 1H, NH), 8.31 - 8.36 (m, 1H, ArH), 8.25 - 8.31 (m, 1H, ArH), 7.94 - 8.03 (m, 2H, ArH), 4.54 - 4.65 (m, 1H, H5), 2.37 (t, *J* = 7.5 Hz, 2H, H7), 2.07 - 2.31 (m, 2H, H6) ppm. ^{13}C NMR (101 MHz, DMSO-d_6) δ = 174.2, 172.8, 169.3, 154.9, 139.1, 132.0, 132.0, 130.0, 129.0, 126.4, 123.3, 120.2, 51.8, 30.7, 26.1 ppm. Mp = 128-130 °C (lit. 128-130 °C)[80], $[\alpha]^{20}_D$ = -6.4 (c = 0.125 in DMSO). HRMS (ESI-TOF) calcd for $C_{15}H_{13}ClN_2NaO_6$ [M+Na$^+$]: 375.0354, found: 375.0352, FT-IR ν_{max} (neat): 2923, 2853, 1709, 1528, 1319, 1214, 766 cm^{-1}.

12.10.4.14 (*R*)-2-(1-chloro-4-hydroxyisoquinoline-3-carboxamido)pentanedioic acid (81b)[80]

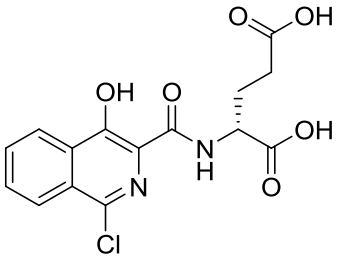

The desired compound (81b) was obtained as a cream white solid (166 mg, 35%) starting from 1-chloro-4-hydroxyisoquinoline-3-carboxylic acid (300 mg, 1.35 mmol).

^{1}H NMR (400 MHz, DMSO-d_6) δ = 13.63 (br. s., 1H, OH), 9.14 (d, *J* = 8.0 Hz, 1H, NH), 8.31 - 8.36 (m, 1H, ArH), 8.25 - 8.31 (m, 1H, ArH), 7.94 - 8.03 (m, 2H, ArH), 4.54 - 4.65 (m, 1H, H5), 2.37 (t, *J* = 7.5 Hz, 2H, H7), 2.07 - 2.31 (m, 2H, H6) ppm. ^{13}C NMR (101 MHz, DMSO-d_6) δ = 174.2, 172.8, 169.3, 154.9, 139.1, 132.0, 132.0, 130.0, 129.0, 126.4, 123.3, 120.2, 51.8, 30.7, 26.1 ppm. Mp = 135-138 °C (lit. 135-138 °C)[80], $[\alpha]^{20}_{D}$ = 6.2 (c = 0.127 in DMSO). HRMS (ESI-TOF) calcd for $C_{15}H_{13}ClN_2NaO_6$ [M+Na$^+$]: 375.0354, found: 375.0342. FT-IR ν_{max} (neat): 2923, 2853, 1709, 1527, 1319, 1214, 766 cm^{-1}.

12.10.4.15 (*S*)-2-(1-chloro-4-hydroxyisoquinoline-3-carboxamido)succinic acid (82a)[80]

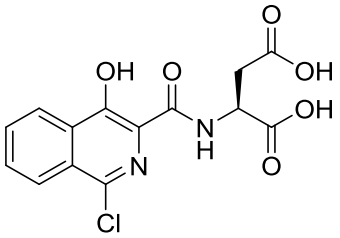

The desired compound (82a) was obtained as a pink solid (186 mg, 41%), starting from 1-chloro-4-hydroxyisoquinoline-3-carboxylic acid (300 mg, 1.35 mmol).

^{1}H NMR (400 MHz, DMSO-d_6) δ =13.56 (br. s., 1H, OH), 9.16 (d, *J* = 8.5 Hz, 1H, NH), 8.22 - 8.43 (m, 2H, ArH), 7.95 - 8.13 (m, 2H, ArH), 4.78 - 5.05 (m, 1H, H5), 2.97 (d, *J* = 6.0 Hz, 2H, H6) ppm. ^{13}C NMR (101 MHz, DMSO-d_6) δ = 172.6, 172.2, 168.7, 154.9, 139.1, 132.3, 132.3, 130.0, 129.1, 126.6, 123.5, 120.8, 48.8, 36.0 ppm. Mp = 240-243 °C (lit. 240-243 °C)[80], $[\alpha]^{20}_{D}$ = -14.2 (c = 0.098 in DMSO). HRMS (ESI-TOF) calcd for $C_{14}H_{11}ClN_2NaO_6$ [M+Na$^+$]: 337.0233, found 337.0247. FT-IR ν_{max} (neat): 3413, 2927, 1707, 1528, 1212, 767 cm^{-1}.

12.10.4.16 (*R*)-2-(1-chloro-4-hydroxyisoquinoline-3-carboxamido)succinic acid (82b)[80]

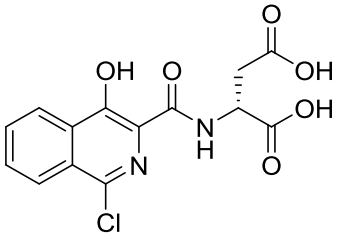

The desired compound (82b) was obtained as a pink solid (177 mg, 39%), starting from 1-chloro-4-hydroxyisoquinoline-3-carboxylic acid (300 mg, 1.35 mmol).

^{1}H NMR (400 MHz, DMSO-d_6) δ = 13.56 (br. s., 1H, OH), 9.16 (d, *J* = 8.5 Hz, 1H, NH), 8.22 - 8.43 (m, 2H, ArH), 7.95 - 8.13 (m, 2H, ArH), 4.78 - 5.05 (m, 1H, H5), 2.97 (d, *J* = 6.0 Hz, 2H, H6), ^{13}C NMR (101 MHz, DMSO-d_6) δ = 172.6, 172.2, 168.7, 154.9, 139.1, 132.3, 132.3, 130.0, 129.1, 126.6, 123.5, 120.8, 48.8, 36.0 ppm. Mp = 239-241 °C (lit. 239-241 °C)[80], $[\alpha]^{20}_{D}$ = 13.8 (c = 0.102 in DMSO). HRMS (ESI-TOF) calcd for $C_{14}H_{11}ClN_2NaO_6$ [M+Na$^+$]: 337.0233, found: 337.0248, FT-IR ν_{max} (neat): 3357, 2926, 1704, 1526, 1194, 765 cm^{-1}.

12.10.5 Synthesis of other bicyclic derivatives

12.10.5.1 (Isoquinoline-3-carbonyl)glycine (83)[78]

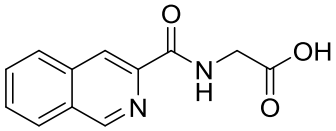

Isoquinoline-3-carboxylic acid (500 mg, 2.89 mmol), glycine methyl ester hydrochloride (363 mg, 2.89 mmol, 1 eq), PyBOP (1.65 g, 3.18 mmol, 1.2 eq) and Et_3N (400 µL, 2.89 mmol, 1 eq) were dissolved in the anhydrous DMF (10 mL) and stirred at room temperature for 24h. Upon completion of the reaction the DMF was evaporated *in vacuo* and the resultant residue was suspended in CH_2Cl_2 (20 mL) and washed with H_2O (2 x 10 mL). The organic phase was dried over $MgSO_4$, filtered and subjected to the column chromatography (eluent system: cHex/EtOAc). The obtained product was dissolved in a mixture of THF/H_2O (1:1, 10 mL) and treated with LiOH · H_2O (600 mg, 14.45 mmol, 5 eq). The reaction was stirred at room temperature for 12h. The THF was evaporated *in vacuo* and the remaining aqueous solution was neutralized with conc. HCl. The precipitate was collected by filtration and dried *in vacuo* to yield the desired product (266 mg, 1.16 mmol, 40%).

^{1}H NMR (400 MHz, DMSO-d_6) δ = 9.42 (s, 1 H, H6), 9.14 (t, *J*=6.0 Hz, 1 H, NH), 8.58 (s1 H, H5), 8.27 (d, *J*=8.0 Hz, 1 H, H3), 8.22 (d, *J*=8.0 Hz, 1 H, H4) 7.90 (ddd, *J*=8.0, 7.0, 1.0 Hz, 1 H, H2) 7.83 (ddd, *J*=8.0, 7.0, 1.0 Hz, 1 H, H1) 4.05 (d, *J*=6.0 Hz, 2 H, H7', H7'')ppm. ^{13}C NMR (101 MHz, DMSO-d_6) δ = 171.7, 164.9, 152.1, 143.8, 135.8, 131.9, 129.8, 129.7, 128.5, 128.3, 120.3, 41.6 ppm. Mp = 208-210 °C (223-224 °C)[78]. HRMS (ESI-TOF) calcd for $C_{12}H_{10}N_2NaO_3$ [M+Na^+]: 253.0584, found: 253.0595, FT-IR ν_{max} (neat): 3378, 1733, 1631, 1531, 1233, 766 cm^{-1}.

12.10.5.2 (1-Hydroxy-2-naphthoyl)glycine (84)

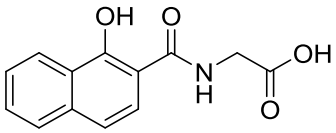

1-Hydroxy-2-naphthoic acid (500 mg, 2.66 mmol) was stirred with CDI (639 mg, 3.94 mmol, 1.5 eq) in the anhydrous DMF (5 mL) for 10 min prior to the addition of mixture of glycine methyl ester hydrochloride (400 mg, 3.18 mmol, 1.2 eq) and Et_3N (440 µL, 3.18 mmol, 1.2 eq). The resultant mixture was stirred at room temperature for 24h. Upon completion of the reaction DMF was evaporated *in vacuo* and the residue was suspended in CH_2Cl_2 (20 mL) and washed with H_2O (2 x 10 mL). The organic phase was dried over $MgSO_4$, filtered and subjected to the column chromatography (eluent system: cHex/EtOAc). The obtained product was dissolved in a mixture of THF/H_2O (1:1, 10 mL) and treated with LiOH · H_2O (560 mg, 13.30 mmol, 5 eq). The reaction was stirred at room temperature for 12h. The THF was evaporated *in vacuo* and the remaining aqueous solution was neutralized with conc. HCl. The precipitate was collected by filtration and dried *in vacuo* to yield the desired product as a solid (325 mg, 1.33 mmol, 50%).

^{1}H NMR (500 MHz, DMSO-d_6) δ = 14.29 (br. s., 1 H, OH), 9.43 (t, *J*=6.0 Hz, 1 H, NH), 8.27 (d, *J*=8.5 Hz, 1 H, ArH), 7.84 - 7.95 (m, 2 H, ArH), 7.65 (ddd, *J*=8.0, 7.0, 1.0 Hz, 1 H, H4), 7.56 (ddd, *J*=8.0, 7.0, 1.0 Hz, 1 H, H3), 7.41 (d, *J*=8.5 Hz, 1 H, ArH), 4.01 (d, *J*=6.0 Hz, 2 H, H7', H7'') ppm. ^{13}C NMR (126 MHz, DMSO-d_6) δ = 171.4, 171.3, 160.1, 136.3, 129.5, 128.0, 126.4, 125.1, 123.5, 122.9, 118.3, 107.3, 41.5 ppm. Mp = 225-227 °C. HRMS (ESI-TOF) calcd for $C_{13}H_{10}N_2O_4$ [M-H$^+$]: 244.0615, found: 244.0615, FT-IR ν_{max} (neat): 3408, 1730, 1622, 1547, 1243, 760 cm^{-1}.

12.10.5.3 (1-Hydroxy-2-naphthoyl)-L-tryptophan (85)

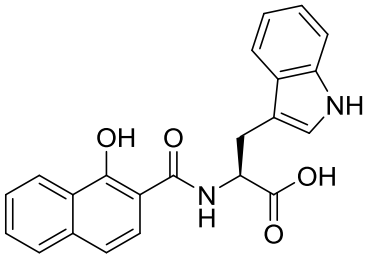

1-Hydroxy-2-naphthoic acid (500 mg, 2.66 mmol) was stirred with CDI (639 mg, 3.94 mmol, 1.5 eq) in anhydrous DMF (5 mL) for 10 min prior to the addition of mixture of tryptophan methyl ester hydrochloride (847 mg, 3.18 mmol, 1.2 eq) and Et_3N (440 µL, 3.18 mmol, 1.2 eq). The resultant mixture was stirred at room temperature for 24h. Upon completion of the reaction DMF was evaporated *in vacuo* and the residue was suspended in CH_2Cl_2 (20 mL) and washed with H_2O (2 x 10 mL). The organic phase was dried over $MgSO_4$, filtered and subjected to the column chromatography (eluent system: cHex/EtOAc). The obtained product was dissolved in a mixture of THF/H_2O (1:1, 10 mL) and treated with LiOH · H_2O (560 mg, 13.30 mmol, 5 eq). The reaction was stirred at room temperature for 12h. The THF was evaporated *in vacuo* and the remaining aqueous solution was neutralized with conc. HCl. The precipitate was collected by filtration and dried *in vacuo* to yield the desired product as a solid (460 mg, 1.22 mmol, 46%).

^{1}H NMR (400 MHz, DMSO-d_6) δ = 14.13 (br. s., 1 H, OH), 10.87 (d, *J*=1.5 Hz, 1 H, NH), 9.17 (d, *J*=8.0 Hz, 1 H, NH), 8.22 (d, *J*=8.5 Hz, 1 H, ArH), 7.97 (d, *J*=9.0 Hz, 1 H, ArH), 7.87 (d, *J*=8.5 Hz, 1 H, ArH), 7.58 - 7.68 (m, 2 H, ArH), 7.54 (ddd, *J*=8.0, 7.0, 1.0 Hz, 1 H, ArH), 7.39 (d, *J*=9.0 Hz, 1 H, ArH), 7.33 (d, *J*=8.0 Hz, 1 H, ArH), 7.25 (d, *J*=2.0 Hz, 1 H, ArH), 7.06 (ddd, *J*=8.0, 7.0, 1.0 Hz, 1 H, ArH), 6.99 (ddd, *J*=8.0, 7.0, 1.0 Hz, 1 H, ArH), 4.75 (ddd, *J*=9.5, 7.5, 5.0 Hz, 1 H, CH), 3.27 - 3.42 (m, 2 H, CH_2) ppm. ^{13}C NMR (101 MHz, DMSO-d_6) δ = 173.5, 171.1, 160.0, 136.5, 136.3, 129.5, 127.9, 127.4, 126.4, 125.0, 124.1, 123.4, 123.2, 121.5, 119.0, 118.5, 118.2, 112.0, 110.6, 107.2, 54.1, 26.8 ppm. Mp = 230-232 °C, $[\alpha]^{20}_D$ = -41.3 (c = 0.100 in DMSO). HRMS (ESI-TOF) calcd for $C_{22}H_{17}N_2O_4$ [M-H$^+$]: 373.1194, found: 373.1197, FT-IR ν_{max} (neat): 3345, 1708, 1620, 1527, 1283, 746 cm^{-1}.

12.10.6 Synthesis of quinoline derivatives

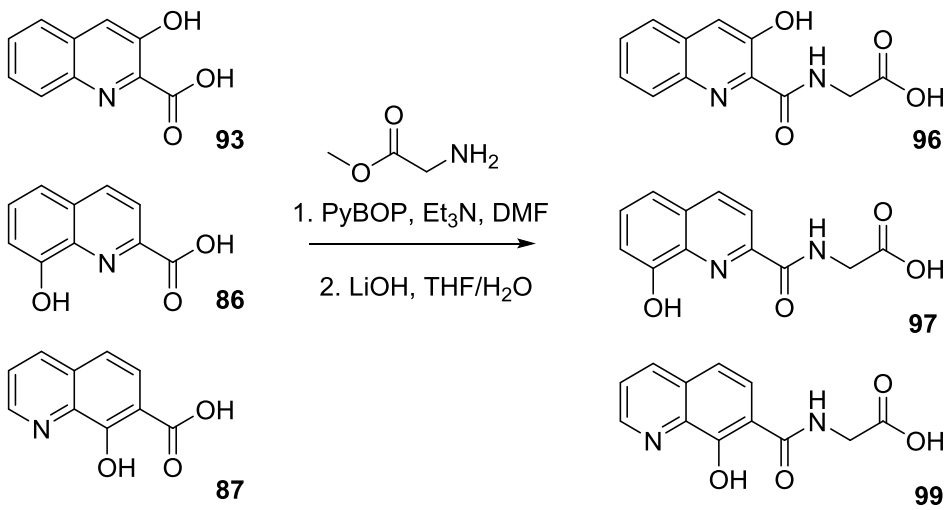

Scheme S6: Synthesis of quinoline based inhibitors.

12.10.7 General procedure for synthesis of glycine conjugates with quinoline derivatives:

The quinoline analogue (300 mg, 1.59 mmol), glycine methyl ester hydrochloride (240 mg, 1.91 mmol, 1.2 eq), PyBOP (990 mg, 1.91 mmol, 1.2 eq) and Et_3N (553 µl, 3.98 mmol, 2.5 mmol) were dissolved in anhydrous DMF (10 mL) and subsequently stirred at room temperature for 24h. Upon the completion of the reaction the DMF was evaporated *in vacuo* and the resultant residue was suspended in DCM (30 mL) and washed with H_2O (2 x 15 mL). The organic phase was dried over $MgSO_4$, filtered and subjected to the column chromatography (Biotage SNAP KP-SIL™ 25 g cartridge, eluent system: cHex/EtOAc). The obtained product was dissolved in a mixture of THF/H_2O (1:1, 10 mL) and subsequently treated with $LiOH \cdot H_2O$ (5 eq). The reaction was stirred at room temperature for 12h. The THF was evaporated *in vacuo* and the resultant aqueous solution was neutralized with conc. HCl. If a precipitate was formed it was filtered-off and dried *in vacuo* to yield the desired product. In case no precipitate was formed, the aqueous solution was extracted with EtOAc (3 x 10 mL). The combined organic layers were dried over $MgSO_4$, filtered and evaporated *in vacuo* to yield the desired product.

12.10.7.1 3-Hydroxyquinoline-2-carboxylic acid (93)[83]

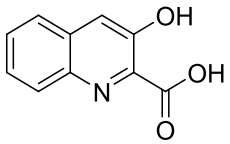

3-hydroxyquinoline-2-carboxylic acid (93) was synthesised according to a literature procedure and obtained as a brown solid[83].

^{1}H NMR (400 MHz, DMSO-d_6) δ = 11.91 (br. s., 1 H, OH), 8.43 - 8.50 (m, 1 H), 8.02 - 8.11 (m, 1 H), 7.77 - 7.84 (m, 3 H) ppm. ^{13}C NMR (101 MHz, DMSO-d_6) δ = 165.5, 163.5, 151.5, 134.0, 130.9, 130.3, 129.9, 127.8, 118.6, 114.4 ppm. Mp = 155-157 °C. HRMS (EI/FI) calcd for $C_{10}H_7NO_3$ [M^+]: 189.0426, found: 189.0426. FT-IR ν_{max} (neat): 3374, 1655, 1510, 1448, 1229, 1141, 763 cm^{-1}.

12.10.7.2 (3-Hydroxyquinoline-2-carbonyl)glycine (96)[73]

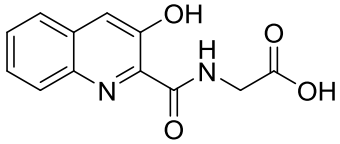

The desired compound (96)[73] was obtained as a yellow solid (150 mg, 0.60 mmol, 38%) starting from 3-hydroxyquinoline-2-carboxylic acid (300 mg, 1.59 mmol) and following the general procedure.

^{1}H NMR (400 MHz, DMSO-d_6) δ = 11.55 (t, *J*=5.0 Hz, 1 H, NH), 8.44 (d, *J*=8.5 Hz, 1 H), 7.92 (d, *J*=7.5 Hz, 1 H), 7.61 - 7.75 (m, 2 H), 7.51 (s, 1 H, OH), 4.17 (d, *J*=5.5 Hz, 2 H, CH_2) ppm. ^{13}C NMR (101 MHz, DMSO-d_6) δ = 170.5, 164.9, 153.9, 136.7, 130.8, 130.4, 128.8, 127.6, 119.6, 111.1, 41.8 ppm. Mp = 218-220°C. HRMS (ESI-TOF) calcd for $C_{12}H_{10}NaN_2O_4$ [M+Na^+]: 269.0533, found: 269.0538. FT-IR ν_{max} (neat): 3346, 1712, 1651, 1332, 835 cm^{-1}.

12.10.7.3 (8-Hydroxyquinoline-2-carbonyl)glycine (97)[84]

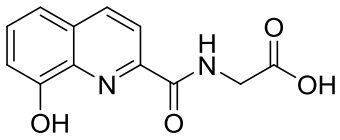

The desired compound (97) was obtained as a yellow solid (160 mg, 0.66 mmol, 42%) starting from 8-hydroxyquinoline-2-carboxylic acid and following the general procedure.

^{1}H NMR (400 MHz, CD_3OD) δ = 8.42 (d, *J*=8.5 Hz, 1 H), 8.18 (d, *J*=8.5 Hz, 1 H), 7.55 (t, *J*=8.0 Hz, 1 H), 7.44 (dd, *J*=8.5, 1.0 Hz, 1 H), 7.18 (dd, *J*=7.5, 1.5 Hz, 1 H), 4.23 (s, 2 H, CH_2) ppm. ^{13}C NMR (101 MHz, CD_3OD) δ = 172.1, 166.2, 154.0, 147.3, 137.9, 137.4, 130.5, 129.7, 118.9, 117.9, 111.7, 40.9 ppm. Mp = 236-238 °C (lit. 292 °C)[84]. HRMS (ESI-TOF) calcd for $C_{12}H_{10}NaN_2O_4$ [M+Na^+]: 269.0533, found: 269.0529. FT-IR ν_{max} (neat): 3344, 1726, 1656, 1504, 1210, 855 cm^{-1}.

12.10.7.4 (8-hydroxyquinoline-7-carbonyl)glycine (99)[85]

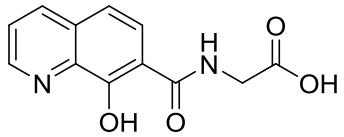

The desired compound (99)[85] was obtained as a yellow solid (160 mg, 0.66 mmol, 42%) starting from 8-hydroxyquinoline-7-carboxylic acid (Sigma-Aldrich) (300 mg, 1.59 mmol) and following the general procedure.

^{1}H NMR (400 MHz, DMSO-d_6) δ = 9.17 (t, *J*=5.5 Hz, 1 H, NH), 8.92 (d, *J*=3.0 Hz, 1 H), 8.37 (d, *J*=8.0 Hz, 1 H), 8.00 (d, *J*=9.0 Hz, 1 H), 7.67 (dd, *J*=8.0, 4.0 Hz, 1 H), 7.45 (d, *J*=9.0 Hz, 1 H), 4.07 (d, *J*=5.0 Hz, 2 H, CH_2) ppm. ^{13}C NMR (101 MHz, DMSO-d_6) δ = 171.5, 168.0, 156.4, 149.5, 139.3, 136.8, 131.1, 126.1, 124.1, 117.6, 113.2, 41.8 ppm. Mp = 224-226°C, HRMS (ESI-TOF) calcd for $C_{12}H_{10}NaN_2O_4$ [M+Na^+]: 269.0533, found: 269.0542. FT-IR ν_{max} (neat): 3350, 2160, 1695, 1632, 1543, 1300, 832 cm^{-1}.

12.10.8 Synthesis of GBB analogues

Synthesis of analogues **1-3**, **203-205**, **207** and **208** is described in Chapter 6. Synthesis of analogues **227-229**, **231-234** and **238** is described in Chapter 4. Analogue **201** was synthesised as described in chapter 2.

12.10.9 General procedure for synthesis of unsaturated GBB analogues

To a solution of corresponding bromide derivative in anhydrous acetonitrile (1 equiv.) a 4.2 M solution of trimethylamine in ethanol was added (1.5 equiv), then the mixture was stirred for 3 h, at which point a white precipitate formed. Solvents and trimethylamine were evaporated *in vacuo*. The residue was taken up in small volume of cold acetonitrile and the solid was filtered off and dried under vacuum to yield the desired product as bromide salt.

12.10.9.1 Nγ-trimethyl-(E)-4-aminobut-2-enoic acid bromide (5)

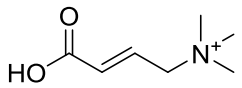

Compound (**5**) was synthesised according to General Procedure starting from (*E*)-4-bromobut-2-enoic acid (100 mg, 0.61 mmol). (**5**) was obtained as a white solid (63 mg, 0.28 mmol, 46%).

^{1}H NMR (700 MHz, D_2O) δ = 6.73 (dt, *J*=15.5, 7.5 Hz, 1 H), 6.28 (d, *J*=15.5 Hz, 1 H), 4.03 (d, *J*=7.5 Hz, 2 H), 3.08 (s, 9 H) ppm, ^{13}C NMR (176 MHz, D_2O) δ = 170.6, 135.5, 130.2, 66.1, 52.8 ppm. Mp = 182-184°C. HRMS (ESI-TOF) calcd for $C_7H_{14}NO_2^+$ [M^+]: 144.1091, found: 144.1015. FT-IR νmax (neat): 3399, 3019, 1720, 1485, 1215, 1003 cm^{-1}.

12.10.9.2 Methyl Nγ-trimethyl-(E)-4-aminobut-2-enoate bromide (196)

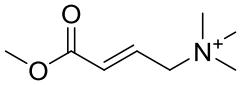

Compound (**196**) was synthesised according to General Procedure starting from methyl (E)-4-bromobut-2-enoate (100 mg, 0.56 mmol). (**196**) was obtained as a white solid (83 mg, 0.35 mmol, 63%).

^{1}H NMR (700 MHz, D_2O) δ = 6.96 (dt, *J*=15.5, 7.5 Hz, 1 H), 6.34 (d, *J*=15.5 Hz, 1 H), 4.08 (d, *J*=7.5 Hz, 2 H), 3.74 (s, 3 H), 3.10 (s, 9 H) ppm, ^{13}C NMR (176 MHz, D_2O) δ = 167.1, 132.6, 131.2, 65.6, 52.7, 52.0 ppm. Mp = 147-149°C. HRMS (ESI-TOF) calcd for $C_8H_{16}NO_2^+$ [M^+]: 158.1176, found: 158.1182. FT-IR νmax (neat): 1724, 1662, 1226, 1183 cm^{-1}.

12.10.9.3 2-(N^{β}-trimethyl-aminomethyl)acrylic acid (197)

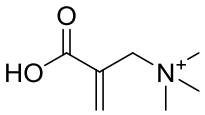

Compound (**197**) was synthesised according to General Procedure starting from 2-(bromomethyl)acrylic acid (100 mg, 0.61 mmol). (**196**) was obtained as a white solid (63 mg, 0.28 mmol, 46%).

^{1}H NMR (700 MHz, D_2O) δ 6.57 (s, 1 H), 6.08 (s, 1 H), 4.15 (s, 2 H), 3.03 (s, 9 H) ppm, ^{13}C NMR (176 MHz, D_2O) δ = 171.4, 136.9, 133.0, 65.9, 52.7 ppm. Mp = 143-145°C. HRMS (ESI-TOF) calcd for $C_8H_{16}NO_2^+$ [M^+]: 144.1019, found: 144.1016. FT-IR νmax (neat): 3003, 2699, 2474, 1640, 1475, 1224, 982 cm^{-1}.

12.10.10 General procedure for synthesis of Mildronate analogues

tert-Butyl 3-bromopropanoate (1 mL, 6.0 mmol) was added dropwise to a solution of amine (12 mmol) and potassium carbonate (1 g, 7.0 mmol) in anhydrous acetonitrile (5 mL) at 0°C and the mixture was stirred for 12 h. Solvents and trimethylamine were evaporated *in vacuo* and the remaining residue was purified on silica (cyclohexane/ethyl acetate) to yield *tert*-butyl ester of desired product as a white solid. The solid was taken into 1 M HCl solution in water (5 mL), stirred for 12 h and then evaporated to dryness. The desired product was obtained as a hydrochloride salt.

12.10.10.1 3-(tert-butylamino)propanoic acid (220)

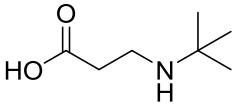

(**220**) was synthesised following General Procedure starting from *tert*-butyl 3-bromopropanoate (1 mL, 6.0 mmol) and *tert*-butylamine (1.26 mL, 12 mmol). (**200**) was obtained as a white solid (hydrochloride salt, 870 mg, 4.8 mmol, 80%).

^{1}H NMR (400 MHz, D_2O) δ = 3.19 (t, *J*=6.5 Hz, 2 H), 2.68 (t, *J*=6.5 Hz, 2 H), 1.27 (s, 9 H) ppm, ^{13}C NMR (101 MHz, D_2O) δ = 174.1, 57.4, 36.9, 30.5, 24.7 ppm. Mp = 225-227°C. HRMS (ESI-TOF) calcd for $C_7H_{16}NO_2^+$ [$M+H^+$]: 146.1176, found: 146.1178. FT-IR νmax (neat): 2937, 2813, 2778, 1733, 1377, 1196, 1004 cm^{-1}.

12.10.10.2 3-(tert-butyl(methyl)amino)propanoic acid (253)

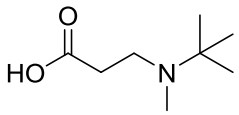

(**246**) was synthesised following General Procedure starting from *tert*-butyl 3-bromopropanoate (1 mL, 6.0 mmol) and *N*-methyl-*N*-*tert*-butylamine (1.40mL, 12 mmol). (**246**) was obtained as a white solid (820 mg, 4.2 mmol, 70%).

^{1}H NMR (400 MHz, D_2O) δ = 3.67 (dt, *J*=14.0, 8.0 Hz, 1 H), 2.97 (dt, *J*=14.0, 6.0 Hz, 1 H), 2.71 - 2.87 (m, 2 H), 2.64 - 2.71 (s, 3 H), 1.31 (s, 9 H) ppm, ^{13}C NMR (101 MHz, D_2O) δ = 173.9, 64.5, 46.7, 34.3, 29.4, 23.6 ppm. Mp = 132-134°C. HRMS (ESI-TOF) calcd for $C_8H_{18}NO_2^+$ [M+H$^+$]: 160.1332, found: 160.1338. FT-IR νmax (neat): 2856, 2650, 1709, 1404, 1225, 1188, 938 cm^{-1}.

12.10.11 Synthesis of N-methyl Mildronate (254)

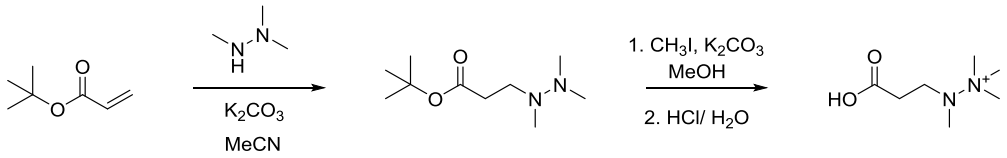

12.10.11.1 3-(1,2,2-trimethylhydrazinyl)propanoic acid

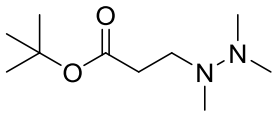

tert-Butyl acrylate (0.95 mL, 6.5 mmol) was added dropwise to a solution of N-methyl-N'-dimethylhydrazine hydrochloride (1 g, 6.8 mmol) and potassium carbonate (2.24 g, 16.2 mmol) in anhydrous acetonitrile (10 mL). The mixture was stirred for 12 h and then the volatiles were evaporated *in vacuo* and the remaining residue was taken in dichloromethane. The mixture was filtered off and the filtrate concentrated *in vacuo* and purified on silica (ethyl acetate/cyclohexane). The desired product was obtained as a yellow oil (100 mg, 0.50 mmol, 7%).

^{1}H NMR (400 MHz, $CDCl_3$) δ = 2.72 (t, *J*=6.5 Hz, 2 H), 2.43 (t, *J*=6.5 Hz, 2 H), 2.30 (s, 6 H), 2.28 (s, 3 H), 1.46 (s, 9 H) ppm, ^{13}C NMR (101 MHz, $CDCl_3$) δ = 172.4, 79.8, 49.8, 38.9, 35.0, 33.8, 28.1 ppm. HRMS (ESI-TOF) calcd for $C_{10}H_{22}N_2NaO_2^+$ [M+Na$^+$]: 225.1573, found: 225.1582.

12.10.11.2 2-(2-carboxyethyl)-1,1,1,2-tetramethylhydrazin-1-ium (254)

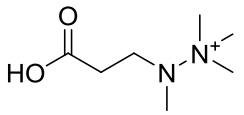

Methyl iodide (17 µL, 0.27 mmol) was added to a solution of 3-(1,2,2-trimethylhydrazinyl)propanoic acid (50 mg, 0.25 mmol) in anhydrous acetonitrile (2 mL) and stirred for 12 h at room temperature. Volatiles were evaporated *in vacuo* and the residue was taken up in 1 M aqueous HCl (1 mL) and stirred for 12 h. The mixture was evaporated *in vacuo* to yield desired compound as chloride salt (50 mg, 0.26 mmol, quant.). For further test crude material was used.
^{1}H NMR (400 MHz, D_2O) δ = 3.22 (s, 9 H), 3.15 (t, *J*=7.5 Hz, 2 H), 2.66 (s, 3 H), 2.56 (t, *J*=7.5 Hz, 2 H) ppm. HRMS (ESI-TOF) calcd for $C_7H_{17}N_2O_2^+$ [M^+]: 161.1285, found: 161.1280.

12.10.12 Synthesis of other GBB analogues

12.10.12.1 Hydroxyamino N^δ-trimethyl-5-aminopentanoate bromide (209)

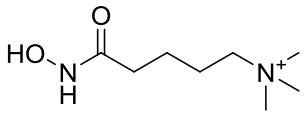

Hydroxylamine hydrochloride (0.58 g, 8.3 mmol) was dissolved in methanol (5 mL) and then added to a stirred solution of KOH (0.46 g, 8.3 mmol) in methanol (2 mL) at 0 °C and stirred for 15 min at 0°C. The precipitate was filtered off and the filtrate kept for further use. Ethyl chloroformate (0.63 mL, 6.6 mmol) and *N*-methylmorpholine (0.79 mL, 7.2 mmol) were added to a solution of 5-bromopentanoic acid (1 g, 5.5 mmol) in diethyl ether (15 mL) at 0 °C. The mixture was stirred for 10 min, then the solid was filtered off and the filtrate was added to a solution of hydroxylamine and stirred for 30 min at room temperature. Volatiles were evaporated *in vacuo* and the remaining residue was purified on silica (dichloromethane/ methanol). Purified bromo derivative was dissolved in anhydrous acetonitrile and treated with 4.2 M solution of trimethylamine (1.5 equiv.) in ethanol. The mixture was stirred for 3 h, upon which a precipitate formed. Solvents and trimethylamine were evaporated *in vacuo*. The residue was taken up in small volume of cold acetonitrile and solid was filtered off and dried under vacuum to yield the desired product as bromide salt (430 mg, 1.7 mmol, 30%).
^{1}H NMR (400 MHz, D_2O) δ = 3.20 - 3.28 (m, 2 H), 3.02 (s, 9 H), 2.16 (t, *J*=7.5 Hz, 2 H), 1.65 - 1.77 (m, 2 H), 1.56 (dt, *J*=14.5, 7.5 Hz, 2 H) ppm, ^{13}C NMR (101 MHz, D_2O) δ = 172.3, 66.0, 52.9, 44.8, 31.6, 21.7 ppm. Mp = 120-123°C. HRMS (ESI-TOF) calcd for $C_8H_{19}NO_2^+$ [M^+]: 175.1441, found: 175.1442. FT-IR νmax (neat): 3210, 3146, 2950, 2862, 1681, 1478, 1176 cm^{-1}.

12.10.12.2 N^{γ}-dimethyl, ethyl-4-aminopropionic acid trifluoroacetate salt (252)

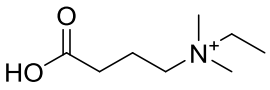

Ethyl iodide (0.12 mL, 1.4 mmol) was added dropwise to a solution of N^{γ}-dimethyl-4-aminopropionic acid hydrochloride (200 mg, 1.2 mmol) and potassium carbonate (0.4 g, 3 mmol) in methanol (5 mL) and mixture was stirred for 12 h at room temperature. Methanol was evaporated and residue re-dissolved in 1 M HCl in water (1 mL) and stirred for 1 h. The aqueous phase was washed with diethyl ether and evaporated *in vacuo* and the resultant residue was purified by HPLC (preparative C-18 reverse phase column; gradient: 50% B in 15 min, where A – water, 0.05% formic acid, B – acetonitrile, 0.1% formic acid; fractions containing product identified using Evaporative Light Scattering Detection (ELSD). The desired fractions were combined and freeze-dried to yield the product as a highly hygroscopic solid. Due to the low level of compound recovery after HPLC purification, IR spectra are not reported. Melting points are not given due to highly hygroscopic nature of obtained material.

^{1}H NMR (700 MHz, D_2O) δ = 3.32 (q, *J*=7.5 Hz, 2 H), 3.20 - 3.26 (m, 2 H), 2.98 (s, 6 H), 2.42 (t, *J*=7.0 Hz, 2 H), 1.98 (dt, *J*=16.5, 7.5 Hz, 2 H), 1.27 (t, *J*=7.0 Hz, 3 H) ppm, ^{13}C NMR (176 MHz, D_2O) δ = 176.6, 62.2, 59.3, 49.6, 30.3, 17.3, 6.8 ppm. HRMS (ESI-TOF) calcd for $C_8H_{18}NO_2^+$ [M^+]: 160.1332, found: 160.1339.

12.10.13 Synthesis of analogues for cell based studies

12.10.13.1 DMOG (Dimethyl *N*-oxalylglycine) (255)

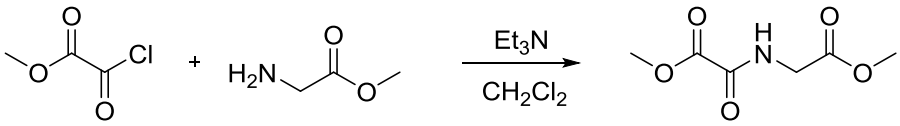

Glycine methyl ester hydrochloride (0.5 g, 4.0 mmol) and triethylamine (1.4 mL, 10 mmol, 2.5 eq) were stirred in anhydrous CH_2Cl_2 (10 mL) at 0°C (ice bath) under nitrogen atmosphere. Oxalyl chloride methyl ester (0.44 mL, 4.8 mmol, 1.2 eq) was added dropwise and the mixture was stirred for 2 h at room temperature. The reaction mixture was extracted with aqueous solutions of 1 M HCl (3×5 mL) and 1M NaOH (3×5 mL), dried over $MgSO_4$, filtered, concentrated *in vacuo* and subjected to column chromatography on silica (elution system: cyclohexane/ethyl acetate) to give desired product as a yellow oil (0.5 g, 2.9 mmol, 72%).

^{1}H NMR (400 MHz, $CDCl_3$) δ = 7.64 (br. s., 1 H, NH), 4.14 (d, *J*=5.5 Hz, 2 H, CH_2), 3.92 (s, 3 H, OCH_3), 3.79 (s, 3 H, OCH_3) ppm. ^{13}C NMR (101 MHz, $CDCl_3$) δ = 169.08, 160.39, 156.41, 53.73, 52.63, 41.36 ppm. TLC chex/EtOAc 1:1 R_f = 0.2. HRMS (ESI-TOF) calcd for $C_6H_9NNaO_5$ [M+Na$^+$]: 198.0373, found: 198.0372. FT-IR ν_{max} (neat): 3379, 2957, 1746, 1689, 1537, 1206 cm^{-1}.

12.10.13.2 DM-NOFD (Dimethyl *N*-oxalyl-(*R*)-phenylalanine) (256)

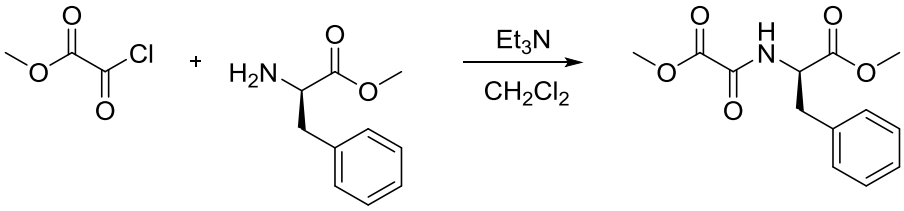

(*R*)-Phenylalanine methyl ester hydrochloride (1.0 g, 4.6 mmol) and triethylamine (1.6 mL, 11.5 mmol, 2.5 eq) were stirred in anhydrous CH_2Cl_2 (10 mL) at 0°C (ice bath) under nitrogen atmosphere. Oxalyl chloride methyl ester (0.50 mL, 5.5 mmol, 1.2 eq) was added dropwise and mixture was stirred for 2 h at room temperature. The reaction mixture was extracted with aqueous solutions of 1 M HCl (3×5 mL) and 1M NaOH (3×5 mL), dried over $MgSO_4$, filtered, concentrated *in vacuo* and subjected to column chromatography on silica (elution system: cyclohexane/ethyl acetate) to give desired product as a yellow oil (0.9 g, 3.5 mmol, 75%).

^{1}H NMR (400 MHz, $CDCl_3$) δ = 7.42 (d, *J*=7.5 Hz, 1 H, NH), 7.15 - 7.28 (m, 3 H, ArH), 7.00 - 7.09 (m, 2 H, ArH), 4.82 (dt, *J*=8.5, 6.0 Hz, 1 H, CH), 3.82 (s, 3 H, OCH_3), 3.67 (s, 3 H, OCH_3), 3.11 (s, 2 H, CH_2) ppm. ^{13}C NMR (101 MHz, $CDCl_3$) δ = 170.7, 160.4, 155.8, 135.1, 129.2, 128.8, 127.4, 53.7, 53.6, 52.6, 37.7 ppm. TLC cyclohexane/EtOAc 1:1 R_f = 0.5. $[\alpha]_D^{20} = +12.3$ (c = 0.28 in MeOH). HRMS (ESI-TOF) calcd for $C_{13}H_{16}NO_5$ [M+H$^+$]: 266.1023, found: 266.1033. FT-IR ν_{max} (neat): 3410, 3030, 2955, 1737, 1701, 1290, 1204, 1031 cm^{-1}.

12.10.13.3 Dimethyl (*R*)-2-hydroxyglutarate (257)

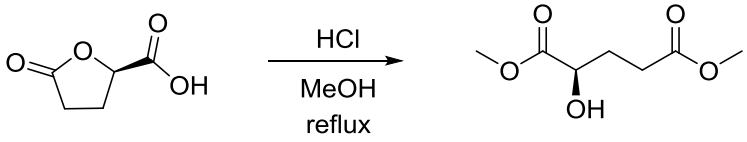

(*R*)-5-oxotetrahydrofuran-2-carboxylic acid (0.5 g, 3.8 mmol) was dissolved in MeOH (5 mL) and a drop of conc. HCl was added. The mixture was refluxed for 12 h, cooled down and solid $NaHCO_3$ was added (until basic). The resultant mixture was stirred for 10 min, filtered and the filtrate concentrated *in vacuo* prior to purification on silica (elution system: cyclohexane/ethyl acetate) to give desired product as a yellow oil (0.6 g, 3.6 mmol, 95%).

^{1}H NMR (400 MHz, $CDCl_3$) δ = 4.18 (ddd, *J*=8.0, 5.5, 4.5 Hz, 1 H, CH), 3.73 (s, 3 H, OCH_3), 3.62 (s, 3 H, OCH_3), 2.97 (d, *J*=5.5 Hz, 1 H, OH), 2.33 - 2.51 (m, 2 H), 2.05 - 2.17 (m, 1 H), 1.81 - 1.94 (m, 1 H) ppm. ^{13}C NMR (101 MHz, $CDCl_3$) δ = 175.0, 173.6, 69.5, 52.6, 51.7, 29.4, 29.3 ppm. TLC chex/EtOAc 1:1 R_f = 0.4. $[\alpha]_D^{20} = +6.2$ (c = 0.30 in MeOH). HRMS (ESI-TOF) calcd for $C_7H_{12}NaO_5$ [M+H$^+$]: 195.0577, found: 195.0578. FT-IR ν_{max} (neat): 3469, 2956, 1731, 1438, 1169, 1104 cm^{-1}.

12.10.13.4 Dimethyl (*S*)-2-hydroxyglutarate (258)

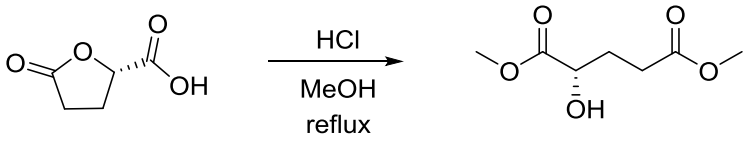

(*S*)-5-oxotetrahydrofuran-2-carboxylic acid (0.5 g, 3.8 mmol) was dissolved in MeOH (5 mL) and a drop of conc. HCl was added. Mixture was refluxed for 12 h, cooled down and solid $NaHCO_3$ was added (until basic). The resultant mixture was stirred for 10 min, filtered and filtrate concentrated in vacuo prior to purification on silica (elution system: cyclohexane/ethyl acetate) to give desired product as a yellow oil (0.6 g, 3.6 mmol, 95%).

Spectroscopic data matched those reported[86]. ^{1}H NMR (400 MHz, $CDCl_3$) δ = 4.22 (ddd, *J*=8.0, 5.5, 4.5 Hz, 1 H, CH), 3.76 (s, 3 H, OCH_3), 3.65 (s, 3 H, OCH_3), 3.16 (d, *J*=5.5 Hz, 1 H, OH), 2.37 - 2.55 (m, 2 H), 2.08 - 2.20 (m, 1 H), 1.91 (dtd, *J*=14.2, 8.1, 8.1, 6.1 Hz, 1 H) ppm. ^{13}C NMR (101 MHz, $CDCl_3$) δ = 175.0, 173.6, 69.4, 52.56, 51.7, 29.4, 29.2 ppm. TLC chex/EtOAc 1:1 R_f = 0.4. $[\alpha]_D^{20} = -7.2$ (c = 0.27 in MeOH). HRMS (ESI-TOF) calcd for $C_7H_{12}NaO_5$ [M+H$^+$]: 195.0577, found: 195.0576. FT-IR ν_{max} (neat): 3469, 2956, 1731, 1438, 1169, 1104 cm^{-1}.

References

1. McMurray, J.J.V. & Pfeffer, M.A. Heart failure. *Lancet* **365**, 1877-1889 (2005).
2. Jaswal, J.S., Keung, W., Wang, W., Ussher, J.R. & Lopaschuk, G.D. Targeting fatty acid and carbohydrate oxidation - A novel therapeutic intervention in the ischemic and failing heart. *Biochimica Et Biophysica Acta-Molecular Cell Research* **1813**, 1333-1350 (2011).
3. Lopaschuk, G.D. Optimizing cardiac fatty acid and glucose metabolism as an approach to treating heart failure. *Seminars in cardiothoracic and vascular anesthesia* **10**, 228-30 (2006).
4. Rigault, C., Le Borgne, F., Tazir, B., Benani, A. & Demarquoy, J. A high-fat diet increases L-carnitine synthesis through a differential maturation of the Bbox1 mRNAs. *Biochimica Et Biophysica Acta-Molecular and Cell Biology of Lipids* **1831**, 370-377 (2013).
5. Galland, S., Georges, B., Le Borgne, F., Conductier, G., Dias, J.V. & Demarquoy, J. Thyroid hormone controls carnitine status through modifications of gamma-butyrobetaine hydroxylase activity and gene expression. *Cellular and Molecular Life Sciences* **59**, 540-545 (2002).
6. Koeth, R.A., Wang, Z.E., Levison, B.S., Buffa, J.A., Org, E., Sheehy, B.T., Britt, E.B., Fu, X.M., Wu, Y.P., Li, L. *et al.* Intestinal microbiota metabolism of L-carnitine, a nutrient in red meat, promotes atherosclerosis. *Nature Medicine* **19**, 576-585 (2013).
7. Petter, R.C., Banerjee, S. & Englard, S. Inhibition of gamma-butyrobetaine hydroxylase by cyclopropyl-substituted gamma-butyrobetaines. *Journal of Organic Chemistry* **55**, 3088-3097 (1990).
8. Ziering, D.L. & Pascal, R.A. Mechanism - based inhibition of bacterial gamma - Butyrobetaine Hydroxylase. *Journal of the American Chemical Society* **112**, 834-838 (1990).
9. Blanchard, J.S. & Englard, S. gamma-Butyrobetaine hydroxylase - primary and secondary tritium kinetic isotopic effects. *Biochemistry* **22**, 5922-5929 (1983).
10. Dambrova, M., Liepinsh, E. & Kalvinsh, I. Mildronate: Cardioprotective action through carnitine-lowering effect. *Trends in Cardiovascular Medicine* **12**, 275-279 (2002).
11. Liepinsh, E., Kalvinsh, I. & Dambrova, M. The Regulation of Energy Metabolism Pathways Through L-Carnitine Homeostasis. in *Role of the Adipocyte in Development of Type 2 Diabetes* (ed. Croniger, C.) (2011).
12. Rydzik, A.M., Leung, I.K.H., Kochan, G.T., Thalhammer, A., Oppermann, U., Claridge, T.D.W. & Schofield, C.J. Development and Application of a Fluoride-Detection-Based Fluorescence Assay for gamma-Butyrobetaine Hydroxylase. *Chembiochem* **13**, 1559-1563 (2012).
13. Tars, K., Rumnieks, J., Zeltins, A., Kazaks, A., Kotelovica, S., Leonciks, A., Sharipo, J., Viksna, A., Kuka, J., Liepinsh, E. *et al.* Crystal structure of human gamma-butyrobetaine hydroxylase. *Biochemical and Biophysical Research Communications* **398**, 634-639 (2010).
14. Leung, I.K.H., Krojer, T.J., Kochan, G.T., Henry, L., von Delft, F., Claridge, T.D.W., Oppermann, U., McDonough, M.A. & Schofield, C.J. Structural and Mechanistic Studies on gamma-Butyrobetaine Hydroxylase. *Chemistry & Biology* **17**, 1316-1324 (2010).
15. Henry, L., Leung, I.K.H., Claridge, T.D.W. & Schofield, C.J. gamma-Butyrobetaine hydroxylase catalyses a Stevens type rearrangement. *Bioorganic & Medicinal Chemistry Letters* **22**, 4975-4978 (2012).
16. Yoshisue, K., Yamamoto, Y., Yoshida, K., Saeki, M., Minami, Y., Esumi, Y. & Kawaguchi, Y. Pharmacokinetics and biological fate of 3-(2,2,2-trimethylhydrazinium) propionate dihydrate (MET-88), a novel cardioprotective agent, in rats. *Drug Metabolism and Disposition* **28**, 687-694 (2000).
17. Jaudzems, K., Kuka, J., Gutsaits, A., Zinovjevs, K., Kalvinsh, I., Liepinsh, E., Liepinsh, E. & Dambrova, M. Inhibition of carnitine acetyltransferase by mildronate, a regulator of energy metabolism. *Journal of Enzyme Inhibition and Medicinal Chemistry* **24**, 1269-1275 (2009).

18. Sjakste, N., Gutcaits, A. & Kalvinsh, I. Mildronate: An antiischernic drug for neurological indications. *Cns Drug Reviews* **11**, 151-168 (2005).
19. Galland, S., Le Borgne, F., Guyonnet, D., Clouet, P. & Demarquoy, J. Purification and characterization of the rat liver gamma-butyrobetaine hydroxylase. *Molecular and Cellular Biochemistry* **178**, 163-168 (1998).
20. Lindsted.G, Lindsted.S & Tofft, M. Gamma-butyrobetaine hydroxylase from Pseudomonas-sp-AK-1. *Biochemistry* **9**, 4336-& (1970).
21. Ng, S.F., Hanauskeabel, H.M. & Englard, S. Cosubstrate binding site of Pseudomonas Sp AK1 gamma-butyrobetaine hydroxylase - interactions with structural analogs of alpha-ketoglutarate. *Journal of Biological Chemistry* **266**, 1526-1533 (1991).
22. Wehbie, R.S., Punekar, N.S. & Lardy, H.A. Rat liver gamma-butyrobetaine hydroxylase catalyzed reaction: influence of potassium, substrates, and substrate analogues on hydroxylation and decarboxylation. *Biochemistry* **27**, 2222-8 (1988).
23. Lindstedt, G. Effect of metal ions on the hydroxylation of gamma-butyrobetaine to carnitine in rat liver homogenages. *Biochimica et Biophysica Acta* **141**, 492-8 (1967).
24. Chowdhury, R., Candela-Lena, J.I., Chan, M.C., Greenald, D.J., Yeoh, K.K., Tian, Y.M., McDonough, M.A., Tumber, A., Rose, N.R., Conejo-Garcia, A. *et al.* Selective Small Molecule Probes for the Hypoxia Inducible Factor (HIF) Prolyl Hydroxylases. *ACS Chemical Biology* (2013).
25. Poppe, L., Tegley, C.M., Li, V., Lewis, J., Zondlo, J., Yang, E., Kurzeja, R.J. & Syed, R. Different modes of inhibitor binding to prolyl hydroxylase by combined use of X-ray crystallography and NMR spectroscopy of paramagnetic complexes. *Jornal of the American Chemical Society* **131**, 16654-5 (2009).
26. Chowdhury, R., Candela-Lena, J.I., Chan, M.C., Greenald, D.J., Yeoh, K.K., Tian, Y.-M., McDonough, M.A., Tumber, A., Rose, N.R., Conejo-Garcia, A. *et al.* Selective Small Molecule Probes for the Hypoxia Inducible Factor (HIF) Prolyl Hydroxylases. *ACS Chemical Biology* **8**, 1488-1496 (2013).
27. King, O.N., Li, X.S., Sakurai, M., Kawamura, A., Rose, N.R., Ng, S.S., Quinn, A.M., Rai, G., Mott, B.T., Beswick, P. *et al.* Quantitative high-throughput screening identifies 8-hydroxyquinolines as cell-active histone demethylase inhibitors. *PLoS One* **5**, e15535 (2010).
28. Hopkinson, R.J., Tumber, A., Yapp, C., Chowdhury, R., Aik, W., Che, K.H., Li, X.S., Kristensen, J.B.L., King, O.N.F., Chan, M.C. *et al.* 5-Carboxy-8-hydroxyquinoline is a broad spectrum 2-oxoglutarate oxygenase inhibitor which causes iron translocation. *Chemical Science* **4**, 3110-3117 (2013).
29. Rose, N.R., Woon, E.C.Y., Tumber, A., Walport, L.J., Chowdhury, R., Li, X.S., King, O.N.F., Lejeune, C., Ng, S.S., Krojer, T. *et al.* Plant Growth Regulator Daminozide Is a Selective Inhibitor of Human KDM2/7 Histone Demethylases. *Journal of Medicinal Chemistry* **55**, 6639-6643 (2012).
30. McDonough, M.A., Li, V., Flashman, E., Chowdhury, R., Mohr, C., Liénard, B.M.R., Zondlo, J., Oldham, N.J., Clifton, I.J., Lewis, J. *et al.* Cellular oxygen sensing: Crystal structure of hypoxia-inducible factor prolyl hydroxylase (PHD2). *Proceedings of the National Academy of Sciences of the United States of America* **103**, 9814-9819 (2006).
31. Clifton, I.J., McDonough, M.A., Ehrismann, D., Kershaw, N.J., Granatino, N. & Schofield, C.J. Structural studies on 2-oxoglutarate oxygenases and related double-stranded beta-helix fold proteins. *Journal of Inorganic Biochemistry* **100**, 644-69 (2006).
32. Aik, W., McDonough, M.A., Thalhammer, A., Chowdhury, R. & Schofield, C.J. Role of the jelly-roll fold in substrate binding by 2-oxoglutarate oxygenases. *Current Opinion in Structural Biology* **22**, 691-700 (2012).
33. Dougherty, D.A. Cation-pi interactions involving aromatic amino acids. *Journal of Nutrition* **137**, 1504S-1508S (2007).
34. Cheng, J.G., Luo, X.M., Yan, X.H., Li, Z., Tang, Y., Jiang, H.L. & Zhu, W.L. Research progress in cation-pi interactions. *Science in China Series B-Chemistry* **51**, 709-717 (2008).

35. Gallivan, J.P. & Dougherty, D.A. Cation-pi interactions in structural biology. *Proceedings of the National Academy of Sciences of the United States of America* **96**, 9459-9464 (1999).
36. Lindstedt, G., Lindstedt, S. & Nordin, I. gamma - Butyrobetaine hydroxylase in human kidney. *Scandinavian Journal of Clinical & Laboratory Investigation* **42**, 477-485 (1982).
37. Hausinger, R.P. Fe(II)/α-ketoglutarate-dependent hydroxylases and related enzymes. *Critical Reviews in Biochemistry and Molecular Biology* **39**, 21-68 (2004).
38. Tegley, C.M., Viswanadhan, V.N., Biswas, K., Frohn, M.J., Peterkin, T.A., Chang, C., Burli, R.W., Dao, J.H., Veith, H., Rogers, N. *et al.* Discovery of novel hydroxy-thiazoles as HIF-alpha prolyl hydroxylase inhibitors: SAR, synthesis, and modeling evaluation. *Bioorganic and Medicinal Chemistry Letters* **18**, 3925-8 (2008).
39. Fleming, F.F., Yao, L., Ravikumar, P.C., Funk, L. & Shook, B.C. Nitrile-Containing Pharmaceuticals: Efficacious Roles of the Nitrile Pharmacophore. *Journal of Medicinal Chemistry* **53**, 7902-7917 (2010).
40. Metzen, E. & Ratcliffe, P.J. HIF hydroxylation and cellular oxygen sensing. *Biological Chemistry* **385**, 223-30 (2004).
41. Schofield, C.J. & Ratcliffe, P.J. Signalling hypoxia by HIF hydroxylases. *Biochemical and Biophysical Research Communications* **338**, 617-26 (2005).
42. Chowdhury, R., McDonough, M.A., Mecinovic, J., Loenarz, C., Flashman, E., Hewitson, K.S., Domene, C. & Schofield, C.J. Structural basis for binding of hypoxia-inducible factor to the oxygen-sensing prolyl hydroxylases. *Structure* **17**, 981-9 (2009).
43. Hewitson, K.S., McNeill, L.A. & Schofield, C.J. Modulating the hypoxia-inducible factor signaling pathway: applications from cardiovascular disease to cancer. *Current Pharmacetical Design* **10**, 821-33 (2004).
44. Shohet, R.V. & Garcia, J.A. Keeping the engine primed: HIF factors as key regulators of cardiac metabolism and angiogenesis during ischemia. *Journal of Molecular Medicine-Jmm* **85**, 1309-1315 (2007).
45. Mole, D.R., Schlemminger, I., McNeill, L.A., Hewitson, K.S., Pugh, C.W., Ratcliffe, P.J. & Schofield, C.J. 2-oxoglutarate analogue inhibitors of HIF prolyl hydroxylase. *Bioorganic and Medicinal Chemistry Letters* **13**, 2677-80 (2003).
46. Nagel, S., Talbot, N.P., Mecinovic, J., Smith, T.G., Buchan, A.M. & Schofield, C.J. Therapeutic manipulation of the HIF hydroxylases. *Antioxidants & Redox Signaling* **12**, 481-501 (2010).
47. Bruegge, K., Jelkmann, W. & Metzen, E. Hydroxylation of hypoxia-inducible transcription factors and chemical compounds targeting the HIF-alpha hydroxylases. *Current Medicinal Chemistry* **14**, 1853-62 (2007).
48. Flagg, S.C., Martin, C.B., Taabazuing, C.Y., Holmes, B.E. & Knapp, M.J. Screening chelating inhibitors of HIF-prolyl hydroxylase domain 2 (PHD2) and factor inhibiting HIF (FIH). *Journal of Inorganic Biochemistry* **113**, 25-30 (2012).
49. Yeoh, K.K., Chan, M.C., Thalhammer, A., Demetriades, M., Chowdhury, R., Tian, Y.M., Stolze, I., McNeill, L.A., Lee, M.K., Woon, E.C.Y. *et al.* Dual-action inhibitors of HIF prolyl hydroxylases that induce binding of a second iron ion. *Organic & Biomolecular Chemistry* **11**, 732-745 (2013).
50. Dang, L., White, D.W., Gross, S., Bennett, B.D., Bittinger, M.A., Driggers, E.M., Fantin, V.R., Jang, H.G., Jin, S., Keenan, M.C. *et al.* Cancer-associated IDH1 mutations produce 2-hydroxyglutarate. *Nature* **462**, 739-744 (2009).
51. Ye, D., Ma, S., Xiong, Y. & Guan, K.-L. R-2-Hydroxyglutarate as the Key Effector of IDH Mutations Promoting Oncogenesis. *Cancer Cell* **23**, 274-276 (2013).
52. Chowdhury, R., Yeoh, K.K., Tian, Y.M., Hillringhaus, L., Bagg, E.A., Rose, N.R., Leung, I.K., Li, X.S., Woon, E.C., Yang, M. *et al.* The oncometabolite 2-hydroxyglutarate inhibits histone lysine demethylases. *EMBO Reports* **12**, 463-9 (2011).
53. McDonough, M.A., Loenarz, C., Chowdhury, R., Clifton, I.J. & Schofield, C.J. Structural studies on human 2-oxoglutarate dependent oxygenases. *Current Opinion in Structural Biology* **20**, 659-672 (2010).

54. Chen, Z., Zang, J., Whetstine, J., Hong, X., Davrazou, F., Kutateladze, T.G., Simpson, M., Mao, Q., Pan, C.H., Dai, S. *et al.* Structural insights into histone demethylation by JMJD2 family members. *Cell* **125**, 691-702 (2006).
55. Sekirnik, R., Rose, N.R., Thalhammer, A., Seden, P.T., Mecinovic, J. & Schofield, C.J. Inhibition of the histone lysine demethylase JMJD2A by ejection of structural Zn(ii). *Chemical Communications*, 6376-6378 (2009).
56. Song, D., Li, L.S., Heaton-Johnson, K.J., Arsenault, P.R., Master, S.R. & Lee, F.S. Prolyl hydroxylase domain protein 2 (PHD2) binds a Pro-Xaa-Leu-Glu motif, linking it to the heat shock protein 90 pathway. *Journal of Biological Chemistry* **288**, 9662-74 (2013).
57. Frauer, C., Rottach, A., Meilinger, D., Bultmann, S., Fellinger, K., Hasenöder, S., Wang, M., Qin, W., Söding, J., Spada, F. *et al.* Different Binding Properties and Function of CXXC Zinc Finger Domains in Dnmt1 and Tet1. *PLoS ONE* **6**, e16627 (2011).
58. Rose, N.R., McDonough, M.A., King, O.N., Kawamura, A. & Schofield, C.J. Inhibition of 2-oxoglutarate dependent oxygenases. *Chemical Society Reviews* **40**, 4364-97 (2011).
59. Chowdhury, R., Flashman, E., Mecinović, J., Kramer, H.B., Kessler, B.M., Frapart, Y.M., Boucher, J.-L., Clifton, I.J., McDonough, M.A. & Schofield, C.J. Studies on the Reaction of Nitric Oxide with the Hypoxia-Inducible Factor Prolyl Hydroxylase Domain 2 (EGLN1). *Journal of Molecular Biology* **410**, 268-279 (2011).
60. Aik, W., Scotti, J.S., Choi, H., Gong, L., Demetriades, M., Schofield, C.J. & McDonough, M.A. Structure of human RNA N6-methyladenine demethylase ALKBH5 provides insights into its mechanisms of nucleic acid recognition and demethylation. *Nucleic Acids Research* (2014).
61. Aik, W., Demetriades, M., Hamdan, M.K.K., Bagg, E.A.L., Yeoh, K.K., Lejeune, C., Zhang, Z., McDonough, M.A. & Schofield, C.J. Structural Basis for Inhibition of the Fat Mass and Obesity Associated Protein (FTO). *Journal of Medicinal Chemistry* **56**, 3680-3688 (2013).
62. Jacob, C., Maret, W. & Vallee, B.L. Ebselen, a Selenium-Containing Redox Drug, Releases Zinc from Metallothionein. *Biochemical and Biophysical Research Communications* **248**, 569-573 (1998).
63. Parnham, M.J. & Sies, H. The early research and development of ebselen. *Biochemical Pharmacology* **86**, 1248-1253 (2013).
64. Parnham, M. & Sies, H. Ebselen: prospective therapy for cerebral ischaemia. *Expert Opinion on Investigational Drugs* **9**, 607-619 (2000).
65. Yamaguchi, T., Sano, K., Takakura, K., Saito, I., Shinohara, Y., Asano, T., Yasuhara, H. & Group, f.t.E.S. Ebselen in Acute Ischemic Stroke: A Placebo-Controlled, Double-blind Clinical Trial. *Stroke* **29**, 12-17 (1998).
66. Bush, M.F., Hall, Z., Giles, K., Hoyes, J., Robinson, C.V. & Ruotolo, B.T. Collision cross sections of proteins and their complexes: a calibration framework and database for gas-phase structural biology. *Analytical Chemistry* **82**, 9557-65 (2010).
67. Otwinowski, Z., Minor, W. & Jr., C.W.C. Processing of X-ray diffraction data collected in oscillation mode. in *Methods in Enzymology*, Vol. **276**, 307-326 (Academic Press, 1997).
68. McCoy, A.J., Grosse-Kunstleve, R.W., Adams, P.D., Winn, M.D., Storoni, L.C. & Read, R.J. Phaser crystallographic software. *Journal of Applied Crystallography* **40**, 658-674 (2007).
69. Schuttelkopf, A.W. & van Aalten, D.M. PRODRG: a tool for high-throughput crystallography of protein-ligand complexes. *Acta Crystallographica D Biological Crystallography* **60**, 1355-1363 (2004).
70. Brunger, A.T., Adams, P.D., Clore, G.M., DeLano, W.L., Gros, P., Grosse-Kunstleve, R.W., Jiang, J.S., Kuszewski, J., Nilges, M., Pannu, N.S. *et al.* Crystallography & NMR system: A new software suite for macromolecular structure determination. *Acta Crystallographica D Biological Crystallography* **54**, 905-921 (1998).
71. Emsley, P. & Cowtan, K. Coot: model-building tools for molecular graphics. *Acta Crystallographica D Biological Crystallography* **60**, 2126-2132 (2004).

72. Laskowski, R.A., MacArthur, M.W., Moss, D.S. & Thornton, J.M. PROCHECK: a program to check the stereochemical quality of protein structures. *Journal of Applied Crystallography* **26**, 283-291 (1993).
73. Woon, E.C.Y., Demetriades, M., Bagg, E.A.L., Aik, W., Krylova, S.M., Ma, J.H.Y., Chan, M., Walport, L.J., Wegman, D.W., Dack, K.N. *et al.* Dynamic Combinatorial Mass Spectrometry Leads to Inhibitors of a 2-Oxoglutarate-Dependent Nucleic Acid Demethylase. *Journal of Medicinal Chemistry* **55**, 2173-2184 (2012).
74. Villalgordo, J.M. & Heimgartner, H. Synthesis of Cyclic Depsipeptides and Peptides via Direct Amide Cyclization. *Helvetica Chimica Acta* **80**, 748-766 (1997).
75. Burdick, D.J., Marsters Jr, J.C., Aliagas-Martin, I., Stanley, M., Beresini, M., Clark, K., McDowell, R.S. & Gadek, T.R. N-Benzoyl amino acids as ICAM/LFA-1 inhibitors. Part 2: Structure–activity relationship of the benzoyl moiety. *Bioorganic & Medicinal Chemistry Letters* **14**, 2055-2059 (2004).
76. He, H., Morley, J.E., Twamley, B., Groeneman, R.H., Bučar, D.-K.i., MacGillivray, L.R. & Benny, P.D. Investigation of the Coordination Interactions of S-(Pyridin-2-ylmethyl)-l-Cysteine Ligands with M(CO)3+ (M = Re, 99mTc). *Inorganic Chemistry* **48**, 10625-10634 (2009).
77. Gosden, A., Macrae, R. & Young, G.T. Amino-acids and peptides. Part XL. Protection removable by electrolytic reduction: the use of S-4-picolyl-L-cysteine and O-4-picolyl-L-tyrosine in synthesis. *Journal of Chemical Research, Part S (Synop.)*, 22-23 (1977).
78. Yuan, Y., Elbegdorj, O., Beletskaya, I.O., Selley, D.E. & Zhang, Y. Structure activity relationship studies of 17-cyclopropylmethyl-3,14β-dihydroxy-4,5α-epoxy-6α-(isoquinoline-3′-carboxamido)morphinan (NAQ) analogues as potent opioid receptor ligands: Preliminary results on the role of electronic characteristics for affinity and function. *Bioorganic & Medicinal Chemistry Letters* **23**, 5045-5048 (2013).
79. Thevis, M., Kohler, M., Schlorer, N. & Schanzer, W. Gas phase reaction of substituted isoquinolines to carboxylic acids in ion trap and triple quadrupole mass spectrometers after electrospray ionization and collision-induced dissociation. *Jornal of the American Society of Mass Spectrometry* **19**, 151-8 (2008).
80. van Berkel, S.S., Brem, J., Rydzik, A.M., Salimraj, R., Cain, R., Verma, A., Owens, R.J., Fishwick, C.W., Spencer, J. & Schofield, C.J. Assay platform for clinically relevant metallo-beta-lactamases. *Journal of Medicinal Chemistry* **56**, 6945-53 (2013).
81. Stubbs, C.J., Loenarz, C., Mecinović, J., Yeoh, K.K., Hindley, N., Liénard, B.t.M., Sobott, F., Schofield, C.J. & Flashman, E. Application of a Proteolysis/Mass Spectrometry Method for Investigating the Effects of Inhibitors on Hydroxylase Structure. *Journal of Medicinal Chemistry* **52**, 2799-2805 (2009).
82. Leung, I.K.H., Flashman, E., Yeoh, K.K., Schofield, C.J. & Claridge, T.D.W. Using NMR Solvent Water Relaxation to Investigate Metalloenzyme−Ligand Binding Interactions. *Journal of Medicinal Chemistry* **53**, 867-875 (2009).
83. Riego, E., Bayó, N., Cuevas, C., Albericio, F. & Álvarez, M. A new approach to 3-hydroxyquinoline-2-carboxylic acid. *Tetrahedron* **61**, 1407-1411 (2005).
84. Reddy, K.V., Jin, S.J., Arora, P.K., Sfeir, D.S., Maloney, S.C.F., Urbach, F.L. & Sayre, L.M. Copper-mediated oxidative C-terminal N-dealkylation of peptide-derived ligands. A possible model for enzymatic generation of desglycine peptide amides. *Journal of the American Chemical Society* **112**, 2332-2340 (1990).
85. Warshakoon, N.C., Wu, S., Boyer, A., Kawamoto, R., Sheville, J., Renock, S., Xu, K., Pokross, M., Zhou, S., Winter, C. *et al.* Structure-based design, synthesis, and SAR evaluation of a new series of 8-hydroxyquinolines as HIF-1α prolyl hydroxylase inhibitors. *Bioorganic & Medicinal Chemistry Letters* **16**, 5517-5522 (2006).
86. Ashoorzadeh, A., Archibald, G. & Caprio, V. Synthetic evaluation of an enantiopure tetrahydropyridine N-oxide. Synthesis of (+)-febrifugine. *Tetrahedron* **65**, 4671-4680 (2009).

Chapter 6

Studies on BBOX from *Pseudomonas* sp. AK1

Abstract

Chapter 6 describes studies on BBOX from *Pseudomonas* sp. AK1. The gene for the *Pseudomonas* BBOX homologue (psBBOX) was cloned, expressed in *E. coli* and purified to homogeneity. A structural model of psBBOX was obtained by homology modelling using the existing hBBOX structure as a template. Kinetic parameters were determined and compared with the corresponding parameters for human BBOX (hBBOX). The results revealed substantial differences between hBBOX and psBBOX. The behaviour of both enzymes in the presence and absence of KCl and ascorbate were studied. The results from reaction of GBB analogues, including fluorinated GBB derivatives, reveal different substrate preferences for hBBOX and psBBOX. psBBOX is likely to be more flexible in the aromatic cage region; analogues substituted at the trimethylammonium group, such as GBBNF, are almost as good substrates as GBB itself, which is not the case for hBBOX. Shorter and longer GBB analogues, such as GBB-5 and GBB-3, are not well tolerated by psBBOX, in contrast with hBBOX, where both GBB-5 and GBB-3 were reasonably good substrates. psBBOX can tolerate substitutions in position 3 of GBB (as in the case of GBBF and D-carnitine).

Contents

1 Introduction

1.1 Bacterial carnitine metabolism

Carnitine is a ubiquitous substance, which plays important roles in animals, e.g. in the transport of long chain fatty acids through mitochondrial membrane or modulation of the ratio between acyl-CoA/CoA.[1-3]. In bacteria, the biological role of carnitine is incompletely defined. Carnitine has been proposed to serve as an osmoprotectant[4] or growth stimulant[5]; some microorganisms can utilise carnitine as a carbon and nitrogen source.[6] The biosynthetic pathway in microorganisms has not been identified and most existing literature on bacterial carnitine metabolism is limited to degradation pathways.[6,7] This situation contrasts with animal systems, where the biosynthetic pathway is well characterised,[8,9] but little is known about carnitine catabolism.[6] Apparently, most bacteria are not able to synthesise carnitine *de novo*; however some species, including certain *Pseudomonas* strains,[10] produce a homologue of γ-butyrobetaine hydroxylase (BBOX),[11-13] which is able to convert γ-butyrobetaine to L-carnitine. The discovery of bacterial enzymes producing carnitine was prompted by increasing demand for a cheap carnitine source. Carnitine is widely used as food supplement or in the pharmaceutical industry for treatment of carnitine deficiencies or cardiac conditions and therefore microbial based production presents an efficient method towards carnitine synthesis.[14,15]

1.2 BBOX from *Pseudomonas* sp. AK1 – previous studies

BBOX from *Pseudomonas* sp. AK1 (psBBOX) was previously isolated from *Pseudomonas* sp. AK1 and characterised as a protein of 383 amino acids per subunit, which in solution exists as a homodimer.[12,13] psBBOX was reported to be fully dependent on the presence of Fe(II) with $K_{M,\ app}$ = 0.06 mM. For purified psBBOX an apparent K_M for γ-butyrobetaine (GBB) and 2-oxoglutarate (2OG) were determined, with values of 2.4 mM and 0.45 mM respectively.[11] Lindstedt *et al.* have studied substrate specificity of psBBOX[11] and reported that neither 3-trimethylaminopropionate, 5-trimethylaminovalerate, 6-trimethylaminocaproate, 4-dimethylaminobutyrate or 4-trimethylaminocrotonate can substitute GBB (i.e. no 2OG conversion to succinate was observed). However, all the tested GBB analogues were moderately good inhibitors. None of the 2OG analogues (succinic semialdehyde, pyruvate, 2-ketobutyrate, 2-ketovalerate, p-hydroxyphenylpyruvate, oxalacetate, 2-ketoadipate, 2-ketopimelate, glutarate, 2-hydroxyglutarate, glutamate, citrate, isocitrate, cis-aconitate, succinate, fumarate, or malate) serves as a co-substrate (i.e. no GBB hydroxylation was observed). Oxalacetate, 2-ketopimelate, citrate and 2-ketoadipate were found to be moderately good inhibitors. Several metal ions were potent inhibitors;[11] the most active ones were Co^{2+}, Ni^{2+}, Cu^{2+}, Zn^{2+}, Cd^{2+}, and Hg^{2+}. The 2OG binding site of BBOX from *Pseudomonas* sp. AK1 has been studied by Ng *et al*.[16] A library of 2OG analogues was tested as

inhibitors resulting in the assignment of 2,4-pyridine dicarboxylate and 3,4-dihydroxybenzoate as the most potent inhibitors. Two functional groups in the inhibitors were assigned as vital for efficient binding: one substituting for the C-5 carboxylate of 2OG and the other one enabling metal chelation. The distance between these two moieties is important, as reflected in the failure of 2OG analogues with longer (2-ketoadipate) or shorter (oxaloacetate) carbon chain length to sustain BBOX catalysis (no hydroxylation observed, when these analogues were used as co-substrates).

2 Sequence and structural comparison

2.1 Sequence alignments

Human and bacterial BBOX homologues share about 30% sequence identity, as determined by BLAST analysis. Several bacterial BBOX sequences were aligned with the human BBOX homologue to reveal that crucial residues involved in substrate and metal binding are conserved among species (Fig. 1). The Zn(II)-binding domain is present in both *Pseudomonas* and human BBOX[17] and residues responsible for Zn(II) binding (marked with yellow stars) are highly conserved. The HxD/E…H – an iron binding motif characteristic for 2OG oxygenase family (indicated by green stars) and the arginine binding C-5 carboxylate of 2OG (red star) are well conserved.[18] Blue circles indicate residues involved in formation of an aromatic cage, which interacts with the trimethyammonium group of GBB via π-cation interactions. For both human and *Pseudomonas* species, these residues are represented by aromatic amino acids such as phenylalanine and tyrosine (psBBOX) or tyrosine and tryptophan (hBBOX). Residues involved in binding of the GBB carboxylate are indicated as pink hexagons. In the human homologue they are both asparagines, whereas psBBOX contains an aspartic acid and an alanine, which might suggest why binding of GBB is less tight in the case of the bacterial BBOX homologue.

2.2 Structural comparisons

Several crystal structures are available for human BBOX. Based on the crystal structure of human BBOX complexed with Ni(II), GBB and NOG (*N*-oxalylglycine, a close 2OG mimic), a model for psBBOX was built using the SWISS-MODEL[19-21] server. The hBBOX structural (PDB id: 3O2G) alignment with the psBBOX model reveals a similar position of all vital residues, including the metal and ligand binding residues and similar overall fold of the enzyme (Fig. 2). A slight difference can be observed in the active site loop region (residues 183-199 in human BBOX), in which human BBOX forms a short helix linking the βI and βII strands of the DSBH (double-stranded β-helix characteristic fold for 2OG dependent oxygenases) (for comparison see Fig. 2B and C). However, prediction of the overall fold of psBBOX has to be taken with care, as BBOX has been shown to display substantial conformational flexibility (see Chapter 5). Nevertheless, the model enables estimation of the differences between the GBB and 2OG binding pockets, which may reflect the

differences in catalytic properties of ps- and hBBOX. Metal and 2OG binding sites are well conserved between bacterial and human BBOX. The metal is coordinated by two histidine and aspartate residues; the 2OG C-5 carboxylate interacts with two arginine residues, one of which forms interactions characteristic for 2OG binding in the active sites of 2OG dependent oxygenases (Arg360/362). Differences are predominantly in the GBB binding region. The predicted aromatic cage in the psBBOX structural model consists of aromatic amino acids; however the Trp181 and Tyr177 which are present in the human BBOX structure are replaced with phenylalanine 188 and 184, respectively, which results in a looser trimethylammonium binding pocket. In both ps- and hBBOX an active site loop 'lid' is formed by a tyrosine residue (Tyr194 in human and Tyr 201 in psBBOX). GBB carboxylate binding residues are not conserved; Asn191 and Asn292 are responsible for GBB carboxylate interactions in the hBBOX in the bacterial homologue are apparently replaced with Ser198 and Ala296, respectively.

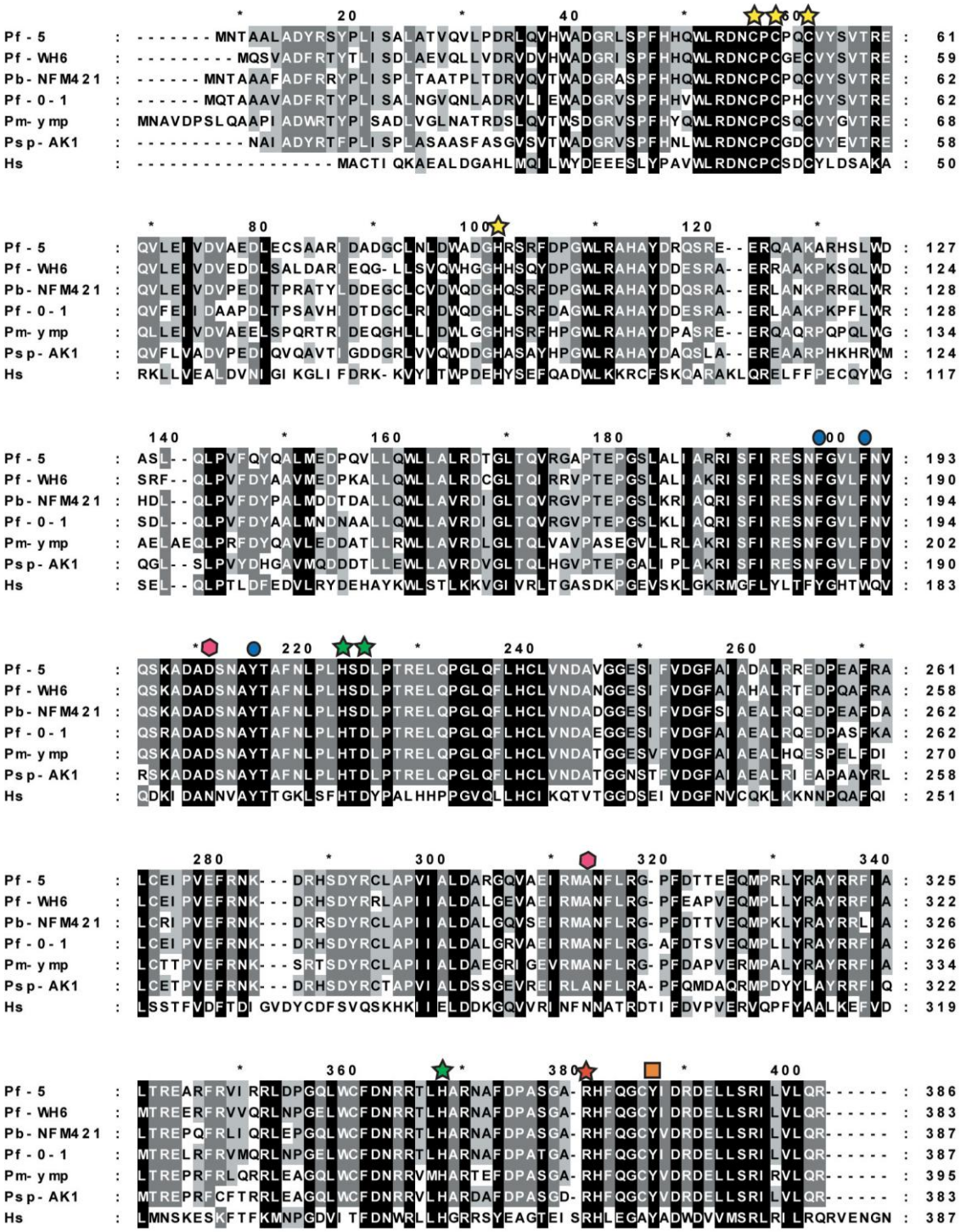

Figure 1 Sequence alignment of BBOX homologues from human (Hs, gi|158261239) and *Pseudomonas* (*Pseudomonas fluorescens* Pf-5, gi|70733041; *Pseudomonas fluorescens* WH6, gi|312963522; *Pseudomonas brassicacearum subsp. brassicacearum* NFM421, gi|330812266; *Pseudomonas fluorescens* Pf0-1, gi|77461455; *Pseudomonas mendocina* ymp, gi|146305540; *Pseudomonas* sp. AK1, gi|231642). Yellow stars represents residues involved in Zn(II) binding, blue circles – involved in formation of an aromatic cage, which interacts with trimethylammonium group of GBB via π-cation interactions; pink pentagons – residues involved in GBB carboxylate binding, green stars represent HxD/E…H (an iron binding motif), red star represent residue involved in binding of 2OG C-5 carboxylate.

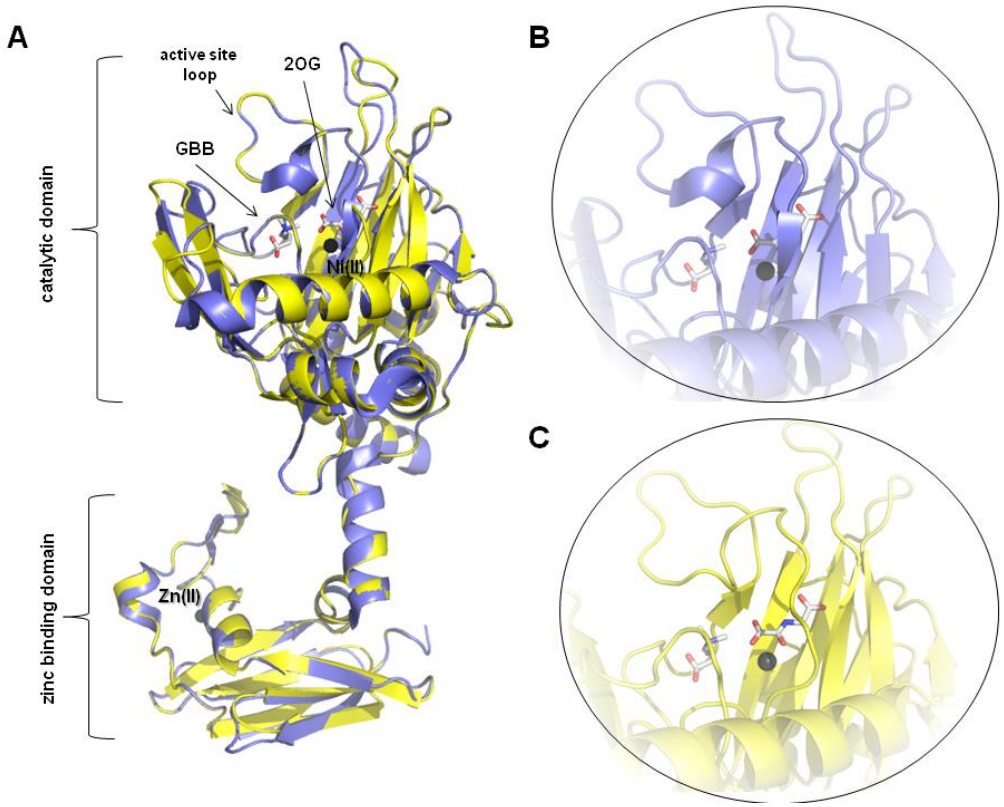

Figure 2 Overlay of an hBBOX structure (blue, PDB id: 3O2G) and the generated model of psBBOX (yellow). Catalytic, zinc binding domains, the active site are indicated (A). Close-up comparison of the active sites of hBBOX (B) and psBBOX (C) show a difference in the observed active site loop fold.

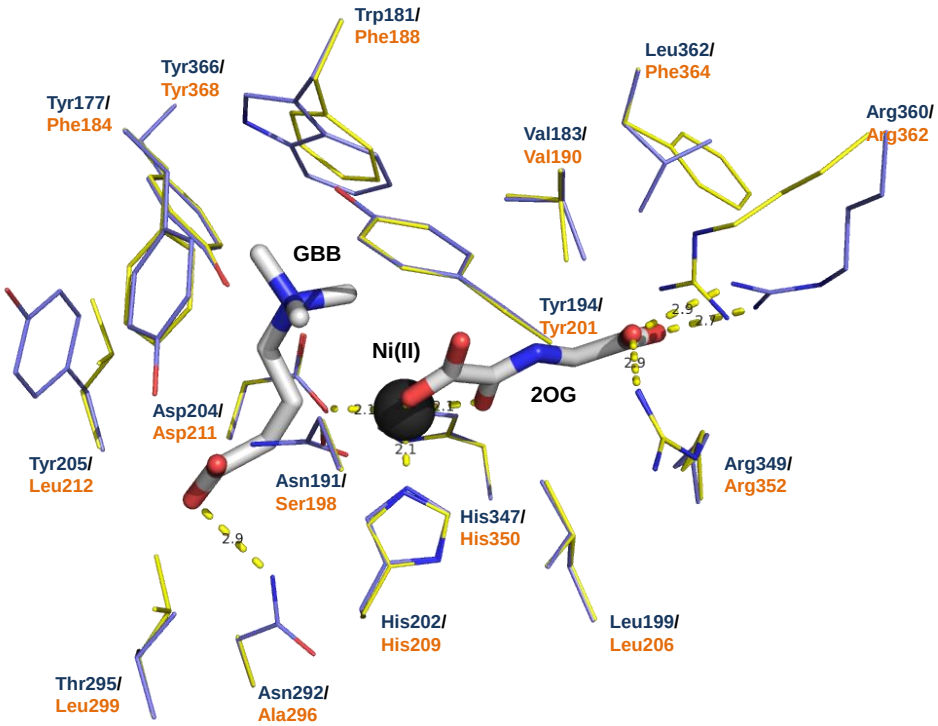

Figure 3 Overlay of GBB and 2OG binding pockets of hBBOX (blue, PDB id: 3O2G) and the model of psBBOX (yellow).

3 Pseudomonas BBOX cloning and purification

3.1 Cloning and expression trials

The gene encoding psBBOX was obtained from GeneArt Life Sciences gene synthesis services, and supplied in a pMA-T plasmid which contained the ampicillin resistance gene. Additional restriction sites for NdeI and BamHI were introduced. Codons were optimised for expression in *E. coli* with lowered GC content compared to the wild type psBBOX DNA sequence. The DNA sequence was designed by reverse transcription of the 383 residue γ-butyrobetaine hydroxylase from *Pseudomonas* sp. AK1 (gi 385463). The supplied plasmid was transformed into XL1 Blue *E. coli* cells and grown overnight prior to plasmid DNA purification using the GeneJet DNA extraction kit (Thermo Fisher). The obtained plasmid and empty pCOLDI (Takara) and pET28a(+) (Novagen) vectors were digested with NdeI and BamHI restriction enzymes (New England Biolabs) using the following conditions: 10 μL of plasmid DNA (conc. 200 μg/μL) was mixed with 1.5 μL of NdeI and BamHI HF and 1.5 μL of NEB 4 buffer (10 ×) and incubated for 3 h at 37°C. The digested DNA was run on a 1% agarose gel at 60V for 40 min; the desired bands were cut out and the resultant DNA was purified using a Gel Extraction Kit (Quiagen). The insert containing psBBOX was ligated with the digested pCOLDI and pET28a vectors using T4 DNA ligase and the following conditions: 1 μL of vector (15 μg/μL), 4 μL of insert (5 μg/μL), 1 μL of T4 DNA ligase, 1 μL of T4 DNA ligase buffer (10 ×) and 3 μL of Milli-Q water were mixed and incubated for 3 h at 37°C. 2 μL of the ligation mixture was then transformed into XL10 Gold competent cells and grown on agar plates containing kanamycin for the pET28a(+) construct and ampicillin for the pCOLDI construct. Obtained colonies were inoculated into fresh media containing the appropriate antibiotic and then grown overnight. Plasmid DNA was purified using a DNA purification kit and the identity of the constructs was confirmed by sequencing (Source Bio Science).

Constructs were transformed in *E. coli* BL21 (DE3) competent cells, which were grow overnight on agar plates containing ampicillin (pCOLDI constructs) and kanamycin (pET28a constructs). A single colony was grown in fresh media overnight and the resultant cell suspension was used for glycerol stock preparation. Expression trials for both constructs were performed. The IPTG concentration, incubation temperature and time were varied. The pET28a construct displayed satisfactory levels of protein expression, however protein production was higher for the pCOLDI based construct (Fig. 4). Therefore, the latter was used in further experiments. The pCOLDI vector utilises a promoter derived from the cspA gene, which is one of the cold-shock genes. When the temperature of the culture is sufficiently reduced, growth as well as expression of endogenous proteins is decreased, while expression of 'cold-shock' proteins is induced, which can lead to high expression levels of the desired protein.

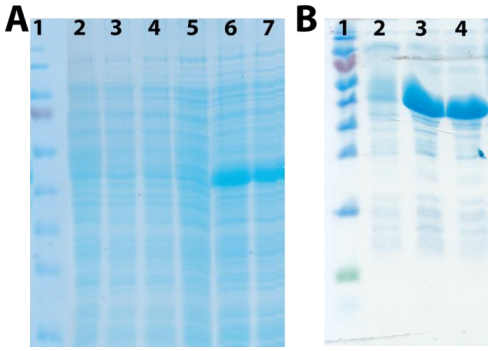

Figure 4 SDS-PAGE analysis of expression trials of psBBOX constructs in pET28a (A) and pCOLDI (B) vectors. A – Lane 1: molecular weight marker, lanes 2-7: soluble fractions of expression trials cell lysates. Lanes 2-4: cells grown for 4 h at 37°C after treatment with 0 mM (2), 0.2 mM (3) and 0.5 mM (4) of IPTG. Lanes 5-7: cells grown for 18 h at 15°C after treatment with 0 mM (5), 0.2 mM (6) and 0.5 mM (7) of IPTG. B – Lane 1: protein ladder. Lanes 2-4 soluble fractions of expression trials cell lysates obtained from cells grown for 18h at 15°C after treatment with 0 mM (2), 0.2 mM (3) and 0.5 mM (4) of IPTG.

3.2 Expression

2TY media (600 mL) containing ampicillin was inoculated with 6 mL of an overnight starter culture and grown at 37°C with shaking (200 rpm) until $O.D._{600}$ reached 0.7; the temperature was then reduced to 15°C and cultures were allowed to stand without shaking for 30 min, when IPTG was then added to final concentration of 0.2 mM. The culture was incubated overnight at 15°C with shaking, after which cells were pelleted by centrifugation (10 min, 7000 rpm). The cell pellet was frozen at -80°C overnight. Cells were lysed according to the lysis protocol (Appendix 1) and lysate was subjected to Ni(II)-affinity chromatography (as described in Appendix 1). Purified protein was stored at a concentration of 20 mg/mL in 50 mM Tris-HCl buffer containing 200 mM NaCl at -80°C. Produced protein contained extra *N*-terminal amino acids originating from the vector sequence: MNHKVHHHHHHIEGRHM, which gives protein product of 399 amino acids, MW = 45.35 kDa (as determined by MS analyses, Fig. 5) and calculated ε = 56.88 and theoretical pI = 6.1(ProtParam tool on the ExPASy server). Expression yielded around 80 mg of protein per 1 L of bacterial culture.

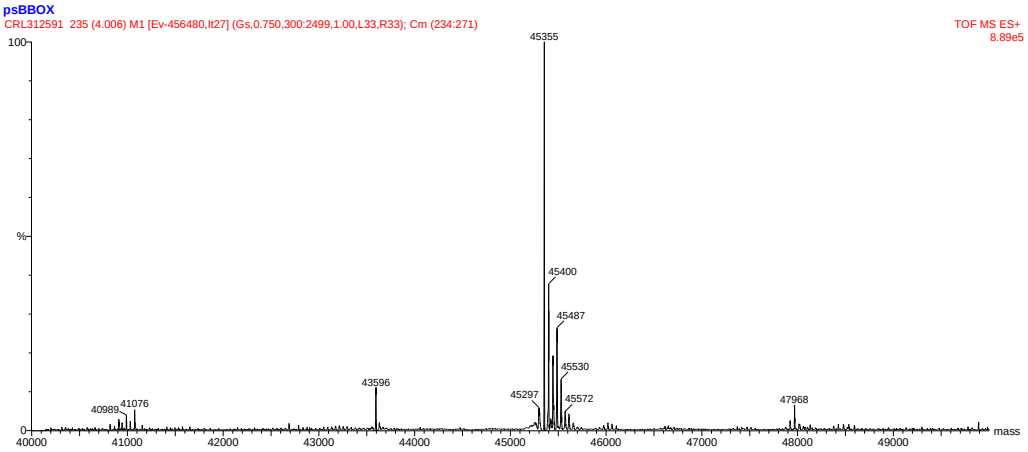

Figure 5 MS spectra of purified psBBOX.

A **B**

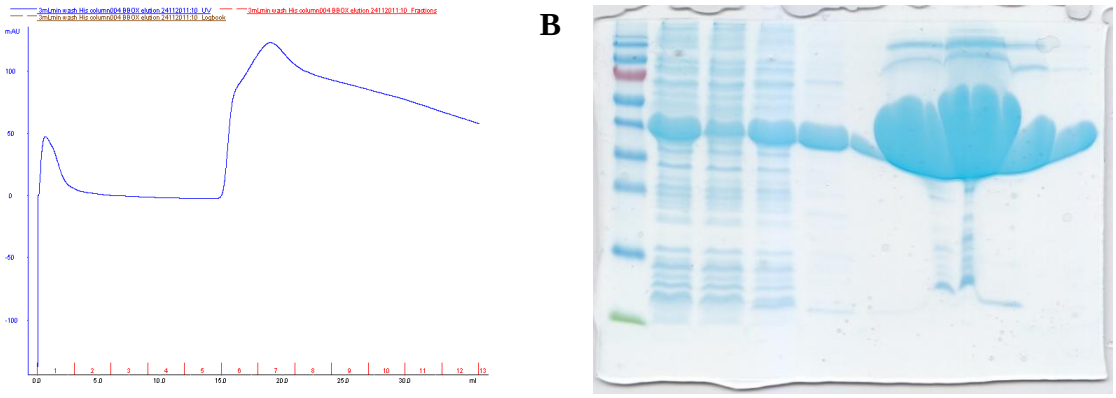

Figure 6 Ni-NTA chromatogram, B. SDS PAGE gel, lanes: 1. Molecular weight marker, 2. Total cell lysate, 3. Cell lysate flow through, 4. Wash flow through, then fractions 6-11.

Further purification for crystallography trials was performed using size exclusion chromatography (Superdex S200, 300 mL column) and ion exchange chromatography (Source-Q column) as described in Experimental Section. Unfortunately, the crystallization trials were unsuccessful.

A **B**

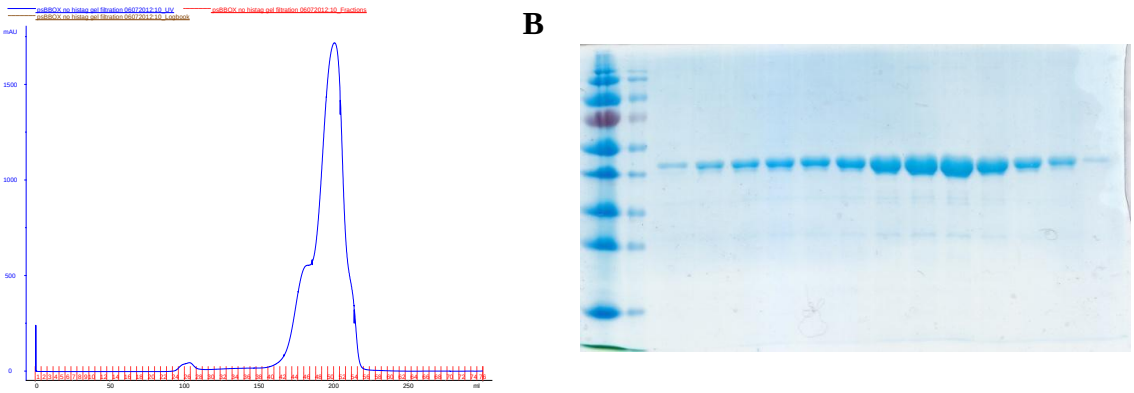

Figure 7 S200 column gel filtration chromatogram, B. SDS PAGE gel, lanes: 1. Molecular weight marker, 2. empty, then fractions 43-55.

A **B**

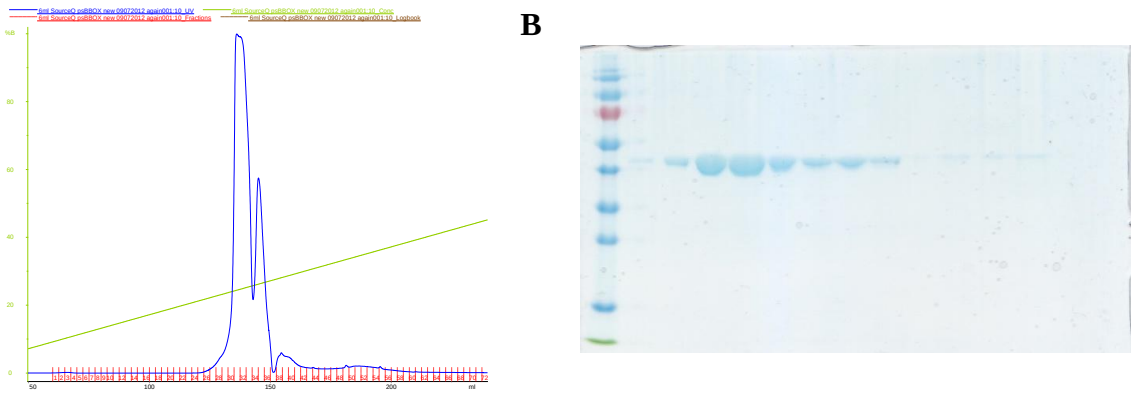

Figure 8 SourceQ column ion exchange chromatogram, B. SDS PAGE gel, lanes: 1. Molecular weight marker, then fractions 29-40. Protein was eluted with 200-250 mM NaCl concentration.

4 Kinetic analyses – comparison with human enzyme.

4.1 Kinetics of substrate turnover

Cofactor requirements and kinetic parameters for 2OG and GBB substrates were determined using an NMR based assay (see Experimental Section for details). Both psBBOX and hBBOX were shown to efficiently hydroxylate GBB, however psBBOX was more active compared with the human counterpart (Fig. 9, Table 1). The shape of the time-course curve was different for the human and *Pseudomonas* BBOX. psBBOX catalysed GBB hydroxylation presents a typical product accumulation curve. For the human enzyme, a short burst phase is observed followed by a linear rise (Fig. 9). For both enzymes GBB hydroxylation was coupled to 2OG decarboxylation.

Table 1 Initial rates of carnitine and succinate formation catalysed by human and psBBOX.

Enzyme	Initial rate of hydroxylation [µM/s]	Initial rate of succinate formation [µM/s]	Ratio of succinate formation to hydroxylation
hBBOX	0.13	0.16	1.2
psBBOX	0.29	0.32	1.1

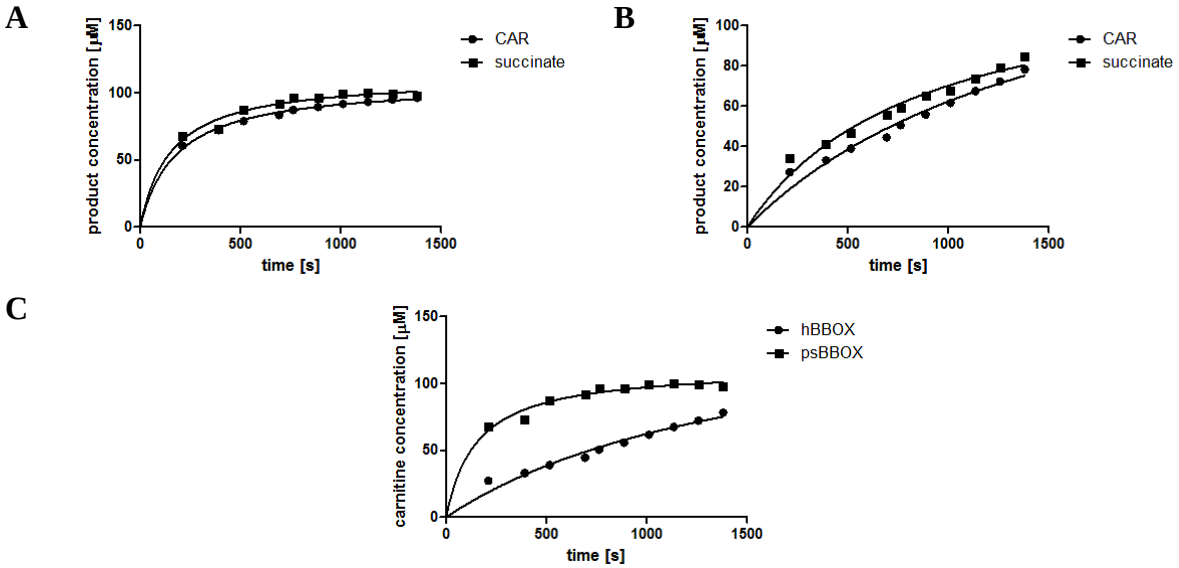

Figure 9 Time course of psBBOX (A) and hBBOX (B) catalysed reaction as observed by carnitine and succinate formation. Overlay of hBBOX and psBBOX catalysed GBB hydroxylation (C).

4.1.1 2-Oxoglutarate kinetics

Kinetic parameters for 2OG were assigned using both succinate and carnitine formation ratios (Table 2). The parameters obtained from these two approaches are different as a large amount of uncoupled 2OG turnover at high 2OG concentrations was observed. GBB was not hydroxylated in the absence of 2OG, therefore the observed amount of GBB hydroxylation was always equal to or lower than the

amount of 2OG decarboxylation. The parameters for GBB were only calculated by observation of carnitine formation, which is specific to GBB hydroxylation and the amount of uncoupled 2OG turnover was not taken into account. 2OG turnover was generally faster for psBBOX with a 6 fold higher v_{max} value, however K_M for 2OG was lower in the case of human BBOX. Human BBOX also displayed inhibition by high levels of 2OG with a K_I value of 5 mM. In general, values obtained from processing the data for succinate formation were higher than those from carnitine formation, consistent with high uncoupled 2OG turnover observed at higher 2OG concentrations (Fig. 10).

Table 2 Kinetic properties of 2OG turnover by psBBOX and hBBOX.

enzyme	K_M [μM]		V_{max} [μMs^{-1}]		k_{cat} [s^{-1}]		K_I [mM]
	carnitine levels	succinate levels	carnitine levels	succinate levels	carnitine levels	succinate levels	carnitine levels
psBBOX	271±65	532±135	0.24	0.35	2.3±0.2	3.5±0.3	-
hBBOX	41±3*	153±44	0.044*	0.080	0.89±0.02*	1.6±0.1	5.2±0.8*

* value obtained by fitting with substrate inhibition equation. Other values were fitted with standard Michaelis-Menten kinetic equation (see experimental section)

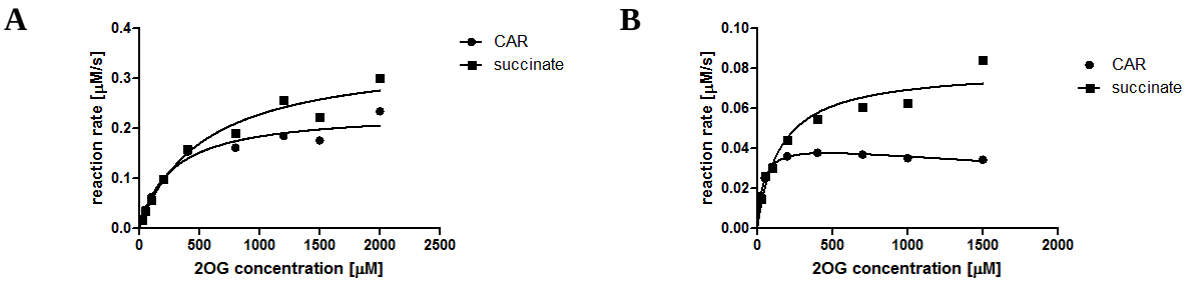

Figure 10 Dependence of initial reaction rate on the 2OG concentration for psBBOX (A) and hBBOX (B). Both initial rate of carnitine and succinate formation are plotted.

4.1.2 γ-Butyrobetaine kinetics

Data obtained for GBB were fitted with a substrate inhibition equation (Table 3, Fig. 11, details of curve fitting are summarised in the Experimental section). hBBOX and psBBOX differ in their affinity towards GBB. For psBBOX a K_M value of 2.5 mM (consistent with the previously reported value of 2.4 mM[11]) was 3 orders of magnitude higher than the K_M of 4 μM for hBBOX. psBBOX displayed only slight substrate mediated inhibition at high concentrations of GBB (>0.6 mM). Fitting range without inhibition with the Michaelis-Menten equation gave a K_M value of 163 μM, V_{max} = 0.12 μM/s and k_{cat} = 2.5 1/s. In contrast, hBBOX was inhibited by GBB at very low concentrations of substrate (>20 μM). These are key differences in the properties of human and bacterial BBOX homologues. The GBB mediated substrate inhibition of human BBOX[17], mentioned

in Chapter 5 (also in the context of cell based studies) is a significant feature of hBBOX catalysis, presumably important for regulation of carnitine biosynthesis. In the case of the bacterial homologue, where the full biosynthesis pathway is most likely not present, the role of BBOX is limited purely to turnover of GBB/CAR production and therefore substrate inhibition by GBB was lost (or gained by the human enzyme during evolution). Lack of GBB substrate inhibition in the psBBOX catalysed reaction gives further evidence for a potential physiological role of this phenomenon in the regulation of carnitine biosynthesis in animals.

Table 3 Kinetic properties of GBB turnover by psBBOX and hBBOX.

Enzyme	K_M [µM]	V_{max} [µMs^{-1}]	k_{cat} [s^{-1}]	K_I [µM]
psBBOX	2474±1466	1.1±0.6	21.3	125±74
hBBOX	4.2±3.9	0.041±0.02	0.83	24±14

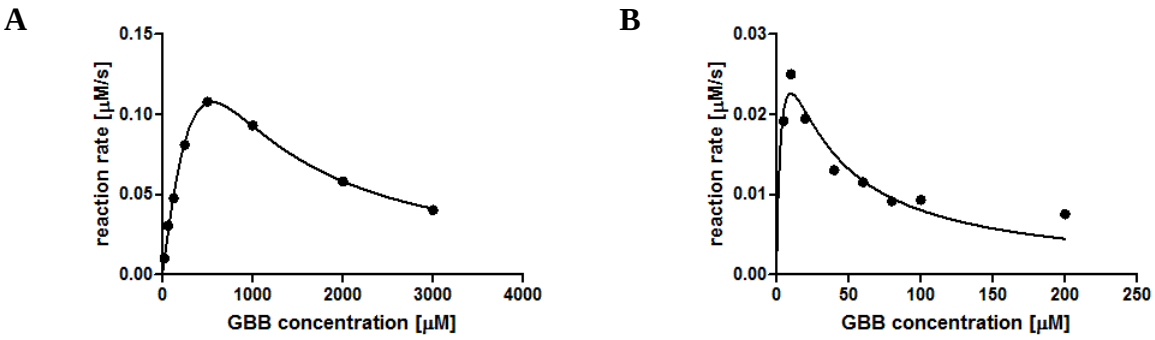

Figure 11 Dependence of initial reaction rate on the GBB concentration for psBBOX (A) and hBBOX (B).

4.2 Uncoupled turnover

Some 2OG dependent oxygenases catalyse turnover of 2OG, independent of substrate transformation (uncoupled 2OG turnover).[22-25] The amount of uncoupled 2OG turnover (in the absence of GBB) was examined and revealed that a small amount of 2OG can be slowly turned into succinate by both h- and psBBOX (Fig. 12). A control experiment with no enzyme added showed no decomposition of 2OG over the investigated time scale, so the observed succinate formation has to be attributed to an enzymatic reaction.

4.3 Ascorbate dependence

Ascorbate was previously shown to aid the activation of some 2OG dependent oxygenases, in part, by preventing oxidation of Fe(II).[26-28] In animals the link between ascorbate deficiency to decreased concentrations of tissue carnitine levels has been made, suggesting ascorbate is an important cofactor in carnitine biosynthesis.[29,30] The presence of ascorbate was found to stimulate hBBOX activity; however it did not have significant influence on the activity of psBBOX (Fig. 13). In the case of both enzymes, ascorbate did not affect the amount of uncoupling (data not shown).

For the hBBOX, initial rate of carnitine formation was similar in the presence or absence of ascorbate, however the rate of carnitine formation changed significantly over time, as without ascorbate the reaction did not proceed any further after certain amount of time. This observation suggests that ascorbate can play a role in the protection of the enzyme against reactive oxygen species, which leads to enzyme deactivation. The insensitivity of psBBOX towards the variation of ascorbate concentrations suggests psBBOX might be less sensitive towards reactive oxygen species than hBBOX. The mechanism of enzyme protection by ascorbate has been studied. It is known that the way ascorbate affects certain 2OG dependent oxygenases is not limited to its properties as a reducing agent, because other reducing agents were not as effective as ascorbate. The dramatically different behaviour of human and bacterial BBOX homologues towards the presence of ascorbate, combined with substantial sequence, structural and catalytic similarities of both enzymes makes BBOX an interesting system for further mechanistic studies on the influence of ascorbate on 2OG oxygenase catalysed reactions.

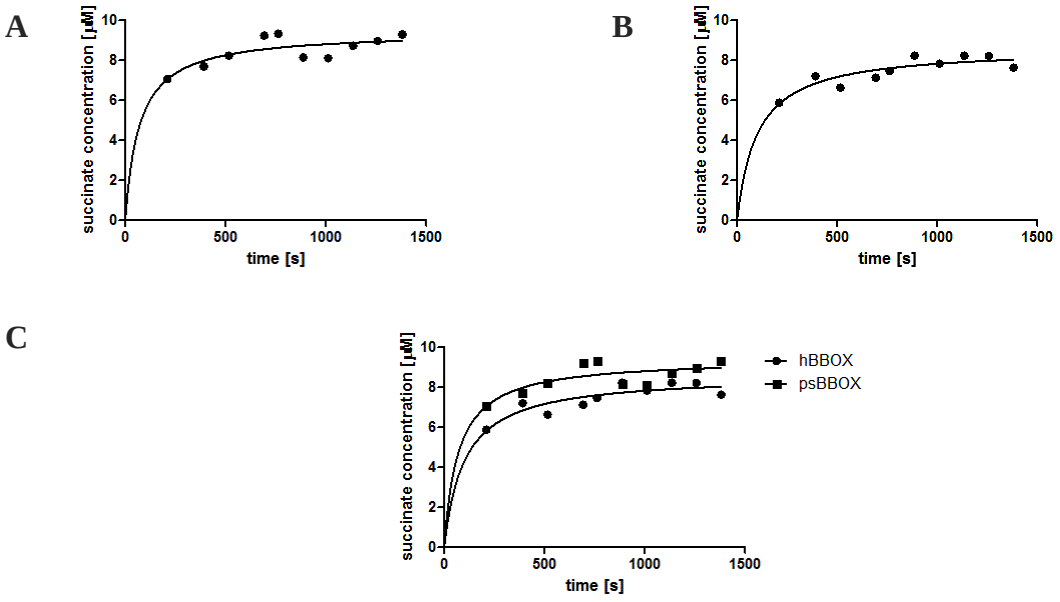

Figure 12 Uncoupled turnover in the absence of substrate for psBBOX (A) and hBBOX (B) catalysed reaction as observed by succinate formation (i.e. in the absence of GBB). Overlay of hBBOX and psBBOX catalysed uncoupled 2OG turnover (C).

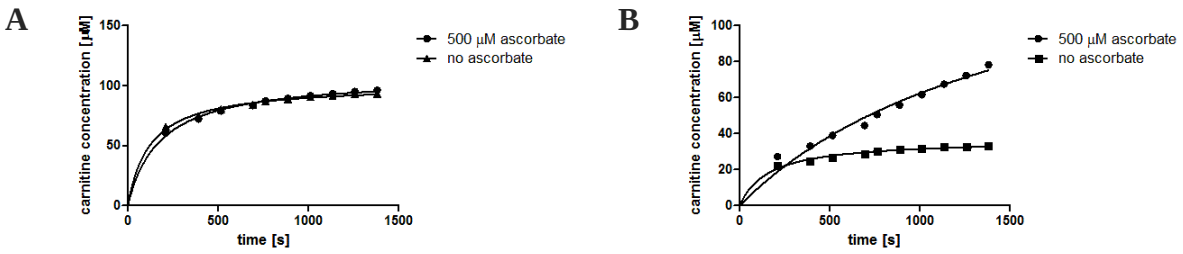

Figure 13 Comparison of time courses of psBBOX (A) and hBBOX (B) catalysed oxidations of GBB, in the presence and absence of ascorbate.

4.4 Influence of KCl

KCl was found to stimulate hBBOX activity, which is consistent with the literature data on human kidney[31] and rat liver BBOX.[32] In the case of hBBOX it also improved the coupling between decarboxylation of 2OG and GBB hydroxylation (Fig 14). On the other hand, for psBBOX, increasing concentrations of KCl had an inhibitory effect, but it did not have significant influence on the coupling between decarboxylation and GBB hydroxylation (Fig 14).

The stabilisation of human BBOX by potassium ions has been previously reported, however the mechanism of this phenomenon remains unknown. Again the ps/h BBOX system because of its dissimilarity when it comes to KCl influence on activity, presents a good system for further study.

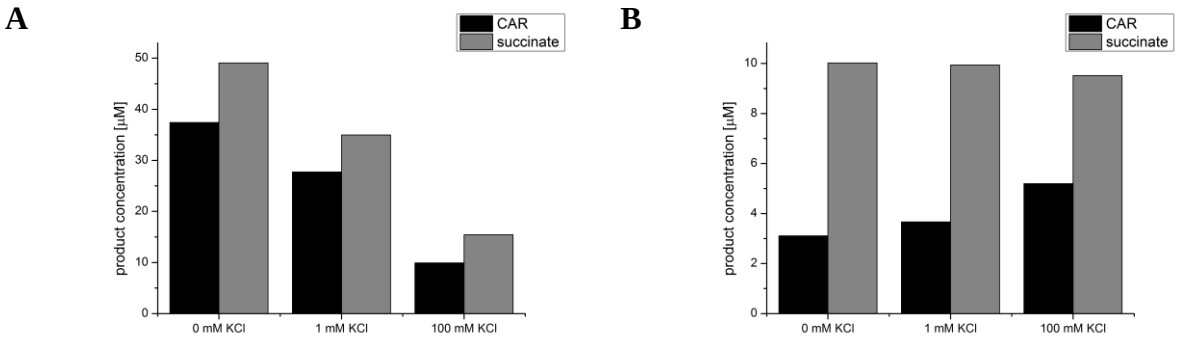

Figure 14 Dependence of product formation (black – carnitine, grey – succinate) on amount of KCl present in the reaction mixture for psBBOX (A) and hBBOX (B) catalysed oxidations of GBB as monitored by product formation by ^{1}H NMR.

5 Kinetic studies using fluorinated GBB analogues

Fluorinated GBB analogues were shown to be useful tools for determining activity of hBBOX, as described in Chapter 2. (*3S*)-Fluoro-GBB (GBBF) was shown to undergo hBBOX catalysed hydroxylation with subsequent fluoride ion release;[33] this was used as the basis for the development of a BBOX activity assay (Chapter 2). psBBOX turnover GBBF in an analogous fashion to hBBOX as determined by ^{1}H NMR. *N*-Fluoromethylated GBB (GBBNF) also gives the same product as hBBOX upon reaction with psBBOX (Chapter 2) (Scheme 1).

For both enzymes, GBBNF was a better substrate than GBBF, which is consistent with crystallographic analyses revealing only little space available for substituents in position 3 (Fig. 15) and possibly a higher tolerance for the substitutions placed in the aromatic cage region (Fig. 3).

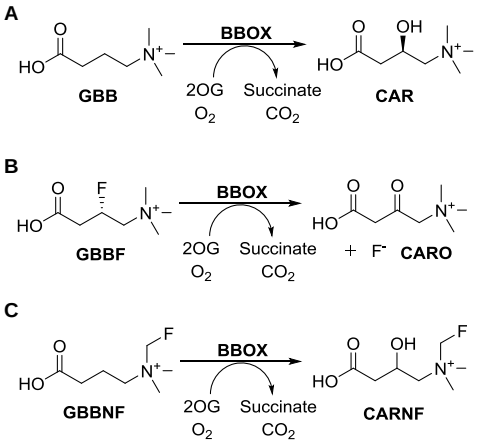

Scheme 1 BBOX catalysed turnover of GBB (A), GBBF (B) and GBBNF (C).

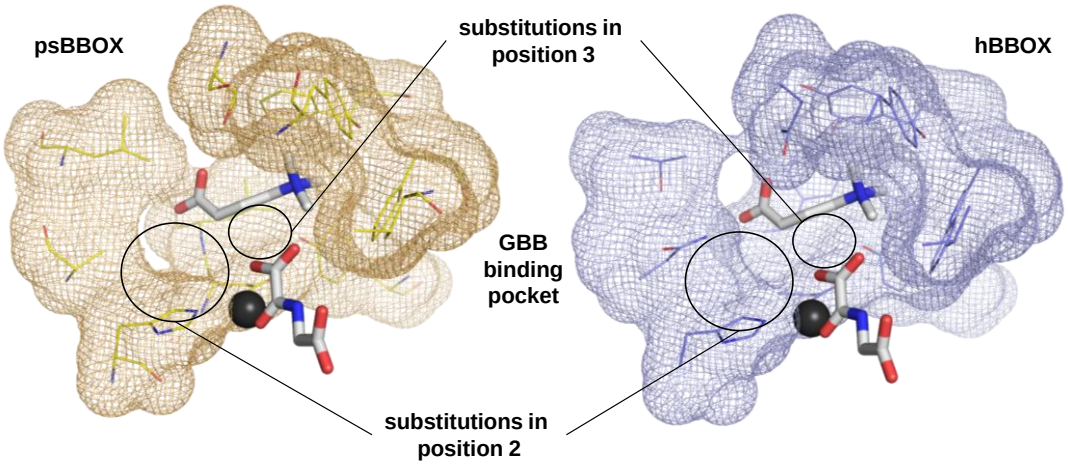

Figure 15 Comparison of GBB binding pockets from the psBBOX model (left, with GBB, NOG and metal modelled in based on hBBOX structure) and hBBOX structure (right, PDB id: 3O2G). It implies there is only limited space for substituents at C-3 of GBB chain in case of both hBBOX and psBBOX. The psBBOX active site offers more space to fit GBB analogues substituted in position 2.

With psBBOX, GBBNF was hydroxylated nearly as well as GBB, likely reflecting the larger size of the trimethylammonium binding pocket in psBBOX compared to hBBOX (Tyr177 and Trp181 present in hBBOX are replaced with phenylalanines in psBBOX, Fig. 3). GBBF was turnovered at a similar rate by both human and psBBOX and it was a poorer substrate than GBBNF, suggesting that substitutions at the hydroxylation site are not well tolerated, possibly because of the steric reasons in both enzymes' binding pockets. In general the coupling between 2OG decarboxylation and hydroxylation was good in case of GBBNF. Some uncoupling was observed when GBBF was a substrate, further indicating it is a poorer substrate than GBBNF[22]. Data is summarized in Table 4 and visualised in Fig. 16-18.

Table 4 Initial rates of BBOX catalysed hydroxylation reactions of GBB analogues.

Enzyme	Substrate	Initial rate of hydroxylation [μM/s]	Initial rate of succinate formation [μM/s]	Ratio of succinate formation to hydroxylation
psBBOX	GBB	0.29	0.32	1.1
	GBBF	0.028	0.059	2.1
	GBBNF	0.21	0.24	1.1
hBBOX	GBB	0.13	0.16	1.2
	GBBF	0.027	0.063	2.3
	GBBNF	0.083	0.097	1.2

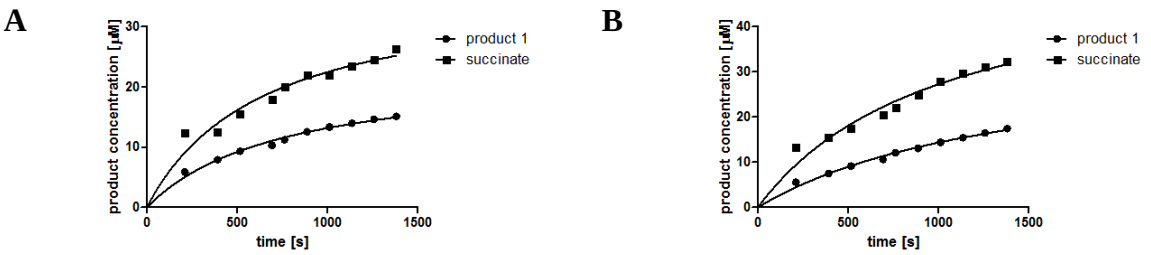

Figure 16 Comparison of time courses of psBBOX (A) and hBBOX (B) catalysed oxidations of GBBF, as observed by carnitine and succinate formation.

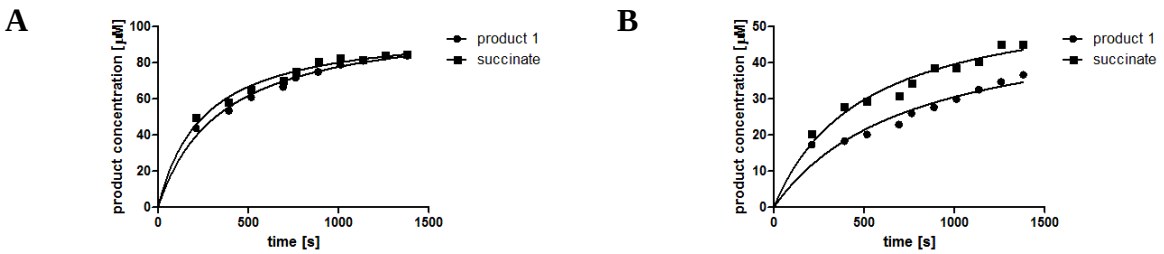

Figure 17 Comparison of time courses of psBBOX (A) and hBBOX (B) catalysed oxidations of GBBNF, as observed by carnitine and succinate formation.

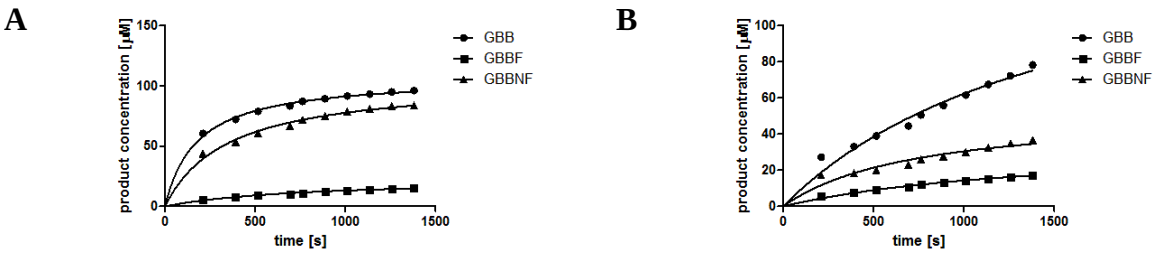

Figure 18 Comparison of time courses of psBBOX (left) and hBBOX (right) catalysed oxidations of GBB, GBBF and GBBNF.

As in the case of GBB, psBBOX displayed much higher K_M values towards the fluorinated GBB analogues than hBBOX (around an order of magnitude difference). psBBOX seemed not to be inhibited by GBBF nor GBBNF, at least up to 0.5 mM concentration of substrate. hBBOX was inhibited by low concentrations of GBBF, but much less inhibition was observed with GBBNF, which is discussed in Chapter 2. This is consistent with the proposed mechanism of substrate inhibition, where an *N*-fluoromethyl group alters interactions within the trimethylammonium binding pocket. Because GBB inhibition was not observed at low concentrations with psBBOX, the lack of substrate inhibition by GBBF or GBBNF is not surprising.

Table 5 Kinetic properties of GBBF turnover by psBBOX and hBBOX.

enzyme	KM [µM]	Vmax [µMs-1]	kcat [s-1]	KI [µM]
psBBOX	623±102	0.47±0.05	0.59	-
hBBOX	20±9	0.11±0.02	0.14	136±44

Table 6 Kinetic properties of GBBNF turnover by psBBOX and hBBOX.

enzyme	K_M [µM]	V_{max} [μMs^{-1}]	k_{cat} [s^{-1}]	K_I [µM]
psBBOX	412±48	1.0±0.07	5.0	-
hBBOX	17±13	0.12±0.04	0.30	224±209

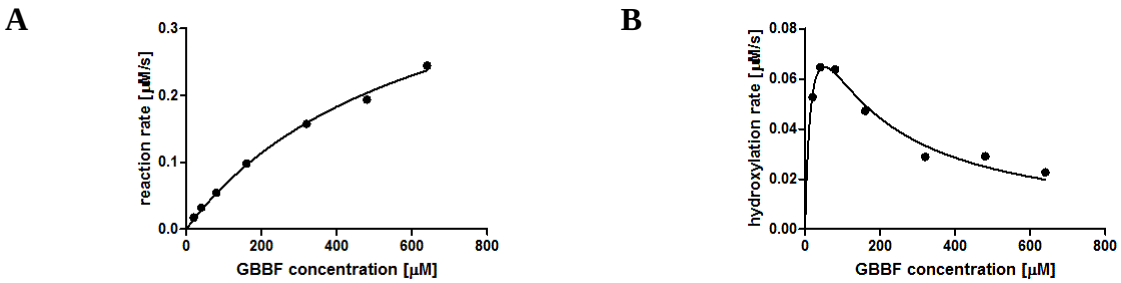

Figure 19 Dependence of initial reaction rate on the GBBF concentration for psBBOX (A) and hBBOX (B).

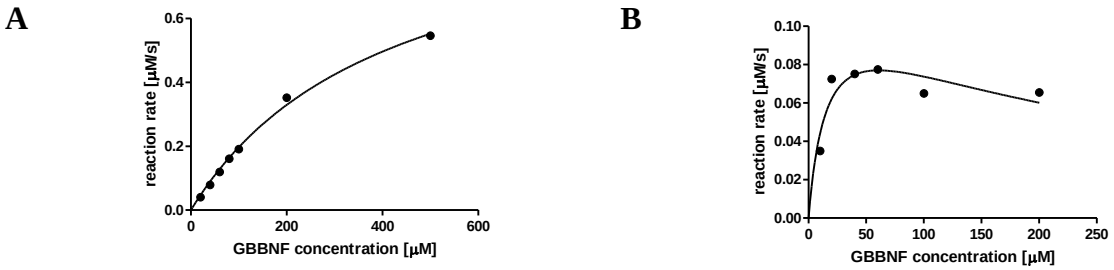

Figure 20 Dependence of initial reaction rate on the GBBNF concentration for psBBOX (A) and hBBOX (B).

6 Reaction with L- and D-carnitine

D-Carnitine (*S*-carnitine) is the enantiomer of physiologically active L-carnitine (*R*-carnitine). It is not produced in animals but some bacteria are able to synthesise and metabolize D-carnitine,[6] with the most common catabolic pathways involving carnitine racemase and carnitine dehydrogenase.[34,35] It was previously shown that human BBOX can hydroxylate D-carnitine to yield 3-keto-GBB[17] (Scheme 2), presumably via the same mechanism by which GBBF, is converted.[33] psBBOX was also able to oxidise D-carnitine in a similar fashion to the human enzyme, yielding the same set of products, as determined by ^{1}H NMR (i.e. 3-keto-GBB). D-Carnitine was a poor psBBOX substrate with the initial rate only at approximately 6% of the psBBOX catalysed GBB hydroxylation. A high level of uncoupled turnover was also observed (Table 7, Fig. 21). The rate of hydroxylation was comparable to that for GBBF (initial rate of 0.018 μM/s vs 0.028 μM/s for GBBF). D-Carnitine is a better substrate for hBBOX with the initial rate at a level of 42% of hBBOX catalysed GBB hydroxylation. The level of uncoupled 2OG turnover is similar to that measured for the psBBOX catalysed reaction.

L-Carnitine is the product of BBOX catalysed hydroxylation of GBB. It was previously demonstrated that human BBOX can further oxidise L-carnitine *in vitro* to yield its keto form, which then spontaneously decarboxylates to yield trimetylaminoacetone.[17] The proposed mechanism of GBB hydroxylation by BBOX consists of a hydrogen abstraction/oxygen insertion step[36]. The reaction is stereospecific and in a native form, this is ensured by positioning of a substrate in the active site, which enables only pro-(*R*) C-H bond cleavage.[33] However, in L-carnitine the pro-(*R*) position is occupied by a hydroxyl group, implying that L-carnitine has to adopt a different arrangement in the active site or that a different mechanism has to be employed for catalysis to take place. A similar observation was made with the fluorinated L-carnitine analogue, (*3R*)-fluoro-GBB, which was shown to slowly undergo hBBOX catalysed oxidation with subsequent fluoride release, yielding same products as (*3S*)-fluoro-GBB in the hBBOX catalysed reaction[33] (Chapter 2). It was found that L-carnitine was not a substrate for psBBOX under the tested reaction conditions (see Experimental section). However, it stimulates uncoupled 2OG turnover at a level of around 13% of the total 2OG turnover measured for native psBBOX catalysed GBB hydroxylation. L-Carnitine was a rather poor substrate for hBBOX with the initial rate at approximately 4% of hBBOX catalysed GBB hydroxylation. A large amount of uncoupled 2OG turnover was also observed, consistent with data obtained before.[17]

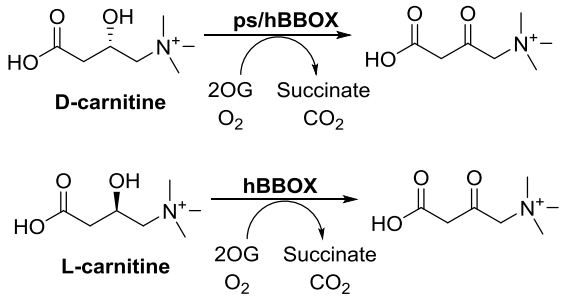

Scheme 2 BBOX catalysed D- and L-carnitine oxidation.

Table 7 Rates of D-carnitine hydroxylation by human and psBBOX.

Enzyme	Initial rate of hydroxylation [µM/s]	Initial rate of succinate formation [µM/s]	Ratio of succinate formation to hydroxylation
hBBOX	0.055	0.127	2.3
psBBOX	0.018	0.054	3.0

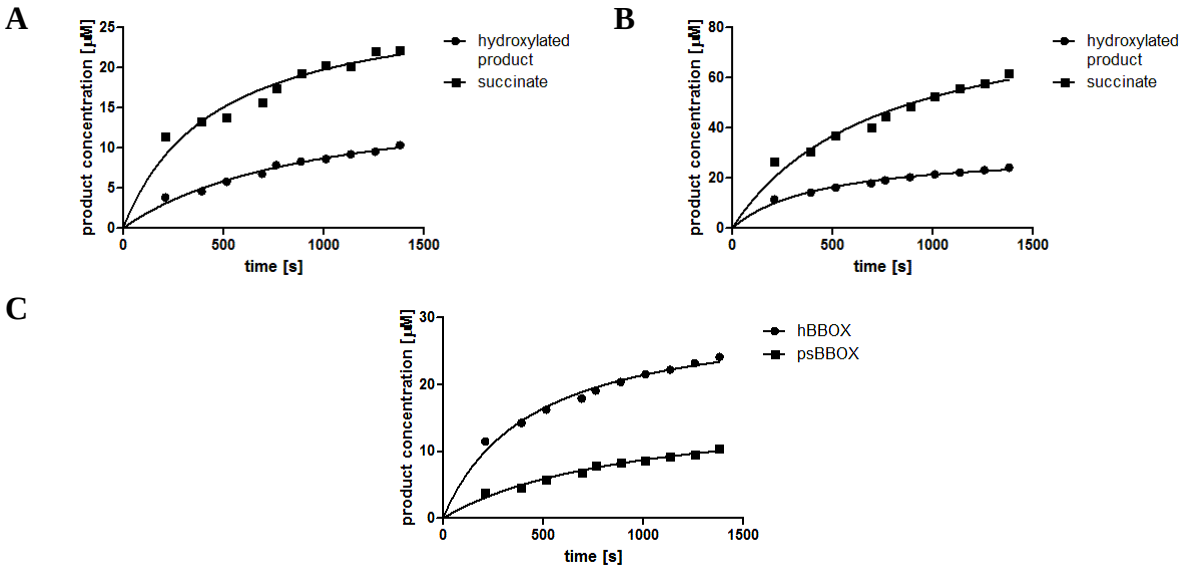

Figure 21 Time course of psBBOX (A) and hBBOX (B) catalysed reaction with D-carnitine as observed by oxo-GBB and succinate formation. Overlay of hBBOX and psBBOX catalysed GBB hydroxylation (C).

Table 8 Rates of L-carnitine hydroxylation by human and psBBOX.

enzyme	Initial rate of hydroxylation [µM/s]	Initial rate of succinate formation [µM/s]	Ratio of succinate formation to hydroxylation
BBOX	0.0048	0.0760	15.8
psBBOX	0	0.0440	-

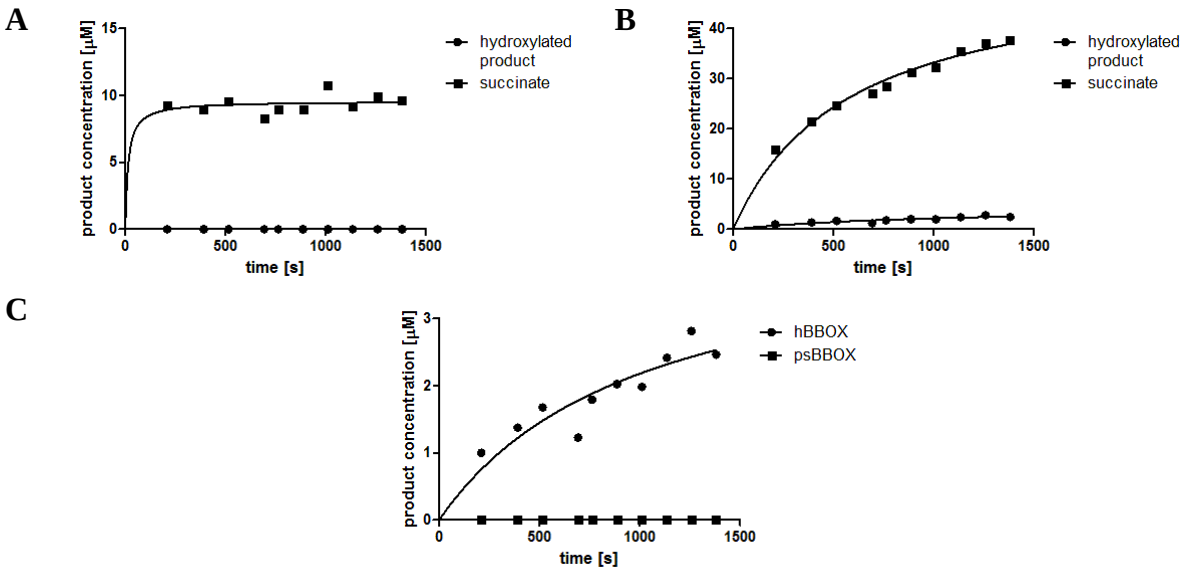

Figure 22 Time course of psBBOX (A) and hBBOX (B) catalysed reaction with L-carnitine as observed by oxo-GBB and succinate formation. Overlay of hBBOX and psBBOX catalysed GBB hydroxylation (C).

7 Alternative substrates

7.1 GBB analogues with different carbon chain lengths

Structural analogues of GBB have been reported to be substrates for hBBOX. 3-Trimethylaminopropionate (GBB-3) and 5-trimethylaminovalerate (GBB-5) were found to be hydroxylated by hBBOX at C-2 and C-3, respectively.[17] A similar experiment with psBBOX revealed that only GBB-5 was a substrate, being hydroxylated at C-3, the same as for hBBOX (assignments were made by ^{1}H and ^{1}H-^{13}C HSQC NMR spectra, Fig. 23). In the case of hBBOX, GBB-3 was a reasonably good and GBB-5 a fair substrate, with GBB-3 hydroxylated at 58% and GBB-5 at 12% of initial hydroxylation rate of GBB. Even though psBBOX did catalyse hyroxylation of GBB-5, it was found to be a poor substrate (1.4% of the initial hydroxylation rate compared to GBB). GBB-3 was not hydroxylated even when a high concentration of psBBOX was used (13 μM). Both GBB-5 and GBB-3 stimulated uncoupled 2OG turnover with psBBOX, which suggest that they, at least weakly, bind to the active site, however in a predominantly unproductive manner.

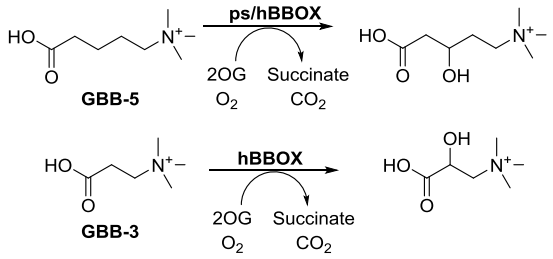

Scheme 3 BBOX catalysed GBB-5 and GBB-3 oxidation.

A

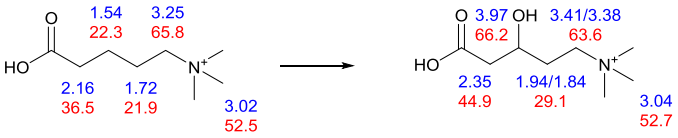

B

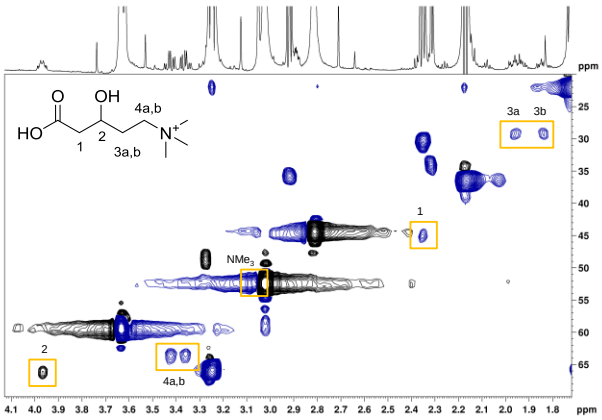

Figure 23 ^{1}H and ^{13}C NMR assignments of GBB-5 and its hydroxylation product (A). GBB-5 hydroxylation by psBBOX – ^{1}H-^{13}C HSQC NMR spectra of reaction mixture (B).

Table 9 Rates of GBB-5 and GBB-3 hydroxylation as catalysed by human and psBBOX.

Enzyme	Substrate	Initial rate of hydroxylation [µM/s]	Initial rate of succinate formation [µM/s]	Ratio of succinate formation to hydroxylation
hBBOX	GBB-5	0.016	0.029	1.8
	GBB-3	0.075	0.087	1.2
psBBOX	GBB-5	0.004	0.035	8.8
	GBB-3	0	0.036	-

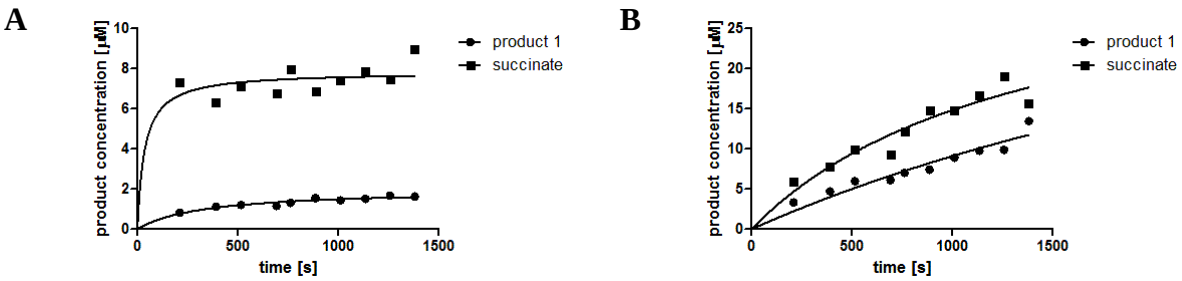

Figure 24 Time course of psBBOX (A) and hBBOX (B) catalysed reaction with GBB-5 as observed by hydroxylated product and succinate formation.

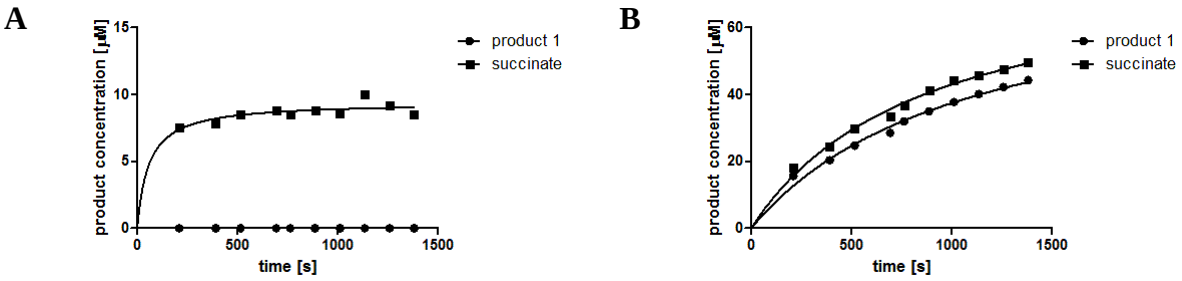

Figure 25 Time course of psBBOX (A) and hBBOX (B) catalysed reaction with GBB-3 as observed by hydroxylated product and succinate formation.

7.2 Amino acid hydroxylation

psBBOX was found to hydroxylate both (*R*) and (*S*) enantiomers of 2-amino-GBB (denoted as GBB-NH(R) and GBB-NH(S) respectively). This is the first example of BBOX catalysed α-amino acid hydroxylation. This process enables production of 1,2-aminoalcohols (as assigned by ^{1}H and ^{1}H-^{13}C HSQC NMR (Scheme 4, Fig. 26)). GBB-NH(S) and GBB-NH(R) where much poorer substrates for psBBOX compared to GBB (Table 10, Fig. 27), nevertheless full conversion to 1,2-aminoalcohol can be reached after prolonged reaction times. In contrast, hBBOX was not able to hydroxylate 2-substituted derivatives of GBB, which is consistent with crystallographic analyses demonstrating that the hBBOX GBB binding site may have less space to accommodate 2-susbtituted GBB analogues compared with psBBOX (Fig. 15).

Uncovering new synthetic routes to α,β-aminoacids is interesting, as this class of compounds presents a common motif in many biologically relevant systems including peptidyl motifs hydroxylated by other 2OG dependent oxygenases. Further engineering of BBOX could allow obtaining of broader range of β-hydroxylated amino acids to be used e.g. as standards in identification of products of enzyme catalysed hydroxylations or non-natural amino acids for incorporation into peptide structures.

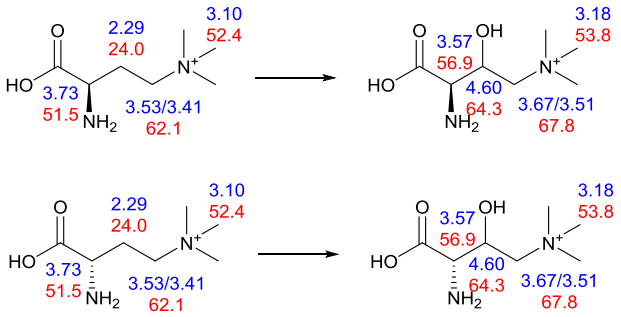

Scheme 4 ^{1}H (blue) and ^{13}C (red) NMR assignments of GBB-NH(R), GBB-NH(S) and substrates and their hydroxylation product at 280K.

A

B

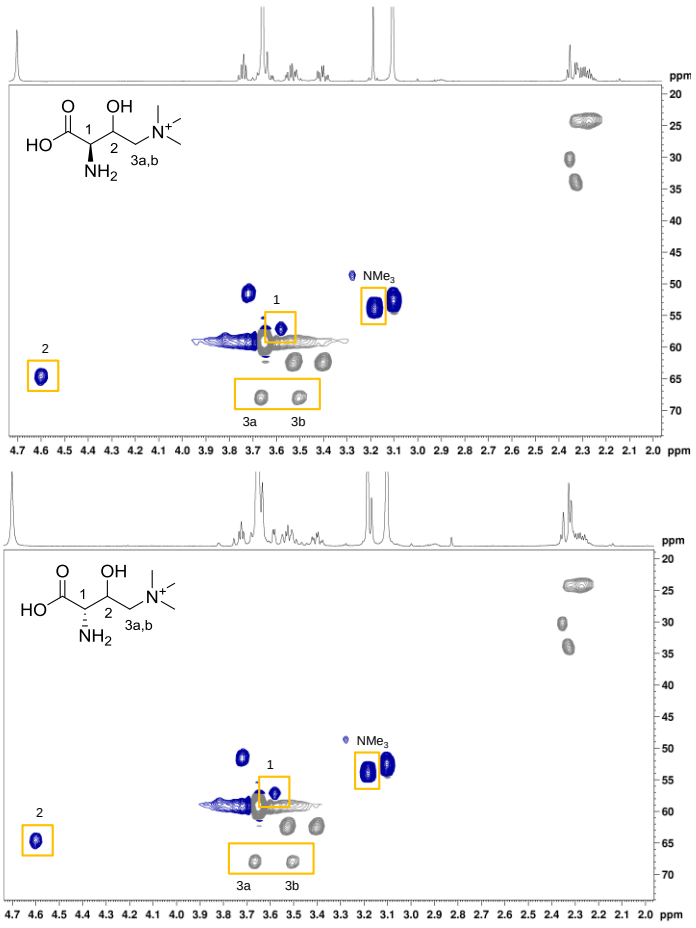

Figure 26 NMR assignments of GBB-NH(R) and GBB-NH(S) hydroxylation products. ^{1}H-^{13}C HSQC assignment of enzymatic reaction mixture containing hydroxylated (A) – GBB-NH(R), (B) – GBB-NH(S).

Table 10 Rates of GBB-NH(R) and GBB-NH(S) hydroxylation by psBBOX.

substrate	Initial rate of hydroxylation [µM/s]	Initial rate of succinate formation [µM/s]	Ratio of succinate formation to hydroxylation
GBB-NH(R)	0.006	0.032	5.3
GBB-NH(S)	0.006	0.018	3.0

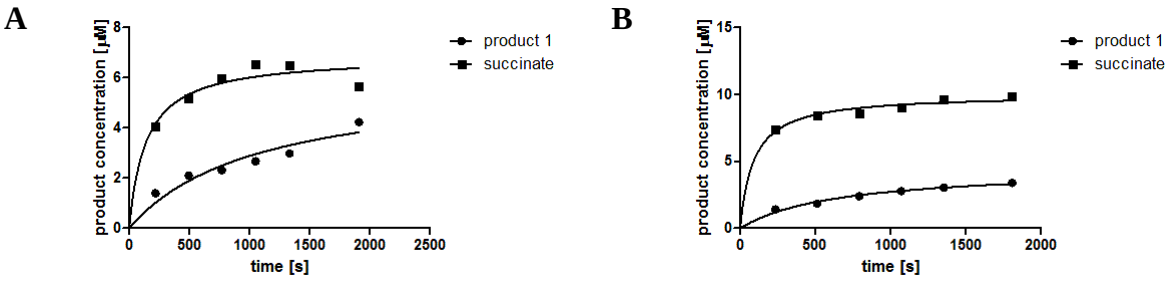

Figure 27 Time course of psBBOX catalysed hydroxylation of GBB-NH(S) (A) and GBB-NH(R) (B) as observed by hydroxylated product and succinate formation.

7.3 Synthesis of an anthopleurine analogue

Anthopleuirne is an alarm pheromone produced by sea anemone *Anthopleura elegantissima* in response to danger. Production of anthopleurine triggers the contraction of species being nearby wounded anemones[37]. Anthopleurine is a close structural analogue of GBB, dihydroxylated at C-2 and C-3, with the (2*R*, 3*S*) stereochemistry assigned[38] (Fig. 27). A few synthetic efforts towards anthopleurine were reported[38], including a cross-metathesis/dihydroxylation sequence[39].

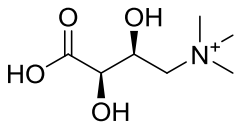

Figure 28 Structure of anthopleurine.

In the previous section, psBBOX catalysed hydroxylation of 2-amino GBB derivatives was discussed. In a similar manner it was found that vicinal diols can also be obtained using 2-hydroxy GBB as a substrate analogue. (*2S*)-hydroxy GBB (denoted as GBB-OH(S)) underwent psBBOX catalysed oxidation similarly to the amino GBB analogues (Scheme 5, Fig. 30). However, GBB-OH(S) was a much better substrate than the corresponding amino analogue with an 8 times higher initial rate of hydroxylation than GBB-NH and a lower level of uncoupling between hydroxylation and 2OG decarboxylation being observed (Table 11, Fig. 29). This is consistent with the reduced steric requirements of the hydroxyl compared to the amino group. However, the stereochemistry of hydroxylation of GBB-OH(S) was unassigned; the most likely stereochemical outcome of hydroxylation is consistent with that for GBB, where the pro-(*R*) hydrogen is abstracted (pro-(*S*) in

the case of GBB-OH(S), because of nomenclature differences), to yield (*2S*, *3S*)-diastereomer of anthopleurine. Judging from psBBOX catalysed hydroxylation of GBB-NH(R), (*2S*)-hydroxy-GBB should be hydroxylated similarly at C-3 in a similar manner to GBB-NH(R), yielding (*2S,3R*)-dihydroxy-GBB (anthopleurine). This work is under further investigation, however these initial studies demonstrate that BBOX is able to efficiently catalyse synthesis of anthopleuirne and raises the question of whether a similar enzyme could not be responsible for the biosynthesis of anthopleurine in sea anemone.

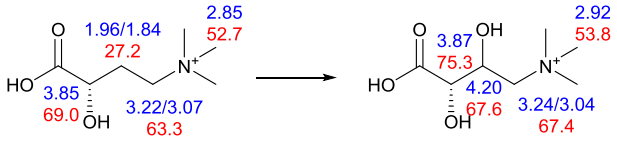

Scheme 5 ^{1}H (blue) and ^{13}C (red) NMR assignments of GBB-OH(S) and its hydroxylation product at 280K.

Table 11 Rate of GBB-OH(S) hydroxylation by psBBOX.

Substrate	Initial rate of hydroxylation [µM/s]	Initial rate of succinate formation [µM/s]	Ratio of succinate formation to hydroxylation
GBB-OH(S)	0.048	0.069	1.4

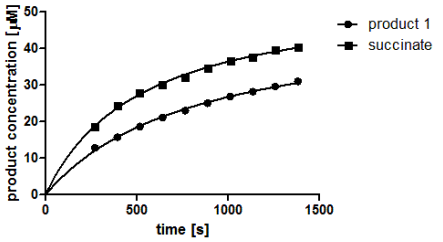

Figure 29 Time course of psBBOX catalysed hydroxylation of GBB-OH(S) as observed by hydroxylated product and succinate formation.

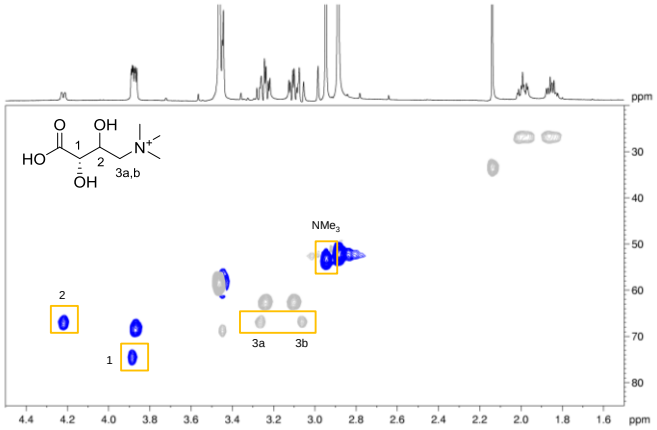

Figure 30 NMR assignments of GBB-OH(S) hydroxylation products. ^{1}H-^{13}C HSQC assignment of enzymatic reaction mixture containing hydroxylated GBB-OH(S).

7.4 Non-substrate GBB analogues

Several other GBB analogues were also screened by MS to determine if they could be hydroxylated by human or psBBOX. Analogues which underwent hydroxylation were discussed in the previous sections, however, non-substrate analogues are worth mentioning because this may give information of the size/flexibility of the active site. BBOX catalysis of GBB analogues with different carbon chain lengths is limited to 5 and 3 carbons (hBBOX being able to catalyse hydroxylation of both GBB-5 and GBB-3, psBBOX hydroxylating GBB-5 only). Neither hBBOX nor psBBOX were able to hydroxylate GBB analogues with a 2- or 6-carbon chain (GBB-2 and GBB-6, Scheme 5A). psBBOX was shown to hydroxylate 2-substituted GBB analogues (GBB-NH analogues) and one carbon longer GBB derivative (GBB-5). Therefore N^{ϵ}-trimethyl ornithine derivatives: (*S*)-TMO and (*R*)-TMO (Scheme 5B) were synthesized; however they were found not to be hydroxylated by either psBBOX nor hBBOX. GBB analogues without a free carboxylate, i.e. the GBB methyl ester (GBB-OMe) or the keto-GBB derivative (GBB-CH3) (Scheme 5C) were also found not to be substrates for either ps- nor hBBOX. Finally, the neurotransmitter acetylcholine and its structural analogues thioacetylcholine, carbachol and phosphocholine (Scheme 6), which were tested because of their similarity to the GBB structure, were not substrates for human nor psBBOX.

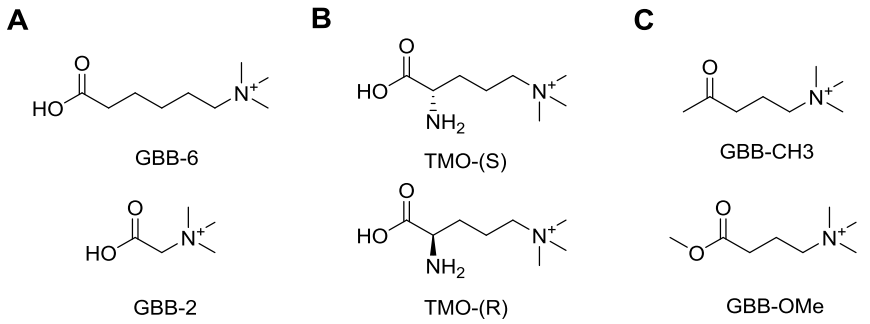

Scheme 6 Structures of GBB analogues, which were not susbtrates for psBBOX nor hBBOX.

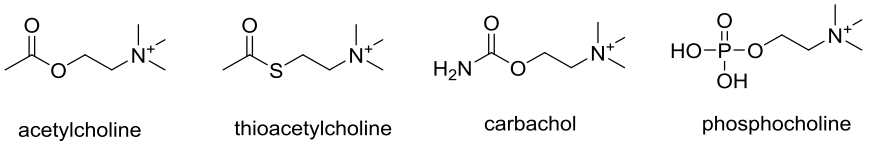

Scheme 7 Structures of acetylcholine derivatives.

8 Summary and perspective

psBBOX can be readily expressed in *E. coli*, is high yielding and a stable enzyme. psBBOX was shown to catalyse chemically interesting transformations, i.e. synthesis of 1,2-aminoalcohols and 1,2-diols, likely in a stereospecific manner. Betaines are somewhat understudied group of chemicals, probably because of difficulty in purification and low solubility in organic solvents. However, the effective preparation of optically pure quaternary ammonium salts could be of use in chemical industry (e.g. as phase transfer catalysts), antimicrobials or pharmaceuticals, where this functional group has not yet shown its full potential. In this chapter, similarities and differences between human and *Pseudomonas* BBOX homologues were studied. The results, especially in view of the tolerance of BBOX homologues towards different substrates, may be useful for engineering psBBOX to perform an even wider range of reactions. Further structural and kinetic studies on the psBBOX/ hBBOX system could aid in the elucidation of the role of ascorbate in 2OG oxygenase catalysis, as well as shed light on the role of KCl in hBBOX stabilisation. Finally, the good system for studies on substrate inhibition in hBBOX is presented, which hopefully will help in understanding the mechanistic basis of GBB inhibition phenomena, which likely regulates carnitine biosynthesis in human cells.

9 Acknowledgements

Human BBOX used in these studies was supplied by Dr. Grazyna T. Kochan (Structural Genomics Consortium, Oxford). I would like to thank Dr. Ivanhoe K.H. Leung (Department of Chemistry, University of Oxford) for useful discussions on NMR assignments of GBB analogues hydroxylation products and Dr. Nikita Loik (Department of Chemistry, University of Oxford) for his assistance and advice on the initial MS screen used in the search for BBOX substrates.

The work in this chapter was be published in an altered form:

A. M. Rydzik, I. K. H. Leung, G. T. Kochan, N. D. Loik, L. Henry, M. A. McDonough, T. D. W. Claridge, C. J. Schofield, Organic & Biomolecular Chemistry, DOI: 10.1039/c4ob01167h

10 Experimental section

10.1 NMR

NMR assays were performed on a Bruker AVIII 700 with an inverse TCI cryoprobe using 3 mm MATCH tubes. Pulses were calibrated using single-pulse nutation method (Bruker pulsecal routine). Water suppression was achieved using the excitation sculpting method.

10.1.1 Enzymatic assays

10.1.1.1 Reagents

Reagents were from Sigma-Aldrich. Tris-d_{11} was from Cambridge Isotopes. The standard solution of Tris-d_{11} buffer was 50 mM in H_2O, pH 7.5 and contained 0.1% NaN_3 to prevent microbial growth. 2OG was used as its sodium salt, ascorbate as its potassium salt, and GBB as its hydrochloride salt. Fe(II) stock solution was prepared by dissolving $Fe(NH_4)_2(SO_4)_2$ in 20 mM HCl to give a final concentration of 100 mM. The total reaction volume was 160 μL. Spectra were recorded 240 s after enzyme addition and the typical experiment length was 16 scans.

10.1.1.2 2OG kinetic parameters

2OG kinetic parameters were assigned by ^{1}H NMR using the following procedure. To a mixture containing 0.5 mM ascorbate, 0.2 M KCl, 0.1 mM GBB (in case of psBBOX)/ 0.04 mM GBB (hBBOX assays), 10% D_2O, the desired concentration of 2OG in 50 mM Tris-d_{11} pH 7.5, and a freshly prepared solution of the Fe(II) salt was added to final concentration of 0.05 mM. The reaction was then initiated by the addition of the enzyme to the reaction mixture to final concentration of 100 nM (psBBOX) or 50 nM (hBBOX).

10.1.1.3 GBB kinetic parameters

GBB kinetic parameters were assigned by ^{1}H NMR using the following procedure. To a mixture containing 0.5 mM ascorbate, 0.2 M KCl, 1 mM 2OG, 10% D_2O and the desired concentration of GBB in 50 mM Tris-d_{11} pH 7.5 a freshly prepared of solution of Fe(II) salt was added to a final concentration of 0.05 mM. The reaction was initiated by addition of enzyme to the reaction mixture to final concentration of 50 nM.

10.1.1.4 Uncoupled turnover assays

Uncoupled turnover assays used the following conditions: 0.5 mM 2OG, 0.5 mM ascorbate, 0.2 M KCl, 50 μM Fe, 10% D_2O in 50 mM Tris-d_{11} pH 7.5. The reaction was initiated by the addition of enzyme to a final concentration of 400 nM. A control with no enzyme added was performed to ensure there was no measurable non-enzymatic 2OG turnover in the assay conditions.

10.1.1.5 Ascorbate dependence assays

Ascorbate dependence assays used the following conditions: 0.5 mM 2OG, 0.1 mM GBB, 0.2 M KCl, 50 μM Fe, 0.5 mM or 0 mM ascorbate, 10% D_2O in 50 mM Tris-d_{11} pH 7.5. Reactions were initiated by the addition of enzyme to a final concentration of 400 nM.

10.1.1.6 KCl dependence assays

KCl dependence assays used the following conditions: 0.1 mM GBB, 0.5 mM 2OG, 0.5 mM ascorbate, the desired amount of KCl, 50 μM Fe, 10% D_2O in 50 mM Tris-d_{11} pH 7.5. Reactions were initiated by the addition of enzyme to a final concentration of 50 nM.

10.1.1.7 GBBF/GBBNF kinetic parameters

GBBF/GBBNF kinetic parameters were assigned by ^1H NMR using the following procedure. To a mixture containing 0.5 mM ascorbate, 0.2 M KCl, 1 mM 2OG, 10% D_2O and the desired concentration of GBBF/GBBNF in 50 mM Tris-d_{11} pH 7.5, was added a freshly prepared solution of Fe(II) salt (final concentration of 0.05 mM). The reaction was initiated by addition of enzyme to the reaction mixture to give a final concentration of 800 nM (for GBBF assays)/200 nM (psBBOX, GBBNF assays, 400 nM (hBBOX, GBBNF assays).

10.1.1.8 Time-course assays of GBB/ GBBF/ GBBNF hydroxylations

Time-course assays of GBB/GBBF/GBBNF hydroxylations were measured using the following conditions: 100 μM GBB analogue, 0.5 mM 2OG, 0.5 mM ascorbate, 0.2 M KCl, 50 μM Fe, 10% D_2O in 50 mM Tris-d_{11} pH 7.5. The reaction was initiated by addition of enzyme to final concentration of 400 nM.

10.1.1.9 Time-course assays of D- and L-carnitine hydroxylations

Time-course assays of D- and L-carnitine hydroxylations were measured using following conditions: 100 μM carnitine analogue, 0.5 mM 2OG, 0.5 mM ascorbate, 0.2 M KCl, 50 μM Fe, 10% D_2O in 50 mM Tris-d_{11} pH 7.5. Reaction was initiated by the addition of enzyme to a final concentration of 400 nM.

10.1.1.10 Time-course assays of other GBB analogues hydroxylations

Time-course assays of GBB-5, GBB-3, GBB-NH(R), GBB-NH(S) and GBB-OH(S) hydroxylations were measured using following conditions: 100 μM GBB analogue, 0.5 mM 2OG, 0.5 mM ascorbate, 0.2 M KCl, 50 μM Fe, 10% D_2O in 50 mM Tris-d_{11} pH 7.5. Reaction was initiated by addition of enzyme to final concentration of 400 nM.

10.1.1.11 NMR assignments

Assignment for GBB-5, GBB-NH(R), GBB-NH(S) and GBB-OH(S) hydroxylation products was done using 0.2 mM GBB-5, 0.5 mM 2OG, 0.2 M KCl, 50 μM Fe, in 50 mM Tris-d_{11} pH 7.5 in D_2O, using a 10 μM final concentration of psBBOX added in two portions with a 2 h interval in between additions. Assignment for GBB-NH(R), GBB-NH(S) and GBB-OH(S) was performed at 280 K.

10.2 MS screening

Initial screens for BBOX substrates were performed on a Waters LCT Premier Instrument, fitted with time of flight (ToF) analyser and employing Electron impact Chemical Ionisation. Samples were measured using direct injection (no column attached) and analysed for the presence of a +16 peak to the initial mass of a substrate.

Enzymatic assays were run in the following conditions: 100 µM substrate, 1 mM 2-oxoglutarate disodium salt, 100 µM Fe(II) ($Fe(NH_4)_2(SO_4)_2$ salt), solution prepared fresh before experiment from concentrated stock in 20 mM HCl), 200 mM KCl, 500 µM ascorbic acid sodium salt, 1 µM enzyme, buffer: 50 mM phosphate pH 7.0, final volume 200 µL. Each assay contained samples run with hBBOX, psBBOX and control with no enzyme added.

10.3 Modelling and alignments

10.3.1 Homology modelling

Homology modelling was done using the SWISS-MODEL server (available from the EXPASY website: http://swissmodel.expasy.org/), using an automatic alignment mode and the human BBOX structure with PDB id: 3O2G as a template. Template for homology modelling was chosen by user, sequence alignment was performed in the automatic mode, theoretical model was obtained with a QMEAN score of 0.62 (QMEAN score estimates model quality on the scale 0-1). Protein structures were visualised using PyMOL software.

10.3.2 Sequence alignments

Sequence alignments were done using the Clustal Omega program for multiple sequence alignment, accessible from EMBL-EBI servers (http://www.ebi.ac.uk/Tools/msa/clustalo/). Alignment was visualised using GeneDoc software.

10.4 Protein preparation

γ-Butyrobetaine hydroxylase from *Pseudomonas* sp. AK1 (gi 385463), was produced with the sequence below. The first N-terminal 17 residues (in bold) result from the vector encoding sequence.

MNHKVHHHHHHIEGRHMNAIADYRTFPLISPLASAASFASGVSVTWADGRVSPFHNLWL
RDNCPCGDCVYEVTREQVFLVADVPEDIQVQAVTIGDDGRLVVQWDDGHASAYHPGWLR
AHAYDAQSLAEREAARPHKHRWMQGLSLPVYDHGAVMQDDDTLLEWLLAVRDVGLTQL
HGVPTEPGALIPLAKRISFIRESNFGVLFDVRSKADADSNAYTAFNLPLHTDLPTRELQPGLQ
FLHCLVNDATGGNSTFVDGFAIAEALRIEAPAAYRLLCETPVEFRNKDRHSDYRCTAPVIAL
DSSGEVREIRLANFLRAPFQMDAQRMPDYYLAYRRFIQMTREPRFCFTRRLEAGQLWCFDN
RRVLHARDAFDPASGDRHFQGCYVDRDELLSRILVLQR

10.4.1 Size exclusion chromatography

Size exclusion chromatography was performed using a Superdex S200 (300 mL) column, which was equilibrated with 1CV of water and 1 CV gel filtration buffer (50 mM Tris-HCl pH 7.5, 200 mM NaCl) at flow rate of 2 mL/min. The protein solution was loaded using a 2 mL loop. Protein was eluted with gel filtration buffer and fractions were UV level was above 10 mAU (absorbance at 280 nm) were collected (5 mL each) and analysed by SDS-PAGE. The desired fractions were combined, concentrated if desired, aliquoted and stored at -80°C, unless further purification was required.

10.4.2 Ion exchange chromatography

Ion exchange chromatography was performed using a Source-Q exchange column using 25 mM Tris-HCl buffer pH 7.5 and gradient of 0-200 mM NaCl.

10.5 Data processing

NMR data were processed using TopSpin 3.1 software (Bruker). Kinetic analyses were carried out using GraphPad Prism software. The standard Michaelis-Menten model was used for most fits. Substrate inhibition was fitted with the built-in equation from GraphPad Prism: $Y=V_{max}*X/(K_M + X*(1+X/K_i))$, where V_{max} is the maximum enzyme velocity, if the substrate did not also inhibit enzyme activity, expressed in the same units as Y. K_M is the Michaelis-Menten constant, expressed in the same units as X. K_i is the dissociation constant for substrate binding in such a way that two substrates can bind to an enzyme. It is expressed in the same units as X. The equation is based on equation 5.44, in RA Copeland, *Enzymes*, 2nd edition, Wiley, 2000.

10.6 Synthesis

10.6.1 Reagents

General synthetic considerations were according to those described in the Synthesis section of Appendix 1. γ-Butyrobetaine, L-carnitine, D-carnitine, glycine betaine (GBB-2), 2-oxoglutarate, acetylcholine, thioacetylcholine, carbachol, phosphocholine and synthetic precursors were from Sigma-Aldrich. GBBF and GBBNF were synthesized as described in Chapter 2.

10.6.2 General procedure I

To a solution of corresponding bromide derivative in anhydrous acetonitrile (1 equiv.) a 4.2 M solution of trimethylamine in ethanol was added (1.5 equiv), then the mixture was stirred for 3 h, upon which a white precipitate formed. Solvents and trimethylamine were evaporated *in vacuo*. Residues was taken up in small volume of cold acetonitrile and solid was filtered off and dried under vacuum to yield the desired product as bromide salt.

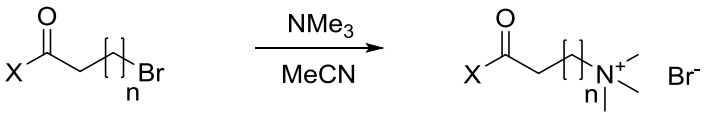

compound	n	X
GBB-3	1	H
GBB-5	3	H
GBB-6	4	H
GBB-OMe	2	OCH_3
GBB-CH3	2	CH_3

10.6.2.1 N^{β}-trimethyl-3-aminopropionic acid bromide (GBB-3)

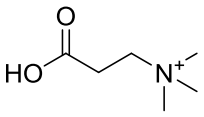

GBB-3 (125 mg, 0.6 mmol, 80%) was obtained as a white solid starting from 3-bromopropionic acid (100 mg, 0.66 mmol) and following the General Procedure I. ^{1}H NMR (400 MHz, D_2O) δ = 3.53 (t, *J*=7.5 Hz, 2 H), 3.04 (s, 9 H), 2.74 (tt, *J*=7.5, 1.5 Hz, 2 H) ppm, ^{13}C NMR (101 MHz, D_2O) δ = 174.9, 62.5, 52.9, 29.5 ppm. Mp = 170-172°C. HRMS (ESI-TOF) calcd for $C_6H_{14}NO_2^+$ [M^+]: 132.1019, found: 132.1023. FT-IR νmax (neat): 2950, 1704, 1489, 1386, 1256 cm^{-1}.

10.6.2.2 N^{δ}-trimethyl-5-aminopentanoic acid bromide (GBB-5)

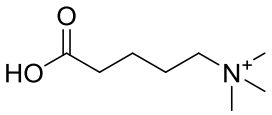

GBB-5 (105 mg, 0.40 mmol, 88%) was obtained as a white solid starting from 5-bromopentanoic acid (100 mg, 0.50 mmol) and following the General Procedure I. ^{1}H NMR (400 MHz, D_2O) δ = 3.20 - 3.29 (m, 2 H), 3.01 (s, 10 H), 2.37 (t, *J*=7.0 Hz, 2 H), 1.73 (d, *J*=8.0 Hz, 2 H), 1.49 - 1.63 (m, 2 H) ppm, ^{13}C NMR (101 MHz, D_2O) δ = 178.0, 66.1, 52.8, 44.7, 33.0, 21.8, 21.0 ppm. Mp = 160-162°C. HRMS (ESI-TOF) calcd for $C_8H_{18}NO_2^+$ [M^+]: 160.1332, found: 160.1336. FT-IR νmax (neat): 2955, 2472, 2160, 1709, 1401, 1167 cm^{-1}.

10.6.2.3 N^{ε}-trimethyl-6-aminohexanoic acid bromide (GBB-6)

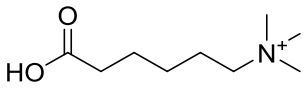

GBB-6 (105 mg, 0.40 mmol, 78%) was obtained as a white solid starting from 5-bromohexanoic acid (100 mg, 0.50 mmol) and following the General Procedure I. ^{1}H NMR (400 MHz, D_2O) δ = 3.16 - 3.26 (m, 2 H), 3.00 (s, 9 H), 2.31 (t, *J*=7.5 Hz, 2 H), 1.71 (dt, *J*=8.0, 4.0 Hz, 2 H), 1.49 - 1.62 (m, 2 H), 1.24 - 1.36 (m, 2 H) ppm, ^{13}C NMR (101 MHz, D_2O) δ = 178.8, 66.4, 52.8, 33.5, 24.9, 23.7, 22.0 ppm. Mp = 177-179°C. HRMS (ESI-TOF) calcd for $C_9H_{20}NO_2^+$ [M^+]: 174.1489, found: 174.1492. FT-IR νmax (neat): 2910, 1720, 1483, 1396, 1174 cm^{-1}.

10.6.2.4 N^{ε}-trimethyl-4-aminobutanoic acid methyl ester bromide (GBB-OMe)

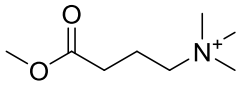

GBB-OMe (60 mg, 0.40 mmol, 75%) was obtained as a white solid starting from 4-bromobutanoic acid methyl ester (50 mg, 0.50 mmol) and following the General Procedure I. ^{1}H NMR (400 MHz, D_2O) δ = 3.59 (s, 3 H), 3.19 - 3.30 (m, 2 H), 3.02 (s, 9 H), 2.40 (t, *J*=7.0 Hz, 2 H), 1.91 - 2.06 (m, 2 H) ppm, ^{13}C NMR (101 MHz, D_2O) δ = 175.0, 65.3, 52.8, 52.3, 29.9, 17.8 ppm. Mp = 75-77°C. HRMS (ESI-TOF) calcd for $C_8H_{18}NO_2^+$ [M^+]: 160.1332, found: 160.1330. FT-IR νmax (neat): 1736, 1480, 1380, 1193 cm^{-1}.

10.6.2.5 N^{ε}-trimethyl-4-amino-2-oxopentane bromide (GBB-CH3)

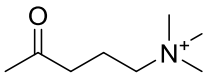

GBB-OMe (54 mg, 0.20 mmol, 80%) was obtained as a white hygroscopic solid following the general procedure I, starting from 4-bromo-2-oxopentane (50 mg, 0.30 mmol), which was prepared from α-acetylbytyrolactone according to literature procedure[40]. ^{1}H NMR (400 MHz, D_2O) δ = 3.19 - 3.27 (m, 2 H), 3.05 (s, 9 H), 2.64 (t, *J*=7.0 Hz, 2 H), 2.14 (s, 3 H), 1.88 - 1.99 (m, 2 H) ppm, ^{13}C NMR (101 MHz, D_2O) δ = 213.2, 65.4, 65.4, 52.8, 38.9, 29.2, 16.6 ppm. Mp = 97-99°C. HRMS (ESI-TOF) calcd for $C_8H_{18}NO^+$ [M^+]: 144.1383, found: 144.1382. FT-IR νmax (neat): 1708, 1484, 1362, 1174 cm^{-1}.

10.6.3 General Procedure II

The appropriate *N*-Boc amino derivative (1 equiv.) was dissolved in methanol (5 mL) along with K_2CO_3 (4 equiv.), treated with an excess of iodomethane (5 equiv.) and stirred at room temperature for 24 h. The methanol was evaporated, and resultant residue dissolved in water (1 mL) and acidified with concentrated HCl. The mixture was stirred for 1 h and then washed with diethyl ether. Water was then evaporated *in vacuo* and resultant residue was purified by HPLC (preparative C-18 reverse phase column; gradient: 50% B in 15 min, where A – water, 0.05% formic acid, B – acetonitrile, 0.1% formic acid; fractions containing product identified using Evaporative Light Scattering Detection (ELSD). The desired fractions were combined and freeze-dried to yield the product as a highly hygroscopic solid. Due to low level of compound recovery after HPLC purification, some of the assays used crude products if pure by ^{1}H NMR (which contained compound and KCl mixture, concentration of organic sample was determined by ^{1}H NMR). Due to small amounts of purified product IR spectra and optical rotation values are not reported. Melting points are not given due to highly hygroscopic nature of obtained material.

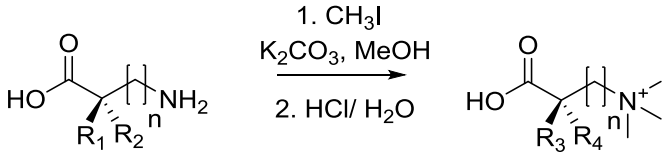

compound	n	R_1	R_2	R_3	R_4
GBB-NH(S)	2	H	NHBoc	H	NH_2
GBB-NH(R)	2	NHBoc	H	NH_2	H
TMO-(S)	3	H	NHBoc	H	NH_2
TMO-(R)	3	NHBoc	H	NH_2	H
GBB-OH(S)	2	H	OH	H	OH

10.6.3.1 Nγ-trimethyl-(S)-2,4-diaminobutanoic acid (GBB-NH(S))

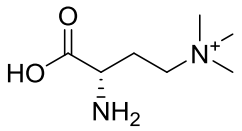

GBB-NH(S) trifluoroacetic acid (TFA) salt (6 mg, 0.022 mmol, 10%) was obtained starting from (*S*)-4-amino-2-((tert-butoxycarbonyl)amino)butanoic acid (50 mg, 0.23 mmol) and following the general procedure 2. ^{1}H NMR (700 MHz, D_2O) δ = 3.81 (t, *J*=6.5 Hz, 1 H), 3.55 (td, *J* = 12.5, 4.5 Hz, 1 H), 3.41 (td, *J* = 12.5, 4.5 Hz, 1 H), 3.10 (s, 9 H), 2.25 - 2.38 (m, 2 H) ppm, ^{13}C NMR (126 MHz, D_2O) δ = 172.1, 62.6, 53.0, 51.5, 24.1 ppm. HRMS (ESI-TOF) calcd for $C_7H_{17}N_2O_2^+$ [M^+]: 161.1285, found: 161.1283.

10.6.3.2 Nγ-trimethyl-(R)-2,4-diaminobutanoic acid (GBB-NH(R))

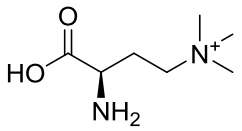

GBB-NH(R) TFA salt (5.0 mg, 0.018 mmol, 8%) was obtained starting from (*R*)-4-amino-2-((tert-butoxycarbonyl)amino)butanoic acid (50 mg, 0.23 mmol) and following the general procedure 2. ^{1}H NMR (700 MHz, D_2O) δ = 3.81 (t, *J*=6.5 Hz, 1 H), 3.55 (td, *J* = 12.5, 4.5 Hz, 1 H), 3.41 (td, *J* = 12.5, 4.5 Hz, 1 H), 3.10 (s, 9 H), 2.25 - 2.38 (m, 2 H) ppm, ^{13}C NMR (126 MHz, D_2O) δ = 172.1, 62.6, 53.0, 51.5, 24.1 ppm. HRMS (ESI-TOF) calcd for $C_7H_{17}N_2O_2^+$ [M^+]: 161.1285, found: 161.1283.

10.6.3.3 Nδ-trimethyl-(S)-2,5-diaminopentanoic acid (TMO-(S), Nε-trimethylamino-(S)-ornithine)

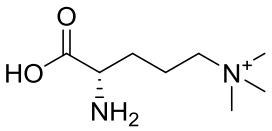

TMO-(S) trifluoroacetic acid (TFA) salt (7 mg, 0.025 mmol, 11%) was obtained starting from (*S*)-5-amino-2-((tert-butoxycarbonyl)amino)pentanoic acid (50 mg, 0.22 mmol) and following the general procedure 2. ^{1}H NMR (700 MHz, D_2O) δ = 4.05 (t, *J* = 6.0 Hz, 1 H), 3.36 (t, *J* = 8.0, 2 H), 3.09 (s, 9 H), 1.86 - 2.04 ppm, ^{13}C NMR (101 MHz, D_2O) δ = 171.8, 65.4, 53.1, 38.8, 26.6, 18.7 ppm. HRMS (ESI-TOF) calcd for $C_8H_{19}N_2O_2^+$ [M^+]: 175.1441, found: 175.1448.

10.6.3.4 Nδ-trimethyl-(R)-2,5-diaminopentanoic acid (TMO-(R), Nε-trimethylamino-(R)-ornithine)

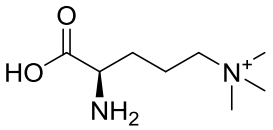

TMO-(R) trifluoroacetic acid (TFA) salt (7 mg, 0.025 mmol, 11%) was obtained starting from (*S*)-5-amino-2-((tert-butoxycarbonyl)amino)pentanoic acid (50 mg, 0.22 mmol) and following the general procedure 2. ^{1}H NMR (700 MHz, D_2O) δ = 4.05 (t, *J* = 6.0 Hz, 1 H), 3.36 (t, *J* = 8.0, 2 H), 3.09 (s, 9 H), 1.86 - 2.04 ppm, ^{13}C NMR (101 MHz, D_2O) δ = 171.8, 65.4, 53.1, 38.8, 26.6, 18.7 ppm. HRMS (ESI-TOF) calcd for $C_8H_{19}N_2O_2^+$ [M^+]: 175.1441, found: 175.1434.

10.6.3.5 Nγ-trimethyl-(S)-4-amino-2-hydroxybutanoic acid (GBB-OH(S))

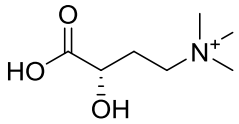

GBB-OH(S) was obtained starting from 4-amino-2-hydroxybutanoic acid hydrochloride and following the general procedure 2. ^{1}H NMR (400 MHz, D_2O) δ = 4.09 (dd, *J* = 7.3, 4.2 Hz, 1 H), 3.40 - 3.52 (m, 1 H), 3.27 - 3.38 (m, 1 H), 3.11 (s, 10 H), 2.21 (tt, *J* = 12.6, 4.4 Hz, 1 H), 2.06 (tdd, *J* = 12.5, 12.5, 7.2, 5.1 Hz, 1 H) ppm, ^{13}C NMR (101 MHz, D_2O) δ = 179.5, 69.3, 63.6, 53.2, 27.8 ppm. HRMS (ESI-TOF) calcd for $C_8H_{18}NO_2^+$ [M^+]: 162.1125, found: 162.1125.

References

1. Bremer, J. Carnitine--metabolism and functions. *Physiological Reviews* **63**, 1420-80 (1983).
2. Hoppel, C. The role of carnitine in normal and altered fatty acid metabolism. *American Journal of Kidney Disease* **41**, S4-12 (2003).
3. Kerner, J. & Hoppel, C. Fatty acid import into mitochondria. *Biochimica et Biophysica Acta* **1486**, 1-17 (2000).
4. Jung, H., Jung, K. & Kleber, H.P. L-carnitine metabolization and osmotic stress response in Escherichia coli. *Journal of Basic Microbiology* **30**, 409-13 (1990).
5. Emaus, R.K. & Bieber, L.L. A biosynthetic role for carnitine in the yeast Torulopsis bovina. *Journal of Biological Chemistry* **258**, 13160-5 (1983).
6. Kleber, H.P. Bacterial carnitine metabolism. *FEMS Microbiol Lett* **147**, 1-9 (1997).
7. Rebouche, C.J. & Seim, H. Carnitine metabolism and its regulation in microorganisms and mammals. Vol. 18 39-61 (1998).
8. Vaz, F.M. & Wanders, R.J. Carnitine biosynthesis in mammals. *Biochemical Journal* **361**, 417-29 (2002).
9. Strijbis, K., Vaz, F.M. & Distel, B. Enzymology of the carnitine biosynthesis pathway. *IUBMB Life* **62**, 357-62 (2010).
10. Lindstedt, G., Lindstedt, S., Midtvedt, T. & Tofft, M. The Formation and Degradation of Carnitine in Pseudomonas*. *Biochemistry* **6**, 1262-1270 (1967).
11. Lindstedt, G., Lindstedt, S. & Tofft, M. Gamma-butyrobetaine hydroxylase from Pseudomonas sp AK 1. *Biochemistry* **9**, 4336-42 (1970).
12. Lindstedt, G., Lindstedt, S. & Nordin, I. Purification and properties of gamma-butyrobetaine hydroxylase from Pseudomonas sp AK 1. *Biochemistry* **16**, 2181-8 (1977).
13. Ruetschi, U., Nordin, I., Odelhog, B., Jornvall, H. & Lindstedt, S. gamma-Butyrobetaine hydroxylase. Structural characterization of the Pseudomonas enzyme. *European Journal of Biochemistry* **213**, 1075-80 (1993).
14. Bernal, V., Sevilla, A., Canovas, M. & Iborra, J.L. Production of L-carnitine by secondary metabolism of bacteria. *Microb Cell Fact* **6**, 31 (2007).
15. Arense, P., Bernal, V., Charlier, D., Iborra, J.L., Foulquie-Moreno, M.R. & Canovas, M. Metabolic engineering for high yielding L(-)-carnitine production in Escherichia coli. *Microb Cell Fact* **12**, 56 (2013).
16. Ng, S.F., Hanauske-Abel, H.M. & Englard, S. Cosubstrate binding site of Pseudomonas sp. AK1 gamma-butyrobetaine hydroxylase. Interactions with structural analogs of alpha-ketoglutarate. *Journal of Biological Chemistry* **266**, 1526-33 (1991).
17. Leung, I.K.H., Krojer, T.J., Kochan, G.T., Henry, L., von Delft, F., Claridge, T.D.W., Oppermann, U., McDonough, M.A. & Schofield, C.J. Structural and Mechanistic Studies on gamma-Butyrobetaine Hydroxylase. *Chemistry & Biology* **17**, 1316-1324 (2010).
18. McDonough, M.A., Loenarz, C., Chowdhury, R., Clifton, I.J. & Schofield, C.J. Structural studies on human 2-oxoglutarate dependent oxygenases. *Current Opinion in Structural Biology* **20**, 659-672 (2010).
19. Arnold, K., Bordoli, L., Kopp, J. & Schwede, T. The SWISS-MODEL workspace: a web-based environment for protein structure homology modelling. *Bioinformatics* **22**, 195-201 (2006).
20. Kiefer, F., Arnold, K., Kunzli, M., Bordoli, L. & Schwede, T. The SWISS-MODEL Repository and associated resources. *Nucleic Acids Research* **37**, D387-92 (2009).
21. Peitsch, M.C. Protein Modeling by E-mail. *Nature Biotechnology* **13**, 658-660 (1995).
22. Hausinger, R.P. Fe(II)/α-ketoglutarate-dependent hydroxylases and related enzymes. *Critical Reviews in Biochemistry and Molecular Biology* **39**, 21-68 (2004).
23. Flashman, E., Davies, S.L., Yeoh, K.K. & Schofield, C.J. Investigating the dependence of the hypoxia-inducible factor hydroxylases (factor inhibiting HIF and prolyl hydroxylase domain 2) on ascorbate and other reducing agents. *Biochemical Journal* **427**, 135-142 (2010).

24. Prescott, A.G. & Lloyd, M.D. The iron(II) and 2-oxoacid-dependent dioxygenases and their role in metabolism. *Natural Product Reports* **17**, 367-383 (2000).
25. Costas, M., Mehn, M.P., Jensen, M.P. & Que, L. Dioxygen Activation at Mononuclear Nonheme Iron Active Sites: Enzymes, Models, and Intermediates. *Chemical Reviews* **104**, 939-986 (2004).
26. Hewitson, K.S., Granatino, N., Welford, R.W.D., McDonough, M.A. & Schofield, C.J. Oxidation by 2-oxoglutarate oxygenases: non-haem iron systems in catalysis and signalling. *Philosophical Transactions of the Royal Society A: Mathematical, Physical and Engineering Sciences* **363**, 807-828 (2005).
27. Myllylä, R., Kuutti-Savolainen, E.-R. & Kivirikko, K.I. The role of ascorbate in the prolyl hydroxylase reaction. *Biochemical and Biophysical Research Communications* **83**, 441-448 (1978).
28. Schofield, C.J. & Zhang, Z. Structural and mechanistic studies on 2-oxoglutarate-dependent oxygenases and related enzymes. *Current Opinion in Structural Biology* **9**, 722-731 (1999).
29. Rebouche, C.J. Ascorbic acid and carnitine biosynthesis. *American Journal of Clinical Nutrition* **54**, 1147S-1152S (1991).
30. Englard, S. & Seifter, S. The biochemical functions of ascorbic acid. *Annual Review of Nutrition* **6**, 365-406 (1986).
31. Lindstedt, G., Lindstedt, S. & Nordin, I. Gamma-butyrobetaine hydroxylase in human kidney. *Scand J Clin Lab Invest* **42**, 477-85 (1982).
32. Lindstedt, G. Effect of metal ions on the hydroxylation of gamma-butyrobetaine to carnitine in rat liver homogenates. *Biochimica et Biophysica Acta* **141**, 492-8 (1967).
33. Rydzik, A.M., Leung, I.K.H., Kochan, G.T., Thalhammer, A., Oppermann, U., Claridge, T.D.W. & Schofield, C.J. Development and Application of a Fluoride-Detection-Based Fluorescence Assay for gamma-Butyrobetaine Hydroxylase. *Chembiochem* **13**, 1559-1563 (2012).
34. Mönnich, K., Hanschmann, H. & Kleber, H.-P. Utilization of d-carnitine by Pseudomonas sp. AK 1. *FEMS Microbiology Letters* **132**, 51-55 (1995).
35. Hanschmann, H. & Kleber, H.-P. Conversion of D-carnitine into L-carnitine with stereospecific carnitine dehydrogenases. *Biotechnology Letters* **19**, 679-682 (1997).
36. Englard, S., Blanchard, J.S. & Midelfort, C.F. Gamma-butyrobetaine hydroxylase: stereochemical course of the hydroxylation reaction. *Biochemistry* **24**, 1110-6 (1985).
37. Howe, N.R. & Sheikh, Y.M. Anthopleurine: a sea anemone alarm pheromone. *Science* **189**, 386-8 (1975).
38. Musich, J.A. & Rapoport, H. Synthesis of anthopleurine, the alarm pheromone from Anthopleura elegantissima. *Journal of the American Chemical Society* **100**, 4865-4872 (1978).
39. Neisius, N.M. & Plietker, B. Diastereoselective Ru-catalyzed cross-metathesis-dihydroxylation sequence. an efficient approach toward enantiomerically enriched syn-diols. *Journal of Organic Chemistry* **73**, 3218-27 (2008).
40. Miller, D.J., Yu, F., Knight, D.W. & Allemann, R.K. 6- and 14-Fluoro farnesyl diphosphate: mechanistic probes for the reaction catalysed by aristolochene synthase. *Organic and Biomolecular Chemistry* **7**, 962-75 (2009).

Appendix 1

Materials and Methods

Contents

1 Molecular Biology

1.1 General

1.1.1 Reagents

Reagents were obtained from Sigma-Aldrich, Stratagene, New England Biolabs, Invitrogen, Bio-Rad or Roche unless stated otherwise. Purified (Milli-Q) water used for experiments was from a Millipore Elix® Reverse Osmosis system which was further purified by a Millipore Milli-Q® Synthesis system with a 0.22 μm filter on the outlet.

1.2 Microbiology

Work involving bacterial strains was carried out following standard sterile practices, employing either open flame or Heraeus laminar flow hood. Media and plasticware were sterilized by autoclaving at 121 °C for 20 min. Solutions of IPTG, antibiotic etc. were sterilized using 0.2 μm filters (Minisart®, Sartorious Stedim).

1.2.1 Bacterial cultures

Bacterial plate cultures were prepared in petri dishes with LB media containing 2% (w/v) agar with the appropriate antibiotic. Standard procedure involved incubation of plate overnight in 37°C. Plates were stored at 4°C if desired.

Liquid cultures were prepared using 2TY medium and appropriate antibiotic either in 500 mL conical flasks (100 mL cultures) or in 50 mL falcon tubes (10 mL cultures). Following inoculation by single bacterial colony from plate or glycerol stock cultures were incubated overnight at 37°C with shaking (200 rpm). Large scale growths were performed in 2 L conical flasks containing 600 mL 2TY media supplemented with appropriate antibiotic, with shaking (100 rpm). Growth was initiated by addition of 6 mL of small starter culture prepared night before.

Optical density readings were taken at 600 nm using a Novaspec® II spectrophotometer (Pharmacia) in 1 ml cuvettes and referenced to the growth media at zero time.

1.2.2 Growth media

All media were autoclaved at 121 °C for 20 min before use. LB (Luria-Bertani) medium contained 10g Bacto tryptone, 5g Yeast extracts, 10g NaCl, 15g Agar per liter. 2TY (2x Tryptone/Yeast) medium contained: 16 g Bacto tryptone, 10g Yeast extracts, 5g NaCl. SOC media contained: 2TY media supplemented with 10 mL of 1M $MgCl_2$ and 20 mL of 2M glucose solutions per liter of media.

1.2.3 Bacterial strains

E. coli strains used:

BL21(DE3): F^- *ompT hsd*S_B ($r_B^- m_B^-$) *gal dcm* (DE3).

XL1(Blue): recA1 endA1 gyrA96 thi-1 hsdR17 supE44 relA1 lac [F'proAB lacI^{q}Z□M15 Tn10(Tet^{r})]

XL10 (Gold): Tet^{r} D(mcrA)183 D(mcrCB-hsdSMR-mrr)173 endA1 supE44 thi-1 recA1 gyrA96 relA1 lac The [F' proAB lacIqZDM15 Tn10 (Tet^{r}) Amy Cam^{r}].

1.2.4 Competent cells

Competent cells were either from Stratagene or prepared following protocol: 100 mL of 2TY media was inoculated with 0.2 mL of overnight starter culture and grown to OD_{600} 0.6-0.8 with shaking (220 rpm, 37°C). Cells were centrifuged at 750 x g, 4°C for 5 minutes, gently resuspended in 50 mL sterile 100 mM $CaCl_2$/20% (v/v) glycerol solution and incubated on ice for 20 min prior to another centrifugation at 750 x g, 4°C for 5 minutes. Cell pellets were resuspended in 2 mL of 100 mM $CaCl_2$/20% (v/v) glycerol solution, aliquoted into sterile Eppendorf vials and stored immediately at -80°C.

1.2.5 Antibiotics

Final concentrations of antibiotics unless indicated otherwise were: ampicillin, 50 μg/ml; kanamycin 30 μg/ml, chloramphenicol 50 μg/ml.

1.2.6 Cell lysis

Cell pellets were collected by centrifugation and frozen overnight in -80°C. Frozen cell pellet was weight out and resuspended in 5× weight of His column binding buffer (section 1.6) with addition of protease inhibitor cocktail tablet (Roche) and 0.5 mg of DNAse I. Cells were kept on ice and lysed by sonication (in a sequence of 10 sec bursts followed by 10 sec break for 10 min in total) using a Vibra Cell VCX 500 with a 13 mm probe. Cell suspension was centrifuged at 14,000 rpm for 20 minutes at 4°C and the supernatant was decanted from the resulting pellet. The supernatant was then filtered using a 0.4 μM Omnipore™ filter (Millipore U.K.).

Small scale lysis (e.g. expression trials growths) was performed on Soniprep 150 sonicator (Sanyo) at an amplitude of 10 microns and micro-centrifuged at room temperature for 10 minutes.

1.2.7 Transformations

Competent cells (30 μl) were thawed on ice prior to addition of 2 μl of plasmid DNA. Mixture was incubated on ice for 30 minutes and then placed in the 42°C water bath for 30 sec or 45 sec. Cells were incubated on ice for further 2 min and then preheated to 37°C SOC medium (0.5 mL) was added. Mixture was stirred gently and incubated in 37°C water bath for an hour and then 0.1 mL of mixture was streaked on the agar plate containing appropriate antibiotic. Plates were inverted and incubated at 37°C overnight.

Transformations for co-expressions were carried out in an analogous way with 2 µl of each plasmid DNA mixed into competent cell suspension. Colonies were selected on agar plates containing mixture of appropriate antibiotics (co-transformed plasmids bear different antibiotic resistance genes).

1.2.8 Glycerol stocks

Glycerol stock of bacterial cell cultures was prepared by the addition of 75% (v/v) glycerol (250µL) to cell culture (650µL), with gentle mixing. The glycerol stocks were stored at -80°C.

1.3 DNA purification and quantification

DNA purification was done using DNA purification kit (Quiagen). DNA concentration was measured using a NanoDropR ND-1000 spectrometer (absorbance at 260 nm). A 260/280 nm absorbance ratio was calculated as purity reference (at 280 nM single stranded DNA/ RNA and proteins absorb)

1.4 Cloning

1.4.1 Plasmids

pCOLD I plasmid and Chaperone Plasmid Set were from Takara Bio. pET28a(+) plasmid was from Novagen.

1.4.2 Genes

psBBOX gene was obtained from Life Technologies GeneArt gene synthesis services supplied as constructs in p-MA-T vector, cloned on NdeI and BamHI restriction sites. pFASTbac vector containing human BBOX gene was obtained from Dr Grażyna Kochan (SGC, Oxford).

1.5 Sequencing

Sequencing was performed by Geneservice Ltd., Department of Biochemistry, University of Oxford. Constructs under T7 promoter were sequenced using standard T7 primers:
T7 forward: 5'- TAATACGACTCACTATAGGG -3'
T7 reverse: 5'- GCTAGTTATTGCTCAGCGG -3'
pCOLDI constructs were sequence using plasmids recommended by manufacturer:
pCOLDI forward: 5'-ACGCCATATCGCCGAAAGG
pCOLDI reverse: 5'-GGCAGGGATCTTAGATTCTG

1.6 Agarose gels

DNA samples were analysed employing horizontal agarose gel electrophoresis. Gels were prepared by boiling 1.5% agarose in TAE buffer (40 mM Tris-HCl, 20 mM acetic acid, 1 mM EDTA, pH adjusted to 8.3). Sybr Safe DNA gel stain (Invitrogen) was added before gel casting (1/10000 v/v)

into gel tray up to 0.7 cm depth. Comb was inserted and gel was allowed to solidify at room temperature. Samples were mixed with loading buffer (6 ×, New England Biolabs), loaded on gel and run in TAE buffer on a Bio-Rad microprocessor (Model 1000/500 or Model 200/2.0) system at 80 V. As a reference 1 kb DNA ladder (GeneRuler, Fermentas) was used. Visualisation was done by UV irradiation in a Gel Logic 200 imaging system (Kodak) and 535 nm emission filter. For purification bands were cut using sharp blade and purified using Gel extraction kit (Qiagen) following the manufacturers protocol.

1.7 Protein purification

Protein purification was on an Amersham Pharmacia Biotech Äkta FPLC System (P920 pump system, IPC900 UV detector, Frac900 fraction collector, controlled by Amersham Pharmacia Unicorn Software v4.00.16).

1.7.1 His-tagged protein purification

1.7.1.1 General method

Purification of the His.tagged proteins was carried out on a 5 ml nickel affinity column HisTrap (Novagen). Column was pre-equilibrated with 10 CV (column volumes) of binding buffer, then cell lysate was loaded using FPLC pump and column was washed with 5 CV of binding buffer, followed by washing by wash buffer until absorbance reached base line (usually 5-10 CV). Usual flow rate was 1 mL/min. Protein was eluted with elution buffer (5 CV) using FPLC fraction collector (3 mL fractions) and fractions which displayed absorbance at 280 nm were analysed by SDS-PAGE. The desired fractions were combined and concentrated to 2.5 mL and applied to PD10 desalting column to exchange into desired buffer. Protein was aliquoted and frozen at -80^{o}C, unless further purification was required. HisTrap column was treated with 5CV of strip buffer, followed by 10 CV of Milli-Q water, 3 CV of charge buffer and 20 CV of Milli-Q water to be ready for next use.

1.7.1.2 Buffers

Buffers used in HisTrap purifications were as follows:

charge buffer – 100 mM $NiSO_4$

binding buffer – 50mM HEPES pH 7.6, 0.5M NaCl, 5 mM imidazole

wash buffer – 50mM HEPES pH 7.6, 0.5M NaCl, 30 mM imidazole

elution buffer – 50mM HEPES pH 7.6, 0.5M NaCl, 500 mM imidazole

strip buffer – 50mM HEPES pH 7.6, 0.5M NaCl, 100 mM EDTA

1.7.2 Size exclusion chromatography

Size exclusion chromatography was performed using Superdex S200 (300 mL) column, which was equilibrated with 1CV of water and 1 CV gel filtration buffer (50 mM Tris-HCl pH 7.5, 200 mM NaCl) at flow rate of 2 mL/min. Protein solution was loaded using 2 mL loop. Protein was eluted

with gel filtration buffer and fractions were UV level was above 10 mAU (absorbance at 280 nm) were collected (5 mL each) and analysed by SDS-PAGE. Desired fractions were combined, concentrated if desired, aliquoted and stored at -80°C, unless further purification was required.

1.7.3 Ion exchange chromatography

Ion exchange chromatography was performed using Source-Q exchange column using 25 mM Tris-HCl buffer pH 7.5 and gradient of 0-200 mM NaCl.

1.8 Protein concentration

Protein solutions were concentrated using Amicon® Ultra-4 or Ultra-15 Ultracel® PL ultrafiltration devices (Millipore) with 10,000 or 30,000 Da nominal molecular weight limit membranes in an Allegra™ 21R centrifuge (Beckman Coulter; S4180 rotor, 3500 rpm, 4°C).

1.9 Buffer exchange

Buffer exchange was achieved using PD10 desalting columns (GE Healthcare) according to manufacturer's gravity based protocol or Amicon® ultrafiltration devices (Millipore) employing centrifugation.

1.10 Determination of protein concentration

Protein concentrations were determined using an ND-1000 spectrophotometer (NanoDrop® Technologies) and measuring absorbance at 280 nm according to manufacturer's instructions. Molecular weights and extinction coefficients (ε) of proteins of interest were calculated using the ProtParam tool (http://www.expasy.ch/tools/protparam.html).

1.11 SDS-PAGE gel electrophoresis

Gels were casted using glass plates and contained of separating and stacking gel layer. Samples were loaded after mixing 1:1 with 2× SDS-PAGE loading buffer and heating at 95°C for 5 minutes. Gels were run on a Mini-PROTEAN Tetra Electrophoresis System (Bio-Rad) at 200 V in SDS-PAGE running buffer. Protein ladder was used as a molecular weight marker (Thermo Scientific PageRuler Pre-stained Protein Ladder 10-170 kDa). Gel staining was achieved by 15 min incubation with InstantBlue™ Coomassie® stain (Expedeon).

1.11.1 Buffers

SDS-PAGE buffers were prepared as follows:

2×SDS-PAGE separating gel buffer consisted of 750 mM Tris-HCl pH 8.8 and 0.2% (w/v) SDS.

2×SDS-PAGE stacking gel buffer consisted of 250 mM Tris-HCl pH 6.8 and 0.2% (w/v) SDS.

2×SDS-PAGE loading buffer (per 100 mL) consisted of 10 mL Tris-HCl 0.5 M pH 6.8, 0.2 g Bromophenol blue 0.2% w/v, 20 mL SDS 10% w/v, 12 mL glycerol, 5 mL β-mercaptoethanol.

SDS-PAGE running buffer (per 1 L) consisted of: 30.2 g Tris base, 144 g glycine, 100 mL SDS 10% (w/v), 900 mL H_2O.

1.11.2 Gels

Gels were prepared as follows:

Separating gel was prepared by mixing 2.5 mL 2×SDS-PAGE separating gel buffer and 2.5 mL of 30% acrylamide. Just before pouring 10 μL of TEMED (N,N,N',N'-tetramethylethylenediamine) and 30 μL of 25% (w/v) APS (ammonium persulphate) were added.

Stacking gel was prepared by mixing 1 mL of 2×SDS-PAGE stacking gel buffer, 0.7 mL Milli-Q H2O and 0.3 mL 30% acrylamide. Just before pouring 5 μL of TEMED and 15 μL of 25% (w/v) APS were added.

2 NMR

Deuterated solvents were from Sigma and Apollo Scientific Ltd. Tris-d_{11} was obtained from Cambridge Isotope Laboratories. ^{1}H NMR and ^{13}C NMR spectra were recorded using Bruker AVANCE AV400 (400 MHz), Bruker AV 500 MHz with ^{13}C cryoprobe and variable temperature setup, Bruker AVIII 700 with inverse TCI cryoprobe or Bruker AVII 500 machines. ^{19}F NMR experiments were recorded on Bruker AVII 500. Pulses were calibrated using Bruker Pulsecal routine. Data was processed using TopSpin 3.1 (Bruker), ACD/Labs Software.

3 Synthesis and product characterization

Chemicals were from Sigma-Aldrich (Dorset, UK) and used without further purification. Solvents for chemical transformations, work-up and chromatography were from Aldrich at HPLC grade, and used without further purification. Silica gel 60 F254 analytical thin layer chromatography (TLC) plates were from Merck (Darmstadt, Germany) and visualized under UV light, or with potassium permanganate. Chromatographic purifications were performed using prepacked SNAP columns on a Biotage SP1 Purification system (Uppsala, Sweden). Deuterated solvents were from Sigma and Apollo Scientific Ltd. ^{1}H NMR spectra were recorded using Bruker AVANCE AV400 (400 MHz), Bruker AV 500 MHz with ^{13}C cryoprobe and variable temperature setup, Bruker AVIII 700 with inverse TCI cryoprobe or Bruker AVII 500 machines. Signal positions were recorded in δ ppm with the abbreviations s, d, t, q, and m denoting singlet, doublet, triplet, quartet and multiplet respectively. NMR chemical shifts were referenced to residual solvent peaks. Coupling constants, *J*, are registered in Hz to a resolution of 0.5 Hz. High Resolution (HR) mass spectrometry data (m/z) were obtained from a Bruker MicroTOF instrument using an ESI source and Time of Flight (TOF) analyzer. Values are reported as ratio of mass to charge in Daltons. Melting points were obtained using a Leica VMTG heated-stage microscope or Stuart SMP-40 automatic melting point apparatus. Fourier transform Infrared (FT-IR) spectra were recorded on a Bruker Tensor 27 instrument. Optical rotations were recorded using a Perkin Elmer 241 Polarimeter.